DIPLOME D'HABILITATION A DIRIGER DES RECHERCHES

"MICROMETEORITES CONCORDIA : DES NEIGES ANTARCTIQUES AUX GLACES COMETAIRES"

Cécile ENGRAND

Soutenance du 14 Novembre 2008 devant le jury constitué de :

- Mme Dominique BOCKELEE-MORVAN (Rapporteur)
- M. Marc CHAUSSIDON (Rapporteur)
- Mme Odile DUTUIT
- M. François GUYOT (Président)
- M. Louis d'HENDECOURT
- M. François ROBERT (Rapporteur)

CSNSM – CNRS/IN2P3

UNIVERSITE PARIS SUD-ORSAY

TABLE DES MATIERES

Introduction

Les analyses en laboratoire d'échantillons extraterrestres ont apporté des éléments essentiels à la connaissance de la formation de notre Système Solaire, il y a 4,5 milliards d'années. Une large partie des contraintes dont nous disposons pour comprendre cette époque lointaine provient des analyses chimiques, minéralogiques et isotopiques de 3 principales familles de matériau extraterrestre primitif : 1) les météorites primitives (principalement les chondrites carbonées) ; 2) les poussières interplanétaires collectées par la NASA dans la stratosphère (IDPs pour Interplanetary Dust Particles) (Brownlee 1985) ; et 3) les micrométéorites (MMs) collectées dans les glaces et les neiges polaires (Maurette *et al.* 1987; Maurette *et al.* 1991; Taylor *et al.* 1998; Yada et Kojima 2000; Duprat *et al.* 2007).

Les météorites proviennent (sauf pour les roches lunaires et martiennes) de la ceinture principale d'astéroïdes. La poussière cosmique (micrométéorites et IDPs) provient à la fois des astéroïdes et des comètes, dans des proportions mal définies. Les comètes à courte période sont des objets formés dans la ceinture de Kuiper lors de la naissance du système solaire. N'étant parvenues dans les régions internes du système solaire que récemment, elles ont échappé à l'évolution qui a conduit à la formation des corps planétaires et aux phénomènes secondaires (différenciation, altération aqueuse…) pouvant agir sur les astéroïdes. Les comètes auraient donc préservé une meilleure "mémoire" des tous premiers instants de la formation du système solaire que les météorites. Toutefois, du point de vue astronomique, une dichotomie stricte entre comètes et astéroïdes est remise en question : des objets identifiés comme des astéroïdes se sont révélés posséder une activité cométaire (Hsieh et Jewitt 2006) alors que les récentes observations de noyaux cométaires par des sondes spatiales (Wild 2, Borrelly, Temple 1) ont révélé des structures de surfaces présentant peu de différences avec celles des astéroïdes. De même, plusieurs auteurs ont proposé que certaines météorites réputées astéroïdales pourraient en fait avoir une origine cométaire (e.g. McSween et Weissman 1989; Gounelle *et al.* 2006b). La mission spatiale Stardust de la NASA a rapporté sur Terre en janvier 2006 des échantillons de poussière de la comète Wild 2. Malgré la dégradation des échantillons due à leur méthode de collecte (impact à 6 km/s dans un aerogel de silice), les analyses préliminaires des grains de poussière de Wild 2 montrent une matière "solaire normale" (e.g. Brownlee *et al.* 2006). Les modèles classiques de grains cométaires formés d'agrégats exotiques de grains interstellaires cimentés par une matière organique abondante (Greenberg et Hage 1990) seraient donc remis en question dans le cas de cette comète. La question est de savoir si les comètes forment un réservoir relativement homogène, ou s'il y a une grande hétérogénéité de composition au sein de la population des comètes. Seuls les échantillons collectés sur Terre, identifiés comme cométaires, pourraient nous permettre d'aborder ce point, le coût d'une mission spatiale étant trop élevé pour analyser un nombre statistiquement représentatif de comètes.

Les questions auxquelles nous tentons de répondre sont donc les suivantes :

- La poussière cométaire est-elle très différente de la poussière astéroïdale? En quelle proportion les comètes ont-elles accrétés des grains issus du milieu interstellaire froid et des poussières issues des régions internes chaudes du système solaire naissant? Cette question essentielle permettrait d'aborder des problèmes tels que la dynamique de la nébuleuse protosolaire, l'efficacité des vents stellaires pour éjecter la matière formée dans le système solaire interne vers l'extérieur, le degré de turbulence de la nébuleuse, sa viscosité ou encore les perturbations gravitationnelles liées à la formation des planètes géantes. La détermination de ces proportions est également essentielle pour comprendre comment se termine le cycle de la poussière interstellaire par son injection dans les

étoiles en formation et donc pour étudier comment elle contribue à l'évolution chimique de la galaxie, et comment elle est préservée et modifiée dans le milieu interstellaire froid.

- Les poussières astéroïdales ou cométaires ont-elles contribué à l'apparition de la vie sur Terre (ou sur d'autres corps planétaires comme Mars, Titan, Europe, Encelade…)? Répondre à cette question impose d'étudier l'origine et l'évolution de la matière organique dans le système solaire. Plusieurs voies de synthèses abiotiques (catalyse minérale, réactions en phase gazeuse, irradiation d'analogues de glaces interstellaires…) peuvent conduire à la formation de composés prébiotiques tels que les acides aminés. Il est donc important de déterminer la composition et la structure chimique de la matière organique météoritique pour déterminer quels types de molécules ont pu être apportés aux corps planétaires.

L'analyse des micrométéorites (MMs) peut apporter des éléments de réponse à ces questions. Notre groupe d'astrophysique du solide du CSNSM, avec Michel Maurette comme pionnier, collecte les micrométéorites dans les glaces antarctiques depuis 1984 (Maurette *et al.* 1987; Maurette *et al.* 1991) et dans la neige des régions centrales Antarctiques depuis 2000 (Duprat *et al.* 2007). Ces poussières extraterrestres se sont révélées constituer une nouvelle population d'objets extraterrestres : leur compositions et distributions se rapprochent uniquement d'une classe rare de météorites, les chondrites carbonées (~ 4% des chutes de météorites), mais elles s'en distinguent par des caractéristiques primitives : taille et nature des minéraux, composition isotopique de l'hydrogène… (e.g. Kurat *et al.* 1994; Engrand et Maurette 1998; Engrand *et al.* 1999a). Les MMs contiennent des minéraux hydratés et environ 2 % en poids de matière carbonée (Engrand et Maurette 1998; Matrajt *et al.* 2001). Les MMs représentent l'essentiel de l'apport extraterrestre sur Terre, environ 1000 fois plus que les météorites (Love et Brownlee 1993; Bland *et al.* 1996). En raison de leurs petites tailles, elles subissent peu le phénomène de focalisation gravitationnelle qui influence la chute des météorites sur Terre, et leur mode de récolte minimise les biais de collecte. La composition du flux de MMs parait également globalement invariante dans le temps et en fonction de la taille des grains (Gounelle *et al.* 2003; Gounelle *et al.* 2005b). Les MMs représentent donc probablement mieux la matière interplanétaire que les météorites. Leur teneur en matière carbonée et en volatils en font des candidats intéressants pour un apport de matière prébiotiques sur Terre, il y a 4 milliards d'années au moment de l'apparition de la vie.

En parallèle avec ces études, je me suis intéressée à la technique d'analyse isotopique la plus adaptée à la petite taille de nos échantillons : la microsonde ionique. En coopération avec G. Slodzian qui a rejoint notre groupe fin 2002, nous avons tenté de créer un pôle de microsonde ionique à Orsay. Notre tentative n'a pas été totalement couronnée de succès, mais beaucoup d'efforts ont été investis dans l'étude de cet instrument, en particulier pour essayer de développer la cosmochimie isotopique du silicium à l'aide de la microsonde ionique.

Je suis également impliquée en tant que CoI ("Co-investigator") dans la qualification scientifique de l'analyseur de poussière COSIMA (COmetary Secondary Ion Mass Analyzer) de la mission cométaire ROSETTA, lancée le 2 Mars 2004, qui atteindra la comète 67P/Churyumov-Gerasimenko en 2014. COSIMA est une microsonde ionique statique (ou encore "à temps de vol", TOF-SIMS) conçue par J. Kissel, qui analysera la poussière cométaire (Kissel *et al.* 2007). Les opérations de qualification de COSIMA sont réalisées en collaboration avec l'équipe COSIMA du LPCE (Orléans) qui en possède un prototype, et de l'équipe de M. Hilchenbach (Max Planck Institut für Sonnensystemforschung de Lindau, Allemagne) où se trouve le modèle au sol (Reference Model) de COSIMA. Nous utilisons nos collections de micrométéorites antarctiques, qui ont été proposées comme échantillons de calibration du fait de leur possible origine cométaire (e.g. Maurette *et al.* 2000), et d'échantillons de minéraux utilisés comme standards analytiques.

Récemment, j'ai également été associée à une aventure me ramenant en pensée à Dôme C où j'ai passé 3 semaines en Janvier et Février 2002 pour collecter les micrométéorites: deux niveaux de poussières ont été découverts dans le grand carottage EPICA-Dôme C, datés à – 430 000 et – 480 000 ans. Nous avons montré l'origine extraterrestre de ces poussières et cherché à comprendre les mécanismes qui ont provoqué ces couches de débris : impacts ou augmentation du flux sporadique de poussières cosmiques ?

Je finirai ce manuscrit par la brève description des axes de recherche que j'envisage pour les prochaines années.

1 Les micrométéorites : archives de la formation du système solaire et artisans de la vie sur Terre?

1.1 Les collectes de micrométéorites

Les petits corps du système solaire (astéroïdes et comètes) sont actuellement les seules archives relativement intactes de la formation du système solaire. Leur devenir lors de l'évolution du système solaire a également pu influencer l'histoire de la Terre, en particulier en ce qui concerne l'apport de volatiles sur Terre et l'origine de la vie (voir section 1.3).

Des particules de poussières d'origines astéroïdale et cométaire, de taille inférieures au millimètre, arrivent sur Terre avec des vitesses allant de ~ 15 km/s à plus de 50 km/s. On appelle micrométéorites les poussières qui sont transmises à la surface terrestre sans avoir été vaporisées dans l'atmosphère. Le flux de micrométéoroïdes avant l'entrée atmosphérique est estimé à ~ 30 000 ± 20 000 tonnes (**Figure 1-1**) (d'après Love et Brownlee 1993), et constitue l'essentiel du flux de matière extraterrestre arrivant actuellement sur Terre, apportant environ 1000 fois plus de masse que les météorites (Bland *et al.* 1996).

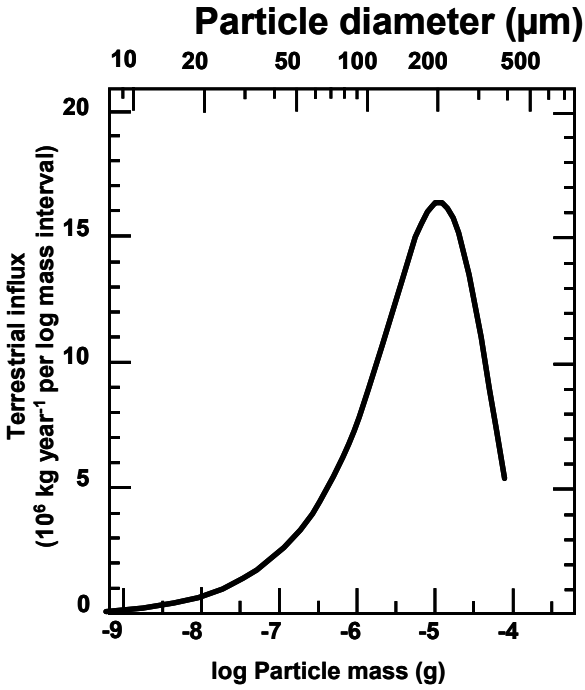

Figure 1-1 : Flux de micrométéoroïdes à 1 unité astronomique (UA) (LDEF) (Love et Brownlee 1993)

Les micrométéorites ne peuvent être collectées efficacement que dans les régions de faible accumulation de matière terrestre, dans les sédiments marins de grande profondeur (e.g. Ganapathy *et al.* 1978; Blanchard *et al.* 1980; Brownlee *et al.* 1997), dans la stratosphère (e.g. Brownlee 1985; Rietmeijer 1998) ou dans les calottes polaires arctiques et antarctiques (e.g. Maurette *et al.* 1986; Harvey et Maurette 1991; Maurette *et al.* 1991; Taylor *et al.* 1998; Nakamura *et al.* 1999; Taylor *et al.* 2000; Terada *et al.* 2001; Duprat *et al.* 2005a; Duprat *et al.* 2007). Notre groupe les collecte dans les glaces et les neiges polaires depuis les années 1990.

1.1.1 Collectes glaciaires en Terre Adélie : Collection de micrométéorites de Cap Prudhomme

Les premières collectes de micrométéorites non fondues furent réalisées par Michel Maurette au Groenland (Maurette *et al.* 1986; Maurette *et al.* 1987). De par les énormes quantités de glace fondues annuellement et aboutissant dans les lacs bleus, les collectes groenlandaises, réalisées à partir des sédiments accumulés au fond des lacs bleus, offrent l'avantage de donner accès aux micrométéorites statistiquement rares de grandes tailles (>300 µm). Un inconvénient inhérent à ces collectes est le développement de sidérobacteries filamentaires au fond de ces lacs bleus qui enserrent les micrométéorites et qu'il est nécessaire de désagréger pour en extraire les particules extraterrestres.

Pour remédier à ces problèmes de contamination en matière organique terrestre et de destruction des grains les plus friables, Michel Maurette décida de tenter la collecte des micrométéorites en Antarctique. Le processus utilisé consiste à former dans un champ de glace bleue, au cours d'une journée, une poche d'eau de fusion de la glace qui sera ensuite pompée et filtrée sur 4 tamis métalliques (de 25 µm à 400 µm) pour en extraire les micrométéorites initialement contenues dans la glace (Maurette *et al.* 1991). Le sable glaciaire obtenu contient jusqu'à 20% de micrométéorites non fondues (Engrand 1995).

Au cours de ma thèse et de mes séjours postdoctoraux, j'ai principalement travaillé sur la caractérisation des micrométéorites de Cap Prudhomme collectées en 1991 et 1994. J'ai contribué à montrer que les micrométéorites ne sont reliées qu'à une classe relativement rare de météorites, les chondrites carbonées (Engrand et Maurette 1998; Engrand *et al.* 1999a; Engrand *et al.* 1999b; Engrand *et al.* 2005). Dans l'article *"The classification of micrometeorites"* (Genge *et al.* 2008), nous considérons cette collecte de Cap Prudhomme comme référence pour établir une classification des micrométéorites, plus simple que celle des météorites puisqu'elle est essentiellement basée sur le degré d'échauffement atmosphérique souffert par les grains lors de l'entrée atmosphérique (**Figure 1-2**).

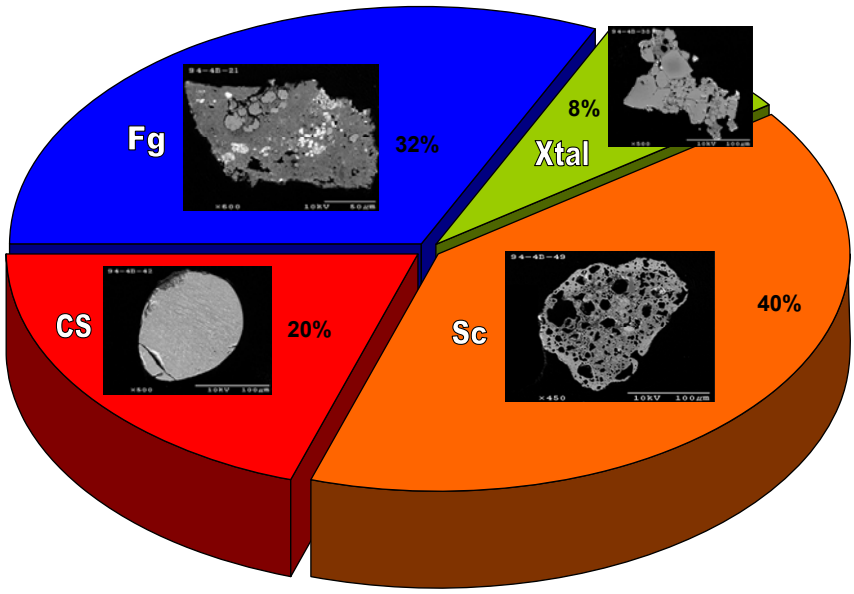

Figure 1-2 : Classification texturale des micrométéorites et abondances de chaque type, établie d'après la collection de micrométéorite de Cap Prudhomme. Cette classification est basée sur leur degré d'échauffement des micrométéorites lors de l'entrée atmosphérique : Fg = Fine-grained (non fondu à grain fin); Xtal = cristalline (non fondu à gros grain); Sc = Scorie (partiellement fondu); CS = Cosmic spherule (micrométéorite majoritairement ou totalement fondue).

Les collectes de Cap Prudhomme montrent une grande différence avec les collectes stratosphériques d'IDPs ("Interplanetary Dust Particles", nom historiquement attribué aux poussières collectées par la NASA dans la stratosphère) : les grains les plus friables en sont absents. Cette différence aurait pu s'expliquer par une variation de la composition du flux de poussières en fonction de la taille (les IDPs étant généralement < 10µm, alors que les micrométéorites sont collectées dans un domaine de taille > 25 µm), ou par un biais de collecte. Avec la collection Concordia (voir section suivante 1.1.2), nous avons montré qu'il s'agissait principalement d'un biais de collecte.

1.1.2 Collectes dans la neige de Dôme C : Collection de micrométéorites CONCORDIA

Depuis 2000, nous collectons les micrométéorites dans la neige des régions centrales antarctiques, sur le site de Dôme C (S75°, E123°) où se trouve la nouvelle base franco-italienne "CONCORDIA" (e.g. Duprat *et al.* 2001; Duprat *et al.* 2003; Duprat *et al.* 2005a; Duprat *et al.* 2007). Ce programme "Micrométéorites à CONCORDIA", est piloté par mon collègue J. Duprat, avec le soutien de l'IPEV (Institut Polaire Français - Paul-Emile-Victor). Trois expéditions de collectes de micrométéorites ont été réalisées à ce jour : en 2000 pour une étude de faisabilité, en 2002 pour une première collecte dans des conditions logistiques assez difficiles, et en 2006 avec un matériel de collecte optimisé. Nous avons, pour ce programme, bénéficié d'un partenariat avec le groupe industriel Chaffoteaux & Maury. J'ai participé à la collecte sur le terrain de 2002.

Par rapport aux collectes de micrométéorites précédemment réalisées, par fonte et filtration de la glace bleue dans les régions côtières, le site de Dôme C présente plusieurs avantages pour la recherche de poussières d'origine extraterrestre : **(i)** sa neige de surface est isolée des sources de poussières terrestres par une épaisseur de glace de plus de 3 kms, et par une distance des côtes de plus de 1100 kms ; **(ii)** le taux de précipitation y étant faible et régulier, il est possible de mesurer le flux de micrométéorites accrétées par la Terre; **(iii)** la température varie de – 30°C à – 80°C, avec un taux d'humidité très faible, ce qui limite les processus d'altération aqueuse dans les micrométéorites; **(iv)** les micrométéorites sont collectées dans la neige et n'ont pas été soumises aux fortes contraintes mécaniques qui transforment la neige en glace à grande profondeur.

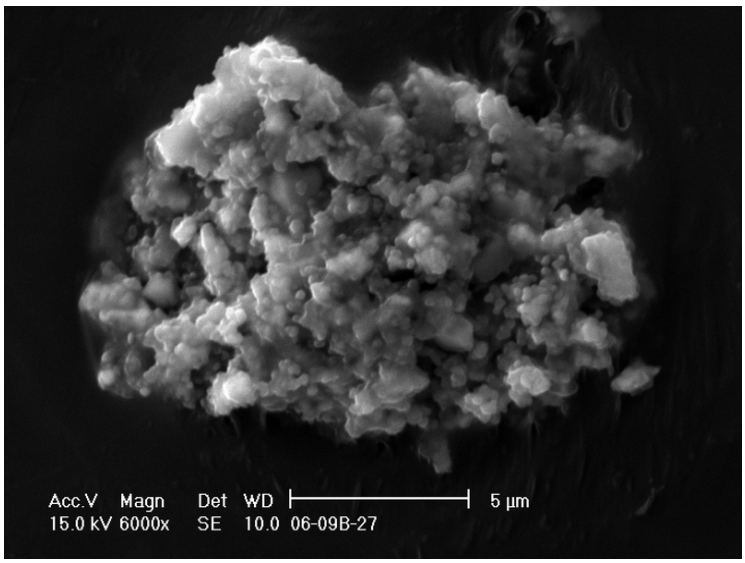

Figure 1-3 : Micrographie électronique de la surface extérieure d'un fragment d'une micrométéorite friable de la collection Concordia 2006 (image en électrons secondaires).

Les collectes de 2002 et 2006 ont en particulier mis en lumière une nouvelle famille de grains très poreux et friables (**Figure 1-3**) et des micrométéorites ultracarbonées (voir section 1.2.5.1). Des phases solubles (sulfures de fer, carbonates) n'existant pas dans les collections précédentes effectuées dans les glaces des régions côtières ont également été mises en évidence dans les micrométéorites Concordia (**Figure 1-4**).

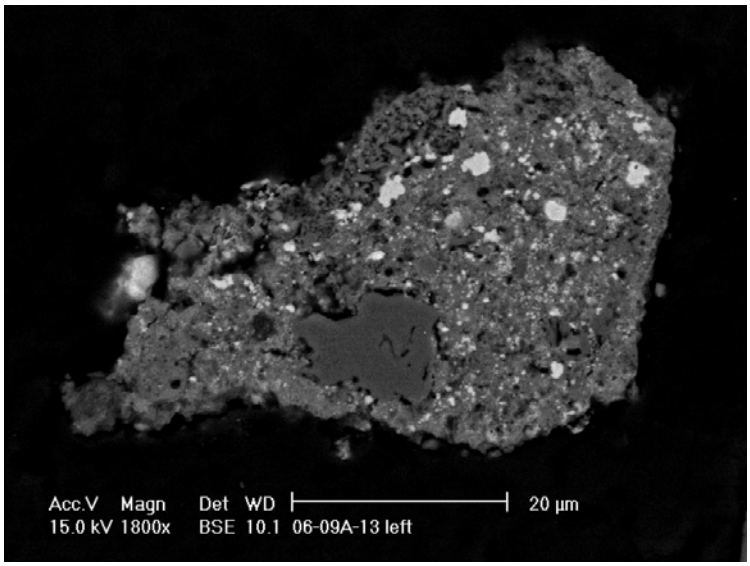

Figure 1-4 : Micrographie électronique d'une section polie d'un fragment de micrométéorite Concordia (image en électrons rétrodiffusés). Les phases blanches sont des sulfures de fer primitifs.

En 2002 et 2006, nous avons pu collecter plusieurs milliers de micrométéorites dans la neige prélevée à 3 kilomètres de la station Concordia à Dôme C. Environ 600 grains sont classifiés à ce jour, chaque grain extraterrestre étant cassé en plusieurs fragments dont le plus petit est caractérisé par microscopie électronique à balayage, pour s'assurer de sa nature extraterrestre. Dans la collecte 2006, environ 80% des grains analysés sont extraterrestres, ce qui est un degré de pureté exceptionnel pour une collection de micrométéorites.

Les caractéristiques de la collection Concordia et les implications de leurs études sont décrites dans la section 1.2.5.

1.2 Vers un continuum astéroïde-comète

Les compositions isotopiques de certains éléments comme l'oxygène et l'hydrogène dans la matière extraterrestre, traduisent la distribution des réservoirs isotopiques dans la nébuleuse solaire et peuvent être utilisées comme traceurs des processus de formation et d'évolution de ces matériaux extraterrestres.

L'utilisation de la microsonde ionique a révolutionné la cosmochimie isotopique ; c'est actuellement le seul instrument capable de réaliser des mesures isotopiques localement à l'échelle de quelques micromètres (voir aussi section 2.1). Etant donnée la petite taille des phases minérales des micrométéorites, et la nécessité de les comparer à des phases de même nature présentes dans les météorites, nous avons réalisé l'ensemble de ces études à l'aide de la microsonde ionique CAMECA IMS1270 de la facilité nationale de Nancy (CRPG-CNRS).

Les analyses ont été réalisées dans différents échantillons extraterrestres : **i)** des micrométéorites antarctiques modernes (MMAs) ; **ii)** des micrométéorites juvéniles,

piégées depuis plus de 4 Ga dans des météorites ; **iii)** des IDPs, particules de poussières interplanétaires collectées dans la stratosphère par la NASA ; **iv)** une météorite de type nouveau, Tagish Lake, qui a été proposée comme un corps parent possible des micrométéorites (Noguchi et Nakamura 2001).

1.2.1 Les micrométéorites de Cap Prud'homme : compositions isotopiques (H et O)

1.2.1.1 Composition isotopique de l'hydrogène des MMAs

Dans l'article "*Extraterrestrial water in micrometeorites and cosmic spherules from Antarctica : an ion microprobe study*", j'ai mesuré la composition isotopique de l'hydrogène des phases hydratées des micrométéorites antarctiques (Engrand *et al.* 1999a). L'utilisation d'un faisceau primaire d'O^- sur la microsonde ionique permet de favoriser l'émission de l'hydrogène des phases hydratées par rapport à l'hydrogène organique (Deloule et Robert 1995). Nous avons montré que la distribution des rapports D/H des micrométéorites recoupe celle des CCs, et est centrée sur la valeur terrestre SMOW (Standard Mean Ocean Water) (**Figure 1-5**) (Engrand *et al.* 1999a). Les micrométéorites antarctiques (MMAs) n'ont pas été contaminées par l'eau terrestre dont la valeur en antarctique est beaucoup plus basse (voir **Figure 1-5**). Cette étude fait un lien entre les MMAs et les chondrites carbonées, tout en démontrant qu'il n'y a pas de similarité parfaite entre ces deux familles d'objets extraterrestres.

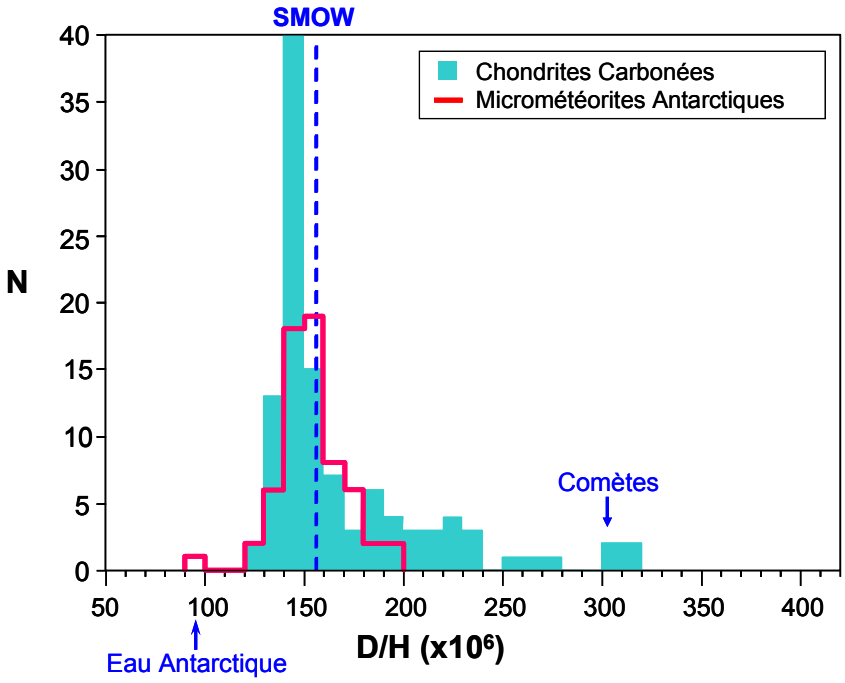

Figure 1-5 : Distribution des rapports D/H dans les micrométéorites antarctiques de Cap Prudhomme (ligne rouge) comparée à celle des chondrites carbonées (données extraites de (Kerridge 1985; Pearson *et al.* 2001; Eiler et Kitchen 2004). D'après (Engrand *et al.* 1999a).

La similitude de la valeur moyenne de la composition isotopique de l'hydrogène des micrométéorites avec la valeur terrestre a également suggéré un scénario d'accrétion de l'eau terrestre par les poussières cosmiques ((Maurette *et al.* 2000) et voir section 1.3.1). La valeur du rapport D/H de la vapeur d'eau des comètes est d'environ deux fois la valeur terrestre (Balsiger *et al.* 1995; Bockelée-Morvan *et al.* 1997; Meier *et al.* 1998b; Meier et Owen 1999; Weaver *et al.* 2008). Cette valeur haute montre que les comètes n'ont pu apporter plus de quelques pourcents de l'eau terrestre.

1.2.1.2 Composition isotopique de l'oxygène des MMAs et des sphérules cosmiques

Dès les années 1970, les analyses de la composition isotopique de l'oxygène des météorites en roche totale par spectrométrie de masse classique, ont montré que la nébuleuse solaire était isotopiquement hétérogène pour l'oxygène, chaque classe de météorite ayant une signature individuelle (e.g. Clayton *et al.* 1973; Clayton *et al.* 1976). De plus, des anomalies isotopiques de l'oxygène ont été découvertes dans les inclusions réfractaires de météorites primitives, les premiers assemblages minéraux formés dans le système solaire primitif (e.g. Clayton 1993; Clayton et Mayeda 1999). Les processus ayant conduit à cette distribution de la composition isotopique de l'oxygène dans les météorites ne sont pas encore clairement établis. Le scénario classique reposant sur les analyses en roche totale des météorites (Clayton et Mayeda 1999) a été remis en question dès le début des années 2000 en particulier par des analyses à la microsonde ionique de phases individuelles de météorites (e.g. Krot *et al.* 2002). A ce jour, trois scenarios ont été envisagés pour expliquer la distribution des réservoirs isotopiques primitifs de l'oxygène : **i)** contamination du système solaire par une supernova apportant de l'^{16}O pur (Clayton *et al.* 1973; Clayton 1993); **ii)** fractionnement isotopique indépendant de la masse semblable à celui observé dans l'ozone atmosphérique (Thiemens et Heidenreich 1983; Gao et Marcus 2001; Robert et Camy-Peyret 2001) agissant dans la nébuleuse solaire (Marcus 2004); **iii)** effet photochimique dû à la photodissociation sélective de molécules CO enrichies en isotopes lourds (self-shielding) produisant de l'oxygène atomique riche en ^{17}O et ^{18}O (Clayton 2002; Yurimoto et Kuramoto 2004; Lyons et Young 2005).

Presque 40 ans après la découverte de l'anomalie isotopique en ^{16}O des inclusions réfractaires et de la droite des CAIs, la composition isotopique de l'oxygène météoritique n'est pas expliquée par un scénario unique auto-cohérent.

Constituées d'assemblages déséquilibrés de matériau carboné-hydraté, les micrométéorites devraient représenter un échantillonnage plus représentatif de la population d'objets présents dans le système solaire que les météorites conventionnelles (e.g. Engrand et Maurette 1998). Dans l'article "*Oxygen isotopic compositions of individual minerals in Antarctic micrometeorites : further links to carbonaceous chondrites*" nous avons montré que la composition isotopique de l'oxygène des minéraux anhydres des MMAs est similaire à celle des météorites les plus primitives, les chondrites carbonées (Engrand *et al.* 1999b) (**Figure 1-6**). Toutefois, il existe des différences entre ces deux populations d'objets, telles que de forts rapports d'abondance pyroxène/olivine dans les MMAs.

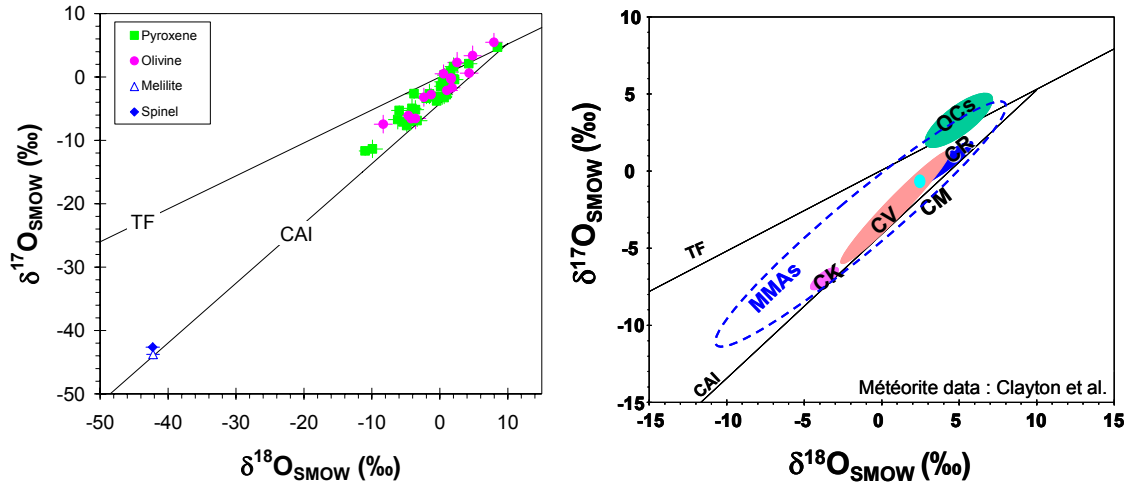

Figure 1-6 : Comparaison de la composition isotopique de l'oxygène des minéraux anhydres des micrométéorites (gauche) et des chondres des chondrites carbonées (droite, d'après Clayton 1993 – le domaine de variation des micrométéorites y est indiqué par le contour pointillé MMAs). D'après (Engrand *et al.* 1999b).

La composition isotopique de l'oxygène des micrométéorites est comparable à celle des échantillons de Wild2 mesurés à ce jour (McKeegan *et al.* 2006) (**Figure 1-7**).

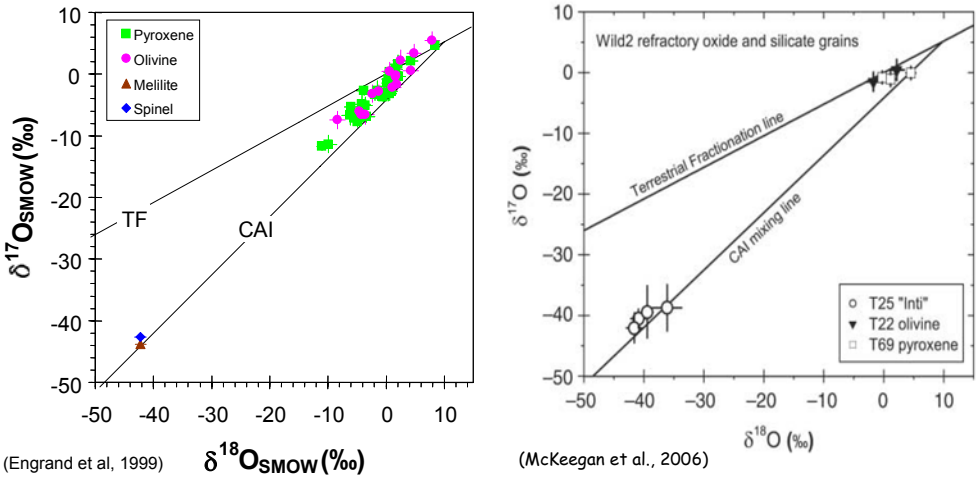

Figure 1-7 : Composition isotopique de l'oxygène des micrométéorites antarctiques (Engrand *et al.* 1999b) comparée à celle des échantillons de la comète Wild2 (McKeegan *et al.* 2006).

Les résultats des études de l'oxygène des micrométéorites indiquent une similarité à la fois avec les chondrites carbonées et les échantillons de la comète Wild2, suggérant un continuum entre la matière astéroïdale primitive et la matière cométaire.

Dans l'article *"Isotopic compositions of oxygen, iron, chromium, and nickel in cosmic spherules: Toward a better comprehension of atmospheric entry heating effects"*, nous avons cherché à mieux comprendre le stress subi par les micrométéorites lors de l'entrée atmosphérique, en étudiant les sphérules cosmiques (Engrand *et al.* 2005). Cette étude a montré que les sphérules cosmiques de type I (composés d'oxyde de fer) collectés dans les sédiments de grande profondeur (e.g. Brownlee *et al.* 1984) étaient initialement du métal chondritique qui s'est oxydé avec l'oxygène atmosphérique et a perdu une grande partie de sa masse sous forme de métal puis d'oxyde par évaporation lors de l'entrée atmosphérique (Engrand *et al.* 2005). Les sphérules cosmiques antarctique silicatés n'ont subi que de petits effets de fractionnement isotopique, soulignant la rapidité du flash heating qu'ils ont subi (Toppani *et al.* 2001) et pouvant être expliqués pour la plupart par un mélange entre l'oxygène extraterrestre et atmosphérique pendant les quelques secondes où le grain est fondu (e.g. Engrand *et al.* 2005). La composition isotopique de l'oxygène de ces sphérules cosmiques est en accord avec une origine du précurseur micrométéoroïde de type chondrite carbonée. Il n'y a donc pas d'incohérence entre la nature des micrométéorites non fondues et celle des sphérules cosmiques, en accord avec le travail de Brownlee (1997).

1.2.2 Variation du flux de micrométéorites en fonction du temps? Micrométéorites juvéniles piégées dans les météorites HED

La distribution des rapports D/H dans les MMAs est centrée sur la valeur des océans terrestres (Engrand *et al.* 1999a). Cette similarité a incité M. Maurette à développer le scénario "EMMA", qui évalue le rôle des micrométéorites dans la formation de l'air et des océans de la Terre primitive (voir (Maurette *et al.* 2000) et section 1.3.1). Ce scénario fait l'hypothèse que la composition des micrométéorites accrétées par la Terre il y a environ 4 Ga, sont similaires à celles des micrométéorites contemporaines.

Gounelle *et al.* (2003) ont identifié des micrométéorites juvéniles, piégées dans plusieurs météorites HED formées il y a environ 4,2 Ga par la compaction de la couche superficielle (régolite) de leur astéroïde parent (probablement Vesta). La minéralogie de ces micrométéorites juvéniles est similaire à celle des MMAs (Gounelle *et al.* 2003).

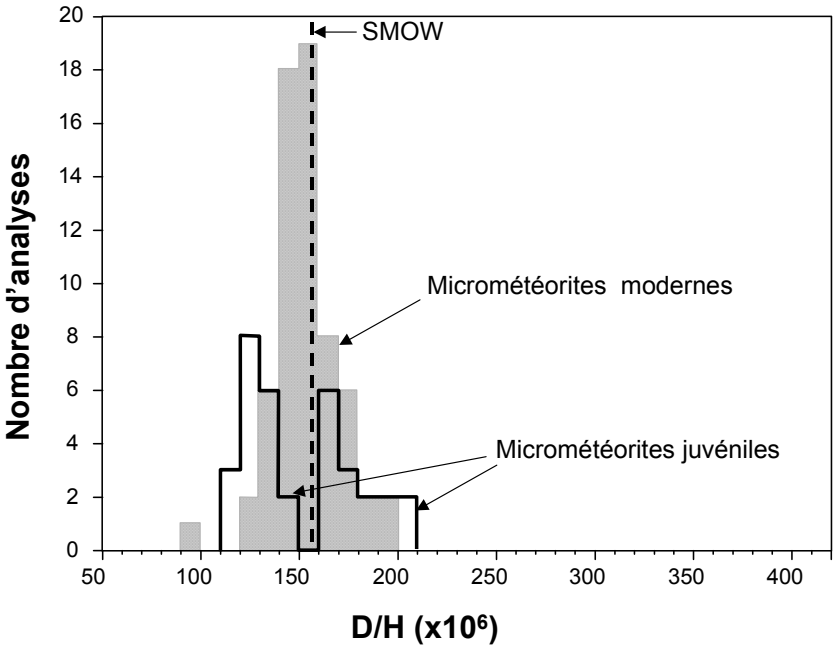

Figure 1-8 : Distributions des rapports D/H dans les phases hydratées des micrométéorites "juvéniles" et des micrométéorites antarctiques modernes. Les deux distributions sont comparables. La valeur des océans terrestres (SMOW, pour Standard Mean Ocean Water) est indiquée pour référence. D'après (Gounelle *et al.* 2005a)

Dans l'article "*Hydrogen isotopic composition of water from fossil micrometeorites in howardites*", nous avons pu mesurer grâce à la facilité nationale de microsonde ionique (CRPG de Nancy) la composition isotopique de l'hydrogène de ces micrométéorites juvéniles (Gounelle *et al.* 2005a). Dans cette étude, nous avons utilisé un faisceau d'ions primaires d'oxygène qui donne accès principalement à la contribution des phases hydratées (voir Deloule et Robert 1995; Engrand *et al.* 1999a). La distribution des rapports D/H dans les micrométéorites juvéniles présente une plage de variation similaire à celle des MMAs (**Figure 1-8**). Cette étude confirme que la composition isotopique de l'hydrogène du flux de micrométéorites de tailles voisines de 100 µm n'a pas varié depuis au moins 4 Ga. Elle valide l'utilisation de la composition isotopique de l'hydrogène des MMAs actuelles pour le scenario EMMA (voir section 1.3.1).

1.2.3 Variation du flux en fonction de la taille? Petites MMs de Cap Prudhomme et Interplanetary Dust particles (IDPs)

Nous collectons les micrométéorites antarctiques dans un domaine de taille allant de 25 µm à ~ 400 µm, qui correspond à la fraction dominante du flux de matière extraterrestre accrété par la Terre. Des micrométéorites de plus petites tailles (1 - 30 µm, les IDPs) sont collectées dans la stratosphère par la NASA. Pour tester une éventuelle variation de la composition du flux de poussières cosmiques en fonction de la taille, nous avons caractérisé des micrométéorites de petites tailles de Cap Prudhomme et des IDPs.

Dans l'article "*Small Antarctic micrometeorites (25-50µm): a mineralogical and in situ oxygen isotopic study*", nous avons montré que la composition isotopique de l'oxygène des petites micrométéorites était semblable à celle de leurs consœurs de plus grandes tailles décrites ci-dessus (Gounelle *et al.* 2005b). Ce résultat, couplé aux observations

minéralogiques, donne une indication que la composition du flux de micrométéorites ne semble pas varier drastiquement en fonction de la taille.

Dans l'article "*Clues on the origin of interplanetary dust particles from the isotopic study of their hydrogen-bearing phases*", nous avons analysé 5 IDPs à l'aide de la microsonde ionique de Nancy pour préciser la phase porteuse des enrichissements en deutérium observés dans les IDPs (Aléon *et al.* 2001). Avec un microfaisceau d'ions primaires Cs^+, nous avons réalisé des cartographies ioniques de répartition de différentes espèces (H, D, C, Al, Si, K) dans ces IDPs. Ce faisceau primaire d'ions Cs^+ permet d'analyser l'hydrogène provenant à la fois les phases hydratées et les phases organiques. La distribution des rapports D/H dans les IDPs est très étendue, avec des valeurs jusqu'à 20 fois la valeur terrestre SMOW (McKeegan *et al.* 1985; Messenger 2000). Ces valeurs anormalement élevées, qui traduisent un enrichissement important en deutérium, sont attribuées à la préservation de phases d'origine interstellaire dans ces grains (e.g. Messenger 2000).

La **Figure 1-9** représente le diagramme de corrélation obtenu pour l'une de ces IDPs, donnant les variations du rapport D/H en fonction des rapports C/H. Il reflète l'existence d'au moins 4 phases porteuses de l'hydrogène : une eau semblable à celle que l'on trouve dans les chondrites carbonées de type CM2 et CI et dans les micrométéorites ; et 3 sortes de matière organique, MO1, MO2 et MO3. "MO1" correspond à la matière organique insoluble météoritique, légèrement enrichi en deutérium. Avec un rapport C/H égal à 1, et une valeur D/H proche de celle mesurée pour l'acide cyanhydrique (HCN) dans le coma de la comète de Hale-Bopp (Meier *et al.* 1998a), "MO2" pourrait être identifiée à du HCN cométaire. MO3 est une phase organique non identifiée.

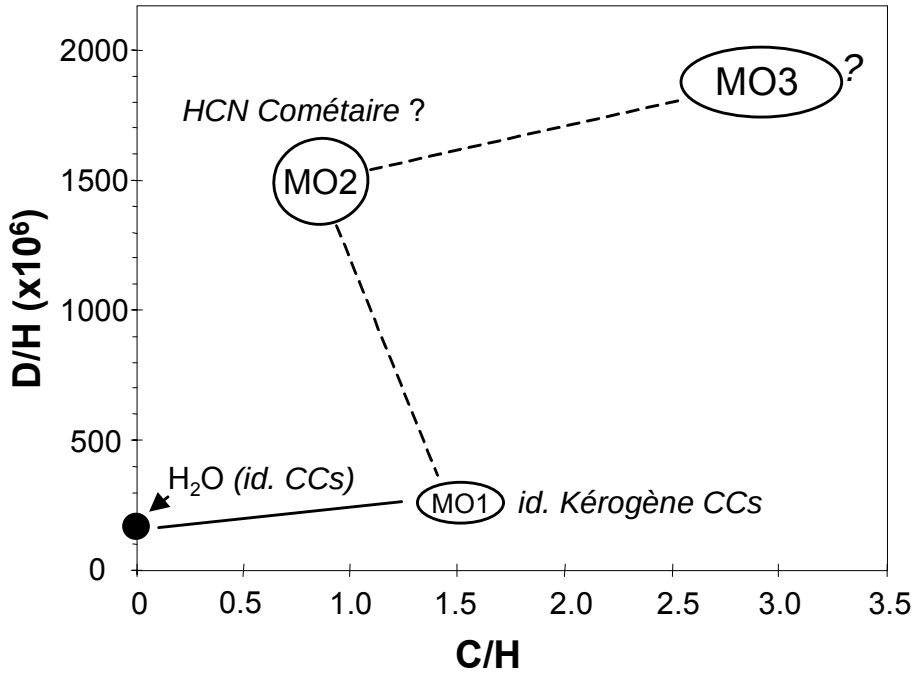

Figure 1-9 : Diagramme de corrélation montrant l'identification de 4 phases porteuses d'hydrogène dans une même IDPs : l'eau et 3 sortes de matière organique (MO) de rapports C/H différents. D'après (Aléon *et al.* 2001).

Dans une même IDP dont la taille ne dépasse pas 50 µm, l'association à l'échelle du micron de phases typiques des chondrites carbonées (CCs) et de composants cométaires (HCN?) suggère de nouveau un lien entre les corps parents des chondrites carbonées et des comètes.

1.2.4 Une météorite exceptionnelle : Tagish Lake

Tagish Lake est une météorite très primitive, d'un type nouveau (CI2). Elle a été collectée en Janvier 2000 dans des conditions propres dans les régions très froides du nord-ouest du Canada, après observation du météore causé par sa rentrée atmosphérique (Brown *et al.* 2000). Certains auteurs ont proposé que Tagish Lake pourrait représenter le corps parent des micrométéorites (Noguchi et Nakamura 2001). Pour mieux comparer les MMAs et cette nouvelle météorite, nous avons mesuré la composition isotopique de l'oxygène et de l'hydrogène de Tagish Lake, grâce à la facilité nationale de microsonde ionique (CAMECA IMS1270) du CRPG de Nancy (Engrand *et al.* 2001a; Engrand *et al.* 2001b; Engrand *et al.* 2003b).

1.2.4.1 Isotopes de l'oxygène de Tagish Lake

Cette météorite présente deux lithologies principales, qui diffèrent fortement par leurs teneurs en carbonates, ce qui suggère un historique de formation ou d'altération différents pour chaque lithologie (Gounelle *et al.* 2001b; Zolensky *et al.* 2002). La composition isotopique de l'oxygène des minéraux primaires formés à haute température (olivines, pyroxènes, minéraux réfractaires) est similaire dans les deux lithologies (voir **Figure 1-10a**), ce qui suggère qu'elles se sont formées à partir d'un précurseur anhydre commun. Cette composition isotopique est également similaire à celle des chondrites carbonées. Des inclusions d'olivine réfractaires montrent un enrichissement en ^{16}O typique des inclusions réfractaires (CAIs). La présence de ces olivines confirme la nature primitive de cette météorite, et suggère un même lieu de formation pour ces olivines et les minéraux constitutifs des CAIs.

L'étude de la composition isotopique de l'oxygène des minéraux secondaires (phyllosilicates, carbonates, magnétites) présents dans l'une ou l'autre des lithologies (voir **Figure 1-10b**) suggère une formation en équilibre et à basse température de la matrice et des carbonates, alors que la magnétite aurait été formée lors d'un épisode ultérieur d'altération.

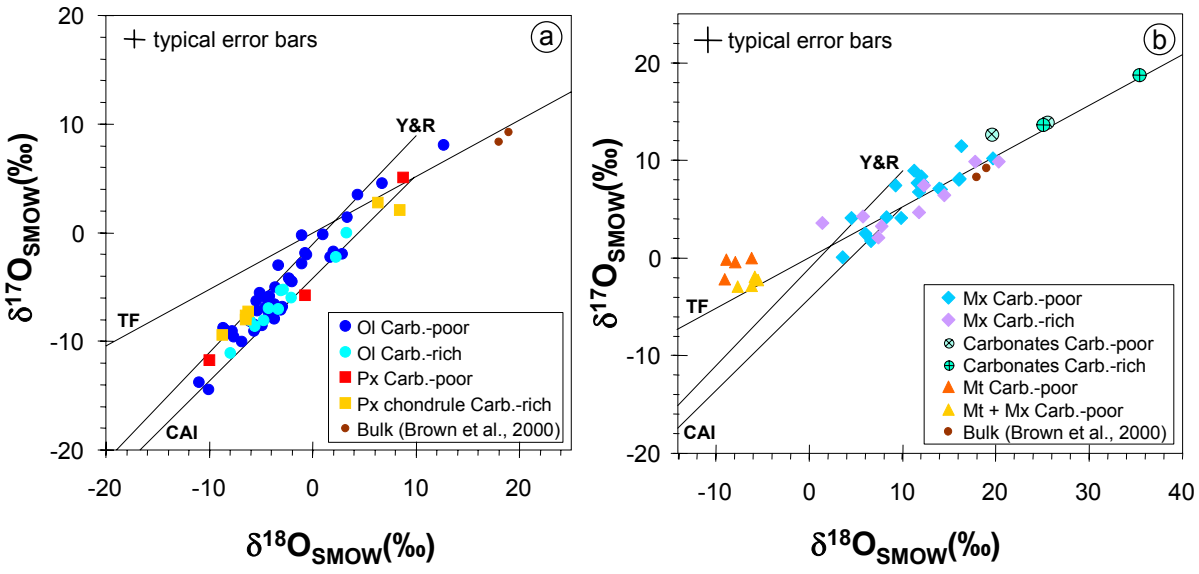

Figure 1-10 : Représentation de la composition isotopique de l'oxygène mesurée dans la météorite Tagish Lake par microsonde ionique (Cameca IMS1270, Nancy) dans les deux lithologies, riche/pauvre en carbonates : a) minéraux anhydres (Ol : olivines et Px : pyroxènes); b) minéraux secondaires (matrice, Mx; carbonates; magnétite, Mt). La droite de fractionnement terrestre (TF), la droite définie par les inclusions réfractaires (CAI, réf. Clayton et Mayeda 1999), et la droite de Young et Russell (Y&R, réf. Young et Russell 1998) sont indiquées pour référence.

La composition isotopique de l'oxygène de Tagish Lake est similaire à celle des chondrites carbonées et des micrométéorites. Elle ne permet pas d'écarter la possibilité que Tagish Lake soit l'un des corps parents des micrométéorites. Nous avons donc mesuré sa composition isotopique de l'hydrogène pour la comparer à celle des MMAs.

1.2.4.2 Isotopes de l'hydrogène de Tagish Lake

La composition isotopique de l'hydrogène des micrométéorites antarctiques (MMAs) présente des similarités avec celle des chondrites carbonées (si l'on exclut le groupe particulier des CR2) (e.g. Engrand *et al.* 1999a et section 1.2.1.1). Nous avons mesuré la composition isotopique de l'hydrogène de Tagish Lake, suggérée comme possible corps parent des micrométéorites (Noguchi et Nakamura 2001). Cette étude montre que les silicates hydratés dans les deux lithologies de Tagish Lake ont la même composition isotopique, et qu'elle est distincte de celle mesurée pour les MMAs ((**Figure 1-11**) et (Engrand *et al.* 2003b)).

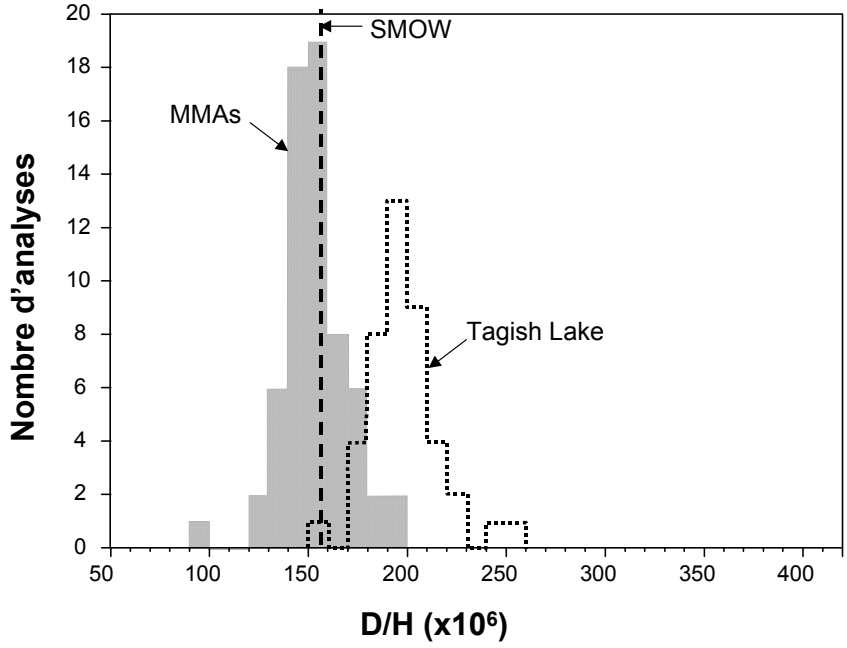

Figure 1-11 : Distributions des rapports D/H dans les micrométéorites antarctiques (MMAs) et dans la météorite Tagish Lake, obtenues avec le faisceau d'ions primaires O^- de la microsonde ionique du CRPG (Nancy). Ces analyses représentent la composition isotopique de l'hydrogène provenant des phases hydratées de l'échantillon, car l'hydrogène organique n'est pas analysé avec ce type d'ions primaires. La valeur des océans terrestres (SMOW, pour Standard Mean Ocean Water) est indiquée pour référence. D'après (Engrand *et al.* 2003b).

Messenger (2001) a mesuré des rapports D/H pour Tagish Lake légèrement supérieurs à nos valeurs. Grâce à l'utilisation d'un faisceau primaire de Cs^+ , Messenger (2001) analyse le D/H des silicates hydratés et de la matière organique. Dans notre cas, avec un faisceau primaire d'oxygène, nous n'analysons que les silicates hydratés (Deloule et Robert 1995). Cette différence met en évidence la présence de composés organique enrichis en deutérium dans Tagish Lake, comme cela a été trouvé par la suite (Busemann *et al.* 2005). Le décalage entre les distributions des rapports D/H dans Tagish Lake et les MMAs analysés par la même méthode va à l'encontre de la suggestion de Noguchi & Nakamura (2001), et montre que cette météorite n'est probablement pas le corps parent des micrométéorites.

1.2.5 La collection de micrométéorites CONCORDIA & la mission spatiale STARDUST

Les premiers résultats de la mission Stardust soulignent une possible continuité entre la matière astéroïdale et cométaire (e.g. Brownlee *et al.* 2006). La découverte de minéraux réfractaires dans le collecteur de Stardust montre que des objets formés près du soleil à haute température peuvent être éjectés dans le système solaire externe dans les régions de formation des comètes (McKeegan *et al.* 2006; Zolensky *et al.* 2006a; Zolensky *et al.* 2008). Nous faisons partie du consortium français Stardust. Notre but est de pouvoir comparer suffisamment de matériel de Stardust avec les micrométéorites pour pouvoir reconnaître les micrométéorites cométaires. En effet, les grains collectés par Stardust ont été endommagés lors de leur entrée à 6 km/s dans l'aérogel du collecteur, et les micrométéorites collectées sur Terre ou dans la stratosphère sont beaucoup mieux préservées. L'identification de ces micrométéorites cométaires serait également un atout majeur pour une meilleure interprétation des données de ROSETTA en 2014 (voir section 2.2). Les caractéristiques générales de la collection Concordia sont décrites dans l'article *"Micrometeorites from Central Antarctic snow: The CONCORDIA collection"* (Duprat *et al.* 2007).

1.2.5.1 Grains friables et micrométéorites ultracarbonées

La découverte de micrométéorites friables-poreuses (FgF, pour "Fine-grained Fluffy" dans la **Figure 1-13**) dans la collection Concordia fait le lien avec la collection de poussières collectées dans la stratosphère (IDPs). Ces poussières friables sont probablement détruites dans les collections glaciaires pour plusieurs raisons : **i)** lors de la compaction de neige en glace; **ii)** lors de cycles de congélation/décongélation des grains suffisamment proches de la surface de glace pour absorber la lumière solaire et faire fondre superficiellement la glace qui les recouvre, ou l'eau qu'elle contiennent sous forme de silicates hydratés ; **iii)** par le pompage mécanique des grains lors de la collecte.

Une nouvelle population de grains tout d'abord décrite par Nakamura *et al*. (2005) a également été découverte dans les MMs Concordia : les micrométéorites ultracarbonées, constituées à plus de 50% en volume de matière carbonée (voir un exemple en **Figure 1-12**). Les micrométéorites ultracarbonées n'ont pas d'équivalent dans les collections de météorites. Elles représentent 3% des micrométéorites non fondues et sont classifiées comme FgF.

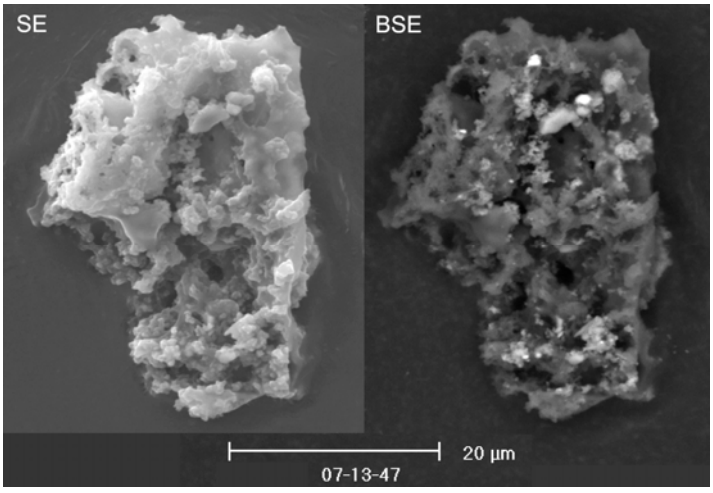

Figure 1-12 : Fragment d'une micrométéorite ultracarbonée (taille initiale : 100 x 250 µm). A gauche : micrographie électronique en électrons secondaires (SE), montrant une grande porosité et une granulométrie fine. A droite : micrographie électronique en électrons rétrodiffusés (BSE) montrant que le poids moléculaire moyen de la micrométéorite est proche de celui du scotch de carbone l'entourant. Les phases plus claires sont des silicates et des sulfures de fer.

Ces deux nouvelles populations donnent lieu à une classification revisitée (**Figure 1-13**).

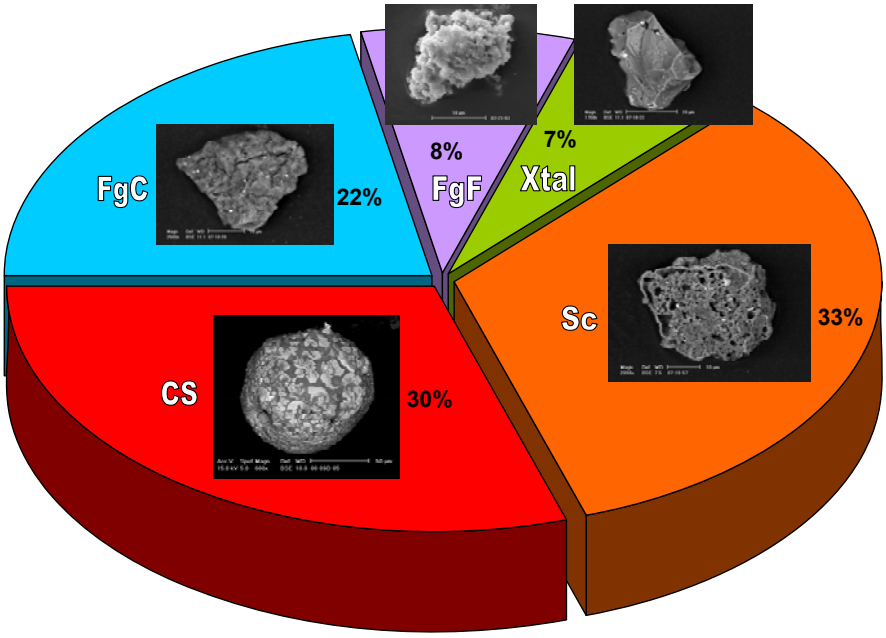

Figure 1-13 : Classification texturale revisitée d'après la collection de micrométéorites Concordia. Par rapport à la classification des MMs de Cap Prudhomme (voir **Figure 1-2**), une nouvelle classe de MMs apparaît : les particules friables (FgF). Cette classification est basée sur le degré d'échauffement des micrométéorites lors de l'entrée atmosphérique : FgC = Fine-grained compact (non fondu à grain fin compact); FgF = Fine-grained Fluffy (non fondu à grain fin poreux)- les MMs ultracarbonées font partie de cette catégorie et représentent 3% des micrométéorites non fondues; Xtal = cristalline (non fondu à gros grain); Sc = Scorie (partiellement fondu); CS = Cosmic spherule (micrométéorite fondue).

Les compositions chimiques moyennes des micrométéorites de la collection Concordia ne montrent plus les appauvrissements en S, Ni et Ca qui étaient caractéristiques des micrométéorites collectées dans la glace bleue (e.g. Kurat *et al.* 1994; Engrand et Maurette 1998) (**Figure 1-14**).

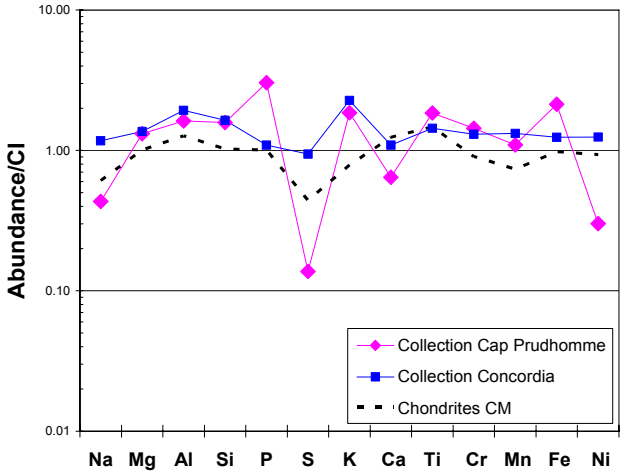

Figure 1-14 : Comparaison des abondances chimiques en éléments majeurs et mineurs des micrométéorites collectées dans la glace (en rose) et dans la neige (en bleu), normalisées par rapport à la composition de référence des météorites CI. La composition des météorites de type CM2 est représentée pour référence. Ce type de météorite est celui dont les micrométéorites se rapprochent le plus par leurs compositions minéralogiques, chimiques et isotopiques.

Ce résultat confirme le fait que ces appauvrissements sont dûs, dans le cas des collections côtières, à la dissolution des phases solubles (sulfures de fer et carbonates) porteuses de ces éléments. Les micrométéorites de la collection Concordia ont donc encore mieux préservé leurs signatures extraterrestres que les micrométéorites collectées précédemment dans la glace bleue.

1.2.5.2 Minéralogie des silicates. Comparaison avec les IDPs et Stardust.

En étudiant plus de 100 micrométéorites Concordia, j'ai trouvé 23 olivines et 52 pyroxènes de plus de 5 microns que j'ai donc pu analyser avec la microsonde électronique CAMECA SX100 du service d'analyse CAMPARIS de l'Université Paris VI. Les conditions d'analyses étaient de 15 kV et 10 nA pour les silicates, et 4 nA ou 10 nA pour les sulfures de fer.

Le rapport d'abondance pyroxène/olivine dépasse 2 dans la collection Concordia. Il est d'environ 1 dans les micrométéorites de Cap Prudhomme (184 pyroxènes pour 201 olivines) (Engrand 1995). Ce rapport 1 est bien supérieur au rapport d'abondance pyroxène/olivine des chondrites CM et avait suggéré un rapprochement des micrométéorites avec les chondrites CR (Kurat *et al.* 1994). La valeur encore supérieure trouvée pour les micrométéorites Concordia pourrait être reliée à la nouvelle population de particules friables poreuses (voir plus haut et Duprat *et al.* 2005b). Il faut noter que les échantillons de la comète Wild 2 (Stardust) sont également dominés par les pyroxènes pauvres en calcium (Zolensky *et al.* 2006b; Tomeoka *et al.* 2008; Zolensky *et al.* 2008).

La composition des olivines des MMS Concordia varie de $Fo_{47.1}$ and $Fo_{99.5}$. Ce domaine de variation est comparable à celui précédemment observé pour les micrométéorites de Cap Prudhomme, avec peut-être une distribution bimodale plus clairement marquée, mais statistiquement peu significative (**Figure 1-15**). Comme précédemment observé, bien que les météorites les plus proches des micrométéorites soient les chondrites CM2 (e.g. Kurat *et al.* 1994), la distribution des compositions en Fo des olivines des micrométéorites se différencie de celle des CM2 (**Figure 1-15**).

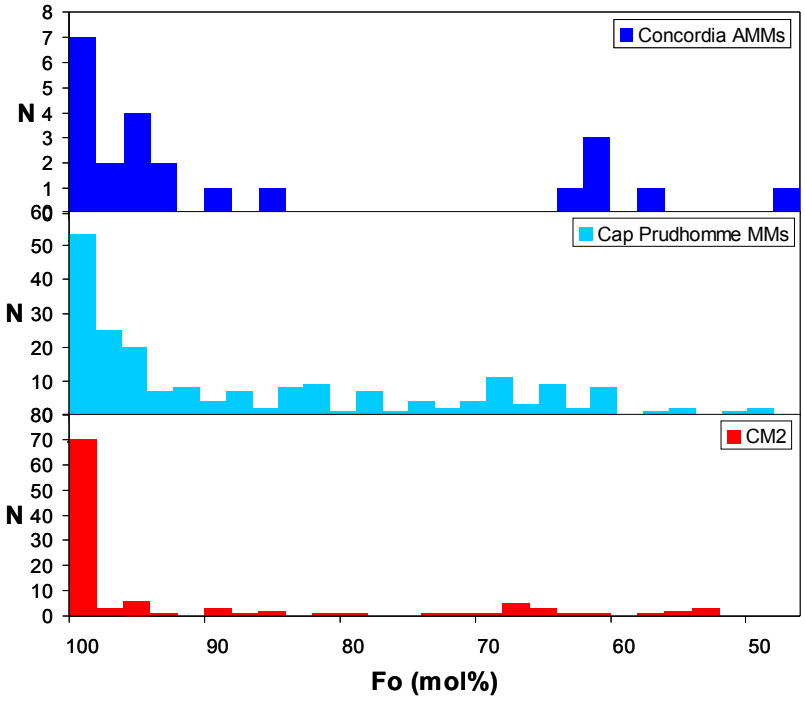

Figure 1-15 : Comparaison des teneurs en fer des olivines exprimées en Fo = Mg/(Mg+Fe) des micrométéorites antarctiques (AMMs) de Cap Prudhomme, de Concordia et des chondrites CM2.

On observe alors que cette distribution de composition des olivines se rapproche de celle des IDPs anhydres et des échantillons récemment rapportés sur Terre de la comète Wild2 (Stardust) (**Figure 1-16** et (Zolensky *et al.* 2006b; Tomeoka *et al.* 2008; Zolensky *et al.* 2008)).

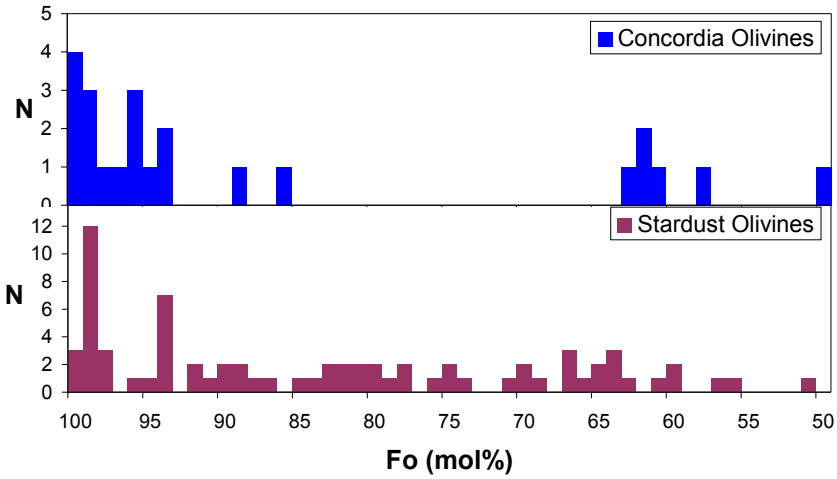

Figure 1-16 : Distribution de la teneur en fer des olivines exprimé comme Fo = Mg/(Mg+Fe) pour les micrométéorites Concordia et la comète Wild2 (Echantillons Stardust) (Zolensky *et al.* 2006b; Tomeoka *et al.* 2008; Zolensky *et al.* 2008).

Les compositions des pyroxènes dans les micrométéorites Concordia suivent la même tendance: le domaine de variation et la distribution de leurs teneurs en fer exprimée sous forme de En = Mg/(Mg+Fe) ressemble à ceux des échantillons Stardust, avec toutefois un domaine de variation plus restreint (**Figure 1-17**). Dans le cas des échantillons de Stardust, on ne peut pas exclure que certains pyroxènes riches en fer aient été formés lors de l'échauffement provoqué par l'entrée dans l'aerogel (e.g. Tomeoka *et al.* 2008).

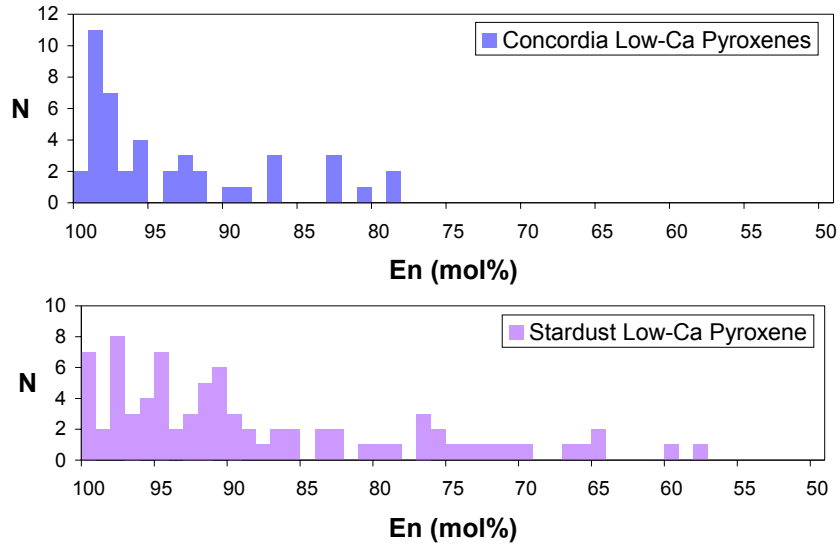

Figure 1-17 : Teneur en fer des pyroxènes pauvres en calcium des micrométéorites Concordia (haut) et des échantillons Stardust (bas). En = Mg/(Mg+Fe) en mole%. (Données Stardust d'après Zolensky *et al.* 2006b; Tomeoka *et al.* 2008; Zolensky *et al.* 2008).

La minéralogie des silicates des micrométéorites de Concordia est donc similaire à celle des micrométéorites de Cap Prudhomme, confirmant ainsi le rapprochement avec les chondrites carbonées, mais également avec les analyses des échantillons de Stardust. Certains auteurs discutent la validité de la comète Wild 2 comme étant représentative de la population des comètes les plus primitives, proposant que les IDPs d'origine (présumée)

cométaire soient de meilleurs échantillons pour caractériser la matière la plus primitive du système solaire (Ishii *et al.* 2008). Les IDPs et les micrométéorites d'origine cométaire sont dans meilleur état de préservation que les échantillons de Stardust et pourraient donner des informations cruciales sur la composante volatile des comètes.

1.2.5.3 Minéralogie des sulfures de fer. Comparaison avec les IDPs et Stardust.

Les sulfures de Fe-Ni sont abondants dans tous les types de matériaux extraterrestres et peuvent donc être utilisés comme moyen de comparaison. Plusieurs types de sulfures de fer sont formés dans divers modes de formation et d'altérations. La troilite (FeS) est considérée comme étant le premier sulfure de fer à se former dans la nébuleuse solaire, par sulfuration du métal Fe-Ni par H_2S, S_2, ou d'autres espèces gazeuses comportant du S (Lauretta et Fegley 1994). La pyrrhotite ($\{Fe,Ni\}_{1-x}S$) résulte probablement de l'altération aqueuse d'une troilite primaire sur le corps parent (Herndon *et al.* 1975). La formation de la pentlandite ($\{Fe,Ni\}_9S_8$) est fréquemment interprétée comme étant un indicateur de métamorphisme à basse température en conditions oxydantes, et/ou d'une altération aqueuse sur le corps parent chondritique (Zolensky et Thomas 1995). Alternativement, il a été proposé que la pentlandite ait pu se former lors d'une sulfuration primaire (Lauretta *et al.* 1996).

La pyrrhotite et la pentlandite sont présentes dans les chondrites primitives, avec une prédominance nette de la pyrrhotite (e.g. Bullock *et al.* 2005 et références citées). Dans les IDPs, la troilite, la pyrrhotite et la pentlandite sont présentes. La pyrrhotite domine la population des sulfures dans un domaine de tailles allant de 15 nm a 10 µm (Zolensky et Thomas 1995). La pentlandite n'est présente que dans les IDPs hydratés et non dans les IDPs anhydres.

Les sulfures de Fe-Ni n'étaient présents que dans moins de 10% des micrométéorites antarctiques des collectes glaciaires. Leur présence a été mentionnée dans les micrométéorites collectées dans la neige à Dôme Fuji, mais n'ont pas été caractérisés en composition (Nakamura *et al.* 2001). Les sulfures de Fe-Ni sont abondants dans les micrométéorites Concordia (e.g. **Figure 1-18**).

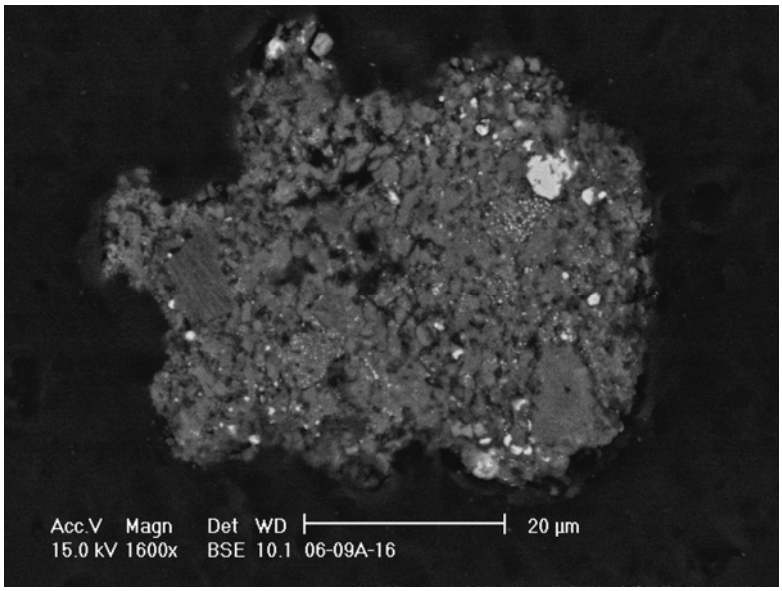

Figure 1-18 : Micrographie électronique (en électrons rétrodiffusés) d'une section polie d'un fragment de micrométéorite Concordia comportant quelques sulfures de Fe-Ni (inclusions blanches) de tailles suffisantes pour être analysés par microsonde électronique.

Dans une centaine de micrométéorites Concordia, j'ai trouvé 44 sulfures de fer de taille suffisante pour être analysés à la microsonde électronique du service Camparis de Jussieu. Ces sulfures de fer sont la troilite, la pyrrhotite et la pentlandite, comme représenté sur le diagramme ternaire Fe-S-Ni sur la **Figure 1-19** (Engrand *et al.* 2007b). Les inclusions de sulfure de fer se concentrent autour du pôle de la troilite.

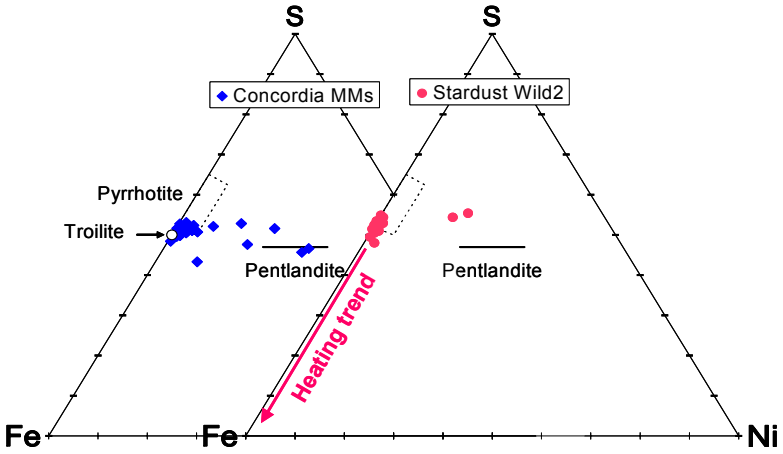

Figure 1-19 : Diagrammes ternaires Fe-S-Ni (at%) pour les micrométéorites Concordia et la comète Wild2 (échantillons Stardust) (données de Wild 2 d'après Zolensky *et al.* 2008). D'après (Engrand *et al.* 2007b).

Les sulfures de Fe-Ni montrant les plus fortes teneurs en Ni (19.7 < Ni at% < 45.9) se trouvent dans des micrométéorites scoriacées qui ont été fortement chauffées lors de l'entrée atmosphérique. La composition la plus extrême (45.9 at% Ni, 0.8 at% Co, 0.3 at% Cu) est probablement le résultat de l'altération d'un sulfure primaire lors de l'entrée atmosphérique. Cette observation suggère un mode de formation de la pentlandite lors de l'échauffement rapide de sulfures primaires pendant l'entrée atmosphérique. On remarque que cet effet serait totalement différent de celui observé lors de l'explosion des grains cométaires dans l'aerogel de Stardust qui appauvrit les sulfures en soufre.

Trente-deux des 44 inclusions de sulfures contiennent moins de 5% de Ni (de 0.2 à 4.8 at%). Lorsque l'on représente ces données le long de l'axe Fe-S, la distribution de leurs teneurs en soufre montre que cette population de sulfures de fer est dominée par la troilite primitive, avec une contribution minoritaire de pyrrhotite (**Figure 1-20**).

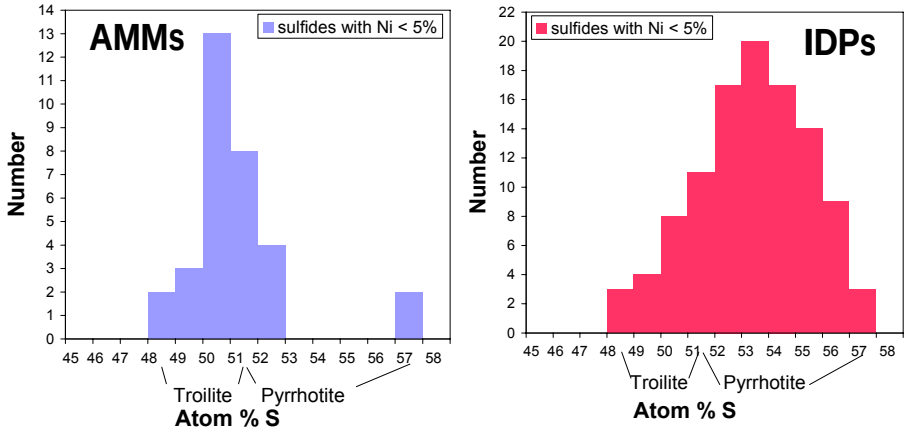

Figure 1-20 : Composition (le long de l'axe Fe-S) des sulfures de fer pauvres en Ni (< 5 at % Ni) dans les micrométéorites Concordia (AMMs, à gauche) et dans les interplanetary dust particles (IDPs, à droite). Adapté de Engrand *et al*. (2007b).

Les compositions des sulfures de Fe-Ni des échantillons de Stardust ont été altérées lors de l'impact des grains cométaires dans l'aerogel, mais quelques grains de troilite, pyrrhotite et pentlandite grains semblent avoir survécu (**Figure 1-19**) (Zolensky *et al.* 2008). La composition des sulfures de Fe-Ni des échantillons de Wild2 sont compatible avec celle des IDPs anhydres et avec une large proportion de sulfures de fer des micrométéorites Concordia.

1.2.5.4 Analyses isotopiques des micrométéorites Concordia

L'analyse isotopique des échantillons de la collection Concordia est en cours pour rechercher parmi ces micrométéorites des grains exotiques (présolaires) et les micrométéorites pouvant être d'origine cométaire. Grâce à l'utilisation de la facilité nationale NanoSIMS50 du LEME au Muséum National d'Histoire Naturelle, nous avons pu mesurer la composition isotopique de l'hydrogène dans une micrométéorite à grain fin (FgF) et 2 micrométéorites ultracarbonées (UCAMMs). Les analyses mettent en évidence une composition isotopique normale pour la MM FgF, et une valeur D/H globale élevée pour les deux particules ultracarbonées, avec un δD de l'ordre de 7000‰ sur des zones d'environ 100 μm^2. Dans une des deux UCAMMs, un fort enrichissement en deutérium de la matière carbonée est observé (jusqu'à δD ~ 25 000‰), associé à de forts rapports C/H (jusqu'à C/H ~ 7) sur de petites zones (~1µm). Le dépouillement de ces données est en cours, mais il pourrait apporter des informations cruciales sur l'origine de la matière organique du système solaire primitif (voir aussi section 4.1).

Nous n'avons pas découvert de grains présolaires dans les micrométéorites Concordia. Gounelle *et al*. (2008) ont reporté la découverte d'un SiC présolaire dans une micrométéorite antarctique de Cap Prudhomme, donc la composition isotopique est compatible avec celle des SiC mainstream isolés de matrices de chondrites carbonées (Zinner 1998). L'abondance de grains présolaires est estimée à ~ 0,1% dans cette micrométéorite, compatible avec la limite supérieure de quelques ppm pour la population des micrométéorites antarctiques. Cette valeur est plus faible que pour les IDPs, mais comparable à celle des échantillons de Wild2 (Stadermann *et al.* 2008). L'abondance en grains présolaires ne peut donc pas être utilisée comme un critère fiable d'origine cométaire.

1.2.5.5 La matière carbonée des micrométéorites Concordia

Dans le cadre d'une collaboration avec E. Quirico (LPG Grenoble), nous avons entamé une étude visant à caractériser le degré d'ordre de la matière carbonée dans les micrométéorites Concordia par micro-spectrométrie Raman (Labram micro-spectromètre à excitation 514 nm and 244 nm, voir Quirico *et al.* 2005b), et à évaluer son éventuelle altération due à l'échauffement atmosphérique. Pour cela, nous avons analysé une suite de micrométéorites allant des Fine-grained Fluffy (FgF) (dont 2 ultracarbonées) aux sphérules cosmiques, en passant par les scories. Les premiers résultats montrent que la matière carbonée des micrométéorites est très désorganisée (Dobrica *et al.* 2008b) (**Figure 1-21**). Certaines similarités sont observées avec la matière organique insoluble (MOI) des chondrites carbonées, mais il n'y a pas de similarité stricte avec un groupe de chondrites donné. Les données sont compatibles avec les analyses d'IDPs (Quirico *et al.* 2005a) et d'échantillons de Wild2 (e.g. Sandford *et al.* 2006; Rotundi *et al.* 2008) et plaident pour une origine très immature (et donc très primitive) de cette matière carbonée micrométéoritique.

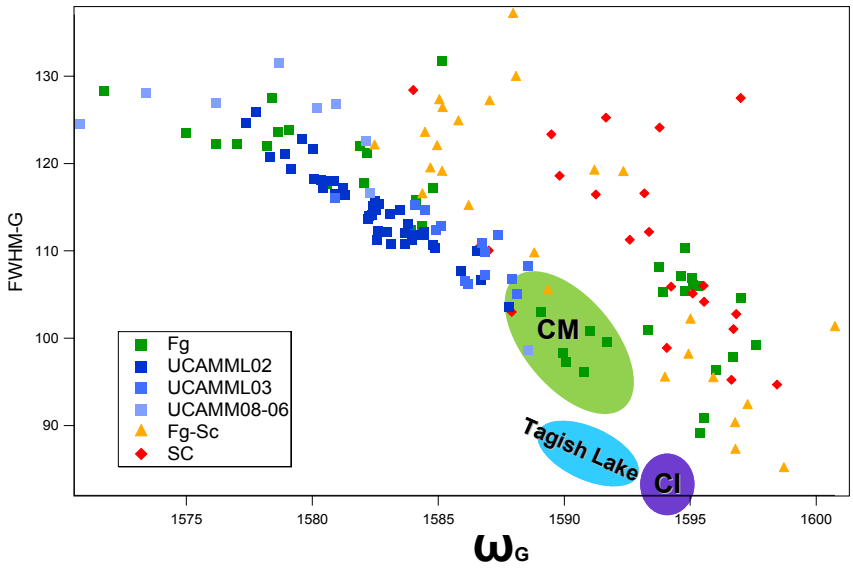

Figure 1-21 : Représentation des données Raman obtenues sur une série de micrométéorites de classes texturales différentes dans l'espace des paramètres de la bande G (largeur à mi-hauteur en fonction de la position de la bande): Fg = Fine-grained, MM à grain fin non fondue; UCAMM = Ultracarbonaceous micrometeorite, contenant plus de 50vol% de matière carbonée; Fg-Sc = Fine-grained/Scorie, MM intermédiaire entre Fg et Sc; Sc = Scorie, micrométéorite partiellement fondue. (D'après Dobrica *et al.* 2008b).

Lors de l'entrée atmosphérique, on observe un faible effet systématique de transformation de la structure de la matière carbonée (voir **Figure 1-21**, symboles jaunes et oranges). Cette tendance n'est absolument pas comparable au métamorphisme subi par certaines météorites de type pétrologique élevé. La durée de l'échauffement subi lors de l'entrée atmosphérique des micrométéorites non fondues ne suffit donc pas à modifier de manière drastique la structure de la matière carbonée. Ce résultat est en accord avec le flash heating des micrométéorites lors de l'entrée atmosphérique (e.g. Toppani *et al.* 2000) et avec les travaux de Beny-Bassez & Rouzaud (1985) montrant que de plus longues durées (> plusieurs minutes) sont nécessaires pour graphitiser significativement la matière carbonée.

Les micrométéorites Concordia contiennent donc vraisemblablement une forte proportion d'objets d'origine cométaire. Avant le retour de la mission Stardust, les analyses des poussières cosmiques suggéraient déjà la possibilité d'un continuum entre matière astéroïdale et cométaire, résultat qui semble conforté par les analyses des échantillons de Wild2 et par la découverte de corps montrant une activité cométaire dans la ceinture principale d'astéroïdes (Hsieh et Jewitt 2006). Les micrométéorites ultracarbonées n'ont pas d'équivalent dans les collections de météorites et pourraient constituer les particules CHON détectées par les missions Giotto et Vega dans la comète de Halley (Lawler et Brownlee 1992; Fomenkova et al. 1994). En dehors de ces particules ultracarbonées très exotiques, nous ne disposons toutefois pas de critère fiable d'identification des micrométéorites cométaires dans la population des poussières cosmiques. Une des raisons à cette difficulté est probablement la faible différence existant entre les astéroïdes primitifs et certaines comètes.

L'utilisation des micrométéorites comme échantillons témoins dans le cadre de la mission Rosetta devrait permettre d'optimiser le retour scientifique de COSIMA, un des analyseurs de poussières de Rosetta. La mission de retour d'échantillon MARCO POLO, présélectionnée dans le cadre du programme Cosmic Vision de l'ESA devrait également rapporter un échantillon d'astéroïde primitif qui donnera des informations de première main sur ce continuum astéroïde-comète.

1.3 Vers l'exobiologie

1.3.1 EMMA : Early MicroMeteorite Accretion

La mesure des rapports D/H dans les micrométéorites centrée sur la valeur terrestre a été le déclenchement d'un scénario appelle EMMA : Early MicroMeteorite Accretion, développé par M. Maurette (Maurette *et al.* 2000; Maurette 2006a, b; Maurette *et al.* 2006). En effet, la Terre s'est probablement formée à partir de matière sèche, et l'eau est apparue plus tardivement. Le scénario EMMA prévoit qu'une grande partie de l'atmosphère et de l'hydrosphère aurait pu être apportée par les micrométéorites, en extrapolant l'augmentation du flux de poussières dans le passé à partir d'une courbe de flux proposée par Hartmann (1999). Il reproduit les teneurs en Ne, CO_2 normalisées à N_2 de l'atmosphère terrestre, et environ la moitié du volume des océans actuels par un apport des MMs (e.g. Maurette 2006a, b; Maurette *et al.* 2006).

Ce scénario est en compétition avec un modèle proposé par le groupe de l'observatoire de Nice (Gomes *et al.* 2005; Morbidelli *et al.* 2005; Tsiganis *et al.* 2005) qui explique la configuration actuelle des astéroïdes troyens par une migration rapide des planètes géantes, environ 700 millions d'années après la formation des planètes. Ces mouvements auraient déstabilisé la ceinture d'astéroïde et envoyé des petits corps astéroïdaux vers le soleil, apportant de ce fait de l'eau sur Terre par l'intermédiaire de planétésimaux de type chondrites carbonées. Ce modèle s'appuie sur l'existence d'un pic d'augmentation du flux de matière extraterrestre qui serait observé sur la lune (voir discussion dans Hartmann *et al.* 2000), et non une augmentation graduelle vers le passé comme dans le scénario proposé par Hartmann (1999) et utilisé dans EMMA. L'existence de ce pic de bombardement sur la lune reste une source de débat (voir Maurette 2006a, pp 223-225: "A questionable clustering of the ages of lunar breccias around 3.85 year ago").

Le débat réside donc toujours sur l'espèce ayant apporté l'eau sur Terre, mais la composition isotopique des phases hydratées des micrométéorites reproduit mieux la valeur terrestre que celle d'une classe donnée (CM ou CI) de chondrite carbonée hydratée. Il existe toutefois un consensus sur le fait que cette eau a été apportée par de la matière de type 'chondrite carbonée' et que la composante cométaire est négligeable, si elle est présente.

1.3.2 Participation des poussières cosmiques à l'origine de la vie

Les micrométéorites auraient pu jouer un rôle dans l'origine moléculaire de la vie sur Terre. Dès 1988, sur la base d'analyses préliminaires montrant que les micrométéorites contenaient de fortes concentrations en matière carbonée en contact avec de nombreuses phases minérales connues pour leurs propriétés catalytiques (sulfures, oxydes métalliques, argiles), il avait été proposé que les micrométéorites auraient pu fonctionner comme des "micro-réacteurs chimiques chondritiques" pour la synthèse de molécules prébiotiques sur Terre, il y a environ 4 milliards d'années, lors d'une hydrolyse catalysée de leur matière carbonée. Ce scénario est maintenant étoffé par de nouveaux résultats (Maurette *et al.* 1995; Maurette 1998a, b; Maurette *et al.* 2001; Maurette *et al.* 2003; Matrajt *et al.* 2004; Maurette 2006a, b), et il est considéré avec attention par la communauté d'exobiologie.

Je poursuis mon intérêt pour l'exobiologie en suivant les manifestations organisées au niveau national, en participant au GDR d'exobiologie (1999-2006) et au groupe thématique Exo/Astrobiologie du CNES depuis sa création. La collection de micrométéorite Concordia pourrait nous permettre d'ouvrir une nouvelle fenêtre dans ce domaine (voir section 4.3).

2 Des microsondes ioniques terrestre et spatiale : l'IMS Orsay & COSIMA

2.1 L'IMS-Orsay et la cosmochimie isotopique du silicium avec une microsonde ionique : un essai non transformé

Les météorites et les micrométéorites contiennent des inclusions réfractaires qui font partie des premiers solides à s'être formés dans la nébuleuse solaire primitive. Ces inclusions sont appelées CAIs (pour "Ca-Al-rich inclusions"). Les chondres sont les principaux composants des météorites chondritiques. Ce sont des sphères de dimensions submillimétriques cristallisées à partir de gouttelettes de silicates fondus. Les différences minéralogiques et isotopiques entres les CAIs et les chondres suggèrent qu'ils furent formés dans deux emplacements différents de la nébuleuse protosolaire et à différentes époques. L'étude des propriétés de ces objets permet de contraindre les propriétés physiques et chimiques de leur endroit et date de formation, en termes de température, pression, rapport gaz/poussière, etc. En particulier, les interactions entre les silicates et le gaz nébulaire à ce moment pourrait également avoir joué un rôle important dans la formation et la différenciation des premiers solides présents dans le système solaire (e.g. Libourel *et al.* 2006; Libourel et Krot 2007).

Molini-Velsko *et al.* (1986) ont étudié la composition isotopique *globale* du silicium de météorites et n'ont pas détecté de variations isotopiques notables. Des études expérimentales ont toutefois montré que SiO avait interagi avec les précurseurs des chondres à l'état fondu pour donner leur texture et compositions actuelles (Tissandier *et al.* 2002; Libourel *et al.* 2006). Un tel processus pourrait être mis en évidence par la mesure de la composition isotopique du silicium de composants *individuels* des météorites. La technique utilisable pour ces études est la microsonde ionique, et nous avons souhaité développer la mesure de la composition isotopique du silicium par microsonde ionique dans une suite de minéraux adaptés à l'étude des CAIs et des chondres.

Pour cela, nous avons déménagé au CSNSM en septembre 2002 la microsonde ionique IMS-Orsay provenant du Laboratoire de Physique du Solide (**Figure 2.1**). Cet instrument a été modifié à partir d'une machine commerciale Cameca IMS4F par le concepteur de cette technique d'analyse, G. Slozian, qui a rejoint notre groupe à cette occasion. Ces modifications ont permis de donner à cet instrument une meilleure précision sur les analyses isotopiques (moins de 1‰, ce qui est unique pour ce type de 'petite' microsonde ionique), mais ont rendu la machine moins flexible d'utilisation, car de nombreuses alimentations et composants ont été figés pour une utilisation spécifique. Lors de sa venue au laboratoire, nous avions le projet de rénover l'électronique et l'informatique de la machine, qui sont obsolètes, pour redonner à l'instrument sa souplesse d'utilisation, et fiabiliser son utilisation dans le temps. Nous avions établi dans ce cadre un partenariat avec Cameca par l'entremise de l'ANVAR. Cameca devait bénéficier des innovations technologiques de notre machine pour créer un instrument 'isotopes' en échange d'une jouvence électronique et informatique de l'IMS-Orsay. Cette jouvence n'a pu voir le jour en raison de la démission (pour raisons personnelles) de l'ingénieur Cameca responsable du projet. Nous avons ensuite recherché une solution en interne au laboratoire mais la complexité de l'instrument ne nous a pas permis à ce jour de pratiquer cette jouvence.

Figure 2.1 : Microsonde ionique IMS-Orsay du CSNSM. Cet instrument a été modifié par l'équipe de G. Slodzian du laboratoire de physique des solides d'Orsay sur la base d'une machine commerciale Cameca IMS4F. Elle a été déménagée au CSNSM en septembre 2002.

Pour développer la mesure isotopique du silicium par microsonde ionique, nous avons analysé de nombreux standards terrestres (séries d'olivines et de pyroxènes, feldspaths, melilites, quartz) dont la liste et les compositions mesurées à la microsonde électronique sont présentées dans le **Tableau 1**.

Les conditions analytiques utilisées dans ce travail diffèrent de celles utilisées classiquement dans les laboratoires de cosmochimie isotopique par microsonde ionique. Nous avons utilisé un courant primaire Cs^+ de 0,1 à 3nA accélérés à 14,5 kV et nous avons compté les ions Si^- sur un multiplicateur d'électrons en monocollection. La taille du faisceau d'ions primaires était d'environ 50 µm, avec un diaphragme de sélection d'aire limitant la zone d'analyse aux 10 µm centraux. Les trois isotopes du silicium ont été mesurés grâce à l'utilisation d'un tube électrostatique à champ magnétique constant. La résolution en masse était de l'ordre de 3000, de façon à séparer l'interférence ^{28}SiH de ^{29}Si. Les lentilles de transfert furent réglées de façon à augmenter l'efficacité de collection et la transmission du spectromètre de masse sur de petites zones d'analyse (champ imagé de 25 µm). La compensation de charge s'effectue par un canon à électrons. Grâce à l'utilisation du tube électrostatique, il est possible de réaliser des distributions en énergie de l'échantillon sans changer sa haute tension, pour vérifier la qualité de la compensation de charge électronique.

Nous avons utilisé l'olivine de San Carlos (Fo_{91}) comme standard de référence. Toutes les analyses furent ensuite normalisées à NBS28 grâce à la mesure de la composition isotopique de cette olivine par rapport au standard international NBS28 avec le MC-ICPMS haute résolution de l'ETH Zürich (Nu Plasma 1700) en collaboration avec Ben Reynolds (e.g. Georg *et al.* 2006). Dans le cadre de cette coopération, 5 autres minéraux ont été mesurés, dont 3 minéraux synthétiques (forsterite synthétique fournie par le Prof. A. Revcolevski, Univ. Orsay, et akermanite & gehlenite du Dr. Morioka, Japon). Gary Huss (ASU) nous a également fourni un échantillon d'enstatite et de fayalite de compositions isotopiques connues (voir **Tableau 1**). Pour les autres minéraux naturels, leur composition isotopique a été approximée à zéro, ce qui est raisonnable compte tenu de notre précision (voir Douthitt 1982, la variation de $\delta 30Si$ est < 0,3‰ pour ce type de minéraux).

	Wt%	Na	Mg	Al	Si	K	Ca	Ti	Cr	Mn	Fe	Ni	O	Total	Fo	En	Wo	An	Alb	Ak	δ^{30}Si (‰)	δ^{29}Si (‰)
Olivine	Forstérite synthétique (transp)	b.d.	34.22	b.d.	20.12	b.d.	b.d.	b.d.	0.02	b.d.	b.d.	b.d.	45.44	99.77	100.0						-1.37 ± 0.06	-0.68 ± 0.04
Olivine	Forstérite synthétique (bleutée)	b.d.	34.19	b.d.	20.25	0.02	0.01	0.02	0.02	b.d.	b.d.	b.d.	45.59	100.08	100.0						-0.14 ± 0.06	-0.10 ± 0.05
Olivine	San Carlos (NHM London)	0.01	29.64	0.01	19.30	0.01	0.06	0.02	0.03	0.10	6.73	0.29	43.64	99.86	91.0						-0.25 ± 0.06	-0.12 ± 0.02
Olivine	San Carlos (UCLA)	b.d.	29.65	b.d.	18.92	0.01	0.04	b.d.	0.02	0.16	7.08	0.33	43.28	99.49	90.6							
Olivine	San Carlos (L.A. Museum)	0.02	28.01	0.18	18.89	b.d.	0.05	b.d.	0.05	0.20	9.02	0.37	42.93	99.73	87.7						-0.21 ± 0.08	-0.10 ± 0.03
Olivine	Jacupiranga (NHM Wien)	0.01	27.80	0.01	18.95	b.d.	0.47	0.01	b.d.	0.90	9.59	0.03	43.10	100.86	86.9							
Olivine	Eagle Station	b.d.	25.28	0.01	18.40	b.d.	0.02	0.01	0.01	0.22	14.62	0.01	41.91	100.50	79.9							
Olivine	Kiglapait Intrusion	b.d.	14.66	b.d.	16.43	b.d.	0.03	0.01	0.01	0.40	30.24	0.05	37.19	99.02	52.7							
Olivine	Kiglapait Intrusion	0.01	14.74	b.d.	16.28	b.d.	0.02	b.d.	b.d.	0.41	30.59	0.05	37.17	99.27	52.6							
Olivine	Kiglapait Intrusion	0.01	14.52	b.d.	16.23	0.01	0.04	0.01	b.d.	0.39	30.55	0.01	36.94	98.71	52.2							
Olivine	Kiglapait Intrusion	0.02	5.87	b.d.	14.72	b.d.	0.16	0.04	b.d.	0.84	43.92	0.01	33.56	99.11	23.5							
Olivine	Kiglapait Intrusion	b.d.	5.82	b.d.	14.57	b.d.	0.14	0.01	b.d.	0.83	44.10	b.d.	33.38	98.81	23.3							
Olivine	Kiglapait Intrusion	b.d.	5.82	b.d.	14.68	b.d.	0.15	0.03	0.02	0.82	44.59	0.01	33.64	99.72	23.1							
Olivine	Fayalite (ASU)	0.01	0.02	b.d.	13.68	b.d.	0.04	b.d.	b.d.	1.98	52.59	0.02	31.24	99.53	0.1						-0.64	-0.32
Pyroxène	Enstatite (ASU)	b.d.	23.38	0.42	27.79	b.d.	0.05	0.03	b.d.	b.d.	0.86	b.d.	47.71	100.25		98.3	0.1				-0.17	-0.07
Pyroxène	Enstatite (UCLA)	0.01	19.33	0.03	27.02	b.d.	0.16	0.02	0.02	0.01	7.79	0.03	45.87	100.31		84.7	0.4					
Pyroxène	L.A. Muséum	0.02	15.24	1.09	24.85	b.d.	0.43	0.11	0.09	0.23	14.26	0.02	43.76	100.10		70.2	1.2					
Pyroxène	Diopside Piemont (NHM Wien)	0.08	10.58	0.21	25.94	b.d.	18.49	0.01	b.d.	0.02	0.80	b.d.	44.36	100.50		47.8	50.6					
Pyroxène	Diopside Madagascar (NHM Wien)	0.20	10.21	1.27	24.95	0.01	17.70	0.04	0.01	0.12	1.66	0.01	43.97	100.14		47.1	49.6					
Pyroxène	diopside Ruthenkopf (NHM Wien)	0.06	10.07	0.18	25.40	b.d.	18.03	0.04	0.02	0.15	1.80	b.d.	43.55	99.29		46.2	50.2					
Pyroxène	Augite Eifel, Germany (NHM London)	0.44	7.91	3.21	22.51	b.d.	16.47	0.74	0.20	0.13	5.19	0.04	42.56	99.40		39.2	49.5					
Feldspath	SudTyrol	0.01	b.d.	18.88	19.78	b.d.	14.27	0.01	b.d.	0.03	0.05	b.d.	45.06	98.10				99.8	0.2			
Feldspath		0.66	0.02	17.94	20.82	0.02	12.80	0.02	b.d.	b.d.	0.38	0.01	45.17	97.86				91.7	8.2			
Feldspath	Sri Lanka (NHM London)	2.92	b.d.	10.22	30.99	9.04	0.16	0.01	0.01	0.04	0.03	b.d.	47.39	100.84				1.1	35.1			
Feldspath	Taos County	8.85	b.d.	10.45	31.95	0.06	0.09	0.01	0.05	0.02	0.04	b.d.	48.89	100.43				0.6	99.1			
Melilite	Akermanite synthétique (Japon)	b.d.	8.80	b.d.	20.61	b.d.	28.98	b.d.	0.02	0.02	b.d.	b.d.	40.84	99.22						100.0	0.07 ±0.08	0.01 ± 0.03
Melilite	Beaver Creek (MNHN Paris)	2.57	4.55	3.76	20.28	0.02	23.42	0.01	0.03	0.23	1.98	0.01	40.35	97.20						72.9		
Melilite	Vésuve (MNHN Paris)	2.55	3.99	6.52	18.63	0.13	24.69	0.01	0.02	0.08	1.30	0.01	40.86	98.82						57.6		
Melilite	Vésuve (NHM London)	1.02	2.93	9.45	16.08	0.19	26.63	0.01	0.01	0.02	2.05	b.d.	40.28	98.66						40.8		
Melilite	Gehlenite synthétique (Japon)	b.d.	b.d.	19.82	10.27	b.d.	28.91	0.04	b.d.	b.d.	0.02	b.d.	40.89	99.92						0.0	0.30 ± 0.06	0.21 ± 0.05

Tableau 1 : Liste des minéraux analysés comme standards, compositions minéralogiques (en poids%), et compositions isotopiques du silicium (certains minéraux). Fo = (Mg/Mg+Fe) pour les olivines; En = Mg/(Mg+Fe+Ca) et Wo = Ca/(Mg+Fe+Ca) pour les pyroxènes; An = Ca/(Na+K+Ca), Alb = Na/(Na+K+Ca) pour les feldspaths; Ak = Mg/(Mg+Al/2) pour les melilites. Les valeurs δ^{30}Si et δ^{29}Si sont exprimées en pourmil par rapport à NBS28. b.d. : en dessous de la limite de détection de la microsonde électronique (~ 0,01wt%).

2.1.1 Reproductibilité et effets de matrice

Les compositions isotopiques sont exprimées en valeurs delta en pourmil par rapport à un standard, ici NBS28 : $\delta^{29}Si = (((^{29}Si/^{28}Si)_{éch}/(^{29}Si/^{28}Si)_{NBS28} - 1) \times 1000$, de même pour $\delta^{30}Si$. Le fractionnement instrumental (IMF) représente la différence entre la composition isotopique mesurée et la valeur vraie. Nous avons obtenu une précision de 0,4‰sur le $\delta^{29}Si$ et 0,5‰ sur le $\delta^{30}Si$ (1σ) (**Figure 2.2**).

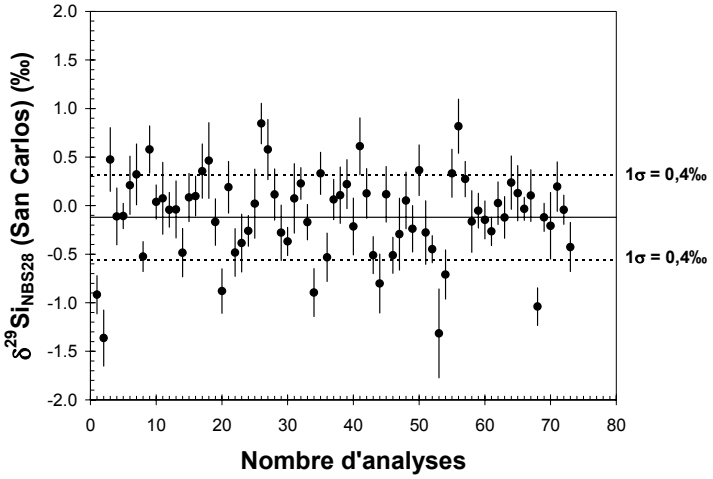

Figure 2.2 : Reproductibilité des analyses isotopiques du silicium sur notre standard d'olivine de San Carlos Olivine. La précision obtenue est de 0,4‰ (1σ)

Nous nous sommes heurtés au problème majeur de "l'effet de matrice", qui modifie la réponse instrumentale de la microsonde ionique en fonction de la phase minérale analysée. Cet effet est particulièrement important dans le cas de l'olivine: il y a un effet de matrice de 20‰/uma (unité de masse atomique) entre la forstérite (Mg_2SiO_4) et la fayalite (Fe_2SiO_4) (Axe vertical sur **Figure 2.3**), et il n'existe pas de corrélation simple entre le fractionnement instrumental des olivines et leur composition (teneurs en silicium, ou autre élément ou combinaison d'éléments) (**Figure 2.3**). Dans le domaine de composition des olivines forstéritiques (Fo_{80-100}), il n'y a pas d'effet de matrice notable. Il est intéressant de noter que cette tendance observée pour le silicium est l'inverse de celle intervenant (dans une moindre mesure) pour les isotopes de l'oxygène dans les olivines, pour lesquels le fractionnement instrumental est plus faible dans les olivines riches en fer que dans les olivines magnésiennes.

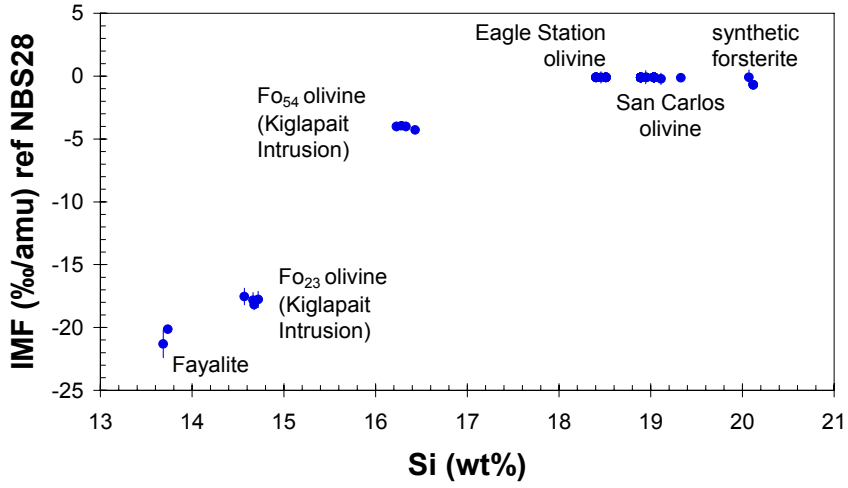

Figure 2.3 : Fractionnement instrumental (Instrumental Mass Fractionation, IMF) normalisé à l'olivine de San Carlos et à la référence NBS28. Les barres d'erreurs représentées sont 1σ.

Nous n'avons eu accès qu'à une gamme limitée de compositions d'orthopyroxènes (En_{70} à En_{98}) et de clinopyroxènes ($En_{39.2}Wo_{49.5}$ à $En_{47.8}Wo_{50.6}$). Nous n'avons pas trouvé d'effet de matrice pour ces orthopyroxènes, et il se limite à 1,5‰/uma pour les clinopyroxènes analysés, avec une possible corrélation linéaire entre le fractionnement isotopique et les concentrations pondérales de Si (**Figure 2.4**).

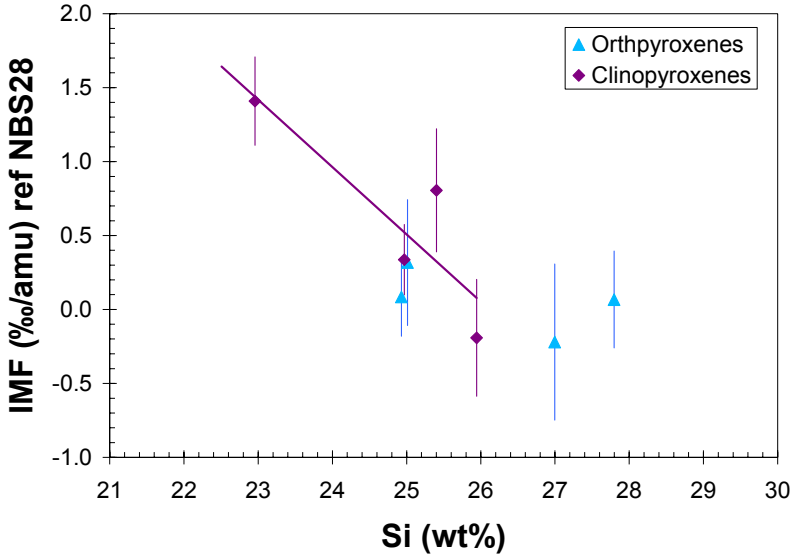

Figure 2.4 : Fractionnement instrumental (Instrumental Mass Fractionation, IMF) pour les pyroxènes exprimés en fonction de Si (poids%). Les barres d'erreurs représentées sont 1σ.

Les feldspaths et les mélilites montrent également des corrélations linéaires entre leur IMF et leurs concentrations pondérales en Si, avec un maximum de 8‰/uma entre l'albite et l'anorthite, et de 6‰ entre la gehlenite et l'akermanite (**Figure 2.5**).

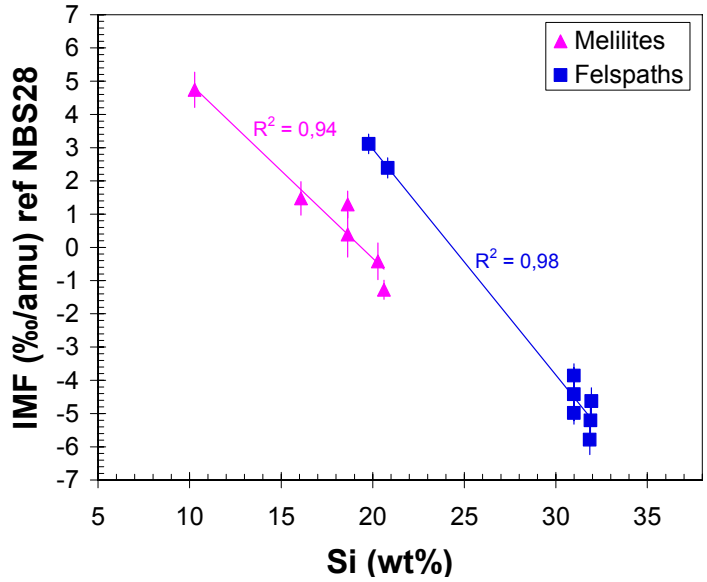

Figure 2.5 : Fractionnement instrumental (Instrumental Mass Fractionation, IMF) pour les feldspaths (en bleu) et pour les mélilites (en rose), exprimés en fonction de Si (poids%). Les barres d'erreurs représentées sont 1σ.

Grâce à la mesure des profondeurs de cratères dans l'olivine et le quartz, nous avons pu calculer la probabilité de production d'ions secondaires silicium ($P^{28}Si$ pour ^{28}Si) et la concentration de Cs^+ implanté dans l'échantillon. On peut montrer analytiquement et

observer que l'IMF est négativement corrélée à $1/P^{28}Si$ (**Figure 2.6**), alors que $P^{28}Si$ est positivement corrélé à la concentration d'ions Cs^+ implantés.

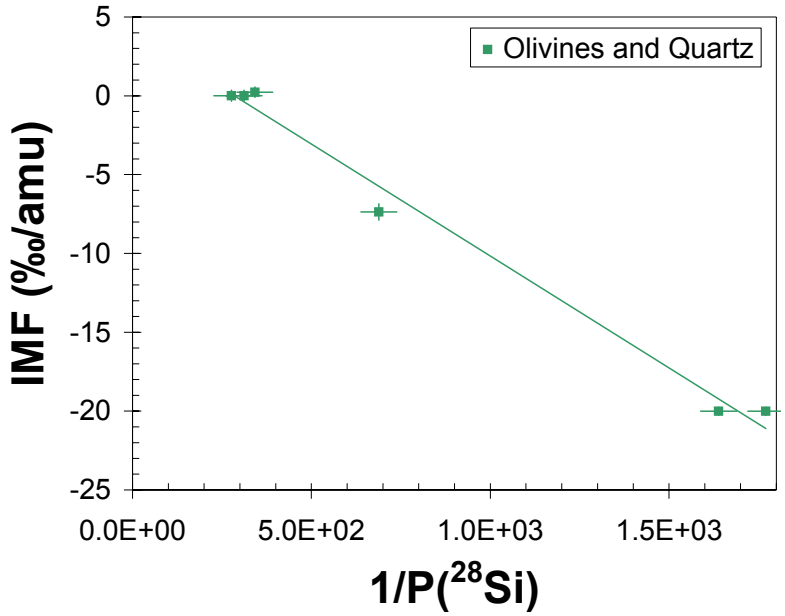

Figure 2.6 : Le fractionnement instrumental (Instrumental Mass Fractionation, IMF) (IMF) est inversement corrélé à la probabilité de production d'ions secondaires $P(^{28}Si)$.

2.1.2 Analyse d'une inclusion réfractaire de Leoville (MRS6)

Grâce à ces calibrations détaillées, nous avons tenté de mesurer la composition isotopique du silicium de l'inclusion réfractaire MRS6 de la météorite Leoville (Engrand *et al.* 2007c) dont nous avions également caractérisé la composition isotopique de l'oxygène à l'aide de la facilité nationale Cameca IMS1270 du CRPG Nancy. Nous avons caractérisé pour ces deux éléments les phases minérales dans lesquelles le ^{10}Be avait été précédemment recherché (Chaussidon *et al.* 2003). Les isotopes de l'oxygène suivent la ligne des CAIs, avec les valeurs $\delta^{18}O$ variant de -7,4‰ à +8,3‰ pour la mélilite; de -27,6‰ à -31,1‰ pour la fassaite; de -30,8‰ à -33,1‰ pour les spinels; et le $\delta^{18}O$ = -33,8‰ pour l'anorthite.

Les trois isotopes du silicium pour MRS6 se placent sur une droite de fractionnement en masse. Après correction des effets de matrice, nous obtenons des valeurs proches de zéro pour l'anorthite et les melilites (**Figure 2.7**) et des valeurs élevées pour les fassaites ($\delta^{30}Si$ entre 13,2‰ et 16,9‰). Dans un autre contexte, ces valeurs élevées de la composition isotopique du silicium de la fassaite pourraient s'expliquer par un processus de distillation par évaporation. Nous pensons que ce n'est pas le cas, car la composition isotopique de l'oxygène n'est pas enrichie en isotopes lourds ($\delta^{18}O \sim \delta^{17}O \sim$ -30‰), la CAI a une texture ignée, et la mélilite et l'anorthite ont des valeurs proches de zéro. Ces valeurs très élevées résultent donc probablement d'une mauvaise correction de l'effet de matrice pour la fassaite. Il n'y a en effet pas d'équivalent terrestre à la fassaite, et nous avons utilisé une extrapolation de la corrélation observée sur les clinopyroxènes (**Figure 2.4**) pour corriger les analyses.

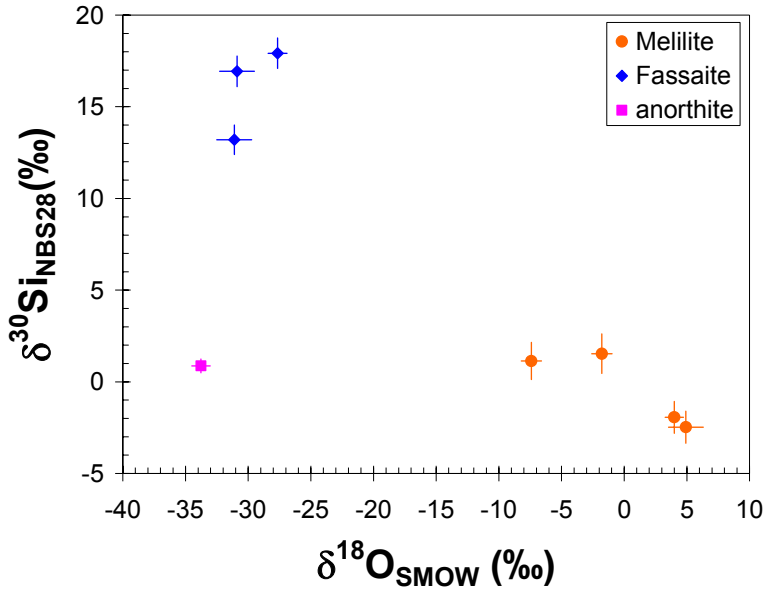

Figure 2.7 : Compositions isotopiques du silicium et de l'oxygène des phases silicatées de l'inclusion réfractaire MRS6 de la météorite Leoville (CV3). Les données élevées observées pour la fassaite résultent probablement d'un artefact instrumental.

La mesure de la composition isotopique du silicium par microsonde ionique dans des échantillons naturels variés se heurte donc au problème d'effet de matrice, en particulier dans les olivines, mais aussi pour des minéraux dont il n'y a pas d'équivalent terrestre. Nous n'avons pas trouvé de méthode adéquate pour corriger ces effets de manière satisfaisante, étant donné les faibles effets isotopiques attendus.

2.2 Mission ROSETTA : l'analyseur de poussières COSIMA

2.2.1 Co-I pour COSIMA

La mission cométaire ROSETTA de l'ESA, lancée le 2 Mars 2004, atteindra la comète 67P/Churyumov-Gerasimenko en 2014. Les instruments embarqués sur la mission permettront de faire des analyses *in situ* de la comète. En particulier, une microsonde ionique statique (ou encore "à temps de vol", TOF-SIMS) conçue par J. Kissel, COSIMA (COmetary Secondary Ion Mass Analyzer), analysera la poussière cométaire (Kissel *et al.* 2007). Je suis associée comme Co-I (Co-Investigator) à COSIMA. Mon rôle consiste à définir les problématiques dans le domaine 'inorganique' que COSIMA pourra contribuer à résoudre, et à participer à la qualification scientifique de l'instrument grâce aux échantillons de calibration que nous avons développés pour la microsonde ionique dynamique (voir section 2.1.1 plus haut) et aux micrométéorites antarctiques qui sont utilisées comme proxies de grains cométaires (e.g. Engrand *et al.* 2007a). Fin 2007, j'ai également été nommée co-responsable (avec D. Bockelée-Morvan) du groupe de travail 'Chemical Properties' du SWT (Science Working Team) de l'ESA pour ROSETTA. Nous devons organiser la concertation entre les différents scientifiques responsables d'instruments pour assurer un retour scientifique maximum des analyses en ce qui concerne la caractérisation des propriétés chimiques des grains. Ce travail est particulièrement ardu en raison du grand nombre d'instruments et d'analyses (plus ou moins complémentaires) présents sur ROSETTA.

Pour ce travail, je collabore avec le groupe COSIMA du Laboratoire de Physique et Chimie de l'Environnement (Orléans), qui a conçu la colonne d'ions primaires de COSIMA, et qui possède un prototype de laboratoire. J'utilise également le modèle au sol de COSIMA en collaboration avec l'équipe du MPI de Katlenburg-Lindau (M. Hilchenbach, actuel PI de COSIMA et H. Krueger).

Les collections de micrométéorites jouent un rôle important car elles présentent les avantages uniques suivants : 1) La collection de Cap Prudhomme (issue des glaces côtières antarctiques) est la seule collection disponible actuellement qui contienne un nombre suffisant de grains pour assurer les besoins de nos partenaires; 2) ces grains présentent un degré de complexité adéquat pour simuler le matériau cométaire complexe, étant constitués d'agrégats chondritiques de minéraux très fins en contact avec une abondante composante carbonée à l'échelle du nanomètre; 3) La collection de micrométéorites Concordia provenant des collectes 2000, 2002 et 2006 dans les neiges des régions centrales antarctiques contient de nouveaux objets friables et montre un degré de préservation des caractéristiques pré-atmosphériques inégalées dans un domaine de taille de 30 à 500 µm (voir section 1.2.5 et Duprat *et al.* 2007). Les analyses des échantillons cométaires de la mission STARDUST (Brownlee *et al.* 2006; Zolensky *et al.* 2008) renforcent notre hypothèse d'une continuité entre les chondrites carbonées et les comètes. Les micrométéorites antarctiques sont actuellement les seuls échantillons potentiellement cométaires disponibles en quantités suffisantes pour assurer la qualification scientifique des analyseurs de poussières de la mission ROSETTA.

2.2.2 Problématique d'analyse

De par nos analyses sur les micrométéorites antarctiques, nous avons défini les questions suivantes concernant le potentiel analytique de COSIMA pour des analyses *in situ* des grains cométaires :

i) Peut-on identifier les silicates les plus abondants de la matière extraterrestre (olivines et pyroxènes)? Peut-on déterminer leur rapport d'abondance pour le comparer à ceux dans la queue de la comète de Hale-Bopp (Wooden *et al.* 1999), ou directement dans les échantillons de Stardust (Zolensky *et al.* 2006b; Tomeoka *et al.* 2008; Zolensky *et al.* 2008). Le rapport Px/Ol >1 mesuré dans Hale-Bopp et dans Stardust est très supérieur à celui des autres échantillons extraterrestres, à l'exception des micrométéorites et d'une famille rare de chondrites carbonées, de type CR2. Ces météorites ont par ailleurs des valeurs de rapports D/H comparables à celles mesurées dans l'eau cométaire (Kerridge 1985; Meier *et al.* 1998b).

ii) la comète contient-elle des phases formées à haute température (chondres et inclusions réfractaires)? Des olivines et pyroxènes magnésiens cristallins et amorphes constituent une part importante de la matière cométaire (e.g. Hanner et Bradley 2004), ces mêmes minéraux ainsi que des inclusions réfractaires et des chondres ont également été décrits dans les échantillons de la comète Wild2 (Stardust) (Zolensky *et al.* 2006b; Zolensky *et al.* 2008). La présence de ces phases haute température suggère une formation près du soleil et un transport dans le système solaire externe, par un processus physique tel que le vent-x (Shu *et al.* 1996; Gounelle *et al.* 2001a; Shu *et al.* 2001) ou la turbulence (e.g. Bockelée-Morvan *et al.* 2002).

iii) Peut-on identifier des phases comme les phyllosilicates ou les carbonates, dont l'origine dans les météorites est couramment attribuée à une altération sur le corps parent? Bien que la présence de carbonate soit suggérée dans Tempel 1 (Deep Impact) et Wild 2 (Stardust) (Lisse *et al.* 2006; Lisse *et al.* 2007; Crovisier et Bockelée-Morvan 2008; Flynn *et al.* 2008), la présence de phyllosilicates dans les comètes est controversée (Crovisier et Bockelée-Morvan 2008; Zolensky *et al.* 2008).

iv) Quelles sont les compositions isotopiques d'éléments légers (H, C, O, N…) des grains cométaires et comment se comparent-ils aux météorites et à la poussière interplanétaire? Peut-on mesurer simultanément les rapports D/H et C/H pour identifier les composantes hydratées et organiques présentes dans les grains cométaires ? (voir Aléon *et al.* 2001 et Figure 1.9 dans section 1.2.3.).

2.2.2.1 Analyses d'échantillons terrestres

Les micrométéorites et les météorites proposées comme échantillons de calibration pour COSIMA sont des échantillons complexes dont les compositions chimiques et isotopiques peuvent varier à l'échelle du micron. Nous avons donc choisi de commencer ces études en utilisant tout d'abord des minéraux simples de composition homogène, qui sont susceptibles d'être présents dans la matière cométaire (olivine, pyroxène, minéraux hydratés, sulfures de fer, carbonates). Nous avons également effectué des analyses (encore préliminaires) d'échantillons de météorites et de micrométéorites, pour mesurer leur composition chimique inorganique, et tenter d'identifier certains de leurs composés organiques. Nous avons en particulier recueilli le spectre d'un acide aminé extraterrestre (AIB), fait quelques tests de mesures de composition isotopique de l'hydrogène dans une météorite dont le rapport D/H est très élevé (Renazzo), et testé s'il sera possible de réaliser des mesures isotopiques du carbone ($^{12}C/^{13}C$) avec COSIMA. La technique d'analyse par TOF-SIMS est extrêmement sensible aux contaminations de surface. Nous avons préparé des échantillons de minéraux en conditions ultra-propres, en les pressant dans l'indium ou dans l'or.

Dans les articles *"Multi-correlation analyses of TOF-SIMS spectra for mineralogical studies*" et "*Chemometric evaluation of time-of-flight secondary ion mass spectrometry data of minerals in the frame of future in situ analyses of cometary material by COSIMA onboard ROSETTA"*, nous montrons que l'exploitation des spectres nécessitent l'utilisation de méthodes statistiques pour essayer de reconstruire la composition des grains analysés (Engrand *et al.* 2004; Engrand *et al.* 2006).

Nous avons en particulier tenté de différencier les couples de minéraux suivants analysés avec le prototype d'Orléans :

- Olivine magnésienne ($Mg_{1.8}Fe_{0.2}SiO_4$) et pyroxène magnésien ($Mg_{0.9}Fe_{0.1}SiO_3$) ;
- Olivine magnésienne ($Mg_{1.8}Fe_{0.2}SiO_4$) et serpentine $Mg_{2.7}Al_{0.3}(Si_{1.9}Fe_{0.10}O_5)(OH)_4$
- Pyroxène magnésien ($Mg_{0.9}Fe_{0.1}SiO_3$) and talc ($Mg_{2.6}Si_{2.8}O_{4.5}(OH)_{7.5}$
- Pyroxène pauvre en Ca ($Mg_{0.9}Fe_{0.1}SiO_3$) et riche en calcium ($Mg_{0.94}Fe_{0.06}Ca_{0.95}Al_{0.10}Si_{1.95}O_6$)

Les spectres montrent peu ou pas de fragments moléculaires, les masses principales observées dans le spectre dans le cas de l'olivine sont par exemple Mg^+, Al^+ (avec une contribution non résolue en masse de $C_2H_3^+$), Ca^+ et Fe^+ (**Figure 2.8 haut**). Les spectres d'une olivine et d'un pyroxène ne sont pas drastiquement différents. Une quantification des pics permet de différencier les deux minéraux, mais il faut pour cela connaître les coefficients d'émission corrects pour chaque minéral. Dans le cas d'un mélange complexe de minéraux, le problème de la quantification se pose.

L'analyse des minéraux hydratés donnent des résultats similaires en ce qui concerne leurs compositions en éléments majeurs (voir **Figure 2.8**). Le problème d'interférence de masses est important, et peut provoquer des erreurs d'attribution de masses dans le cas d'un matériau totalement inconnu.

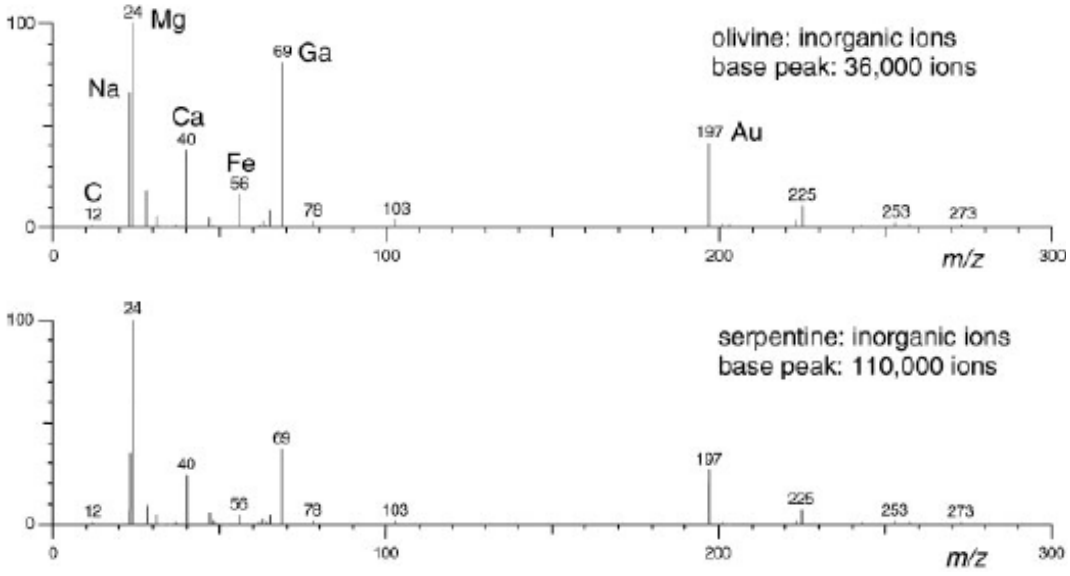

Figure 2.8 : spectres de masses en ions positifs pour une olivine (haut) et une serpentine (bas) obtenus à l'aide du prototype COSIMA du LPCE d'Orléans. Les pics de Ga et Au correspondent respectivement à l'implantation des ions primaires et au substrat dans lequel les minéraux ont été écrasés. D'après (Engrand *et al.* 2006).

Les deux spectres de la **Figure 2.8** se ressemblent fortement, mais un traitement statistique avec CORICO (Lesty 1999) permet de distinguer les familles de minéraux (**Figure 2.9**) (Engrand *et al.* 2004; Engrand *et al.* 2006). Une étude réalisée en aveugle à partir de la base de données construite pour ces minéraux a permis de reconnaitre le bon minéral avec 90% de réussite, mais le problème de l'identification des minéraux présents dans le cas d'un mélange reste encore non résolu. Un carbonate analysé (calcite, $CaCO_3$) n'a pas de signature significative en ions secondaire positifs : le spectre montre principalement un pic de Ca^+, donc la présence de ce carbonate serait difficile à identifier dans le cadre de l'analyse d'un mélange de minéraux.

Nous avons établi la liste des minéraux d'intérêt cométaire, et une banque de données de spectres de ces minéraux est en cours de construction avec le prototype d'Orléans et le modèle au sol de COSIMA au MPI de Lindau.

Cette étude menée avec le LPCE se poursuit également en étroite collaboration avec K. Varmuza (Laboratory for Chemometrics, TU, Vienne), pour essayer d'identifier les phases inorganiques et organiques présentes à partir de ses fragments moléculaires ionisés que l'on observe dans le spectre à temps de vol obtenu par COSIMA, par une approche de "virtual analytical chemometry".

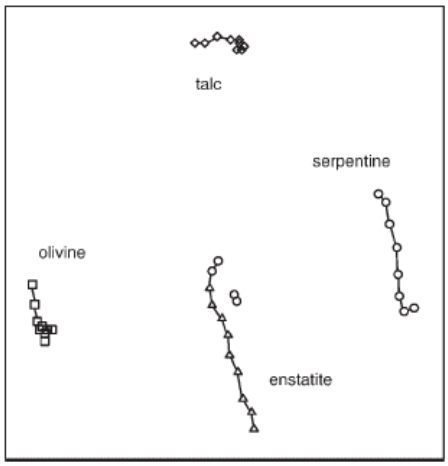

Figure 2.9 : Diagramme de corrélation dans un espace sans dimension obtenu à l'aide du traitement statistique de CORICO de spectres de masse de 4 minéraux obtenus avec le prototype de COSIMA au LPCE d'Orléans. Chaque point correspond à un spectre en masse; la corrélation est représentée par les lignes reliant les points (d'après Engrand *et al.* 2006).

L'analyse d'une solution 100mMol de l'un des acides aminés les plus abondants dans la matière extraterrestre, l'AIB (NH_2-C_3H_7-COOH) produit un nombre assez réduit de pics dans le spectre en ions secondaires positifs, qui pourraient représenter une signature significative, aux masses 18 (NH_4), 45 (COOH?), 58 (AIB – COOH?) et 104 (AIB + H). Le spectre correspondant en ions secondaires négatifs comporte également peu de pics, principalement aux masses 26 (CN?), 31 (CH_2OH, probablement résultant d'une contamination avec de l'éthanol), 42 (CNO), 102 (AIB – H). La faible résolution en masse rend l'identification des pics parfois incertaines, mais la combinaison des spectres en ions secondaires positifs et négatifs permet une meilleure identification des composes analysés, particulièrement pour les produits organiques car peu d'éléments inorganiques émettent en ions secondaires négatifs, ce qui révèle d'autant mieux la matière carbonée.

2.2.2.2 Analyses d'échantillons extraterrestres

La campagne de mesure avec l'équipe du LPCE s'est poursuivie par l'analyse de la chondrite carbonée Murchison et d'une micrométéorite Concordia, dont un fragment avait déjà été utilisé comme échantillon de référence pour préparer la communauté française au retour des échantillons STARDUST (Gounelle *et al.* 2006a; Engrand *et al.* 2007a). Les spectres de COSIMA en ions positifs montrent des pics significatifs de Mg^+, Si^+, Ca^+ et Fe^+ associés aux minéraux présents dans la micrométéorite. On observe un pic à la masse 19 (H_3O^+) qui pourrait provenir d'un silicate hydraté ou de la matière organique micrométéoritique. Les spectres en ions négatifs montrent principalement des signatures de produits soufrés (S^-, SO_2^-, SO_3^- et SO_4^-) probablement reliés à la présence de sulfures de fer dans la micrométéorite. D'autres pics moléculaires pourraient également provenir de la micrométéorite (C_2H^-, CN^-…), mais le risque de contamination de surface en organiques est à considérer également.

Nous avons poursuivi cette campagne de mesure en analysant les mêmes échantillons à l'aide d'un TOF-SIMS de laboratoire (ION-TOF5) à l'Université Technique de Vienne (Autriche). Cet instrument possède des performances théoriquement supérieures à celles des prototypes de COSIMA (possibilité d'imagerie, très haute résolution en masse), qui seront utiles pour une meilleure interprétation des spectres COSIMA (résolution des interférences, meilleure identification des pics, etc…). Nous nous sommes toutefois heurtés pour ces analyses à un problème de manque de planéité de l'échantillon : la méthode d'écrasement des grains dans des feuilles d'or utilisée pour COSIMA ne donne pas

des surfaces suffisamment planes, ce qui dégrade la résolution en masse des spectres obtenus avec l'ION-TOF5. Nous sommes en train d'essayer de résoudre ce problème en sélectionnant dans les images obtenues de zones de même hauteur. Le logiciel d'analyse d'image temps de vol est coûteux, et nous dépendons actuellement de nos collègues autrichiens pour le dépouillement des images. Nous réfléchissons également à d'autres modes de préparation d'échantillons permettant de garantir une meilleure planéité des surfaces à analyser (par ultramicrotomie, par exemple).

Nos tentatives pour mesurer la composition isotopique de l'hydrogène se sont jusqu'à présent soldées par un échec. Nous avons analysé la météorite Renazzo, qui a un rapport D/H égal à deux fois la valeur moyenne terrestre (δD_{-} ~ 1000‰). Nous avons réalisé la mesure en ions secondaires négatifs, car l'émission de H_2^- est négligeable devant celle de D^- (McKeegan *et al.* 1985), ce qui résout le problème d'interférence de masse entre D^+ et H_2^+. Les résultats que nous avons obtenus sont incohérents avec la valeur connue de la météorite. Etant donnée la sensibilité de la méthode aux contaminations de surface, il semble que nous ayons mesuré la composition isotopique de l'hydrogène du vide résiduel présent dans la chambre objet de COSIMA, qui domine le signal provenant de l'échantillon.

Pour la mesure des isotopes du carbone, la résolution en masse de l'instrument est à priori insuffisante pour séparer la masse interférente $^{12}CH^-$ de $^{13}C^-$. Nous nous sommes procuré un montage de grains de graphite présolaires (très riches en ^{13}C) provenant de Washington University (St. Louis) qui a déjà été analysé par SIMS dynamique. A l'aide de cet échantillon test, nous pourrons comparer les deux méthodes (SIMS dynamique et le TOF-SIMS de COSIMA) et estimer l'erreur introduite par la présence de l'interférence en masse $^{12}CH^-$ dans le cas de COSIMA.

2.2.2.3 Tests du modèle de vol de COSIMA :

Dans le laboratoire de développement de Schwetzingen (Allemagne), j'ai participé aux tests du modèle de vol de COSIMA actuellement à bord de la sonde ROSETTA. La priorité des développements étaient de montrer la capacité fonctionnelle du modèle de vol, mais j'ai tout de même pu obtenir du temps de mesure pour réaliser des spectres de fragments d'olivine déposés sur une cible de noir d'or.

Ces spectres réalisés en conditions réelles, ont montré toute la difficulté de leur dépouillement, car des éléments comme le fer semble sous-représentés dans ces spectres, par rapport aux autres éléments majeurs de l'olivine (Mg, Si, O). Cet effet a peut-être un lien avec la taille des grains analysés (~ 20 µm dans ce cas), alors que pour les analyses à Orléans, nous utilisons des minéraux écrasés dont la taille est compatible avec celle du faisceau incident (~100 µm). Les résultats obtenus sur les deux instruments doivent être comparés plus finement, et interprétés.

3 EPICA - Dôme C: deux niveaux de poussières inattendus

3.1 Contexte de la découverte

Dans l'article "*First discovery of meteoritic events in deep Antarctic (EPICA-Dome C) ice cores*", deux couches de poussières extraterrestres ont été identifiées dans la carotte de glace EPICA à Dôme C (75°06'S, 123°21'E) à l'est du plateau Antarctique (**Figure 3-1**) (Narcisi *et al.* 2007). Ces couches de poussières avaient tout d'abord été considérées comme étant d'origine volcanique, mais leur origine extraterrestre ne fait actuellement aucun doute. Elles ont ensuite également été identifiées dans le carottage de Dôme Fuji, situé à 2000 km de Dôme C (Misawa *et al.* 2008) (**Figure 3-2**). Ces deux couches de poussières, L1 (2788 m de profondeur) et L2 (2833 m), correspondent à deux événements distincts datés à 434 ± 6 ka et 481 ± 6 ka, respectivement (Narcisi *et al.* 2007; Parrenin *et al.* 2007). Le flux de poussières correspondant à ces événements correspond à 10^4 fois le flux sporadique de poussières de tailles >30µm mesuré à Dôme C (Duprat *et al.* 2006). Il est difficile d'estimer la durée de ces événements, car les couches de glaces sont perturbées à de telles profondeurs, mais on peut estimer que la période de dépôt de ces poussières est inférieure à ~ un an.

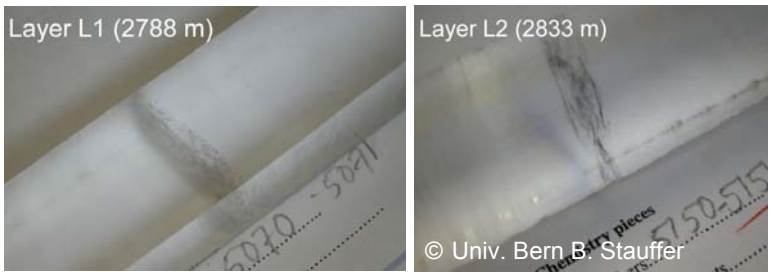

Figure 3-1 : Vue optique des deux niveaux de poussières dans la carotte EPICA-Dôme C (diamètre apparent de la carotte : 10 cm).

Des particules de la couche L2 pourraient également avoir été isolées dans la collection de micrométéorites de Frontier Mountains (Montagnes Transantarctiques) (van Ginneken *et al.* 2008).

Figure 3-2 : Localisation des sites où les niveaux de poussières ont été observés sur le continent Antarctique: L1 et L2 à Dôme C et Dôme Fuji; L2 peut-être également présent dans les montagnes transantarctiques (Frontier Mountains).

3.2 Caractérisations texturales et chimiques

Nous avons caractérisé la morphologie des grains de L1 et L2 par microscopie électronique à balayage sur leur surface externe et la composition de 47 grains de L1 et 70 grains de L2 ont et caractérisées en sections polies à l'aide de la microsonde électronique de Jussieu (service Camparis), avec 2 à 5 analyses par grain (Engrand *et al.* 2008a; Engrand *et al.* 2008b).

Les particules de poussières de L1 et L2 montrent des morphologies différentes : L1 est dominée par des fragments angulaires avec une taille maximum d'environ 100 µm (**Figure 3-3**). Certains grains de L1 ont une structure poreuse qui semble résulter de la compaction de grains de tailles micrométriques (**Figure 3-3 droite)**.

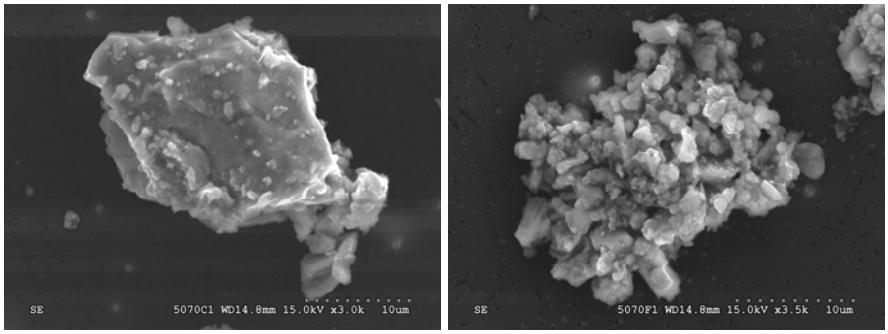

Figure 3-3 : Micrographies électroniques en électrons secondaires des surfaces externes d'un grain compact (gauche) et d'un grain poreux (droite) de la couche de poussières L1 de la carotte EPICA-Dome C.

La couche L2 est dominée par des sphérules de tailles inférieures à ~ 30 µm (**Figure 3-4**) et ne contient que de rares fragments anguleux.

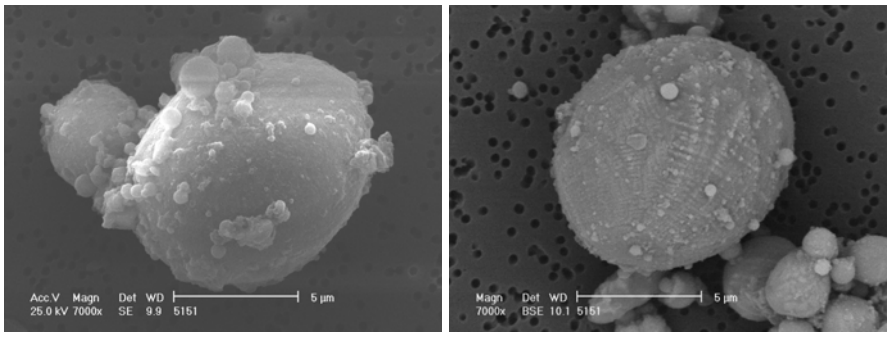

Figure 3-4: Micrographies électroniques (électrons secondaires à gauche, électrons rétrodiffusés à droite) des surfaces externes de sphérules de la couche de poussières L2 de la carotte de glace EPICA-Dôme C.

Les compositions des grains analysés pour chaque couche sont globalement chondritiques, avec une faible fraction des grains (2 pour L1 et 3 pour L2) ayant une composition déviant du champ défini par les sphérules cosmiques, et considérés comme d'origine terrestre (**Figure 3-5**). Cette très forte abondance (> 95%) de grains extraterrestre doit être comparée au rapport d'abondance de grains extraterrestres/terrestres d'environ 1/4000 que nous avons observé dans une carotte de glace pour des grains de moins de 10 µm (VanderWood *et al.* 1995; VanderWood *et al.* 1996).

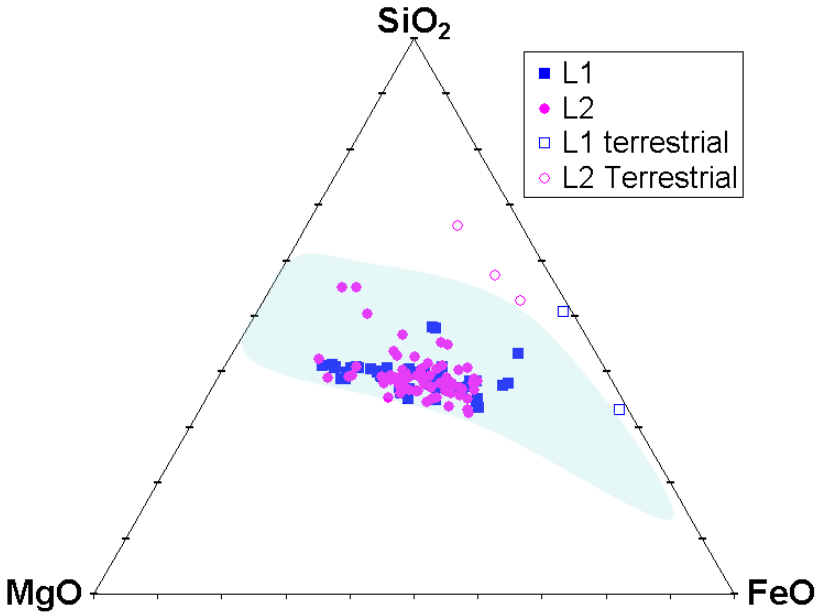

Figure 3-5 : Représentation des compositions des grains sur un diagramme ternaire MgO-SiO_2-FeO pour les deux niveaux de poussières L1 et L2 de la carotte de glace EPICA-Dome C. La zone bleue représente les analyses de sphérules cosmiques antarctiques (d'après Engrand *et al.* 2005 ; Taylor *et al.* 2005; Yada *et al.* 2005 et données non publiées). Quelques grains ont été classifiés comme terrestres d'après leur composition chimique en dehors de cette zone.

Les sphérules de L2 montrent des réseaux de dendrites de magnétite (voir **Figure 3-4 droite**) plus denses que les sphérules cosmiques du flux sporadique de tailles similaires collectés en Antarctique. Les sphérules de L2 ne montrent pas de barres d'olivine, et il faut également noter la présence de sphérules de très petites tailles <1µm. Ces observations suggèrent un processus de formation de ces sphérules par fragmentation, échauffement et refroidissement violents du précurseur de L2.

J'ai pu mesurer la composition de quelques olivines dans L1 et L2 (**Figure 3-6**). Leurs teneurs en fer sont différentes de celles des olivines primitives dans les micrométéorites et reliques dans les sphérules cosmiques (voir **Figure 1.15** dans la section 1.2.5) et sont typiques d'olivines secondaires, formées par recristallisation du liquide silicate fondu lors de la formation de L1 et L2. Tous les grains observés (même les particules anguleuses) ont des textures et de compositions de grains ayant fondus lors de leur arrivée sur Terre. Je n'ai pas trouvé de grain ou de minéral relique. Les grains anguleux semblent résulter de fragmentation de particules plus grandes.

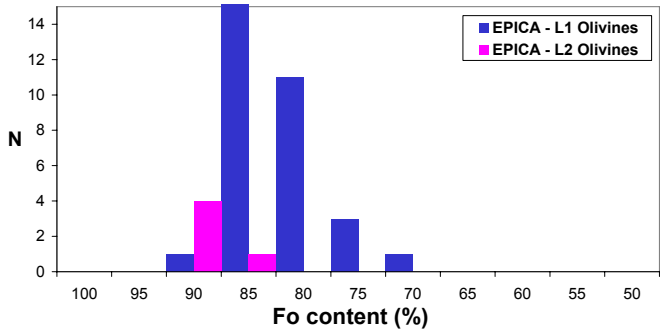

Figure 3-6 : Composition des olivines des échantillons L1 et L2 de la carotte de glace EPICA-Dôme C, exprimées par leurs teneurs en forstérite (Fo = Mg/(Mg+Fe) en nombre de cations).

Les compositions moyennes des particules de deux niveaux de poussières sont représentées sur la **Figure 3-7**. Elles sont globalement chondritiques pour tous les éléments, sauf pour le soufre qui est très appauvri dans les deux échantillons.

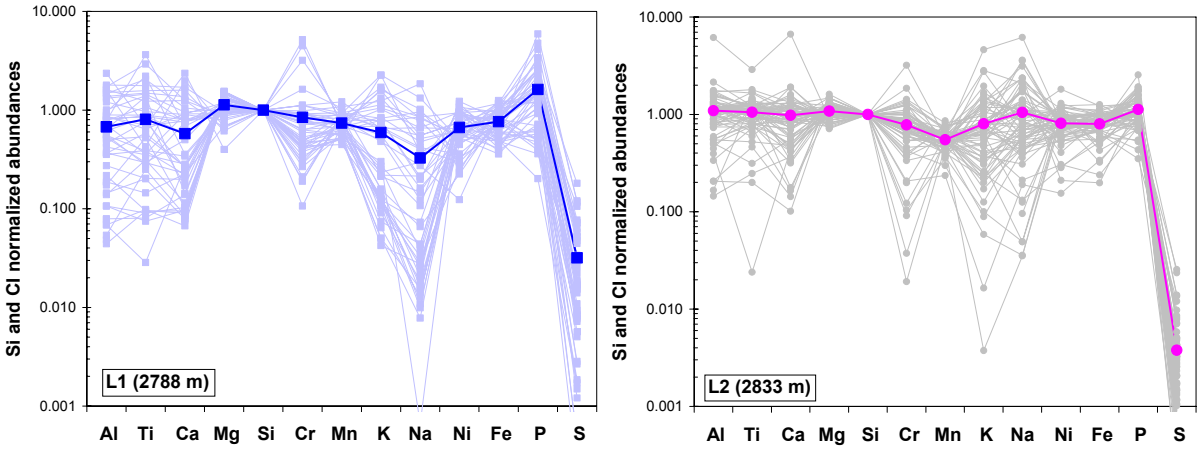

Figure 3-7 : Compositions chimiques de particules des niveaux L1 (en bleu) et L2 (en rose) de la carotte de glace EPICA-Dôme C mesurées à la microsonde électronique et normalisées à Si et CI (valeurs CI d'après Lodders 2003). Les traits forts bleus et roses représentent les valeurs moyennes des analyses des particules individuelles représentées en couleurs plus claires. D'après (Engrand *et al.* 2008a).

Si l'on s'intéresse plus en détail à la distribution des compositions en éléments majeurs et mineurs normalisées à Si et CI (**Figure 3-8**), L1 est légèrement appauvri à la fois en éléments réfractaires (Al, Ca, Ti) et volatils (Na, S). Le Ni est chondritique. La composition de L2 est nettement plus chondritique, avec toutefois un appauvrissement en S plus marqué que pour L1. Excepté un enrichissement en Ni et Na, L2 est globalement compatible avec les sphérules cosmiques (**Figure 3-8**).

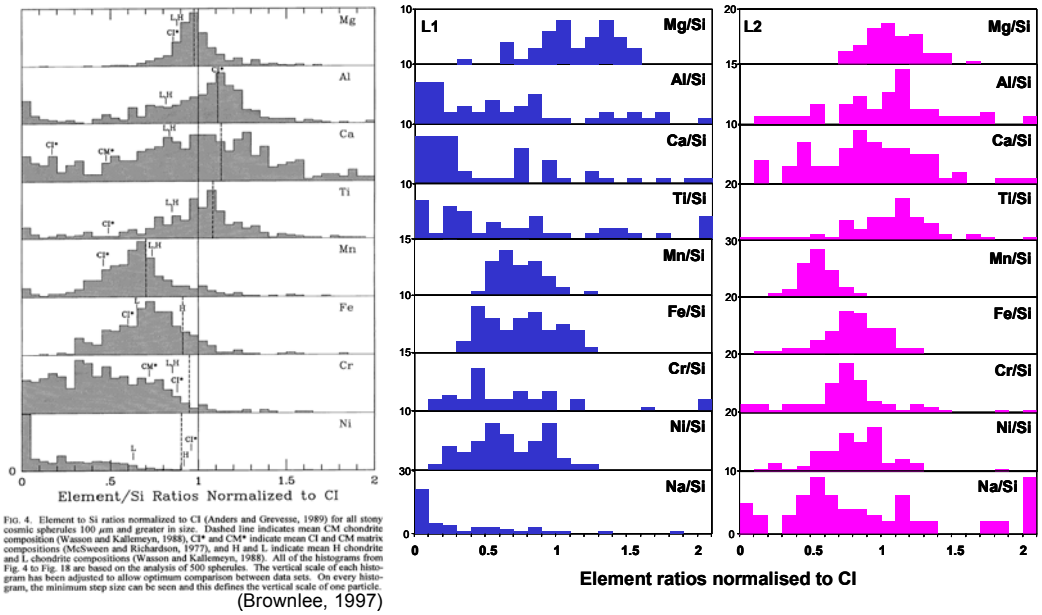

(Brownlee, 1997)

Figure 3-8 : Rapports élémentaires normalisés à CI (Lodders 2003) et Si pour les sphérules cosmiques (Brownlee *et al.* 1997), et les particules des niveaux de poussières L1 (en bleu) et L2 (en rose) de la carotte de glace EPICA-Dôme C. D'après (Engrand *et al.* 2008a).

Les informations texturales et compositionnelles suggèrent que les impacteurs responsables de la déposition de deux niveaux de poussières étaient différents, ou qu'ils ont eu des histoires thermiques totalement différentes lors de la rencontre avec la Terre.

3.3 Composition isotopique de l'oxygène de L1 et L2

Pour une meilleure compréhension de la nature de événements ayant produit ces deux niveaux de poussières, nous avons pu mesurer la composition isotopique de l'oxygène de 5 particules de L1 et 18 grains de L2 grâce à l'utilisation de la facilité nationale de microsonde ionique du CRPG de Nancy (Cameca IMS1270). Les données sont représentées sur la **Figure 3-9**. Les données de L1 et L2 sont sur ou proches de la droite de fractionnement terrestre (TF), avec $\delta^{18}O$ (L1) variant de -41,8‰ à -32,5‰; $\delta^{17}O$ (L1) de -24,2‰ à -18,1‰; $\delta^{18}O$ (L2) de -17,5‰ à +20,1‰ et $\delta^{17}O$ (L2) de -10,2‰ à +8,2‰. Une régression linéaire des données de L2 intercepte la droite TF à la composition mesurée de la glace de la carotte : $\delta^{18}O \sim \delta D/8$ (Craig 1961) avec δD variant entre -380 et -420 ‰ (Jouzel *et al.* 2007).

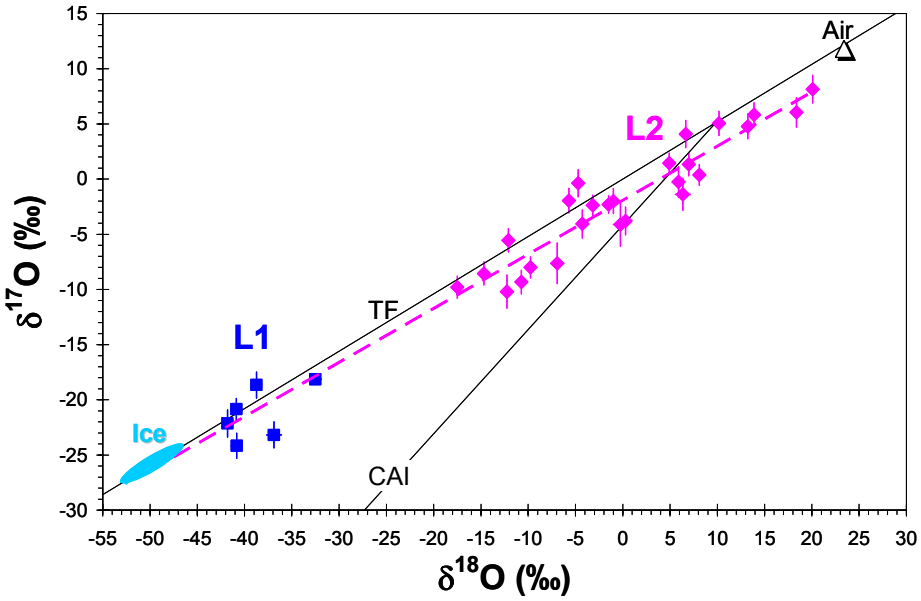

Figure 3-9 : Composition isotopique de l'oxygène dans des particules des deux niveaux de poussières L1 et L2 de la carotte de glace EPICA-Dôme C. La composition isotopique de la glace ("Ice", d'après Jouzel *et al.* 2007), celle de l'oxygène atmosphérique à haute altitude ("Air", d'après Thiemens *et al.* 1995), la ligne de fractionnement terrestre (TF) et la ligne des minéraux anhydres des météorites ("CAI", d'après Clayton 1993) sont indiquées pour référence.

Ces données isotopiques s'expliquent différemment pour les deux échantillons :

- L1 montre des valeurs isotopiques très proches de celles de la glace, suggérant 70 à 85% d'échange isotopique avec la glace ; des calculs de diffusion classiques prédisent qu'une exposition de ~ 50s à 1800°C peuvent reproduire ces taux d'échange pour une particule de 10µm. Les 430 ka de résidence dans la glace à basse température ne peuvent pas expliquer un tel effet d'échange isotopique.
- Certaines valeurs de L2 sont compatibles avec des données isotopiques de sphérules cosmiques (**Figure 3-10 gauche**) ou peuvent s'expliquer par évaporation/mélange avec l'oxygène atmosphérique. Les autres données peuvent s'interpréter comme résultant d'un échange isotopique avec la glace à partir d'un précurseur de type CM/CV/CR dont la composition isotopique est compatible avec la zone de croisement entre les données L2 et la droite CAI (**Figure 3-10 droite**). Dans ce cas, de 0 to 40% d'échange isotopique avec la glace peuvent s'expliquer par un contact de quelques secondes à 1800°C pour un grain de 10 µm.

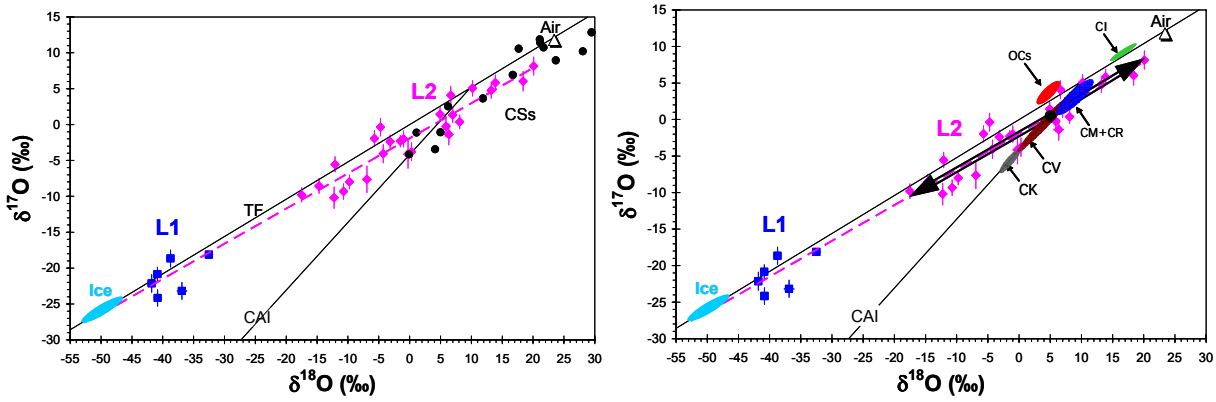

Figure 3-10 : Scénarios possibles pour expliquer les compositions isotopiques de l'oxygène observées dans les niveaux de poussières L1 et L2 de la carotte de glace EPICA-Dôme C. A gauche : L1 montre un fort taux d'échange isotopique avec la glace de la carotte ("Ice", d'après Jouzel *et al.* 2007). Certains points de L2 sont compatibles avec des analyses de sphérules cosmiques antarctiques (CSs, en noir) (Engrand *et al.* 2005); A droite : A partir d'un précurseur CM/CR/CV (croisement des données de L2 avec la ligne CAI) on peut expliquer les données par un échange isotopique avec la glace (Ice) et par évaporation/mélange avec l'oxygène atmosphérique (Air, Thiemens *et al.* 1995).

3.4 Origine des niveaux de poussières et implications

Les caractéristiques texturales et compositionnelles des échantillons de L1 et L2 suggèrent que les impacteurs responsables des deux niveaux de poussières observés dans la carotte de glace EPICA-Dôme C et Dôme Fuji étaient probablement de compositions et de structures différentes.

L'origine de ces événements par impact semble la plus naturelle : **i)** il n'est dynamiquement pas possible (J. Vaubaillon pers. comm.) d'augmenter de façon aussi massive le flux sporadique de poussières (x 10^4) sur des périodes aussi courtes (<1 an); **ii)** la composition isotopique de l'oxygène des deux échantillons s'explique naturellement par un échange isotopique avec la glace, ce qui implique une interaction à haute température entre les gouttelettes de roche fondues et un nuage de vapeur d'eau provenant de la calotte glaciaire impactée. Cet impact a nécessairement dû avoir lieu sur la glace (ou dans l'atmosphère au dessus de la calotte) car les échantillons ne sont pas mélangés avec de la matière rocheuse terrestre.

Les échantillons retrouvés dans la carotte de glace à Dôme Fuji à un âge correspondant à L1 (~ 430 ka) comportent des sphérules allant jusqu'à plusieurs centaines de microns (Misawa *et al.* 2008). Leurs fortes teneurs en ^{10}Be (Nishiizumi *et al.* 2008a) sont interprétées comme une contamination par la glace lors de l'impact, et l'absence d'^{26}Al (Nishiizumi *et al.* 2008b) soutient l'hypothèse de l'impact d'un corps massif. La grande taille des sphérules de L1 dans les échantillons de la carotte de glace de Dôme Fuji suggère un lieu d'impact plus proche de Dôme Fuji que de Dôme C.

Les échantillons de L2 sont compatibles avec la matière la plus abondante actuellement accrétée par la Terre (micrométéorites, de type C2), comme le montrent leurs compositions chimiques compatibles avec celle des sphérules cosmiques et leurs compositions isotopiques de l'oxygène. La distribution en taille ce ces poussières est inhabituelle en particulier par la présence simultanée de très petites (<1µm) et de grandes (>10µm) sphérules. Les échantillons de L2 n'ont pas perdu de Ni, alors que c'est couramment le cas pour les sphérules cosmiques, par ségrégation et séparation physique

de minuscules pépites de métaux du groupe du platine. Cela conforte le processus d'impact, fragmentant et fondant efficacement le précurseur de L2 sur Terre.

La nature de L1 est plus difficile à évaluer, sa composition chimique diffère de celle des sphérules cosmiques et sa composition isotopique de l'oxygène est trop proche de celle de la glace pour apporter des informations très précises.

La probabilité d'obtenir deux impacts de ce type à 50,000 ans de différence est raisonnable pour des corps dans la gamme de 50-500m (Bland et Artemieva 2003). L'hypothèse de l'impact sur la calotte glaciaire limite la taille du corps à environ 150m. Au delà de cette taille, l'explosion aurait lieu dans l'atmosphère, ce qui n'est toutefois pas contraignant pour notre interprétation car l'onde de choc pourrait vaporiser la calotte glaciaire (Svetsov et Wasson 2007). Encore faut-il comprendre s'il y a une raison physique à la présence de ces deux impacts sur une zone géographique limitée, et si ces impacts auraient pu avoir une influence sur le climat à grande échelle.

4 Perspectives de recherche

4.1 Recherche de micrométéorites cométaires dans la collection Concordia

4.1.1 Micrométéorites cométaires chondritiques ?

L'étude de la composition chimique et minéralogique des micrométéorites Concordia a mis en lumière de nombreuses similarités avec les chondrites carbonées et les échantillons de la comète Wild2 rapportés sur Terre par la mission Stardust (voir section 1.2). Cette observation soutient la proposition d'un continuum entre matière astéroïdale et cométaire, dont la population des micrométéorites pourrait être un échantillon représentatif.

Dans le futur, je continuerai à comparer les données recueillies sur les micrométéorites Concordia avec celles des échantillons Stardust, pour tenter de quantifier la proportion d'objets astéroïdaux et cométaires dans nos collections, et ainsi essayer de mieux préciser la distribution et la nature de la matière interplanétaire.

Ce travail se concentrera sur la caractérisation des micrométéorites à toutes les échelles (de la microscopie optique à la microscopie électronique à transmission) et sur des études isotopiques.

4.1.1.1 Structure fine et composition des micrométéorites Concordia chondritiques

Cette étude se fera dans le cadre de la thèse d'E. Dobrica, en collaboration avec Hugues Leroux (LSPES Lille). Les micrométéorites présentent un degré de complexité qui requiert une caractérisation par microscopie électronique transmission (MET). Nous nous attacherons à étudier les relations de phases minérales à l'échelle du MET pour mieux préciser les conditions de formation des micrométéorites. Les IDPs poreux anhydres d'origine cométaire présumée présentent de nombreuses inclusions vitreuses "GEMS" (Glass Embedded with Metal and Sulfides) dont l'origine interstellaire est débattue (Bradley 1994; Davoisne *et al.* 2006). Ils contiennent également des whiskers d'enstatite, orientés selon la direction [100] et avec de nombreux défauts d'empilement, qui auraient pu être condensés directement à partir de la phase vapeur et dont la présence attesterait de l'origine cométaire de ces IDPs (e.g. Bradley *et al.* 1983; Ishii *et al.* 2008). Nous avons identifié un whisker d'enstatite similaire dans une micrométéorite friable Concordia (Dobrica *et al.* 2008a). La minéralogie de cette micrométéorite contient des minéraux magnésiens et riches en calcium inclus dans une matrice poreuse riche en SiO_2. Nous devons poursuivre cette étude, rechercher des inclusions GEMS et caractériser la minéralogie des sulfures de fer à l'échelle du MET dans une large gamme de micrométéorites Concordia. Dans les grains les plus friables, nous rechercherons également la présence de traces de fission attestant de l'irradiation par le rayonnement cosmique lors de leur exposition dans l'espace interplanétaire. Jusqu'à présent nous n'avons pu observer ces traces de fission, probablement recuites lors de l'échauffement à l'entrée atmosphérique.

4.1.1.2 Composition isotopique de l'oxygène des MMs Concordia

Dans Engrand *et al*. (1999b), nous avions mesuré la composition isotopique de l'oxygène des minéraux individuels (olivines, pyroxènes et minéraux réfractaires). La composition isotopique de l'oxygène *globale* des micrométéorites n'avait jamais été mesurée. Des résultats obtenus sur des MMAs non fondues de la collection pôle sud (South Pole Water Well) (Matrajt *et al.* 2005) montrent des valeurs très enrichies en isotopes lourds de l'oxygène, contrairement aux mesures que nous avions réalisées sur les minéraux anhydres. Les auteurs interprètent cet effet comme une caractéristique intrinsèque des micrométéorites. Les isotopes de l'oxygène constituant un outil taxonomique majeur pour

la matière extraterrestre (e.g. Clayton 1993), les auteurs de ce travail proposent que les micrométéorites constituent une population *très exotique* de petits corps du milieu interplanétaire. Il faut noter que ces compositions sont différentes de celles mesurées dans les météorites ou échantillons cométaires de Wild2.

Je vois trois explications supplémentaires à cette observation : **i)** cet enrichissement en isotopes lourds de l'oxygène pourrait résulter d'une forte évaporation de l'eau contenue dans les minéraux hydratés des micrométéorites lors de leur entrée atmosphérique; **ii)** une évaporation importante des silicates de la micrométéorite incidente pourrait également donner, par distillation, une composition isotopique enrichie en isotopes lourds; **iii)** les zones analysées lors des mesures globales contiennent une fraction importante de magnétite formée lors de l'entrée atmosphérique, qui pourrait être isotopiquement lourde.

Les hypothèses i) et ii) semblent peu probables. Des compositions isotopiques aussi fractionnées ont été observées dans des micrométéorites fondues, ou sphérules cosmiques (Yada *et al.* 2003; Engrand *et al.* 2005; Taylor *et al.* 2005), mais ne pourraient probablement pas expliquer ces résultats dans des particules non (ou peu) fondues. De plus, si l'enrichissement en isotopes lourds (^{17}O, ^{18}O) de l'oxygène des MMAs résultait de l'évaporation d'une fraction importante de l'eau structurale des minéraux hydratés lors de l'entrée atmosphérique, on s'attendrait à observer un effet isotopique important sur la composition isotopique de l'hydrogène de l'eau résiduelle de ces minéraux hydratés, ce qui n'a pas été observé dans d'autres MMs de même type (e.g. Engrand *et al.* 1999a et section 1.2.1.1). Par contre, l'hypothèse iii) semble raisonnable : la composition isotopique de l'oxygène de la magnétite formée lors de l'entrée atmosphérique pourrait être enrichie en isotopes lourds. L'oxygène de l'air à ces altitudes est déjà lourd ($\delta^{18}O$ = 23,5‰ (Thiemens *et al.* 1995)) et cette magnétite pourrait s'enrichir en isotopes lourds par distillation lors de l'entrée atmosphérique.

Pour tester cette hypothèse que les micrométéorites puissent représenter une population très exotique de matière interplanétaire, je propose donc de mesurer les isotopes de l'oxygène dans des micrométéorites contenant plus ou moins de magnétite (plus ou moins scoriacées), et de mesurer directement la composition isotopique de la fine couche de magnétite qui se forme à la surface des micrométéorites les plus échauffées.

Etant donné la similarité entre la composition isotopique de l'oxygène des échantillons de Wild2 et la matière solaire 'normale', si les compositions isotopiques mesurées sont conformes à l'hypothèse iii), cela ne nous permettra pas de prouver l'origine cométaire des MMs, mais renforcera la nature représentative du continuum astéroïde-comète des micrométéorites, plutôt que de leur conférer un statut de particules exotiques.

4.1.1.3 Composition isotopique de l'hydrogène et de l'azote des MMs Concordia

Le rapport D/H de l'eau cométaire a été mesuré dans 4 comètes : Halley (Balsiger *et al.* 1995; Eberhardt *et al.* 1995), Hyakutake (Bockelée-Morvan *et al.* 1997), Hale-Bopp (Meier *et al.* 1998b) et C/2001 Q4 (NEAT) (Weaver *et al.* 2008). Les mesures s'accordent sur une valeur D/H égale à environ 2 fois la valeur SMOW (δD ~ 1000 ‰). Le rapport D/H de Wild2 est difficile à mesurer, du fait de la forte hydroscopie de l'aerogel. Les valeurs publiées varie de la valeur terrestre jusqu'à environ 3 fois la valeur SMOW (McKeegan *et al.* 2006).

Le $\delta^{15}N$ dans HCN et CN des comètes Hale-Bopp et Holmes a été récemment revisité et est enrichi en ^{15}N par rapport a la valeur terrestre ($^{15}N/^{14}N_{air}$ = 272): $^{14}N/^{15}N$ = 139 ± 26 dans HCN and $^{14}N/^{15}N$ = 165 ± 40 dans CN (Bockelée-Morvan *et al.* 2008).

Si une grande fraction des MMs sont d'origine cométaire, on pourrait s'attendre à trouver des compositions isotopiques de l'hydrogène des silicates hydratés compatibles avec les valeurs de l'eau cométaire. Ce n'est pas le cas pour les MMs de Cap Prudhomme dont le D/H moyen est centré sur la valeur terrestre (Engrand *et al.* 1999a; Gounelle *et al.* 2005a) suggérant d'ailleurs qu'elles auraient pu avoir un rôle important dans la formation des océans terrestres (e.g. Maurette 2006a). La distribution des rapports D/H dans les micrométéorites antarctique est également marginalement cohérente avec celle des chondrites carbonées, mais est incompatible avec les mesures réalisées dans les autres classes de météorites et dans une large fraction des IDPs (~ 35%) (e.g. Messenger 2000).

Je souhaite approfondir l'analyse isotopique globale des micrométéorites Concordia collectées à Dôme C en 2002 et 2006 (Duprat *et al.* 2007). En effet, cette collection possède des micrométéorites friables, qui n'existaient pas dans les collectes précédentes, et qui pourraient faire le lien avec les collectes stratosphériques d'IDPs. Cette collection contient potentiellement une plus grande proportion de grains cométaires que nous cherchons à identifier.

Un autre aspect de cette étude concerne le débat toujours sous-jacent d'un possible échange isotopique entre l'eau antarctique (de faible rapport D/H) et les micrométéorites, lors de leur séjour dans la glace. Bien que nous ayons montré que l'échange isotopique est négligeable lorsque l'on immerge des fragments de météorites dans de l'eau deutérée à 60°C (voir Engrand *et al.* 1999a), certains collègues ont récemment invoqué la possible déshydratation d'une saponite présente dans certaines MMs lors de l'entrée atmosphérique, qui pourrait se réhydrater 'instantanément' au contact de la calotte antarctique lors de la chute du grain extraterrestre dans la glace (lorsque la température n'est pas très négative, l'énergie solaire absorbée par le grain noir qu'est la micrométéorite peut très localement faire fondre la glace dans l'environnement immédiat du grain). La distribution des D/H mesurés dans les MMs de Cap Prudhomme pourrait dans ce cas être un mélange entre l'eau indigène et l'eau antarctique appauvrie en deutérium. On peut noter dans ce sens qu'il y a un léger décalage vers les basses valeurs de D/H des distributions des rapports D/H mesurés dans des micrométéorites japonaises dont le temps de résidence dans la glace est plus long que celui des MMs de Cap Prudhomme (Engrand *et al.* 2003a). Les micrométéorites de Dôme C sont conservées à très basse températures dans le névé, et elles n'ont jamais vu l'eau liquide avant leur collecte : toute possibilité d'échange isotopique avec la neige est exclu.

Jusqu'à présent, nous n'avons pas mesuré la composition isotopique de l'azote des micrométéorites chondritiques. Toujours dans l'optique d'une comparaison avec les comètes et pour préciser l'origine de la matière carbonée des micrométéorites, je souhaite donc pouvoir réaliser ces analyses.

4.1.2 Micrométéorites cométaires ultracarbonées :

4.1.2.1 Minéralogie des micrométéorites ultracarbonées

Les micrométéorites ultracarbonées (UCAMMs, pour UltraCarbonaceous Antarctic Micrometeorites) découvertes dans la collection Concordia sont de bons candidats de grains cométaires (voir section 1.2.5.1 et **Figure 4.1**). Elles n'ont pas d'équivalent dans les collections de météorites et pourraient constituer les particules CHON détectées par les missions Giotto et Vega dans la comète de Halley (Lawler et Brownlee 1992; Fomenkova *et al.* 1994). Ces particules présentent une fine association de matière carbonée et de minéraux qu'il convient de caractériser à l'échelle du microscope électronique à transmission, dans le cadre de la thèse d'E. Dobrica, en collaboration avec Hugues Leroux (LSPES Lille) et J.-N. Rouzaud (ENS Paris).

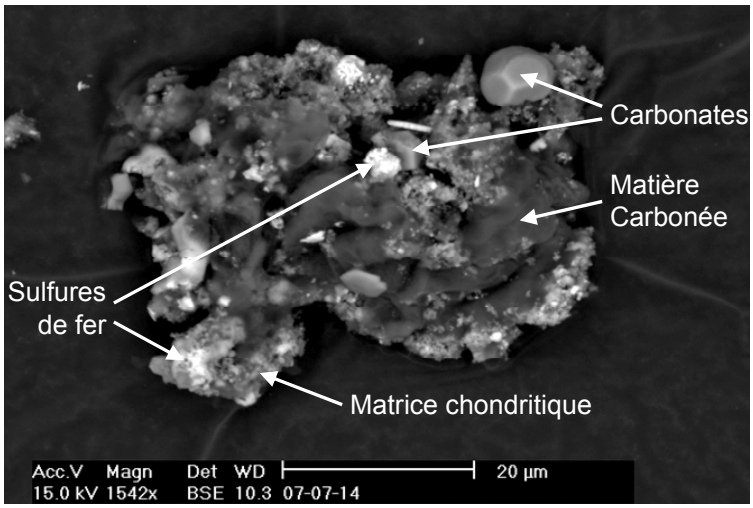

Figure 4.1 : Micrographie électronique en électrons rétrodiffusés d'un fragment d'une micrométéorite ultracarbonée montrant une forte abondance de matière carbonée (gris foncé) associée à des silicates chondritiques (matrice à grains fins), des sulfures de fer (inclusions blanches) et des carbonates de calcium.

Certaines micrométéorites ultracarbonées montrent une association avec des carbonates de calcium de tailles supérieures au micromètre (**Figure 4.1**). Dans les chondrites carbonées, les carbonates sont interprétés comme étant des phases secondaires résultant d'une altération aqueuse. Dans ces micrométéorites ultracarbonées il semble difficile de réconcilier les forts enrichissements en deutérium observés dans la matière carbonée (voir section 1.2.5.4) avec la présence de carbonates secondaires résultant d'une altération aqueuse. On peut envisager un processus de formation par condensation tel que celui décrit par Toppani *et al*. (2005), mais ces carbonates doivent être étudiés en détail dans le contexte de leur matrice carbonée pour mieux comprendre leur processus de formation.

4.1.2.2 Structure de la matière carbonée.

Dans le cadre d'une collaboration avec E. Quirico (LPG Grenoble), nous avons débuté la caractérisation de la matière carbonée des micrométéorites Concordia par micro-spectrométrie Raman, y compris dans deux micrométéorites ultracarbonées ((Dobrica *et al.* 2008b) et section 1.2.5.5). Nous devons complémenter ces analyses par une caractérisation de la structure de la matière carbonée par microscopie électronique à transmission à haute résolution en collaboration avec J.-N. Rouzaud. Ces études permettront de comparer la matière carbonée ayant une probable origine cométaire avec les matières organiques insolubles météoritiques, et d'apporter des précisions sur l'origine de cette matière.

Nous utiliserons également la microscopie IR (collaboration E. Quirico) pour caractériser la composition de cette matière carbonée.

4.1.2.3 Analyses isotopiques des MMs ultracarbonées

Certaines IDPs d'origine cométaire présumée sont très enrichies en D et ^{15}N (e.g. Messenger 2000; Aléon *et al.* 2001; Aléon *et al.* 2003; Aléon et Robert 2004). De fortes anomalies isotopiques ("hotspots") sont également trouvées très localement dans la matière organique des météorites primitives (Busemann *et al.* 2006; Robert *et al.* 2006). Ces enrichissements sont parfois interprétés comme résultant d'un héritage interstellaire ou d'un échange isotopique avec un réservoir riche en D dans la nébuleuse solaire primitive (e.g. Busemann *et al.* 2006; Remusat *et al.* 2006; Robert *et al.* 2006; Alexander *et al.*

2007). La présence d'eau deutérée a par ailleurs été mise en évidence dans un disque protosolaire (Ceccarelli *et al.* 2005).

Les premières analyses de la composition isotopique de l'hydrogène réalisées sur deux micrométéorites ultracarbonées montrent un fort enrichissement en deutérium de la matière carbonée. Les valeurs D/H globales des micrométéorites sont également élevées, de l'ordre de 7000‰ (voir section 1.2.5.4). Nous poursuivrons cette étude pour essayer de trancher sur l'origine interstellaire (e.g. Messenger 2000) vs deutération dans le système solaire (Remusat *et al.* 2006) de ces enrichissements en D, qui pourraient également contraindre le lieu de formation de cette matière organique.

Nous poursuivrons par des analyses isotopiques de l'azote de cette même matière carbonée. La composition isotopique de HCN et CN cométaires a récemment été revisitée et est enrichie en ^{15}N (Bockelée-Morvan *et al.* 2008), montrant un fractionnement isotopique important par rapport à la valeur solaire appauvrie en ^{15}N (Meibom *et al.* 2007). Nous nous intéresserons également aux isotopes du carbone des carbonates présents dans certaines UCAMMs pour retracer leur origine.

4.2 Des radioactivités éteintes dans les micrométéorites ?

4.2.1 Contexte de l'étude : Radioactivités éteintes dans les météorites

Les inclusions réfractaires météoritiques (CAIs) sont parmi les premiers solides à s'être formés dans la nébuleuse solaire. Elles contiennent des radioactivités éteintes, éléments radioactifs à courtes périodes (inférieures à quelques millions d'années) qui étaient encore en cours de décroissance au moment de la cristallisation de ces inclusions et dont l'abondance est supérieure à celle prédite par l'évolution chimique de la galaxie. L'^{26}Al est la plus emblématique de ces radioactivités éteintes, et celle qui a été découverte en premier (Lee *et al.* 1976). L'importance de ces radioactivités est multiple : **i)** l'énergie générée par leur décroissance radioactive a pu contribuer à différencier des corps de tailles suffisantes; **ii)** si la distribution en ^{26}Al est homogène, il fournit un chronomètre de grande précision (Russell *et al.* 1996); **iii)** l'origine de ces radioactivités éteintes dans ces inclusions peut donner des informations sur les conditions physiques et chimiques de la nébuleuse solaire primitive. Depuis la découverte de l'^{26}Al, d'autres radioactivité éteintes ont été découvertes (**Tableau 2**), comme le ^{53}Mn (Birck et Allegre 1985; Birck et Allegre 1988; Lugmair et Shukolyukov 1998), le ^{41}Ca (Srinivasan *et al.* 1994), le ^{10}Be (McKeegan *et al.* 2000), le ^{36}Cl (Lin *et al.* 2005), peut-être le ^{7}Be (Chaussidon *et al.* 2006) et le ^{60}Fe (Tachibana et Huss 2003; Mostefaoui *et al.* 2004) (voir Wasserburg *et al.* 2006 pour une revue récente).

Radioactivité	^{26}Al	^{53}Mn	^{41}Ca	^{10}Be	^{36}Cl	^{7}Be?	^{60}Fe?
$T_{1/2}$ (Ma)	0,7	3,7	0,1	1,5	0,3	53,2 jours	1,5

Tableau 2 : Nature des radioactivités éteintes identifiées dans les inclusions réfractaires météoritiques (CAIs). L'abondance du ^{60}Fe fait encore débat.

L'origine de ces radioactivités éteintes est encore vivement débattue, en particulier pour l'^{26}Al: **i)** l'^{26}Al des CAIs aurait pu provenir de l'injection de dernière minute provenant de l'explosion d'une supernova dans l'environnement proche du nuage moléculaire protosolaire ; **ii)** un modèle d'irradiation basé sur celui développé par Lee *et al*. (1998) avait été proposé pour expliquer la formation concomitante de plusieurs radioactivités éteintes dans la même inclusion réfractaire (Gounelle *et al.* 2001a; Fitoussi *et al.* 2008) dans le cadre du modèle x-wind proposé par Shu *et al*. (2001). Les deux alternatives ont leurs pros et cons. La probabilité d'avoir une explosion de supernova ayant pu ensemencer

le nuage protosolaire en ^{26}Al très tôt lors de sa formation est très faible (Gounelle et Meibom 2008), mais un calcul de l'énergie totale nécessaire pour former la totalité de l'^{26}Al par irradiation dans le disque protosolaire (en faisant l'hypothèse d'une distribution homogène) montre qu'il n'y a pas suffisamment d'énergie disponible pour former l'^{26}Al par irradiation (Duprat et Tatischeff 2007). En particulier, selon Duprat & Tatischeff (2007), si les échantillons cométaires contiennent de l'^{26}Al éteint, l'hypothèse de formation de l'^{26}Al par irradiation est caduque. Si la présence de ^{60}Fe éteint dans les météorites était confirmée (mais voir Chaussidon et Barrat 2008), l'origine nucléosynthétique serait requise car le ^{60}Fe ne peut être produit par irradiation. D'autre part, l'irradiation était également un mécanisme actif car on ne peut simplement expliquer autrement la présence de ^{10}Be dans les CAIs. Il semble donc que les deux processus soient nécessaires pour expliquer l'abondance des radioactivités éteintes dans les météorites primitives. L'étude de ces radioactivités éteintes apporte donc une information sur le contexte astrophysique de la formation du système solaire.

4.2.2 Recherche d'^{26}Al éteint dans les inclusions réfractaires de MMs

Dans le contexte d'une meilleure compréhension de l'origine des radioactivités éteintes, nous proposons de rechercher l'^{26}Al éteint dans les inclusions réfractaires de MMs. Nous disposons à ce jour d'une dizaine d'inclusions réfractaires (**Figure 4.2**) dont nous proposons de mesurer la composition isotopique du Mg pour rechercher un excès en ^{26}Mg provenant de la décroissance de l'^{26}Al maintenant éteint.

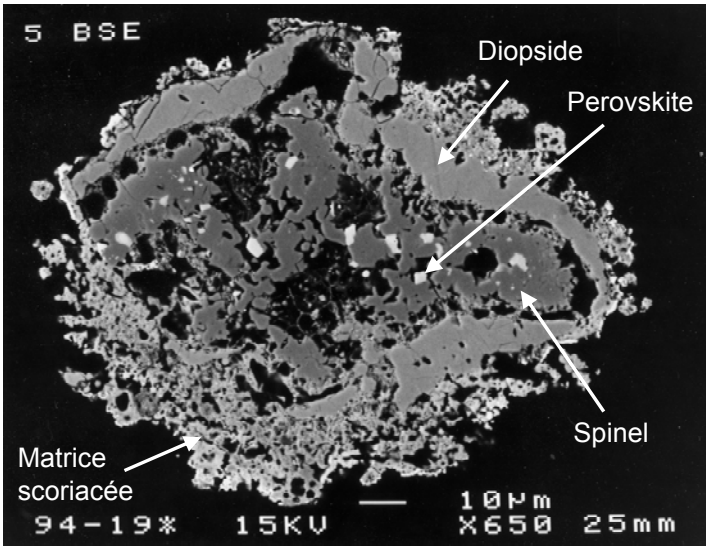

Figure 4.2 : Micrographie électronique en électrons rétrodiffusés d'une inclusion réfractaire dans une micrométéorite antarctique de Cap Prudhomme.

L'abondance d'inclusions réfractaires dans la collection de micrométéorites (Cap-Prudhomme et Concordia) ne dépasse pas quelques pourcents. Ce type d'analyse n'a jamais été réalisé dans les IDPs ou les échantillons de Stardust.

4.2.3 Recherche d'anomalies en ^{60}Fe dans les sulfures de fer des micrométéorites Concordia

Dans le même contexte, l'abondance initiale de ^{60}Fe dans les météorites est mal contrainte (Tachibana et Huss 2003; Mostefaoui *et al.* 2004), et sa présence au delà des abondances prévues par l'évolution chimique de la galaxie est actuellement remise en question (Chaussidon et Barrat 2008). Les micrométéorites Concordia contiennent une population de sulfures de fer très primitifs, qui seraient potentiellement les phases adéquates pour rechercher le ^{60}Fe (voir section 1.2.5.3). Les sulfures de fer identifiés à ce jour dans les micrométéorites Concordia contiennent du nickel, ce qui est un facteur

limitant pour rechercher la présence passée de ^{60}Fe dans ces phases minérales. Nous poursuivrons notre quête de sulfures de fer sans nickel, en particulier dans les micrométéorites ultracarbonées où les sulfures n'ont pas encore été caractérisés.

4.3 Exobiologie

Depuis ma thèse, j'ai gardé la motivation d'essayer de comprendre nos origines. L'exobiologie est un domaine stimulant car il nécessite de rencontrer des collègues de disciplines très différentes (biologiste, géologues, chimistes, astronomes), et de comprendre leur langage scientifique. Depuis ma thèse, mon implication en exobiologie s'est limitée à essayer de caractériser la matière carbonée des micrométéorites. J'ai également fait partie du conseil de groupement du GDR d'exobiologie et du groupe thématique Exo/Astrobiologie du CNES.

4.3.1 Recherche d'acides aminés dans les micrométéorites Concordia

La découverte des micrométéorites ultracarbonées a relancé les études concernant la connexion possible entre les MMs et l'origine de la vie. Lors de ma thèse, nous avions mis en évidence que les MMs de Cap-Prudhomme contenaient des molécules organiques comme des PAHs et potentiellement des acides aminés, en particulier l'AIB (Brinton *et al.* 1998; Clemett *et al.* 1998). La présence d'AIB dans les MMs a été récemment confirmée par Matrajt *et al*. (2004) après plusieurs résultats négatifs (Matrajt 2001; Glavin *et al.* 2004).

Les MMs analysées à ce jour montrent une contamination en acides aminés provenant de la glace antarctique (voir Brinton *et al.* 1998), et seuls les acides aminés non biologiques (comme l'AIB et l'isovaline) peuvent raisonnablement n'être attribués qu'à l'échantillon analysé.

Les micrométéorites Concordia présentent l'avantage d'avoir des temps de résidence courts dans la neige (moins de 50 ans), à des températures très basses (-30 à -80°C), et dans des zones où la vie est virtuellement absente. Ils constituent donc les échantillons adéquats pour une recherche d'acides aminés, mais nous ne pouvons nous permettre de sacrifier 50 à 100 micrométéorites pour ces analyses, comme cela a été le cas jusqu'à présent. Martin *et al*. (2008) ont développé une méthode permettant d'analyser une particule individuelle d'environ 50 µm. En collaboration avec cette équipe, nous tenterons donc la recherche d'acides aminés dans quelques fragments de micrométéorites ultracarbonées.

4.3.2 Un spectromètre de masse pour l'exobiologie : ILMA

Dans le cadre de la mission spatiale MARCO POLO en compétition pour le programme Cosmic Vision de l'ESA, j'avais été mandatée par le GDR d'exobiologie en 2006 pour proposer un spectromètre de masse pouvant répondre à des thématiques exobiologiques. Cette proposition a vu le jour sous la forme d'un spectromètre de masse à transformée de Fourier dont le détail est donné dans la section 4.6.

4.4 Des niveaux de poussières inattendus dans EPICA : influence sur le climat global?

La présence de deux niveaux de poussières d'origine extraterrestre dans les grands carottages EPICA-Dôme C et de Dôme Fuji est attribuée à deux impacts de corps de tailles ~ 100m sur la calotte glaciaire antarctique, il y a 430 et 480 ka (voir section 3).

Je poursuivrai le travail en cours sur ces niveaux de poussières, en collaboration avec B. Narcisi (ENEA Italie) et J.-R.Petit (LGGE Grenoble). J'essaierai de préciser la nature

des impacteurs en mesurant la composition en éléments en trace (collaboration avec O. Alard, Montpellier), en recherchant d'éventuelles traces de choc dans les échantillons, et en recherchant et comparant la nature des impacteurs et la taille des cratères connus sur Terre. Nous essayerons d'évaluer si ces impacts auraient pu avoir une influence sur le climat global.

Nous avons également entamé une collaboration avec J. Vaubaillon et F. Colas (IMCCE Paris) pour tenter d'élucider les mécanismes de dynamique céleste ayant pu lancer ces corps sur la calotte glaciaire avec un intervalle de temps de 50 ka.

4.5 Mission ROSETTA : COSIMA

Je poursuivrai les études autour de COSIMA (voir section 2.2) en collaboration étroite avec l'équipe COSIMA du LPCE d'Orléans, du MPI de Lindau, et avec K. Varmuza (Laboratory for Chemometrics, TU, Vienna), pour essayer de déterminer les phases présentes dans les spectres TOF-SIMS par une approche de chémométrie. Nous collaborons également avec H. Cottin (LISA, Creteil) qui est plus apte à interpréter la partie organique du spectre de masses. Nous avons de plus entamé une collaboration à Vienne pour l'utilisation d'un TOF-SIMS à haute résolution en masse et haute résolution spatiale pour calibrer les données des prototypes de COSIMA d'Orléans et de Lindau. Un des principaux objectifs de cette étude est également de fabriquer une base de données de spectres de références pour des minéraux d'intérêt cométaire. Grâce aux données recueillies par Deep Impact et Stardust, nous avons défini une liste de minéraux qui sont en cours d'analyses ou seront préparés prochainement. Nous utiliserons également des échantillons extraterrestres (micrométéorites et météorites primitives) pour participer à la qualification scientifique de COSIMA.

Nous avons également fait appel a notre collègue A. Kearsley qui a fabriqué des agrégats d'olivine et de matière organique reproduisant la structure des cratères observés sur les feuilles d'aluminium du collecteur de Stardust (Kearsley *et al.* 2008). Nous allons tester le comportement de ces grains sur une cible COSIMA à l'aide du canon à poussière développé à Munich par K. Hornung.

Nous reprendrons enfin nos tentatives de mesures isotopiques à l'aide de l'instrument d'Orléans. La résolution en masse de COSIMA devrait nous permettre de mesurer au moins la composition isotopique de l'oxygène $^{18}O/^{16}O$. La composition isotopique de l'hydrogène ne pose pas de problème quant à la résolution en masse, mais la qualité du vide est cruciale. Les isotopes du carbone sont à tester : la résolution en masse n'est théoriquement pas suffisante pour séparer ^{13}C de ^{12}CH, mais de forts effets isotopiques sont peut-être détectables. Nous nous sommes procuré un montage de SiC présolaires présentant de fortes anomalies isotopiques du carbone et un montage témoin pour faire un test de faisabilité en aveugle (de S. Messenger JSC Houston). Nous testerons aussi la possibilité de mesurer les isotopes du soufre.

Je poursuivrai également ma participation au WG2 'Chemical Properties' en tant que co-chairman pour la planification des analyses lors du rendez-vous en 2014. Nous devons fournir une première version d'un protocole d'analyses coordonnées pour fin 2008. L'étape suivante consistera à vérifier s'il existe des conflits avec des opérations désirées par les autres groupes de travail. La définition des opérations de la mission pour toutes les phases de mission devra être finalisée pour mi-2010.

4.6 Mission MARCO POLO : ILMA

MARCO POLO est une mission d'analyse et de retour d'échantillons d'un astéroïde géocroiseur primitif de type C ou D, proposée en réponse à l'appel d'offre Cosmic Vision de l'ESA dans le cadre d'une collaboration avec la JAXA (Japon): http://www.lesia.obspm.fr/cosmicvision/neosr/ (mot de passe : sifnos07). Les objectifs de la mission sont principalement axés sur une meilleure compréhension des processus du système solaire primitif accompagnant la formation planétaire et l'origine de la matière carbonée et de la vie dans le système solaire.

En 2006, j'avais été mandatée par le conseil de groupement du GDR Exobiologie pour proposer d'inclure un spectromètre de masse à transformée de Fourier : ILMA – Ion Laser Mass Analyzer, capable de réaliser des mesures de compositions chimiques et isotopiques.

Ce spectromètre de masse, initialement accepté par l'équipe de la proposition MARCO POLO, a fait également l'objet d'une proposition indépendante en réponse à l'appel d'offre de l'ESA pour charge utile scientifique de MARCO POLO. Une équipe de 23 scientifiques, appartenant à une quinzaine d'instituts dans 5 pays européens s'est constituée autour de cet instrument. La base de l'équipe est française avec Hervé Cottin (LISA) comme PI, Christelle Briois (LPCE) et moi-même comme Co-PIs, L. Thirkell (LPCE) comme ingénieur système et N. Grand (LISA) comme chef de projet. Ce projet serait financé par le CNES, DLR, CNRS, MPI, et plusieurs autres universités et institutions de recherche européens.

ILMA est un SIMS (Secondary Ion Mass Spectrometry) à transformée de Fourier de nouvelle génération, à haute résolution en masse (**Figure 4.3**).

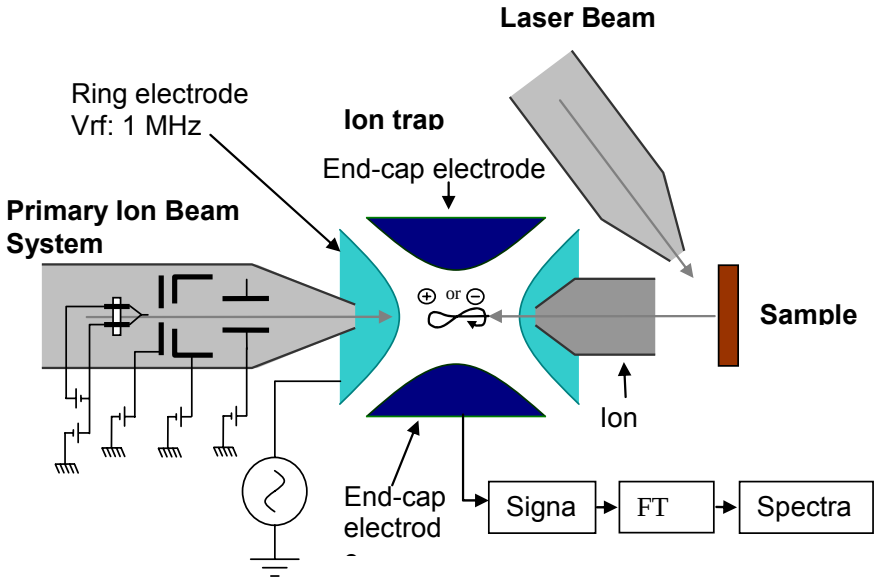

Figure 4.3 : vue schématique d'ILMA (Ion Laser Mass Analyzer), un spectromètre de masse a transformée de Fourier haute résolution proposé dans le cadre de la mission de retour d'échantillon d'astéroïde MARCO POLO.

ILMA est le seul instrument sur MARCO POLO qui pouvoir répondre à des thématiques d'exobiologie. Sans ILMA, cet aspect, présenté comme faisant partie des premières priorités de la mission, repose sur le retour d'échantillons sur Terre, avec le risque de perte et de contamination inhérent à ce type de mission. Dans la configuration optimale, ILMA serait placé sur l'atterrisseur de MARCO POLO. Il pourrait caractériser le site de prélèvement d'échantillons, permettant ainsi de replacer ceux-ci dans leur

contexte local, mais aussi réaliser des analyses d'échantillons *in situ*, sans risque de contamination.

4.6.1 ILMA et la formation du système solaire

Quelle est la matière la plus abondance du milieu interplanétaire? Les météorites sont-elles représentatives de cette matière? Quels sont les processus ayant formé les astéroïdes et comment ont-ils évolué? Quel était le contexte astrophysique de la formation du système solaire?

L'approche la plus directe pour répondre à ces questions consistera à comparer les analyses *in situ* d'ILMA de l'astéroïde avec la composition des différentes météorites et micrométéorites recueillies sur Terre. On pense que les chondrites carbonées proviennent des astéroïdes de type C, et que les astéroïdes D n'ont pas de représentants dans les collections de météorites, sauf peut-être Tagish Lake (Hiroi *et al.* 2001). De telles assertions sont difficile à vérifier du sol, car elles reposent sur les propriétés spectroscopiques des astéroïdes, dont la surface est altérée par leur résidence dans l'espace, alors que les météorites perdent ~90% de leur masse (et leur surface externe) par ablation lors de l'entrée sur Terre. Les micrométéorites, qui représentent actuellement l'apport dominant de matière extraterrestre sur Terre (environ 1000 fois plus que les météorites) sont seulement reliées à la classe relativement rare des chondrites carbonées, qui représentent moins de 5% des chutes de météorites (e.g. Engrand et Maurette 1998). La vaste majorité des météorites présentes dans les collections (>80%) est de type "chondrite ordinaire". Cette apparente divergence entre les types de météorites et micrométéorites pourrait s'expliquer par la prédominance d'astéroïdes C et D dans la ceinture prinipale, impliquant que la poussière cosmique serait plus représentative de la matière interplanétaire que les météorites. Alternativement, la poussière cosmique pourrait provenir préférentiellement des corps les plus facilement désagrégés lors d'un impact (Bottke *et al.* 2008). Les analyses de Wild 2 (Stardust) (e.g. Brownlee *et al.* 2006), et la découverte de comètes dans la ceinture principale d'astéroïdes (Hsieh et Jewitt 2006) confortent l'existence d'un continuum entre matière astéroïdale et cométaire. La caractérisation d'un astéroïde in situ dans l'espace interplanétaire permettra de mieux contraindre le lien génétique entre le type de l'astéroïde, les classes de météorites et les micrométéorites.

Les analyses isotopiques réalisées par ILMA sur l'astéroïde carboné pourraient également révéler la présence de grains présolaires interstellaires tels que ceux identifiés dans les météorites primitives (e.g. Zinner 1998). La nature et l'abondance de tels grains présolaires dans cet astéroïde apporteraient des informations sur le contexte astrophysique de la formation du système solaire.

4.6.2 ILMA et l'origine de la vie dans le système solaire

Quel est la nature et l'origine des composés organiques présents dans un astéroïde de type C? Que peuvent apporter ces produits organiques à la compréhension de l'origine de la vie? Quel est le rôle de l'apport extraterrestre pour l'origine de la vie?

Les astéroïdes de type C pourraient être les corps parents des chondrites carbonées, qui sont des mélanges de chondres et de minéraux formés à haute température, associés à une matrice formée à basse température et à de la matière carbonée. Les chondrites carbonées contiennent typiquement quelques pourcents de carbone, dont plus de 80% est sous forme de matière organique insoluble (MOI) (e.g. Remusat *et al.* 2006). Des composés organiques de plus faibles poids moléculaires, comme les acides aminés (ou leurs précurseurs) sont également présents en faible quantités (100 ppm - 250 ppm) dans les chondrites carbonées (e.g Botta et Bada 2002; Martins *et al.* 2007)

Les scénarios actuels d'exobiologie font appel à un apport extraterrestre de matière organique sur la terre primitive. Il a été proposé que cette matière organique pourrait avoir fourni des molécules organiques complexes capables de déclencher la synthèse prébiotiques de composes biochimiques sur la Terre primitive (e.g. Maurette 2006a). Il est intéressant de noter dans ce contexte que les acides amines météoritiques, formés en conditions abiotiques, présentent parfois un excès énantiomérique L allant jusqu'à ~15% (e.g. Pizzarello *et al.* 2003).

La surface de l'astéroïde ayant été exposée au vide interplanétaire et au rayonnement cosmique pendant plusieurs millions (voire milliards) d'années, il semble improbable de trouver des composés organique volatiles à sa surface. L'analyse clé pour l'exobiologie dans le cadre de la mission MARCO POLO serait donc de pouvoir faire le lien entre ce type d'astéroïdes et une classe de chondrites carbonées, permettant de mieux contraindre la nature de la matière organique apportée sur Terre à l'époque de la chimie prébiotique.

Bibliographie

Aléon J., Engrand C., Robert F. and Chaussidon M. (2001) Clues on the origin of interplanetary dust particles from the isotopic study of their hydrogen-bearing phases. *Geochim. Cosmochim. Acta* **65**, 4399-4412.

Aléon J., Robert F., Chaussidon M. and Marty B. (2003) Nitrogen isotopic composition of macromolecular organic matter in interplanetary dust particles. *Geochim. Cosmochim. Acta* **67**, 3773-3783.

Aléon J. and Robert F. (2004) Interstellar chemistry recorded by nitrogen isotopes in Solar System organic matter. *Icarus* **167**, 424-430.

Alexander C.M.O.D., Fogel M., Yabuta H. and Cody G.D. (2007) The origin and evolution of chondrites recorded in the elemental and isotopic compositions of their macromolecular organic matter. *Geochim. Cosmochim. Acta* **71**, 4380-4403.

Balsiger H., Altwegg K. and Geiss J. (1995) D/H and $^{18}O/^{16}O$ ratio in the hydronium ion and in the neutral water from in situ ion measurements in comet Halley. *J. Geophys. Res.* **100**, 5827-5834.

Beny-Bassez C. and Rouzaud J.N. (1985) Characterization of carbonaceous materials by correlated electron and optical microscopy and Raman microspectroscopy. *Scanning Electron Microscopy* **1**, 119-132.

Birck J.-L. and Allegre C.-J. (1985) Evidence for the presence of ^{53}Mn in the early solar system. *Geophys. Res. Lett.* **12**, 745-748.

Birck J.L. and Allegre C.J. (1988) Manganese-chromium isotope systematics and the development of the early solar system. *Nature* **331**, 579-584.

Blanchard M.B., Brownlee D.E., Bunch T.E., Hodge P.W. and Kyte F.T. (1980) Meteoroid ablation spheres from deep-sea sediments. *Earth Planet. Sci. Lett.* **46**, 179-190.

Bland P.A., Smith T.B., Jull A.J.T., Berry F.J., Bevan A.W.R., Couldt S. and Pillinger C.T. (1996) The flux of meteorites to the Earth over the last 50,000 years. *Mon. Not. R. Astron. Soc.* **283**, 551-565.

Bland P.A. and Artemieva N.A. (2003) Efficient disruption of small asteroids by Earth's atmosphere. *Nature* **424**, 288-291.

Bockelée-Morvan D., et al. (1997) Deuterated water in comet C/1996 B2 (Hyakutake) and its implications for the origin of comets. *Icarus* **133**, 147-162.

Bockelée-Morvan D., Gautier D., Hersant F., Huré J.M. and Robert F. (2002) Turbulent radial mixing in the solar nebula as the source of crystalline silicates in comets. *Astron. Astrophys.* **384**, 1107-1118.

Bockelée-Morvan D., et al. (2008) Large excess of heavy nitrogen in both hydrogen cyanide and cyanogen from comet 17P/Holmes. *Astrophys. J.* **679**, L49-L52.

Botta O. and Bada J.L. (2002) Extraterrestrial organic compounds in meteorites. *Surveys in Geophysics* **23**, 411-467.

Bottke W.F., Levison H.F., Nesvorny D., Morbidelli A. and Gounelle M. (2008) The collisional evolution of objects captured in the outer asteroid belt during the late heavy bombardment. In *Asteroids, Comets, Meteors*, pp. #8096, Baltimore.

Bradley J.P., Brownlee D.E. and Veblen D.R. (1983) Pyroxene whiskers and platelets in interplanetary dust: evidence for vapour phase growth. *Nature* **310**, 473-477.

Bradley J.P. (1994) Chemically anomalous preaccretionally irradiated grains in interplanetary dust from comets. *Science* **265**, 925-929.

Brinton K.L.F., Engrand C., Glavin D.P., Bada J.L. and Maurette M. (1998) A search for extraterrestrial amino acids in carbonaceous Antarctic micrometeorites. *Orig. Life Evol. Biosph.* **28**, 413-424.

Brown P.G., et al. (2000) The fall, recovery, orbit, and composition of the Tagish Lake meteorite: a new type of carbonaceous chondrite. *Science* **290**, 320-325.

Brownlee D., et al. (2006) Comet 81P/Wild 2 under a microscope. *Science* **314**, 1711-1716.

Brownlee D.E., Bates B.A. and Wheelock M.M. (1984) Extraterrestrial platinum group nuggets in deep-sea sediments. *Nature* **309**, . 693-695.

Brownlee D.E. (1985) Cosmic dust : collection and research. *Ann. Rev. Earth Planet. Sci.* **13**, 147-173.

Brownlee D.E., Bates B. and Schramm L. (1997) The elemental composition of stony cosmic spherules. *Meteoritics Planet. Sci.* **32**, 157-175.

Bullock E.S., Gounelle M., Lauretta D.S., Grady M.M. and Russell S.S. (2005) Mineralogy and texture of Fe-Ni sulfides in CI1 chondrites: Clues to the extent of aqueous alteration on the CI1 parent body. *Geochim. Cosmochim. Acta* **69**, 2687-2700.

Busemann H., Alexander C.M.O.D., Hoppe P., Nittler L.R. and Young A.F. (2005) Extreme H isotopic anomalies in chondritic organic matter. *Meteoritics Planet. Sci.* **40 (Suppl)**, #5255.

Busemann H., Young A.F., Alexander C.M.O.D., Hoppe P., Mukhopadhyay S. and Nittler L.R. (2006) Interstellar chemistry recorded in organic matter from primitive meteorites. *Science* **312**, 727-730.

Ceccarelli C., Dominik C., Caux E., Lefloch B. and Caselli P. (2005) Discovery of deuterated water in a young protoplanetary disk. *Astrophys. J.* **631**, L81-L84.

Chaussidon M., Robert F., Russell S.S., Gounelle M. and Ash R.D. (2003) Variations of apparent $^{10}Be/^{9}Be$ ratios in Leoville MRS-06 type B1 CAI: constraints on the origin of ^{10}Be and ^{26}Al. *Lunar Planet. Sci.* **XXXIV**, #1347 (CD-ROM).

Chaussidon M., Robert F. and McKeegan K.D. (2006) Li and B isotopic variations in an Allende CAI: Evidence for the in situ decay of short-lived 10Be and for the possible presence of the short-lived nuclide 7Be in the early solar system. *Geochim. Cosmochim. Acta* **70**, 224-245.

Chaussidon M. and Barrat J.A. (2008) Extinct Fe-60 in the eucrite NWA 4523. *Meteoritics Planet. Sci.* **43**, A31-A31.

Clayton R.N., Grossman L. and Mayeda T.K. (1973) A component of primitive nuclear composition in carbonaceous meteorites. *Science* **182**, 485-488.

Clayton R.N., Onuma N. and Mayeda T.K. (1976) A classification of meteorites based on oxygen isotopes. *Earth Planet. Sci. Lett.* **30**, 10-18.

Clayton R.N. (1993) Oxygen isotopes in meteorites. *Ann. Rev. Earth Planet. Sci.* **21**, 115-149.

Clayton R.N. and Mayeda T.K. (1999) Oxygen isotope studies of carbonaceous chondrites. *Geochim. Cosmochim. Acta* **63**, 2089-2104.

Clayton R.N. (2002) Solar System : self shielding in the solar nebula. *Nature* **415**, 860-861.

Clemett S.J., Chillier X.D.F., Gillette S., Zare R.N., Maurette M., Engrand C. and Kurat G. (1998) Observation of indigeneous polycyclic aromatic hydrocarbons in 'giant' carbonaceous Antarctic micrometeorites. *Orig. Life and Evol. Biosphere* **28**, 425-448.

Craig H. (1961) Isotopic variations in meteoric waters. *Science* **133**, 1702-1703.

Crovisier J. and Bockelée-Morvan D. (2008) Comment on ``Comparison of the composition of the Tempel 1 ejecta to the dust in Comet C/Hale--Bopp 1995 O1 and YSO HD 100546" by C.M. Lisse, K.E. Kraemer, J.A. Nuth III, A. Li, D. Joswiak [2007. Icarus 187, 69--86]. *Icarus* **195**, 938-940.

Davoisne C., Djouadi Z., Leroux H., D'Hendecourt L., Jones A. and Deboffle D. (2006) The origin of GEMS in IDPs as deduced from microstructural evolution of amorphous silicates with annealing. *Astron. Astrophys.* **448**, L1-L4.

Deloule E. and Robert F. (1995) Interstellar water in meteorites? *Geochim. Cosmochim. Acta* **59**, 4695-4706.

Dobrica E., Engrand C., Leroux H., Duprat J. and Gounelle M. (2008a) Classic and exotic particles in the 2006 Concordia Antarctic micrometeorite collection. *Lunar Planet. Sci.* **XXXIX**, #1672 (CD-ROM).

Dobrica E., Engrand C., Quirico E., Montagnac G. and Duprat J. (2008b) New clues on composition and structure of carbonaceous matter in Antarctic micrometeorites. *Meteoritics Planet. Sci.* **43**, A38-A38.

Douthitt C.B. (1982) The geochemistry of the stable isotopes of silicon. *Geochim. Cosmochim. Acta* **46**, 1449-1458.

Duprat J., Maurette M., Engrand C., Matrajt G., Immel G., Hammer C., Gounelle M. and Kurat G. (2001) An estimation of the contemporary micrometeorite flux obtained from surface snow samples collected in central Antarctica. *Meteoritics Planet. Sci.* **36 Suppl.**, A52.

Duprat J., Engrand C., Maurette M., Gounelle M., Hammer C. and Kurat G. (2003) The CONCORDIA-collection : pristine contemporary micrometeorites from central Antarctica surface snow. *Lunar Planet. Sci.* **XXXIV**, #1727 (CD-ROM).

Duprat J., Engrand C., Maurette M., Gounelle M., Kurat G. and Hammer C. (2005a) The micrometeorite program at Dome C. In *Dome C Astronomy and Astrophysics Meeting* (eds. M. Giard, F. Casoli and F. Paletou), pp. 51-56. EAS Pub. Series.

Duprat J., Engrand C., Maurette M., Gounelle M., Kurat G. and Leroux H. (2005b) Friable micrometeorites from central Antarctica snow. *Lunar Planet. Sci.* **XXXVI**, #1678 (CD-ROM).

Duprat J., Engrand C., Maurette M., Naulin F., Kurat G. and Gounelle M. (2006) The micrometeorite mass flux as recorded in Dome C central Antarctic surface snow. *Meteoritics Planet. Sci.* **41 Suppl.**, A48.

Duprat J., Engrand C., Maurette M., Kurat G., Gounelle M. and Hammer C. (2007) Micrometeorites from Central Antarctic snow: The CONCORDIA collection. *Adv. Space Res.* **39**, 605-611.

Duprat J. and Tatischeff V. (2007) Energetic constraints on in situ production of short-lived radionuclei in the early Solar System. *Astrophys. J.* **671**, L69-L72.

Eberhardt P., Reber M., Krankowsky D. and Hodges R.R. (1995) The D/H and $^{18}O/^{16}O$ ratios in water from comet P/Halley. *Astron. Astrophys.* **302**, 301-316.

Eiler J.M. and Kitchen N. (2004) Hydrogen isotope evidence for the origin and evolution of the carbonaceous chondrites. *Geochim. Cosmochim. Acta* **68**, 1395-1411.

Engrand C. (1995) Micrométéorites antarctiques: vers l'exobiologie et la mission cométaire "ROSETTA". Ph. D. thesis thesis. Université de Paris Sud, Centre d'Orsay.

Engrand C. and Maurette M. (1998) Carbonaceous micrometeorites from Antarctica. *Meteoritics Planet. Sci.* **33**, 565-580.

Engrand C., Deloule E., Robert F., Maurette M. and Kurat G. (1999a) Extraterrestrial water in micrometeorites and cosmic spherules from Antarctica : an ion microprobe study. *Meteoritics Planet. Sci.* **34**, 773-787.

Engrand C., McKeegan K.D. and Leshin L.A. (1999b) Oxygen isotopic compositions of individual minerals in Antarctic micrometeorites : further links to carbonaceous chondrites. *Geochim. Cosmochim. Acta* **63**, 2623-2636.

Engrand C., Gounelle M., Duprat J. and Zolensky M.E. (2001a) In-situ oxygen isotopic composition of individual minerals in Tagish Lake, a new type 2 carbonaceous meteorite. *Lunar Planet. Sci.* **XXXII**, #1568 (CD-ROM).

Engrand C., Gounelle M. and Zolensky M.E. (2001b) Oxygen isotopic composition of Tagish Lake. *Meteoritics Planet. Sci.* **36 Suppl.**, A54.

Engrand C., Duprat J. and Gounelle M. (2003a) Comparison of the hydrogen isotopic compositions of Antarctic micrometeorites from the French and Japanese collections. *Meteoritics Planet. Sci.* **38 Suppl.**, A108.

Engrand C., Gounelle M., Zolensky M.E. and Duprat J. (2003b) About Tagish Lake as a potential parent body for polar micrometeorites ; clues from their hydrogen isotopic compositions. *Lunar Planet. Sci.* **XXXIV**, #1688 (CD-ROM).

Engrand C., Lespagnol J., Martin P., Thirkell L. and Thomas R. (2004) Multi-correlation analyses of TOF-SIMS spectra for mineralogical studies. *Applied Surf. Sci.* **231**, 883-887.

Engrand C., McKeegan K.D., Leshin L.A., Herzog G.F., Schnabel C., Nyquist L.E. and Brownlee D.E. (2005) Isotopic compositions of oxygen, iron, chromium, and nickel in cosmic spherules: Toward a better comprehension of atmospheric entry heating effects. *Geochim. Cosmochim. Acta* **69**, 5365-5385.

Engrand C., Kissel J., Krueger F.R., Martin P., Silén J., Thirkell L., Thomas R. and Varmuza K. (2006) Chemometric evaluation of time-of-flight secondary ion mass spectrometry data of minerals in the frame of future *in situ* analyses of cometary material by COSIMA onboard ROSETTA. *Rapid. Commun. Mass Spectrom.* **20**, 1361-1368.

Engrand C., Briois C., Thirkell L. and Cottin H. (2007a) A Concordia Antarctic micrometeorite used as a cometary proxy for the analyses of COSIMA onboard ROSETTA. *Meteoritics Planet. Sci.* **42 suppl.**, A42.

Engrand C., Duprat J., Maurette M. and Gounelle M. (2007b) Fe-Ni sulfides in Concordia Antarctic micrometeorites. *Lunar Planet. Sci.* **XXXVIII**, #1668 (CD-ROM).

Engrand C., Duprat J., Slodzian G., Reynolds B.C., Dennebouy R., Gounelle M. and Russell S.S. (2007c) SIMS analysis of silicon isotopes: instrumental effects and application to a Leoville refractory inclusion. *Lunar Planet. Sci.* **XXXVIII**, #1723 (CD-ROM).

Engrand C., Narcisi B., Petit J.-R., Dobrica E. and Duprat J. (2008a) Cosmic dust layers in EPICA-Dome C deep ice core. *Lunar Planet. Sci.* **XXXIX**, #1554 (CD-ROM).

Engrand C., Narcisi B., Petit J.R., Dobrica E., Duprat J., Vaubaillon J. and Colas F. (2008b) More clues about the EPICA-Dome C extraterrestrial events. *Meteoritics Planet. Sci.* **43**, A41-A41.

Fitoussi C., et al. (2008) Measurement of the $^{24}Mg(^{3}He,p)^{26}Al$ cross section, implication for ^{26}Al production in the early Solar System. *Phys. Rev. C* **78**, 044613.

Flynn G.J., Leroux H., Tomeoka K., Tomioka N., Ohnishi I., Mikouchi T., Wirick S., Keller L.P., Jacobsen C. and Sandford S.A. (2008) Carbonate in Comets: A Comparison of Comets 1P/Halley, 9P/Temple 1, and 81P/Wild 2. *Lunar Planet. Sci.* **XXXIX**, #1979 (CD-ROM).

Fomenkova M.N., Chang S. and Mukhin L.M. (1994) Carbonaceous components in the comet Halley dust. *Geochim. Cosmochim. Acta* **58**, 4503-4512.

Ganapathy R., Brownlee D.E. and Hodge P.W. (1978) Silicate spherules from deep-sea sediments: confirmation of extraterrestrial origin. *Science* **201**, 1119-1121.

Gao Y.Q. and Marcus R.A. (2001) Strange and unconventional isotope effects in ozone formation. *Science* **293**, 259-263.

Genge M.J., Engrand C., Gounelle M. and Taylor S. (2008) The classification of micrometeorites. *Meteoritics Planet. Sci.* **43**, 497-515.

Georg R.B., Reynolds B.C., Frank M. and Halliday A.N. (2006) New sample preparation techniques for determination of Si isotope composition using MC-ICPMS. *Chem. Geology* **235**, 95-104.

Glavin D., Matrajt G. and Bada J.L. (2004) Re-examination of amino-acids in Antarctic micrometeorites. *Adv. Space Res.* **33**, 106-113.

Gomes R., Levison H.F., Tsiganis K. and Morbidelli A. (2005) Origin of the cataclysmic Late Heavy Bombardment period of the terrestrial planets. *Nature* **435**, 466-469.

Gounelle M., Shu F.H., Shang H., Glassgold A.E., Rehm K.E. and Lee T. (2001a) Extinct radioactivities and protosolar cosmic-rays: self-shielding and light elements. *Astrophys. J.* **548**, 1051-1070.

Gounelle M., Zolensky M.E., Tonui E. and Mikouchi T. (2001b) Mineralogy of Tagish Lake, a new type 2 carbonaceous chondrite. *Lunar Planet. Sci.* **XXXII**, #1616 (CD-ROM).

Gounelle M., Zolensky M.E., Liou J.-C., Bland P.A. and Alard O. (2003) Mineralogy of carbonaceous chondritic microclasts in howardites: identification of C2 fossil micrometeorites. *Geochim. Cosmochim. Acta* **67**, 507-527.

Gounelle M., Engrand C., Alard O., Bland P.A., Zolensky M.E., Russell S.S. and Duprat J. (2005a) Hydrogen isotopic composition of water from fossil micrometeorites in howardites. *Geochim. Cosmochim. Acta* **69**, 3431-3443.

Gounelle M., Engrand C., Maurette M., Kurat G., McKeegan K.D. and Brandstätter F. (2005b) Small Antarctic micrometeorites (25-50μm): a mineralogical and in situ oxygen isotopic study. *Meteoritics Planet. Sci.* **40**, 917-932.

Gounelle M., et al. (2006a) Coordinated studies of pristine Concordia micrometeorites. *Lunar Planet. Sci.* **XXXVII**, #1613 (CD-ROM).

Gounelle M., Spurny P. and Bland P.A. (2006b) The orbit and atmospheric trajectory of the Orgueil meteorite from historical records. *Meteoritics Planet. Sci.* **41**, 135-150.

Gounelle M. and Meibom A. (2008) The origin of short-lived radionuclides and the astrophysical environment of solar system formation. *Astrophys. J.* **680**, 781-792.

Gounelle M., Mostefaoui S., Meibom A., Engrand C. and Duprat J. (2008) The discovery of an in situ presolar silicon carbide in an Antarctic micrometeorite. *Lunar Planet. Sci.* **XXXIX**, #1612 (CD-ROM).

Greenberg J.M. and Hage J.I. (1990) From interstellar dust to comets - a unification of observational constraints. *Astrophys. J.* **361**, 260-274.

Hanner M.S. and Bradley J.P. (2004) Composition and mineralogy of cometary dust. In *Comets II*, pp. 555-564.

Hartmann W.K. (1999) *Moons & planets*. Wadsworth Pub. Co., Belmont, CA. pp. 1-428.

Hartmann W.K., Ryder G., Dones L. and Grinspoon D. (2000) The time-dependent intense bombardment of the primordial Earth/Moon system. In *Origin of the Earth and Moon* (eds. R. M. Canup, K. Righter and 69 collaborating authors), pp. 493-512. University of Arizona Press, Tucson.

Harvey R.P. and Maurette M. (1991) The origin and significance of cosmic dust from the Walcott Neve, Antarctica. *Proc. Lunar Planet. Sci. Conf.* **21**, 569-578.

Herndon J.M., Rowe M.W., Larson E.E. and Watson D.E. (1975) Origin of magnetite and pyrrhotite in carbonaceous chondrites. *Nature* **253**, 516-518.

Hiroi T., Zolensky M.E. and Pieters C.M. (2001) The Tagish Lake meteorite : a possible sample from a D-type asteroid. *Science* **293**, 2234-2236.

Hsieh H.H. and Jewitt D. (2006) A population of comets in the main asteroid belt. *Science* **312**, 561-563.

Ishii H.A., Bradley J.P., Dai Z.R., Chi M., Kearsley A.T., Burchell M.J., Browning N.D. and Molster F. (2008) Comparison of comet 81P/Wild 2 dust with interplanetary dust from comets. *Science* **319**, 447-.

Jouzel J., et al. (2007) Orbital and millennial Antarctic climate variability over the past 800,000 years. *Science* **317**, 793-796.

Kearsley A.T., et al. (2008) Dust from comet Wild 2: Interpreting particle size, shape, structure, and composition from impact features on the Stardust aluminum foils. *Meteoritics Planet. Sci.* **43**, 41-73.

Kerridge J.F. (1985) Carbon, hydrogen and nitrogen in carbonaceous chondrites: abundances and isotopic compositions in bulk samples. *Geochim. Cosmochim. Acta* **49**, 1707-1714.

Kissel J., et al. (2007) Cosima - High Resolution Time-of-Flight Secondary Ion Mass Spectrometer for the Analysis of Cometary Dust Particles onboard Rosetta. *Space Sci. Rev.* **128**, 823-867.

Krot A.N., McKeegan K.D., Leshin L.A., MacPherson G.J. and Scott E.R.D. (2002) Existence of an ^{16}O-rich gaseous reservoir in the solar nebula. *Science* **295**, 1051-1054.

Kurat G., Koeberl C., Presper T., Brandstätter F. and Maurette M. (1994) Petrology and geochemistry of Antarctic micrometeorites. *Geochim. Cosmochim. Acta* **58**, 3879-3904.

Lauretta D.S. and Fegley B., Jr. (1994) Troilite formation kinetics and growth mechanism in the solar nebula. *Meteoritics* **29**, 490.

Lauretta D.S., Kremser D.T. and Fegley B., Jr. (1996) A comparative study of experimental and meteoritic metal-sulfide assemblages. *Antarctic Met. Res.* **9**, 97-110.

Lawler M.E. and Brownlee D.E. (1992) CHON as a component of dust from Comet Halley. *Nature* **359**, 810-812.

Lee T., Papanastassiou D.A. and Wasserburg G.J. (1976) Demonstration of Mg-26 excess in Allende and evidence for Al-26. *Geophys. Res. Lett.* **3**, 41-44.

Lee T., Shu F.H., Shang H., Glassgold A.E. and Rehm K.E. (1998) Protostellar cosmic rays and extinct radioactivities in meteorites. *Astrophys. J.* **506**, 898-912.

Lesty M. (1999) *La revue Modulad* **22**, 41-77.

Libourel G., Krot A.N. and Tissandier L. (2006) Role of gas-melt interaction during chondrule formation. *Earth Planet. Sci. Lett.* **251**, 232-240.

Libourel G. and Krot A.N. (2007) Evidence for the presence of planetesimal material among the precursors of magnesian chondrules of nebular origin. *Earth Planet. Sci. Lett.* **254**, 1-8.

Lin Y., Guan Y., Leshin L.A., Ouyang Z. and Wang D. (2005) Short-lived chlorine-36 in a Ca- and Al-rich inclusion from the Ningqiang carbonaceous chondrite. *Proceedings of the National Academy of Science* **102**, 1306-1311.

Lisse C.M., et al. (2006) Spitzer spectral observations of the Deep Impact ejecta. *Science* **313**, 635-640.

Lisse C.M., Kraemer K.E., Nuth Iii J.A., Li A. and Joswiak D. (2007) Comparison of the composition of the Tempel 1 ejecta to the dust in Comet C/Hale-Bopp 1995 O1 and YSO HD 100546. *Icarus* **187**, 69-86.

Lodders K. (2003) Solar system abundances and condensation temperatures of the elements. *Astrophys. J.* **591**, 1220-1247.

Love S.G. and Brownlee D.E. (1993) A direct measurement of the terrestrial mass accretion rate of cosmic dust. *Science* **262**, 550-553.

Lugmair G.W. and Shukolyukov A. (1998) Early solar system timescales according to ^{53}Mn-^{53}Cr systematics. *Geochim. Cosmochim. Acta* **62**, 2863-2886.

Lyons J.R. and Young E.D. (2005) CO self-shielding as the origin of oxygen isotope anomalies in the early solar nebula. *Nature* **435**, 317-320.

Marcus R.A. (2004) Mass-independent isotope effect in the earliest processed solids in the solar system: A possible chemical mechanism. *J. Chem. Phys.* **121**, 8201-8211.

Martin M.P., Glavin D.P. and Dworkin J.P. (2008) Nanoflow separation of amino acids for the analysis of cosmic sust. *Lunar Planet. Sci.* **XXXIX**, #2055 (CD-ROM).

Martins Z., Alexander C.M.O., Orzechowska G.E., Fogel M.L. and Ehrenfreund P. (2007) Indigenous amino acids in primitive CR meteorites. *Meteoritics Planet. Sci.* **42**, 2125-2136.

Matrajt G. (2001) La contribution des micrométéorites à l'origine de la vie sur Terre. Ph.D. thesis thesis. Paris VI, Paris.

Matrajt G., Gallien J.P. and Maurette M. (2001) Nuclear microprobe analysis of carbon and nitrogen in Murchison and Antarctic micrometeorites : preliminary results. *Meteoritics Planet. Sci.* **36 Suppl.**, A127.

Matrajt G., Pizzarello S., Taylor S. and Brownlee D. (2004) Concentration and variability of the AIB amino acid in polar micrometeorites: Implications for the exogenous delivery of amino acids to the primitive Earth. *Meteoritics Planet. Sci.* **39**, 1849-1858.

Matrajt G., Guan Y., Leshin L., Taylor S., Genge M., Joswiak D. and Brownlee D.E. (2005) Oxygen isotope measurement of bulk unmelted Antarctic micrometeorites (abstract). In *Workshop on Dust in Planetary Systems*, pp. abstract #4060, Kauai, Hawaii.

Maurette M., Hammer C., Brownlee D.E., Reeh N. and Thomsen H.H. (1986) Placers of cosmic dust in the blue ice lakes of Greenland. *Science* **233**, 869-872.

Maurette M., Jéhano C., Robin E. and Hammer C. (1987) Characteristics and mass distribution of extraterrestrial dust from the Greenland ice cap. *Nature* **328**, 699-702.

Maurette M., Olinger C., Christophe M., Kurat G., Pourchet M., Brandstätter F. and Bourot-Denise M. (1991) A collection of diverse micrometeorites recovered from 100 tons of Antarctic blue ice. *Nature* **351**, 44-47.

Maurette M., Brack A., Kurat G., Perreau M. and Engrand C. (1995) Were micrometeorites a source of prebiotic molecules on the early Earth? *ASR* **15**, (3)113-(3)126.

Maurette M. (1998a) Carbonaceous micrometeorites and the origin of life. *Orig. Life and Evol. Biosphere* **28**, 385-412.

Maurette M. (1998b) Micrometeorites on the early Earth. In *The molecular origin of life: assembling pieces of the puzzle* (ed. A. Brack), pp. 147-186. Cambridge Univ. Press.

Maurette M., Duprat J., Engrand C., Gounelle M., Kurat G., Matrajt G. and Toppani A. (2000) Accretion of neon, organics, CO_2, nitrogen and water from large interplanetary dust particles on the early Earth. *Planet. Space Sci.* **48**, 1117-1137.

Maurette M., Matrajt G., Gounelle M., Engrand C. and Duprat J. (2001) La matière extraterrestre primitive et les mystères de nos origines. In *Éléments d'exobiologie I: l'environnement de la Terre primitive et l'origine de la vie* (eds. M. Gargaud, D. Despois and J. P. Parisot), pp. 99-127. Presses Univ. Bordeaux.

Maurette M., Matrajt G., Gounelle M., Duprat J., Engrand C. and Blanot D. (2003) "Juvenile" KBOs dust and prebiotic organic chemistry. In *Frontiers of life* (eds. L. M. Celniquier and J. Trân Thanh Vân), pp. 7-22. Thê Gioi, Hanoï, Vietnam, Château de Blois, France.

Maurette M. (2006a) *Micrometeorites and the mysteries of our origins*. Springer, Berlin Heidelberg New York. pp. 330.

Maurette M. (2006b) Cometary Micrometeorites in Planetology, Exobiology, and Early Climatology. In *Comets and the Origin and Evolution of Life*, pp. 69-111.

Maurette M., Duprat J., Engrand C. and Kurat G. (2006) From Earth to Mars with micrometeorite volatiles. *Adv. Space Res.* **38**, 701-708.

McKeegan K.D., Walker R.M. and Zinner E. (1985) Ion microprobe isotopic measurements of individual interplanetary dust particles. *Geochim. Cosmochim. Acta* **49**, 1971-1987.

McKeegan K.D., Chaussidon M. and Robert F. (2000) Incorporation of short-lived ^{10}Be in a calcium-aluminium-rich inclusion from the Allende meteorite. *Science* **289**, 1334-1337.

McKeegan K.D., et al. (2006) Isotopic compositions of cometary matter returned by Stardust. *Science* **314**, 1724-1728.

McSween H.Y., Jr. and Weissman P.R. (1989) Cosmochemical implications of the physical processing of cometary nuclei. *Geochim. Cosmochim. Acta* **53**, 3263-3271.

Meibom A., Krot A.N., Robert F., Mostefaoui S., Russell S.S., Petaev M.I. and Gounelle M. (2007) Nitrogen and carbon isotopic composition of the Sun inferred from a high-temperature solar nebular condensate. *Astrophys. J.* **656**, L33-L36.

Meier R., Owen T.C., Jewitts D.C., Matthews H.E., Senay M., Biver N., Bockelée-Morvan D., Crovisier J. and Gautier D. (1998a) Deuterium in Comet C/1995 O1 (Hale-Bopp) : Detection of DCN. *Science* **279**, 1707-1710.

Meier R., Owen T.C., Matthews H.E., Jewitts D.C., Bockelée-Morvan D., Biver N., Crovisier J. and Gautier D. (1998b) A determination of the HDO/H_2O ratio in comet C/1995 O1 (Hale-Bopp). *Science* **279**, 842-844.

Meier R. and Owen T.C. (1999) Cometary deuterium. *Space Sci. Rev.* **90**, 33-43.

Messenger S. (2000) Identification of molecular-cloud material in interplanetary dust particles. *Nature* **404**, 968-971.

Messenger S. (2001) Hydrogen isotopic measurements of the Tagish Lake meteorite. *Lunar Planet. Sci.* **XXXII**, #1916 (CD-ROM).

Misawa K., Tomiyama T., Kohno M., Noguchi T., Nagao K., Nakamura T., Mikouchi T., Nishiizumi K. and Motoyama H. (2008) Extraterrestrial dust layers in Dome Fuji ice core, East Antarctica. *Lunar Planet. Sci.* **XXXIX**, #1690 (CD-ROM).

Molini-Velsko C., Mayeda T.K. and Clayton R.N. (1986) Isotopic composition of silicon in meteorites. *Geochim. Cosmochim. Acta* **50**, 2719-2726.

Morbidelli A., Levison H.F., Tsiganis K. and Gomes R. (2005) Chaotic capture of Jupiter's Trojan asteroids in the early Solar System. *Nature* **435**, 462-465.

Mostefaoui S., Lugmair G.W., Hoppe P. and El Goresy A. (2004) Evidence for live ^{60}Fe in meteorites. *New Astron. Rev.* **48**, 155-159.

Nakamura T., et al. (1999) Antarctic micrometeorites collected at the Dome Fuji Station. *Antarctic Met. Res.* **12**, 183-198.

Nakamura T., Noguchi T., Yada T., Nakamuta Y. and Takaoka N. (2001) Bulk mineralogy of individual micrometeorites determined by X-ray diffraction analysis and transmission microscopy. *Geochim. Cosmochim. Acta* **65**, 4385-4397.

Nakamura T., Noguchi T., Ozono Y., Osawa T. and Nagao K. (2005) Mineralogy of ultracarbonaceous large micrometeorites. *Meteoritics Planet. Sci.* **40 Suppl.**, #5046.

Narcisi B., Petit J.R. and Engrand C. (2007) First discovery of meteoritic events in deep Antarctic (EPICA-Dome C) ice cores. *Geophys. Res. Lett.* **34**, L15502.

Nishiizumi K., Caffee M.W., Kohno M., Misawa K., Nagao K. and Tomiyama T. (2008a) Exposure histories of micrometeorites found in a 434 kyr old layer in the Dome Fuji ice core, Antarctica. *Lunar Planet. Sci.* **XXXIX**, #2231 (CD-ROM).

Nishiizumi K., Caffee M.W., Kohno M., Misawa K. and Tomiyama T. (2008b) Large meteoritic impact on Antarctic ice sheet 434 kyr ago - Micrometeorites found in the Dome Fuji ice core. *Meteoritics Planet. Sci.* **43 Suppl.**, A116.

Noguchi T. and Nakamura T. (2001) Mineralogy of phyllosilicate-rich micrometeorites and comparison with Tagish Lake CI and Sayama CM chondrites. *Lunar Planet. Sci.* **XXXII**, #1541 (CD-ROM).

Parrenin F., et al. (2007) The EDC3 chronology for the EPICA dome C ice core. *Clim. Past* **3**, 485-497.

Pearson V.K., Sephton M.A., Gilmour I. and Franchi I.A. (2001) Hydrogen isotopic composition of the Tagish Lake meteorite : comparison with other carbonaceous chondrites. *Lunar Planet. Sci.* **XXXII**, #1861 (CD-ROM).

Pizzarello S., Zolensky M. and Turk K.A. (2003) Nonracemic isovaline in the Murchison meteorite: chiral distribution and mineral association. *Geochim. Cosmochim. Acta* **67**, 1589-1595.

Quirico E., Borg J., Raynal P.-I., Montagnac G. and D'Hendecourt L. (2005a) A micro-Raman survey of 10 IDPs and 6 carbonaceous chondrites. *Planet. Space Sci.* **53**, 1443-1448.

Quirico E., Rouzaud J.-N., Bonal L. and Montagnac G. (2005b) Maturation grade of coals as revealed by Raman spectroscopy: Progress and problems. *Spectr. Acta Part A* **61**, 2368-2377.

Remusat L., Palhol F., Robert F., Derenne S. and France-Lanord C. (2006) Enrichment of deuterium in insoluble organic matter from primitive meteorites: A solar system origin? *Earth Planet. Sci. Lett.* **243**, 15-25.

Rietmeijer F.J.M. (1998) Interplanetary dust particles. In *Planetary Materials* (ed. J. J. Papike), pp. 2/1-2/95. Mineralogical Society of America, Washington DC.

Robert F. and Camy-Peyret C. (2001) Ozone isotopic composition: an angular effect in scattering processes? *Ann.Geophys.* **19**, 229-244.

Robert F., Mostefaoui S., Aléon J., Derenne S., Remusat L. and Meibom A. (2006) NanoSIMS H, C, N, and O-Isotopic Study of Insoluble Organic Matter in Murchison. *Lunar Planet. Sci.* **XXXVII**, #1301 (CD-ROM).

Rotundi A., et al. (2008) Combined micro-Raman, micro-infrared, and field emission scanning electron microscope analyses of comet 81P/Wild 2 particles collected by Stardust. *Meteoritics Planet. Sci.* **43**, 367-397.

Russell S.S., Srinivasan G., Huss G.R., Wasserburg G.J. and MacPherson G.J. (1996) Evidence for widespread ^{26}Al in the solar nebula and constraints for nebula time scales. *Science* **273**, 757-762.

Sandford S.A., et al. (2006) Organics captured from comet 81P/Wild 2 by the Stardust spacecraft. *Science* **314**, 1720-1724.

Shu F.H., Shang H. and Lee T. (1996) Toward an astrophysical theory of chondrites. *Science* **271**, 1545-1552.

Shu F.H., Shang S., Gounelle M., Glassgold A.E. and Lee T. (2001) The origin of chondrules and refractory inclusions in chondritic meteorites. *Astrophys. J.* **548**, 1029-1050.

Srinivasan G., Ulyanov A.A. and Goswami J.N. (1994) Ca-41 in the early solar system. *Astrophys. J.* **431**, L67-L70.

Stadermann F.J., Hoppe P., Floss C., Heck P.R., Horz F., Huth J., Kearsley A.T., Leitner J., Marhas K.K., McKeegan K.D. and Stephan T. (2008) Stardust in Stardust - The C, N, and O isotopic compositions of Wild 2 cometary matter in Al foil impacts. *Meteoritics Planet. Sci.* **43**, 299-313.

Svetsov V.V. and Wasson J.T. (2007) Melting of soil rich in quartz by radiation from aerial bursts - A possible cause of formation of Libyan desert glass and layered tektites. *Lunar Planet. Sci.* **XXXVIII**, #1499 (CD-ROM).

Tachibana S. and Huss G.R. (2003) The initial abundance of ^{60}Fe in the solar system. *Astrophys. J.* **588**, L41-L44.

Taylor S., Lever J.H. and Harvey R.P. (1998) Accretion rate of cosmic spherules measured at the South Pole. *Nature* **392**, 899-903.

Taylor S., Lever J.H. and Harvey R.P. (2000) Numbers, types and compositions of an unbiased collection of cosmic spherules. *Meteoritics Planet. Sci.* **35**, 651-666.

Taylor S., Alexander C.M.O.D., Delaney J., Ma P., Herzog G.F. and Engrand C. (2005) Isotopic fractionation of iron, potassium, and oxygen in stony cosmic spherules : implications for heating histories and sources. *Geochim. Cosmochim. Acta* **69**, 2647-2662.

Terada K., et al. (2001) General characterization of Antarctic micrometeorites collected by the 39th Japanese Antarctic Research Expedition: Consortium studies of JARE AMMs (III). *Antarctic Met. Res.* **14**, 89.

Thiemens M., Jackson T., Zipf E.C., Erdman P.W. and Van Egmond C. (1995) Carbon dioxide and oxygen isotope anomalies in the mesosphere and stratosphere. *Science* **270**, 969-972.

Thiemens M.H. and Heidenreich J.E.I. (1983) The mass-independent fractionation of oxygen: A novel isotope effect and its possible cosmochemical implications. *Science* **219**, 1073-1075.

Tissandier L., Libourel G. and Robert F. (2002) Gas-melt interactions and their bearing on chondrule formation. *Meteoritics Planet. Sci.* **37**, 1377-1389.

Tomeoka K., Tomioka N. and Ohnishi I. (2008) Silicate minerals and Si-O glass in comet Wild 2 samples: Transmission electron microscopy. *Meteoritics Planet. Sci.* **43**, 273-284.

Toppani A., Libourel G., Engrand C. and Maurette M. (2000) Experimental simulation and modeling of atmospheric entry of micrometeorites. *Meteoritics Planet. Sci.* **35 suppl.**, A158.

Toppani A., Libourel G., Engrand C. and Maurette M. (2001) Experimental simulation of atmospheric entry of micrometeorites. *Meteoritics Planet. Sci.* **36**, 1377-1396.

Toppani A., Robert F., Libourel G., de Donato P., Barres O., D'Hendecourt L. and Ghanbaja J. (2005) A `dry' condensation origin for circumstellar carbonates. *Nature* **437**, 1121-1124.

Tsiganis K., Gomes R., Morbidelli A. and Levison H.F. (2005) Origin of the orbital architecture of the giant planets of the Solar System. *Nature* **435**, 459-461.

van Ginneken M., Folco L., Rochette P. and Perchiazzi N. (2008) An unusual particle from the Transantarctic mountain micrometeorite collection likely related to the ca. 480 ka cosmic dust layer in the EPICA-Dome C and Dome Fuji ice cores. *Meteoritics Planet. Sci.* **43 suppl.**, A161.

VanderWood T.B., Bradley J.P., Maurette M., Petit J.R., Barkov N.I. and Kurat G. (1995) Automated SEM-search for micrometer-sized Antarctica micrometeorites from East Antarctica (Dôme B) ice core samples. *Lunar Planet. Sci.* **XXVI**, 1443-1444.

VanderWood T.B., Maurette M., Bradley J.P., Engrand C., Kurat G., Petit J.R. and Barkov N.I. (1996) Automated SEM analysis of fine grained dust from Antarctica ice cores. *Lunar Planet. Sci.* **XXVII**, 1355-1356.

Wasserburg G.J., Busso M., Gallino R. and Nollett K.M. (2006) Short-lived nuclei in the early Solar System: Possible AGB sources. *Nuclear Physics A* **777**, 5-69.

Weaver H.A., A'Hearn M.F., Arpigny C., Combi M.R., Feldman P.D., Tozzi G.-P., Dello Russo N., Feaga L.M. and Festou M.C. (2008) Atomic deuterium emission and the D/H ration in comets. In *Asteroids, Comets, Meteors*, pp. #8216, Baltimore.

Wooden D.H., Harker D.E., Woodward C.E., Butner H.M., Koike C., Witteborn F.C. and McMurtry C.W. (1999) Silicate mineralogy of the dust in the inner coma of comet C/1995 01 (Hale-Bopp) pre- and post-perihelion. *The Astrophysical Journal* **517**, 1034-1058.

Yada T. and Kojima H. (2000) The collection of micrometeorites in the Yamato meteorite ice field of Antarctica in 1998. *Antarctic Met. Res.* **13**, 9-18.

Yada T., Nakamura T., Noguchi T., Ushikubo T., Matsumoto N., Kojima H. and Takaoka N. (2003) Variations of oxygen isotopic compositions of silicate spherules collected from Antarctic blue ice. *Lunar Planet. Sci.* **XXXIV**, #1587 (CD-ROM).

Yada T., Nakamura T., Noguchi T., Matsumoto N., Kusakabe M., Hiyagon H., Ushikubo T., Sugiura N., Kojima H. and Takaoka N. (2005) Oxygen isotopic and chemical

compositions of cosmic spherules collected from the Antarctic ice sheet: Implications for their precursor materials. *Geochim. Cosmochim. Acta* **69**, 5789-5804.

Young E. and Russell S. (1998) Oxygen reservoirs in the early solar nebula inferred from an Allende CAI. *Science* **282**, 452-455.

Yurimoto H. and Kuramoto K. (2004) Molecular cloud origin for the oxygen isotope heterogeneity in the solar system. *Science* **305**, 1763-1766.

Zinner E. (1998) Trends in the study of presolar dust grains from primitive meteorites. *Meteoritics Planet. Sci.* **33**, 549-564.

Zolensky M., et al. (2006a) Mineralogy and Petrology of Comet Wild2 Nucleus Samples - Final Results of the Preliminary Examination Team. *Meteoritics Planet. Sci.* **41 suppl.**, A167.

Zolensky M., et al. (2008) Comparing Wild 2 particles to chondrites and IDPs. *Meteoritics Planet. Sci.* **43**, 261-272.

Zolensky M.E. and Thomas K.L. (1995) Iron and iron-nickel sulfides in chondritic interplanetary dust particles. *Geochim. Cosmochim. Acta* **59**, 4707-4712.

Zolensky M.E., Nakamura K., Gounelle M., Mikouchi T., Kasama T., Tachikawa O. and Tonui E. (2002) Mineralogy of Tagish Lake: An ungrouped type 2 carbonaceous chondrite. *Meteoritics Planet. Sci.* **37**, 737-761.

Zolensky M.E., et al. (2006b) Mineralogy and Petrology of Comet 81P/Wild 2 Nucleus Samples. *Science* **314**, 1735-1739.

CURRICULUM VITAE

ENGRAND Cécile
Née le 21 Octobre 1968 (40 ans)
Union libre, 1 fille (25/10/2004)
☎ : 01 69 15 52 95
Fax: 01 69 15 50 08
Cecile.Engrand@csnsm.in2p3.fr

Centre de Spectrométrie Nucléaire et de Spectrométrie de Masse (CSNSM)
CNRS - Univ. Paris Sud
Bâtiment 104
91405 Orsay Campus

Chargée de Recherche 1ère classe au CNRS (section 17)

CSNSM Orsay - Equipe d'Astrophysique du Solide

PROJETS PROFESSIONNELS

- Système solaire primitif : conditions de formation des micrométéorites et des météorites (mesures isotopiques de l'oxygène, de l'hydrogène et du silicium par microsonde ionique)
- Composition et origine des comètes :
  - Préparation des analyses de la mission cométaire ROSETTA ;
  - Participation au consortium national pour l'analyse d'échantillons cométaires de la mission spatiale STARDUST
- Exobiologie : rôle des apports extraterrestres dans l'apparition de la vie sur Terre.

FORMATION

1995 Doctorat de l'Université Paris XI Orsay. "Micrométéorites antarctiques : vers l'exobiologie et la mission cométaire Rosetta". Directeur de thèse : M. Maurette. Mention très honorable avec félicitations du jury.
1992 DEA Spécialité “Sciences des Matériaux”, Université Paris XI, Mention AB.
1991 Diplôme d'Ingénieur FIUPSO. Spécialité “Sciences et Génie des Matériaux”, Mention AB.
1988 DEUG A “Sciences des Structures et de la Matière”, Université Paris XI, Mention AB.
1986 Baccalauréat Série D “Mathématiques et Sciences de la Nature”. Mention AB.

DIRECTION DE THESE :

- Elena DOBRICĂ (bourse RTN Marie-Curie "ORIGINS") depuis septembre 2007.

RESPONSABILITES et ANIMATION DE LA RECHERCHE (présent et passé) :

- Membre nommé de la Section 17 du Comité National de la Recherche Scientifique (2007-2008)
- Expert AERES Vague C (2008) pour l'UMS Nanoanalyses (MNHN Paris)
- Membre externe de la Commission de Spécialistes de Paris VII (section 34 – Astronomie, astrophysique) (2004-2006 titulaire, suppléant depuis 2007)
- Membre du Comité Scientifique du Programme National de Planétologie (2000-2003 et depuis 2007)
- Co-Investigateur de l'analyseur COSIMA (mission spatiale ROSETTA)
- Co-Responsable du Groupe de Travail WG2 mis en place par l'ESA pour l'exploitation de la mission spatiale ROSETTA (depuis 2007)
- Membre du Conseil de Groupement du GdR Exobiologie du CNRS (1999-2006)
- Membre du Groupe Thématique Exo/Astrobiologie du CNES depuis sa création (2004)
- Editeur associé de Geochemical Journal
- Responsable du groupe d'Astrophysique du Solide du CSNSM (1999-2004)
- Reviewer de proposition de recherche NASA (programme OSS) et de propositions ANR, du PID OPV, membre du comité national d'évaluation des propositions pour la facilité IMS1270 de Nancy (2004-2005)
- Reviewer de publications (Geochim. Cosmochim. Acta, Geology, Meteoritics Planet. Sci., Phil. Trans. Roy. Soc., Earth Planet. Sci. Lett.…)

VULGARISATION :
Nombreuses participations aux manifestations de dissémination de la science (fêtes de la science, bars des sciences, interviews pour revues scientifiques de vulgarisation…)

AFFILIATION PROFESSIONNELLE
Meteoritical Society, American Geophysical Union

LANGUES ETRANGERES
Allemand (courant, 12 mois de postdoc en Autriche), Anglais (courant, 22 mois de postdoc aux U.S.A.).

PUBLICATIONS CHOISIES :

- Genge M.J., Engrand C., Gounelle M. and Taylor S. (2008) The classification of micrometeorites. *Meteoritics Planet. Sci.* **43**, 497-515.
- Narcisi B., Petit J.R. and Engrand C. (2007) First discovery of meteoritic events in deep Antarctic (EPICA-Dome C) ice cores. *Geophys. Res. Lett.* **34**, L15502.
- Duprat J., Engrand C., Maurette M., Kurat G., Gounelle M. and Hammer C. (2007) Micrometeorites from Central Antarctic snow: The CONCORDIA collection. *Adv. Space Res.* **39**, 605-611.
- Engrand C., Kissel J., Krueger F. R., Martin P., Silén J., Thirkell L., Thomas R. and Varmuza K. (2006) Chemometric evaluation of time-of-flight secondary ion mass spectrometry data of minerals in the frame of future *in situ* analyses of cometary material by COSIMA onboard ROSETTA. *Rapid. Commun. Mass Spectrom.* **20**, 1361-1368.
- Duprat J., Engrand C., Maurette M., Gounelle M., Kurat G. and Hammer C. (2005) The micrometeorite program at Dome C. In *Dome C Astronomy and Astrophysics Meeting* (eds. M. Giard, F. Casoli and F. Paletou), pp. 51-56. EAS Pub. Series.
- Engrand C., McKeegan K. D., Leshin L. A., Herzog G. F., Schnabel C., Nyquist L. E. and Brownlee D. E. (2005) Isotopic compositions of oxygen, iron, chromium, and nickel in cosmic spherules: Toward a better comprehension of atmospheric entry heating effects. *Geochim. Cosmochim. Acta* **69**, 5365-5385.
- Gounelle M., Engrand C., Alard O., Bland P. A., Zolensky M. E., Russell S. S. and Duprat J. (2005) Hydrogen isotopic composition of water from fossil micrometeorites in howardites. *Geochim. Cosmochim. Acta* **69**, 3431-3443.
- Gounelle M., Engrand C., Maurette M., Kurat G., McKeegan K. D. and Brandstätter F. (2005) Small Antarctic micrometeorites (25-50µm): a mineralogical and in situ oxygen isotopic study. *Meteoritics Planet. Sci.* **40**, 917-932.
- Engrand C., Lespagnol J., Martin P., Thirkell L. and Thomas R. (2004) Multi-correlation analyses of TOF-SIMS spectra for mineralogical studies. *Applied Surf. Sci.* **231-231**, 883-887.
- Aléon J., Engrand C., Robert F. and Chaussidon M. (2001) Clues on the origin of interplanetary dust particles from the isotopic study of their hydrogen-bearing phases. *Geochim. Cosmochim. Acta* **65**, 4399-4412.
- Engrand C., Deloule E., Robert F., Maurette M. and Kurat G. (1999) Extraterrestrial water in micrometeorites and cosmic spherules from Antarctica : an ion microprobe study. *Meteoritics Planet. Sci.* **34**, 773-787.
- Engrand C., McKeegan K. D. and Leshin L. A. (1999) Oxygen isotopic compositions of individual minerals in Antarctic micrometeorites : further links to carbonaceous chondrites. *Geochim. Cosmochim. Acta* **63**, 2623-2636.
- Engrand C. and Maurette M. (1998) Carbonaceous micrometeorites from Antarctica. *Meteoritics Planet. Sci.* **33**, 565-580.

Sélection d'articles dont les résultats sont décrits dans le texte (par ordre d'apparition) :

1. Genge M.J., Engrand C., Gounelle M. and Taylor S. (2008) The classification of micrometeorites. *Meteoritics Planet. Sci.* **43**, 497-515.
2. Engrand C., Deloule E., Robert F., Maurette M. and Kurat G. (1999) Extraterrestrial water in micrometeorites and cosmic spherules from Antarctica : an ion microprobe study. *Meteoritics Planet. Sci.* **34**, 773-787.
3. Engrand C., McKeegan K.D. and Leshin L.A. (1999) Oxygen isotopic compositions of individual minerals in Antarctic micrometeorites : further links to carbonaceous chondrites. *Geochim. Cosmochim. Acta* **63**, 2623-2636.
4. Engrand C., McKeegan K.D., Leshin L.A., Herzog G.F., Schnabel C., Nyquist L.E. and Brownlee D.E. (2005) Isotopic compositions of oxygen, iron, chromium, and nickel in cosmic spherules: Toward a better comprehension of atmospheric entry heating effects. *Geochim. Cosmochim. Acta* **69**, 5365-5385.
5. Gounelle M., Engrand C., Alard O., Bland P.A., Zolensky M.E., Russell S.S. and Duprat J. (2005) Hydrogen isotopic composition of water from fossil micrometeorites in howardites. *Geochim. Cosmochim. Acta* **69**, 3431-3443.
6. Gounelle M., Engrand C., Maurette M., Kurat G., McKeegan K.D. and Brandstätter F. (2005) Small Antarctic micrometeorites (25-50µm): a mineralogical and in situ oxygen isotopic study. *Meteoritics Planet. Sci.* **40**, 917-932.
7. Aléon J., Engrand C., Robert F. and Chaussidon M. (2001) Clues on the origin of interplanetary dust particles from the isotopic study of their hydrogen-bearing phases. *Geochim. Cosmochim. Acta* **65**, 4399-4412.
8. Duprat J., Engrand C., Maurette M., Kurat G., Gounelle M. and Hammer C. (2007) Micrometeorites from Central Antarctic snow: The CONCORDIA collection. *Adv. Space Res.* **39**, 605-611.
9. Engrand C., Lespagnol J., Martin P., Thirkell L. and Thomas R. (2004) Multi-correlation analyses of TOF-SIMS spectra for mineralogical studies. *Applied Surf. Sci.* **231**, 883-887.
10. Engrand C., Kissel J., Krueger F.R., Martin P., Silén J., Thirkell L., Thomas R. and Varmuza K. (2006) Chemometric evaluation of time-of-flight secondary ion mass spectrometry data of minerals in the frame of future *in situ* analyses of cometary material by COSIMA onboard ROSETTA. *Rapid. Commun. Mass Spectrom.* **20**, 1361-1368.
11. Narcisi B., Petit J.R. and Engrand C. (2007) First discovery of meteoritic events in deep Antarctic (EPICA-Dome C) ice cores. *Geophys. Res. Lett.* **34**, L15502.

The Meteoritical Society

Meteoritics & Planetary Science 43, Nr 3, 497–515 (2008)
Abstract available online at http://meteoritics.org

The classification of micrometeorites

M. J. GENGE[1†], C. ENGRAND[2], M. GOUNELLE[2*], and S. TAYLOR[3]

[1]IARC, Department of Earth Science and Engineering, Imperial College London, Exhibition Road, London SW7 2AZ, UK
and The Natural History Museum, Exhibition Road, London SW7 2BT, UK
[2]Centre de Spectrométrie Nucléaire et de Spectrométrie de Masse, CNRS/IN2P3—Univ. Paris XI, 91405 Orsay-Campus, France
[3]U.S. Army Cold Regions Research and Engineering Laboratory, Hanover, New Hampshire 03755, USA
[*]Present address: Laboratoire d'Étude de la Matière Extraterrestre, Muséum National d'Histoire Naturelle,
Case Postale 52, 57 rue Cuvier, 75005 Paris, France
[†]Corresponding author. E-mail: m.genge@imperial.ac.uk

(Received 04 April 2006; revision accepted 06 July 2007)

Abstract–Due to their small size, the mineralogical and chemical properties of micrometeorites (MMs) are not representative of their parent bodies on the centimeter to meter scales that are used to define parent body groups through the petrological study of meteorites. Identifying which groups of MM are derived from the same type of parent body is problematic and requires particles to be rigorously grouped on the basis of mineralogical, textural, and chemical properties that reflect the fundamental genetic differences between meteorite parent bodies, albeit with minimal bias towards preconceived genetic models. Specifically, the interpretation of MMs requires a rigorous and meaningful classification scheme. At present the classification of MMs is, however, at best ambiguous. A unified petrological-chemical classification scheme is proposed in the current study and is based on observations of several thousand MMs collected from Antarctic ice.

INTRODUCTION

Micrometeorites (MMs) are extraterrestrial dust particles that have been captured by the Earth and are thought to mainly represent samples of asteroids and comets. In interplanetary space dust particles are inherently transported sunwards by P-R light drag (Dohnanyi 1967) and once captured by the Earth their deceleration occurs at high altitudes allowing fragile micrometeoroids to survive atmospheric entry (Love and Brownlee 1991). The parent bodies of MMs, therefore, are likely to differ from those of meteorites. Enormous numbers of particles can be recovered (up to tens of thousands during a single collecting expedition) (Maurette et al. 1991; Taylor et al. 1998), and provide us with a unique opportunity to study a diverse sample of solar system small bodies in the laboratory.

Studies of micrometeorites recovered from the Earth's surface and interplanetary dust particles (IDPs) collected in the stratosphere have shown that these include two distinct populations of materials. The larger micrometeorites (~30–1000 μm) recovered from the Earth's surface, which are mainly collected by filtering of melted Antarctic ice and snow (Duprat et al. 2003; Iwata and Imae 2001; Maurette et al. 1991; Taylor et al. 1998; Yada and Kojima 2000) mostly have strong mineralogical and chemical affinities with the carbonaceous chondrites, and thus appear to be derived principally from asteroids (Genge et al. 1997a; Kurat et al. 1994) although cometary materials are also present (Engrand and Maurette 1998a; Nakamura et al. 2005). Meteorite-like materials also occur among the smaller particles (<30 μm) collected directly from the Earth's stratosphere, however, around 40% of IDPs, known as anhydrous IDPs, are very different from meteorites and are highly volatile-rich. These have been suggested to be derived from comets (Bradley 1994; Rietmeijer 1998). Extraterrestrial dust particles collected in the stratosphere have come to be known as interplanetary dust particles, whereas those recovered from the Earth's surface are most commonly referred to as micrometeorites. Previously, only particles that survived atmospheric entry without melting were termed MMs (Whipple 1951); however, because of the gradational nature of melting, all extraterrestrial dust particles that survive to reach the Earth's surface, including melted particles, are here classified as MMs.

The small size of extraterrestrial dust particles restricts the information that individual particles can provide on the nature and origins of their parent bodies. Meteorites indicate that even the most primitive are relatively heterogeneous on

scales equivalent to the dimensions of MMs since they are composed of chondrules, refractory inclusions, and fine-grained matrix. Individual asteroidal MMs, therefore, provide us with samples of the components of their parent bodies, whether these are matrix, chondrules or refractory inclusions (Genge et al. 1997a; Kurat et al. 1994). In contrast, although anhydrous IDPs are mineralogically relatively homogeneous at scales larger than tens of microns (Rietmeijer 1998), the nature of cometary materials is uncertain.

The challenge with MMs, therefore, is that their mineralogical and chemical properties are unlikely to be representative of their parent bodies on the centimeter to meter scales that are used to define parent body groups through the petrological study of meteorites (Brearley and Jones 1998). Identifying which groups of MM are derived from the same type of parent body is problematic and requires particles to be rigorously grouped on the basis of mineralogical, textural, and chemical properties that reflect the fundamental genetic differences between meteorite parent bodies, albeit with minimal bias towards preconceived genetic models. Specifically the interpretation of MMs requires a rigorous and meaningful classification scheme.

Here we present a unified classification system for MMs intended to reflect the genetic relationships between different groups of MMs that may derive from related parent bodies. The classification system is based on the combined observations of several thousand particles recovered from Antarctic ice from both the vicinity of Cap Prudhomme (Maurette et al. 1991) and the South Pole Water Well (Taylor et al. 1998) by the authors. Descriptions of the techniques used to select, prepare, and analyze these materials are given in Engrand et al. (1998a), Genge et al. (1997a), and Taylor et al. (2000). Groups of MM proposed herein are all based on backscattered imaging of polished grain mounts of particles and, in some cases, quantitative microanalysis of mineral phases, however, throughout this paper we also provide descriptions of features by which MM types can be approximately identified under a binocular microscope during the selection procedure.

NON-ISOTOPIC CRITERIA FOR EXTRATERRESTRIAL ORIGIN

Definitive evidence for the extraterrestrial origin of MMs has been made on the basis of cosmogenic nuclei and noble gas measurements (Olinger 1990; Raisbeck and Yiou 1987); however, the identification of dust particles recovered from the Earth's surface as micrometeorites can be made on one or more of a number of criteria. Features that strongly suggest an extraterrestrial origin are any of: (1) the presence of a partial or complete shell of magnetite around MMs, which is thought to arise from entry heating (Toppani et al. 2001; Toppani and Libourel 2003), (2) the presence of Ni-bearing iron metal, and (3) a chondritic bulk composition for major and minor elements, at least for particles with a small grain-size relative to particle-size. Features that are less determinative are: (1) high CaO, Cr_2O_3 olivines and very FeO-poor olivines that are exceedingly rare in terrestrial rocks (Brearley et al. 1998), (2) evidence for surface heating consistent with atmospheric entry, and (3) spherical particle morphologies.

Spherical particle morphologies are particularly ambiguous since anthropogenic particulates, impact spherules, meteorite ablation spheres and even some small-scale volcanic dust may have similar morphologies. Iron-rich industrial/diesel spherules are, for example, very common in the terrestrial environment and many consist primarily of magnetite and are thus mineralogically indistinguishable from some melted micrometeorites. Isotopic data of iron-rich spherules recovered from the deep sea have confirmed their extraterrestrial origins (Clayton et al. 1986; Engrand et al. 1998, 2005; Herzog et al. 1999; Raisbeck and Yiou 1989). These make up a large fraction of the deep sea spherules (25 to 50%), but are present in abundances of a few percent in polar regions (Genge et al. 1997a; Taylor et al. 1998). In early collections in continental areas outside the polar regions, iron-dominated spherules were found to be abundant, and studies have shown these are of anthropogenic origin (Fisher et al. 1976).

METEORITE ABLATION SPHERES AND MICROTEKTITES VERSUS MICROMETEORITES

Meteorite ablation spheres, produced during the atmospheric entry of larger meteoroids, and microtektites, condensed from vapor plumes or separated from impact melt produced during the collision of asteroids and comets with the Earth, could also be considered extraterrestrial in origin. In the case of microtektites a small extraterrestrial component is intimately mixed with terrestrial materials from target rocks (Glass 1990). Micrometeorites are extraterrestrial particles that were present as dust-sized particles in interplanetary space and were not part of larger meteoroids. Spallogenic and cosmogenic isotope abundances consistent with exposure to solar energetic particles and galactic cosmic rays as small particles allow MMs to be unequivocally distinguished from ablation spherules and microtektites (Harvey et al. 1998; Raisbeck and Yiou 1987, 1989). However, there are also several mineralogical and chemical features that can be used to distinguish these groups of materials in routine particle surveys.

For unmelted dust-sized debris the presence of a magnetite-rim unequivocally distinguishes MMs since this is developed during hypervelocity deceleration at high altitudes (Toppani et al. 2001; Topponi and Libourel 2003). Discrete magnetite rims are not present either on meteorite fusion crusts (Genge et al. 1999), ablation spheres (Harvey et al.

1998), or on microtektites (Glass 1990). However, MMs that have experienced a high degree of melting during atmospheric entry heating (e.g., cosmic spherules) or very low degrees of heating likewise generally lack magnetite rims.

Studies of meteorite fusion crusts (Genge et al. 1999) and spherules from the one known meteorite ablation spherule layer (Harvey et al. 1998) suggest that ablation spherules will have bulk compositions very close to that of their parent meteoroid and are enriched in volatile and moderately volatile elements such as Na and S relative to most melted MMs, which have lost volatiles by evaporation. Microtektites usually consist of a mixture of target and projectile materials and thus have major element compositions that diverge significantly from chondritic (Glass 1990), allowing them to be distinguished from MMs. Metallic impact spherules, associated with iron projectiles and commonly associated with smaller craters such as the Barringer crater are, however, broadly similar in composition to iron-rich melted MMs, except in their Cr contents.

Probably the most significant feature of meteorite ablation spheres and impact spherules, however, is their localized temporal, spatial, and chemical distribution. The Bit-58 meteorite ablation layer in the Antarctic, for example, contains spherules with a very limited range of chemical and isotopic characteristics related to a H-chondrite parent body (Harvey et al. 1998). Close to Barringer Crater likewise iron-spherules are found in much higher abundances than iron-rich melted MMs (Nininger 1956). Silicate dominated impact spherules, associated with larger impacts, are stratigraphically restricted. Impact and ablation spherules can, therefore, be distinguished on the basis of their localized distribution.

CLASSIFICATION OF MICROMETEORITES

Two main groups of micrometeorite can be identified on the basis of their preatmospheric textures: (1) fine-grained MMs (FgMMs), which are dominated by a fine-grained porous groundmass of micron-sized mineral grains, and (2) coarse-grained MMs (CgMMs), which are dominated by anhydrous silicates with grain-sizes larger than several microns, often with glassy mesostasis. Heating of MMs during atmospheric entry, however, complicates the classification of particles on the basis of their preatmospheric nature because it results in significant changes in the primary mineralogy, texture and even the compositions of particles. Micrometeorites are, therefore, also divided into several groups (Table 1) depending on the extent of thermal reprocessing during atmospheric entry. The proportion of melted, partially melted, and unmelted micrometeorites is not well known but varies with particle size (Maurette et al. 1991; Taylor et al. 2000). For sizes >100 μm melted MMs make up 70–90% of particles (Maurette et al. 1991; Taylor et al. 2000), for those 50–100 mm in size melted and partially melted MMs make up ~50% of particles (Genge et al. 1997a), although a partially melted MMs to unmelted ratio of 1 in this size range is found using a different classification (Engrand and Maurette 1998), and for those 25–50 mm in size melted and partially melted MMs comprise only 22% of the particles (Gounelle et al. 2005b). It is stressed that changes due to atmospheric heating are largely gradational and, therefore, assigning micrometeorites into a discrete group is not always possible. This has lead to differences in how MMs have been classified.

Melted Micrometeorites: Cosmic Spherules

Melted micrometeorites are classified as spherical to subspherical particles formed as molten droplets during atmospheric entry. These particles that have experienced large degrees of fusion of primary phases (defined in the current manuscript as those existing prior to atmospheric entry) during atmospheric entry and thus behave as low viscosity melts (Fig. 1). Igneous particles that experienced melting prior to capture by Earth are thus not included in this group and are classified as unmelted MMs. It is, however, not always straightforward to distinguish particles that have melted in the atmosphere from those that were primarily melted.

Evidence that significant fusion occurred during atmospheric entry is an important criteria for identifying a melted MM as compared to an igneous unmelted particle. The fundamental characteristic of atmospheric entry heating is that it is a surface process. Surface correlated heating or particle shapes suggesting melting with no subsequent thermal overprint thus strongly imply that heating occurred during atmospheric entry. Fusion is identified in melted MMs on the basis of textures and mineralogy. Particles dominated by a glassy mesostasis, with or without microphenocrysts, are demonstrably formed by crystallization of a melt. Vesicles are also often present within the mesostases of melted MMs, however, they are not necessarily characteristic of these particles since subspherical voids also occur in unmelted varieties.

Cosmic spherules show considerable diversity in textures, compositions and mineralogy and can be subdivided into several chemical and textural groups (Fig. 1). The basic chemical subtypes of CSs, which are also reflected in their principle mineralogy, are the iron-rich spherules (I-type), a glass with magnetite (G-type) group (Blanchard et al. 1980) and silicate-type (S-type) CSs.

I-type CSs (Figa. 1a and 1b) are dominated by FeO with minor amounts of other oxides (principally MgO and SiO^2), mineralogically they are dominated by the iron oxides wüstite and magnetite, however, Ni-rich iron metal, sometimes with nugget of the platinum group elements, can occur as spheres within spherules. I-type spherules often contain a single large spherical void that may form by the

Table 1. An outline of the classification of micrometeorites.

Groups	Class	Type	Subtype	Description
Melted MMs	Cosmic spherules (CSs)	S	CAT	Spherules with Mg/Si > 1.7 that are enriched in Ca, Ti, and Al. They have barred olivine textures.
		S	Glass	Spherules consisting almost entirely of glass.
		S	Cryptocrystalline	Spherules dominated by submicron crystallites and magnetite. Some include multiple domains.
		S	Barred olivine (BO)	Spherules dominated by parallel growth olivine within glass.
		S	Porphyritic olivine (Po)	Spherules dominated by equant and skeletal olivine within glass. Relict-bearing varieties contain unmelted minerals.
		S	Coarse-grained	These spherules contain >50% volume relict minerals.
		G		Spherules are dominated by magnetite dendrites within silicate glass.
		I		Spherules dominated by magnetite, wüstite.
Partially melted MMs	Scoriaceous MMs (ScMMs)	–	–	Vesicular particles dominated by a mesostasis of fayalitic olivine microphenocrysts within glass. ScMMs often contain relict minerals and relict matrix areas.
Unmelted MMs	Fine-grained MMs (FgMMs)	C1		Compact, chemically homogeneous FgMMs. Often contain framboidal magnetite.
		C2		Compact, chemically heterogeneous fine-grained MMs. Often contain isolated silicates and/or tochilinite.
		C3		Highly porous FgMMs. Often contain isolated silicates and framboidal magnetite.
	Coarse-grained MMs (CgMMs)	Chondritic CgMMs	Porphyritic olivine and/or pyroxene	Igneous MMs dominated by pyroxene and/or pyroxene phenocrysts within glass.
			Granular olivine and/or pyroxene	Igneous MMs dominated by pyroxene and/or olivine without significant glass.
			Barred olivine	Igneous MMs dominated by parallel growth olivine within glass.
			Radiate pyroxene	Igneous MMs dominated by radiating pyroxene dendrites within glass.
			Type I/type II	Type I CgMMs are reduced particles containing Fs and/or Fa < 10 mol%. Type II CgMMs are oxidized particles with Fs and/or Fa > 10 mol%.
		Achondritic CgMMs	–	Differentiated igneous CgMMs.
	Refractory MMs	Porous	–	Porous particles dominated by refractory minerals.
		Compact	–	Compact particles dominated by refractory minerals.
		Hydrated	–	Particles dominated by refractory minerals surrounded by Fe-rich phyllosilicates or their dehydroxylates.
	Ultracarbonaceous MMs		–	Particles dominated by carbonaceous materials with embedded

loss of a molten metal bead from the particle. They also often exhibit an irregular void space in their centre which could result from the rapid cooling of the melt from the surface inwards (Feng et al. 2005). I-type spherules are abundant in deep sea collections, as they are very resistant to weathering, but they constitute only 2% of 1600 cosmic spherules collected at the bottom of the South Pole Water Well (SPWW) (Taylor et al. 2000).

G-type CSs have major element compositions that are intermediate between the broadly chondritic S-type spherules and the I-type CSs. G-type spherules are typically dominated by magnetite dendrites within a mesostasis of silicate glass, some have subspherical voids similar to those found within I-type spherules which may likewise have formed by the loss of metal beads (Figs. 1c and 1d). G-type spherules, however, can have a wide range of textures and include particles that differ in texture and mineralogy from typical spherules. G-type spherules are only present at the level of 1% among 1600 CSs from the SPWW (Taylor et al. 2000).

The silicate S-type are by far the most common, making up 97% of 1600 cosmic spherules analyzed from the South Pole Water Well (Taylor et al. 2000). Most have broadly chondritic compositions (Brownlee et al. 1997); notable exceptions are the CAT spherules that have Mg/Si ratios >1.7 and are highly enriched in Ca, Al, and Ti (Taylor et al. 2000). S-type CSs are dominated by olivine microphenocrysts,

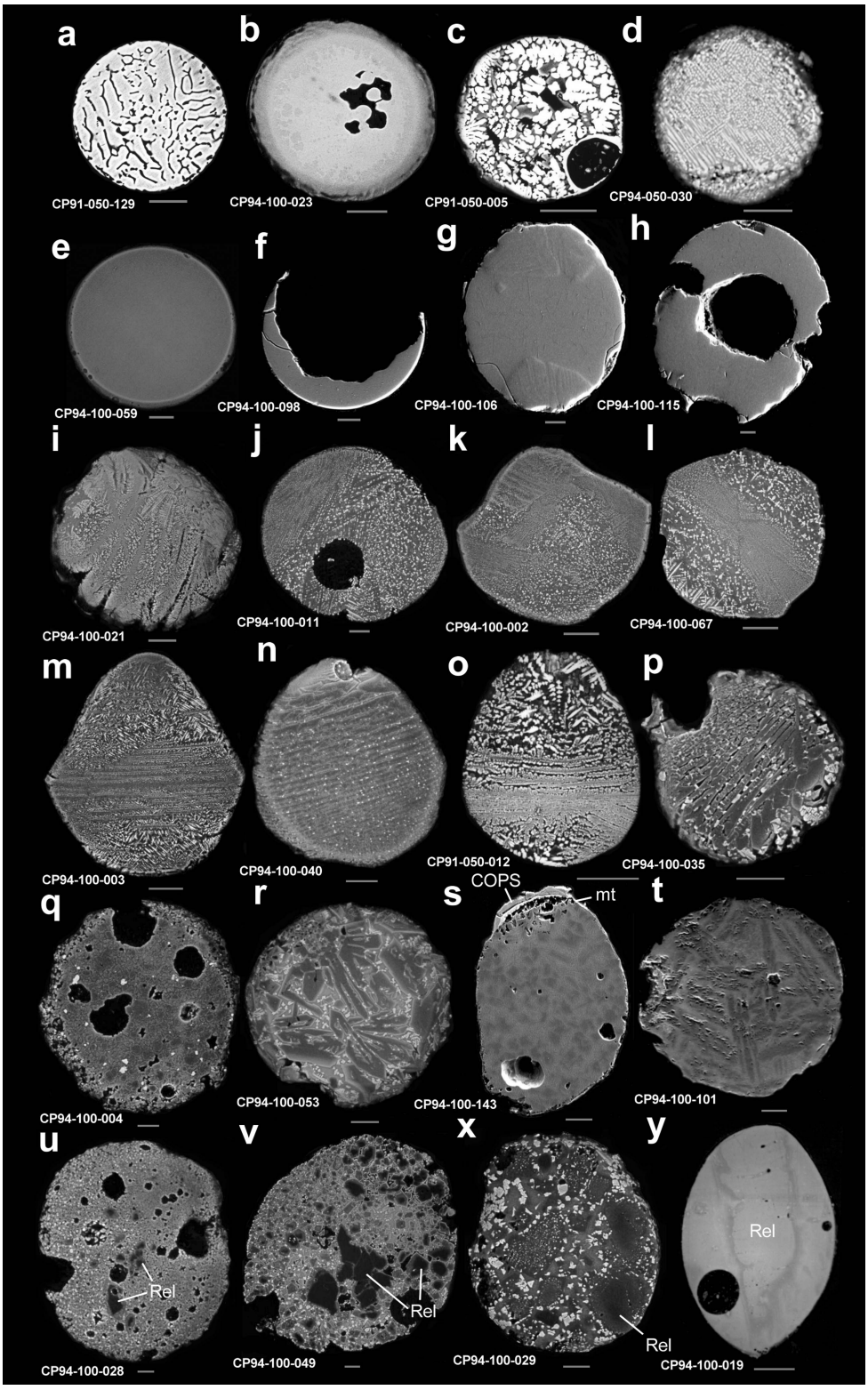

Fig. 1. Backscattered electron images of cosmic spherules. a), b) I-type spherules dominated by magnetite and wüstite. c), d) G-type spherules containing magnetite dendrites in a silica-rich glass. e–h) Glass S-type spherules. i–k) Cryptocrystalline S-type spherules. l–p) Barred olivine S-type spherules, where l is probably transitional to cryptocrystalline spherules. (q–t) Porphyritic olivine S-type spherules. Spherule s has a magnetite rim (mt) associated with COPS. u), v) Relict-bearing PO spherules containing relict anhydrous silicates (Rel) that have survived atmospheric melting. x), y) Coarse-grained spherules, which are dominated by relict grains (Rel). In particle x some relict contain iron-oxide inclusions. The scale bar is 20 μm.

silicate glass and often contain magnetite and/or chromite. They may also contain relict grains, principally Mg-rich pyroxene and olivine, that survived melting in the atmosphere and sometimes have FeNi metal droplets.

S-type spherules can be subdivided into several subclasses depending on their quench textures, which are thought to reflect their peak atmospheric temperatures (Taylor et al. 1991). CAT spherules, have barred olivine textures, lack Fe, have high Mg/Si ratios, and high Ca, Al, and Ti values. These appear white under the microscope and weather quickly in the acidic Antarctic melt water (Taylor et al. 2000). Isotopic analyses (Mg, Si, and O) confirm that they have been partial evaporated during atmospheric entry heating (Alexander 2002) and compared to all other S-type spherules were subjected to the highest temperatures.

Glass spherules (Figs. 1e–h) lack olivine microphenocrysts and are thought to have formed at the next highest peak temperatures. Under a binocular microscope these tend to be transparent brown, yellow, or green in color and go extinct under crossed polarization. Glass spherules sometimes contain large vesicles. They are usually spherical, can be highly vesiculated, and some contain FeNi metal beads. They should not be confused with the G-type spherules that were described above.

Cryptocrystalline (CC) spherules (Figs. 1 i–l) contain submicron crystallites and can have significant submicron magnetite. There are two distinct textures. Olivine microcrystals can grow from the surface inward producing a knobbly surface. Under a binocular microscope the knobbly protrusions on the surface of CC spherules are characteristic and were called "turtleback" (Brownlee and Bates 1983). Other cryptocrystalline spherules have multiple regions that crystallized simultaneously producing extremely fine-grained regions surrounded by a more iron rich phase. CC spherules are thought to have experienced slightly lower peak temperatures than the glass spheres, because some of crystallization nuclei survive (Brownlee et al. 1991).

Barred olivine (BO) spherules (Figs. 1m–p) are dominated by parallel growth olivine, which is seen as parallel bars in polished sections, within a glassy mesostasis that often contains magnetite. Most BO spherules have ovoid (egg-like) shapes that are easily identified under a binocular microscope, although some are elliptical. In ovoid BO spherules, olivine bars are usually orientated approximately perpendicular to the long-axes of the particles. Some BO spherules exhibit FeNi metal beads that have sometimes oxidized to form iron-oxide, often with a cubic morphology, located at one end of the particle. The Fe-Ni-oxides frequently contain S, C, and P, and are probably dominated by ferrihydrite (Engrand et al. 1999) and might represent weathering products of metal (Genge et al. 1998a). These iron-rich bodies, therefore, probably formed as immiscible Fe-Ni-metal liquids that were separating from the silicate melt of the spherule (Genge et al. 1998a). Barred olivine spherules are thought to form at lower peak temperatures than CC spherules (Taylor et al. 2000). Barred olivine spherules are usually opaque under a binocular microscope, except for those containing a metal/ferrihydrite bead which are often brown/green transparent.

Porphyritic olivine (PO) spherules (Figs. 1q–t) are dominated by olivine microphenocrysts with equant, euhedral or skeletal morphologies within a glassy mesostasis, usually with accessory magnetite and/or chromite. Relict olivine (and rare pyroxene), often with overgrowths of more Fe-rich olivine grown from the melt, are common in PO spherules and together with the olivine microphenocrysts, which indicate abundant crystallization nuclei, suggest that PO spherules experienced the lowest peak temperatures of any cosmic spherules, especially those that contain relict minerals.

Porphyritic spherules show a wide range of crystallinities and crystal sizes. Those with the smallest microphenocrysts tend to be the most vesicular and are likely to be gradational to partially melted MMs. Some PO spherules also contain areas dominated by Fe-Ni-ferrihydrite and/or Ni-bearing sulfides. These are thought to form as immiscible metallic liquids during heating and are often found at the margins of spherules, suggesting they were in the processes of separating during cooling (Genge et al. 1998a).

Relict pyroxene and olivine within cosmic spherules that have survived atmospheric melting are usually forsterite and enstatite, however, occasionally Fe-rich varieties are observed and identified by more Mg-rich overgrowths. The abundance of relict grains varies greatly from those containing small volumes of isolated grains, often present as cores to olivine microphenocrysts grown from the melt, to spherules in which relicts are volumetrically dominant. The latter particles probably represent melted coarse-grained or composite particles (see below for definition of these materials) and are, thus, distinct from other CSs that form by melting of fine-grained particles.

The presence of relict minerals within CSs should be denoted by a prefix of "relict-bearing" (Taylor et al. [1998] and Figs. 1u and 1v). Those spherules that appear to have formed by melting of a coarse-grained precursor should be described as CG spherules. These spherules include those containing large volumes (>25%) of relict grains or having non-chondritic compositions suggesting formation by melting of a coarse-grained precursor (Figs. 1x and 1y).

Partially Melted MMs

Scoriaceous Fine-Grained MMs

Scoriaceous micrometeorites (ScMMs) are irregular, but smooth, highly vesicular particles (Fig. 2). Particle shape and vesicularity alone are not, however, particularly

discriminative properties for these particles since they represent a gradational series from the more intensely heating CSs to the less heated ScMMs. The presence of envelopes of magnetite (magnetite rims) surrounding ScMMs and their absence on CSs, however, seems to be much more characteristic even if the reason for this difference is, as yet, largely uncertain (Toppani et al. 2001).

Scoriaceous micrometeorites are dominated by a mesostasis of microporphyritic olivine, usually with crystal sizes <1 μm, within an interstitial silicate glass phase (Fig. 2). Although the textures of the mesostasis implies crystallization of a melt, probably at temperatures just above the melting point, ScMMs commonly contain areas of relict fine-grained matrix similar to that of many unmelted MMs. Many ScMMs are, therefore, partially melted and are a gradational group to unmelted particles. Under a binocular microscope ScMMs often have lobate, smooth exteriors with vesicles impinging on their surfaces.

The most common relict grains in ScMMs and are Mg-rich pyroxene and olivine. Enstatite grains are frequently highly fractured and are surrounded by more Fe-rich pyroxene that appears to have formed by reaction with the surrounding melt. Relict olivines are usually forsterites. Vesicle abundances in ScMMs are frequently high and sometimes exceed 50% by volume. Occasionally ScMMs contain Fe-Ni metal/oxides or Ni-bearing sulfides and like those of CSs these may have formed as immiscible metallic/sulfide liquids.

One ScMM has been reported (Genge and Grady 1998a) with large volumes of Fe-Ni-oxides and a mesostasis dominated by enstatite microphenocrysts rather than olivine. No additional similar ScMMs have yet been recognized, however, it remains a possibility that there are a subgroup of Mg-rich ScMMs formed by separation of significant Fe-Ni-metal liquids under highly reducing conditions. Such particles may have formed from C-rich precursors.

Distinguishing partially melted mesostasis and relict matrix is difficult since in reality both have probably experienced a degree of fusion. Partially melted mesostasis, however, is probably best defined as areas that have melted to a sufficient degree during entry heating to behave as a viscous fluid, whereas relict matrix retains the rheological properties of a rigid solid. Partially melted mesostasis, therefore, lacks irregular pore space, except that which can be attributed to etching of interstitial glass, and irregular dehydration cracks. Both partially melted mesostasis and relict matrix, however, contain subspherical to rounded vesicles, although these tend to have more irregular shapes within relict matrix. The presence of Fe-rich olivine microphenocrysts within the partially melted mesostasis of ScMMs also gives it a higher backscattered electron potential than relict matrix (Figs. 2 and 3).

Studies of the thermal evolution of micrometeoroids during entry heating (Flynn 1995; Genge 2006) and heating experiments (Toppani et al. 2001) indicate that the survival of relict matrix within ScMMs occurs due to thermal discontinuities supported by decomposition of volatile-bearing phases such as phyllosilicates and carbonaceous matter. Consequently the fusion of FgMMs occurs through surface melting and is a gradational process in which the unmelted core is progressively consumed.

In the current classification system it is proposed that ScMMs with relict fine-grained cores that comprise less than 50% by volume of the particle are termed Sc/FgMMs; where Fg denotes fine-grained matrix. Particles in which the relict fine-grained core exceeds 50% by volume of the particle are denoted as Fg/ScMM particles.

The matrix mineralogies and textures of relict matrix are described in detail below since thermal alteration of fine-grained matrix is a gradational and complex process that is likely to be dependent on the duration of heating as well as peak temperature. Consequently thermally altered, relict matrix is also often observed in particles lacking scoriaceous mesostasis.

Scoriaceous Coarse-Grained MMs

Scoriaceous coarse-grained MMs are formed by partial melting of CgMMs, which are described below amongst unmelted particles. Incorporating the degree of thermal alteration within CgMMs in a classification scheme is complicated due to the gradational nature of thermal alteration affects within these materials. The lowest temperature changes in mineralogy occur in the glassy mesostases of particles with the remobilization of the glass, the formation of vesicles and growth of fayalitic olivine overgrowths on olivine phenocrysts (Genge et al. 1996). Partial melting occurs at temperatures above the solidus and can produce CSs. Igneous rims found on many CgMMs may be melted fine-grained matrix that was attached to the exterior of the particle (Genge 2006) and provide a direct relationship to the thermal alteration of fine-grained particles. As defined for scoriaceous/fine-grained particles, scoriaceous MMs which have retained an large (>50%) fraction of unmelted coarse-grained minerals will be noted as Cg/ScMMs (Figs. 9a and 9b). If the particle shows large amounts of scoriaceous matrix associated with coarse-grained minerals, the MM will be described as Sc/CgMM (Fig. 6).

Unmelted Micrometeorites

Unmelted fine-grained MMs are those dominated by a fine-grained porous groundmass of micron-sized mineral grains and are similar to the fine-grained matrices of chondritic meteorites (Figs. 3 and 4). Like these materials they have broadly chondritic compositions, mostly in the range of CI, CM, and CR chondrite matrices, for most major and minor elements (Genge et al. 1997a; Kurat et al. 1994). The depletions in Ca, Ni, and S present within Cap

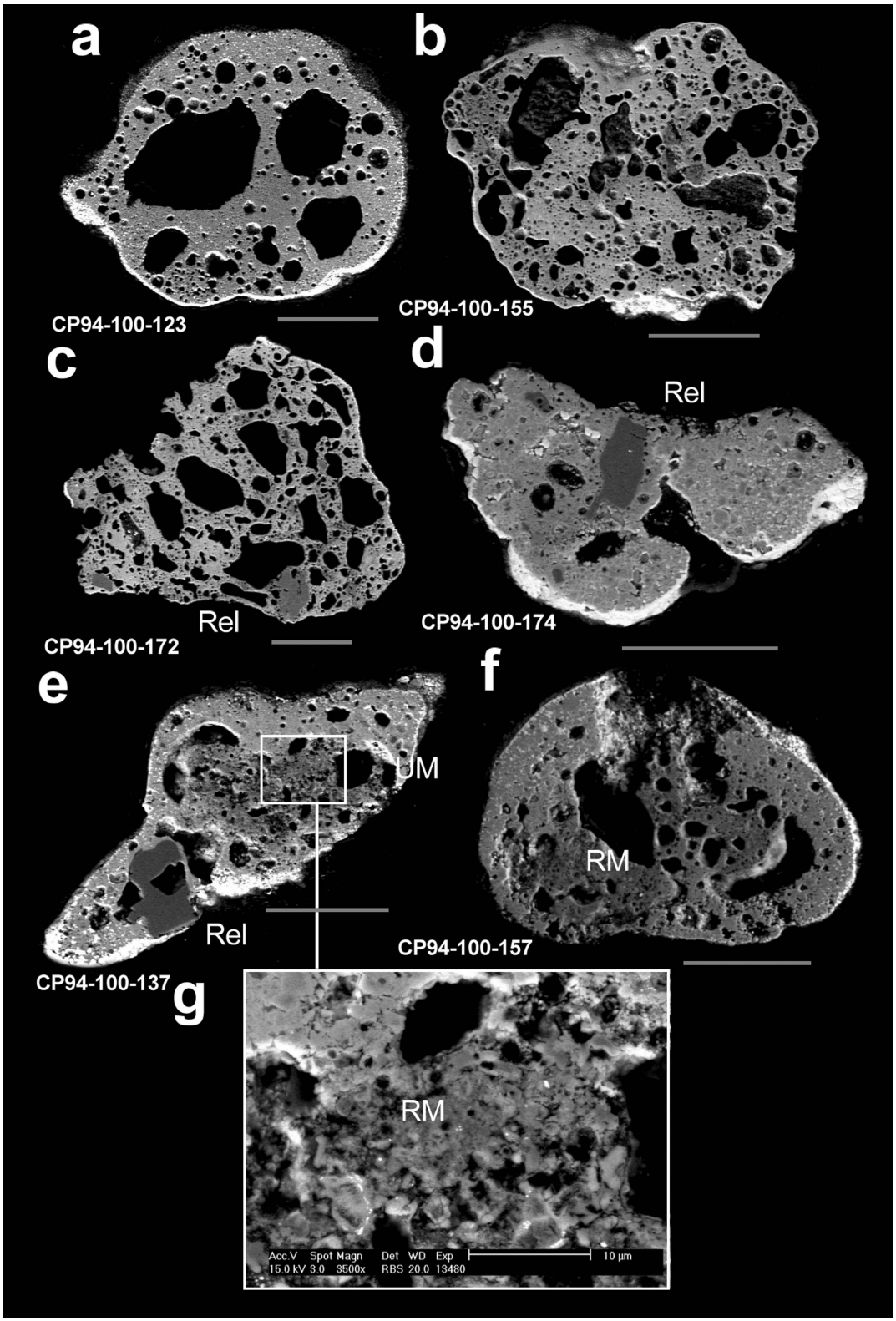

Fig. 2. Backscattered electron images of scoriaceous micrometeorites. Particles c and d are relict-bearing (Rel) since they contain anhydrous silicates (forsterite and enstatite) that have survived atmospheric heating. Particles e and d both contain cores of relict fine-grained matrix (RM). g) A high-resolution backscattered electron image of particle e showing the melted mesostasis of the ScMM (top of image; dominated by fayalitic olivine microphenocrysts) and unmelted matrix (center of image; dominated by lower backscattered potential porous materials). The scale bar is 50 µm.

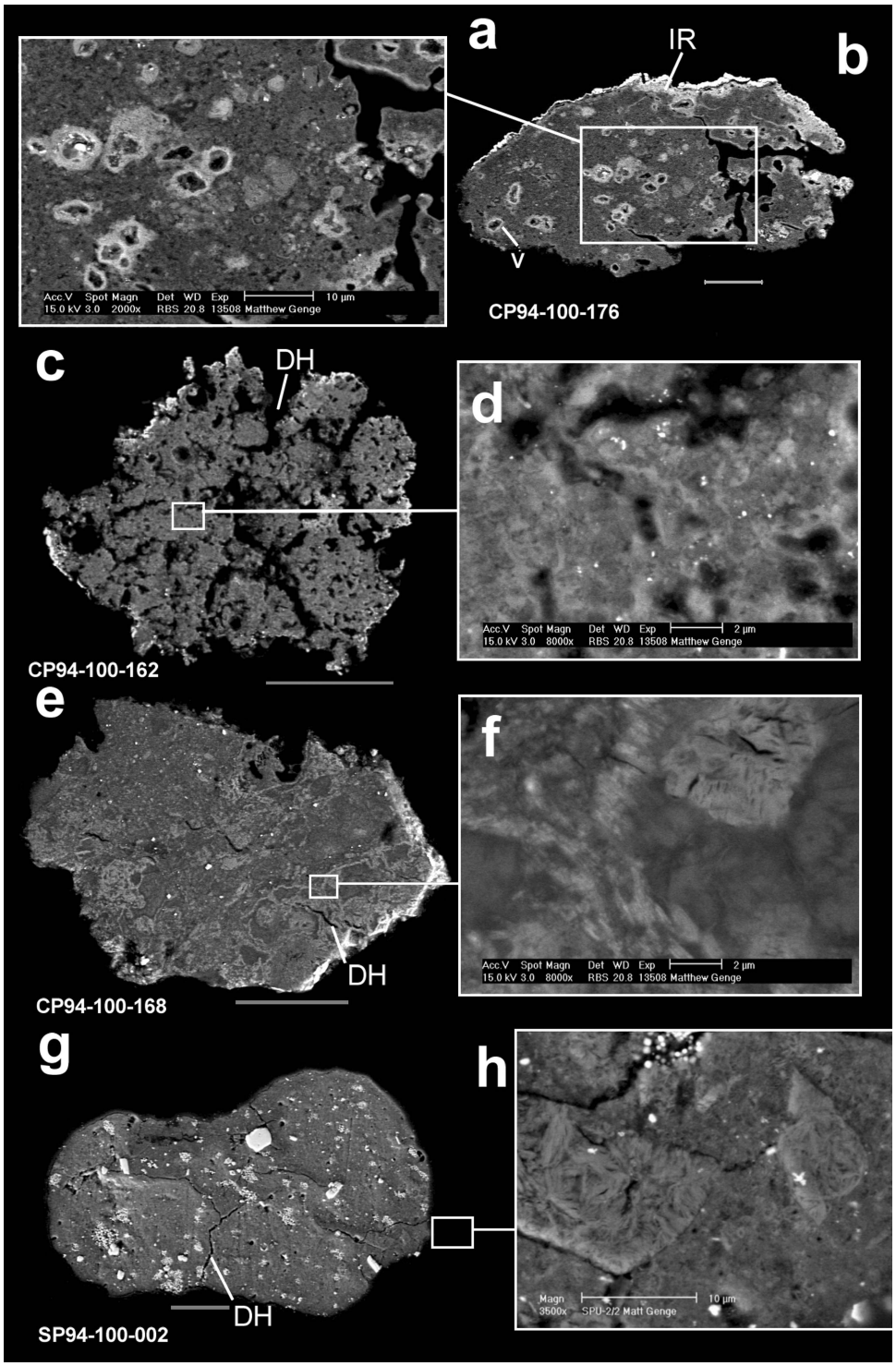

Fig. 3. Backscattered electron images of unmelted micrometeorites. a), b) An unmelted MM with an igneous rim (IR) consisting of microphenocrysts of fayalitic olivine within a glassy mesostasis surrounding unmelted, but altered, matrix with vesicles. c), d) An altered MM dominated by fine-grained matrix lacking textural evidence for acicular/sheet-like phases but with irregular dehydration cracks (DH). This particle also has a thin igneous rim and is transitional to ScMM. e), f) An unmelted MM consisting of fine-grained matrix with textural evidence for acicular/sheet-like phases. Transmission electron microscopy of this particle (Genge et al. 2001) indicates that phyllosilicates have decomposed to amorphous dehydroxylates. g), h) An unmelted MM consisting of fine-grained matrix with textural evidence for acicular/sheet-like phases. Transmission electron microscopy of this particle confirms the presence of serpentine and saponite. The presence of unaltered phyllosilicates cannot be determined from textures observed in backscattered electron images, however, the absence of a magnetite rim may be indicative of its low degree of heating. Scale bar is 50 μm.

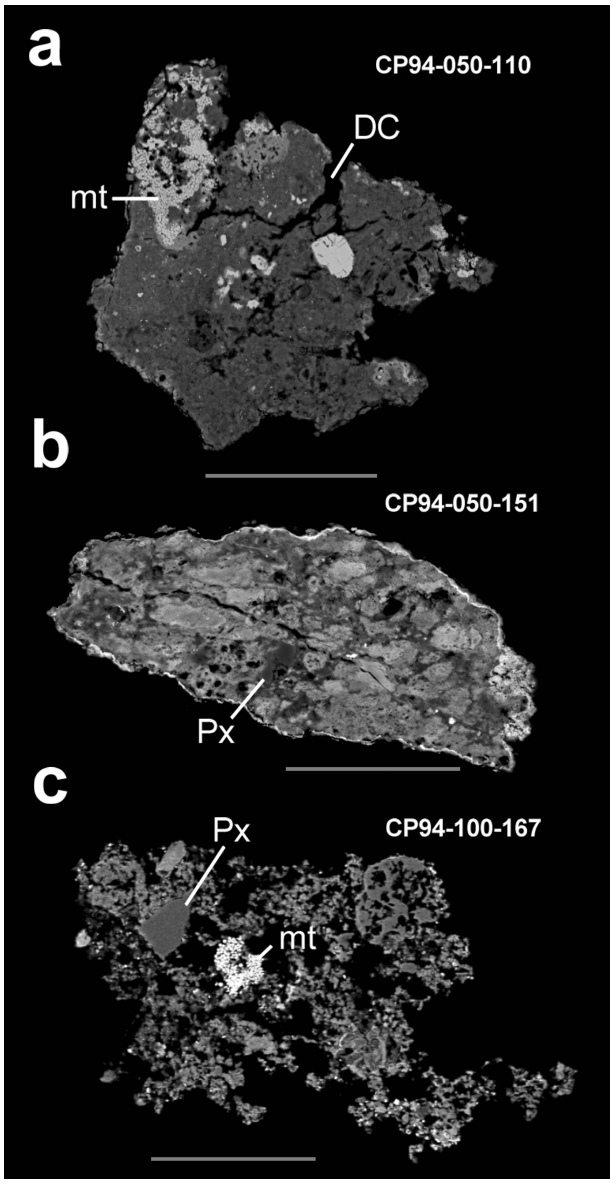

Fig. 4. Backscattered electron images of textural types of MM suggested by Genge et al. 2002a. a) A compact C1 MM containing framboidal magnetite (mt) and showing dehydration cracks (DC); Fig. 3g also shows a C1 particle. b) A compact C2 MM with significant spatial variation in the Fe/Mg ratio of the matrix. This particle contains a small isolated silicate mineral (IS), in this case pyroxene. Figure 3e also shows a C2 particle. c) A porous C3 MM dominated by anhydrous silicates with framboidal magnetite. The matrix of the composite particle in Fig. 7 is also C3 material. Scale bar is 50 μm.

Prudhomme and SPWW micrometeorites may be in part due to the leaching of soluble phases like sulfides and carbonates while in the ice/water, as they are not found in Concordia MMs (Duprat et al. 2005). Primary differences from chondrites, for example, in the high pyroxene to olivine ratios of MMs are also evident (Maurette et al. 1991).

Unmelted coarse-grained micrometeorites are defined as dominated by anhydrous silicates, primarily pyroxene with subordinate pyroxene, with grain sizes larger than ~1 micron. Often CgMMs have igneous textures with olivine and/or pyroxene contained within a glassy mesostasis, however, some CgMMs are merely fragments of single crystals of olivine or pyroxene, or are granular aggregates of anhydrous silicates (Fig. 5).

Composite unmelted micrometeorites have also been observed that contain both portions characteristic of both CgMM and FgMM (Genge 2006). Such particles usually consist of a coarse-grained, igneous-textured object dominated by anhydrous silicates and glassy mesostasis, surrounded by a partial rim of fine-grained matrix (Fig. 7). To denote the composite nature of these particles the notation Fg/CgMM and Cg/FgMM is used to describe particles in which the fine-grained and coarse-grained portions dominate respectively.

Unmelted MMs: Fine-Grained MMs

Thermal Alteration of Hydrous Matrix in Fine-Grained MMs

Genge et al. (1997a) suggested that FgMMs could be split into altered and unaltered subtypes due to thermal alteration during atmospheric entry in which unaltered particles are those containing acicular to sheet-like, submicron mineral grains in the matrix. These were suggested to be phyllosilicates or their thermal decomposition products. Particles whose matrices are dominated by submicron anhedral, equant grains, often within a interstitial homogeneous material were defined as altered and suggested to consist of matrix in which the amorphous dehydroxylates of phyllosilicates that have decomposed into olivine, pyroxene, and glass (Greshake et al. 1998). Such particles frequently contain subspherical vesicles that are probably formed by decomposition of volatile-bearing phases and often have rims of redeposited amorphous material (Genge et al. 2001).

Transmission electron microscope (TEM) and X-ray diffraction studies of the matrices of FgMM have confirmed that phyllosilicates with measurable basal spacings are rare and are dominated by smectite (Genge et al. 2001; Gounelle et al. 2002; Nakamura et al. 2001; Noguchi et al. 2000, 2002) although serpentine has also been identified. Most FgMMs whose matrices contain submicron acicular to sheet-like phases are dominated by amorphous, often iron-rich silicates. These appear to be pseudomorphs after original hydrous minerals and are thought to be dehydroxylates after phyllosilicates (Genge et al. 2001; Gounelle et al. 2002; Noguchi et al. 2000).

Transmission electron microscope studies of more intensely heated FgMMs and the relict fine-grained matrices of ScMM indicate they are dominated by submicron, anhedral olivine and pyroxene with interstitial glass and thus probably are the thermal decomposition products of dehydroxylates. It is likely, however, that the transition from phyllosilicates-

bearing MMs to those in which amorphous dehydroxylates of phyllosilicates have recrystallized to olivine and pyroxene is gradational. Genge et al. (2001) suggested FgMMs lacking magnetite rims are probably the least heated and most likely to contain undecomposed phyllosilicates.

Many FgMMs preserve the original texture of the fine-grained matrix to a large extent since the amorphous dehydroxylates pseudomorph the pre-existing phyllosilicates. Those FgMMs that preserve phyllosilicates with measurable basal-spacings are the least heated and should be prefixed with phyllosilicate-bearing.

Primary Variations

It has been suggested that FgMMs may also be subdivided on the basis of their textures and chemical homogeneity into one of three groups (Genge and Grady 2002): CU1, CU2, and CU3 FgMMs. Chemical homogeneity in Fe/Si ratio, which is reflected in significant variation in backscattered electron potential, in particular can also be distinguished in thermally altered FgMMs (Genge et al. 2000).

CU1 particles are compact FgMMs with low apparent porosities that are chemically homogeneous over scales of 10 microns (Fig. 4a). CU1 particles rarely contain large (>4 μm), "isolated" anhydrous silicates. These particles are suggested to have affinities to carbonaceous chondrite type 1 meteorite matrices (i.e., those which have experienced intense aqueous alteration such as the CI1 chondrites and the Tagish Lake chondrite (Brearley and Jones 1998; Zolensky et al. 2002).

CU2 particles are compact FgMMs with low porosities that are chemically heterogeneous, in particular in their Fe/Mg, Fe/Si ratios, over distances of 10 microns (Fig. 4b). Isolated, anhydrous pyroxenes and olivines more than 4 μm across are more abundant in CU2 particles than in CU1. These particles may have affinities to carbonaceous chondrite type 2 meteorite matrices that, although aqueously altered, have not been chemically homogenized on small scales.

CU3 particles are porous FgMMs, sometimes with a porosity up to 50% by volume, that are dominated by subhedral to euhedral magnesian olivine and pyroxene grains, which are up to several microns in size, with minor amounts of interstitial acicular to sheet-like phases (Fig. 4c). A TEM investigation of one CU3 particle suggests the sheet-like phase is a dehydroxylate after phyllosilicate (Genge and Grady 2002). Based on the higher visible irregular porosity and the paucity of phases after hydrous silicates CU3 particles might have affinities with carbonaceous chondrite type 3 meteorite matrices that have experienced lower degrees of aqueous alteration than type 1 or type 2.

Under a binocular microscope FgMMs have irregular shapes and vary from smooth compact particles (generally CU1 and CU2) to highly re-entrant fluffy particles (CU3). In altered FgMMs subspherical voids can often be observed on their surfaces and particles with igneous rims can resemble ScMMs.

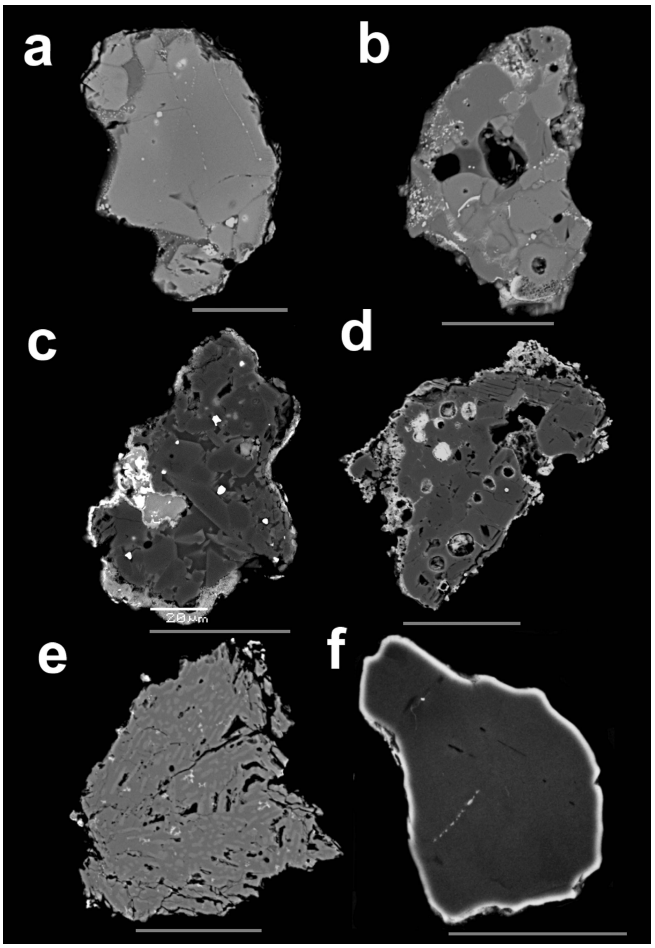

Fig. 5. Backscattered electron images of chondritic CgMMs. a) Porphyritic pyroxene type I CgMM with interstitial glass and FeNi droplets, some of which have been altered to ferrihydrite-dominated assemblages. b) Granular pyroxene and olivine type 1 CgMM with altered FeNi metal. c) Porphyritic olivine type 2 CgMM with an interstitial Na-bearing aluminosilicate glass. d) Porphyritic olivine and pyroxene type 2 CgMM with interstitial glassy mesostasis. This particle also contains some diopside. e) Radiate pyroxene type 2 particle with small iron-oxide dendrites in the interstitial glass. f) A single crystal CgMM of diopside. This particle lacks a magnetite rim (the bright exterior is charging), however, its extraterrestrial nature is indicated by the FeNi metal droplets it contains. Note that particles c and d both exhibit igneous rims similar to those of ScMM and unmelted MMs (cf. Genge 2005). Scale bar is 50 μm.

Minor Phases in FgMMs

In addition to isolated pyroxene and olivine, minor primary phases found in FgMMs include magnetite, tochilinite, metal, sulfide, and refractory minerals typical of CAIs. These presence of these phases have some implications for the parent body associations of micrometeorites but are not usually strongly discriminative. Magnetite framboids and platelets, for example, although most common in CI1 chondrites are also found in Tagish Lake, CM2 and CR2 chondrites, and more rarely in CV3 and CO3 chondrites. Tochilinite, or at least its thermal decomposition products, nevertheless, may be

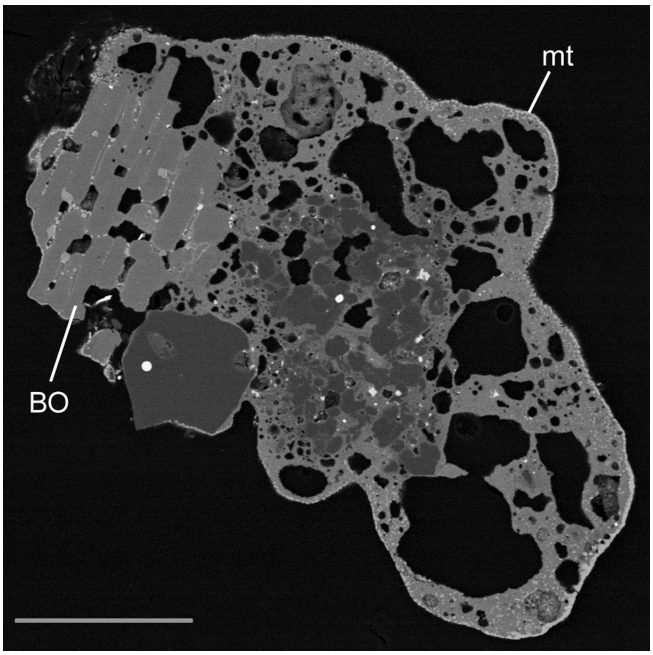

Fig. 6. Backscattered electron image of a Sc/CgMM from the South Pole water well containing a fragment of a barred olivine igneous object (BO) covering the upper quarter of the particle. The particle has a well developed igneous rim. Scale bar is 50 μm.

diagnostic of a CM2 affinity (Brearley et al. 1998). The presence of minor phases in FgMMs is probably, therefore, best recorded as a prefix giving classifications, such as, "framboidal magnetite-bearing FgMM" or "spinel-bearing FgMM."

A special case of minor phases in FgMMs, however, are those that contain refractory phases, such as Mg-Al-spinel, surrounded by iron-rich phyllosilicates. These particles are strongly reminiscent of aqueously altered CAIs from CM2 chondrites and are discussed in more detail below.

Unmelted MMs: Coarse-Grained MMs

The majority of CgMMs have igneous textures and are dominated by pyroxene and/or olivine within a glassy mesostasis which can contain accessory metal, sulfide, and/or iron oxides. The majority of these particles have broadly chondritic mineral assemblages similar to chondrules or the primitive achondrites. Most other CgMMs are fragments of single crystals of olivine and pyroxene and thus provide little genetic information to suggest an adequate parent body association. Very rare achondritic particles, with textures and mineralogies suggesting derivation from differentiated parent have been recognized such as a single particle containing pigeonite with augite exsolution and anorthite that may have an affinity to basaltic achondrites (Gounelle et al. 2005a). Consequently CgMMs should probably be subdivided into (a) chondritic CgMMs, which have broadly chondritic mineralogies (Figs. 5a–e), (b) rare achondritic CgMMs, which have non-chondritic, non-refractory mineralogies, and (c) single crystal CgMMs (Fig. 5f). Under a binocular microscope CgMMs can sometimes be identified by their facetted surfaces, however, they are often difficult to distinguish from ScMMs, particularly when they have igneous rims.

Chondritic CgMMs

Chondritic CgMMs can be subdivided using a petrological scheme (Genge et al. 2005) in which particles are classified in a similar fashion to chondrules. Coarse-grained MMs can, therefore, be porphyritic (P), granular (G) or radiating pyroxene (Rp). Porphyritic and granular particles, like chondrules, are prefixed with their dominant mineralogies following their textural classification, for example, into porphyritic olivine (Po), porphyritic pyroxene (PP), porphyritic olivine and pyroxene (POP) (Fig. 5). A single Sc/CgMM containing an area of barred olivine similar to barred olivine chondrules has been identified (S. Taylor, unpublished data; Fig. 6), the term barred olivine (Bo) should be used for such particles, when dominated by the coarse-grained portion.

Chondritic, porphyritic, and granular CgMMs fall into two main chemical populations based on the compositions of their olivines and pyroxenes, and the abundance of metal and sulfide (Genge 2006). This scheme is analogous to that of chondrules. Type 1 CgMMs are those with Mg-rich olivines and/or pyroxenes, and usually contain abundant FeNi metal and sulfides (Figs. 5a and 5b). Type 2 CgMMs are those with more Fe-rich olivines and pyroxenes, less abundant metal and sulfides, and sometimes contain iron oxides (Figs. 5c, 5d, and 5e). The boundary between the two groups, as with chondrules, is 10 mol% fayalite or ferrosilite (Grossman et al. 1988). Coarse-grained MMs consisting of single crystals are also observed (Fig. 5f).

In classifying primitive CgMMs into type 1 and type 2 particles it should not be assumed that these necessarily originated as fragments of chondrules. A derivation from a primitive achondrite source or even shock melts is possible for many individual particles.

Chondritic CgMMs sometimes include selvages of fine-grained matrix similar to that of FgMMs (Fig. 7). These particles indicate that at least a proportion of CgMMs and FgMMs are derived from the same parent bodies and have been termed composite MMs (Genge 2006). Such particles are classified as Fg/CgMMs.

Chondritic CgMMs with subspherical particle shapes (Fig. 8) are difficult to distinguish from cosmic spherules since both can have similar igneous textures formed by crystallization during rapid cooling. Chondritic CgMMs, however, can be identified on the basis of any of the following criteria: (1) the presence of pyroxene phenocrysts, which are absent within cosmic spherules since pyroxene crystallization is inhibited by the extremely rapid cooling rates (several hundred °C s^{-1}) experienced by spherules (Taylor and Brownlee 1991), (2) the occurrence of a magnetite rim, which

is rare on cosmic spherules and usually associated with metal separation, and (3) the presence of an igneous rim similar to that found on some fine-grained micrometeorites. It should be noted, however, that pyroxene dendrites can occasionally be found in cosmic spherules within the mesostasis and are probably formed at very large supercoolings (Genge et al. 1997a).

Unmelted MMs: Refractory MMs

Micrometeorites that potentially represent samples of components other than chondrules (i.e., other than chondritic igneous objects) and matrix have been reported but are present in low abundances within MM collections such that sufficient numbers have yet to be characterized to facilitate a reliable classification scheme. Principal among these are unmelted FgMM containing refractory minerals that are likely to be fragments of refractory inclusions. Fine-grained micrometeorites containing isolated grains of spinel, perovskite, melilite, fassaite, and hibonite have been reported by previous studies (Beckerling and Bischoff 1995; Engrand and Maurette 1998; Engrand 1999; Gounelle 2000; Greshake et al. 1996; Hoppe et al. 1995; Kurat et al. 1994; Lindstrom et al. 1992) and some have been classified on the basis of their trace element systematics following the scheme used for CAIs (Greshake et al. 1996). In the current system it is recommended that such particles are classified as FgMMs and prefixed with the refractory mineral name (e.g., hibonite-bearing FgMM) since the refractory minerals comprise a volumetrically small component of the particles.

Several micrometeorites, however, have been discovered that are dominated by refractory minerals, or their alteration products, that warrant a separate classification. Particles containing spinels surrounded by Fe-rich phyllosilicates (or their thermal decomposition products) bear a close resemblance to aqueous-altered CAIs from CM2 chondrites (Fig. 10a) (Gounelle 2000; Kurat et al. 1994). These particles are classified as hydrated refractory MMs.

Only three micrometeorite (BI54B3-31, 94-4-36, and 94-19-5) dominated by refractory minerals have been previously reported. B154B3-31 is a porous aggregate of anhedral fassaite with a smaller region dominated by enstatite (Greshake et al. 1996). Particles 94-4-36 and 94-19-5 are dominated by spinel containing inclusions of perovskite and surrounded by Fe-rich phyllosilicates in the case of 94-4-5 (Fig. 10c) and by Ca-rich pyroxene and matrix in the case of 94-4-36 (Fig. 10b) (Engrand et al. 1995). Figure 10d shows a fourth refractory particle dominated by aluminous diopside with minor forsterite (Genge, unpublished data). Classifying these refractory MMs is problematic due to the low numbers of particles so far discovered and the lack of a unified petrological CAI classification system. It is suggested, therefore, that refractory particles should simply be subdivided into porous and compact varieties and prefixed with their dominant mineralogy. Particle BI54B3-31 would, therefore, be a fassaite-enstatite-bearing, porous refractory MM. The low abundance of CAI-related MMs, although similar to CM2 abundances, may be a result of separation techniques used in the laboratory, which focus on dark or spherical particles. The mineralogy and grain-sizes of refractory MMs are, however, subtly different from those of CM2 chondrites (Brearley and Jones 1998).

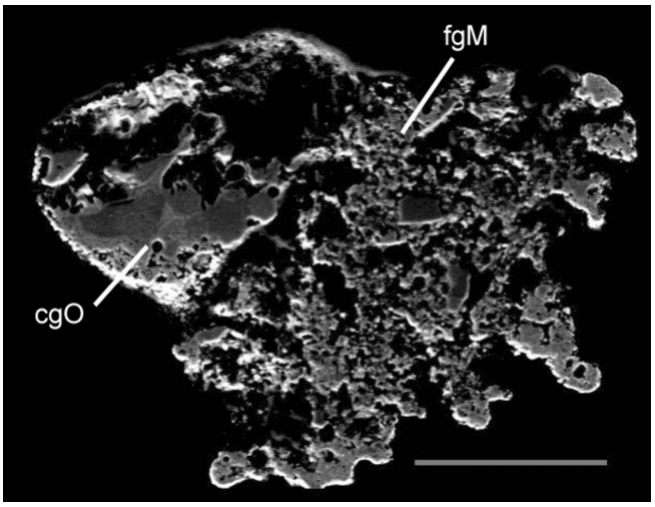

Fig. 7. A backscattered electron image of a Fg/CgMM micrometeorite (SP94-100-001) consisting of both fine-grained (FGM) and coarse-grained (IO) portions. Scale bar is 50 μm.

Unmelted MMs: Ultracarbonaceous MMs

Three large particles (>200 μm) have now been identified amongst those collected from Antarctic snow that contain considerably higher abundances of carbon than CI chondrites (Nakamura et al. 2005). The MMs are dominated by networks of amorphous carbon containing olivine, low-Ca pyroxene, pyrrhotite, and kamacite. The silicate components of these MMs have heteorogeneous compositions that suggest they are unequilibrated. One of the particles, KWP3F5, contained melted silicates suggesting intense atmospheric heating, however, another contained high abundances of presolar silicates and had evidently survived atmospheric entry without significant heating. These MMs may be cometary in origin and are termed ultracarbonaceous MMs by their discoverers.

DISCUSSION

A discussion of the more controversial aspects of micrometeorite origins and their implications is not appropriate within the current work which aims to provide a balanced framework for particle classification based on features likely to be of genetic importance. There are,

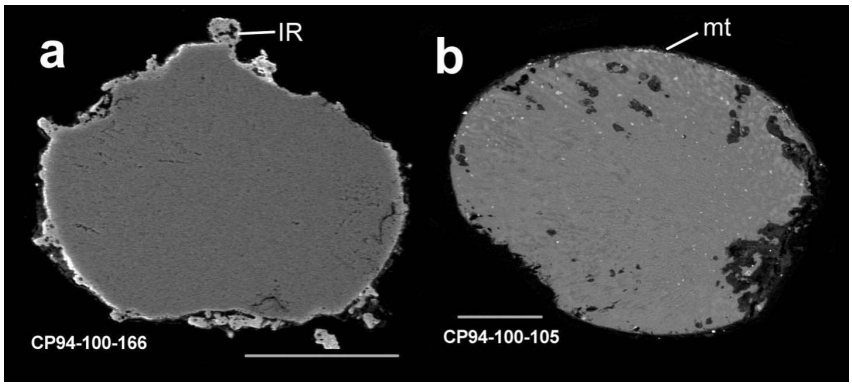

Fig. 8. Backscattered electron images of subspherical CgMMs. a) A radiating pyroxene type 2 CgMM. This particle has a vesicular igneous rim (IR) consisting fayalitic olivine microphenocrysts with interstitial glass. b) A radiating pyroxene type 2 CgMM with interstitial olivine and glass. This particle has a magnetite rim (mt). Scale bar is 50 μm.

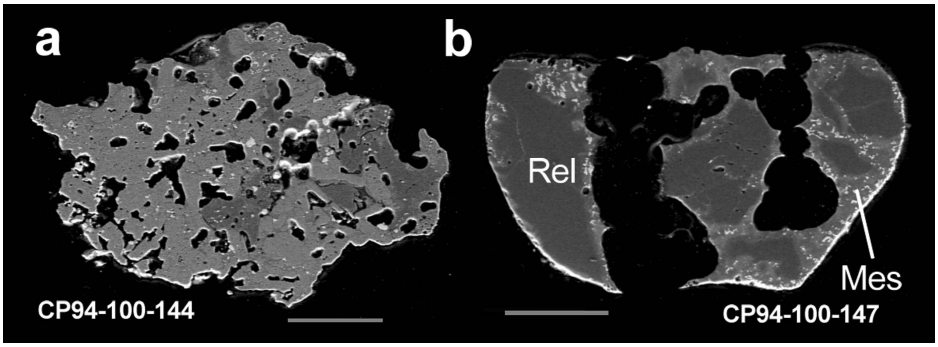

Fig. 9. Atmospheric heating effects in CgMMs. a) A vesicular CgMM in which vesicles have formed within glassy mesostasis. Note Fig. 5b, 5d, and 5e are also vesicular particles. b) A partially melted CgMM containing relict anhydrous silicates (Rel) within melted mesostasis (Mes). Although having experienced a significant degree of melting this particle retains an irregular shape. Coarse-grained spherules are shown in Figs. 1x and 1y. Scale bar is 50 μm.

however, a number of outstanding problems relating to the genetic interpretation of particles that are worthy of mention here. In particular these relate to particle types that we might expect to find among micrometeorite collections that have yet to be recognized since potentially these will require the current classification system to be extended.

In the following we discuss particle types we might expect to be present within micrometeorite collections based on the assumptions that: (1) both asteroidal and cometary dust 30–1000 μm contribute to collections retrieved from the Earth's surface, (2) asteroidal dust will include particles derived from asteroids with similar components to both chondritic and achondritic meteorites, and (3) cometary dust, at least prior to atmospheric entry, will probably include highly primitive materials similar to anhydrous IDPs.

There is, however, little agreement, even amongst the coauthors of this paper, on the exact distinction between cometary and asteroidal materials. It has often been assumed, for example, that liquid water cannot exist on cometary nuclei and thus cometary materials will not include phyllosilicates. The recent preliminary detection of hydrous silicates in comet Temple 1 by the Deep Impact mission (unpublished press release), however, indicates that some FgMMs and even CI chondrites may have a cometary origin (Gounelle et al. 2004, 2006; Lodders and Osborne 1999; McSween and Weissman 1989). The occurrence of chondrules and refractory inclusions within cometary materials has also been postulated to explain rare dense compact particles observed within cometary meteor streams (Swindle and Campins 2004) and is not precluded by models of the transport of these objects in the early solar system such as the X-wind model (Shu et al. 2001). The presence of chondrule or CAI fragments in MMs, therefore, is not conclusive evidence of an asteroidal origin. Similarly ultracarbonaceous MMs and anhydrous IDPs are assumed to be derived from comets on the basis of the presence of abundant presolar silicates and their high C-contents (Bradley 1994; Nakamura et al. 2005), however, these might also be derived from highly primitive objects in the main asteroid belt. The additional particle types, discussed below, therefore, are where possible presented without reference to parent body type since it is entirely possible that cometary and primitive asteroidal matter are closely related.

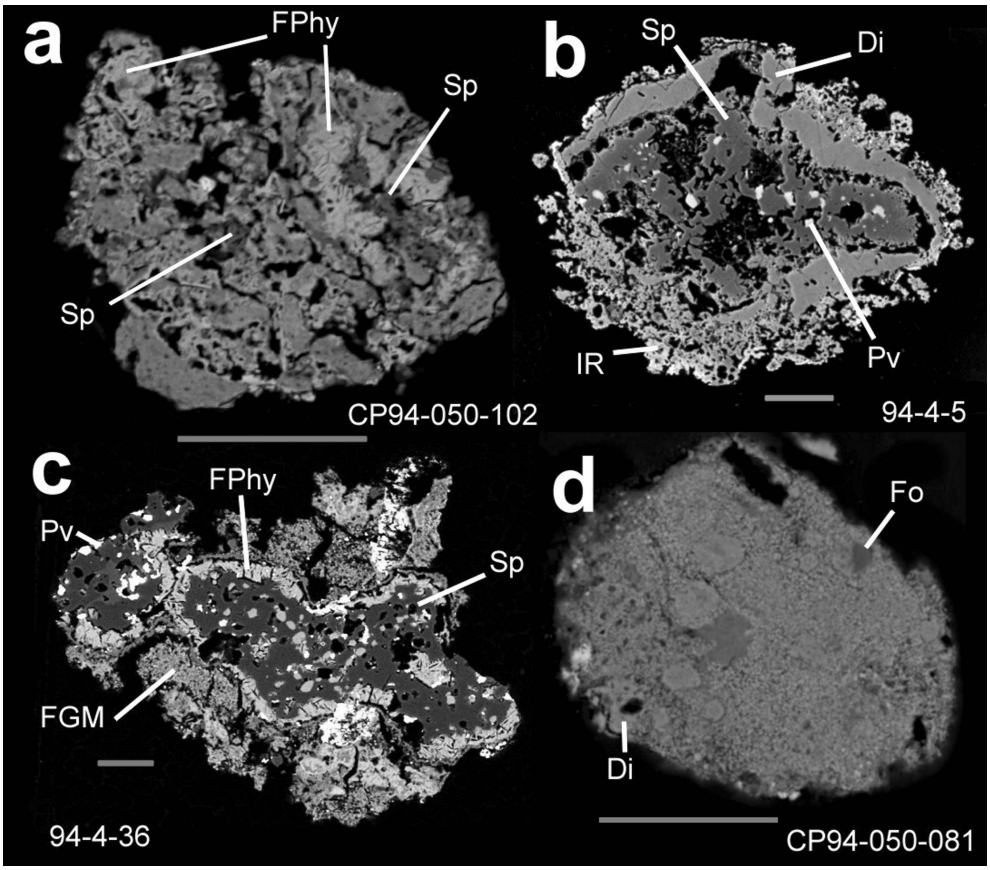

Fig. 10. Backscattered electron images of CgMMs. a) A hydrated refractory MM dominated by coarse-grained Fe-rich phyllosilicates (FPhy) and containing spinel (Sp, $MgAl_2O_4$). b) A compact spinel-diopside (Di)–perovskite (Pv) refractory MM with a scoriaceous igneous rim. c) A hydrated spinel-perovskite refractory MM with fine-grained matrix (FGM). d) A porous diopside-forsterite (Fo) refractory MM. Scale bar is 50 μm.

Achondritic Micrometeorites

Currently only a single particle has been reported that is demonstrably achondritic since it contains a large pigeonite crystal with augite exsolution lamellae and so demonstrably experienced slow cooling. This particle, which contains plagioclase, also has a depleted differentiated REE pattern suggesting crystallization from a melt generated from a depleted lithosphere (Gounelle et al. 2005a).

Several problems exist in the identification of achondritic particles, of which grain-size is probably the most significant. The large grain-sizes of most achondrites are likely to mean that dust derived from stony achondritic sources are present as single crystals, primarily of olivine or pyroxene that are unlikely to be distinct from those of primitive meteorites. Identifying an achondritic source for single crystal particles would involve trace element analyses and/or isotopic data. Consequently surveys of large numbers of particles are not practical. Only those phases with distinctive major element chemistries, such as kirschsteinite (angrites) and augite (basaltic achondrites), may be readily identified. Exsolution, in particular within pyroxenes, which indicates slow cooling may, however, also provide an indicator of an achondritic origin by which particles may be selected for more detailed chemical or isotopic analysis. Materials from primitive achondrites are likely to be particularly problematic due to their broadly chondritic mineral assemblages and trace element systematics (Mittlefehdt et al. 1998). Martian or lunar MMs that might be expected to occur within dust collections would be classified as achondritic MMs and their identification would rely on their petrology and isotopic analysis. Martian MMs are likely to be exceedingly rare since martian interplanetary dust particles will inherently evolve to Earth-crossing orbits on short timescales (Dohnanyi 1976) and they can only be produced by relatively recent impacts on Mars. In contrast, lunar MMs are likely to contribute significantly to the terrestrial dust flux for short periods following impact events on the Moon.

Entirely metallic MMs, representing dust-sized debris from metallic asteroids, or primitive metal from chondrites, have also yet to be recognized. Isotopic analyses of iron-type spherules (Engrand et al. 1998, 2005; Herzog et al. 1999), however, suggest that many of these particles may have been metallic FeNi micrometeoroids that have been oxidized

during atmospheric entry heating. The absence of unmelted metallic MMs, however, is puzzling since photometry studies of M-type asteroids imply the presence of regolith (Belskaya and Lagerkrist 1996). The presence of metal within CgMMs certainly suggests it can survive long term storage in Antarctic ice without complete oxidation. A density bias during collection of melt water is a possible explanation, however, collections derived from melting of Antarctic snow have also not yet reported metallic unmelted MMs (Duprat et al. 2003; Nakamura et al. 1999).

Chondrite-Like Micrometeorites

There are a significant number of unresolved issues related to particles derived from chondrite-like parent bodies. Materials similar to components within the known chondritic meteorite groups would be expected to occur within MM collections, however, to date most micrometeorites appear to have affinities with C1 and C2 parent bodies. These also appear to sample mainly matrix, isolated minerals, and chondrules, with rare materials from CAIs. It is likely that the absence of MMs with affinities to other chondrite groups and components of chondrites relate to either a lower abundance within the asteroid belt or selection biases due to dust production, capture by the Earth, or survival of atmospheric entry.

The absence of FgMMs with affinities to CV3 or CO3 matrix is particularly surprising considering the significant number of meteorites of these classes. One possible reason for this under-representation may be if the Eos family of main belt asteroids are the parent bodies of C3 meteorites, as suggested by asteroid spectroscopy (Nesvorny et al. 2003), since the dust band associated with this asteroid has a relatively high inclination. The latitude of CV3 and CO3 dust at 1 AU may, therefore, result in less of this material being captured by the Earth than from other, lower inclination sources (Kortenkamp and Dermett 1999). CV3 and CO3 dust may be present in low abundances in MM collections, however, particles dominated by porous assemblages of relatively fayalitic olivine, that might be analogous to CV3 and CO3 matrix (Brearley and Jones 1998), have yet to be identified.

Particles with affinities to reduced, primitive parent bodies such as the enstatite chondrites, and from highly oxidized parent bodies, such as R-chondrites, have also yet to be discovered. One type I Po CgMM, containing Si-bearing metal and silica, could have affinities to the K-chondrites or enstatite chondrites (Genge et al. 1997b), and several type II CgMMs with highly fayalitic olivines (e.g., Fa_{48}) have been identified (Genge, unpublished data) that could be derived from oxidized chondrite groups. Currently the low abundance of such particles does not warrant extension of the classification scheme for CgMMs.

Classifying CgMMs derived as chondrule fragments from parent bodies with affinities to ordinary chondrites is a particular problem since without the additional information on chondrule abundances and bulk chemistry provided by macroscopic samples these materials will be difficult to distinguish as individual particles from those derived from carbonaceous chondrites. It has been suggested that CgMMs could potentially be classified into equilibrated or unequilibrated particles, relating to type 1–3 and type 4–7 chondrites, on the basis of textural, mineralogical and chemical properties (Genge and Grady 1998b). Coarse-grained MMs containing glassy mesostases, having chemical zoning in their phenocrysts, are demonstrably unequilibrated, although such features must be shown not to have arisen during atmospheric entry. Identifying equilibrated particles is more problematic since lack of chemical zoning or glassy mesostasis does not necessarily indicate equilibration. FeO, MnO, CaO, and Cr_2O_3 abundances within olivines may, however, provide one diagnostic test (Brearley and Jones 1998).

Several C2 FgMMs have been reported in which the fine-grained matrix had spatial chemical variations of Fe/Mg closely resembling relict hydrated chondrules found in CM2 chondrites (Genge 2002). Whether such particles should be given a classification denoting such an origin is debatable since recognizing such particles is dependent on preservation of their pseudomorphed textures and it is, therefore, difficult to give quantitative criteria for their identification.

One further possibility must be considered for those particles classified as altered FgMMs that relates directly to the nature of their parent body. Implicit in the classification of a FgMM as altered is that the thermal alteration occurred during atmospheric entry. Another possibility, however, is that some altered FgMMs may represent hydrous matrix that was dehydrated due to parent body metamorphism, similar to the suggested origin of dark clasts found in a range of meteorites (Brearley and Jones 1998). Distinguishing between the effects of parent body and atmospheric heating is likely to involve detailed characterization of textures and mineralogies at the submicron scale and thus would be difficult to apply in particle surveys. The complete absence of a magnetite rim would, perhaps, be one criteria that could be used to indicate minimal entry heating. Conversely, those particles with igneous rims, which are supported by the exothermic dehydration reactions, demonstrably contained hydrated silicates during atmospheric entry (Genge 2006).

Shock State

No studies have yet examined the shock state of MMs, mainly because standard thin-section techniques for the identification of shock features in particular phases are difficult to apply to small particulates. Several textural features, which can be characterized in backscattered electron images, may, however, prove to be useful in characterizing shock in MMs. Metal-sulfide veining within anhydrous silicates is a common shock feature within chondritic

meteorites that can be readily identified, but gives little correlation with the shock scale used for meteorites (Stoeffler et al. 1991). Mosaicism within olivine may provide a means of identifying particles shocked to S4 and above, however, discriminating mosaicism from annealed granular textures in BEI images is likely to be inconclusive. Both metal-sulfide veining and mosaicism may, nevertheless, provide criteria by which particles can be selected for TEM characterization of microstructural defects to better constrain their shock state. Annealing during atmospheric entry will also complicate analysis of shock features.

Micrometeorites sampling shock melts are also likely to be difficult to distinguish from fragments of chondrules and primitive achondrites since these have broadly similar mineralogies and textures. The presence of abundant submicron FeNi metal blebs and annealed relicts may, however, provide criteria for their identification.

Highly Primitive Micrometeorites

Models of atmospheric entry heating suggest that at least a proportion of low geocentric velocity cometary dust, which would be expected to be highly primitive dust, should survive atmospheric entry at diameters up to ~100 μm (Flynn 1991; Genge 2003; Liou and Zook 1996; Love and Brownlee 1991). Most of these cometary MMs are predicted to experience significant thermal alteration, however, a small proportion are expected to survive atmospheric entry without melting. To date only the ultracarbonaceous MMs have been identified as such highly primitive, potentially cometary, micrometeorites.

One possible explanation for the paucity of MMs equivalent to anhydrous IDPs may be that these particles are extremely fragile and become disaggregated during atmospheric flight, storage in Antarctic ice and/or collection. Certainly preliminary results of a new collection made by melting of Antarctic snow indicate the presence of larger numbers of fluffy, fragile particles (Duprat et al. 2003, 2005). An alternative explanation is that cometary particles are present among MMs but more closely resemble asteroidal materials than has previously been thought.

Intensely heated cometary particles have also not been identified with any certainty. An unusual Mg-rich ScMM containing segregated FeNi metal droplets might represent one such particle on the basis of the carbon-enriched nature of anhydrous IDPs and the significant reduction of the particle (Genge and Grady 1998c). No other similar particles, however, have yet been discovered.

CONCLUSIONS

The field of "micrometeoritics" has progressed considerably in the last two decades since the pioneering collection of particles from the deep sea (Brownlee 1985) and Antarctic ice (Maurette et al. 1991). The characterization of many thousands of MMs by authors of this paper and others has now allowed groups and classes of particle to be identified and placed into a genetically significant framework. In the future, as the work of characterization of these materials progresses, rare types of MM will undoubtedly be recognized and allow MMs to be used to better constraint the diversity of asteroidal and cometary bodies within our solar system.

Acknowledgments—This paper owes much to previous authors and workers in the field of micrometeorite studies. There are too many to mention everyone, however, in particular we would like to acknowledge the pioneering efforts of Michel Maurette in the collection of Antarctic micrometeorites and Gero Kurat for his thorough characterization of these materials. We also would like to acknowledge the significant contributions made by Don Brownlee in the study of deep sea particles and the contributions of Jean Duprat and Ralph Harvey in collection and characterization of micrometeorites.

Editorial Handling—Dr. Donald Brownlee

REFERENCES

Alexander C. M. O'D. 2002. Mass-dependent fractionation of Mg, Si, and Fe isotopes in five stony cosmic spherules. *Geochimica et Cosmochimica Acta* 66:173–183.

Beckerling W. and Bischoff A. 1995. Occurrence and composition of relict minerals in micrometeorites from Greenland and Antarctica—Implications for their origins. *Planetary and Space Science* 43:435–449.

Belskaya I. N. and Lagerkvist C. I. 1996. Physical properties of M class asteroids. *Planetary and Space Science* 44:783–794.

Blanchard M. B., Brownlee D. E., Bunch T. E., Hodge P. W., and Kyte F. T. 1980. Meteoroid ablation spheres from deep sea sediments. *Earth and Planetary Science Letters* 46:178–190.

Bradley J. P. 1994. Chemically anomalous, preaccretionally irradiated grains in interplanetary dust from comets. *Science* 265: 925–929.

Brearley A. J. and Jones R. H. 1998. Chondritic meteorites. In *Planetary materials*, vol. 36, edited by Papike J. J. Washington, D.C.: Mineralogical Society of America. pp. 1–191.

Brownlee D. E. and Bates B. 1983. Meteor ablation spherules as chondrule analogs. In *Chondrules and their origins*, edited by King E. A. Houston: Lunar and Planetary Institute. pp. 10–25.

Brownlee D. E. 1985. Cosmic dust: Collection and research. *Annual Reviews of Earth and Planetary Sciences* 13:147–173.

Brownlee D. E., Love S., and Schramm L. S. 1991. Cosmic spherules and giant micrometeorites as samples of main belt asteroids (abstract). 22nd Lunar and Planetary Science Conference. p. 147.

Brownlee D. E., Bates B., and Schramm L. 1997. The elemental composition of stony cosmic spherules. *Meteoritics & Planetary Science* 32:157–175.

Clayton R. N., Mayeda T. M., and Brownlee D. E. 1986. Oxygen isotopes in deep-sea spherules. *Earth and Planetary Science Letters* 79:235–240.

Dohnanyi J. S. 1967. Sources of interplanetary dust: Asteroids. In

Interplanetary dust and the zodiacal light, vol. 48, edited by Elsasser H. and Fechtig H. Berlin: Springer-Verlag. pp. 187–206.
Dohnanyi J. S. 1976. Sources of interplanetary dust: Asteroids. In *Interplanetary dust and zodiacal light*, edited by Elsasser H. Berlin: Springer-Verlag. pp. 569–639.
Duprat J., Engrand C., Maurette M., Gounelle M., Hammer C., and Kurat G. 2003. The CONCORDIA collection: Pristine contemporary micrometeorites from central Antarctica surface snow (abstract #1727). 34th Lunar and Planetary Science Conference. CD-ROM.
Duprat J., Engrand C., Maurette M., Gounelle M., Kurat G., and Leroux H. 2005. Friable micrometeorites from central Antarctic snow (abstract #1678). 36th Lunar and Planetary Science Conference. CD-ROM.
Engrand C., Maurette M., Zolensky M. E., Kurat G., and Walter J. 1995. Electron microprobe analyses of Antarctic micrometeorites and interplanetary dust particles collected in the stratosphere (abstract). 26th Lunar and Planetary Science Conference. p. 375.
Engrand C. and Maurette M. 1998. Carbonaceous micrometeorites from Antarctica. *Meteoritics & Planetary Science* 33:565–580.
Engrand C., McKeegan K. D., Leshin L. A., and Brownlee D. E. 1998b. In situ measurement of oxygen isotopic compositions of deep-sea and Antarctic cosmic spherules (abstract #1473). 29th Lunar and Planetary Science Conference. CD-ROM.
Engrand C. 1999. Oxygen isotopic compositions of individual minerals in Antarctic micrometeorites: Further links to carbonaceous chondrites. *Geochimica et Cosmochimica Acta* 63: 2623–2636.
Engrand C., Deloule E., Robert F., Maurette M., and Kurat G. 1999. Extraterrestrial water in micrometeorites and cosmic spherules from Antarctica: An ion microprobe study. *Meteoritics & Planetary Science* 34:773–786.
Engrand C., McKeegan K. D., Leshin L. A., Herzog G. F., Schnabel C., Nyquist L. E., and Brownlee D. E. 2005. Isotopic compositions oxygen, iron, chromium, and nickel in cosmic spherules: Toward a better comprehension of atmospheric entry heating effects. *Geochimica et Cosmochimica Acta* 69:5365–5385.
Feng H., Jones K. W., Tomov S., Stewart B., Herzog G. F., Schnabel C., and Brownlee D. E. 2005. Internal structure of type I deep-sea spherules by X-ray computed microtomography. *Meteoritics & Planetary Science* 40:195–206.
Fisher G. L., Chang D. P. Y., and Brummer M. 1976. Fly ash collected from electrostatic precipitators: Microcrystalline structures and the mystery of the spheres. *Science* 7:553–555.
Flynn G. J. 1991. Survival of large micrometeorites on atmospheric entry: Implications for their sources and the flux of cometary dust (abstract). 22nd Lunar and Planetary Science Conference. p. 393.
Flynn G. J. 1995. Thermal gradients in interplanetary dust particles: The effect of an endothermic phase transition (abstract). 26th Lunar and Planetary Science Conference. p. 405.
Genge M. J., Hutchison R., and Grady M. M. 1996. Atmospheric alteration of coarse-grained Antarctic micrometeorites (abstract). *Meteoritics & Planetary Science* 31:A49.
Genge M. J., Grady M. M., and Hutchison R. 1997a. The textures and compositions of fine-grained Antarctic micrometeorites—Implications for comparisons with meteorites. *Geochimica et Cosmochimica Acta* 61:5149–5162.
Genge M. J., Grady M. M., and Hutchison R. 1997b. Free-silica in a non-chondritic micrometeorite from Antarctic ice (abstract). 28th Lunar and Planetary Science Conference. p. 405.
Genge M. J. and Grady M. M. 1998a. Melted micrometeorites from Antarctic ice with evidence for the separation of immiscible Fe-Ni-S liquids during entry heating. *Meteoritics & Planetary Science* 33:425–434.
Genge M. J. and Grady M. M. 1998b. A petrological-chemical classification scheme for coarse-grained micrometeorites. *Meteoritics & Planetary Science* 33:A56.
Genge M. J. and Grady M. M. 1998c. Melted micrometeorites from Antarctic ice with evidence for the separation of immiscible Fe-Ni-S liquids during entry heating. *Meteoritics & Planetary Science* 33:425–434.
Genge M. J. and Grady M. M. 1999. The fusion crusts of stony meteorites: Implications for the atmospheric reprocessing of extraterrestrial materials. *Meteoritics & Planetary Science* 34: 341–356.
Genge M. J., Engrand C., and Grady M. M. 2000. The parent bodies of thermally altered fine-grained micrometeorites: Comparisons with CI and CM fusion crusts (abstract). *Meteoritics & Planetary Science* 35:A59.
Genge M. J., Bradley J. P., Engrand C., Gounelle M., Harvey R. P., and Grady M. M. 2001. The petrology of fine-grained micrometeorites: Evidence for the diversity of primitive asteroids (abstract #1546). 32nd Lunar and Planetary Science Conference. CD-ROM.
Genge M. J. 2002. Hydrated chondrule fragments among micrometeorites (abstract). *Meteoritics & Planetary Science* 37: A51.
Genge M. J. and Grady M. M. 2002. The distribution of asteroids: Evidence from Antarctic micrometeorites (abstract #1010). 33rd Lunar and Planetary Science Conference. CD-ROM.
Genge M. J. 2003. Primary variations in micrometeorites with entry velocity (abstract #1151). 34th Lunar and Planetary Science Conference. CD-ROM.
Genge M. J., Gileski A., and Grady M. M. 2005. Chondrules in Antarctic micrometeorites. *Meteoritics & Planetary Science* 40: 225–238.
Genge M. J. 2006. Igneous rims on micrometeorites. *Geochimica et Cosmochimica Acta* 70:2603–2621.
Glass B. P. 1990. Tektites and microtektites: Key facts and interferences. *Tectonophysics* 171:393–404.
Gounelle M. 2000. Matière extraterrestre sur Terre: Des Océans aux protoétoiles. Ph.D. thesis, Universite Paris. In French.
Gounelle M., Devouard B., Engrand C., Genge M. J., Toppani A., and Leroux H. 2002. TEM study of Antarctic micrometeorites: A preliminary report (abstract). *Meteoritics & Planetary Science* 37:A55.
Gounelle M., Spurný P., and Bland P. 2004. The orbit of the Orgueil meteorite from historical records (abstract). *Meteoritics & Planetary Science* 39:A45.
Gounelle M., Engrand C., Chaussidon M., Zolenksy M. E., and Maurette M. 2005a. An achondritic micrometeorite from Antarctica: Expanding the solar system inventory of basaltic asteroids (abstract #1655). 36th Lunar and Planetary Science Conference. CD-ROM.
Gounelle M., Engrand C., Maurette M., Kurat G., McKeegan K. D., and Brandstaetter F. 2005b. Small Antarctic micrometeorites: A mineralogical and in site mineralogical study. *Meteoritics & Planetary Science* 40:917–932.
Gounelle M., Spurný P., and Bland P. A. 2006. The orbit and atmospheric trajectory of the Orgueil meteorite from historical records. *Meteoritics & Planetary Science* 41:135–150.
Greshake A., Hoppe P., and Bischoff A. 1996. Mineralogy, chemistry, and oxygen isotopes of refractory inclusions from stratospheric interplanetary dust particles and micrometeorites. *Meteoritics* 31:739–748.
Greshake A., Kloeck W., Arndt P., Maetz M., Flynn G. J., Bajt S., and Bischoff A. 1998. Heating experiments simulating atmospheric entry heating of micrometeorites: Clues to their parent body sources. *Meteoritics & Planetary Science* 33:267–290.
Grossman J. N., Rubin A. E., Nagahara H., and King E. A. 1988.

Properties of chondrules. In *Meteorites and the early solar system*, edited by Kerridge J. F. and Matthews M. S. Tucson, Arizona: The University of Arizona Press. pp. 619–659.

Harvey R. P., Dunbar N. W., McIntosh W. C., Esser R. P., Nishiizumi K., Taylor S., and Caffee M. W. 1998. Meteoritic event recorded in Antarctic ice. *Geology* 26:607–610.

Herzog G. F., Xue S., Hall G. S., Nyquist L. E., Shih C. Y., Weismann H., and Brownlee D. E. 1999. Isotopic and elemental composition of iron, nickel, and chromium in type I deep-sea spherules: Implications for origin and composition of the parent micrometeoroids. *Geochimica et Cosmochimica Acta* 63:1443–1457.

Hoppe P., Kurat G., Walter J., and Maurette M. 1995. Trace elements and oxygen isotopes in a CAI-bearing micrometeorite from Antarctica (abstract). 26th Lunar and Planetary Science Conference. p. 623.

Iwata N. and Imae N. 2001. The collection of Antarctic micrometeorites by JARE-41 in 2000 (abstract). *Meteoritics & Planetary Science* 36:A89.

Kortenkamp S. J. and Dermott S. F. 1999. Accretion of interplanetary dust particles by the Earth. *Icarus* 135:469–495.

Kurat G., Koeberl C., Presper T., Franz B., and Maurette M. 1994. Petrology and geochemistry of Antarctic micrometeorites. *Geochimica et Cosmochimica Acta* 58:3879–3904.

Lindstrom D. J. and Klock E. 1992. Analyses of 24 unmelted Antarctic micrometeorites by instrumental neutron activation analysis. *Meteoritics* 27:250.

Liou J. C. and Zook H. A. 1996. Comets as a source of low eccentricity and low inclination interplanetary dust particles. *Icarus* 123:491–502.

Lodders K. and Osborne R. 1999. Perspectives on the comet-asteroid-meteorite link. *Space Science Reviews* 90:289–297.

Love S. G. and Brownlee D. E. 1991. Heating and thermal transformation of micrometeoroids entering the Earth's atmosphere. *Icarus* 89:26–43.

Maurette M., Olinger C., Michel-Levy M. C., Kurat G., Pourchet M., Brandstatter F., and Bourot-Denise M. 1991. A collection of diverse micrometeorites recovered from 100 tonnes of Antarctic blue ice. *Nature* 351:44–47.

McSween H. Y. Jr. and Weissman P. R. 1989. Cosmochemical implications of the physical processing of cometary nuclei. *Geochimica et Cosmochimica Acta* 53:3263–3271.

Mittlefehdt D. W., McCoy T. J., Goodrich C. A., and Kracher A. 1998. Non-chondritic meteorites from asteroidal bodies. In *Planetary materials*, vol. 36, edited by Papike J. J. Washington, D.C.: Mineralogical Society of America. pp. 4-1–4-195.

Nakamura K., Nogushi T., Ozono Y., Osawa T., and Nagao K. 2005. Mineralogy of ultracarbonaceous large micrometeorites (abstract). *Meteoritics & Planetary Science* 40:A110.

Nakamura T., Imae N., Nakai I., Noguchi T., Yano H., Terada K., Murakami T., Fukuoka T., Nogami K.-I., Ohashi H., Nozaki W., Hashimoto M., Kondo N., Matsuzaki H., Ichikawa O., and Ohmori R. 1999. Antarctic micrometeorites collected at the Dome Fuji Station. 23rd Symposium on Antarctic Meteorites. p. 183.

Nakamura T., Noguchi T., Yada T., Nakamuta Y., and Takaoka N. 2001. Bulk mineralogy of individual micrometeorites determined by X-ray diffraction analysis and transmission electron microscopy. *Geochimica et Cosmochimica Acta* 65: 4385–4397.

Nesvorny D., Bottke W. F., Levison H. F., and Dones L. 2003. Recent origin of the solar system dust bands. *The Astrophysical Journal* 591:486–497.

Nininger H. H. 1956. *Arizona's Meteor Crater*. Sedona, Arizona: World Press. 232 p.

Noguchi T. and Nakamura T. 2000. Mineralogy of Antarctic micrometeorites recovered from the Dome Fuji Station. 24th Symposium on Antarctic Meteorites, p. 285.

Noguchi T., Nakamura T., and Nozaki W. 2002. Mineralogy of phyllosilicate-rich micrometeorites and comparison with Tagish Lake and Sayama meteorites. *Earth and Planetary Science Letters* 202:229–246.

Olinger C. T. 1990. Isotopic measurements of solar noble gases in individual micrometeorites from Greenland and Antarctica. Ph.D. thesis, University of Washington.

Raisbeck G. M. and Yiou F. 1987. ^{10}Be and ^{26}Al in micrometeorites from Greenland ice. *Meteoritics* 22:485–486.

Raisbeck G. M. and Yiou F. 1989. Cosmic-ray exposure ages of cosmic spherules (abstract). *Meteoritics* 24:318.

Rietmeijer F. J. M. 1998. Interplanetary dust particles. In *Planetary materials*, vol. 36, edited by Papike J. J. Washington, D. C.: Mineralogical Society of America. pp. 28–119.

Shu F. H., Shang H., Gounelle M., Glassgold A. E., and Lee T. 2001. The origin of chondrules and refractory inclusions in chondritic meteorites. *The Astrophysical Journal* 548:1029–1050.

Stöffler D., Keil K., and Scott E. R. D. 1991. Shock metamorphism of ordinary chondrites. *Geochimica et Cosmochimica Acta* 55: 3845–3867.

Swindle T. D. and Campins H. 2004. Do comets have chondrules and CAIs? Evidence from the Leonid meteors. *Meteoritics & Planetary Science* 39:1733–1740.

Taylor S. and Brownlee D. E. 1991. Cosmic spherules in the geological record. *Meteoritics* 26:203–211.

Taylor S., Lever J. H., and Harvey R. P. 1998. Accretion rate of cosmic spherules measured at the South Pole. *Nature* 392: 899–903.

Taylor S., Lever J. H., and Harvey R. P. 2000. Numbers, types, and compositions of an unbiased collection of cosmic spherules. *Meteoritics & Planetary Science* 55:651–666.

Toppani A., Libourel G., Engrand C., and Maurette M. 2001. Experimental simulation of atmospheric entry of micrometeorites. *Meteoritics & Planetary Science* 36:1377–1396.

Toppani A. and Libourel G. 2003. Factors controlling compositions of cosmic spinerls: Application to atmospheric entry conditions of meteoritic materials. *Geochimica et Cosmochimica Acta* 67: 4621–4638.

Whipple F. 1951. The theory of micrometeorites. Part II. In heterothermal atmospheres. *Proceedings of the National Academy of Sciences* 36:687–695.

Yada T. and Kojima H. 2000. The collection of micrometeorites from bare ice of the Yamato Mountains in Antarctica in austral summer of 1998 (abstract #1528). 31st Lunar and Planetary Science Conference. CD-ROM.

Zolensky M. E., Nakamura K., Gounelle M., Mikouchi T., Kasama T., Tachikawa O., and Tonui E. 2002. Mineralogy of Tagish Lake: An ungrouped type 2 carbonaceous chondrite. *Meteoritics & Planetary Science* 37:737–761.

Meteoritics & Planetary Science 34, 773–786 (1999)

Extraterrestrial water in micrometeorites and cosmic spherules from Antarctica: An ion microprobe study

CÉCILE ENGRAND[1]*, ETIENNE DELOULE[2], FRANÇOIS ROBERT[3], MICHEL MAURETTE[1] AND GERO KURAT[4]

[1]C.S.N.S.M. Bâtiment 104, F-91405 Orsay Campus, France
[2]CRPG-CNRS, 15 rue Notre-Dame des Pauvres, BP20, F-54501 Vandoeuvre les Nancy Cedex, France
[3]Laboratoire de Minéralogie, CNRS-URA736, Muséum d'Histoire Naturelle, 61 rue Buffon, F-75005 Paris, France
[4]Naturhistorisches Museum, Mineralogische Abteilung, Postfach 417, A-1014 Vienna, Austria
*Correspondence author's e-mail address: engrand@csnsm.in2p3.fr

(Received 1998 August 27; accepted in revised form 1999 June 17)

Abstract–The D/H ratios and water contents were measured by ion microprobe analysis in 52 individual Antarctic micrometeorites (AMMs) and 10 Antarctic cosmic spherules (ACSs) containing nuggets of iron hydroxide (COPS phase). In AMMs, δD values vary from –366 to +249‰ and water contents lie between 0.4–3.7 wt%. The COPS nuggets in cosmic spherules have high water contents (2 to 8 wt%) and exhibit δD values from –144 to +167‰, which is indicative of an extraterrestrial origin of their constituent water. The silicate portion of ACSs also contain extraterrestrial H equivalent to ~0.1 to 1.2 wt% water. Deuterium-exchange experiments were performed with isotopically spiked water. These experiments demonstrate that water in mineral phases of AMMs and ACSs is indigenous and does not result from contamination during residence in Antarctic ice. The frequency distribution of D/H ratios in AMMs allows us to further narrow the relationship between AMMs and carbonaceous chondrites to CM and CI chondrites but contrasts with that of stratospheric interplanetary dust particles (IDPs) of similar sizes (from ~10 to 50 μm). The relatively narrow range of D/H ratios measured in AMMs as well as in ACSs (which are more resistant and thus less susceptible to collection biases) suggests that D-rich IDP-like particles are very rare in our AMMs collections. This indicates that these D-rich grains might constitute a minor fraction of the micrometeorite flux in the interplanetary medium and that possible collection biases in Antarctica would not be responsible for their strong depletion in the AMMs collections.

INTRODUCTION

The most recent estimate for the meteorite flux onto the Earth (~10 tons per year; Bland *et al.*, 1996) amounts to only a fraction of the dust flux (~10 000–20 000 tons per year) as estimated from abundances in the Greenland (Hammer and Maurette, 1996) and Antarctica ice sheets (Taylor *et al.*, 1998) as well as in other types of sediments (Peucker-Ehrenbrink, 1996). Direct measurements in near-Earth interplanetary space gives a flux of 40 000 ± 20 000 tons per year (Love and Brownlee, 1993), which was subsequently revised downward to a value of 30 000 tons per year (Brownlee, pers. comm.), and which is mainly carried by particles with a mean diameter of ~200 μm. Large Antarctic micrometeorites (AMMs) of the 50–400 μm size range are samples of such matter that survived the hypervelocity impact with the Earth's atmosphere without being volatilized or transformed into cosmic spherules, and they represent by far the dominant extraterrestrial material reaching the Earth's surface today. Cosmogenic isotope studies, such as ^{21}Ne (Olinger *et al.*, 1990), ^{10}Be and ^{26}Al (Nishiizumi *et al.*, 1991; Raisbeck and Yiou, 1987; Raisbeck *et al.*, 1986), show that AMMs were individually exposed in space and therefore are not fragments of larger meteoroids.

Chemical and mineralogical data (see Kurat, 1998; Kurat *et al.*, 1994) indicate that ~99% of the AMMs are related to carbonaceous chondrites (which constitute only ~4% of the meteorite falls). The closest meteoritic equivalents appear to be a matter similar to CI, CM, and CR chondrites (Kurat, 1998; Kurat *et al.*, 1994). However, AMMs exhibit higher C/O ratios than CI and CM chondrites (Engrand and Maurette, 1998), a marked depletion of chondrules (Walter *et al.*, 1995a), and other mineralogical differences (Kurat, 1998). Thus, the most abundant matter accreted by the Earth today is not represented in the meteorite collections (Engrand and Maurette, 1998; Kurat *et al.*, 1994; Maurette *et al.*, 1996).

Micrometeorites are also collected in the stratosphere (*e.g.*, Brownlee, 1985). These so-called stratospheric interplanetary dust particles (IDPs) show differences with both AMMs and carbonaceous chondrites. In particular, stratospheric IDP collections contain a subgroup of porous-anhydrous particles, many of which show marked anomalies in their H and/or N-isotopic compositions (Messenger and Walker, 1997), and a unique component (GEMS: "glass embedded with metal and sulfides"; Bradley, 1994) that has no equivalent in AMMs and carbonaceous chondrites.

We report here ion microprobe measurements of the D/H ratios and water contents of 52 AMMs and 10 Antarctic cosmic spherules (ACSs) selected from the 1991 and 1994 collections in the blue ice fields of Cap-Prudhomme, Antarctica (Maurette *et al.*, 1991, 1994). Our major objectives were to get further clues about the relationships between AMMs and both meteorites and stratospheric IDPs; the effects of frictional heating and Antarctic weathering on D/H ratios; and hopefully, on the parent bodies of AMMs and IDPs.

EXPERIMENTAL

Sampling

Micrometeorites were collected in Antarctica during the 1991 and 1994 field expeditions by melting large quantities of clean blue ice and gently filtering the melt ice water using a stack of four stainless steel sieves (see Maurette *et al.*, 1994; for more details). In 1994, the use of stainless steel or Teflon for all parts in contact with hot water, as well as the heaviest snow falls recorded over the last 44 years, yielded the cleanest collection in terms of both the chemical composition of AMMs and their higher concentration (in number of grains) in the glacial sand. The 1994 samples were kept in

TABLE 1a. Electron microprobe analyses of micrometeorites mounted in polished sections (oxide wt%).

Sample	Type	Size range (μm)	Year of collect	Number of analyses	Na_2O	MgO	Al_2O_3	SiO_2	P_2O_5	SO_3	K_2O	CaO	TiO_2	Cr_2O_3	MnO	FeO	NiO
5M2	FG	100–400	1991	1	0.19	24.5	1.84	33.1	n.a.	0.13	0.05	0.48	0.11	0.94	0.20	25.2	0.02
5M3	FG	100–400	1991	1	0.19	14.2	1.80	34.3	n.a.	0.66	0.08	1.20	0.08	0.47	0.27	21.6	0.21
5M5	FG	100–400	1991	1	0.29	11.0	2.21	24.8	n.a.	0.38	0.13	0.99	0.12	0.30	0.17	30.6	0.14
5M10	FG	100–400	1991	1	0.38	10.8	1.65	20.2	n.a.	n.a.	0.00	0.19	0.14	0.64	0.03	26.6	0.21
5M10(2)	FG	100–400	1991	1	0.19	7.7	1.39	17.7	n.a.	0.36	0.00	0.16	0.10	0.54	0.04	35.6	0.13
92-14-06	FG	100–400	1991	1	n.a.	17.6	1.71	16.9	n.a.	n.a.	n.a.	n.a.	n.a.	0.23	0.14	38.2	n.a.
92-14-08	FG	100–400	1991	1	n.a.	14.9	2.59	26.6	n.a.	n.a.	n.a.	n.a.	n.a.	0.28	0.24	44.1	n.a.
92-14-12	FG	100–400	1991	1	n.a.	20.3	2.52	42.2	n.a.	n.a.	n.a.	n.a.	n.a.	0.55	0.28	20.3	n.a.
94-10-09	FG	100–400	1994	1	0.11	22.7	2.01	33.0	n.a.	0.85	0.00	0.15	0.13	0.61	0.29	30.1	0.11
94-10-11	FG	100–400	1994	1	0.27	16.2	2.57	37.3	n.a.	1.55	0.03	0.35	0.14	0.49	0.23	21.3	0.20
94-10-14	FG	100–400	1994	1	0.11	11.4	1.39	36.0	n.a.	1.18	0.00	0.99	0.11	0.35	0.17	24.8	0.73
94-10-24	FG	100–400	1994	1	0.15	19.8	1.87	32.5	n.a.	1.58	0.00	0.06	0.12	0.35	0.27	33.3	0.19
94-10-26	FG	100–400	1994	1	0.10	11.3	2.03	25.5	n.a.	7.50	0.00	0.25	0.06	0.52	0.08	33.1	0.57
94-10-31	FG	100–400	1994	1	0.16	19.5	1.95	33.9	n.a.	1.58	0.00	0.10	0.10	0.53	0.30	28.8	0.26
94-10-34	FG	100–400	1994	1	0.09	13.1	1.34	24.1	n.a.	1.90	0.00	0.19	0.10	0.60	0.28	39.8	0.38
93-7-03	FG	25–50	1991	1	1.29	15.3	5.10	40.5	0.00	0.00	0.24	8.11	0.00	0.37	0.00	28.0	1.14
93-7-06	FG	25–50	1991	1	0.51	12.5	3.62	29.0	0.96	4.86	0.30	0.30	0.45	0.69	0.32	45.6	0.91
93-7-10	FG	25–50	1991	1	0.92	15.3	3.31	32.7	0.04	1.31	0.16	2.58	0.00	0.40	0.68	42.5	0.08
93-7-14	FG	25–50	1991	1	1.57	19.3	3.19	36.1	0.02	4.09	0.06	0.46	0.00	0.61	0.33	33.6	0.66
93-7-19	FG	25–50	1991	1	0.81	26.5	3.05	45.7	0.47	2.14	0.11	1.95	0.00	0.26	0.50	17.6	0.96
93-7-25	FG	25–50	1991	1	0.14	12.6	2.59	35.5	0.00	0.57	0.00	0.16	0.09	0.14	0.39	47.6	0.26
5M8	SC	100–400	1991	1	0.01	13.7	1.08	19.4	n.a.	0.06	0.03	0.16	0.08	0.36	0.24	31.0	0.10
94-10-36	SC	100–400	1994	1	0.21	17.1	1.48	28.9	n.a.	1.59	0.00	0.64	0.10	0.45	0.26	27.5	0.21
93-7-01	SC	25–50	1991	1	0.58	20.8	2.43	27.5	0.00	0.36	0.02	0.00	0.06	0.68	0.15	45.8	1.57
93-7-09	SC	25–50	1991	1	0.76	19.8	4.36	52.0	0.00	0.00	0.13	0.94	0.00	1.00	0.76	19.9	0.46
93-7-21	SC	25–50	1991	1	0.90	15.9	4.11	31.7	0.79	2.06	0.35	1.19	0.49	1.18	0.06	40.7	0.55
5M1	ACS	100–400	1991	1	0.01	26.4	2.89	37.3	n.a.	0.15	0.00	1.08	0.18	0.43	0.28	27.3	0.03
5M1(2)	ACS	100–400	1991	1	0.00	20.6	1.59	29.0	n.a.	0.22	0.00	0.63	0.11	0.35	0.17	38.7	0.09
92-23B-77	ACS	100–400	1991	1	n.a.	28.8	2.29	44.0	n.a.	n.a.	n.a.	n.a.	n.a.	0.43	0.64	20.8	n.a.
93-6C	ACS	100–400	1991	2	0.00	25.8	2.43	43.0	n.a.	0.03	0.00	0.30	0.09	0.29	0.14	18.4	0.00
95-11-01	ACS	100–400	1994	1	0.00	23.7	1.82	40.8	0.08	0.01	0.00	1.99	0.12	0.48	0.33	26.5	0.01
95-11-01 (2)	ACS	100–400	1994	1	0.00	25.2	1.56	40.4	0.06	0.04	0.00	1.71	0.08	0.47	0.35	26.1	0.00
95-11-02	ACS	100–400	1994	1	0.01	27.5	2.40	41.1	0.05	0.03	0.00	1.84	0.10	0.43	0.17	23.2	0.00
95-11-02 (2)	ACS	100–400	1994	1	0.00	27.2	2.41	41.7	0.04	0.07	0.00	1.83	0.10	0.49	0.18	23.5	0.00
95-11-03	ACS	100–400	1994	1	0.00	23.7	3.35	42.6	0.07	0.14	0.00	3.30	n.a.	0.42	0.36	24.8	0.02
n.a.	ACS	100–400	1994	1	0.01	23.2	3.15	42.4	0.06	0.12	0.00	3.30	n.a.	0.53	0.39	25.6	0.00
95-7A	ACS	100–400	1994	1	0.01	23.9	1.87	37.6	n.a.	0.04	0.00	1.71	0.10	0.56	0.29	22.2	0.01
95-7B(+glass)	ACS	100–400	1994	1	0.01	17.5	2.03	32.3	n.a.	0.07	0.00	2.58	0.06	0.41	0.27	30.3	0.01
95-7B(-glass)	ACS	100–400	1994	1	0.00	18.6	0.65	28.4	n.a.	0.07	0.00	0.71	0.06	0.46	0.24	35.5	0.00
95-7C	ACS	100–400	1994	1	0.00	29.7	6.90	42.6	n.a.	0.01	0.00	6.53	0.27	0.26	0.10	6.2	0.00
95-7D	ACS	100–400	1994	1	0.02	21.3	2.49	39.1	n.a.	0.07	0.05	2.40	0.10	0.57	0.45	14.8	0.02
92-23B-77	COPS	nugget	1991	2	n.a.	1.2	0.42	4.1	n.a.	n.a.	n.a.	n.a.	n.a.	0.11	0.08	71.5	n.a.
93-6C	COPS	nugget	1991	2	0.06	0.0	0.49	1.6	n.a.	1.84	0.00	0.04	0.04	0.01	0.02	56.4	1.84
95-11-01	COPS	nugget	1994	1	0.02	0.0	0.08	1.3	2.48	2.05	0.00	0.05	n.a.	0.10	0.01	71.8	2.67
95-11-02	COPS	nugget	1994	1	0.03	0.0	0.28	1.5	0.52	1.98	0.00	0.02	n.a.	0.12	0.00	73.0	3.15
95-11-03	COPS	nugget	1994	1	0.00	0.0	0.07	1.3	0.02	6.30	0.00	0.05	n.a.	0.01	0.00	76.3	5.80
95-7A	COPS	nugget	1994	1	0.02	0.0	0.36	2.8	n.a.	4.00	0.00	0.00	0.03	0.12	0.02	74.1	7.72
95-7D	COPS	nugget	1994	1	0.05	0.0	0.39	5.5	n.a.	6.00	0.00	0.07	0.03	0.33	0.08	66.0	1.27

n.a. = not analyzed.
These analyses are used to calculate the isotopic instrumental fractionation factor for the ion microprobe analyses (see Fig. 1 and Table 3). Two types of preparation were used: polished sections (Table 1a) and fragments crushed on Au foils (Table 1b). The samples are arranged by textural type for each half of the table (FG = fine-grained particle, SC = scoriaceous particle, ACS = Antarctic cosmic spherule, COPS = ferrihydrite "COPS" nugget; see Fig. 3 and text for details). The size range of the grains, their year of collection in Antarctica, and the number of D/H analyses on each micrometeorite are given in columns 3 to 5, respectively.

refrozen melt ice water since the time of their recovery whereas the particles from the 1991 collection were dried in the field at 70 °C for one hour. Since 1994, the preselection and the microhandling of the particles has been done in a clean room at C.S.N.S.M. in Orsay.

Antarctic micrometeorites and ACSs were extracted from three size fractions (25–50, 50–100, and 100–400 μm). Whereas AMMs were selected at random in the glacial sand, the preselected ACSs were of a particular type, exhibiting nuggets of an iron oxyhydroxide ("COPS" phase, see Engrand *et al.*, 1993; Genge and Grady, 1998) protruding on their external surface (see Results and Discussion). Antarctic micrometeorites from the two largest size fractions were broken into three or more fragments, one of which

TABLE 1b. Electron microprobe analyses of micrometeorites crushed on Au foils (oxide wt%).

Sample	Type	Size range (μm)	Year of collect	Number of analyses	Na_2O	MgO	Al_2O_3	SiO_2	P_2O_5	SO_3	K_2O	CaO	TiO_2	Cr_2O_3	MnO	FeO	NiO
94-10-11	FG	100–400	1994	1	0.27	16.2	2.57	37.3	n.a.	1.55	0.03	0.35	0.14	0.49	0.23	21.3	0.20
94-10-31	FG	100–400	1994	1	0.16	19.5	1.95	33.9	n.a.	1.58	0.00	0.10	0.10	0.53	0.30	28.8	0.26
94-18-03	FG	100–400	1994	1	0.47	16.4	2.71	40.3	0.37	0.54	0.07	0.37	0.13	0.50	0.16	21.8	0.29
94-18-07	FG	100–400	1994	1	0.14	14.3	2.11	21.9	0.24	0.49	0.02	0.50	0.12	0.74	0.20	41.1	0.36
94-18-12	FG	100–400	1994	1	0.10	13.9	1.77	24.3	0.49	0.52	0.03	0.14	0.16	0.56	0.15	20.8	0.18
94-18-13	FG	100–400	1994	1	0.11	17.7	2.18	36.0	0.13	0.99	0.05	3.03	0.10	0.43	0.31	27.1	0.41
94-18-17	FG	100–400	1994	5	0.16	17.1	1.69	25.2	0.29	0.34	0.01	0.95	0.09	0.58	0.37	37.0	0.17
94-18-20	FG	100–400	1994	3	0.14	19.8	1.13	23.0	0.12	0.31	0.06	0.78	0.03	0.37	0.34	40.0	0.38
94-18-21	FG	100–400	1994	2	0.27	15.5	2.34	28.0	0.25	0.43	0.03	0.23	0.10	0.34	0.25	39.0	0.46
94-18-23	FG	100–400	1994	2	0.31	17.3	2.52	27.1	0.38	0.37	0.08	1.12	0.10	0.58	0.43	35.3	0.42
94-18-26	FG	100–400	1994	1	0.14	8.6	1.16	20.3	1.00	1.46	0.03	0.36	0.15	0.55	0.08	34.3	0.13
94-18-27	FG	100–400	1994	1	0.28	21.2	2.59	35.7	0.75	5.03	0.04	0.44	0.09	0.57	0.15	23.1	1.05
94-18-28	FG	100–400	1994	1	0.50	14.2	1.82	30.1	0.22	0.84	0.14	0.53	0.16	0.59	0.20	31.6	0.16
94-18-29	FG	100–400	1994	1	0.10	12.4	1.76	23.8	0.58	0.75	0.04	0.12	0.16	1.05	0.19	38.7	0.25
95-1-04	FG	50–100	1994	1	0.25	17.4	3.39	40.7	1.04	0.57	0.15	0.13	0.16	0.50	0.09	17.9	0.11
95-1-08	FG	50–100	1994	2	0.34	16.5	2.42	37.9	0.24	0.64	0.09	0.16	0.05	0.55	0.13	19.5	0.43
95-1-12	FG	50–100	1994	1	0.40	15.0	2.53	32.0	0.69	0.14	0.11	0.11	0.16	0.50	0.15	30.3	0.13
95-1-22	FG	50–100	1994	1	0.51	14.9	1.41	29.8	0.88	0.34	0.17	0.33	0.09	0.28	0.15	34.2	0.01
95-1-24	FG	50–100	1994	1	0.38	19.1	2.25	37.0	0.35	0.77	0.10	0.11	0.18	0.59	0.19	21.0	0.12
95-1-25	FG	50–100	1994	1	0.19	15.0	2.31	31.6	1.27	0.56	0.08	0.70	0.13	0.26	0.20	29.5	0.26
94-18-04	SC	100–400	1994	1	0.46	13.6	2.16	26.3	0.68	0.46	0.11	0.84	0.13	0.56	0.23	41.5	0.26
94-18-05	SC	100–400	1994	1	0.29	17.3	1.42	28.1	0.13	0.26	0.02	0.47	0.12	0.41	0.39	35.4	0.07
94-18-25	SC	100–400	1994	1	0.49	20.7	2.13	33.1	0.67	0.67	0.09	0.59	0.10	0.55	0.33	27.1	0.07
95-1-06	SC	50–100	1994	1	0.41	12.7	2.09	25.7	0.74	0.42	0.10	0.65	0.12	0.71	0.30	35.8	0.19
95-1-11	SC	50–100	1994	1	0.18	20.9	2.14	31.2	0.31	0.42	0.05	0.53	0.09	0.44	0.26	31.0	0.32
95-1-14	SC	50–100	1994	1	0.22	13.1	1.76	24.7	2.01	0.36	0.08	0.26	0.10	0.33	0.27	31.8	0.09
95-1-16	SC	50–100	1994	1	0.79	20.9	2.14	34.8	0.15	0.16	0.20	0.26	0.08	0.43	0.34	26.5	0.15
95-1-18	SC	50–100	1994	1	0.29	23.8	0.99	32.4	0.83	0.26	0.12	0.91	0.10	0.40	0.83	26.4	0.14
95-1-19	SC	50–100	1994	1	0.83	17.0	2.49	39.4	0.74	0.33	0.21	0.23	0.16	0.49	0.18	23.4	0.17

n.a. = not analyzed.
These analyses are used to calculate the isotopic instrumental fractionation factor for the ion microprobe analyses (see Fig. 1 and Table 3). Two types of preparation were used: polished sections (Table 1a) and fragments crushed on Au foils (Table 1b). The samples are arranged by textural type for each half of the table (FG = fine-grained particle, SC = scoriaceous particle; see Fig. 3 and text for details). The size range of the grains, their year of collection in Antarctica, and the number of D/H analyses on each micrometeorite are given in columns 3 to 5, respectively.

was embedded in epoxy resin and polished. For some AMMs, a second fragment was crushed into a Au foil in order to test the influence of the resin on the D/H ratio (see below). The 25–50 μm size particles and the ACSs were mounted in polished sections but not crushed on Au foils.

Analytical scanning electron microscopy (SEM) at the Natural History Museum of Vienna was used for a first characterization of AMMs and ACSs. For taxonomic and ion microprobe calibration purposes, the chemical composition of each AMM and ACS was measured using the electron microprobes at the Natural History Museums of Paris and Vienna. Each value given in Table 1 is the average of two to five analyses obtained on areas of about $5 \times 5\ \mu m^2$ for each particle. For the AMMs, the sum of the analyses, as expressed in oxide weight percent, typically lies between ~75 and ~85%. The resulting mass deficit is attributed to sample porosity and to the presence of light elements (including H and C) that were not analyzed with the electron microprobe.

Thirty-one AMMs and 10 ACSs from the largest size fraction (100–400 μm) as well as 12 AMMs from the intermediate size fraction (50–100 μm) were selected for ion microprobe analyses. Moreover, measurements of nine AMMs from the smallest size fraction (25–50 μm) were also made for comparison with stratospheric IDPs of the same size range. The samples analyzed with their type of preparation, their textural type, their size, their year of collection, and the number of spot analyses are also summarized in Table 1.

Ion Microprobe Analyses

Calibration and Precision–We used the Nancy Cameca IMS 3f ion microprobe, which allows routine measurements of D/H ratios in a volume of ~200 μm^3 using an primary O^- beam (*e.g.*, Deloule *et al.*, 1991; Deloule and Robert, 1995). With this kind of primary beam, the emission of H from the H-bearing silicate phases dominates (by a factor >100) that of organic H from the sample (Deloule and Robert, 1995). We thus assume that the contribution of H coming from organic matter is negligible in our analyses and that we measured the D/H ratios of the constituent water.

Samples were Au coated and then kept in an oven at 50 °C in order to minimize water adsorption. To reduce H contamination, moisture from evaporation of adsorbed water in the ion probe was removed by baking the ion microprobe at 120 °C after each sample introduction, and by using a liquid nitrogen trap (Deloule *et al.*, 1991). A negative primary O beam with a current ranging from 4 to 8 nA was focused to a 10–15 μm diameter spot. Positive secondary ions were collected using a 150 μm imaged field with a 60 μm diameter transmitted field.

The mass resolving power was set at 1800 in order to resolve the H_2^+ interference from D^+. The energy slit was open at ±25 eV and

no energy filtering was applied. Data were collected in peak jumping mode with counting times of 3, 2, and 15 s for H^+, H_2^+, and D^+, respectively. Successive measurement cycles were accumulated for 60–75 min on each point. The electron multiplier was used in pulse counting mode with a dead time of 20 ± 2 ns that resulted in negligible corrections for the counting rates. The H_2/H ratio was used to monitor H contamination at the sample's surface, and analyses with H_2/H ratio higher than 10^{-3} were rejected. The statistical treatment of the analyses usually removes the first few cycles of the analyses, due to a stability problem of the magnet. Note that the counting time (hence counting statistics) was systematically set to a lower value for the smallest AMMs (25–50 μm) than for the largest ones.

The H^+ secondary beam intensity, normalized to the primary beam intensity, was converted into water concentration through calibrations made on hydroxylated minerals (amphibole and micas; cf., Table 2). The relative precision on water concentrations in hydroxylated minerals is ±10%. For lower water contents (<1 wt%) the possible systematic error can reach a factor of 2.

Hydrogen isotopic compositions are reported both as D/H ratios and as δD values: $\delta D\ (‰) = [(D/H)_{sample}/(D/H)_{SMOW} - 1] \times 1000$, with $(D/H)_{SMOW} = 155.76 \times 10^{-6}$.

Instrumental mass fractionation (Shimizu and Hart, 1982; Slodzian *et al.*, 1980) was measured on standards (cf., Table 2) prior to and after each set of analyses. The mineral standards were either mounted on polished sections or pressed into Au foils to match the mode of preparation of the AMMs analyzed. The instrumental isotopic fractionation factor (α_{ins}, defined as the ratio of the measured ratio to the true ratio) in hydroxylated silicate minerals ranges from 0.70 to 0.48 (see Fig. 1). It depends on the chemical composition of the sample and is linearly related to the Mg/(Mg + Fe) atomic ratio (Mg#). Therefore, several silicate standards with different Mg# values were used, and an appropriate α_{ins} value (noted $\alpha_{Mg\#}$ in Table 3) has been determined for each sample. A variation of the Mg# value of 0.1 corresponds to a change in the calculated δD value of ~40‰. Including the possible error on the estimation of the α_{ins} value, the maximum systematic bias on the D/H ratio (*i.e.*, the error on the calibration line definition and on the Mg# value) is 2.5%, and the accuracy (*i.e.*, the analytical error and systematic bias quadratically added) is ±3.5%, including reproducibility (Deloule and Robert, 1995). Due to counting statistical limitations, the overall uncertainty for the smallest samples (25–50 μm) is estimated to be ~±7%.

An iron oxyhydroxide phase has been observed in all textural types of AMMs as well as in ACSs. Therefore the D/H ratio of a terrestrial goethite sample was measured by both ion probe and conventional mass spectrometry (see pisolite, in Table 2). The α_{ins} value for goethite (noted α_{FeOOH} in Table 3) is close to α_{ins} for the Fe-rich silicate endmember (see Fig. 1).

Antarctic Micrometeorites Analyses–In the case of AMM analyses for which the analyzed area (~15 μm in diameter) could include both silicate and iron oxyhydroxide, we used the electron microprobe chemical analysis of the same area to calculate the proportion of each phase, assuming a (Fe + Mg)/(Si + Al) atomic ratio of 1/1.8 in the silicate, which is the ratio observed for two typical AMMs (# 95-1-14 and # 94-18-26). If Fe was in excess, a weighted

TABLE 2. Chemical (wt%) and isotopic composition of the standards used for determination of the H contents and D/H ratios in Antarctic micrometeorites.*

	Mg-Kaersutite Bita Hochee†	Arfvedsonite Illimaussaq†	Mg-Hastingsite Bamble†	Richterite Kip†	Phlogopite C01a†	Goethite Pisolite‡
SiO_2	41.36	49.57	51.48	44.64	37.98	1.79
TiO_2	4.38	0.62	0.34	0.70	0.53	–
Al_2O_3	12.43	0.71	4.08	8.22	16.30	0.08
MgO	12.77	0.01	18.20	13.85	16.68	0.27
CaO	10.72	0.34	11.94	11.24	0.00	–
MnO	0.20	1.40	0.03	0.19	0.71	–
FeO	11.31	32.42	8.45	13.58	9.07	–
Fe_2O_3	–	–	–	–	–	82.84
Na_2O	2.51	7.25	1.59	2.42	0.33	–
K_2O	1.93	3.24	0.27	1.08	9.22	–
H_2O	2.00	1.60	2.03	1.39	2.34	11.83
F	0.00	0.46	0.09	1.16	3.48	–
Cl	–	0.01	0.02	0.16	–	–
M/C ¥	15.72	27.10	15.26	17.35	15.66	¥
Mg/Mg+Fe	0.668	0.001	0.793	0.645	0.738	0.013
δD_{SMOW} (‰)	–52	–142	–61	–88	–80	–148
D/H_{true} ($\times 10^{-6}$)	147.51	133.50	146.11	141.91	143.15	132.57
$D/H_{meas.}$ ($\times 10^{-6}$)	91.15	64.16	97.43	88.35	91.70	51.25
α_{ins}	0.62	0.48	0.67	0.62	0.64	0.39

*The D/H_{meas} values given in this table have been measured during one analysis session and are shown as typical values.
†Hydroxylated silicates were used to calibrate the silicate analyses.
‡Goethite was used for the analyses of the COPS phase.
¥M/C is the mean mass to charge ratio of the octahedral cations in amphibole and mica; this definition is not relevant for the pisolite. A linear relationship between the instrumental isotopic fractionation factor and the M/C ratio is observed (Deloule *et al.*, 1991; and see Fig. 1).

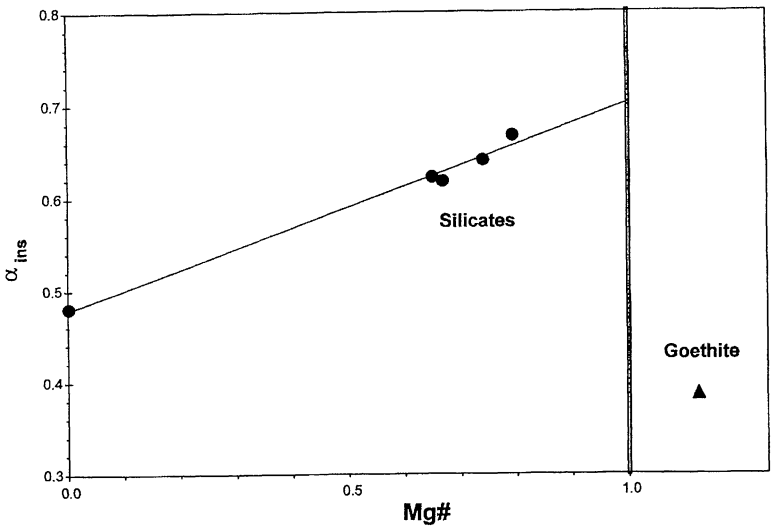

FIG. 1. Instrumental mass fractionation factor (α_{ins}) in hydroxylated silicate minerals as a function of Mg# = Mg/(Mg + Fe), and in an iron hydroxide (goethite). Note that the definition of Mg# ($0 < Mg\# < 1$) is not relevant in the case of goethite, which is thus plotted outside this range. This plot represents the instrumental isotopic fractionation factor measured for one set of analyses and is shown as a representative pattern. Due to electron multiplier aging, the slope of the line varies from one analysis session to another; however, the goodness of the fit as expected from Deloule *et al.* (1991) does not vary significantly (*e.g.*, Deloule *et al.*, 1992).

mean value of α_{ins} (noted α_{mix} in Table 3) was calculated and applied. Due to the difference of α_{ins} values between silicate and goethite, the uncertainty in this calculation could introduce a systematic error that is estimated to be <5% but is nevertheless much larger than the internal precision of a spot analysis (~2%). Otherwise, α_{ins} values for silicates (noted $\alpha_{Mg\#}$) was applied. The potential contribution of organic H to secondary H^+ is likely to be negligible, due to the nature of the O^- primary ion beam (Deloule and Robert, 1995, and see above). Thus the measured D/H ratios should be mainly ascribed to water.

Antarctic Cosmic Spherule Analyses: Nuggets and Spherules–For ACSs nuggets, α_{FeOOH} was directly applied. For the silicate fraction of the ACSs, scanning electron microscopy shows that they are formed of barred olivine, with interstitial glass containing tiny inclusions of a phase thought to be magnetite (Brownlee *et al.*, 1997. and references therein), but which could be, in fact, some type of iron oxyhydroxide. Because this minor phase might be a major source of hydrogen in our ACSs analyses (the proportion of which cannot be estimated), the appropriate instrumental isotopic fractionation factor (α_{ins}) cannot be accurately determined for the silicate fraction of ACSs. From scanning electron micrographs that indicate a maximum "magnetite" to glass ratio of ~1, a conservative estimate can be made by assuming that the proper fractionation factor must lie between two extreme values: (1) $\alpha_{ins} = \alpha_{Mg\#}$ (*i.e.*, H is entirely released by the silicate phases) and (2) $\alpha_{ins} = 0.5 \times \alpha_{Mg\#} + 0.5 \times \alpha_{FeOOH}$ (*i.e.*, 50% H is present in the iron oxyhydroxide). The ranges in α_{ins} obtained by this approach are reported in Table 3 with their corresponding ranges in D/H ratios. Note that because the textures are similar for all analyzed ACSs, the instrumental isotopic fractionation is likely to be approximately constant and, thus, the range of isotopic variation should not be drastically affected by this uncertainty. For example, taking the minimum and maximum α_{ins} values yields ranges in D/H ratios equal to 82×10^{-6} (*i.e.*, from 82 to 164×10^{-6}, or a range in δD values of ~530‰) and 70×10^{-6} (*i.e.*, from 65 to 135×10^{-6}, or a range in δD values of ~450‰), respectively (see Table 3a).

Exchange and Contamination Experiments

During their recovery, the particles were immersed for about eight hours in Antarctic melt ice water having a low δD value ($\delta D \approx -300$‰), at a temperature of a few degrees Celsius. Prior to this recovery, they might also have been subjected to Antarctic cryogenic weathering during residence in the superficial layer of the ice fields. We conducted two distinct types of simulation experiments to assess the importance of a potential terrestrial water contamination. We describe below these experiments and also present their results showing that this contamination is negligible.

Three Deuterium Exchange Tests–(1) Several fragments of the hydrous carbonaceous chondrites Orgueil and Murchison with sizes of a few hundred micrometers were exposed to water (with $\delta D = -149$‰) at 80 °C for 20 h. We did not observe any significant deviation of the D/H ratios measured for the meteorite fragments after exposition to this water from the bulk values given in the literature (see Table 4, compare columns 2 and 3 for Murchison and 4 and 5 for Orgueil); (2) 100 mg of powdered Orgueil whole rock was immersed in heavy water ($\delta D = +1407$‰) for 30 days at room temperature. Water was extracted from Orgueil by stepwise heating pyrolysis, and the concentration and D/H ratios were measured before and after the treatment. Results are reported in Fig. 2 and show that isotopic exchange or contamination is restricted to <4%. (3) An amphibole standard was cut in heavy water ($\delta D = +1407$‰), in order to test the surface contamination during the preparation of large samples (*e.g.*, standards that were used to calibrate our AMMs analyses). In this sample, one analyzed spot showed an increase in the δD value of 120‰. This increase, however, was observed only during the first 10 cycles of the 100 to 150 cycles required for one spot analysis. This surface contamination is eliminated after ~5 min of sputtering (or a depth of ~0.2 μm).

Two Dehydration Tests–Antarctic micrometeorites crushed on Au foil were systematically degassed for eight hours at 120 °C in high vacuum (~10^{-4} Torr) before analysis (in the case of terrestrial clays, adsorbed water is eliminated by heating at 90 °C in vacuum for eight hours). We did not observe any significant difference between the D/H frequency distributions for these samples and for AMMs prepared in polished section (only heated at 60 °C during 12 h for curation of the epoxy). In addition, the D/H ratios measured on the same two fragments of two AMMs (# 94-18-7 and # 94-18-20), which were preheated at 120°C and then reheated at 200 °C for three hours under vacuum (see Table 4, column 3), give indistinguishable values.

Although these experiments might not constitute an exhaustive set of tests, they seem to demonstrate that, as for terrestrial samples, extraterrestrial phyllosilicates are not subject to contamination *via* addition or isotopic exchange with ambient vapor or liquid water.

RESULTS AND DISCUSSION

In this section, chemical and isotopic compositions of AMMs and ACSs are presented successively and discussed in the frame of a comparison between various solar system objects.

TABLE 3a. Water concentrations, type and value of the instrumental isotopic fractionation factors applied to the D/H analyses (see text), and D/H ratios measured in Antarctic micrometeorites and COPS-rich Antarctic cosmic spherules prepared in polished sections.*

Sample	Type	Size range (μm)	H_2O (wt%)	Mean H_2O (wt%)	α_{ins} correction	α_{ins}	D/H ($\times 10^{-6}$)	δD_{SMOW} (‰)
94-10-14	FG	100–400	1.1		$\alpha_{Mg\#}$	0.52	194.5	249
94-10-34	FG	100–400	1.2		α_{mix}	0.48	193.5	242
94-10-11	FG	100–400	2.1		$\alpha_{Mg\#}$	0.54	187.8	206
92-14-06	FG	100–400	3.3		α_{mix}	0.38	184.9	187
5M10(2)	FG	100–400	1.7		$\alpha_{Mg\#}$	0.53	176.5	133
5M10	FG	100–400	1.9		$\alpha_{Mg\#}$	0.56	173.9	116
5M3	FG	100–400	2.1		$\alpha_{Mg\#}$	0.59	169.9	91
93-7-25	FG	25–50	n.d.		$\alpha_{Mg\#}$	0.54	162.5‡	43‡
5M5	FG	100–400	1.4		$\alpha_{Mg\#}$	0.56	162.2	41
5M2	FG	100–400	0.9		$\alpha_{Mg\#}$	0.61	159.0	21
94-10-26	FG	100–400	1.5	1.7	$\alpha_{Mg\#}$	0.51	158.6	18
94-10-31	FG	100–400	2.1		$\alpha_{Mg\#}$	0.53	157.7	12
94-10-24	FG	100–400	2.0		$\alpha_{Mg\#}$	0.53	155.0	–5
94-10-09	FG	100–400	1.9		$\alpha_{Mg\#}$	0.53	154.6	–7
93-7-10	FG	25–50	n.d.		$\alpha_{Mg\#}$	0.56	151.3‡	–29‡
93-7-03	FG	25–50	n.d.		$\alpha_{Mg\#}$	0.58	141.9‡	–89‡
93-7-14	FG	25–50	n.d.		$\alpha_{Mg\#}$	0.58	138.6‡	–110‡
93-7-19	FG	25–50	n.d.		$\alpha_{Mg\#}$	0.63	136.9‡	–121‡
93-7-06	FG	25–50	n.d.		$\alpha_{Mg\#}$	0.54	136.7‡	–122‡
92-14-12	FG	100–400	1.9		$\alpha_{Mg\#}$	0.55	129.6	–168
92-14-08	FG	100–400	1.1		α_{mix}	0.44	128.4	–176
94-10-36	SC	100–400	1.7		$\alpha_{Mg\#}$	0.53	179.6	153
5M8	SC	100–400	2.2		$\alpha_{Mg\#}$	0.57	173.5	114
93-7-21	SC	25–50	n.d.	1.9	$\alpha_{Mg\#}$	0.56	172.0‡	105‡
93-7-09	SC	25–50	n.d.		$\alpha_{Mg\#}$	0.61	170.9‡	97‡
93-7-01	SC	25–50	n.d.		$\alpha_{Mg\#}$	0.57	140.8‡	–96‡
95-11-03	ACS	100–400	0.7		$\alpha_{Mg\#}$ / α_{mix}	0.60 / 0.49†	135 / 164†	–136 / 53†
95-11-03	ACS	100–400	0.7		$\alpha_{Mg\#}$ / α_{mix}	0.60 / 0.50†	129 / 158†	–171 / 12†
95-11-01	ACS	100–400	0.9		$\alpha_{Mg\#}$ / α_{mix}	0.60 / 0.49†	126 / 153†	–193 / –16†
5M1	ACS	100–400	0.6		$\alpha_{Mg\#}$ / α_{mix}	0.58 / 0.48†	125 / 150†	–195 / –36†
92-23B-77	ACS	100–400	n.d.		$\alpha_{Mg\#}$ / α_{mix}	0.57 / 0.43†	125 / 164†	–196 / 51†
95-11-02	ACS	100–400	0.8		$\alpha_{Mg\#}$ / α_{mix}	0.61 / 0.50†	124 / 153†	–201 / –18†
93-6C	ACS	100–400	0.6		$\alpha_{Mg\#}$ / α_{mix}	0.63 / 0.51†	120 / 149†	–227 / –44†
95-11-01	ACS	100–400	0.5	0.6	$\alpha_{Mg\#}$ / α_{mix}	0.61 / 0.50†	117 / 143†	–251 / –85†
95-11-02	ACS	100–400	0.9		$\alpha_{Mg\#}$ / α_{mix}	0.61 / 0.50†	115 / 141†	–263 / –95†
93-6C	ACS	100–400	1.1		$\alpha_{Mg\#}$ / α_{mix}	0.57 / 0.44†	112 / 147†	–279 / –55†
95-7A	ACS	100–400	0.1		$\alpha_{Mg\#}$ / α_{mix}	0.61 / 0.50†	112 / 137†	–283 / –121†
95-7B (1)	ACS	100–400	1.2		$\alpha_{Mg\#}$ / α_{mix}	0.58 / 0.48†	102 / 122†	–345 / –216†
5M1	ACS	100–400	0.1		$\alpha_{Mg\#}$ / α_{mix}	0.61 / 0.50†	97 / 118†	–378 / –240†
95-7D	ACS	100–400	0.2		$\alpha_{Mg\#}$ / α_{mix}	0.62 / 0.50†	95 / 117†	–389 / –246†
95-7B (2)	ACS	100–400	0.2		$\alpha_{Mg\#}$ / α_{mix}	0.58 / 0.48†	83 / 100†	–465 / –357†
95-7C	ACS	100–400	0.1		$\alpha_{Mg\#}$ / α_{mix}	0.66 / 0.52†	65 / 82†	–581 / –472†
93-6C	COPS	nugget	3.8		α_{FeOOH}	0.30	181.7	167
93-6C	COPS	nugget	1.1		α_{FeOOH}	0.39	173.4	113
95-11-02	COPS	nugget	7.9		α_{FeOOH}	0.39	161.8	39
95-11-03	COPS	nugget	5.0	4.3	α_{FeOOH}	0.39	157.7	12
95-11-01	COPS	nugget	5.3		α_{FeOOH}	0.39	146.0	–62
92-23B-77	COPS	nugget	3.4		α_{FeOOH}	0.30	144.1	–75
95-7A	COPS	nugget	5.4		α_{FeOOH}	0.39	135.4	–131
95-7D	COPS	nugget	3.5		α_{FeOOH}	0.39	133.4	–144

*The analyses are arranged by textural type (FG = fine-grained Antarctic micrometeorite, SC = scoriaceous Antarctic micrometeorite, ACS = COPS-rich Antarctic cosmic spherule, COPS = ferrihydrite "COPS" nugget). Within each textural group, results are given by decreasing D/H values.
†The quoted range in α_{ins} for ACSs stands for possible systematic errors in calibration (see text).
‡Reported values for these smallest AMMs (25–50 μm) have higher uncertainty than for the larger AMMs (see text).

Antarctic Micrometeorites

Comparisons between Antarctic Micrometeorites and Carbonaceous Chondrites: Textures and Chemical Compositions– Previous works (Engrand and Maurette, 1998; Kurat *et al.*, 1994; Maurette *et al.*, 1993) have classified micrometeorites according to their textures resulting from the degree of heating during atmospheric entry (see Fig. 3): (1) unmelted AMMs: either fine-grained (FG-AMMs, see Fig. 3a), or coarse-grained crystalline (Xtal-AMMs); (2) partially melted scoriaceous AMMs (SC-AMMs,

TABLE 3b. Water concentrations, type and value of the instrumental isotopic fractionation factors applied to the D/H analyses (see text), and D/H ratios measured in Antarctic micrometeorites crushed on Au foils.*

Sample	Type	Size range (μm)	H_2O (wt%)	Mean H_2O (wt%)	α_{ins} correction	α_{ins}	D/H ($\times 10^{-6}$)	δD_{SMOW} (‰)
94-18-07	FG	100–400	1.8		$\alpha_{Mg\#}$	0.49	169.6	89
94-18-17_3	FG	100–400	2.0†		$\alpha_{Mg\#}$	0.51	165.8	64
94-10-11	FG	100–400	1.0		$\alpha_{Mg\#}$	0.54	164.4	55
94-18-20	FG	100–400	1.2		$\alpha_{Mg\#}$	0.51	161.4	36
95-1-12	FG	50–100	3.1		$\alpha_{Mg\#}$	0.51	160.8	32
95-1-08	FG	50–100	1.0		$\alpha_{Mg\#}$	0.54	157.8	13
94-18-17_3	FG	100–400	2.0†		$\alpha_{Mg\#}$	0.51	157.0	8
94-18-29	FG	100–400	2.4		$\alpha_{Mg\#}$	0.49	156.0	2
95-1-08	FG	50–100	1.2		$\alpha_{Mg\#}$	0.54	155.9	1
95-1-24	FG	50–100	2.1		$\alpha_{Mg\#}$	0.54	155.7	–1
94-18-23	FG	100–400	1.1		$\alpha_{Mg\#}$	0.51	154.7	–7
95-1-04	FG	50–100	3.7		$\alpha_{Mg\#}$	0.55	153.5	–14
94-18-20	FG	100–400	1.1		$\alpha_{Mg\#}$	0.51	153.2	–17
94-18-27	FG	100–400	1.5		$\alpha_{Mg\#}$	0.54	153.1	–17
94-18-28	FG	100–400	1.9	1.8	$\alpha_{Mg\#}$	0.51	150.7	–32
94-18-21	FG	100–400	2.1†		$\alpha_{Mg\#}$	0.50	150.3	–35
94-18-21	FG	100–400	2.0		$\alpha_{Mg\#}$	0.50	149.5	–40
95-1-25	FG	50–100	1.7		$\alpha_{Mg\#}$	0.51	149.3	–42
94-18-12	FG	100–400	2.0		$\alpha_{Mg\#}$	0.53	149.1	–43
94-18-26	FG	100–400	0.9		$\alpha_{Mg\#}$	0.48	146.7	–58
94-18-23	FG	100–400	1.2		$\alpha_{Mg\#}$	0.51	146.6	–59
94-18-17_3	FG	100–400	2.0†		$\alpha_{Mg\#}$	0.5	145.9	–64
94-18-17_3	FG	100–400	1.6		$\alpha_{Mg\#}$	0.510	145.3	–67
94-18-13	FG	100–400	2.0		$\alpha_{Mg\#}$	0.53	143.6	–78
95-1-22	FG	50–100	0.9		$\alpha_{Mg\#}$	0.50	143.5	–79
94-18-20	FG	100–400	1.9		$\alpha_{Mg\#}$	0.51	142.7	–84
94-18-17_3	FG	100–400	2.0†		$\alpha_{Mg\#}$	0.51	140.7	–97
94-10-31	FG	100–400	1.4		$\alpha_{Mg\#}$	0.53	134.3	–138
94-18-03	FG	100–400	3.3		$\alpha_{Mg\#}$	0.53	133.5	–143
94-18-25	SC	100–400	1.8		$\alpha_{Mg\#}$	0.53	159.3	23
95-1-19	SC	50–100	1.5		$\alpha_{Mg\#}$	0.53	157.2	9
95-1-14	SC	50–100	1.9		$\alpha_{Mg\#}$	0.50	149.1	–43
95-1-06	SC	50–100	1.7		$\alpha_{Mg\#}$	0.49	148.5	–47
95-1-11	SC	50–100	1.8	1.5	$\alpha_{Mg\#}$	0.53	144.5	–72
94-18-04	SC	100–400	1.3		$\alpha_{Mg\#}$	0.49	144.2	–74
95-1-18	SC	50–100	1.7		$\alpha_{Mg\#}$	0.54	142.7	–84
94-18-05	SC	100–400	1.0		$\alpha_{Mg\#}$	0.51	134.7	–135
95-1-16	SC	50–100	0.4		$\alpha_{Mg\#}$	0.53	98.7	–366
94-18-07 (200 °C)	FG	100–400	1.4†		$\alpha_{Mg\#}$	0.49	151.3†	–29†
94-18-20 (200 °C)	FG	100–400	1.1†		$\alpha_{Mg\#}$	0.51	149.3†	–42†

*The analyses are arranged by textural type (FG = fine-grained Antarctic micrometeorite, SC = scoriaceous Antarctic micrometeorite). Within each textural group, results are given by decreasing D/H values.
†Values were measured after heating in high vacuum at 200 °C.

see Fig. 3b), and (3) melted grains (ACSs, see Fig. 3c for an example of the peculiar type of ACSs analyzed in this study that contains a nugget of iron oxyhydroxide phase). Note that Xtal-AMMs were not analyzed in this work because of their low-water concentration (estimated to be <100 ppm, as they did not yield a significant H signal). In the case of the cosmic spherules collected at Cap-Prudhomme, only ~10% contain nuggets of a peculiar iron oxyhydroxide phase protruding on their external surface (Fig. 3c). These ACSs have been purposely selected for this work and are referred also as COPS-ACSs. This particular type of spherule is not glassy but is rather related to the most abundant family of nonglassy ACSs, the so-called barred olivine spherules, made of bars of olivines separated by interstitial glass containing small "magnetite" inclusions. However, they have a transparent light green and/or brownish color when observed in transmitted light, whereas barred olivine spherules are usually opaque.

The elemental compositions of the AMMs and ACSs analyzed in this study are reported on a Mg–Fe–Si ternary diagram in Fig. 4 (Table 1). The AMM compositions are similar to those previously reported (Engrand, 1995). In Fig. 4, they typically plot in the chondritic zone defined by analyses of the matrix of carbonaceous chondrites (CCs) containing serpentine and saponite (McSween, 1987; Zolensky and Lindstrom, 1992), which suggests the presence of phyllosilicate in the AMM fine-grained matrix. Relying on textural and chemical studies, phyllosilicates have been identified in AMMs as being mainly serpentine and occasionally smectite (Kurat *et al.*, 1994). The presence of these hydrated silicates in unmelted AMMs has been later confirmed by transmission electron

TABLE 4. Selected exchange and contamination experiments.*

	Murchison		Orgueil		AMMs§	
Treatment	–	water†	–	water†	120 °C	200 °C
Average D/H	150.1‡	136.0	188.9‡	186.8	169.6	151.3
($\times 10^{-6}$)	–	–	–	–	152.4	149.3

*The D/H ratios were measured before and after various treatments in ~200 μm chunks of Murchison and Orgueil, and in two Antarctic micrometeorites (AMMs # 94-18-7 and # 94-18-20) crushed in Au foils.
†Exposure during 20 h to low-D water (δD = –149‰) at 80 °C.
‡Average D/H values for Murchison and Orgueil are from Kerridge (1985).
§The same two fragments of two micrometeorites were measured after heating in high vacuum at 120 °C, and after reheating at 200 °C (see text).

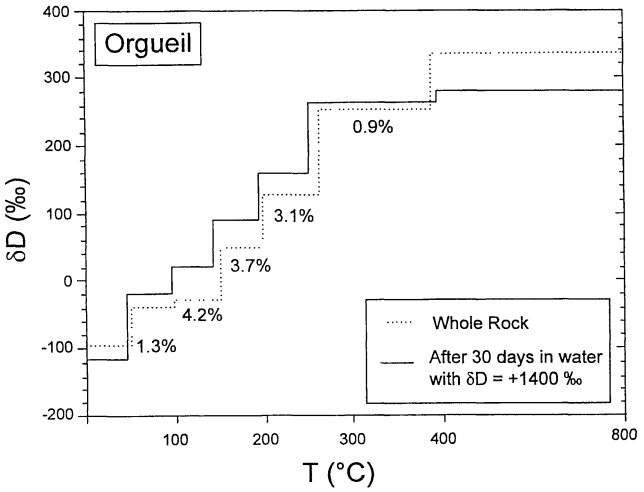

FIG. 2. Stepwise heating measurement of D/H ratios in 100 mg powdered Orgueil sample before and after exposure to heavy water (δD = 1407‰) for 30 days at room temperature. Note that the amount of exchange between the deuterated water and H-bearing phases in Orgueil after this treatment is limited to only ~4% (see text).

microscopy (*e.g.*, Klöck and Stadermann, 1994). Thus, it can be postulated that the H signal measured in AMMs predominantly comes from hydrated silicates, as the organic contribution to the H signal ought to be negligible (see experimental section).

The chemical compositions of ACSs in their silicate phase (see Table 1 and Fig. 4) exhibit a depletion in Fe compared to unmelted AMMs that might explain their light-green brownish color and that probably results from the formation of their nugget. The fact that these ACSs are texturally and compositionally so similar with each other indicates that their parent micrometeoroids were probably closely related to each other. Their nuggets are chemically similar in major element composition to the "COPS" phase observed in all textural types of AMMs. This phase has been identified as a "dirty" variety of ferrihydrite ($5Fe_2O_3$, $9H_2O$; Engrand and Maurette, 1998; Engrand *et al.*, 1993) that can accommodate large amounts (up to several percent) of minor elements, such as Mg, Si, P, S, Fe, and Ni.

Comparisons between Antarctic Micrometeorites and Carbonaceous Chondrites: Water Contents and D/H Ratios–Water contents as well as the corresponding D/H ratios and their frequency distribution of the 52 AMMs (38 FG-AMMs and 14 SC-AMMs) investigated in this work are reported in Table 3 and Figs. 5 and 6.

Water contents in FG-AMMs lie between 0.9 and 3.7 wt% (average value = 1.8 wt%) and between 0.4 and 2.2 wt% (average value = 1.5 wt%) in SC-AMMs (see Table 3). These distributions of water contents, which peak at ~4 wt% for the FG-AMMs and at

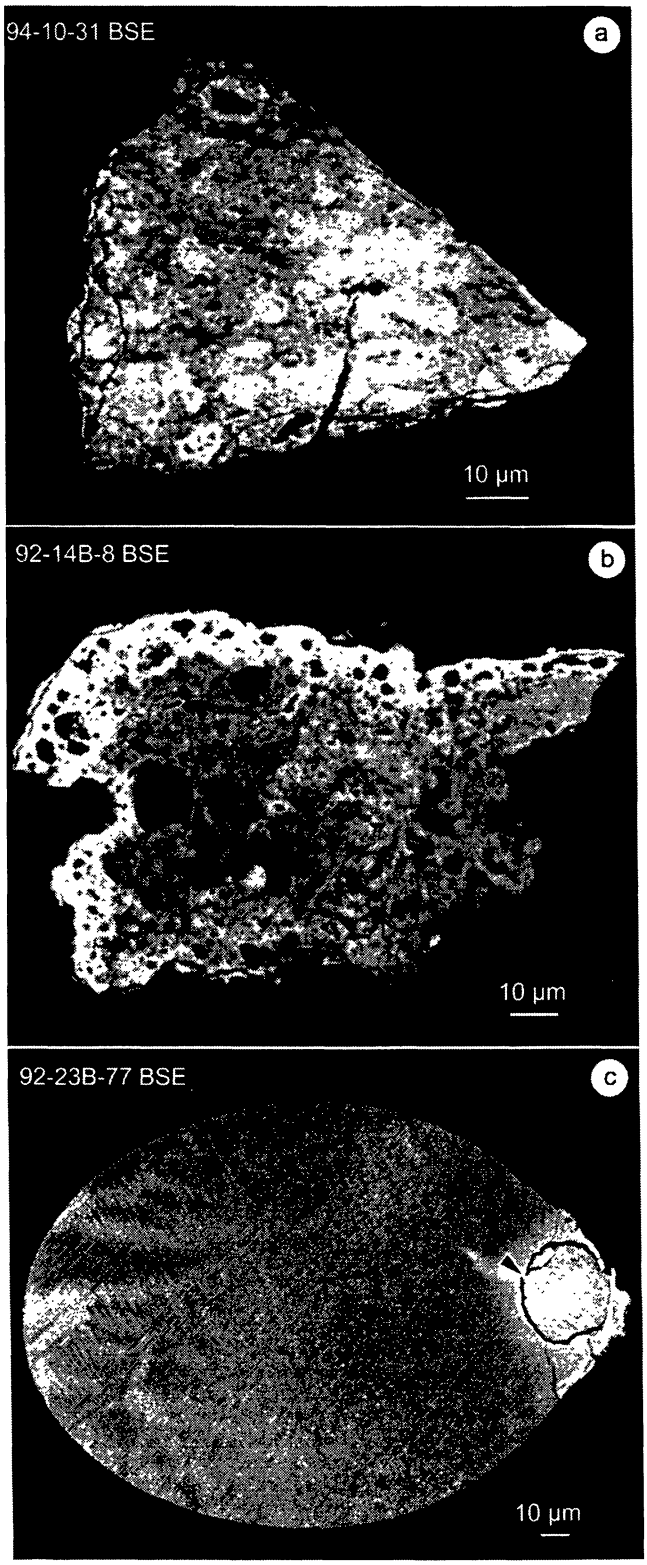

FIG. 3. Scanning electron micrographs of representative samples of (a) an unmelted Antarctic micrometeorite composed of fine-grained matrix (FG-AMM); (b) a partially melted/dehydrated scoriaceous Antarctic micrometeorite (SC-AMM); and (c) a melted micrometeorite (called Antarctic cosmic spherule (ACS) of the peculiar type analyzed in this study) that contains a nugget of ferrihydrite–"COPS" nugget designated by an arrow.

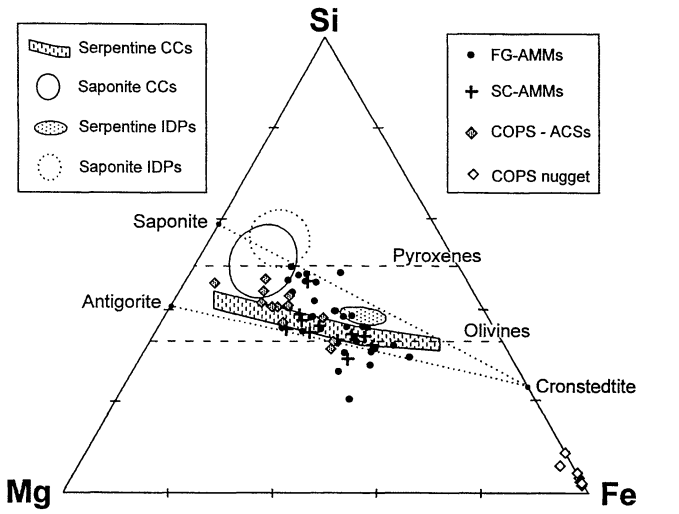

FIG. 4. A Mg–Fe–Si ternary projection of chemical compositions of micrometeorites whose D/H ratios are reported in Table 3. Also shown are the ranges of compositions for serpentines (dashed areas) and saponite (full line and dashed line delimited areas; Zolensky and Lindstrom, 1992) in carbonaceous chondrites (CCs) and in IDPs, and for terrestrial phyllosilicates (saponite, antigorite, and cronstedtite; from Deer *et al.*, 1962, 1992).

~2 wt% for the SC-AMMs, correspond to a content of hydrous silicates (~20 vol% for the least-heated AMMs) that is lower than that of CI chondrites, and intermediate between that of CM (~40–70 vol%), CR (~20–40 vol%), and CO and CV (<0.1 vol%) meteorites.

Some individual AMMs exhibit internal variations in their D/H ratios. For example, FG-AMM n° 94-18-17 was measured on five spots, with the D/H values varying from 140.7×10^{-6} to 165.8×10^{-6} (or δD from –97 to +64‰). The fact that some other AMMs are homogeneous (*e.g.*, in FG-AMM n° 94-18-21, the D/H ratios are 149.5×10^{-6} (or $\delta D = -40‰$) and 150.3×10^{-6} (or $\delta D = -35‰$)) suggests that this heterogeneity does not have instrumental sources. The D/H ratios vary from 128.4×10^{-6} to 194.5×10^{-6} ($\delta D = -176$ to +249‰) and 98.7×10^{-6} to 179.6×10^{-6} ($\delta D = -366$ to +153‰), for the FG-AMMs and SC-AMMs, respectively. No significant difference is observed between the average values of the D/H ratios for FG-AMMs ($\overline{D/H}_{FGs} = 156.3 \times 10^{-6}$; or $\delta D = +3‰$) and SC-AMMs ($\overline{D/H}_{SCs} = 148.4 \times 10^{-6}$; or $\delta D = -47‰$), even if a small trend to lower values could possibly exist in the distribution of D/H ratios for SC-AMMs (see Fig. 7). The D/H ratios measured for the three size fractions (25–50, 50–100, and 100–400 μm) are quite similar, thus reinforcing our previous conclusions in favor of a common source for all micrometeorites recovered from Antarctic ice (Engrand and Maurette, 1998; see also the later section on "Comparison between Antarctic Micrometeorites and Comets").

The high D/H values ($D/H > 160 \times 10^{-6}$) are indicative of an extraterrestrial origin, because they cannot be caused by any known terrestrial contamination processes. This origin is further supported by two observations: the distribution of the D/H ratios in AMMs matches that of carbonaceous chondrites (see hereafter and Fig. 5a) and the water contents of SC-AMMs is systematically lower than those of FG-AMMs (see Table 3), implying that water was partially outgassed during frictional heating upon atmospheric entry.

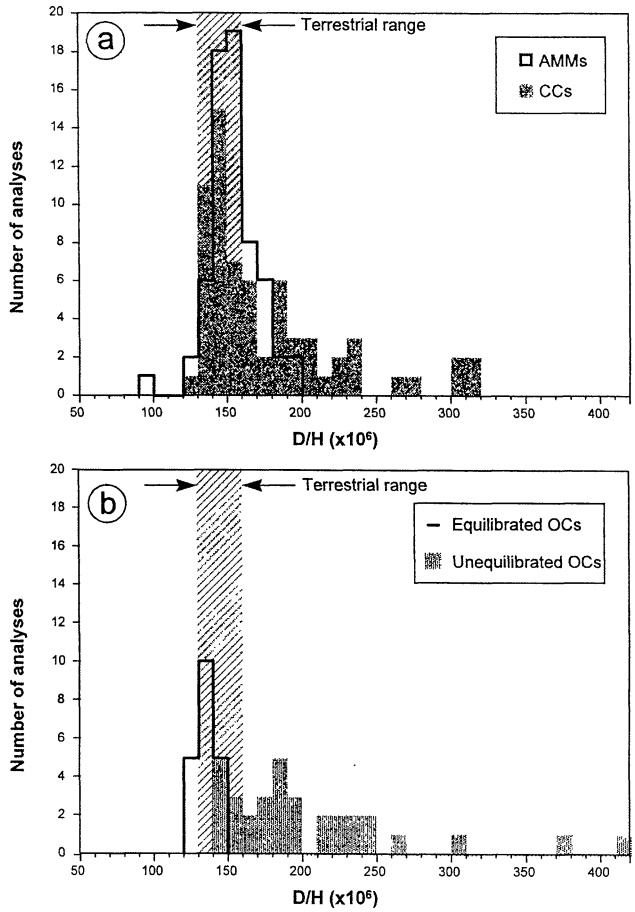

FIG. 5. Comparison of the frequency distributions of D/H ratios for AMMs and meteorites: (a) D/H ratios measured for AMMs (full line), and for a set of carbonaceous chondrites (CCs) (dashed area from Boato, 1954; Kerridge, 1985; Kolodny *et al.*, 1980; Robert and Epstein, 1982; Robert *et al.*, 1979). (b) D/H ratios measured for equilibrated ordinary chondrites (full line from Robert *et al.*, 1979, 1987b), and for unequilibrated ordinary chondrites (dashed area from McNaughton *et al.*, 1981, 1982; Robert *et al.*, 1979, 1987a).

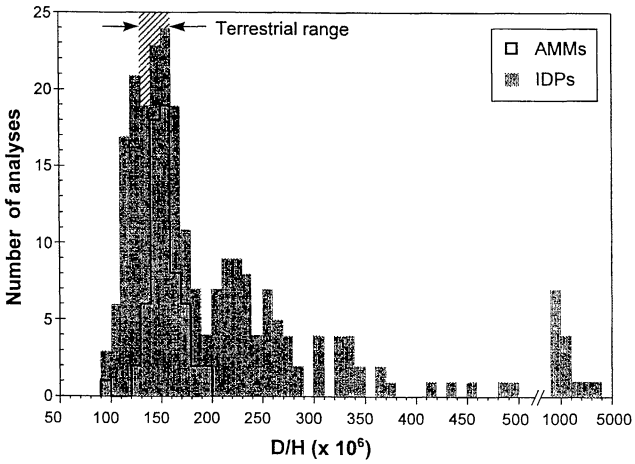

FIG. 6. Comparison of the frequency distributions of D/H ratios for Antarctic micrometeorites (full line, this study), and for stratospheric IDPs (dashed area, data from McKeegan, 1985, 1987; Messenger, 1997; Messenger and Walker, 1997; Zinner *et al.*, 1983). Note that the wide range of D/H ratios measured in IDPs are significantly larger than for AMMs and CCs.

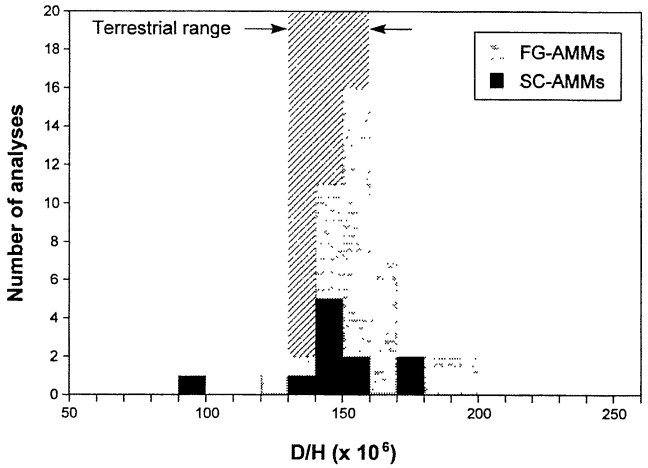

FIG. 7. Distribution of the D/H ratios in the fine-grained unmelted Antarctic micrometeorites (FG-AMMs) compared to that of the scoriaceous partially dehydrated/melted AMMs (SC-AMMs).

Although frictional heating of the incident micrometeoroids has altered the texture of SC-AMMs and caused a partial loss of indigenous water, it apparently did not drastically affect their H-isotopic composition. Until now, the SC-AMMs were reported as being partially melted, but this was already inconsistent with their high solar-Ne contents (Olinger *et al.*, 1990). The close similarity between the D/H frequency distributions of carbonaceous chondrites and SC-AMMs suggest that the D/H ratios in SC-AMMs were not affected by a extensive Rayleigh distillation during their atmospheric entry. Therefore the amount of melting in SC-AMMs is limited, although dehydration can be more pronounced.

The frequency distribution of D/H ratios in AMMs is similar to that in carbonaceous chondrites (Fig. 5a; data from Boato, 1954; Kerridge, 1985; Kolodny *et al.*, 1980; Robert and Epstein, 1982; Robert *et al.*, 1979) and is quite different from that observed in ordinary chondrites (Fig. 5b; data from Robert *et al.*, 1979, 1987b) and unequilibrated ordinary chondrites (data from McNaughton *et al.*, 1981, 1982; Robert *et al.*, 1979, 1987a).

These results suggest that both FG-AMMs and SC-AMMs are derived from a common fine-grained material (made of a mixture of anhydrous and hydrous minerals) essentially related to the hydrous fraction of the carbonaceous chondrites. They also confirm that the ordinary chondrite contribution to the AMM collection is small (~1%, as previously deduced from chemical and mineralogical features; Walter *et al.*, 1995b). This is a new confirmation of the relationship between AMMs and carbonaceous chondrites, previously inferred from neutron activation and electron microprobe data (see for example Kurat *et al.*, 1994).

Because of their high pyroxene/olivine ratio, AMMs could be related to CR chondrites rather than to CM chondrites. Our new D/H measurements make such a relationship with CR chondrites less likely as CR meteorites typically show much higher D/H ratios (Kerridge, 1985) than AMMs. If so, the high pyroxene/olivine ratio of ~1 observed in AMMs (matching that observed in CR chondrites but ~10 times higher than in CM chondrites) would represent an additional major difference between AMMs and CM chondrites.

Comparisons between Antarctic Micrometeorites and Stratospheric Interplanetary Dust Particles: D/H Ratios–Scanning and transmission electron microscopy revealed that a large proportion (~40%) of the stratospheric IDP collection is constituted of chondritic porous-anhydrous particles that contain in particular an exotic component quoted "GEMS" (Bradley, 1994). Both these chondritic porous-anhydrous IDPs and GEMS are virtually absent in the AMM collection or in the fine-grained matrix of carbonaceous chondrites.

The D/H ratios measured in the stratospheric IDPs with a primary beam of Cs^+ further amplified these differences. They revealed large positive D anomalies in the IDPs, mostly observed in the chondritic porous-anhydrous particles (McKeegan, 1987; McKeegan *et al.*, 1985, 1987; Zinner *et al.*, 1983). In sharp contrast, C. Alexander, S. Messenger, and P. Hoppe (pers. comm., and see Alexander *et al.*, 1992; Engrand *et al.*, 1996) did not find any marked positive D anomaly in more than 60 AMMs with sizes of ~200 μm.

In these previous investigations, stratospheric IDPs were quite smaller than AMMs. It has thus been postulated that the D-rich stratospheric IDPs are cometary particles, whereas the "normal" matter found in other types of IDPs and in AMMs has an asteroidal origin (Brownlee *et al.*, 1995). The recent use of a "giant" stratospheric IDP collector (~100 cm^2 instead of 10 cm^2) has allowed the collection of larger IDPs (sizes up to 50 μm), which fragment upon impact with the collector, forming "cluster particles." These new cluster IDPs now overlap in size the smallest size fraction of AMMs (25–50 μm); thus a direct comparison between stratospheric IDPs and AMMs can now be made in the 25–50 μm size range.

Data on the 25–50 μm size AMMs, including SEM observations, electron microprobe analyses (Gounelle *et al.*, 1998), and D/H measurements (this work, with a primary O^- beam, see Table 3a) show that they are similar to the larger AMMs up to the maximum size recovered in Antarctica (~400 μm). In sharp contrast, the range of positive D anomalies in the 25–50 μm size cluster IDPs (as measured with a primary Cs^+ beam) is even more pronounced than in their smaller counterparts (Messenger and Walker, 1997). This is reflected by both the higher proportion (~70%) of particles showing D anomalies and their higher D enrichments (δD values up to +25 000‰). Furthermore, the correlation between the D enrichment and the C signal previously noted by McKeegan (1987) indicating an organic carrier of the D enrichments is not observed anymore, which suggests that both the organic matter and the hydrous component of the IDPs are carriers of the D anomalies (Messenger and Walker, 1997).

In Fig. 6, we compare the distributions of the D/H ratios for AMMs (this study) and stratospheric IDPs (both cluster and individual particles; data from McKeegan, 1987; McKeegan *et al.*, 1985; Messenger, 1997; Messenger and Walker, 1997; Zinner *et al.*, 1983). The discrepancy between the two distributions cannot any longer be attributed to the different size distributions between AMMs and IDPs. Assuming the validity of our comparison between AMMs and IDPs, we outline below four tentative interpretations that still need to be thoroughly checked:

(1) Ion microprobe analyses may not give similar results when performed using a primary O^- or Cs^+ beam. This is likely because the sputtering yields of H^+ or H^-, respectively, from organic/silicate hydrogen differ. As a result, hydrogen from the hydrous phases dominate the analyses performed with the primary O^- beam whereas the Cs^+ beam does not discriminate between organic and hydroxyl hydrogen. A precise quantification of this effect is still needed in order to compare data obtained from both methods, but preliminary analyses of AMMs using a Cs^+ beam (C. Alexander, S. Messenger and P. Hoppe, pers. comm.; and Alexander *et al.*, 1992; Engrand *et al.*,

1996) seem to show that this effect is not large enough to explain the D/H discrepancy between stratospheric IDPs and AMMs.

(2) It has been argued (Messenger and Walker, 1997) that the micrometeoroid flux in the interplanetary medium—reflected in the stratospheric IDPs collected in a narrow time window—may contain a unique set of particles recently captured by the Earth. More recently, Messenger and Walker (1998) proposed that these anomalous cluster IDPs are preferentially of cometary origin, possibly from comet Schwassmann-Wachmann 3. This would imply short-term and drastic variations in the composition of the micrometeorite flux in the recent times and could only be detected by punctual collections at well-defined times. However, prior analyses of IDPs collected from flags flown over a period of years (McKeegan, 1987; McKeegan *et al.*, 1985, 1987; Zinner *et al.*, 1983) yielded D-rich particles as well, thus challenging this interpretation. In addition, micrometeorites with sizes >100 μm have now been recovered from three distinct sites in Antarctica, including the blue ice field of Cap-Prudhomme (Maurette *et al.*, 1994), the bottom of the water well at the South Pole (Taylor *et al.*, 1996), and a meteorite stranding ice field (Harvey and Maurette, 1990). These sites correspond to different terrestrial ages of AMMs: a few decades, 300 years, and 100 000 years, respectively. Preliminary comparisons of micrometeorites recovered from these collections (see Harvey and Maurette, 1990; Maurette *et al.*, 1997) already suggests that they contain the same type of AMMs, which indicates in turn that there is no drastic variations of the flux over this time scale in this size range.

(3) The carrier phases (either organic or inorganic) of the D in micrometeorites for all sizes and/or types could be highly soluble in water. If correct, D-rich soluble phases have been leached from AMMs during cryogenic weathering and/or during their eight hour exposure to melt ice water at a few degrees Celsius upon recovery (such is already the case, for example, of the soluble salts from AMMs; see Presper *et al.*, 1993) but remained unaltered in IDPs during their exposure to stratospheric acid aerosols (Arndt *et al.*, 1996; Jessberger *et al.*, 1992).

(4) Finally, despite the overlap in their size range, stratospheric IDPs and AMMs could represent different populations of extraterrestrial material coming from different parent bodies. This would imply that the two modes of collection would favor the recovery of one population over the other in an opposite way in the IDP and AMM collections. The most friable, fluffy, less-dense micrometeorites carrying the D-excess would be enhanced in IDPs relative to AMMs collections as a result of their low-gravitational settling speeds. Furthermore, upon impacting the collector plate, the most friable IDPs fragment into cluster particles that stick to the 100 μm thick layer of silicone oil whereas the harder and denser ones could be lost as they bounce back off the plate. Contrary to stratospheric IDP collections, the Antarctic ice should initially collect all types of cosmic dust. However, cycles of ice freezing and melting combined with the dissolution of soluble salts of AMMs might disaggregate the most friable particles, that might further break up during their cycling through the pumping system.

Comparisons between Antarctic Micrometeorites and Comets: D/H Ratios–Asteroidal and cometary dust should both contribute to the flux of interplanetary dust accreted by the Earth (*e.g.*, Levasseur-Regourd *et al.*, 1991; Liou *et al.*, 1995, 1996; Liou and Zook, 1996, 1997; Whipple, 1967). Unambiguous identification of cometary material among the Antarctic micrometeorite collection was a central issue of this study. Indeed, compared to other water bearing objects of the solar system, comets seem to have a well-defined D/H signature in their gas phase. Cometary water released by comets Halley, Hyakutake, and Hale-Bopp exhibit D/H ratios equal to $(316 \pm 34) \times 10^{-6}$, $(290 \pm 100) \times 10^{-6}$, and $(330 \pm 80) \times 10^{-6}$, respectively (Balsiger *et al.*, 1995; Bockelée-Morvan *et al.*, 1997; Eberhardt *et al.*, 1995; Meier *et al.*, 1998). Although the size of the error bars on these data may be revised in the future, we take the present central values as the mean D/H ratios of these three comets, thus being significantly different from SMOW. Thus, cometary water has a D/H ratio that is also about twice that measured in AMMs and carbonaceous chondrites.

We propose three independent explanations to account for this isotopic discrepancy: (1) AMMs and most carbonaceous chondrites are not derived from cometary matter; (2) the high D/H ratios measured in three comets cannot be taken as face values for the mean value of cometary materials; and (3) in comets, water and minerals may have drastically different D/H ratios. As a consequence, if AMMs represent the mineral fraction of the cometary material, they could exhibit bulk D/H ratios different from those observed in cometary water. Such an intrinsic tremendous isotopic fractionation, which could be regarded as an *ad-hoc* explanation, is routinely observed, in fact, in LL3 meteorites (Deloule *et al.*, 1998). In meteorites, this large distribution is interpreted as the result of the mixing of two different water reservoirs in the solar system (Drouart *et al.*, 1999). If AMMs are of cometary origin, their water-bearing phases were not formed during some type of aqueous alteration effective in recent times during the percolation of water vapor in the cometary crust near the Sun (as such phases would have retained the high-D content of the cometary water), but probably at a much earlier epoch, in a environment characterized by D/H ratios similar to those observed in the hydrous phases of carbonaceous chondrites.

Antarctic Cosmic Spherules

Comparisons between Antarctic Cosmic Spherule Silicates, Antarctic Micrometeorites, and Carbonaceous Chondrites: Water Contents and D/H Ratios–Antarctic cosmic spherules have water contents in their silicate fraction (0.1 to 1.2 wt%, see Table 3a), which are surprisingly high for melted material. Their average water content (~0.6 wt%) is still about a third of the amount found in the least heated AMMs. Independent observations argue against a terrestrial origin of this water: these cosmic spherules are compact objects showing no detectable porosity and/or microfractures in which water might enter. Furthermore, SEM observations do not show etch features and/or reaction layers along the glass matrix (the most reactive component in melt ice water) that would result from Antarctic weathering (see Callot *et al.*, 1987). Given the large uncertainty on D/H absolute values for ACSs (see Table 3a) due to the ambiguity on the proper choice for α_{ins} , the isotopic results cannot be used to confirm this conclusion. However, it should be noted that this uncertainty does not affect significantly the range defined by their total D/H variations (see in Experimental, Ion Microprobe Analyses) which is comparable to that observed for unmelted AMMs (see Table 3). This is an additional argument against a terrestrial origin of the water in ACSs, because contamination by Antarctic water would define a unique value of the D/H ratio.

The presence of residual H in ACSs, with a range of D/H variation that is virtually indistinguishable from that of AMMs and carbonaceous chondrites, make cosmic spherules from diverse collections (including deep-sea samples) more interesting than previously thought. In particular, Brownlee (1985) quoted a possible relationship between deep-sea cosmic spherules and carbonaceous chondrites (CI and CM types) on the basis of their major chemical element

compositions. The present study supports this interpretation in showing that extraterrestrial water-bearing minerals were indeed present in their parent micrometeoroids. As discussed previously for AMMs, the range of D/H variation in ACSs is much narrower than that in stratospheric IDPs (by up to a factor of ~20). Therefore D-rich IDPs seem to be absent also in the flux of the parent micrometeoroids of ACSs, provided no systematic bias was introduced in our sampling.

Comparisons between Antarctic Cosmic Spherules "COPS" Nuggets and Antarctic Micrometeorites: Water Contents and D/H Ratios–The high water contents of the COPS nuggets (1 to 8 wt%, see Table 3a) are compatible with those of ferrihydrite (nominal water content of 8 wt%) that has been partially dehydrated. The range and frequency distribution of the D/H ratios for the ferrihydrite "COPS" nuggets ($D/H = 133.4 \times 10^{-6}$ to 181.7×10^{-6}; or $\delta D = -144$ to +167‰) is comparable to that of AMMs. Three of the seven nuggets have high D/H ratios, corresponding to positive δD values (up to +167‰) indicative of an extraterrestrial origin of the H. So, the constituent water of the nuggets is likely to have an extraterrestrial origin.

The mechanisms for COPS nuggets formation is unclear, partly because these objects have no counterparts in meteorite collections. Indeed, ferrihydrite is found in CI chondrites (Tomeoka and Buseck, 1988), and rarely in CM-type material (Zolensky *et al.*, 1996), but always appears as a dispersed phase in the fine-grained matrix. Such a nugget texture for ferrihydrite has not been observed in meteorites and suggests that the formation process of these nuggets is likely linked to frictional heating during atmospheric entry. Two processes might tentatively be proposed to account for this peculiar association between an iron hydroxide nugget and a melted silicate host.

(1) The COPS phase is originally present as a dispersed phase throughout the hydrous parent micrometeoroid and is separated from the silicate melt when entering the atmosphere. The phase separation is achieved by centrifugal tumbling. A problem with this idea is that the high initial water concentration in COPS has to be preserved in this process while the silicate fraction is heavily outgassed.

(2) The COPS phase could be a secondary product of a high-temperature oxidation-hydration of a metallic nugget by extraterrestrial water released by the dehydration of hydrous phases. Such nuggets likely formed by reduction of the silicates followed by separation of the metallic phases from the silicate melt formed in the atmosphere. The COPS phase would then be an "aeromineral" formed upon atmospheric entry.

Regardless of which hypothesis for the formation of COPS is correct, the presence of thermally unstable COPS nuggets as well as high-water contents in the ACSs are not expected based on models of frictional heating of micrometeoroids upon atmospheric entry (Bonny, 1990; Bonny and Balageas, 1990; Bonny *et al.*, 1988; Flynn, 1994; Love and Brownlee, 1991). Thus, they place new constraints on such models, which need to be further refined.

CONCLUSIONS

A close relationship between AMMs and carbonaceous chondrites (CI, CM, CR) was previously proposed, based on mineralogical and chemical analyses (see Engrand and Maurette, 1998; Kurat *et al.*, 1994). The D/H ratios measured in AMMs at a scale of ~10 μm support this conclusion. In addition, the possible relationship with CR chondrites, initially suggested by high pyroxene/olivine ratio in AMMs, now seems quite unlikely because CR chondrites have D enrichments exceeding by a factor of 2 those found in the presently measured AMMs. Thus, this high pyroxene/olivine ratio in the AMMs now becomes a primordial difference between most AMMs and their remaining closest meteoritic relative, the CM chondrites. This further strengthens our previous conclusion that the most abundant material present in the contemporary interplanetary space (*e.g.*, "giant" micrometeorites with sizes $\geq 50\ \mu$m, as sampled in Antarctica) is composed of a "carbonaceous chondrite without chondrules" material, not represented in meteorite collections (Engrand and Maurette, 1998, and references therein).

The parent micrometeoroids of the COPS-rich ACSs likely contained water-bearing minerals that had D/H ratios quite comparable to those observed in AMMs and in carbonaceous chondrites, but much lower than those in stratospheric IDPs. The "incomprehension" gap between stratospheric IDPs and extraterrestrial microscopic materials reaching the Antarctic ice sheet has been widened by the present isotopic results but could be explained by an unfortunate succession of "complementary" biases in both the IDP and AMM collections. Nevertheless, the narrow range of D/H variation observed in AMMs as well as in ACSs suggest that D-rich particles are indeed rare in the micrometeoroid flux.

The formation of the COPS phase (ferrihydrite) in ACSs might result from the segregation into nuggets of a ferrihydrite phase initially dispersed in the parent micrometeoroid of the particles or from dehydration reactions between indigenous ingredients during aerodynamic braking in the atmosphere. High-water concentrations both in high-temperature (silicate) and low-temperature (ferrihydrite) phases in cosmic spherules would challenge models proposed to describe the alteration and melting of micrometeoroids upon atmospheric entry. The "COPS" ferrihydrite phases are now observed in micrometeorites, cosmic spherules, CI carbonaceous chondrites (Tomeoka and Buseck, 1988), and CM clasts in the howardite–eucrite–diogenite meteorites (Zolensky *et al.*, 1996). These ferrihydrite phases may represent a common and widespread byproduct of a general hydration process in the solar system.

Cometary water has D/H ratios approximately twice those measured in AMMs and carbonaceous chondrites. To the extent that this high value of the D/H ratio can be taken as representative of cometary silicates, this study did not permit the identification of a clear cometary component in the AMM collection. On the other hand, if (at least some) AMMs originate from comets, their water-bearing phases were not formed by aqueous alteration processes during the percolation of water vapor of in the cometary crust. *In situ* cometary missions are required to ultimately decide whether cometary dust is dominated by a carbonaceous chondrite matter strongly depleted in chondrules (like AMMs) or by a D-rich matter as sampled by a large proportion of stratospheric IDPs.

Acknowledgements–We thank M. Chaussidon, K. D. McKeegan, and L. A. Leshin for comments and helpful discussions. The laboratory assistance of D. Mangin with the ion microprobe is gratefully acknowledged. The paper was improved by thoughtful reviews by K. D. McKeegan and L. R. Nittler. This work was supported by IN2P3, CNES, PNP, and IFRTP in France; and by FWF in Austria (P10688-GEO).

Editorial handling: S. Sandford

REFERENCES

ALEXANDER C. M. O. D., MAURETTE M., SWAN P. AND WALKER R. M. (1992) Studies of Antarctic micrometeorites (abstract). *Lunar Planet. Sci.* **23,** 7–8.

ARNDT P., BOSHUNG J., MAETZ M. AND JESSBERGER E. K. (1996) The elemental abundances in interplanetary dust particles. *Meteorit. Planet. Sci.* **31,** 807–816.

BALSIGER H., ALTWEGG K. AND GEISS J. (1995) D/H and $^{18}O/^{16}O$ ratio in the hydronium ion and in the neutral water from in situ ion measurements in comet Halley. *J. Geophys. Res.* **100,** 5827–5834.

BLAND P. A., SMITH T. B., JULL A. J. T., BERRY F. J., BEVAN A. W. R., COULDT S. AND PILLINGER C. T. (1996) The flux of meteorites to the Earth over the last 50,000 years. *Mon. Not. R. Astron. Soc.* **283,** 551–565.

BOATO G. (1954) The isotopic composition of hydrogen and carbon in the carbonaceous chondrites. *Geochim. Cosmochim. Acta* **6,** 209–220.

BOCKELÉE-MORVAN D., GAUTIER D., LIS D. C., YOUNG K., KEENE J., PHILLIPS T., OWEN T., CROVISIER J., GOLDSMITH P. F., BERGIN E. A., DESPOIS D. AND WOOTEN A. (1997) Deuterated water in comet C/1996 B2 (Hyakutake) and its implications for the origin of comets. *Icarus* **133,** 147–162.

BONNY P. (1990) Transmission atmosphérique des micrométéorites polaires et implications. Ph.D. thesis. Université Paris Sud, Centre d'Orsay.

BONNY P. AND BALAGEAS D. (1990) Entry corridor of micrometeorites containing organic material (abstract). *Lunar Planet. Sci.* **21,** 111–112.

BONNY P., BALAGEAS D., DEVEZEAUX D. AND MAURETTE M. (1988) Atmospheric entry of micrometeorites containing organic material (abstract). *Lunar Planet. Sci.* **19,** 118–119.

BRADLEY J. P. (1994) Chemically anomalous preaccretionally irradiated grains in interplanetary dust from comets. *Science* **265,** 925–929.

BROWNLEE D. E. (1985) Cosmic dust: Collection and research. *Ann. Rev. Earth Planet. Sci.* **13,** 147–173.

BROWNLEE D. E., BATES B. AND SCHRAMM L. (1997) The elemental composition of stony cosmic spherules. *Meteorit. Planet. Sci.* **32,** 157–175.

BROWNLEE D. E., JOSWIAK D. J., SCHLUTTER D. J., PEPIN R. O., BRADLEY J. P. AND LOVE S. G. (1995) Identification of individual cometary IDPs by thermally stepped He release (abstract). *Lunar Planet. Sci.* **26,** 183–184.

CALLOT G., MAURETTE M., POTTIER L. AND DUBOIS A. (1987) Biogenic etching of amorphous and crystalline silicates. *Nature* **328,** 147–149.

DEER W. A., HOWIE R. A. AND ZUSSMAN J. (1962) *Rock-forming Minerals.* Longmans Scientific and Technical, Harlow, England.

DEER W. A., HOWIE R. A. AND ZUSSMAN J. (1992) *An Introduction to the Rock-forming Minerals* (2nd edition). Longmans Scientific and Technical, Harlow, England. 696 pp.

DELOULE E. AND ROBERT F. (1995) Interstellar water in meteorites? *Geochim. Cosmochim. Acta* **59,** 4695–4706.

DELOULE E., FRANCE-LANORD C. AND ALBAREDE F. (1991) D/H analysis of minerals by ion probe. *Geochim. Cosmochim. Acta* **Spec. Pub. 3,** 53–62.

DELOULE E., CHAUSSIDON M. AND ALLÉ P. (1992) Instrumental limitations for isotope measurements with a Cameca IMS-3f ion microprobe: Example of H, B, S and Sr. *Chemical Geology* **101,** 187–192.

DELOULE E., DOUKHAN J. C. AND ROBERT F. (1998) Interstellar hydroxyls in meteorite chondrules: Implications for the origin of water in the inner solar system. *Geochim. Cosmochim. Acta*, **62,** 3367–3378.

DROUART A., DUBRULLE B., GAUTIER D. AND ROBERT F. (1999) Structure and transport in the Solar nebula from constraints on deuterium enrichment and giant planets formation. *Icarus*, in press.

EBERHARDT P., REBER M., KRANKOWSKY D. AND HODGES R. R. (1995) The D/H and $^{18}O/^{16}O$ ratios in water from comet P/Halley. *Astron. Astrophys.* **302,** 301–316.

ENGRAND C. (1995) Micrométéorites antarctiques: Vers l'exobiologie et la mission cométaire "ROSETTA". Ph. D. thesis, Université Paris Sud, Centre d'Orsay, France. 175 pp.

ENGRAND C. AND MAURETTE M. (1998) Carbonaceous micrometeorites from Antarctica. *Meteorit. Planet. Sci.* **33,** 565–580.

ENGRAND C., MAURETTE M., KURAT G., BRANSTÄTTER F. AND PERREAU M. (1993) A new carbon-rich phase ("COPS") in Antarctic micrometeorites (abstract). *Lunar Planet. Sci.* **24,** 441–442.

ENGRAND C., DELOULE E., HOPPE P., KURAT G., MAURETTE M. AND ROBERT F. (1996) Water contents of micrometeorites from Antarctica (abstract). *Lunar Planet. Sci.* **27,** 337–338.

FLYNN G. J. (1994) Cometary dust: A thermal criterion to identify cometary samples among the interplanetary dust collected in the stratosphere. In *Analysis of Interplanetary Dust* (eds. M. E. Zolensky, T. L. Wilson, F. J. M. Rietmeijer and G. J. Flynn), pp. 223–230. AIP Conf. Proc., American Institute of Physics, Houston, Texas, USA.

GENGE M. J. AND GRADY M. M. (1998) Melted micrometeorites from Antarctic ice with evidence for the separation of immiscible Fe-Ni-S liquids during entry heating. *Meteorit. Planet. Sci.* **33,** 425–434.

GOUNELLE M., MAURETTE M., ENGRAND C. AND KURAT G. (1998) Cometary origin for Antarctic micrometeorites: New experimental evidence (abstract). *Meteorit. Planet. Sci.* **33 (Suppl.),** A61.

HAMMER C. AND MAURETTE M. (1996) Micrometeorite flux on the melt zone of the west Greenland ice sheet (abstract). *Meteorit. Planet. Sci.* **31 (Suppl.),** A56.

HARVEY R. P. AND MAURETTE M. (1990) The best cosmic dust source in the world? The origin and significance of the Walcott neve, Antarctica micrometeorites (abstract). *Lunar Planet. Sci.* **21,** 467–468.

JESSBERGER E. K., BOHSUNG J., CHAKAVEH S. AND TRAXEL K. (1992) The volatile element enrichment of chondritic interplanetary dust particles. *Earth Planet. Sci. Lett.* **112,** 91–99.

KERRIDGE J. F. (1985) Carbon, hydrogen and nitrogen in carbonaceous chondrites: Abundances and isotopic compositions in bulk samples. *Geochim. Cosmochim. Acta* **49,** 1707–1714.

KLÖCK W. AND STADERMANN F. J. (1994) Mineralogical and chemical relationships of interplanetary dust particles, micrometeorites and meteorites. In *Analysis of Interplanetary Dust* (eds. M. E. Zolensky, T. L. Wilson, F. J. M. Rietmeijer and G. J. Flynn), pp. 51–87. AIP Conf. Proc., American Institute of Physics, Houston, Texas, USA.

KOLODNY Y., KERRIDGE J. K. AND KAPLAN I. R. (1980) Deuterium in carbonaceous chondrites. *Earth Planet. Sci. Lett.* **46,** 149–158.

KURAT G. (1998) Cosmogenic matter in terrestrial environments. In *Advanced Mineralogy: Mineral Matter in Space, Mantle, Ocean Floor, Biosphere, Environmental Managment, and Jewelry* (ed. A. S. Marfunin), pp. 28–34. Springer-Verlag, Berlin, Germany.

KURAT G., KOEBERL C., PRESPER T., BRANDSTÄTTER F. AND MAURETTE M. (1994) Petrology and geochemistry of Antarctic micrometeorites. *Geochim. Cosmochim. Acta* **58,** 3879–3904.

LEVASSEUR-REGOURD A. C., RENARD J. B. AND DUMONT R. (1991) The zodiacal cloud complex. In *Origin and Evolution of Interplanetary Dust* (eds. A. C. Levasseur-Regourd and H. Hasegawa), pp. 131–138. Kluwer Academic Publishers, Dordrecht, The Netherlands.

LIOU J. C. AND ZOOK H. A. (1996) Comets as a source of low eccentricity and low inclination interplanetary dust particles. *Icarus* **123,** 491–502.

LIOU J. C. AND ZOOK H. A. (1997) Evolution of interplanetary dust particles in mean motion resonances with planets. *Icarus* **128,** 354–367.

LIOU J. C., DERMOTT S. F. AND XU Y. L. (1995) The contribution of cometary dust to the zodiacal cloud. *Planet. Space Sci.* **43,** 717–722.

LIOU J. C., ZOOK H. A. AND DERMOTT S. F. (1996) Kuiper belt dust grains as a source of interplanetary dust particles. *Icarus* **124,** 429–440.

LOVE S. G. AND BROWNLEE D. E. (1991) Heating and thermal transformation of micrometeoroids entering the Earth's atmosphere. *Icarus* **89,** 26–43.

LOVE S. G. AND BROWNLEE D. E. (1993) A direct measurement of the terrestrial mass accretion rate of cosmic dust. *Science* **262,** 550–553.

MAURETTE M., OLINGER C., CHRISTOPHE M., KURAT G., POURCHET M., BRANDSTÄTTER F. AND BOUROT-DENISE M. (1991) A collection of diverse micrometeorites recovered from 100 tons of Antarctic blue ice. *Nature* **351,** 44–47.

MAURETTE M., KURAT G., PERREAU M. AND ENGRAND C. (1993) Micro-analyses of Cap-Prudhomme Antarctic micrometeorites. *Microbeam Analysis* **2,** 239–251.

MAURETTE M., IMMEL G., HAMMER C., HARVEY R., KURAT G. AND TAYLOR S. (1994) Collection and curation of IDPs from the Greenland and Antarctic ice sheets. In *Analysis of Interplanetary Dust* (eds. M. E. Zolensky, T. L. Wilson, F. J. M. Rietmeijer and G. J. Flynn), pp. 277–289. AIP Conf. Proc., American Institute of Physics, Houston, Texas, USA.

MAURETTE M., ENGRAND C. AND KURAT G. (1996) Collection and microanalysis of Antarctic micrometeorites. In *Physics, Chemistry, and Dynamics of Interplanetary Dust—Proceedings of the 150th Colloquium of the International Astronomical Union* (eds. B. A. S. Gustafson and M. S. Hanner), pp. 265–273. Astronomical Society of the Pacific Conferences Series, Gainesville, Florida, USA.

MAURETTE M., TAYLOR S., ENGRAND C., LEVER J., KURAT G. AND NTAFLOS T. (1997) Cosmic dust from Cap-Prudhomme and South Pole, Antarctica (abstract). *EGS Meeting,* Annales Geophysicae, Vienna April 1997.

MCKEEGAN K. D. (1987) Ion microprobe measurements of H, C, O, Mg and Si isotopic abundances in individual interplanetary dust particles. Ph.D. thesis, Washington University, St. Louis, Missouri, USA. 187 pp.

MCKEEGAN K. D., WALKER R. M. AND ZINNER E. (1985) Ion microprobe isotopic measurements of individual interplanetary dust particles. *Geochim. Cosmochim. Acta* **49,** 1971–1987.

MCKEEGAN K. D., SWAN P., WALKER R. M., WOPENKA B. AND ZINNER E. (1987) Hydrogen isotopic variations in interplanetary dust particles (abstract). *Lunar Planet. Sci.* **18,** 627–628.

McNaughton N. J., Borthwick J., Fallick A. E. and Pillinger C. T. (1981) Deuterium/hydrogen ratio in unequilibrated ordinary chondrites. *Nature* **294,** 639–641.

McNaughton N. J., Fallick A. E. and Pillinger C. P. (1982) Deuterium enrichments in Type 3 ordinary chondrites. *Proc. Lunar Planet. Sci. Conf.* **13th**, *J. Geophys. Res.* **87,** A297–302.

McSween H. Y., Jr. (1987) Aqueous alteration in carbonaceous chondrites: Mass balance constraints on matrix mineralogy. *Geochim. Cosmochim. Acta* **51,** 2469–2477.

Meier R., Owen T. C., Matthews H. E., Jewitts D. C., Bockelée-Morvan D., Biver N., Crovisier J. and Gautier D. (1998) A determination of the HDO/H_2O ratio in comet C/1995 O1 (Hale-Bopp). *Science* **279,** 842–844.

Messenger S. (1997) Combined molecular and isotopic analysis of circumstellar and interplanetary dust. Ph.D. thesis, Washington University, St. Louis, Missouri, USA. 191 pp.

Messenger S. and Walker R. M. (1997) Evidence for molecular cloud material in meteorites and interplanetary dust. In *Astrophysical Implications of the Laboratory Study of Presolar Materials* (eds. T. J. Bernadowicz and E. K. Zinner), pp. 545–564. AIP Conf. Proc., American Institute of Physics, St. Louis, Missouri, USA.

Messenger S. and Walker R. M. (1998) Possible association of isotopically anomalous cluster IDPs with comet Schwassmann-Wachmann 3 (abstract). *Lunar Planet. Sci.* **29,** #1906, Lunar and Planetary Institute, Houston, Texas, USA (CD-ROM).

Nishiizumi K., Arnold J. R., Fink D., Klein J., Middleton R., Brownlee D. E. and Maurette M. (1991) Exposure history of individual cosmic particles. *Earth Planet. Sci. Lett.* **104,** 315–324.

Olinger C. T., Maurette M., Walker R. M. and Hohenberg C. M. (1990) Neon measurements of individual Greenland sediment particles: Proof of an extraterrestrial origin and comparison with EDX and morphological analyses. *Earth Planet. Sci. Lett.* **100,** 77–93.

Peucker-Ehrenbrink B. (1996) Accretion of extraterrestrial matter during the last 80 million years and its effect on the marine osmium record. *Geochim. Cosmochim. Acta* **60,** 3187–3196.

Presper T., Kurat G., Koeberl C., Palme H. and Maurette M. (1993) Elemental depletions in Antarctic micrometeorites and Arctic cosmic spherules: Comparison and relationships (abstract). *Lunar Planet. Sci.* **24,** 1177–1178

Raisbeck G. M. and Yiou F. (1987) ^{10}Be and ^{26}Al in micrometeorites from Greenland ice. *Meteoritics* **22,** 485–486.

Raisbeck G. M., Yiou F., Bourles D. and Maurette M. (1986) ^{10}Be and ^{26}Al in Greenland cosmic spherules: Evidence for irradiation in space as small objects and a probable cometary origin (abstract). *Meteoritics* **21,** 487–488.

Robert F. and Epstein S. (1982) The concentration and isotopic composition of hydrogen, carbon and nitrogen in carbonaceous chondrites. *Geochim. Cosmochim. Acta* **46,** 81–95.

Robert F., Merlivat L. and Javoy M. (1979) Deuterium concentration in the early Solar System: Hydrogen and oxygen isotope study. *Nature* **282,** 785–789.

Robert F., Javoy M., Halbout J., Dimon B. and Merlivat L. (1987a) Hydrogen isotope abundances in the solar system: Part I. Unequilibrated chondrites. *Geochim. Cosmochim. Acta* **51,** 1787–1805.

Robert F., Javoy M., Halbout J., Dimon B. and Merlivat L. (1987b) Hydrogen isotope abundances in the solar system: Part II. Meteorites with terrestrial-like D/H ratio. *Geochim. Cosmochim. Acta* **51,** 1807–1822.

Shimizu N. and Hart S. R. (1982) Isotope fractionation in secondary ion mass spectrometry. *J. Appl. Phys.* **53,** 1303–1311.

Slodzian G., Lorin J. C. and Havette A. (1980) Isotopic effect on the ionization probabilities in secondary ion emission. *J. Phys.* **23,** 555–558.

Taylor S., Lever J. and Harvey R. (1996) A new source of micrometeorites: The South Pole water well (abstract). *Lunar Planet. Sci.* **27,** 1319–1320.

Taylor S., Lever J. H. and Harvey R. P. (1998) Accretion rate of cosmic spherules measured at the South Pole. *Nature* **392,** 899–903.

Tomeoka K. and Buseck P. R. (1988) Matrix mineralogy of the Orgueil CI carbonaceous chondrite. *Geochim. Cosmochim. Acta* **52,** 1627–1640.

Walter J., Brandstätter F., Kurat G., Koeberl C. and Maurette M. (1995a) Cosmic spherules, micrometeorites and chondrules (abstract). *Lunar Planet. Sci.* **26,** 1457–1458.

Walter J., Kurat G., Brandstätter F., Koeberl C. and Maurette M. (1995b) The abundance of ordinary chondrite debris among Antarctic micrometeorites (abstract). *Meteoritics* **30,** 592–593.

Whipple F. L. (1967) On maintaining the meteoritic complex. In *The Zodiacal Light and The Interplanetary Medium* (ed. J. L. Weinberg), p. 409. NASA SP-150, U.S. Government Printing Office, Washington D.C., USA.

Zinner E., McKeegan K. D. and Walker R. M. (1983) Laboratory measurements of D/H ratios in interplanetary dust. *Nature* **305,** 119–121.

Zolensky M. E. and Lindstrom D. J. (1992) Mineralogy of 12 large "chondritic" interplanetary dust particles. *Proc. Lunar Planet. Sci. Conf.* **22th,** 161–169.

Zolensky M. E., Weisberg M. K., Buchanan P. C. and Mittlefehldt D. W. (1996) Mineralogy of carbonaceous chondrite clasts in HED achondrites and the Moon. *Meteorit. Planet. Sci.* **31,** 518–537.

Pergamon

Geochimica et Cosmochimica Acta, Vol. 63, No. 17, pp. 2623–2636, 1999

0016-7037/99 $20.00 + .00

PII S0016-7037(99)00160-X

Oxygen isotopic compositions of individual minerals in Antarctic micrometeorites: Further links to carbonaceous chondrites

CÉCILE ENGRAND,*,† KEVIN D. MCKEEGAN, and LAURIE A. LESHIN‡
UCLA, Department of Earth and Space Sciences, 595 Charles Young Drive, Los Angeles, CA 90095-1567, USA

(*Received October* 21, 1998; *accepted in revised form April* 16, 1999)

Abstract—We report in situ measurements of oxygen isotopic abundances in individual silicate and oxide minerals from 16 Antarctic micrometeorites (AMMs). The oxygen isotopic compositions of 10 olivine and 11 pyroxene grains are enriched in ^{16}O relative to terrestrial minerals, and on an oxygen three-isotope diagram they plot on the low $\delta^{18}O$ side of the ^{16}O mixing line defined by calcium-aluminum-rich inclusions (CAI) from chondritic meteorites. AMM olivine and pyroxene $\delta^{18}O$ values range from –9.9‰ to +8.0‰ and $\delta^{17}O$ ranges from –11.3‰ to +5.5‰, similar to values measured in individual olivine grains and whole chondrules from carbonaceous chondrites. These data indicate that the mineral grains preserve their pre-terrestrial oxygen isotopic compositions, and provide another link between AMMs and carbonaceous chondrites. However, no clear relationship with one single subgroup of carbonaceous chondrite can be established. Based on their textures, crystal chemistries, and oxygen isotopes, some coarse-grained crystalline AMMs could originate from chondrule fragmentation. Whether the remaining mineral grains were formed by igneous or condensation processes is unclear. No clear correlation is observed between isotopic compositions and mineral compositions of AMM olivine grains, suggesting that the FeO- and ^{16}O-enrichment processes are not coupled in a simple way. Nor are any relatively large ^{16}O enrichments measured in any of the olivine grains, however two Mg-Al spinels and a melilite grain are ^{16}O enriched at the level of $\delta^{18}O \sim \delta^{17}O \sim -40‰$. The discovery of an ^{16}O-enriched melilite grain in AMMs supports the hypothesis that refractory minerals throughout the solar nebula formed from a relatively uniformly ^{16}O-enriched reservoir. This unique ^{16}O-rich signature of refractory minerals in primitive solar system materials suggests that they either formed from a widespread ^{16}O-rich reservoir in the solar nebula, or that an efficient mechanism (such as bipolar outflows) was acting to spread them from a highly localized ^{16}O-rich region over the early solar nebula.

1. INTRODUCTION

The majority of the mass of extraterrestrial matter presently accreted by Earth is comprised of particles in the 50–400 μm size range (Love and Brownlee, 1993). Much of this material is heated during passage through the atmosphere resulting in partial to total melting, but some particles with low enough velocity and/or shallow entry angles survive as unmelted micrometeorites. These particles may be collected from Antarctic blue ice which contains very low levels of terrestrial dust (Maurette et al., 1991, 1994). Many of these Antarctic micrometeorites (AMMs) consist of unequilibrated mixtures of fine-grained anhydrous minerals, hydrated silicates, and carbonaceous matter, and display chemical and mineralogical affinities to CI, CM and CR carbonaceous chondrites (Engrand and Maurette, 1998; Kurat et al., 1994b). However, differences between AMMs and CI/CM/CR chondrites in terms of relative abundances of major silicate minerals, range of mineral chemistries (e.g., fayalite contents of olivine), bulk C/O ratios, and the extremely low abundance of chondrules in AMMs clearly indicate that they sample a different type of extraterrestrial matter than that represented in conventional meteorite collections (Engrand and Maurette, 1998). This may reflect biases in the macroscopic meteorite collection, such as atmospheric-entry selection effects and/or the predominance of samples from a limited number of asteroidal parent bodies (Meibom and Clark, 1999), that are not as prevalent among the micrometeorite population. Thus, it is of considerable interest to understand the intrinsic properties of micrometeorites which may be more representative of small solar system bodies than are common meteorite types (e.g., ordinary chondrites).

Analyses of whole-rock meteorites have demonstrated that oxygen isotopic abundances are heterogeneously distributed on a planetary scale within the inner solar system and have led to the use of oxygen isotopic composition as an essential parameter in the classification of meteorites (Clayton, 1993 and references therein). The distinctive oxygen isotopic compositions of meteorites within a group is thought to reflect their common origin from a singular parent body or, perhaps, a limited number of related asteroids (e.g., in the case of the carbonaceous chondrites). How micrometeorites fit into this classification scheme based on oxygen isotopic composition is not known.

Isotopic studies of micrometeorites are hampered by their small sizes and by potential problems of contamination or isotopic exchange during atmospheric entry and prolonged terrestrial residence times. Some isotopic data exist for hydrogen (Engrand et al., in press), carbon (Wright et al., 1997), and neon (Olinger, 1990; Olinger et al., 1990) in individual AMMs.

*Author to whom correspondence should be addressed (engrand@csnsm.in2p3.fr).
†*Present address:* C.S.N.S.M. Bat 104, F-91405 Orsay Campus, France; Tel: +33 1 69 15 52 95; Fax: +33 1 69 15 50 08.
‡*Present address:* Department of Geology, Arizona State University, Tempe, AZ 85287-1404, USA; Tel: (602) 965-0796; Fax: (602) 965-8102; E-mail: laurie.leshin@asu.edu.

Oxygen isotope compositions have been reported only for suites of cosmic spherules collected from deep sea sediments (Clayton et al., 1986), for 2 olivines from Greenland micrometeorites (Christophe Michel-Levy and Bourot-Denise, 1992), and for refractory minerals (spinel and pyroxene) from 4 AMMs (Greshake et al., 1996; Hoppe et al., 1995; Kurat et al., 1994a). These limited data do not permit definitive comparisons to meteorite compositional groups because either the indigenous oxygen in the micrometeorites has partially exchanged with terrestrial oxygen reservoirs (as is the case for the cosmic deep sea spherules), or because refractory minerals exhibit ^{16}O-rich compositions regardless of meteorite group (e.g., McKeegan et al., 1998b).

We report in situ ion microprobe analyses of the oxygen isotopic compositions of single olivine and pyroxene grains from 15 AMMs, and of refractory minerals from 2 AMMs. Because these minerals are thought to be relict (i.e., they did not form during atmospheric entry), they are expected to preserve their pre-terrestrial oxygen isotopic compositions. The oxygen isotopic analysis of common mafic silicates allows a more direct comparison to similar mineral phases in chondrites for which a relatively large body of data exist (Choi et al., 1997b; Hervig and Steele, 1992; Jones et al., 1998; Leshin et al., 1998; Leshin et al., 1997; Saxton et al., 1998; Sears et al., 1998; Weinbruch et al., 1993). The primary goals of this work are to better constrain the relationships of AMMs to conventional meteorite groups and to attempt to shed light on the origins of anhydrous mineral grains in AMMs. To the extent that AMMs provide a more complete sampling of primitive extraterrestrial materials, these data may also assist in better defining oxygen isotopic reservoirs in the solar nebula.

2. SAMPLES AND METHODS

Individual AMMs containing mineral grains large enough for in situ ion microprobe analysis of their oxygen isotopic compositions were selected from the 50–100 μm and 100–400 μm size fractions of micrometeorites harvested from the blue ice fields of Cap-Prudhomme, Antarctica, (see Maurette et al., 1994 for details regarding sample collection). A total of 10 olivine and 11 pyroxene grains, ranging in size from about 10–30 μm, were identified from among 15 AMMs. One melilite and one spinel grain (~8–10 μm in diameter) were located within an additional micrometeorite, and a small spinel was also documented within one of the olivine and pyroxene-bearing AMMs. All AMMs were mounted in epoxy and polished to expose the sample interiors (see Figs. 1, 2 and 3 for electron micrographs of typical examples of these AMMs).

The major and minor element compositions of all minerals were determined prior to ion microprobe isotopic analysis by using the UCLA CAMECA Camebax microbeam electron microprobe or the Caltech JEOL JXA-733 Superprobe with a sample current of 10 nA at 15 kV.

The oxygen isotopic compositions of the selected minerals were measured in situ within the AMM polished sections by using the UCLA CAMECA ims 1270 ion microprobe. Samples were coated with ~ 350 Å of gold. The ~0.1–0.4 nA primary Cs^+ beam was shaped into a spot ~ 8–10 μm in diameter (usually in aperture illumination mode). Charge compensation was achieved using a normal-incidence electron flood gun (Slodzian, 1980). Low energy (~0–30 eV) negative secondary ions were measured at high-mass resolving power (M/ΔM) of about 6500. At this mass resolution, the correction for the contribution of the tail of the $^{16}OH^-$ peak to the $^{17}O^-$ signal was typically less than 0.1‰. Measurements were made by magnetic peak switching through 25 cycles of counting $^{16}O^-$ for 3s, $^{17}O^-$ for 10s and $^{18}O^-$ for 5s. The secondary $^{16}O^-$ current was measured in a Faraday cup equipped with a Keithley 642 electrometer, and the $^{17}O^-$ and $^{18}O^-$ signals were pulse-counted on an electron multiplier with a deadtime of typically 20 ns. The analysis conditions typically yielded equivalent count rates of 20–40 million counts per second of $^{16}O^-$. Measured secondary ion intensities were corrected for background ($^{16}O^-$), and for deadtime ($^{17}O^-$ and $^{18}O^-$). With the count rates employed in these experiments, the total magnitude of these corrections is small (<2‰), and thus the additional uncertainties resulting from background and deadtime corrections are negligible (~0.1‰).

San Carlos olivine was used as a standard ($\delta^{18}O = +5.25$‰; Eiler et al., 1995) to correct for instrumental mass fractionation. The olivine data have been corrected for matrix effects, i.e., the change of the instrumental mass fractionation as a function of the chemical composition of the sample. Based on previous analyses of olivine standards ranging in composition from Fa_9[1] to Fa_{100} the magnitude of matrix effect corrections was determined to be ~+0.5‰/amu per increase of Fa_{10} for the analyzed olivine as compared with the standard (San Carlos olivine, $Fa_{9.2}$). Such corrections for the AMM olivine grains were on the order of 1‰, and thus slight inaccuracies in this correction do not affect the interpretation of the data. No matrix effect corrections were made for the other mineral (pyroxene, melilite, spinel) data, because analyses of enstatite, melilite, and spinel standards all show relative variations of instrumental mass fractionation compared to San Carlos olivine of <1‰/amu under our experimental conditions. The reported (1σ) uncertainties reflect the internal measurement precision quadratically summed with the standard deviation of analyses on the primary standard during the analytical session (which represents the uncertainty in the instrumental mass fractionation correction and in the relative collection efficiency of the two detectors). Under our experimental conditions, the precision and accuracy of the analysis is typically 1 to 1.5‰ in both $\delta^{18}O$ and $\delta^{17}O$.

3. RESULTS

3.1. Petrography and Mineral Chemistry

The olivine and pyroxene grains studied here occur in two different textural settings: as coarse-grained crystalline AMMs (Fig. 1) and as isolated mineral grains in a fine-grained matrix (Fig. 2). We analyzed olivine and pyroxene grains in 4 coarse-grained crystalline AMMs (# 92-13C-13, -20, -26; # 94-4B-38; Fig. 1), and in 11 fine-grained AMMs which range in texture from unmelted to scoriaceous (see Fig. 2). The minerals are euhedral to rounded and typically range from 5–50 μm in size (Figs. 1 & 2).

Major and minor element abundances in individual olivine and pyroxene grains from 15 AMMs are reported in Table 1. The pyroxene grains analyzed are all Ca-poor and have compositions $Fs_{1.3\text{-}11}$ $Wo_{0.6\text{-}3}$. Olivine grains range in composition between Fa_1 and Fa_{34}. These compositions are comparable to the range previously reported for AMM olivine and pyroxene grains (Beckerling and Bishoff, 1995; Christophe Michel-Levy and Bourot-Denise, 1992; Kurat et al., 1994b; Presper, 1993; Steele, 1992).

Refractory minerals analyzed in this study include two spinel grains and the first melilite mineral discovered in the AMM collection (see Fig. 3). The spinel grains are nearly pure $MgAl_2O_4$ and the melilite has an intermediate composition, $Åk_{22}$ (Table 1). End-member Mg-Al spinel grains are common in refractory inclusions (CAIs) from carbonaceous chondrites, as are melilite grains with Al-contents comparable with that of the melilite in AMM # 92-13C-23 (MacPherson et al., 1988).

[1] The Fa_x notation is used to represent the fayalite component of the olivine, where x = 100*Fe/(Fe + Mg) with cation concentrations expressed as mole fractions

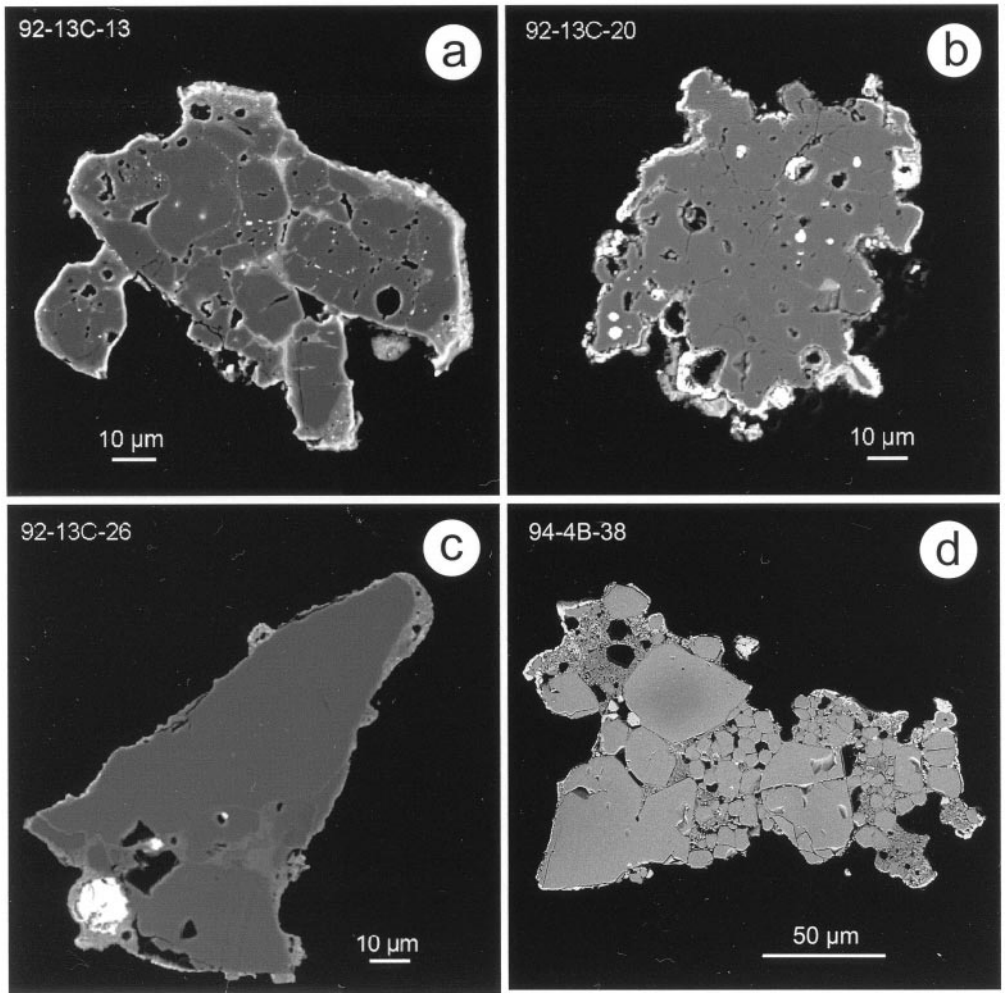

Fig. 1. Backscattered electron micrographs of coarse-grained crystalline Antarctic micrometeorites consisting of assemblages of olivine and pyroxene grains with minor amounts of fine-grained matrix.

3.2. Oxygen Isotopes

The oxygen isotopic compositions of olivine, pyroxene, spinel, and melilite grains from 16 AMMs are reported in Table 2 and shown on a three-isotope diagram in Fig. 4a.

For the 10 olivine grains (Fig. 4b), $\delta^{18}O$ values range from −8.3 ‰ to +8.0 ‰ and $\delta^{17}O$ from –7.4 ‰ to +5.5‰. The $\delta^{18}O$ values for the pyroxenes (Fig. 4b) range from −9.9‰ to +2.2‰, and $\delta^{17}O$ from –11.3‰ to +0.4‰.

The AMM olivine and pyroxene oxygen isotopic compositions plot parallel to, but slightly above, the CAI line and mostly below the terrestrial fractionation (TF) line in the oxygen three-isotope plot. The displacement from the terrestrial fractionation line, expressed as $\Delta^{17}O$ values, are typically in the range of –2 to −4‰ for the olivine and pyroxene grains. As a group, the AMM olivine grains have oxygen isotopic compositions which are slightly poorer in ^{16}O than those of the pyroxene grains. No correlation between the oxygen isotopic composition and the apparent size of the host micrometeorite or the mineral grain size is observed.

In 4 AMMs, individual mineral grains were large enough to permit multiple analyses of the same crystal (1 olivine, in AMM #92-13C-26, and 3 pyroxenes, in AMMs #92-13C-4, -15, -20). No significant ($>2\sigma$) heterogeneity is observed within an individual grain. However, the isotopic compositions of both olivine and pyroxene grains do vary from one AMM to another, and within two AMMs there is slight intergrain heterogeneity between olivine and pyroxene grains of different FeO contents (AMM #94-4b-5) or between olivine grains of different FeO content (AMM #94-4b-38).

A single analyzed melilite ($Åk_{22}$) grain exhibits a large ^{16}O enrichment with $\delta^{18}O = -42.2‰$ and $\delta^{17}O = -43.8‰$. Spinel grains, of nearly pure $MgAl_2O_4$, were analyzed in 2 AMMs. The analysis of spinel in AMM # 94-4b-5 yielded only a moderate ^{16}O enrichment ($\delta^{18}O$ = –21‰ and $\delta^{17}O$ = –27‰) probably due to its small size (<10 μm) which resulted in partial overlap of the ion beam onto adjacent fine-grained matrix material. In particle # 92-13C-23, multiple analyses of the spinel yielded a range of ^{16}O-enrichments between approximately −40‰ and −48‰ with an average composition of $\delta^{18}O = -42‰$ and $\delta^{17}O = -43‰$. It is likely that the range of values observed in the spinel from #92-13C-23 also

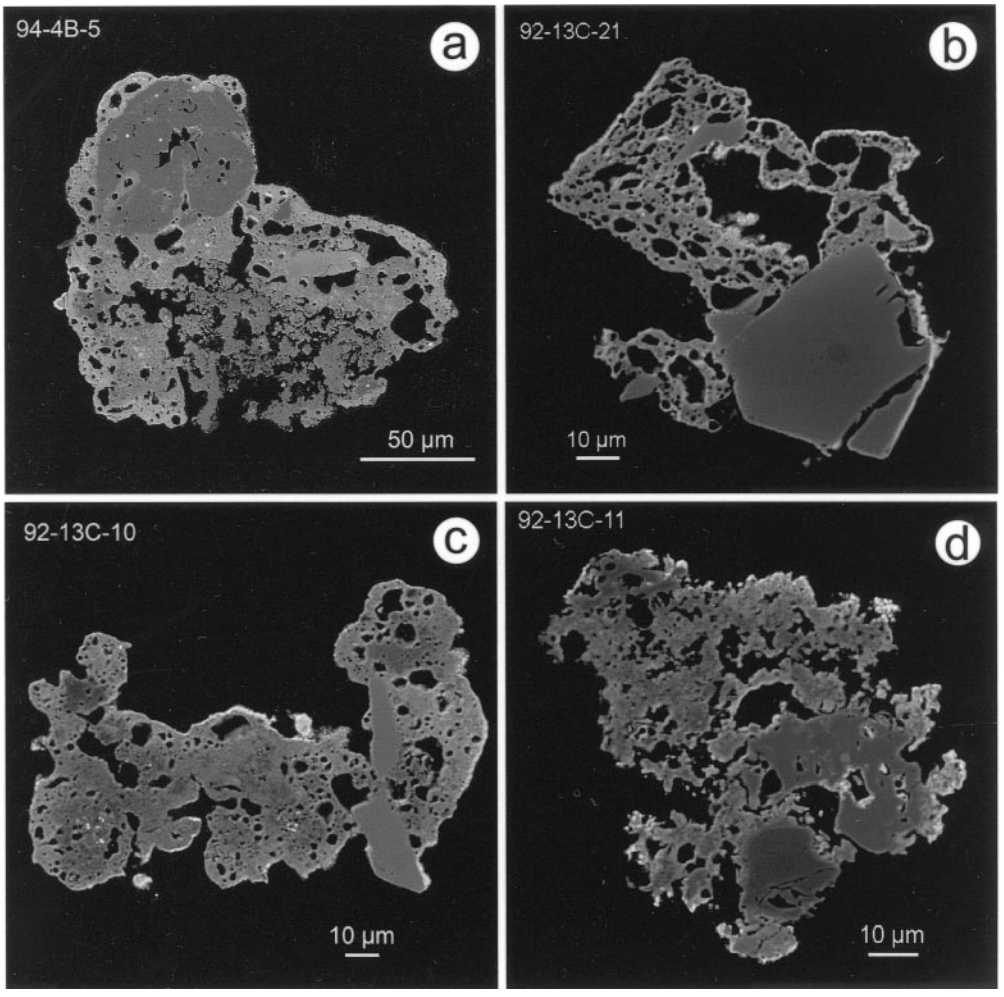

Fig. 2. Backscattered electron micrographs of Antarctic micrometeorites containing individual minerals of olivine (a,b,c) and pyroxene (a,d). The mineral grains are embedded in unmelted to partially-melted (scoriaceous) matrix. The rounded crystalline structure in Fig. 2a consists of an assemblage of coarse Mg-rich olivine and pyroxene grains. An additional FeO-rich olivine grain (Fa_{32}), that is located within the fine-grained matrix of this AMM, was analyzed for oxygen isotopic composition. See Engrand and Maurette (1998) and Kurat et al. (1994b) for the definition of the textural classification of micrometeorites.

reflects minor ion beam mixing rather than true heterogeneity within this single spinel grain.

4. DISCUSSION

We have analyzed the oxygen isotopic compositions of individual mineral grains from 16 AMMs. Based on their textures and chemical compositions, these minerals have been interpreted to be relict and unaltered by atmospheric entry heating. The observed isotopic homogeneity within single AMM mineral grains, as well as the lack of a trend toward isotopically heavy (i.e., ^{18}O and ^{17}O-enriched) oxygen as observed in clearly melted cosmic spheres (Engrand et al., 1998), argues strongly against mass fractionation or isotopic exchange with terrestrial oxygen during atmospheric entry. Thus, these data represent the pre-terrestrial oxygen isotopic composition of the grains and allow a direct comparison to data for similar phases in chondrites.

4.1. Olivine and Pyroxene Data: Comparison to Meteorites and Interplanetary Dust Particles

Chondritic meteorites are unequilibrated with respect to oxygen isotopic composition on size scales ranging from whole-rock (Clayton, 1993) to discrete, mm-sized nebular constituents such as chondrules and inclusions (e.g., Clayton and Mayeda, 1983; Clayton et al., 1991; Clayton et al., 1977) to, in some cases, μm scale, sub-mineralic domains (e.g., McKeegan et al., 1996). The ordinary chondrites are characterized by having whole-rock oxygen isotopic compositions that plot above the terrestrial mass-dependent fractionation line (TF line), while almost all carbonaceous chondrites are more ^{16}O-enriched than ordinary chondrite or terrestrial samples, and thus plot below the TF line (Clayton, 1993 and references therein). The main exception to this general rule are the highly aqueously altered CI chondrites, which have bulk isotopic compositions which plot close to but slightly above the TF line

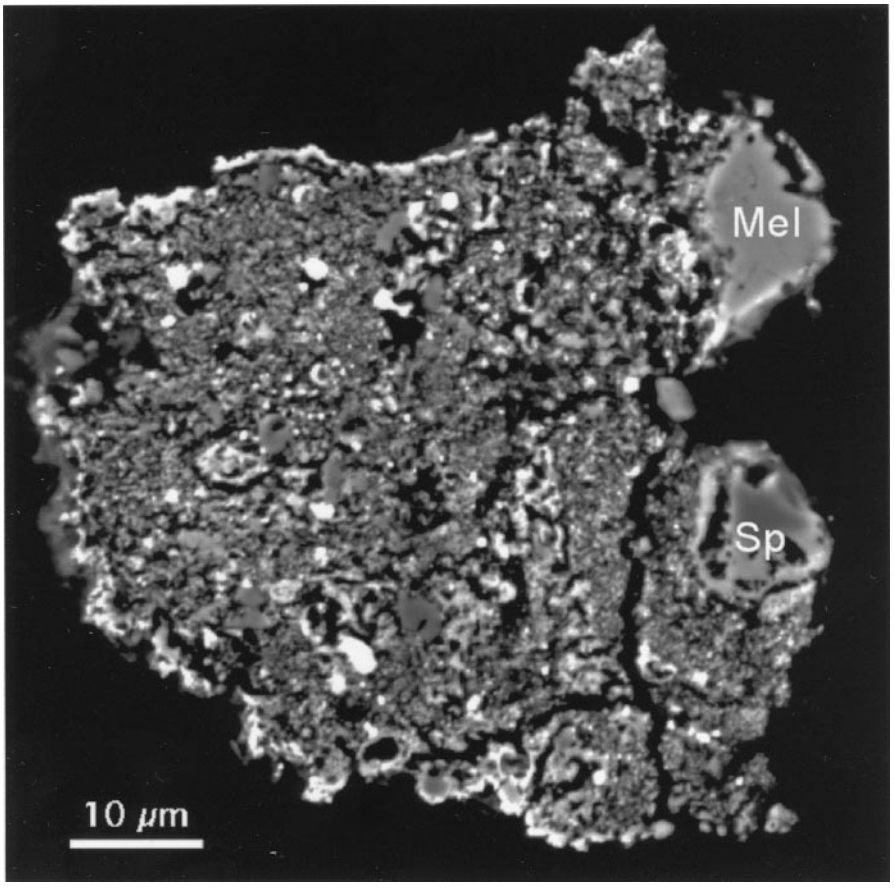

Fig. 3. Backscattered electron micrographs of a fine-grained Antarctic micrometeorite containing a spinel and a melilite ($Åk_{22}$) grain.

(Clayton and Mayeda, 1984; Rowe et al., 1994). Recent ion microprobe studies have demonstrated that oxygen isotopic heterogeneities are even more extensive than previously indicated, further complicating this picture. For example, ^{16}O-enriched material has been identified in ordinary chondrites (McKeegan et al., 1998b; Russell et al., 1997; Saxton et al., 1995; Saxton et al., 1996). However, these are minor components of ordinary chondrites (such as refractory inclusions) and the majority of mafic silicates in these meteorites, e.g., the olivine and pyroxene in chondrules, are characterized by oxygen isotopic compositions that lie above the TF line by a few permil (Ash et al., 1998; Clayton and Mayeda, 1983; Clayton et al., 1991). In addition, other ion microprobe data have confirmed that the anhydrous precursor (olivine and pyroxene) minerals in CI carbonaceous chondrites are ^{16}O-enriched and are likely to have been derived from the breakup of chondrules (Leshin et al., 1997). Thus, although some mixing has undoubtedly occurred, to first order the oxygen isotope data for whole-rock chondrites and their chondrules indicate that the nebular accretion regions of the ordinary and carbonaceous chondrites were distinct with respect to oxygen isotopic composition. It is therefore plausible that the oxygen isotopic signatures of the same minerals from AMMs could provide a distinctive link to one of these classes of meteorites.

Our data on oxygen isotopes in AMM olivine and pyroxene grains plot below the TF line with $\Delta^{17}O$ values typically in the range of –2 to –4‰. Such compositions are distinct from those of olivines measured as single mineral grains (Choi et al., 1998; Sears et al., 1998) or from whole chondrule data (Clayton et al., 1991) in ordinary chondrites, but are compatible with those measured in anhydrous silicate minerals from carbonaceous meteorites (Choi et al., 1997b; Clayton, 1993 and references therein; Clayton and Mayeda, 1983; Clayton et al., 1991; Hervig and Steele, 1992; Jones et al., 1998; Leshin et al., 1998; Leshin et al., 1997; Weinbruch et al., 1993). Thus, these data provide a further link between AMMs and carbonaceous chondrites. However, within the carbonaceous chondrites significant overlap exists in isotopic compositions reported for individual silicate (mostly olivine) mineral grains (CV: Choi et al., 1997b; Hervig and Steele, 1992; Leshin et al., 1998; Weinbruch et al., 1993), (CR: Leshin et al., 1998), (CO: Jones et al., 1998), (CI: Leshin et al., 1997). In addition, our data demonstrate that there is considerable spread within the AMM population (Fig. 4a) which overlaps much of the range of data reported from carbonaceous chondrite chondrules (Fig. 4c). Thus, oxygen isotope data of olivine and pyroxene minerals are not sufficiently diagnostic at the individual grain level to discriminate amongst different groups of carbonaceous chondrites, and our data cannot assign a definite affiliation of AMMs with a single class of carbonaceous chondrite.

In chondritic meteorites, coarse-grained olivine and pyroxene minerals occur predominantly in chondrules and CAIs, or,

Table 1. Electron microprobe analyses of AMM olivine, pyroxene, spinel and melilite grains analyzed for their oxygen isotopic composition.

Sample designation	AMM size fraction (μm)	Mineral	Mineral composition	MgO	Al_2O_3	SiO_2	CaO	TiO_2	Cr_2O_3	MnO	FeO	NiO	Total
92-13C-4	50-100	Px	$Fs_{1.3}Wo_{1.1}$	38.5	1.28	60.3	0.58	n.d.	0.68	0.14	0.8	0.01	102.31
92-13C-5	50-100	Px	$Fs_{2.3}Wo_{1.2}$	38.4	1.10	59.1	0.64	n.d.	0.50	0.06	1.6	0.03	101.38
92-13C-10	50-100	Ol	$Fa_{33.8}$	32.0	0.05	37.4	0.17	n.d.	0.51	0.50	29.1	0.16	99.94
92-13C-11	50-100	Px	$Fs_{2.0}Wo_{0.8}$	38.9	0.96	60.2	0.44	n.d.	0.65	0.09	1.4	0.02	102.62
92-13C-11	50-100	Px	$Fs_{8.2}Wo_{2.9}$	34.0	1.84	57.5	1.52	n.d.	0.98	0.52	5.0	0.08	101.46
92-13C-13	50-100	Ol	$Fa_{2.2}$	54.4	0.21	43.7	0.20	n.d.	0.61	0.33	2.2	0.11	101.90
92-13C-13	50-100	Px	$Fs_{1.6}Wo_{1.1}$	37.8	0.85	59.9	0.59	n.d.	0.81	0.00	1.1	0.05	101.20
92-13C-15	50-100	Px	$Fs_{5.3}Wo_{0.9}$	37.2	0.43	59.1	0.47	n.d.	1.24	0.32	3.4	0.00	102.12
92-13C-20	50-100	Px	$Fs_{3.5}Wo_{1.2}$	37.9	0.68	59.5	0.68	n.d.	0.75	0.20	2.3	0.07	102.02
92-13C-21	50-100	O1	$Fa_{28.7}$	35.8	0.05	38.0	0.19	n.d.	0.53	0.31	25.6	0.07	100.54
92-13C-23	50-100	Mel	$Åk_{22}$	3.6	28.33	26.3	40.5	n.d.	0.03	0.02	0.25	0.00	99.02
92-13C-23	50-100	Sp	Sp	28.8	70.27	0.3	0.52	n.d.	0.38	0.00	0.20	0.08	100.50
92-13C-26	50-100	Ol	$Fa_{3.8}$	53.8	0.02	42.6	0.21	n.d.	0.62	0.29	3.8	0.12	101.53
92-13C-33	50-100	Px	$Fs_{4.4}Wo_{1.1}$	35.9	0.91	57.7	0.58	n.d.	0.62	0.11	2.9	0.00	98.81
92-13C-35	50-100	Px	$Fs_{1.3}Wo_{0.6}$	39.7	0.37	60.7	0.36	n.d.	0.49	0.07	0.9	0.00	102.52
94-4b-2	100-400	Ol	$Fa_{2.6}$	54.7	0.09	42.2	0.13	0.02	0.47	0.29	2.6	0.00	100.46
94-4b-5	100-400	Ol	$Fa_{1.1}$	54.8	0.02	41.7	0.21	0.02	0.48	0.20	1.1	0.01	98.59
94-4b-5	100-400	Ol	$Fa_{32.4}$	33.0	0.02	37.2	0.25	0.00	0.43	0.29	28.1	0.00	99.38
94-4b-5	100-400	Px	$Fs_{2.6}Wo_{1.2}$	37.1	0.75	57.3	0.64	0.12	0.57	0.17	1.6	0.03	98.28
94-4b-5	100-400	Sp	Sp_{99}	27.6	68.09	0.5	0.05	0.11	0.11	0.00	1.23	0.01	97.68
94-4b-32	100-400	Ol	$Fa_{8.9}$	45.5	0.01	39.9	0.18	0.03	0.92	4.51	7.9	0.04	99.00
94-4b-32	100-400	Px	$Fs_{10.9}Wo_{0.8}$	33.6	0.29	55.9	0.41	0.03	0.79	0.42	6.9	0.00	98.38
94-4b-38	100-400	Ol	$Fa_{32.2}$	33.0	0.02	36.4	0.24	0.00	0.40	0.77	27.9	0.00	98.75
94-4b-38	100-400	Ol	$Fa_{22.6}$	39.2	0.01	37.6	0.19	0.00	0.42	0.29	20.4	0.06	98.19

n.d.: not determined.
Note: Na_2O and K_2O were analyzed but omitted in this table because they were always found to be below detection limit.

to a lesser degree, within rims surrounding chondrules and CAIs and as isolated grains in matrix. In AMMs, on the other hand, chondrules are known to be rare (Engrand and Maurette, 1998; Walter et al., 1995). Although most of the olivine and pyroxene analyzed here are petrographically "isolated" grains, the possibility that they represent fragments of disrupted chondrules or refractory inclusions should be considered.

Recent oxygen isotopic analyses of meteoritic olivine grains petrographically associated with CAIs, occurring either within olivine-rich refractory inclusions in CM Murchison (Hiyagon and Hashimoto, 1999) or in the fine-grained accretionary rims of CAIs from CV meteorites (Hiyagon, 1998; McKeegan et al., 1998a), showed large enrichments in ^{16}O to approximately the same level as the most ^{16}O-enriched refractory minerals in CAIs ($\delta^{18}O \approx \delta^{17}O \approx -40$ to -50‰). Although forsteritic, these olivines are not known to be especially chemically distinctive. So far, such isotopically anomalous olivine grains have not been found as isolated crystals (in matrix) or within chondrules. We have not found any such highly ^{16}O-enriched olivines in our selection of AMM grains, including particle #94-4B-5, which contains spinel in addition to olivine.

Most chondrule olivine and pyroxene grains result from igneous crystallization from the chondrule melt, with the exception of relict minerals that may be in chemical and isotopic disequilibrium with phenocrysts. However, the origin of the isolated olivine grains in meteorites is controversial. An origin from direct nebular condensation for some of the grains (particularly the forsterite enriched in refractory elements such as Ca, Ti, Al; Steele, 1986) is supported by several authors (Olsen and Grossman, 1978; Steele, 1986, 1988, 1989, 1992; Weinbruch et al., 1993, 1997). Other researchers favor an origin of isolated grains as fragments of disaggregated chondrules (Desnoyers, 1980; Jones, 1992; Jones and Danielson, 1997; McSween, 1977; Richardson and McSween, 1978). This latter viewpoint is mostly based on textural arguments and chemical characteristics of the olivines, in particular their CaO vs. FeO content (Beckerling and Bishoff, 1995; McSween, 1985; Scott and Taylor, 1983). Recent ion microprobe analyses have demonstrated that oxygen isotopic signatures of isolated olivine grains, even the most refractory forsteritic olivine that might be of nebular condensate origin, are not necessarily distinct from some chondrule olivine (Leshin et al., 1998).

Whether the olivine and pyroxene grains in AMMs formed by igneous crystallization (in chondrule melt) or as direct nebular condensates remains an open question. Five of the AMMs we have examined (#92-13C-13, #92-13C-20, #92-13C-26, #94-4B-5, #94-4B-38) contain coarse-grained aggregates of olivine and/or pyroxene crystals (Figs. 1 & 2a). The textures of these aggregates are consistent with origin of the minerals within a chondrule and their chemistry is plausibly compatible with crystallization of the grains from a single silicate melt composition. With a single exception (AMM #94-4B-38), the olivine and pyroxene minerals in these AMMs within a given mineral aggregate are in equilibrium with regard to their oxygen isotopic composition at the 2σ level (Table 2), consistent with (but not requiring) formation by crystallization from a single chondrule melt. The twelve other mineral grains we analyzed (see Figs. 2b,c,d) are petrographically similar to isolated minerals in carbonaceous chondrites in that they occur as single mineral grains within a fine-grained matrix, although the olivines in AMMs tend to be of smaller size than those studied in carbonaceous chondrites (Steele, 1988). The oxygen isotopic compositions of these grains are also compatible with those measured in carbonaceous chondrite whole chondrules

Table 2. Oxygen isotopic compositions of individual minerals in AMMs.

Sample designation	Mineral	Mineral composition	$\delta^{18}O \pm 1\sigma$ (‰)[†]	$\delta^{17}O \pm 1\sigma$ (‰)[†]	$\Delta^{17}O$ (‰)[†,‡]
92-13C-4	Px	$Fs_{1.3}Wo_{1.1}$	−1.5 ± 1.2	−3.6 ± 1.0	−2.8
92-13C-4	Px	$Fs_{1.3}Wo_{1.1}$	0.8 ± 1.3	−4.0 ± 1.0	−4.4
92-13C-5	Px	$Fs_{2.3}Wo_{1.2}$	−4.5 ± 1.6	−7.0 ± 0.8	−4.7
92-13C-10	Ol	$Fa_{33.8}$	4.3 ± 1.3	0.6 ± 0.8	−1.6
92-13C-11	Px	$Fs_{2.0}Wo_{0.8}$	−6.0 ± 1.1	−5.3 ± 0.7	−2.2
92-13C-11	Px	$Fs_{8.2}Wo_{2.9}$	−3.8 ± 1.3	−2.6 ± 0.8	−0.6
92-13C-13	Ol	$Fa_{2.2}$	−1.3 ± 1.3	−2.8 ± 1.0	−2.1
92-13C-13	Px	$Fs_{1.6}Wo_{1.1}$	2.2 ± 1.3	−0.4 ± 0.9	−1.5
92-13C-15	Px	$Fs_{5.3}Wo_{0.9}$	2.1 ± 1.2	0.0 ± 1.0	−1.1
92-13C-15	Px	$Fs_{5.3}Wo_{0.9}$	−2.0 ± 1.3	−2.9 ± 1.0	−1.9
92-13C-20	Px	$Fs_{3.5}Wo_{1.2}$	−5.4 ± 1.4	−7.4 ± 1.4	−4.6
92-13C-20	Px	$Fs_{3.5}Wo_{1.2}$	−5.5 ± 1.2	−6.9 ± 1.0	−4.0
92-13C-21	Ol	$Fa_{28.7}$	1.0 ± 1.5	−2.1 ± 1.3	−2.6
92-13C-23	Mel	$Åk_{22}$	−39.8 ± 1.3	−41.7 ± 1.1	−21.0
92-13C-23	Mel	$Åk_{22}$	−44.6 ± 1.3	−45.1 ± 0.9	−21.9
92-13C-23	Sp	Sp_{100}	−40.3 ± 1.4	−41.7 ± 1.1	−20.7
92-13C-23	Sp	Sp_{100}	−48.4 ± 2.4	−47.2 ± 1.6	−22.0
92-13C-23	Sp	Sp_{100}	−42.1 ± 1.6	−41.2 ± 1.2	−19.3
92-13C-26	Ol	$Fa_{3.8}$	1.9 ± 1.5	−1.4 ± 1.5	−2.4
92-13C-26	Ol	$Fa_{3.8}$	1.7 ± 1.8	−1.9 ± 1.4	−2.8
92-13C-33	Px	$Fs_{4.4}Wo_{1.1}$	0.6 ± 1.1	−3.2 ± 1.0	−3.5
92-13C-35	Px	$Fs_{1.3}Wo_{0.6}$	−3.4 ± 1.5	−6.9 ± 0.9	−5.1
94-4b-2	Ol	$Fa_{2.6}$	−4.6 ± 1.3	−6.1 ± 1.8	−3.7
94-4b-5	Ol	$Fa_{1.1}$	−8.3 ± 1.3	−7.4 ± 1.4	−3.1
94-4b-5	Ol	$Fa_{32.4}$	−3.6 ± 1.5	−6.5 ± 1.6	−4.6
94-4b-5	Px	$Fs_{2.6}Wo_{1.2}$	−9.9 ± 1.5	−11.3 ± 1.4	−6.2
94-4b-5	Sp	Sp_{99} + matrix	−21.1 ± 1.3	−26.8 ± 1.4	−15.8
94-4b-32	Ol	$Fa_{8.9}$	4.8 ± 1.3	3.4 ± 1.5	0.9
94-4b-32	Px	$Fs_{10.9}Wo_{0.8}$	1.3 ± 1.3	0.4 ± 1.3	−0.3
94-4b-38	Ol	$Fa_{32.2}$	8.0 ± 1.2	5.5 ± 1.4	1.3
94-4b-38	Ol	$Fa_{22.6}$	1.7 ± 1.2	−0.1 ± 1.4	−1.0

[†] Relative to SMOW
[‡] $\Delta^{17}O = \delta^{17}O - 0.52 \times \delta^{18}O$

(Clayton and Mayeda, 1983; Clayton et al., 1977; McSween, 1985; Rowe et al., 1994; Rubin et al., 1990; Weisberg et al., 1993). However, oxygen isotopic composition by itself may not be very diagnostic of mode of origin for either individual olivine grains in carbonaceous meteorites or for AMM olivines.

On the CaO vs. FeO diagram (Fig. 5), the AMM olivine grains analyzed in this study plot within the fields defined by carbonaceous chondrite olivines, including those from both type I and type II chondrules. Additionally, their oxygen isotopic compositions are compatible with those measured in carbonaceous chondrite whole chondrules (Clayton and Mayeda, 1983; Clayton et al., 1977; McSween, 1985; Rowe et al., 1994; Rubin et al., 1990; Weisberg et al., 1993). Thus, it is not possible based on our chemical and isotopic data to rule out a chondrule origin for the AMM olivine and pyroxene grains.

In meteorite olivine grains, the degree of ^{16}O enrichment has often been reported to be broadly negatively correlated with the FeO content of olivine grains (Hervig and Steele, 1992; Leshin et al., 1997; Saxton et al., 1995; Weinbruch et al., 1993). Likewise, an inverse correlation between bulk chondrule ^{16}O-enrichment and FeO content has also been observed (Clayton and Mayeda, 1983; McSween, 1985; Rubin et al., 1990). Various hypotheses have been advanced to account for this apparent correlation. McSween (1985) suggested that a greater degree of isotopic exchange could occur between ^{16}O-enriched chondrule precursors and an ^{16}O-depleted nebular gas during more prolonged melting of the more FeO-rich chondrules, while Rubin et al. (1990) invoked mixing of two solid components with distinctive ^{16}O and FeO contents to form chondrule precursors. Weinbruch et al. (1993) interpreted a correlation of ^{16}O-enrichment with FeO content between the cores and rims of two isolated Allende olivine grains as reflecting condensation processes in the solar nebula.

Although the most forsteritic AMM olivine grain (#94-4B-5) shows the greatest ^{16}O-enrichment, there is no overall correlation of FeO-content and oxygen isotopic composition in our AMM olivines (Fig. 6). In fact, this observation agrees with the most recent ion microprobe studies of the oxygen isotopic compositions of individual minerals in carbonaceous chondrites (Jones et al., 1998; Leshin et al., 1998) which demonstrate that this correlation breaks down upon detailed examination. Thus, the data indicate that the processes responsible for the FeO-content and oxygen isotopic compositions of meteoritic (and AMM) olivine grains are not linked in a straightforward manner.

The oxygen isotope data for olivine and pyroxene from AMMs also overlap the data available for whole chondritic interplanetary dust particles (IDPs) collected from the stratosphere (McKeegan, 1987a; McKeegan, 1987b; Stadermann, 1990). However, a valid comparison is not readily made since the IDPs were measured by crushing the entire particle onto a gold foil. Recent analyses of single silicate mineral grains in 2

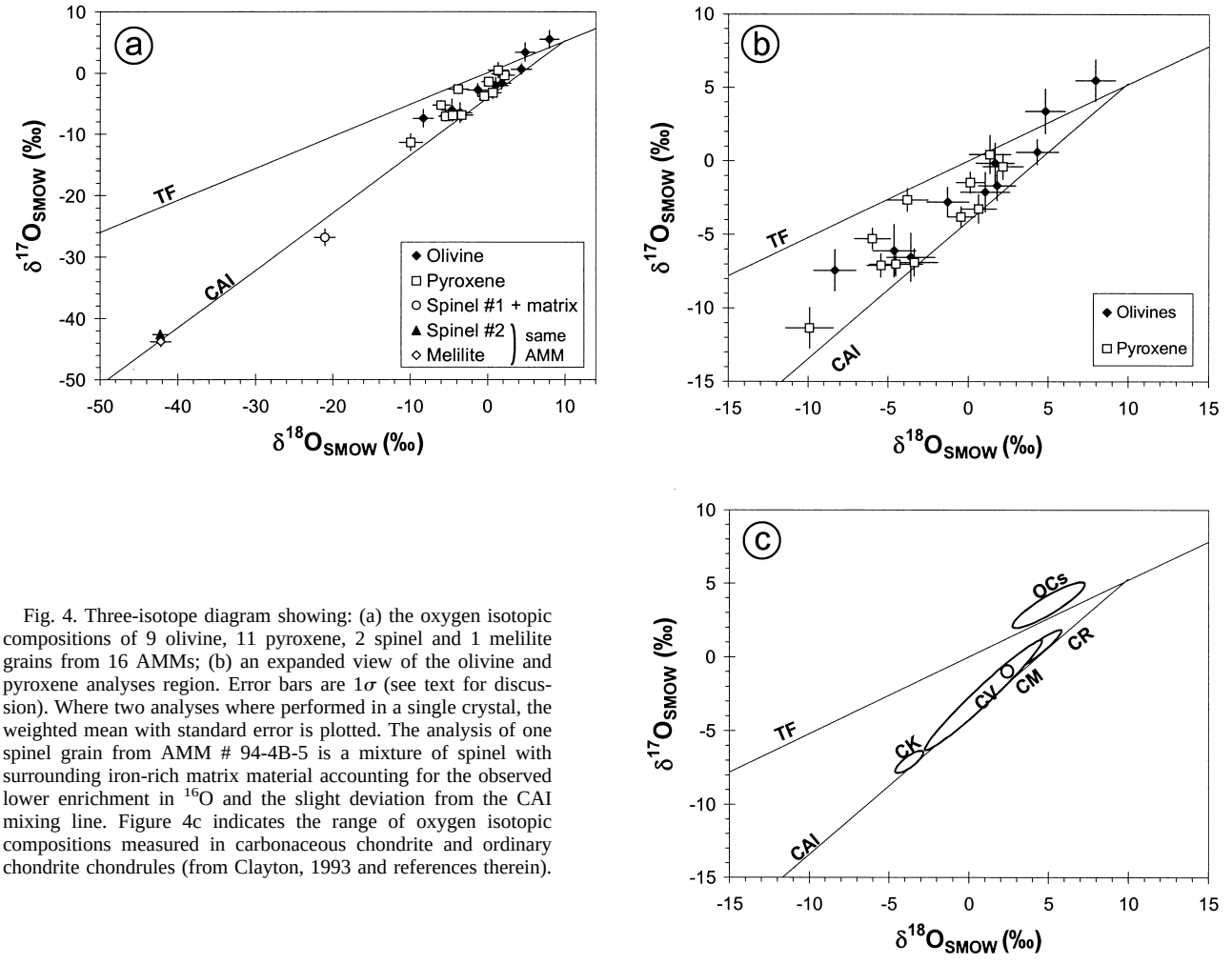

Fig. 4. Three-isotope diagram showing: (a) the oxygen isotopic compositions of 9 olivine, 11 pyroxene, 2 spinel and 1 melilite grains from 16 AMMs; (b) an expanded view of the olivine and pyroxene analyses region. Error bars are 1σ (see text for discussion). Where two analyses where performed in a single crystal, the weighted mean with standard error is plotted. The analysis of one spinel grain from AMM # 94-4B-5 is a mixture of spinel with surrounding iron-rich matrix material accounting for the observed lower enrichment in ^{16}O and the slight deviation from the CAI mixing line. Figure 4c indicates the range of oxygen isotopic compositions measured in carbonaceous chondrite and ordinary chondrite chondrules (from Clayton, 1993 and references therein).

IDPs (Engrand et al., 1999) are compatible with the AMM mafic silicate data presented here.

4.2. Refractory Mineral Data: Comparison to Meteorites and Interplanetary Dust Particles

In chondritic meteorites, with the exception of the recently discovered olivine discussed above, large ^{16}O-excesses are exclusively associated with the refractory oxide and Ti-rich pyroxene (fassaite) minerals found in CAIs. The relative abundance of AMMs that bear refractory mineral phases is at most a few percent (Engrand and Maurette, 1998; Greshake et al., 1996; Kurat et al., 1994b), hence these materials have not been very extensively studied compared to their counterparts in carbonaceous chondrites. The overall mineralogy of refractory phases in AMMs appears to be similar to that for refractory inclusions in CM chondrites (see Greshake et al., 1996; Kurat et al., 1994b). As in CM chondrites, melilite may be relatively rare as only one melilite grain has been identified in AMMs thus far (Engrand et al., 1997, this study).

Previous oxygen isotopic data on 3 spinel-bearing AMMs showed variable ^{16}O-excesses that are broadly consistent with the CAI mixing line (Greshake et al., 1996; Hoppe et al., 1995; Kurat et al., 1994a). Our oxygen isotopic data are in general agreement with these measurements, but for the first time convincingly show that refractory minerals from AMMs fall on the CAI line (Fig. 4a). Although in one particle the small grain size prevented a clean analysis of only refractory material (AMM #94-4B-5), in the other particle examined (AMM #92-13C-23) it is clear that both spinel and melilite are enriched in ^{16}O at the level of $\delta^{18}O \sim -40‰$, as is the case for most spinel grains in CAIs from carbonaceous chondrites (Clayton, 1993 and references therein; McKeegan et al., 1996). The isotopic composition of AMM #92-13C-23 is strikingly similar to that measured in a melilite-spinel-hibonite bearing inclusion from the unequilibrated ordinary chondrite Semarkona (McKeegan et al., 1998b).

The AMM data are also in good agreement with measurements of "bulk" refractory stratospheric IDPs which have oxygen isotopic compositions on the CAI line, with enrichments in ^{16}O up to $\delta^{18}O \approx \delta^{17}O \approx -40‰$ (McKeegan, 1987a, 1987b; Stadermann, 1990, 1991). The refractory mineral assemblages identified in IDPs (Christoffersen and Buseck, 1986; Tomeoka and Buseck, 1985; Zolensky, 1987) consist mainly of spinel, perovskite, fassaite, hibonite, melilite, corundum, diop-

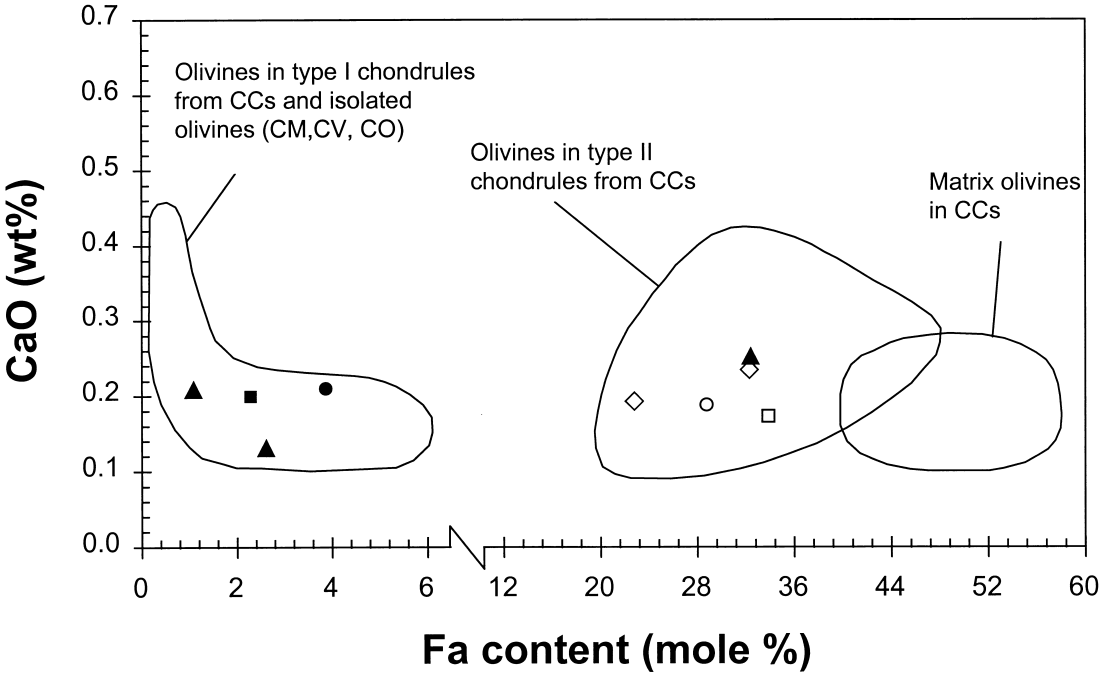

Fig. 5. Weight percent CaO vs. FeO measured in olivines from carbonaceous and ordinary chondrites (adapted from Fig. 4 from Beckerling and Bishoff, 1995), and in the AMM olivines analyzed in this study. Identical symbols are used for olivine grains within a single micrometeorite.

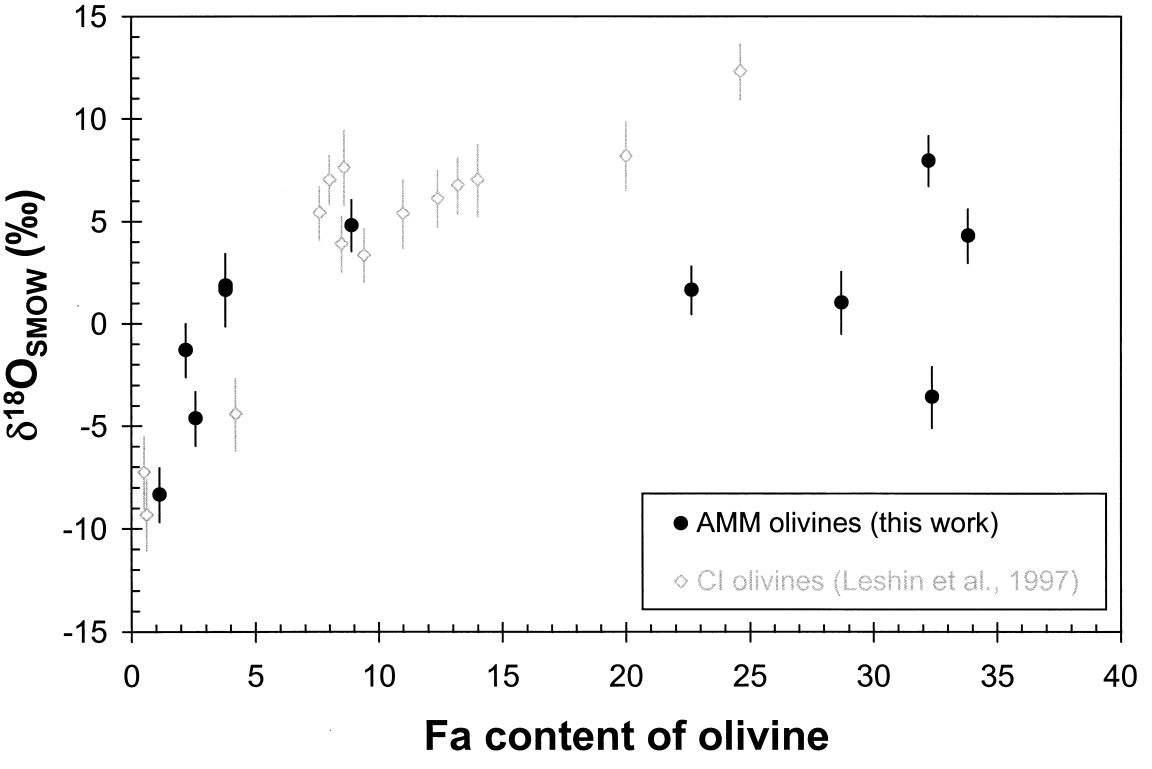

Fig. 6. $\delta^{18}O$ as a function of the fayalite (Fa) content of the olivine. The lack of a definite correlation is consistent with other recent ion microprobe studies of olivine from carbonaceous chondrites. See text for discussion.

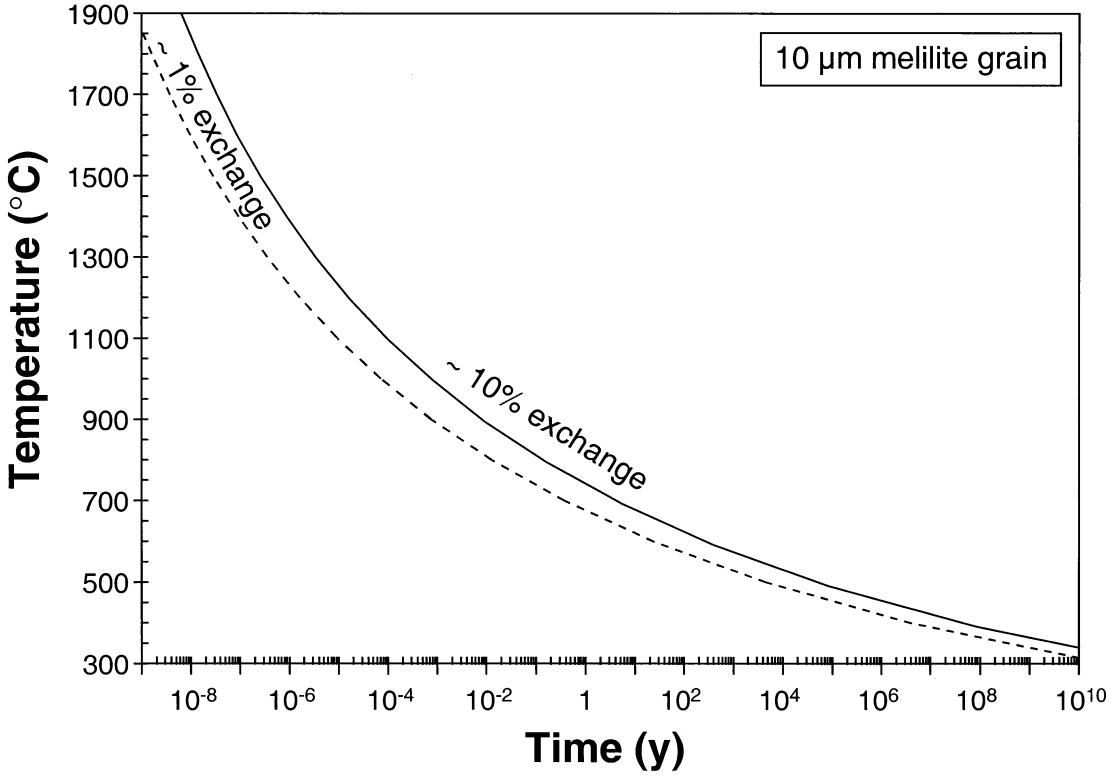

Fig. 7. Time-temperature diagram for a gas-solid exchange diffusion scenario constrained by the isotopic composition of the AMM melilite grain (see text). For a given temperature, the curves represent the time necessary to exchange 10% and 1%, respectively, of the oxygen by gas-solid reaction and diffusion in a 10 μm diameter melilite crystal.

side and anorthite (see Greshake et al., 1996 for a review). The refractory minerals in these particles differ from those in most carbonaceous chondrite CAIs by their sub-micron grain size (e.g., Zolensky, 1987), whereas the typical grain size of AMM CAIs is on the order of microns. Although the data are limited, refractory IDPs also seem to exhibit a wider mineral variety than AMM CAIs. However, from the viewpoint of oxygen isotopes, micrometeorite refractory minerals bear a striking similarity to meteoritic CAIs and refractory IDPs.

A possible exception to this isotopic similarity is provided by the observation of ^{16}O-rich melilite in AMM #92-13C-23. Although recent ion microprobe analyses have uncovered isotopically anomalous (^{16}O-enriched) melilite in CAIs from both unequilibrated ordinary chondrites (McKeegan et al., 1998b) and carbonaceous chondrites (Hiyagon, 1998; Ito et al., 1998; Kim et al., 1998; Kimura et al., 1993), most melilite in CAIs from carbonaceous chondrites has close to a "normal" oxygen isotopic composition (Clayton et al., 1977). The most commonly accepted interpretation to explain the isotopic heterogeneity between melilite and ^{16}O-enriched spinel and fassaite in (type B) carbonaceous chondrite CAIs invokes post-crystallization solid-gas isotopic exchange between initially ^{16}O-enriched refractory minerals and ^{16}O-depleted nebular gas (Clayton and Mayeda, 1977). In this model, the extent of isotopic exchange depends on the rate of oxygen self-diffusion in each mineral phase and on the thermal history of the CAI.

Although it is not yet known how representative it is, the discovery of an isotopically anomalous melilite grain in an AMM supports the hypothesis that refractory minerals throughout the solar nebula formed from a relatively uniformly ^{16}O-enriched reservoir (Clayton, 1993; McKeegan et al., 1998b). Assuming that both the spinel and the melilite grains start with the same initial oxygen isotopic composition, the observed isotopic homogeneity between melilite and spinel in AMM #92-13C-23 implies a low degree of exchange with nebular gas and thus provides some constraints regarding the thermal history experienced by this AMM since the time of its formation. Considering analytical uncertainties, the maximum degree of isotopic exchange that could be permitted by the data would be a change of the δ^{18}O value by $\sim$5‰ which is equivalent to $\sim$10% exchange with a gas reservoir of assumed nebular composition (Clayton, 1993; Rowe et al., 1994). If the diffusion length-scale can be approximated by the grain size ($\sim$10 μm in diameter) and the oxygen self-diffusion coefficient for this melilite ($Åk_{22}$) can be interpolated from the experiments of Yurimoto et al. (1989, see their Fig. 6), then $\sim$10% isotopic exchange can occur in a matter of minutes at high temperatures (>1200°C) but could not be achieved in the lifetime of the solar system for temperatures below 300°C (see Fig. 7).

4.3. Possible Implications for Oxygen Isotopic Reservoirs in the Solar Nebula

Because micrometeorites constitute the majority of the mass flux currently being accreted by the Earth, they may provide a more representative sampling of extraterrestrial materials than

conventional meteorite collections. Therefore, their oxygen isotope compositions could give important insights into the distribution of oxygen isotopic reservoirs in the solar nebula. If the micrometeorite population is mainly derived from asteroids, our data imply that carbonaceous chondrite material is dominant in the asteroid belt, as opposed to the ordinary chondrites which constitute ~80% of meteorites. This is in agreement with conclusions reached by Meibom and Clark (1999) based mostly on spectroscopic observations of asteroids. One important limitation, however, is that the origins of individual micrometeorites, in the sense of locale within the solar system, are not well constrained. Unlike chondrites, which certainly originate in the asteroid belt (Wetherill and Chapman, 1988), some fraction of micrometeorites are probably samples of comets. However, the proportion of cometary particles is uncertain (Levasseur-Regourd et al., 1991; Liou et al., 1995 and references therein; Liou and Zook, 1996, 1997; Liou et al., 1996) and the source of any individual particle—such as those measured here—is a matter of speculation. Current knowledge about the oxygen isotopic compositions of comets is insufficient to provide much useful information regarding possible differences in oxygen isotope reservoirs between inner and outer solar system materials. In the water vapor of comet Halley, Eberhardt et al. (1995) and Balsiger et al. (1995) quoted values of $\delta^{18}O = +12 \pm 74‰$ and $-38 \pm 62‰$, respectively. Within their substantial uncertainties, these values overlap with all terrestrial and meteoritic compositions, including those for AMMs and those inferred for volatile species (e.g., Choi et al., 1997a; Clayton and Mayeda, 1984; Leshin et al., 1997). Note also that this isotopic value, measured in water vapor, might not be representative of that of the cometary silicate grains, for which no direct measurements are available as yet. Despite the uncertainties regarding micrometeorite sources, the most straightforward interpretation of the data presented here is that the oxygen isotopic compositions of the majority of the unequilibrated anhydrous silicates in the solar system are similar to those of carbonaceous chondrites and not ordinary chondrites.

The refractory minerals from CAIs in both carbonaceous and ordinary chondrites as well as from refractory IDPs and AMMs exhibit a nearly constant maximum ^{16}O-enrichment of $\sim +50‰$. This indicates that an ^{16}O-enriched reservoir of refractory dust must have been ubiquitous in the solar nebula or alternatively requires a mechanism for scattering refractory materials, originally formed in a restricted nebular locale, over widely variable heliocentric distances (McKeegan et al., 1998b). One such mechanism could be the bipolar outflows (x-winds) discussed by Shu et al. (1996). Recent studies (Hiyagon, 1998; Ito et al., 1998; Kim et al., 1998; Kimura et al., 1993; McKeegan et al., 1998b, this study) have demonstrated that ^{16}O-enriched melilite exists, and may be more common in small, fine-grained refractory mineral assemblages than in coarse-grained (primarily type-B) CAIs where ^{16}O-enriched melilite appears to be rare. Either these refractory objects, which were incorporated into parent bodies that probably were assembled at different heliocentric distances, experienced distinct thermal histories or they were exposed to different isotopic environments. To what extent a possible correlation of petrographic occurrence and isotopic composition of melilite provides evidence for production of refractory minerals in a highly localized region of the solar nebula, as in the Shu et al. (1996) model, remains an open question that can be addressed by further analyses of refractory minerals in primitive extraterrestrial materials. The answer ultimately has important implications for understanding the origin of the premier isotopic anomaly in the solar system, whether as a manifestation of the chemical memory of interstellar dust (Clayton, 1982; Clayton et al., 1973), or as a product of non-equilibrium chemistry in the solar nebula (Thiemens, 1996; Thiemens and Heidenreich, 1983).

5. CONCLUSIONS

The oxygen isotopic compositions of the individual minerals in AMMs studied here do not show evidence for exchange with terrestrial oxygen upon atmospheric entry. This is consistent with the unmelted texture and pristine chemistry of the minerals. Thus, the oxygen isotopic data can be directly compared to data for similar phases in meteorites.

The oxygen isotopic compositions of olivine and pyroxene grains in AMMs overlap those observed in carbonaceous chondrites. Thus, this work documents an additional important similarity between AMMs and primitive carbonaceous meteorites, adding to the chemical, mineralogical and isotopic similarities previously discussed by Kurat et al. (1994b), Kurat (1998) and Engrand and Maurette (1998).

The petrographic, chemical, and isotopic data presented here do not permit a unique interpretation of the origin of the AMM mineral grains studied. Whole chondrules are extremely rare in the AMM collection, and thus a chondrule origin is not definitively indicated by the petrographic occurrence of the AMM minerals studied. The chemistry and oxygen isotopic compositions of at least some AMM mineral grains, however, are consistent with an origin from the igneous crystallization and subsequent breakage of chondrules, based upon comparison to the available data in chondritic meteorites. Further studies of AMMs, as well as of isolated minerals in chondrites, are necessary to define evidence for igneous versus condensation origin of isolated minerals which are not petrographically associated with chondrules.

We did not observe any extreme ^{16}O enrichments in our selection of olivine grains, such as has been recently reported in carbonaceous chondrite olivines associated with refractory inclusions (Hiyagon, 1998; Hiyagon and Hashimoto, 1999; McKeegan et al., 1998a). Thus the olivine grains studied here probably did not originate in a similar way to the olivine within or rimming refractory inclusions in carbonaceous chondrites.

In agreement with other recent studies (Jones et al., 1998; Leshin et al., 1998), we do not observe a correlation between the ^{16}O-enrichment of the olivine grains and their FeO content, suggesting that the processes responsible for the FeO and ^{16}O abundances are not related in a straightforward way.

The AMM spinel and melilite grains in this study are enriched in ^{16}O at the level of $\delta^{17}O \approx \delta^{18}O \approx -40‰$, similar to refractory minerals in carbonaceous chondrites (Clayton, 1993 and references therein), in bulk refractory IDPs (Greshake et al., 1996; McKeegan, 1987b; Stadermann, 1990), and from a previous study of AMMs (Greshake et al., 1996; Kurat et al., 1994a). The discovery of an isotopically pristine AMM melilite

grain (enriched in ^{16}O at the same level as spinel) supports the model of formation of refractory minerals from an isotopically homogeneous ^{16}O-rich reservoir and subsequent gas-solid isotopic exchange with ^{16}O-depleted nebular gas to yield the mineralogically-dependent oxygen isotopic compositions thus far observed in most carbonaceous chondrite CAIs (e.g., Clayton, 1993 and references therein). ^{16}O-enriched melilite has now been documented in carbonaceous chondrites (Hiyagon, 1998; Ito et al., 1998; Kim et al., 1998; Kimura et al., 1993), ordinary chondrites (McKeegan et al., 1998b), and micrometeorites (this study), suggesting that there could be abundant examples of CAI minerals that escaped the secondary exchange process discussed above and testifying to the variety of environments and/or processes which must have affected materials in the early solar system.

Acknowledgments—We would like to thank M. Maurette for hauling these samples from Antarctica and making them available to the community. We thank A. Rubin, J. Wasson, F. Kyte, G. Kurat and M. Genge for fruitful discussions. The laboratory assistance of C. Coath and G. Jarzebinski is gratefully acknowledged. The paper was improved by thoughtful reviews by P. Hoppe and J. Saxton. This work was supported by NASA grants NAG5-4305 and NAG5-4704. The UCLA ion microprobe is partially supported by a grant from the NSF Instrumentation & Facilities program.

REFERENCES

Ash R. D., Rumble III D., Alexander C. M. O. D., and MacPherson G. J. (1998) Oxygen isotopes in isolated chondrules from the Tieschitz ordinary chondrite: Initial compositions and differential parent body alteration. *Lunar Planet. Sci.* **XXIX,** CD-ROM # 1854.

Balsiger H., Altwegg K., and Geiss J. (1995) D/H and $^{18}O/^{16}O$ ratio in the hydronium ion and in the neutral water from in situ ion measurements in comet Halley. *J. Geophys. Res.* **100,** 5827–5834.

Beckerling W. and Bishoff A. (1995) Occurence and composition of relict minerals in micrometeorites from Greenland and Antarctica: Implications for their origins. *Planet. Space Sci.* **43,** 435–449.

Choi B. G., McKeegan K. D., Krot A. N., and Wasson J. T. (1997a) Magnetite in unequilibrated ordinary chondrites; evidence for an ^{17}O-rich reservoir in the solar nebula. *Lunar Planet. Sci.* **XXVIII,** 227–228.

Choi B. G., McKeegan K. D., Krot A. N., and Wasson J. T. (1998) Extreme oxygen-isotope compositions in magnetite from unequilibrated ordinary chondrites. *Nature* **392,** 577–579.

Choi B.-G., McKeegan K. D., Leshin L. A., and Wasson J. T. (1997b) Origin of magnetite in oxidized CV chondrites; in situ measurement of oxygen isotope compositions of Allende magnetite and olivine. *Earth Planet. Sci. Lett.* **146,** 337–349.

Christoffersen R. and Buseck P. R. (1986) Refractory minerals in interplanetary dust. *Science* **234,** 590–592.

Christophe Michel-Levy M. and Bourot-Denise M. (1992) Mineral composition in Antarctic and Greenland micrometeorites. *Meteoritics* **27,** 73–80.

Clayton D. D. (1982) Cosmic chemical memory - a new astronomy. *Quart. J. Royal Astron. Soc.* **23,** 174.

Clayton R. N. (1993) Oxygen isotopes in meteorites. *Ann. Rev. Earth Planet. Sci.* **21,** 115–149.

Clayton R. N., Grossman L., and Mayeda T. K. (1973) A component of primitive nuclear composition in carbonaceous meteorites. *Science* **182,** 485–488.

Clayton R. N. and Mayeda T. K. (1977) Correlated oxygen and magnesium isotope anomalies in Allende inclusions, I: Oxygen. *Geophys. Res. Lett.* **4,** 295–298.

Clayton R. N. and Mayeda T. K. (1983) Oxygen isotopic composition of chondules in Allende and ordinary chondrites. In *Chondrules and their origin* (ed. A. E. King), pp. 37–43. Lunar and Planetary Institute.

Clayton R. N. and Mayeda T. K. (1984) The oxygen isotope record in Murchison and other carbonaceous chondrites. *Earth Planet. Sci. Lett.* **67,** 151–161.

Clayton R. N., Mayeda T. K., Goswami J. N., and Olsen E. J. (1991) Oxygen isotope studies of ordinary chondrites. *Geochim. Cosmochim. Acta* **55,** 2317–2337.

Clayton R. N., Mayeda T. M., and Brownlee D. E. (1986) Oxygen isotopes in deep-sea spherules. *Earth Planet. Sci. Lett.* **79,** 235–240.

Clayton R. N., Onuma N., Grossman L., and Mayeda T. K. (1977) Distribution of the pre-solar components in Allende and other carbonaceous chondrites. *Earth Planet. Sci. Lett.* **34,** 209–224.

Desnoyers C. (1980) The Niger (I) carbonaceous chondrite and implications for the origin of aggregates and isolated olivine grains in C2 chondrites. *Earth Planet. Sci. Lett.* **47,** 223–234.

Eberhardt P., Reber M., Krankowsky D., and Hodges R. R. (1995) The D/H and $^{18}O/^{16}O$ ratios in water from comet P/Halley. *Astron. Astrophys.* **302,** 301–316.

Eiler J. M., Farley K. A., Valley J. W., Stolper E. M., Hauri E. H., and Craig H. (1995) Oxygen isotope evidence against bulk recycled sediments in the mantle sources of Pitcairn Island lavas. *Nature* **377,** 138–141.

Engrand C., Deloule E., Robert F., Maurette M., and Kurat G. (in press) Extraterrestrial water in micrometeorites and cosmic spherules from Antarctica: An ion microprobe study. *Meteoritics Planet. Sci.* **34**.

Engrand C. and Maurette M. (1998) Carbonaceous micrometeorites from Antarctica. *Meteoritics Planet. Sci.* **33,** 565–580.

Engrand C., McKeegan K. D., and Leshin L. A. (1997) *In situ* analysis of the oxygen isotopic composition of individual minerals in Antarctic micrometeorites. (abstract). *Meteoritics Planet. Sci.* **32,** A39.

Engrand C., McKeegan K. D., Leshin L. A., Bradley J. P., and Brownlee D. E. (1999) Oxygen isotopic compositions of interplanetary dust particles: ^{16}O-excess in a GEMS-rich IDP. *Lunar Planet. Sci.* **XXX,** (CDROM #1690).

Engrand C., McKeegan K. D., Leshin L. A., and Brownlee D. E. (1998) In-situ measurement of oxygen isotopic compositions of deep sea and Antarctic cosmic spherules. *Lunar Planet. Sci.* **XXIX,** #1473 (CR-ROM).

Greshake A., Hoppe P., and Bischoff A. (1996) Mineralogy, chemistry, and oxygen isotopes of refractory inclusions from stratospheric interplanetary dust particles and micrometeorites. *Meteoritics Planet. Sci.* **31,** 739–748.

Hervig R. L. and Steele I. M. (1992) Oxygen isotopic analysis of Allende olivine by ion microprobe and implications for chondrule origin. *Lunar Planet. Sci.* **XXIII,** 525–526.

Hiyagon H. (1998) Distribution of oxygen isotopes in and around some refractory inclusions from Allende. *Lunar Planet. Sci.* **XXIX,** #1582 (CD-ROM).

Hiyagon H. and Hashimoto A. (1999) ^{16}O excesses in olivine inclusions in Yamato-86009 and Murchison chondrites and their relation to CAIs. *Science* **283,** 828–831.

Hoppe P., Kurat G., Walter J., and Maurette M. (1995) Trace elements and oxygen isotopes in a CAI-bearing micrometeorite from Antarctica. *Lunar Planet. Sci.* **XXVI,** 623–624.

Ito M., Yurimoto H., and Nagasawa H. (1998) Oxygen isotope microanalysis of CAI by SIMS; an evidence for isotopically anomalous melilite. *Lunar Planet. Sci.* **XXIX,** #1556 (CD-ROM).

Jones R. H. (1992) On the relationship between isolated and chondrule olivine grains in the carbonaceous chondrite ALH77307. *Geochim. Cosmochim. Acta* **56,** 467–482.

Jones R. H. and Danielson L. R. (1997) A chondrule origin for dusty relict olivine in unequilibrated chondrites. *Meteoritics Planet. Sci.* **32,** 753–760.

Jones R. H., Saxton J. M., Lyon I. C., and Turner G. (1998) Oxygen isotope analyses of chondrule and isolated olivine grains in the CO3 chondrite ALHA77307. *Lunar Planet. Sci.* **XXIX,** #1795 (CD-ROM).

Kim G. L., Yurimoto H., and Sueno S. (1998) ^{16}O-enriched melilite and anorthite coexisting with ^{16}O-depleted melilite in a CAI. *Lunar Planet. Sci.* **XXIX,** #1344 (CD-ROM).

Kimura M., El Goresy A., Palme H., and Zinner E. (1993) Ca-, Al-rich inclusions in the unique chondrite ALH85085; petrology, chemistry, and isotopic compositions. *Geochim. Cosmochim. Acta* **57,** 2329–2359.

Kurat G. (1998) Cosmogenic matter in terrestrial environments. In

Advanced Mineralogy. Mineral Matter in Space, Mantle, Ocean Floor, Biosphere, Environmental Managment, and Jewelry (ed. A. S. Marfunin), Vol. 3, pp. 28–34. Springer-Verlag.

Kurat G., Hoppe P., Walter J., Engrand C., and Maurette M. (1994a) Oxygen isotopes in spinels from Antarctic micrometeorites (abstract). *Meteoritics* **29,** 487–488.

Kurat G., Koeberl C., Presper T., Brandstätter F., and Maurette M. (1994b) Petrology and geochemistry of Antarctic micrometeorites. *Geochim. Cosmochim. Acta* **58,** 3879–3904.

Leshin L. A., McKeegan K. D., Engrand C., Zanda B., Bourot-Denise M., and Hewins R. H. (1998) Oxygen isotopic studies of isolated and chondrule olivine from Renazzo and Allende (abstract). *Meteoritics Planet. Sci.* **33,** A93–A94.

Leshin L. A., Rubin A. E., and McKeegan K. D. (1997) The oxygen isotopic composition of olivine and pyroxene from CI chondrites. *Geochim. Cosmochim. Acta* **61,** 835–845.

Levasseur-Regourd A. C., Renard J. B., and Dumont R. (1991) The zodiacal cloud complex. In *Origin and evolution of interplanetary dust* (ed. A. C. Levasseur-Regourd and H. Hasegawa), pp. 131–138. Kluwer Academic Publishers.

Liou J. C., Dermott S. F., and Xu Y. L. (1995) The contribution of cometary dust to the zodiacal cloud. *Planet. Space Sci.* **43,** 717–722.

Liou J. C. and Zook H. A. (1996) Comets as a source of low eccentricity and low inclination interplanetary dust particles. *Icarus* **123**(2), 491–502.

Liou J. C. and Zook H. A. (1997) Evolution of interplanetary dust particles in mean motion resonances with planets. *Icarus* **128,** 354–367.

Liou J. C., Zook H. A., and Dermott S. F. (1996) Kuiper belt dust grains as a source of interplanetary dust particles. *Icarus* **124,** 429–440.

Love S. G. and Brownlee D. E. (1993) A direct measurement of the terrestrial mass accretion rate of cosmic dust. *Science* **262,** 550–553.

MacPherson G. J., Wark D. A., and Armstrong J. T. (1988) Primitive material surviving in chondrites: refractory inclusions. In *Meteorites and the Early Solar System* (ed. J. F. K. a. M. S. Matthews), pp. 746–807. Univ. of Arizona Press.

Maurette M., Immel G., Hammer C., Harvey R., Kurat G., and Taylor S. (1994) Collection and curation of IDPs from the Greenland and Antarctic ice sheets. In *Analysis of Interplanetary Dust, AIP Conf. Proc.* (ed. M. E. Zolensky, T. L. Wilson, F. J. M. Rietmeijer, and G. J. Flynn), Vol. 310, pp. 277–289. American Institute of Physics.

Maurette M., Olinger C., Christophe M., Kurat G., Pourchet M., Brandstätter F., and Bourot-Denise M. (1991) A collection of diverse micrometeorites recovered from 100 tons of Antarctic blue ice. *Nature* **351,** 44–47.

McKeegan K. D. (1987a) Ion microprobe measurements of H, C, O, Mg and Si isotopic abundances in individual interplanetary dust particles. Ph.D. thesis, Washington Univ., St Louis.

McKeegan K. D. (1987b) Oxygen isotopes in refractory stratospheric dust particles: Proof of extraterrestrial origin. *Science* **237,** 1468–1471.

McKeegan K. D., Leshin L. A., and MacPherson G. J. (1998a) Oxygen isotopic stratigraphy in a Vigarano type-A calcium-aluminium-rich inclusion (abstract). *Meteoritics Planet. Sci.* **33,** A102–A103.

McKeegan K. D., Leshin L. A., Russell S. S., and MacPherson G. J. (1996) In situ measurement of O isotopic anomalies in a type B Alllende CAI. *Meteoritics Planet. Sci.* **31,** A86–A87.

McKeegan K. D., Leshin L. A., Russell S. S., and MacPherson G. J. (1998b) Oxygen isotopic abundances in calcium-aluminum-rich inclusions from ordinary chondrites: Implications for nebular heterogeneity. *Science* **280,** 414–418.

McSween H. Y., Jr. (1977) On the nature and origin of isolated olivine grains in carbonaceous chondrites. *Geochim. Cosmochim. Acta* **41,** 411–418.

McSween H. Y., Jr. (1985) Constraints on chondrule origin from petrology of isotopically characterized chondrules in the Allende meteorite. *Meteoritics* **20,** 523–539.

Meibom A. and Clark B. E. (1999) Evidence for the insignificance of ordinary chondritic material in the asteroid belt. *Meteoritics Planet. Sci.* **34,** 7–24.

Olinger C. T. (1990) Isotopic measurements of solar noble gases in individual micrometeorites from Greenland and Antarctica. Ph.D. thesis, Washington University, St Louis.

Olinger C. T., Maurette M., Walker R. M., and Hohenberg C. M. (1990) Neon measurements of individual Greenland sediment particles: Proof of an extraterrestrial origin and comparison with EDX and morphological analyses. *Earth Planet. Sci. Lett.* **100,** 77–93.

Olsen E. and Grossman L. (1978) On the origin of isolated olivine grains in type 2 carbonaceous chondrites. *Earth Planet. Sci. Lett.* **41,** 111–127.

Presper T. (1993) Pauschalzusammensetzung und Mineralchemie von Arktischen Kosmischen Kügelchen und Antarktischen Mikrometeoriten. Ph.D. thesis, Johannes Gutenberg-Universität in Mainz.

Richardson S. M. and McSween H. Y., Jr. (1978) Textural evidence bearing on the origin of isolated olivine crystals in C2 carbonaceous chondrites. *Earth Planet. Sci. Lett.* **37,** 485–491.

Rowe M. W., Clayton R. N., and Mayeda T. K. (1994) Oxygen isotopes in separated components of CI and CM meteorites. *Geochim. Cosmochim. Acta* **58,** 5341–5347.

Rubin A. E., Wasson J. T., Clayton R. N., and Mayeda T. K. (1990) Oxygen isotopes in chondrules and coarse-grained chondrule rims from the Allende meteorite. *Earth Planet. Sci. Lett.* **96,** 247–255.

Russell S. S., Leshin L. A., McKeegan K. D., and MacPherson G. J. (1997) Oxygen isotopic composition of Al-rich chondrules: Clues to their origin (abstract). *Meteoritics Planet. Sci.* **32,** A111–A112.

Saxton J. M., Lyon I. C., and Turner G. (1995) Oxygen isotopes in forsterite grains from Julesburg and Allende: Oxygen-16-rich material in an ordinary chondrite. *Meteoritics* **30,** 571–572.

Saxton J. M., Lyon I. C., and Turner G. (1996) Oxygen-16-rich olivine in the Julesburg ordinary chondrite. *Meteoritics Planet. Sci.* **31,** 123.

Saxton J. M., Lyon I. C., and Turner G. (1998) Oxygen isotopes in forsterite grains from Julesburg and Allende: Oxygen-16-rich material in an ordinary chondrite. *Meteoritics Planet. Sci.* **33,** 1017–1027.

Scott E. R. D. and Taylor G. J. (1983) Chondrules and other components in C, O, and E chondrites: Similarities in their properties and origins. *Proc. 14th Lunar Planet. Sci. Conf.* **88,** B275–B286.

Sears D. W. G., Lyon I., Saxton J., and Turner G. (1998) The oxygen isotope properties of olivines in the Semarkona ordinary chondrite. *Meteoritics Planet. Sci.* **33,** 1029–1032.

Shu F. H., Shang H., and Lee T. (1996) Toward an astrophysical theory of chondrites. *Science* **271,** 1545–1552.

Slodzian G. (1980) Micronalayzers using secondary ion emission. In *Advances in Electronics and Electron Physics*, Vol. Supplement 13B (ed. A. Septier), pp. 1–44. Acad. Press.

Stadermann F. J. (1990) Messung von Isotopen- und Elementhaufigkeiten in einzelnen Interplanetaren Staubteilchen mittels Sekundaerionen-Massenspektrometrie. Ph.D. thesis, Univ. Heidelberg.

Stadermann F. J. (1991) Rare earth and trace elements abundances in individual IDPs. *Lunar Planet. Sci.* **XXII,** 1311–1312.

Steele I. M. (1986) Compositions and textures of relic forsterite in carbonaceous and unequilibrated ordinary chondrites. *Geochim. Cosmochim. Acta* **50,** 1379–1395.

Steele I. M. (1988) Primitive material surviving in meteorites: Mineral grains. In *Meteorites and the early solar system* (ed. J. F. Kerridge and M. S. Matthews), pp. 808–818. The University of Arizona Press.

Steele I. M. (1989) Compositions of isolated forsterites in Ornans (CO3). *Geochim. Cosmochim. Acta* **53,** 2069–2079.

Steele I. M. (1992) Olivine in Antarctic micrometeorites: Comparison with other extraterrestrial olivine. *Geochim. Cosmochim. Acta* **56,** 2923–2929.

Thiemens M. H. (1996) Mass-independent isotopic effects in chondrites: The role of chemical processes. In *Chondrules and the protoplanetary disk* (ed. R. H. Hewins, R. H. Jones, and E. R. D. Scott), pp. 107–118. Cambridge University Press.

Thiemens M. H. and Heidenreich J. E. I. (1983) The mass-independent fractionation of oxygen: A novel isotope effect and its possible cosmochemical implications. *Science* **219,** 1073–1075.

Tomeoka K. and Buseck P. R. (1985) Hydrated interplanetary dust particle linked with carbonaceous chondrites? *Nature* **314,** 338–340.

Walter J., Brandstätter F., Kurat G., Koeberl C., and Maurette M. (1995) Cosmic spherules, micrometeorites and chondrules. *Lunar Planet. Sci.* **XXVI,** 1457–1458.

Weinbruch S., Palme H., Spettel B., and Steele I. M. (1997) Refractory forsterite in carbonaceous chondrites; an unaltered condensate from the solar nebula. *Workshop on parent-body and nebular modification of chondritic materials*.

Weinbruch S., Zinner E. K., El Goresy A., Steele I. M., and Palme H. (1993) Oxygen isotopic composition of individual olivine grains from the Allende meteorite. *Geochim. Cosmochim. Acta* **57,** 2649–2661.

Weisberg M. K., Prinz M., Clayton R. N., and Mayeda T. K. (1993) The CR (Renazzo-type) carbonaceous chondrite group and its implications. *Geochim. Cosmochim. Acta* **57,** 1567–1586.

Wetherill G. W. and Chapman C. R. (1988) Asteroids and meteorites. In *Meteorites and the early solar system* (ed. J. F. Kerridge and M. S. Matthews), pp. 35–67. The University of Arizona Press.

Wright I. P., Yates P., Hutchison R., and Pillinger C. T. (1997) The content and stable isotopic composition of carbon in individual micrometeorites from Greenland and Antarctica. *Meteoritics Planet. Sci.* **32,** 79–89.

Yurimoto H., Nagasawa H., Mori Y., and Matsubaya O. (1989) Diffusion in single crystals of melilite: I. Oxygen. *Geochim. Cosmochim. Acta* **53,** 2387–2394.

Zolensky M. E. (1987) Refractory interplanetary dust particles. *Science* **237,** 1466–1468.

Geochimica et Cosmochimica Acta, Vol. 69, No. 22, pp. 5365–5385, 2005

0016-7037/05 $30.00 + .00

doi:10.1016/j.gca.2005.07.002

Isotopic compositions of oxygen, iron, chromium, and nickel in cosmic spherules: Toward a better comprehension of atmospheric entry heating effects

Cécile Engrand,[1,*] Kevin D. McKeegan,[1] Laurie A. Leshin,[1,†] Gregory F. Herzog,[2] Christoph Schnabel,[2,‡] Laurence E. Nyquist,[3] and Donald E. Brownlee[4]

[1]Department of Earth and Space Sciences, University of California, Los Angeles, Los Angeles, CA 90095-1567, USA
[2]Department of Chemistry and Chemical Biology, Rutgers University, Piscataway, NJ 08854-8087, USA
[3]NASA Johnson Space Center, Houston, TX 77058, USA
[4]Department of Astronomy, Box 351580, University of Washington, Seattle, WA 98195, USA

(*Received October* 14, 2004; *accepted in revised form July* 5, 2005)

Abstract—Large, correlated, mass-dependent enrichments in the heavier isotopes of O, Cr, Fe, and Ni are observed in type-I (metal/metal oxide) cosmic spherules collected from the deep sea. Limited intraparticle variability of oxygen isotope abundances, typically <5‰ in $\delta^{18}O$, indicates good mixing of the melts and supports the application of the Rayleigh equation for the calculation of fractional evaporative losses during atmospheric entry. Fractional losses for oxygen evaporation from wüstite, assuming a starting isotopic composition equal to that of air ($\delta^{18}O = 23.5‰$; $\delta^{17}O = 11.8‰$), are in the range 55%–77%, and are systematically smaller than evaporative losses calculated for Fe (69%–85%), Cr (81%–95%), and especially Ni (45%–99%). However, as $\delta^{18}O$ values increase, fractional losses for oxygen approach those of Fe, Cr, and Ni indicating a shift in the evaporating species from metallic to oxidized forms as the spherules are progressively oxidized during entry heating. The observed unequal fractional losses of O and Fe can be reconciled by allowing for a kinetic isotope mass-dependent fractionation of atmospheric oxygen during the oxidation process and/or that some metallic Fe may have undergone Rayleigh evaporation before oxidation began.

In situ measurements of oxygen isotopic abundances were also performed in 14 type-S (silicate) cosmic spherules, 13 from the Antarctic ice and one from the deep sea. Additional bulk Fe and Cr isotopic abundances were determined for two type-S deep-sea spherules. The isotopic fractionation of Cr isotopes suggest appreciable evaporative loss of Cr, perhaps as a sulfide. The oxygen isotopic compositions for the type-S spherules range from $\delta^{18}O = -2‰$ to + 27‰. The intraspherule isotopic variations are typically small, ~5% relative, except for the less-heated porphyritic spherules which have preserved large isotopic heterogeneities in at least one case. A plot of $\delta^{17}O$ vs. $\delta^{18}O$ values for these spherules defines a broad parallelogram bounded at higher values of $\delta^{17}O$ by the terrestrial fractionation line, and at lower values of $\delta^{17}O$ by a line parallel to it and anchored near the isotopic composition of $\delta^{18}O = -2.5‰$ and $\delta^{17}O = -5‰$. Lack of independent evidence for substantial evaporative losses suggests that much of this variation reflects the starting isotopic composition of the precursor materials, which likely resembled CO, CM, or CI chondrites. However, the enrichments in heavy isotopes indicate that some mixing with atmospheric oxygen was probably involved during atmospheric entry for some of the spherules. Isotopic fractionation due to evaporation of incoming grain is not required to explain most of the oxygen isotopic data for type-S spherules. However spherules with barred olivine textures that are thought to have experienced a more intense heating than the porphyritic ones might have undergone some distillation. Two cosmic spherules, one classified as a radial pyroxene type and the other showing a glassy texture, show unfractionated oxygen isotopic abundances. They are probably chondrule fragments that survived atmospheric entry unmelted.

Possible reasons type-I spherules show larger degrees of isotopic fractionation than type-S spherules include: a) the short duration of the heating pulse associated with the high volatile content of the type-S spherule precursors compared to type-I spherules; b) higher evaporation temperatures for at least a refractory portion of the silicates compared to that of iron metal or oxide; c) lower duration of heating of type-S spherules compared to type-I spherules as a consequence of their lower densities.

1. INTRODUCTION

Micrometeorites in the size range from 50 μm to 500 μm constitute the dominant source of extraterrestrial material currently accreted by the Earth (Love and Brownlee, 1993). These particles represent mineralogically, chemically, and isotopically primitive materials (e.g., Brownlee, 1985; Engrand and Maurette, 1998) that have undergone varying degrees of terrestrial alteration, first during atmospheric entry and then during residence in such diverse environments as sea water and Antarctic ice (e.g., Kurat et al., 1994; Duprat et al., 2005).

Rapid atmospheric heating melts many of the incoming particles either partially or completely, thereby producing the cosmic spherules (CS). In this work we examine the effects of this heating on: (1) the isotopic composition of oxygen in both

* Author to whom correspondence should be addressed, at CSNSM Bat. 104, 91405 Orsay Campus, France (engrand@csnsm.in2p3.fr).
† *Present address:* Department of Geological Sciences and Center for Meteorite Studies, Arizona State University, Tempe, AZ 85287-1404, USA.
‡ *Present address:* Scottish Universities Environmental Research Centre, Rankine Avenue, East Kilbride G75 0QF, Scotland.

iron-rich (type-I) cosmic spherules and silicate-rich or stony (type-S) cosmic spherules; and (2) the isotopic composition of Cr, Fe, and Ni in type-I CS, and the isotopic composition of Cr in two type-S CS. The changes in isotopic composition are of interest in several contexts. First, because the spherules are flash-heated in the presence of a low pressure gas, isotopic analyses of cosmic spherules may furnish insights into the mechanisms of elemental exchange between chondrule precursors and nebular gas. Second, if the effects of heating are better understood, isotopic analyses may allow the identification of cosmic spherules that formed from chondrules and thereby constrain the abundance of chondrules in the particle flux to Earth. At present that abundance is thought to be very low, <1% (e.g., Engrand and Maurette, 1998) but is poorly constrained (Genge, 2004; Genge et al., 2005). Third, isotopic analyses may permit estimates of mass loss from cosmic spherules through evaporation and thus aid in refining estimates of the mass distribution of the particle flux to Earth.

Evidence for interesting isotopic behavior of oxygen in *iron-rich* (type-I) cosmic spherules came from the work of Clayton et al. (1986) who reported large positive values of $\delta^{17}O$ and $\delta^{18}O$ in groups of size-sorted particles. Davis et al. (1991) and Davis and Brownlee (1993) subsequently observed large, mass-dependent enrichments in the heavier isotopes of iron, attributing both them and the previously reported enrichments in oxygen isotopes to evaporation during atmospheric entry. Later studies showed that the isotopes of Ni and Cr were also fractionated and lent support to the idea of evaporative loss (e.g., Herzog et al., 1999, and references therein). Even so, the lack of oxygen isotopic analyses of *individual* type-I cosmic spherules has hampered the estimation of relative elemental evaporation rates and hence has made it more difficult to reconstruct thermal histories. In this work, we seek to fill the gap by analyzing O, Cr, Fe, and Ni isotopic abundances in several type-I cosmic spherules.

In general, the *stony* or type-S cosmic spherules are thought to preserve the isotopic abundances of the precursor materials more faithfully than do the iron-rich cosmic spherules (Brownlee et al., 1997). Appreciable mass-dependent isotopic fractionation of Fe, Si, and Mg occurs in a few stony cosmic spherules, however, and to an extent that correlates with independent textural and compositional evidence for heating (Alexander et al., 2002; Taylor et al., 2002). Results for oxygen are fragmentary. Clayton et al. (1986) suggested that the oxygen in melted stony cosmic spherules might be related to the oxygen in bulk C3 chondrites and in the anhydrous components of C2 chondrites. It was not clear from that work how much atmospheric heating might have altered the isotopic abundances of the stony cosmic spherule precursor materials. Engrand et al. (1999) analyzed the oxygen isotopic composition of relict olivine and of relict pyroxene grains in Antarctic micrometeorites (AMMs) that did not melt during atmospheric entry. As did Clayton et al., Engrand and colleagues noted affinity but not identity between the AMMs and carbonaceous chondrites. Their results for these unmelted particles tend to disperse over a wider range than those for any one group of bulk carbonaceous chondrites and to approach the terrestrial fractionation line more closely. Left unsettled by these studies were the respective fractions of the differences owed to variations in the starting composition on the one hand and to the effects of atmospheric heating on the other. By determining the oxygen isotopic compositions of individual stony cosmic spherules and comparing them to the earlier results for unmelted particles, we seek a clearer picture of the effects of heating and melting.

2. SAMPLES AND METHODS

Twenty-seven spherules were selected: 11 type-I cosmic spherules (CS) and 3 type-S spherules recovered from deep-sea sediments (DSCS; see Brownlee, 1985), and 13 type-S spherules collected at Cap Prudhomme in 1994 in Antarctica (ACS; see Maurette et al., 1994). The DSCS have sizes >400 μm; the ACS are from the 100–400 μm size fraction. All samples except two type-S deep-sea spherules (S12 and S13) were mounted in epoxy and polished, and their textures and bulk chemical compositions characterized semi-quantitatively with a scanning electron microscope equipped with an energy-dispersive detector. The major and minor element compositions were determined quantitatively, before any ion microprobe analyses, by using the UCLA CAMECA Camebax microbeam electron microprobe with sample currents set to 10 nA at 15 kV. The detection limit and the analytical uncertainties of the electron microprobe analyses are on the order of 0.01 wt%.

The oxygen isotopic compositions of all samples were measured in situ with the UCLA Cameca ims1270 ion microprobe. Measurements of $^{16,17,18}O$ were performed by following the procedure described in Engrand et al. (1999). The diameter of the analysis spot was ~10 μm. The results are given in the standard δ notation relative to Vienna-Standard Mean Ocean Water (V-SMOW, hereafter noted "SMOW"; Gonfiantini et al., 1993, and references therein), $^{18}O/^{16}O = 0.0020052$, and $^{17}O/^{16}O = 0.00038288$.

The iron isotopic compositions ($^{54,56,57}Fe$) were also measured in situ with the UCLA Cameca ims1270 ion microprobe and ~0.5 nA primary O^- beam, but with a spot size of ~15 μm. The mass resolving power, $M/\Delta M \sim 9000$, was sufficient to resolve $^{57}Fe^+$ from the $^{56}FeH^+$ interference (Fahey, 1988). At this mass resolution the correction for the contribution of the tail of the $^{56}FeH^+$ peak to the $^{57}Fe^+$ signal is negligible. The $^{54}Cr^+$ contribution to the $^{54}Fe^+$ signal, typically 1‰-5‰, was removed by measuring the ^{52}Cr signal and assuming a normal Cr isotopic composition ($^{53}Cr/^{52}Cr = 0.113464$, $^{54}Cr/^{52}Cr = 0.028213$; Birck and Allegre, 1985). It is possible to correct for the ^{54}Cr interference in this way because the samples have low Cr contents, <1%, and because ^{54}Cr is a minor isotope. We did not try to measure ^{58}Fe in the face of large interferences from ^{58}Ni, the major isotope of Ni. The iron isotopic composition is expressed relative to ^{54}Fe in the standard δ notation using the terrestrial iron isotopic ratios of Völkening and Papanastassiou (1989), i.e., $^{56}Fe/^{54}Fe = 15.956853$ and $^{57}Fe/^{54}Fe = 0.371172$.

Instrumental fractionation was corrected by assuming a linear mass fractionation law with parameters set for stony CS by analyses of San Carlos olivine, and set for type-I CS by analyses of a natural magnetite standard. We also analyzed the oxygen isotopic composition of a standard containing 10% magnetite and 90% wüstite. No isotopic fractionation ("matrix effect") was observed between the two types of iron oxides. Several samples were so fine-grained that the analysis of mixed phases was unavoidable—mineral + matrix in the case of the stony CS and magnetite + wüstite for the metallic CS. We made no attempt to correct for possible matrix effects in these cases. The precision of the ion microprobe analyses was 1 to 1.5‰ (1σ) for both oxygen and iron isotopes, but accuracy could be slightly worse for O isotopes in stony spherules due to mixed-phase matrix effects.

After the ion microprobe measurements of the type-I DSCS were complete, the sample mount was soaked in acetone for a week and the type-I CS removed from the softened material with a stainless steel needle. The polished spherule fragments were weighed, then dissolved in HCl. Cr and Ni in the solution were separated by ion exchange, and an ICP-MS used to measure the Cr, Fe, and Ni contents of the samples. Cr isotopic abundances were determined by thermal ionization mass spectrometry at the Johnson Space Center (see Nyquist et al., 1994) and Ni isotopic abundances were determined by ICP-MS at Rutgers University (see Herzog et al., 1999). In addition, Fe isotopic abundances for two type-S spherules (S12 and S13) were determined by TIMS at the Johnson Space Center. The reference ratios for nickel by ICP-MS are: $^{60}Ni/^{58}Ni =$

Table 1. Diameters (D, μm)*, masses (μg)[§], textures (Text.)[¥], magnetite rim thicknesses (Mt, μm)[†], and chemical compositions (wt %) of type-I cosmic spherules.

Sample	D*	Mass[§]	Text.[¥]	Mt[†]	O	Na	Al	Ca	Ti	Cr[‡]	Cr[£]	Mn	Fe[‡]	Fe[£]	Ni[‡]	Ni[£]	Total
KK2-97A -1	505	180	C	25	21.1	b.d.	0.01	b.d.	0.02	0.06	0.070	0.02	72.8	71.3	0.56	0.50	94.6
KK2-97A -2	440	147	A	0	21.4	b.d.	0.03	0.03	b.d.	0.03	0.035	0.01	68.9	69.8	5.83	6.70	96.3
KK2-97A -3	408	103	C	20	21.1	0.01	b.d.	b.d.	b.d.	0.07	0.065	b.d.	71.6	75.5	1.88	1.94	94.7
KK2-97A -4	425	117	C	30	21.1	0.01	b.d.	0.01	b.d.	0.11	0.100	b.d.	73.1	75.5	0.47	0.43	94.8
KK2-97A -5	443	117	C	20	21.5	b.d.	0.01	b.d.	b.d.	0.07	0.116	b.d.	72.9	71.9	2.01	1.84	96.5
KK2-97A -6	418	111	B	5	21.3	b.d.	0.01	0.01	0.01	0.26	0.182	0.01	69.7	70.2	4.46	4.34	95.7
KK2-97A -7	430	116	C	10	21.1	b.d.	b.d.	0.01	b.d.	0.20	0.145	0.04	69.4	70.5	4.10	4.70	94.9
KK2-97A -8	420	123	A	0	21.4	b.d.	b.d.	b.d.	0.01	0.08	0.086	0.02	69.2	72.1	5.72	5.96	96.5
-8 (Core)	60		A(N)			b.d.	0.02	0.03	b	0.01		b.d.	7.6		92.7		100.3
KK2-97A -9	555	224	C	30	21.4	b.d.	b.d.	b.d.	b.d.	0.07	0.071	b.d.	74.0	76.6	0.47	0.42	95.9
KK2-97A -10	575	385	B	3	21.5	b.d.	0.01	b.d.	0.01	0.25	0.259	0.04	69.5	69.3	5.5	5.56	96.8
KK2-97A -11	485	157	C	20	21.3	b.d.	0.04	0.05	b.d.	0.17	0.134	0.03	73.4	76.3	0.63	0.66	95.6
Average										0.12	0.11	0.02	71.3	72.6	2.9	3.0	
σ										0.08	0.06	0.01	2.0	2.8	2.3	2.5	
Literature[&]										0.16			68.4		2.5		

b.d.: below detection limit of ~0.01 wt%.

* Average diameters (in μm) were measured on polished sections using transmitted light.

[§] The polished spherules were weighed after extraction from epoxy. Diameters measured on the polished section by reflected light only slightly larger than those measured using transmitted light suggest that the spherules were polished almost to their half.

[¥] The letters A, B, and C refer to the textures shown in Figures 1A (magnetite dendrites in wüstite), 1B (magnetite in higher abundance but not dendritic), and 1C (exsolution of magnetite in wüstite). The letter N signifies the presence of a core (nugget).

[†] Thickness (in μm) of a layer of pure magnetite that rims some, but not all spherules.

[‡] Electron microprobe analysis.

[£] ICP-MS analysis.

[&] Weighted average based on Herzog *et al.* (Table 3; 1999).

0.385196, $^{61}Ni/^{58}Ni = 0.016746$, $^{62}Ni/^{58}Ni = 0.053381$, and $^{64}Ni/^{58}Ni = 0.013602$. For chromium and iron, the measured ratios are fractionated from the natural values during evaporation of the sample from the sample filament. This effect is compensated by making the sample and standard "loads" nearly identical, and by following the same filament heating schedule for sample and standard. Reference values for Cr standard are: $^{50}Cr/^{52}Cr = 0.0518585$ (normalizing ratio, Birck and Allegre, 1985); $^{53}Cr/^{52}Cr = 0.113464$ (normalized); and $^{54}Cr/^{52}Cr = 0.028213$ (normalized). Unnormalized values for standards were typically fractionated by 6.4‰/amu and 5.4‰/amu for standard loads of 160 and 80 ng of Cr, respectively. For Fe analyses by TIMS, ratios were measured relative to ^{56}Fe. The reference values are $^{54}Fe/^{56}Fe = 0.062669$ (normalizing ratio, Völkening and Papanastassiou, 1989); $^{57}Fe/^{56}Fe = 0.0232636$ (normalized); and $^{58}Fe/^{56}Fe = 0.0031103$ (normalized). Unnormalized values for standards were typically fractionated by 9‰/amu for standard loads of 10 μg of Fe. The values for $\delta^{57}Fe$ and $\delta^{56}Fe$ given in Table 3 are renormalized to $\delta^{54}Fe = 0$ from the measured values relative to $\delta^{56}Fe = 0$.

3. RESULTS OF IRON-RICH (TYPE I) COSMIC SPHERULES

3.1. Sizes, Textures, and Elemental Compositions

The mean diameters of the type-I particles were measured using transmitted light. They range from ~400 μm to ~575 μm (Table 1). These diameters are slightly larger than those measured in reflected light, showing that the section was not polished beyond the midsection of the spherules. The textures and chemical compositions of the type-I spherules are comparable to those that Brownlee (1985) described for particles of this type. In particular, they consist of magnetite (Fe_3O_4) intergrown with wüstite (FeO) in different proportions. The presence of wüstite, a metastable phase, indicates high temperature, low oxygen availability, and fast cooling. Figure 1 shows examples of the three typical textures A, B, and C observed in our samples. The abundance of wüstite (light phase on Fig. 1) decreases from type A to C: in type A, wüstite dominates, magnetite being marginally present; in type B, the proportions of the two phases are approximately the same; in type C, the abundance of magnetite is higher than that of wüstite. Spherules of type B and C are also surrounded by a continuous rim of magnetite, while the type A spherules are not (Fig. 1 and Table 1).

The Cr, Fe, and Ni contents, as measured independently by averaging spot analyses with the electron microprobe and by ICP-MS (bulk analysis), agree well (Table 1). The iron contents of the oxides slightly increase from type A to type C spherules, averaging ~72 wt% Fe, while their nickel contents decrease from type A to C (Table 1). In relative terms, the nickel contents vary more, from 0.5 wt% in type C to ~6 wt% in type A, than do the iron contents. One spherule (spherule 8) has a nickel rich metal core (92.5 wt% Ni, 7.5 wt% Fe) in the plane of the polished section (Fig. 1A). There are no systematic variations of the chromium contents with the textural types. They range from the detection limit of ~0.01 wt% in the metal core of spherule 8 to a high of ~0.26 wt% in spherule 6 (Table 1).

3.2. Oxygen Isotopic Composition

Table 2 shows the oxygen isotopic compositions measured relative to standard mean ocean water (SMOW) for two to ten spots in each of eleven type-I spherules. The data fall along the terrestrial fractionation line (TF), $\delta^{17}O \sim 0.52 \times \delta^{18}O$, with $\delta^{18}O$ values ranging from 38.4‰ to 57.4‰, and $\delta^{17}O$ values from 19.1‰ to 29.4‰ (Fig. 2). The mean values for our analyses, $\delta^{18}O = 47.0 \pm 5.5$‰ and $\delta^{17}O = 23.9 \pm 2.9$‰, are consistent with those of Clayton et al. (1986), which fell in a narrower range, $39.9‰ < \delta^{18}O < 47.1‰$. For different spots

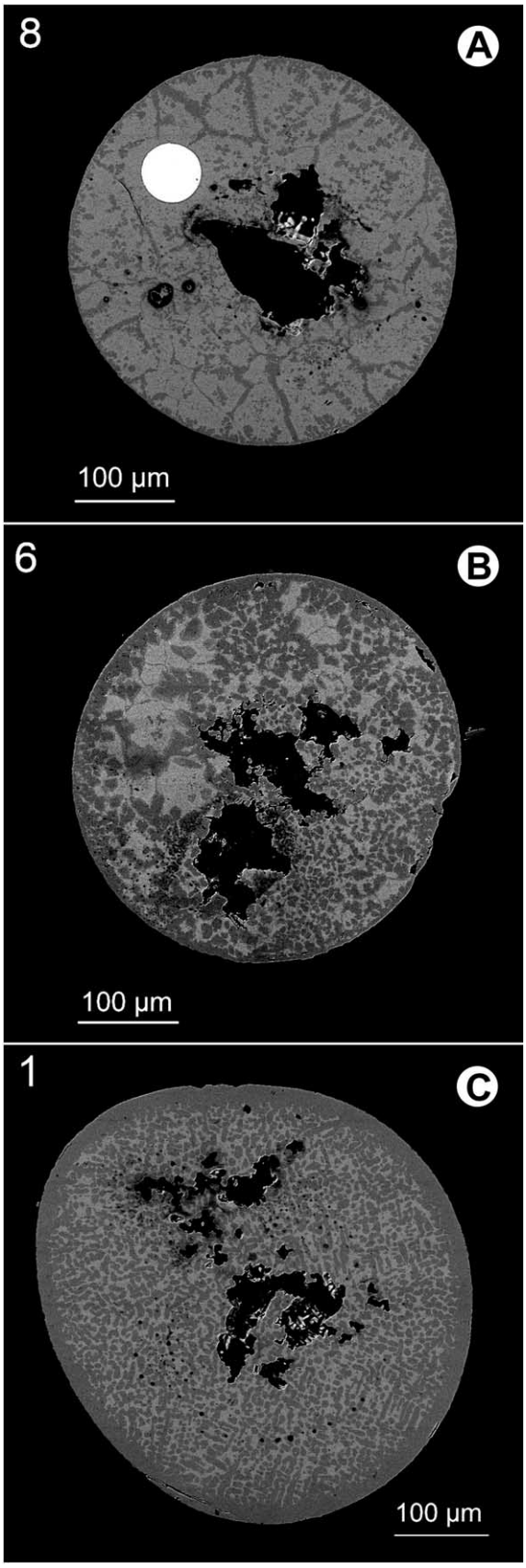

within individual spherules the measured values of $\delta^{18}O$ vary by only a small amount, from 0.3‰ (Table 2, spherule 4) to 6.8‰ (Table 2, spherule 7).

The $\delta^{17,18}O$ values shown in Table 2 do not correlate with the respective proportions of wüstite and magnetite in the ion probe spots as determined by counting pixels in digitized backscattered electron images. This lack of correlation, added to the comparable values measured for a magnetite and a wüstite/magnetite standard (see methods) demonstrate that the variations observed in $\delta^{17,18}O$ in the cosmic spherules do not result from an instrumental artifact, i.e., a matrix effect.

Although no correlation is found between the $\delta^{17,18}O$ values and the magnetite content on single spots, a correlation between the $\delta^{17,18}O$ values in the spherules and the thickness of their magnetite rim is found (Fig. 3a). This suggests that this correlation exists at the scale of the whole spherule but not locally. Within the range of particle sizes analyzed in this work, the degree of heavy oxygen enrichment also correlates well with the particle diameter for the spherules of type C (Fig. 3b). The spherules with textures A and B do not show this correlation with spherule size, as their $\delta^{18}O$ values average ~41‰ for sizes ranging from 400 to 600 μm.

3.3. Iron Isotopic Composition

Table 3 shows the iron isotopic compositions measured in nine of the eleven spherules also analyzed for oxygen. Two to four spots were analyzed for each spherule. No significant isotopic heterogeneity within individual spherules is observed. The data fall on the terrestrial fractionation line (Fig. 4) with $\delta^{57}Fe$ values ranging from 30.3‰ to 50.2‰ (average $\delta^{57}Fe = 43.0 \pm 7.3$‰) and $\delta^{56}Fe$ values from 20.8‰ to 36.2‰ (average $\delta^{56}Fe = 29.3 \pm 5.2$‰). These results are similar to those reported elsewhere (Davis et al., 1991; Davis and Brownlee, 1993; Herzog et al., 1999). The iron isotopic fractionation markedly increases from textural type A to textural type C.

3.4. Chromium and Nickel Isotopic Composition

Table 4 shows the isotopic compositions of chromium and of nickel in type-I spherules. As with iron, the isotopic data for chromium and nickel are consistent with mass-dependent fractionation of material that initially had terrestrial-like isotopic abundances.

Fig. 1. Backscattered electron micrographs of the three textures observed in the section KK2-97A of type-I deep-sea cosmic spherules. There is a systematic increase in the abundance of magnetite (Fe_3O_4, dark phase) over wüstite (FeO, light phase) from type A to type C. (A) Spherule showing magnetite dendrites in wüstite. Wüstite is the most abundant phase. A metal core (92.5 wt% Ni, 7.5 wt% Fe) is visible in the plane of the section; (B) spherule showing about the same proportion of magnetite and wüstite phases. The spherule exhibits a rim of pure magnetite. Magnetite does not have a dendritic texture; (C) exsolution of magnetite in wüstite with a thick rim of magnetite. The abundance of magnetite is well above that of wüstite. These textural differences are probably due to differences in heating and cooling rates: the temperatures and duration of heating probably increased in the order A<B<C.

Table 2. Oxygen isotopic composition measured by ion microprobe of eleven type-I cosmic spherules from deep-sea sediments.

Sample	Text.*	$\delta^{18}O \pm 1\sigma$ (‰)†	$\delta^{17}O \pm 1\sigma$ (‰)†	$\Delta^{17}O \pm 1\sigma$ (‰)†‡
KK2-97A-1_1		56.7 ± 1.0	29.4 ± 0.8	0.0 ± 1.1
KK2-97A-1_2		54.2 ± 1.0	27.5 ± 1.1	−0.7 ± 1.3
Wtd mean	*C*	*55.5 ± 0.7*	*28.8 ± 0.6*	*−0.3 ± 0.8*
KK2-97A-2_1		42.9 ± 0.9	20.4 ± 1.0	−1.9 ± 1.2
KK2-97A-2_2		38.4 ± 1.0	19.5 ± 1.1	−0.5 ± 1.3
Wtd mean	*A*	*40.8 ± 0.7*	*20.0 ± 0.7*	*−1.2 ± 0.9*
KK2-97A-3_1		48.7 ± 0.9	23.5 ± 0.9	−1.8 ± 1.1
KK2-97A-3_2		45.8 ± 0.9	22.2 ± 1.0	−1.6 ± 1.2
KK2-97A-3_3		46.4 ± 0.9	22.3 ± 1.1	−1.8 ± 1.3
KK2-97A-3_4		46.3 ± 0.9	22.4 ± 1.0	−1.7 ± 1.2
KK2-97A-3_5		46.2 ± 0.9	24.3 ± 1.1	0.3 ± 1.3
Wtd mean	*C*	*46.7 ± 0.4*	*23.0 ± 0.4*	*−1.4 ± 0.5*
KK2-97A-4_1		50.2 ± 0.9	24.9 ± 1.0	−1.2 ± 1.2
KK2-97A-4_2		49.9 ± 0.9	24.5 ± 0.9	−1.4 ± 1.1
Wtd mean	*C*	*50.0 ± 0.6*	*24.7 ± 0.7*	*−1.3 ± 0.8*
KK2-97A-5_1		49.1 ± 0.9	24.7 ± 0.9	−0.9 ± 1.1
KK2-97A-5_2		47.7 ± 0.9	24.1 ± 1.0	−0.7 ± 1.2
Wtd mean	*C*	*48.4 ± 0.6*	*24.4 ± 0.7*	*−0.8 ± 0.8*
KK2-97A-6_1		39.2 ± 1.1	19.2 ± 0.9	−1.3 ± 1.0
KK2-97A-6_2		44.3 ± 1.0	23.1 ± 0.9	0.0 ± 1.0
KK2-97A-6_3		39.0 ± 1.0	20.6 ± 0.9	0.3 ± 1.0
Wtd mean	*B*	*40.9 ± 0.6*	*20.9 ± 0.5*	*−0.3 ± 0.6*
KK2-97A-7_1		45.9 ± 0.9	24.2 ± 0.9	0.4 ± 1.0
KK2-97A-7_1b		46.6 ± 0.9	24.4 ± 0.8	−0.8 ± 1.0
KK2-97A-7_2		45.6 ± 0.9	22.9 ± 0.9	−1.2 ± 1.2
KK2-97A-7_3		42.2 ± 1.0	20.8 ± 1.1	1.2 ± 1.1
KK2-97A-7_4		42.8 ± 1.0	23.5 ± 1.0	0.4 ± 1.2
KK2-97A-7_5		46.0 ± 0.9	24.3 ± 1.1	−0.8 ± 1.2
KK2-97A-7_6		47.4 ± 0.9	23.9 ± 1.1	0.7 ± 1.2
KK2-97A-7_7		48.2 ± 1.0	25.8 ± 1.1	0.7 ± 1.2
KK2-97A-7_8		48.9 ± 0.9	26.1 ± 1.2	−0.3 ± 1.1
KK2-97A-7_9		47.8 ± 0.9	24.5 ± 1.0	0.1 ± 1.0
Wtd mean	*C*	*46.2 ± 0.3*	*24.0 ± 0.3*	*0.0 ± 0.3*
KK2-97A-8_1		42.5 ± 1.0	22.6 ± 1.1	0.5 ± 1.2
KK2-97A-8_2		41.9 ± 1.1	21.8 ± 1.1	0.0 ± 1.2
KK2-97A-8_3		41.7 ± 1.0	21.7 ± 0.9	0.0 ± 1.0
Wtd mean	*A*	*42.0 ± 0.6*	*22.0 ± 0.6*	*0.2 ± 0.7*
KK2-97A-9_1		57.4 ± 0.9	29.3 ± 0.9	−0.6 ± 1.0
KK2-97A-9_2		52.1 ± 1.0	25.8 ± 1.0	−1.3 ± 1.1
KK2-97A-9_3		55.5 ± 1.0	26.8 ± 1.1	−2.0 ± 1.2
KK2-97A-9_4		56.8 ± 0.9	29.0 ± 0.9	−0.5 ± 1.0
Wtd mean	*C*	*55.6 ± 0.5*	*27.9 ± 0.5*	*−1.0 ± 0.5*
KK2-97A-10_1		41.5 ± 0.9	21.7 ± 1.0	0.2 ± 1.1
KK2-97A-10_2		39.8 ± 1.0	19.8 ± 0.9	−0.9 ± 1.1
KK2-97A-10_3		43.9 ± 1.0	22.6 ± 1.0	−0.3 ± 1.1
KK2-97A-10_4		40.2 ± 0.9	21.1 ± 0.9	0.2 ± 1.0
Wtd mean	*A*	*41.3 ± 0.5*	*21.2 ± 0.5*	*−0.2 ± 0.5*
KK2-97A-11_1		49.0 ± 0.9	26.8 ± 0.9	1.3 ± 1.0
KK2-97A-11_2		50.0 ± 0.9	26.2 ± 1.0	0.2 ± 1.1
KK2-97A-11_3		50.4 ± 0.9	26.2 ± 0.9	−0.1 ± 1.0
Wtd mean	*A*	*49.8 ± 0.5*	*26.4 ± 0.5*	*0.5 ± 0.6*

* See Figure 1 and caption Table 1.
† Relative to SMOW, errors are 1σ mean.
‡ $\Delta^{17}O = \delta^{17}O - 0.52 \times \delta^{18}O$

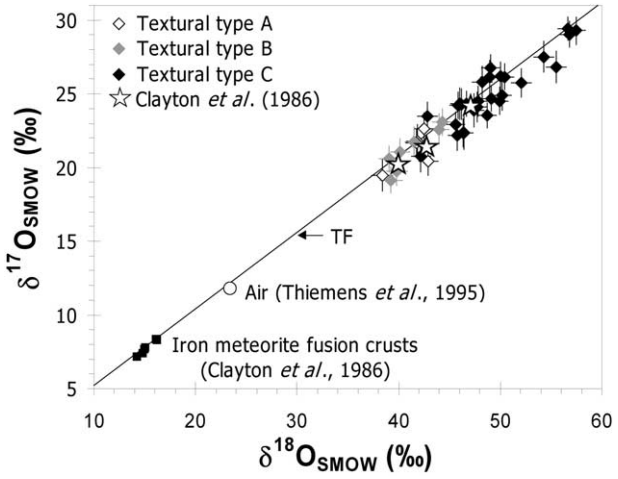

Fig. 2. Oxygen isotope abundances in type-I spherules plot along a mass-dependent fractionation line. The terrestrial fractionation line (TF) passes through both the composition of air (open circle; data taken from Thiemens et al., 1995), and of standard mean ocean water (SMOW). Our data are shown according to the three textural types (A, B, and C) found in the deep-sea spherules, as defined in Figure 1. Data from Clayton et al. (1986) are shown for comparison purposes for three sets of type-I deep-sea spherules (open stars), and for iron meteorite fusion crusts (black squares).

3.5. Φ, a Measure of Overall Mass-Dependent Fractionation

When all the isotopic data for an element fall on a single mass-dependent fractionation line, as our data do, it is convenient to have one measure of the fractionation. For this measure we adopt the slope, Φ, of a plot of δ values vs. the corresponding isotope mass differences for each isotopic system. We calculate the slope from our data by using the weighted least squares fitting routine of Williamson (1968). Qualitatively, larger Φ means a larger degree of mass-dependent fractionation.

Values of Φ (‰/amu) for the type-I spherules appear in Table 5. We have made two different calculations of Φ for oxygen :(1) to ease the comparison with other data, we calculate $\Phi_{O(SMOW)}$ using the classical SMOW value as a reference ($\delta^{18}O_{SMOW}(SMOW) = \delta^{17}O_{SMOW}(SMOW) = 0$ by definition); (2) we use the air isotopic composition ($\delta^{18}O_{SMOW}(AIR) = 23.5‰; \delta^{17}O_{SMOW}(AIR) = 11.8‰$) (Thiemens et al., 1995) as the starting isotopic composition to calculate $\Phi_{O(AIR)}$. The results calculated with air as the starting isotopic value are thus smaller by ~12 ‰/amu than those calculated relative to SMOW. Because the spherule precursors interacted with atmospheric oxygen, we prefer to adopt "air" as the reference value, hence $\Phi_{O(AIR)}$ only represents the overall mass-dependent fractionation relative to air and does not reflect the difference in isotopic composition between atmospheric oxygen and SMOW. For the type-I spherules, the average for $\Phi_{O(AIR)}$ is 11.6 ± 2.7‰/amu, with values for individual spherules ranging from 8.4 to 15.8‰/amu.

In general, the ranges and absolute values of Φ calculated for Cr, Fe, and Ni resemble those reported by others (Davis and Brownlee, 1993; Xue et al., 1995; Herzog et al., 1999). We confirm the tendency of Φ_{Ni} to increase as Ni content decreases, as expected from a well mixed evaporating system of relatively uniform starting composition (Fig. 5). Two of the spherules, 4 and 9, have remarkably large values of Φ_{Ni}, 46.7‰/amu and 43.5‰/amu, respectively, topping the previous record of 38‰/amu (Davis and Brownlee, 1993). Increases in Φ for the three elements correlate with one another (Fig. 6), as was noted by Herzog et al. (1999). For chromium higher values of Φ_{Cr} (or lower values of Φ_{Fe}) are observed with respect to the correlation given in Herzog et al. (1999). The difference may reflect a small systematic bias (~2–3‰) as the iron isotopic compositions were measured in our case by ion microprobe and not by TIMS as in Herzog et al. (1999). In type A spherules the deviations from the correlation Φ_{Cr} vs. Φ_{Fe} are especially large, which suggests that these spherules lost a large proportion of their Cr ab initio thus leading to larger degrees of fractionation of the remaining Cr (see below).

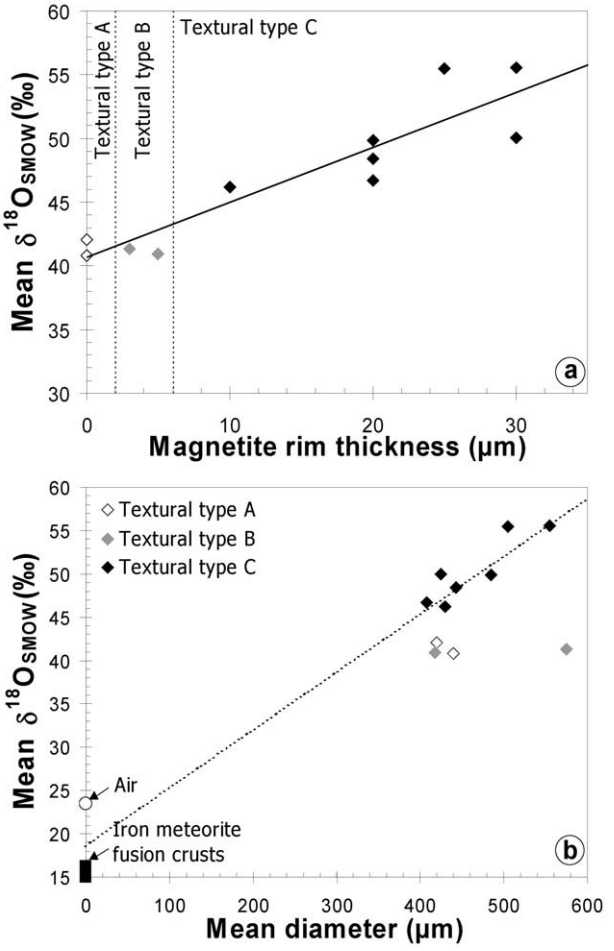

Fig. 3. (a) Correlation plot between $\delta^{18}O$ and the thickness of magnetite rim; (b) Values of $\delta^{18}O$ increase with the diameter of type-I deep-sea spherules belonging to textural type C (see definition of textural types in Fig. 1). Results for type A and type B spherules do not plot on this correlation. The extrapolation of this correlation line to the origin plots close to the oxygen isotopic values found in iron meteorite fusion crusts (see text).

4. DISCUSSION OF TYPE-I SPHERULES

The nature of the extraterrestrial precursors of the type-I spherules is uncertain. Herzog et al. (1999) argued for small

Table 3. Iron isotopic composition of nine type-I and two-type-S cosmic spherules from deep-sea sediments. Type-I: by SIMS; Type-S: by TIMS.

Sample	δ^{57}Fe ± σ (‰)†	δ^{56}Fe ± σ (‰)†
Type-I		
KK2-97A - 1_1	47.0 ± 1.1	33.0 ± 0.7
KK2-97A - 1_1a	46.8 ± 1.1	31.6 ± 0.7
KK2-97A - 1_2a	47.6 ± 1.1	33.6 ± 0.6
KK2-97A - 1_3	48.2 ± 1.6	33.2 ± 1.4
Wtd mean	*47.3 ± 0.6*	*32.8 ± 0.4*
KK2-97A - 2_1	30.3 ± 1.1	20.8 ± 1.0
KK2-97A - 2_2	32.5 ± 1.1	23.1 ± 1.0
KK2-97A - 2_3	32.3 ± 1.1	22.8 ± 0.8
Wtd mean	*31.7 ± 0.6*	*22.3 ± 0.5*
KK2-97A - 3_1	46.4 ± 1.6	31.9 ± 1.4
KK2-97A - 3_2	45.3 ± 1.6	31.4 ± 1.4
Wtd mean	*45.9 ± 1.1*	*31.6 ± 1.0*
KK2-97A - 6_1	41.6 ± 1.1	28.0 ± 0.7
KK2-97A - 6_2	40.3 ± 1.6	26.6 ± 1.5
Wtd mean	*41.2 ± 0.9*	*27.8 ± 0.6*
KK2-97A - 7_1	50.7 ± 1.6	34.1 ± 1.4
KK2-97A - 7_2	50.7 ± 1.6	35.0 ± 1.5
Wtd mean	*50.7 ± 1.1*	*34.5 ± 1.0*
KK2-97A - 8_1	34.7 ± 1.6	21.8 ± 1.5
KK2-97A - 8_2	33.6 ± 1.6	22.2 ± 1.5
KK2-97A - 8_3	31.0 ± 1.6	20.8 ± 1.6
Wtd mean	*33.1 ± 0.9*	*21.6 ± 0.9*
KK2-97A - 9_1	49.2 ± 1.1	34.5 ± 0.8
KK2-97A - 9_2	52.0 ± 1.1	36.2 ± 0.7
Wtd mean	*50.6 ± 0.8*	*35.4 ± 0.5*
KK2-97A - 10_1	37.7 ± 1.6	25.5 ± 1.4
KK2-97A - 10_2	38.7 ± 1.6	25.6 ± 1.6
Wtd mean	*38.2 ± 1.1*	*25.5 ± 1.1*
KK2-97A - 11_1	46.9 ± 1.6	31.5 ± 1.6
KK2-97A - 11_2	49.2 ± 1.6	32.8 ± 1.4
Wtd mean	*48.1 ± 1.1*	*32.2 ± 1.1*
Type-S		
S12	4.8 ± 1.0	3.2 ± 0.9
S13	2.0 ± 0.3	1.4 ± 0.3

† Delta values are normalized to ^{54}Fe.

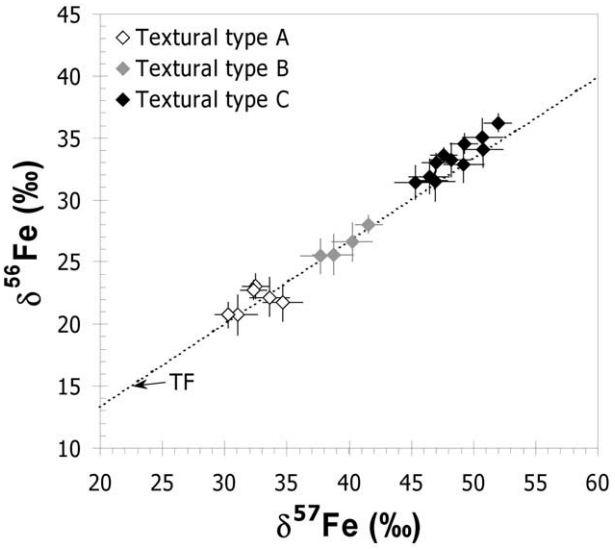

Fig. 4. Iron isotopic composition in the type-I deep-sea spherules. The data lie on a mass fractionation line. The textural types are defined in Figure 1.

metal particles; Brownlee et al. (1997) suggested that the reduction of carbonaceous chondrite material produced metal droplets. Raisbeck et al. (1982) and Yiou et al. (1985) suggested a metal-bearing parent body for the type-I spherules, using arguments based on the unexpected presence in type-I spherules of the cosmogenic radionuclide ^{10}Be. Iron meteorites contain about the same concentrations of ^{10}Be as do type-I spherules, but the chemical composition of type-I spherules cannot be reconciled with that of iron meteorites (see Delaney et al., 2002).

Whatever the extraterrestrial precursors may have been, we will begin with the premise that just after melting, the type-I spherules contained no oxygen, either terrestrial or extraterrestrial, and that they evolved primarily through oxidation, and evaporation of metal and oxide, and perhaps fragmentation. As we shall see, all of the isotope data are consistent with this view.

4.1. Heating Sequence: Hints from Sizes, Textures, and Compositions

The good anticorrelation between the Fe and Ni contents of all spherules (Table 1, Fig. 7) suggests a common precursor that underwent successive stages of melting and fragmentation. The thickness of the magnetite rim, as well as the abundance ratio of magnetite to wüstite, increases from textural type A to C, as do the average O, Fe and Ni isotopic fractionations. The behavior of Cr is more complex. For types B and C, the behavior of Φ_{Cr} is compatible with that of O, Fe, and Ni. For type A, the fractionation observed is about the same as that found for type C spherules. We suggest that type A spherules lost Cr through the evaporation of a Cr-rich nugget, perhaps a sulfide, thus leading to a decreased Cr content and a larger Φ_{Cr} in the spherule.

The growth of magnetite rims, the ever more intimate intergrowth of magnetite and wüstite within the individual spherules, and the increasing isotopic fractionations of the major elements from type A to C spherules suggest a heating sequence, with type A heated least (lowest peak temperatures for the shortest times) and type C heated most strongly. The variations in heating intensity could be due to differences in entry speed, entry angle, or particle size. Also, Lal and Jull (2002) have suggested that an appreciable portion of the particle flux in the spherule size range comes from the atmospheric breakup of bodies larger than 1 cm. If the breakup occurred at moderate altitudes—i.e., <100 km—the resulting debris would be more strongly heated.

4.2. Evaporative Losses

We will use the Rayleigh formula to calculate from Φ (the degree of mass-dependent fractionation; Table 5) the fractions

Table 4. Chromium isotopic composition measured by TIMS and nickel isotopic composition measured by ICP-MS of type-I and type-S cosmic spherules. Error limits are 2σ.

Sample	δ^{50}Cr	δ^{53}Cr	δ^{54}Cr	δ^{60}Ni	δ^{61}Ni	δ^{62}Ni	δ^{64}Ni
type-I							
KK2-97A-1				71 ± 10	110 ± 26	145 ± 11	
KK2-97A-2	−48.3 ± 5.8	23.6 ± 2.8	42.8 ± 8.5	16 ± 7	29 ± 7	32 ± 12	
KK2-97A-3				44 ± 6	63 ± 6	85 ± 9	140 ± 40
KK2-97A-4	−56.0 ± 5.8	28.1 ± 2.8	56.1 ± 5.5	95 ± 3	123 ± 39	174 ± 10	
KK2-97A-5	−51.6 ± 5.8	26.1 ± 2.8	52.4 ± 5.5	45 ± 8	45 ± 33	71 ± 18	
KK2-97A-6	−34.7 ± 5.8	17.6 ± 2.8	34.9 ± 5.5	25 ± 4	35 ± 12	45 ± 9	
KK2-97A-7	−52.3 ± 5.8	26.2 ± 2.8	52.5 ± 5.5	28 ± 10	38 ± 25	56 ± 9	
KK2-97A-8	−44.5 ± 5.8	22.4 ± 2.8	44.4 ± 5.5	9 ± 5	21 ± 12	23 ± 11	
KK2-97A-9	−47.2 ± 5.8	23.7 ± 2.8	48.1 ± 5.5	93 ± 6	124 ± 15	166 ± 10	
KK2-97A-10	−32.4 ± 5.8	16.0 ± 2.8	32.1 ± 5.5	20 ± 4	32 ± 24	42 ± 3	85 ± 30
KK2-97A-11	−37.7 ± 5.8	18.9 ± 2.8	38.1 ± 5.5	61 ± 8	97 ± 28	126 ± 10	
KK1-9				41 ± 12	62 ± 9	80 ± 12	
KK1-9*				37	61	72	
Type-S							
S12	−13.7 ± 1.8	6.6 ± 1.0	13.4 ± 2.0				
S13	−23.3 ± 1.8	11.2 ± 1.0	22.0 ± 2.0				

* Herzog *et al.* (1999)

retained, f_r, of the reference isotopes ^{16}O, ^{52}Cr, ^{54}Fe, and ^{58}Ni after evaporation:

$$\frac{R}{R_o} = f_r^{\left(\frac{1}{\alpha}-1\right)}, \tag{1}$$

where R is an isotopic ratio, ^{18}O/^{16}O for instance for oxygen, and R_o is the starting value of this ratio before evaporation and α is the conventional isotopic fractionation factor. In an ideal system,

$$\alpha = \sqrt{\frac{m'}{m}} \tag{1a}$$

where m and m′ are the isotopic masses of the evaporating species. Then

$$f_r = \left(1 + \frac{\Phi}{1000}\right)^b \tag{1b}$$

The exponent b is related to the conventional fractionation factor α by the expression:

$$b = \frac{\alpha}{1-\alpha} \tag{1c}$$

The relative uniformity (within 10% relative; section 3.2) of isotopic composition within a spherule shows that the oxygen in type-I spherules meets at least one of the requirements for a Rayleigh evaporation, namely, that the melts be well-mixed. As our systems may not be ideal in all respects, the choice of m

Table 5. Average mass-dependent fractionation (Φ, ‰/amu)*, and fraction of element lost§ in type-I and type-S cosmic spherules.

	Φ					f_{lost}				
Sample	$O_{(SMOW)}$¥	$O_{(AIR)}$†	Cr	Fe	Ni	O¥	O†	Cr	Fe	Ni
type-I										
KK2-97A -1	27.9 ± 0.3	15.8 ± 0.3		16.1 ± 0.3	36.1 ± 2.4	0.92	0.77		0.83	0.98
KK2-97A -2	20.3 ± 0.3	8.4 ± 0.3	23.5 ± 1.8	10.9 ± 0.4	9.1 ± 1.7	0.85	0.54	0.91	0.69	0.65
KK2-97A -3	23.2 ± 0.2	11.3 ± 0.2		15.6 ± 0.7	21.5 ± 1.4	0.88	0.64		0.82	0.92
KK2-97A -4	24.9 ± 0.3	12.9 ± 0.3	28.1 ± 1.6		46.7 ± 1.1	0.90	0.69	0.95		0.995
KK2-97A -5	24.2 ± 0.3	12.2 ± 0.3	26.1 ± 1.6		20.0 ± 2.9	0.89	0.68	0.93		0.90
KK2-97A -6	20.5 ± 0.3	8.6 ± 0.3	17.5 ± 1.6	13.8 ± 0.5	11.9 ± 1.3	0.85	0.55	0.84	0.78	0.75
KK2-97A -7	23.2 ± 0.1	11.2 ± 0.1	26.2 ± 1.6	17.1 ± 0.7	14.0 ± 2.0	0.88	0.66	0.93	0.84	0.80
KK2-97A -8	21.2 ± 0.3	9.2 ± 0.3	22.3 ± 1.6	10.9 ± 0.6	5.3 ± 1.7	0.86	0.59	0.90	0.70	0.46
KK2-97A -9	27.7 ± 0.2	15.7 ± 0.2	23.8 ± 1.6	17.3 ± 0.4	43.5 ± 1.8	0.92	0.77	0.92	0.85	0.993
KK2-97A -10	20.7 ± 0.2	8.8 ± 0.2	16.1 ± 1.6	12.7 ± 0.7	10.4 ± 0.7	0.85	0.56	0.81	0.75	0.70
KK2-97A -11	25.2 ± 0.2	13.1 ± 0.2	19.0 ± 1.6	16.1 ± 0.7	31.4 ± 2.1	0.90	0.71	0.86	0.83	0.97
Average ± 1σ	*23.5 ± 2.7*	*11.6 ± 2.7*	*22.5 ± 4.2*	*14.5 ± 2.5*	*22.7 ± 14.5*	*0.88*	*0.65*	*0.89*	*0.79*	*0.83*
Type-S										
S12			6.7 ± 0.6	1.6 ± 0.5				0.51	0.17	
S13			11.3 ± 0.6	0.6 ± 0.2				0.69	0.07	

* From non-linear least squares fits (Williamson, 1968) to isotopic data assuming that the initial isotopic ratios were terrestrial.
§ From the Rayleigh fractionation equation.
¥ Assumes starting isotopic composition is that of standard mean ocean water (SMOW).
† Assumes starting isotopic composition is atmospheric : $\delta^{18}O_{SMOW}(AIR) = 23.5‰$; $\delta^{17}O_{SMOW}(AIR) = 11.8‰$ (Thiemens *et al.*, 1995).

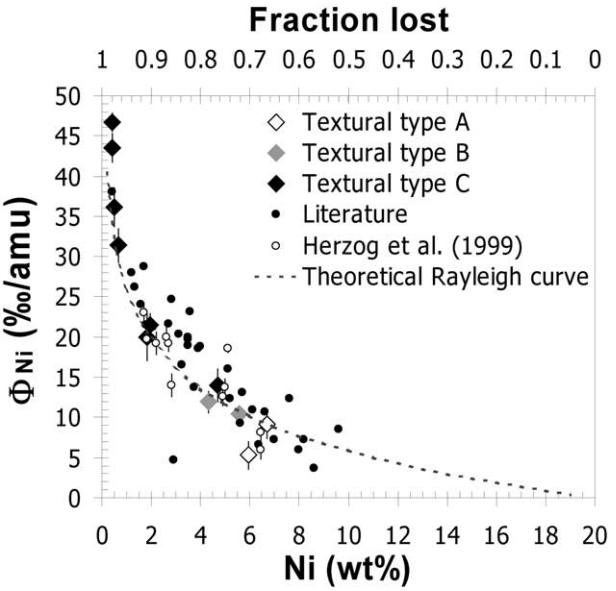

Fig. 5. Values of $\Phi_{Ni,}$ a quantity that measures the degree of mass dependent fractionation of Ni, anticorrelate with Ni content (bottom X-axis), suggesting that the precursor particles have a limited compositional range. Literature values are from Davis and Brownlee (1993) and Xue et al. (1995). The theoretical Rayleigh distillation behavior showing the values of Φ_{Ni} expected as a function of the retained fraction of Ni (top X-axis) is given for comparison (dotted line). Here we assume an initial Ni content of 20 wt%. The textural types are defined in Figure 1.

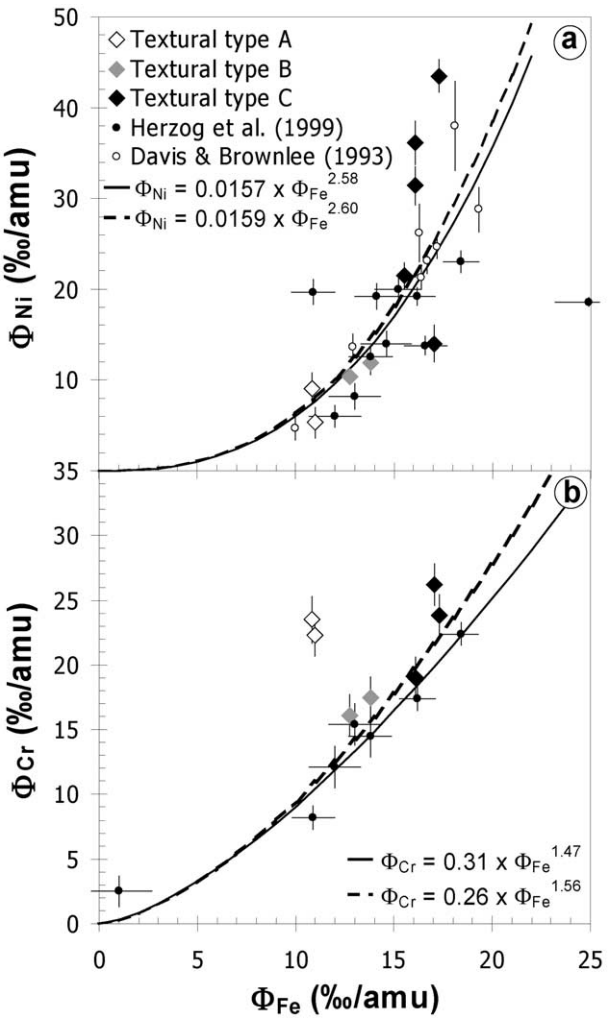

Fig. 6. Values of the quantity Φ are correlated for the elements Fe, Cr, and Ni, in agreement with previous work (e.g., Herzog et al., 1999, and references therein). The textural types are defined in Figure 1.

requires further discussion. For the metals, Cr, Fe, and Ni, we adopt for m the masses of the isotopes themselves, e.g., m = 57.94 for ^{58}Ni. In the case of nickel, this choice seems straightforward. As the most noble of the three metals, nickel oxidizes last, and, indeed, appreciable amounts of metallic Ni remain in many type-I spherules. As metallic nickel is more volatile than the oxide and as it persists through the late stages of evaporation, it is plausible that the element leaves the spherules mainly as the atom. Iron and chromium, on the other hand, are more likely to oxidize completely during descent through the atmosphere and the nature of the evaporating species is not obvious. Wang et al. (1994) studied the evaporation of wüstite in the laboratory and found that use of the atomic mass of iron in Eqn. (1a) described the observations, possibly because the oxide decomposes before evaporation. Lacking experimental data for Cr, we simply assume that we can use the atomic mass of ^{52}Cr. In the case of oxygen, which is bound mainly to iron, we again follow Wang et al. (1994), who determined fractionation factors α = 1.0110 and 1.0217 for ^{17}O and ^{18}O, respectively, corresponding to effective masses (amu) of 45.206 and 45.588, evaporating from wüstite for ^{17}O and ^{18}O, respectively.

4.3. Evaporation Sequence in Type I Spherules

Figure 8 and Table 5 give the calculated fractions of O, Cr, Fe, and Ni lost, $1 - f_r$, by our type-I spherules, taking terrestrial ratios as the starting isotopic composition before evaporation. Herzog et al. (1999) noted that for lower degrees of evaporation—say $\Phi_{Fe} < 5$ ‰/amu and $1 - f_{r(Fe)} < 0.43$—evaporative losses occur in the order: Fe > Cr > Ni > O (see Figs. 6 and 8). If the spherules first formed as metallic droplets, then the order of loss, Fe > Ni, is the one expected based on vapor pressures of the elements (Davis and Brownlee, 1993; Herzog et al., 1999). The inversion of Fe and Cr may result from experimental error or early loss of Cr (see above comment regarding sulfide).

The first stages of evaporation and isotopic fractionation of the spherules almost certainly take place before much oxygen has had a chance to react. It follows that oxygen can only begin to fractionate and "catch up" isotopically with the metals somewhat later in the evaporation process—after the oxygen reacts with the descending droplet and the loss rates of the more volatile metals have slowed. Thus it is not surprising that for spherules that have lost up to 75% of their Fe, the losses of Cr, Fe, and Ni exceed those of O.

For the more strongly heated spherules, the observed order of loss shifts to Ni > Cr ≥ Fe ~ O. Figure 8 shows oxygen "catching up" with iron and chromium in the spherules that have larger degrees of evaporative loss. Meanwhile, the fractionation (and implied loss) of oxygen stays behind that of

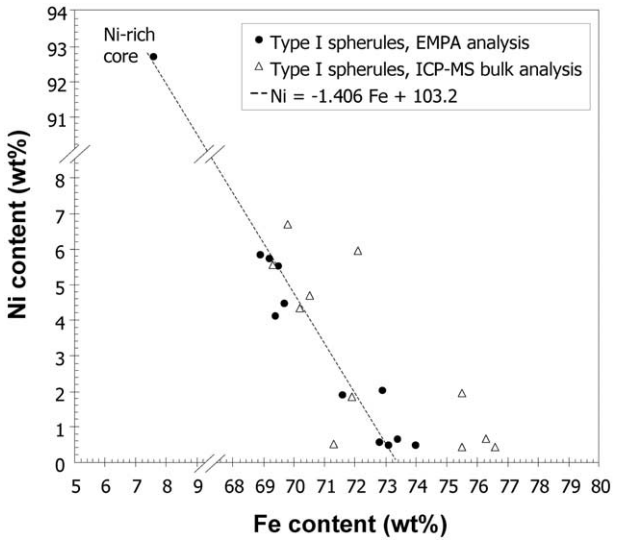

Fig. 7. Iron and nickel compositions (in wt%) of the deep-sea spherules. The solid symbols represent data obtained by averaging 2 to 5 spot analyses measured with the electron microprobe (EMPA) on the polished section. Open symbols are bulk measurements of dissolved spherules by ICP-MS. A good anticorrelation is found between these two composition, suggesting a common precursor for the spherules, which underwent successive stages of melting and fragmentation.

nickel. We interpret these observations as follows. As oxygen strikes the descending droplets, minimization of free energy first favors reaction with Cr. With the formation of the oxides of Cr, the evaporation rate of Cr decreases and, depending on the volatility of the various oxides, fractionation continues, but probably more slowly. Although the details for Cr are unclear, the concentrations of Cr are too low to have much influence on the total oxygen budget.

Once Cr has oxidized, the major element iron should oxidize next. As argued by Davis and Brownlee (1993), the oxidation of Fe should lower its volatility while nickel should continue to evaporate at a more or less constant rate for as long as it remains a metal (assuming constant temperature and ignoring nonideal behavior). In other words, during the latter stages of evaporation, the loss rates of iron and oxygen should approach one another but lag behind that of nickel, for as long as nickel remains unoxidized. Using the Φ_{Cr}, Φ_{Fe} and Φ_{Ni} values given in Table 5, we can calculate preloss Cr/Fe of (3.4 ± 1.6) × 10^{-3} and Fe/Ni of (16.6 ± 4.3) mass/mass ratios which are in good agreement with the data previously reported by others (e.g., Herzog et al., 1999).

4.4. Evaporation of Fe and FeO

Here we consider the degree to which iron evaporates as metal and as oxide. We conjecture that when evaporation of the oxide begins, the iron has a single, characteristic isotopic composition and explore various values for it and their implications.

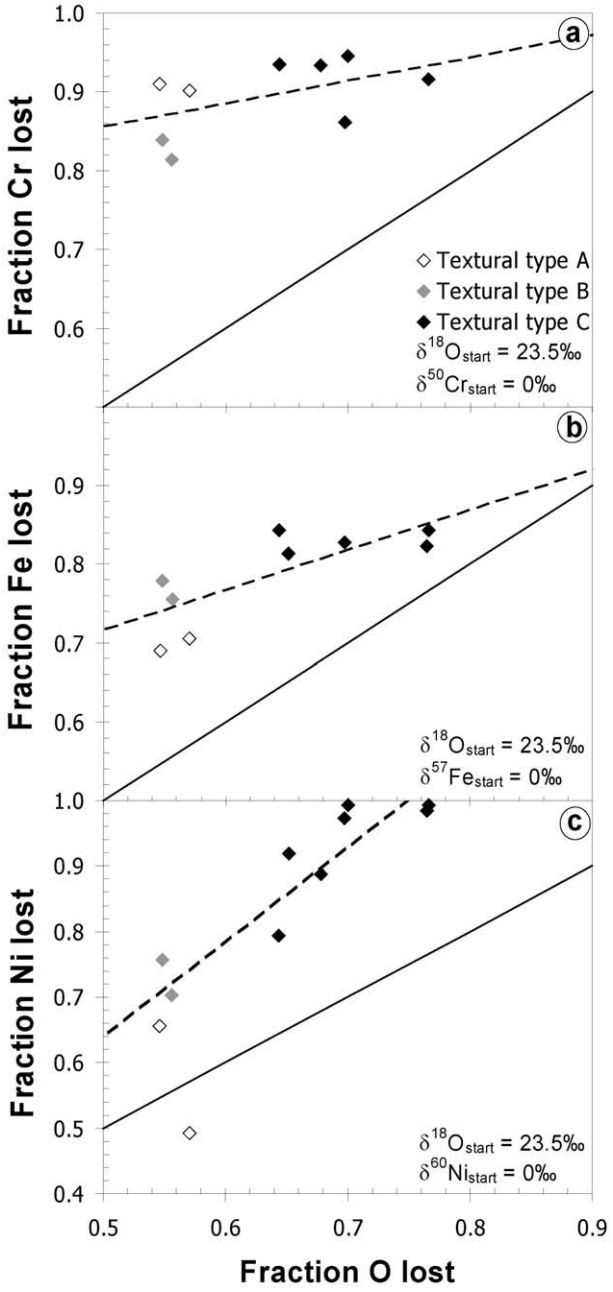

Fig. 8. Fractional evaporative losses of Cr, Fe, Ni, and O from I-type spherules. Starting isotopic compositions at the beginning of *oxygen* evaporation (subscript "start") for this figure are taken as terrestrial (i.e., $\delta^{18}O = 23.5‰$, $\delta^{17}O = 11.8‰$, δFe,Cr,Ni = 0‰). The slope one line (solid) and best linear fit lines through the data (dashed) are given for reference. The best linear fits have the following forms: $1 - f_{r(Cr)} = (0.41 \pm 0.20) \times (1 - f_{r(O)}) + (0.62 \pm 0.13)$; $1 - f_{r(Fe)} = (0.43 \pm 0.23) \times (1 - f_{r(O)}) + (0.53 \pm 0.15)$; $1 - f_{r(Ni)} = (1.7 \pm 0.5) \times (1 - f_{r(O)}) + (-0.30 \pm 0.34)$. The textural types are defined in Figure 1.

4.4.1. *Case 1: If the oxygen entering the spherules has $\delta^{18}O_{SMOW}$ = 23.5‰, i.e., is atmospheric, then evaporation of FeO dominates after 40% of the Fe has evaporated as metallic Fe.*

We take the oxygen isotopic composition to be atmospheric ($\delta^{18}O_{SMOW}$(AIR) = 23.5‰ (Thiemens et al., 1995)). If we

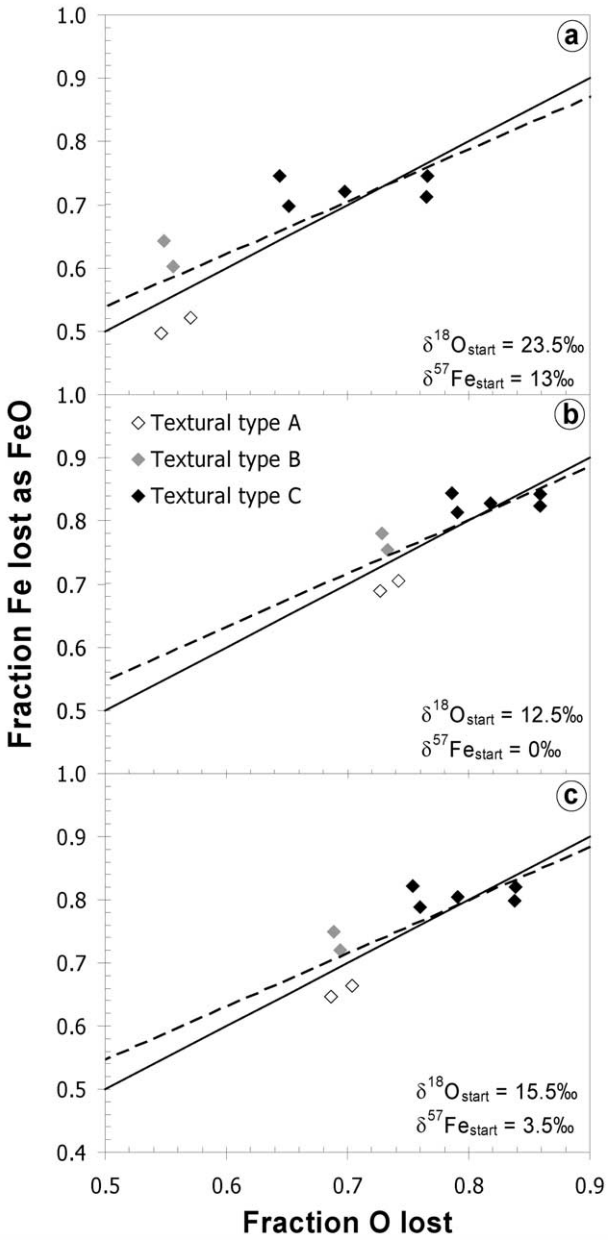

Fig. 9. The isotopic data help constrain how much Fe evaporates as metal before it oxidizes and evaporates as an oxide. The calculation rests on the requirement that after oxidation, any evaporative losses of metal and oxygen must lead to identical degrees of mass-dependent fractionation. In our calculations, the isotopic composition of both elements before evaporation are allowed to vary (see text). (a) Given a terrestrial oxygen isotopic composition equal to that measured by Thiemens et al., 1995 ($\delta^{18}O = 23.5‰$, $\delta^{17}O = 11.8‰$), fractional losses of iron and oxygen can be made approximately equal by calculating iron losses relative to a mass-fractionated (nonterrestrial) isotopic composition of iron that corresponds to the loss of ~40% of the iron originally present; (b) fractional losses of iron and oxygen can also be made equal by considering a terrestrial starting value for iron and a "virtual" starting oxygen isotopic composition of $\delta^{18}O = 12.5‰$; (c) with a starting oxygen isotopic composition of $\delta^{18}O = 15.5‰$, as observed by Clayton et al. (1986) in iron meteorite fusion crusts, a best match between the fractional iron and oxygen losses is achieved by calculating iron losses relative to a mass-fractionated isotopic composition of iron $\Phi_{Fe(start)}$ ~1.2‰/amu, that corresponds to the loss of ~12% of the iron originally present before oxidation and subsequent evaporation of the oxide. The textural types are defined in Figure 1.

recalculate from Eqn. (1b) the losses of Fe (as FeO) relative to a fractionated isotopic composition of iron, those losses should equal the losses calculated for oxygen. By using least squares fitting we find that by decreasing Φ_{Fe} by $(4.5 \pm 0.5)‰$/amu for all samples, we obtain a fairly good match between the fractions of O and Fe lost (Fig. 9a). Because, to a good approximation, a change in the starting isotopic composition of Fe simply shifts all the measured values of Φ_{Fe} by a fixed amount, we can say equivalently that the evaporation of O with FeO begins when the isotopic composition of iron has been fractionated by evaporation of Fe metal to the extent that $\Phi_{Fe(start)} = (4.5 \pm 0.5)‰$/amu, or $\delta^{57}Fe_{start} \sim 13‰$ (the subscript "start" refers to the isotopic composition of the elements (O, Fe, Cr, Ni) when ***oxygen*** starts to evaporate). Application of the Rayleigh equation then shows that oxidation of iron is complete and FeO evaporation begins when ~40% of the metallic Fe has evaporated. The correlation between Φ_{Fe} and Φ_{Ni} (Fig. 6) implies that at this point, only ~10% of the Ni has evaporated. The calculated preloss Cr/Fe and Fe/Ni ratios are not affected by this hypothesis and remain as quoted above.

4.4.2. *Case 2: If no Fe evaporates as metal, but only as FeO, then the oxygen entering the spherules should have $\delta^{18}O_{SMOW(start)} = 12.5‰$.*

For completeness, we consider the case where Fe evaporates not as metal but as an oxide with $\Phi_{Fe(start)} = 0$. We now show that a good match between f_O and f_{Fe} can be obtained by adopting an initial oxygen isotopic composition such that $\Phi_{O(SMOW)start} \sim 6.3‰$/amu, or equivalently, $\delta^{18}O_{SMOW(start)} = 12.5‰$ (Fig. 9b). Choosing a reference state of oxygen different from air might seem to be an ad hoc assumption. Clayton et al. (1986), however, have found oxygen isotopic compositions in iron meteorite fusion crusts with $\delta^{18}O_{SMOW} \sim 15.5‰$, which is ~8‰ lower than that of air ($\delta^{18}O_{SMOW}(AIR) = 23.5‰$, Thiemens et al., 1995). As the oxygen present in these fusion crusts comes from oxidation of incoming meteoritic metal during atmospheric entry, Clayton et al. (1986) concluded that a kinetic isotope effect took place during oxidation of iron. The iron meteorites thus acquired oxygen from the atmosphere with a fractionation of approximately −8‰ in $\delta^{18}O$.

4.4.3. *Case 3: If the oxygen entering the spherules has $\delta^{18}O_{SMOW(start)} = 15.5‰$, the same value as fusion crusts in iron meteorites, then evaporation of FeO dominates after 12% of the Fe has evaporated as metallic Fe.*

If we take $\delta^{18}O_{SMOW} \sim 15.5‰$ as the starting oxygen isotopic composition before evaporation (see above or Clayton et al., 1986), then a best fit between the fractions of O and Fe lost is obtained with an initial $\delta^{57}Fe = 3.5‰$, or $\Phi_{Fe(start)} \sim 1.2‰$/amu (Fig. 9c), which means that ~12% of the iron evaporated as metal before oxidizing and evaporating (more slowly) as oxide. The correlation between Φ_{Fe} and Φ_{Ni} (Fig. 6) implies that at this point, less than a few percent of Ni has evaporated.

In summary, we conclude that the oxygen isotopic composition of the oxygen entering the spherules—the "apparent

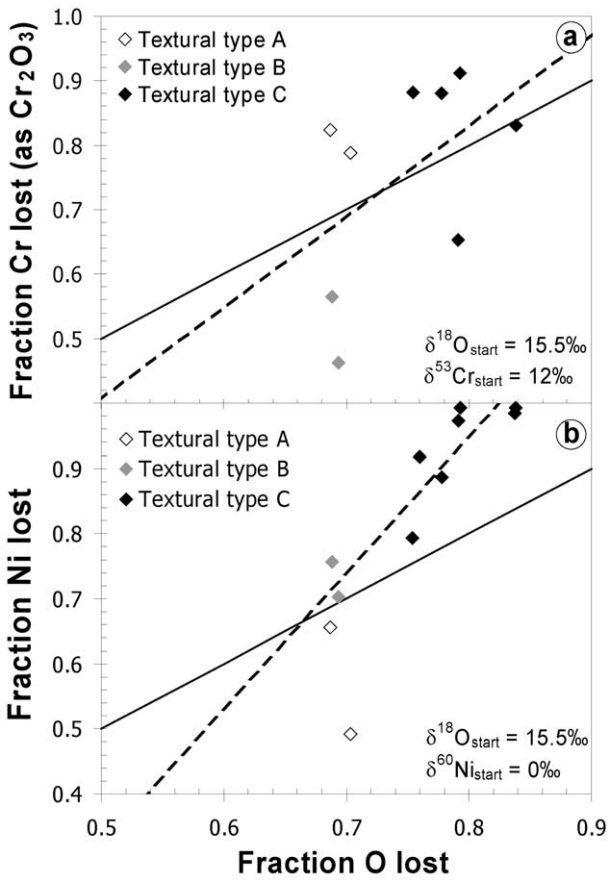

Fig. 10. (a) The isotopic data for Cr constrain how much Cr evaporates as metal before it oxidizes and evaporates as an oxide. With a starting oxygen isotopic composition on the terrestrial fractionation line with $\delta^{18}O = 15.5‰$ (see Fig. 9) the average fractional losses of chromium and oxygen can be made approximately equal by calculating chromium losses relative to a mass-fractionated isotopic composition ($\Phi_{Cr(start)} = 12‰$/amu). However Cr as a very minor element does not control the oxygen budget. The apparent good fit observed here can be explained by the similarity between the observed values of Φ_{Fe} and Φ_{Cr}. (b) By proceeding as in Figure 10a, it is impossible to reconcile the losses of nickel, as calculated from its isotopic composition with those of oxygen. Nickel was probably mostly lost as metal, and not as oxide. The textural types are defined in Figure 1.

atmospheric composition"—must be between $\delta^{18}O = 12.5‰$ and 23.5‰. The corresponding amounts of evaporation of metallic iron before oxidation are between 39 and 0%, respectively. Case 2 does not seem realistic, as evaporation of iron was most probably competing with the oxidation process. Case 1 and 3 seem equally probable, but we rely on the measurements of the oxygen isotopic compositions of iron meteorite fusion crusts by Clayton et al. (1986) to favor case 3. In that case ~12% of iron evaporated as metal before oxidation became essentially complete. The "apparent" oxygen isotopic composition of the atmosphere is that case is $\delta^{18}O_{SMOW} \sim 15.5‰$, with $\delta^{17}O_{SMOW} \sim 8‰$.

With this starting oxygen isotopic composition, one can also calculate a best match between the loss of oxygen and that of Cr_2O_3. It is obtained for a starting $\Phi_{Cr(start)} \sim 12‰$/amu, which means that ~70% of the Cr evaporated as metal (more if the evaporating entity was a heavier sulfide) before loss as oxide (Fig. 10a). The quality of this fit is not as good as with Fe. This might be due to the relatively small amount of Cr available and the associated analytical uncertainty. The behavior of Cr is perhaps also more complex than this two-step mechanism suggests, and the Rayleigh hypothesis of a perfect instantaneous mixing may not be realized during the early states of evaporation.

It is not possible to reconcile the losses of O and Ni by using the methods described above for Fe. In most cases, Ni probably evaporated too fast as metal for it to have had time to oxidize in significant amounts. Figure 10b shows the fractional losses of O and Ni with the starting oxygen isotopic composition of $\delta^{18}O = 15.5‰$.

4.5. Rarity of Spherules with Little Mass-Dependent Fractionation of Cr and Fe

Type-I spherules with little mass-dependent fractionation are of special interest because their compositions should resemble most closely those of the precursor material. Curiously, only 2 of 24 and 2 of 14 type-I spherules, respectively, have values of Φ_{Fe} and Φ_{Cr} less than 10‰/amu, a value that already corresponds to substantial elemental losses, ~60%. For Ni, the fraction of objects with little mass-dependent fractionation is larger: low values of Φ_{Ni}, < 10‰/amu, occur in 9 of 43 spherules (this work, and Herzog et al., 1999, and references therein). We infer that once melting has taken place, evaporation of iron proceeds very quickly relative to the total time available for evaporation, 5–20 s (Yada et al., 1996). An alternative explanation, that subaerial weathering destroys objects that retain more metal, seems unlikely for the corrosion-resistant, Ni-rich spherules. Conceivably only those type-I spherules that are specially armored in some unknown way by atmospheric heating survive for long in ocean sediments. A detailed, systematic study of the surfaces of type-I spherules, which vary considerably (e.g., Czajkowski, 1987) might prove worthwhile.

5. RESULTS OF STONY (TYPE S) COSMIC SPHERULES

5.1. Sizes, Textures, and Chemical Compositions

Table 6 summarizes the sizes, textures, and chemical compositions of all stony spherules except S12 and S13. The apparent diameters of thirteen Antarctic *S*-type spherules range from ~100 μm to ~200 μm; the deep-sea particle is larger, with a diameter of ~400 μm. Three spherules are of the barred olivine type (BO; e.g., Fig. 11a), one consists of radial pyroxene (RP; Fig. 11b), and one looks like a glass spherule (Gl; Fig. 11c). The remaining nine stony spherules are porphyritic olivine (PO; e.g., Fig. 11d) with two of them being very fine-grained (94-4-14 and 94-4B-45), and four of them only partially melted with relict grains (94-4-14B, 94-4B-6, 94-4B-12 and 94-4B-43, e.g., Figs. 11e and 11f).

As we do not have direct access to the bulk chemical compositions of the stony spherules, we make the assumption that the means of our electron microprobe analyses (Table 6) give reasonable proxies for these bulk compositions. In our sampling of 14 spherules, we find depleted Mg/Si and Al/Si average atomic ratios (0.95 and 0.074, respectively) compared to the corresponding average values for 68 Antarctic stony spherules of 1.06 and 0.091 given by Brownlee et al. (1997), and of 1.05 and 0.090, respectively, for 46 BO spherules analyzed by Taylor et al. (2000). The

Table 6. Chemical composition (wt%) of 13 stony cosmic spherules from Antarctica (94-4 and 94-4B series) and one stony deep sea spherule (KK2-97A-23) measured by electron microprobe at the location of the ion microprobe spots. The data are arranged by textural type.

Sample	D* (μm)	Type§	Phases analyzed¥	O	Na	Mg	Al	Si	P	S	K	Ca	Ti	Cr	Mn	Fe	Ni	Total
94-4-11_1	195	BO	Ol + Gl + Mt	36.5	0.02	12.8	0.71	15.9	b.d.	0.04	b.d.	0.89	0.08	0.21	0.15	30.4	0.10	97.80
94-4-11_2	195	BO	Ol + Gl + Mt	37.0	0.02	14.5	0.66	16.1	b.d.	0.02	b.d.	0.73	0.03	0.22	0.14	28.1	0.01	97.49
94-4B_42_1–3	150	BO	Ol + Gl + Mt	38.0	0.01	13.6	1.45	16.5	0.04	b.d.	0.02	1.86	0.06	0.20	0.19	27.0	0.80	99.88
KK297A-23_1–4	400	BO	Ol + Gl + Mt	42.3	b.d.	16.8	1.40	21.5	n.a.	n.a.	n.a.	0.56	0.06	0.07	0.30	17.1	0.90	101.08
94-4B-25_1,2	135	Gl	Gl	43.1	b.d.	17.5	1.84	23.0	n.a.	n.a.	n.a.	2.13	0.15	0.13	0.11	9.3	0.01	97.23
94-4-32_1	140	RP	Px + Plag	38.3	0.69	14.1	1.49	17.5	0.19	0.04	0.08	1.50	0.10	0.27	0.30	21.8	0.06	96.36
94-4-32_2	140	RP	Px + Plag	38.5	0.57	15.4	1.27	17.0	0.18	0.03	0.06	1.40	0.07	0.42	0.25	22.5	0.08	97.76
94-4-32_3	140	RP	Px + Plag	38.0	0.46	14.4	1.55	16.9	0.17	0.08	0.17	1.46	0.07	0.44	0.32	22.2	0.04	96.27
94-4-32_4	140	RP	Px + Plag	40.0	0.31	13.7	1.39	19.0	0.21	0.06	0.03	4.75	0.15	0.52	0.27	18.8	0.04	99.23
94-4-14_1	180	PO	Ol + Gl + Mt	36.9	b.d.	12.9	0.81	15.4	0.02	0.20	0.01	1.69	0.04	0.29	0.27	31.0	0.24	99.77
94-4-14_2	180	PO	Ol + Gl + Mt	35.9	0.04	12.5	1.02	14.1	0.05	0.38	b.d.	1.77	0.04	0.43	0.31	31.4	0.27	98.18
94-4B-45_1,2	160	PO	Ol + Gl + Mt	40.1	0.02	17.8	1.17	17.6	0.08	0.01	0.01	1.00	0.09	0.24	0.25	22.2	0.37	100.91
94-4B_26_1	160	PO	Ol + Gl	43.3	0.05	12.2	2.61	23.6	0.09	0.12	0.01	2.83	0.16	0.54	0.41	14.3	0.03	100.33
94-4B_26_2	160	PO	Ol + Gl	30.0	0.05	5.4	0.21	11.7	0.09	0.13	0.03	0.59	0.10	0.26	0.42	42.1	0.10	91.07
94-4-13_1	185	PO	Ol + Gl + Mt	36.9	0.01	4.2	3.22	17.8	0.17	0.02	b.d.	4.74	0.11	0.12	0.18	30.0	0.08	97.52
94-4-13_2	185	PO	Ol + Gl + Mt	36.8	0.02	9.4	2.29	16.2	0.12	b.d.	b.d.	2.46	0.10	0.23	0.26	30.0	0.30	98.14
94-4-8_1	125	PO	Ol + Gl + Mt	33.9	b.d.	3.0	2.61	15.6	0.10	b.d.	0.01	3.76	0.11	0.13	0.43	34.6	0.12	94.44
94-4-8_2	125	PO	Ol + Gl + Mt	37.6	0.01	16.1	0.74	16.1	0.03	0.01	b.d.	0.86	0.04	0.44	0.30	24.9	0.47	97.59
94-4-14B_1	190	PO‡	Ol + Mx + Mt	40.1	0.01	21.2	0.36	18.3	0.06	0.01	0.01	0.93	0.02	0.08	0.26	14.7	0.27	96.34
94-4-14B_2	190	PO‡	Ol + Mx + Mt	39.7	b.d.	20.6	0.16	17.7	0.04	0.01	0.02	0.64	0.03	0.20	0.30	18.3	0.16	97.96
94-4B-6	140	PO‡	Ol + Mx + Mt	44.5	0.23	17.9	1.42	23.5	0.15	0.50	0.01	1.63	0.11	0.57	0.25	8.7	0.34	99.74
94-4B-12	130	PO‡	Ol + GI	43.7	0.08	17.0	1.46	23.3	0.11	0.02	0.01	1.56	0.09	0.56	0.35	12.1	0.04	100.33
94-4B-43_1	140	PO‡	$Fo_{98.8}$	45.1	0.01	33.5	0.02	19.7	n.a.	n.a	n.a	0.12	0.03	0.36	0.38	1.0	b.d.	100.19
94-4B-43_2	140	PO‡	$Fo_{98.7}$ + Mx	45.5	b.d.	32.3	0.82	20.0	n.a.	n.a.	n.a.	0.69	0.01	0.23	0.10	1.0	0.02	100.60
94-4B_43_3	140	PO‡	$Fo_{98.6}$ + zoning	45.2	0.01	33.6	0.02	19.6	n.a.	n.a.	n.a.	0.13	0.01	0.37	0.55	1.1	b.d.	100.66
94-4B_43_4	140	PO‡	Mx	39.4	0.28	14.0	1.28	17.7	0.12	0.23	0.05	1.09	0.07	0.37	0.27	26.1	0.19	101.13
94-4B_43_5	140	PO‡	Fo + Mx	43.0	0.03	26.9	0.77	18.3	0.05	0.05	b.d.	0.53	0.03	0.36	0.20	10.6	0.35	101.25

b.d.: below detection limit of ~0.01 wt%; n.a.: not analyzed.

* Average diameter as measured on the polished section.

§ Textural type of cosmic spherules: BO = barred olivine; Gl = Glass; RP = radial pyroxene; PO = porphyritic olivine; ‡ PO = Porphyritic olivine but only partially melted.

¥ The ion microprobe beam spot included sometimes several mineral phases: Ol = olivine; Gl = glass; Mt = magnetite; Mx = matrix material; Px = pyroxene; Plag = plagioclase. The Fo numbers refer to the forsterite content (in mol%) of the olivine grains analyzed in spherule #94-4B-43.

average Mg/Si and Al/Si atomic ratios calculated for our three BO spherules are 0.95 and 0.068, respectively.

The mean Ca/Si and Fe/Si atomic ratios found for our 14 spherules (0.062 and 0.61, respectively) are intermediate between the mean ratios of 0.056 and 0.53 measured by Brownlee et al. (1997) in Antarctic spherules and that of 0.073 and 0.61 reported by Taylor et al. (2000) in 46 BO spherules. In our 14 spherules, the average Mg/Si, Al/Si, and Fe/Si atomic ratios normalized to CI values (Anders and Grevesse, 1989) are slightly less than one (0.88, 0.88, and 0.68, respectively). The Ca/Si atomic ratio is chondritic (Ca/Si = 1.02 normalized to CI).

5.2. Oxygen Isotopic Composition

Because of the small sizes of the mineral grains, the beam of the ion microprobe sometimes included several phases (Table 7). The oxygen in the stony cosmic spherules is generally enriched in ^{17}O and ^{18}O relative to SMOW, although to a lesser degree than the oxygen in the type-I spherules (Table 7; Fig. 12). The values of $\delta^{18}O$ range from -0.1‰ to 29.8‰ and of $\delta^{17}O$ from -5.0‰ to 13.8‰. The oxygen isotope enrichment broadly correlates with textural type (Fig. 12): the barred olivine ("BO") and the totally melted porphyritic olivine ("PO melted") spherules have the heaviest oxygen; the glass ("Gl") and the porphyritic olivine spherules which were only partially melted ("PO part. melted") have a low degree of heavy isotope enrichment, with variable isotopic compositions, especially for 94-4B-43 with 1.5 ‰ $< \delta^{18}O <$ 24.7‰ (Table 7); the radiating pyroxene spherule ("RP") plots in the range of unmelted minerals in AMMs (Engrand et al., 1999). There is no correlation between the apparent sizes (or masses) of the stony cosmic spherules and their oxygen isotopic compositions.

5.3. Variability of Oxygen Isotope Composition within Spherules

In particle 94-4B-43, a porphyritic spherule with an apparent radius of 140 μm, the values of $\delta^{18}O$ range from 1.5‰ to 24.7‰, thus covering most of the spread established by the other 13 samples (Table 7, Fig. 13). This large variability may be due to the presence of unmelted, relict grains. The $\delta^{18}O$ variability within the other type-S spherules with two or more measurements is considerably smaller, only (3.2 ± 2.3)‰ on average. This spread is roughly comparable to the ranges observed in individual type-I spherules, and is consistent with variability expected given the measurement error on any one spot. Only one other particle, the porphyritic spherule 94-4-14B, has a range in $\delta^{18}O$ greater than 6‰. We might expect smaller spreads in the range of oxygen isotopic values in the more strongly heated samples but the average for the barred olivine spherules (3.9 ± 1.5)‰ is not significantly different from the average for the entire set; moreover, in two of the barred olivine spherules, $\delta^{18}O$ varies by ~4‰. We conclude that most of the particle melts were generally isotopically homogeneous.

5.4. Isotopic Composition of Fe and Cr in Two Type-S Spherules

Tables 3 and 4 include the Cr and Fe isotopic compositions of two type-S deep-sea spherules of unknown petro-

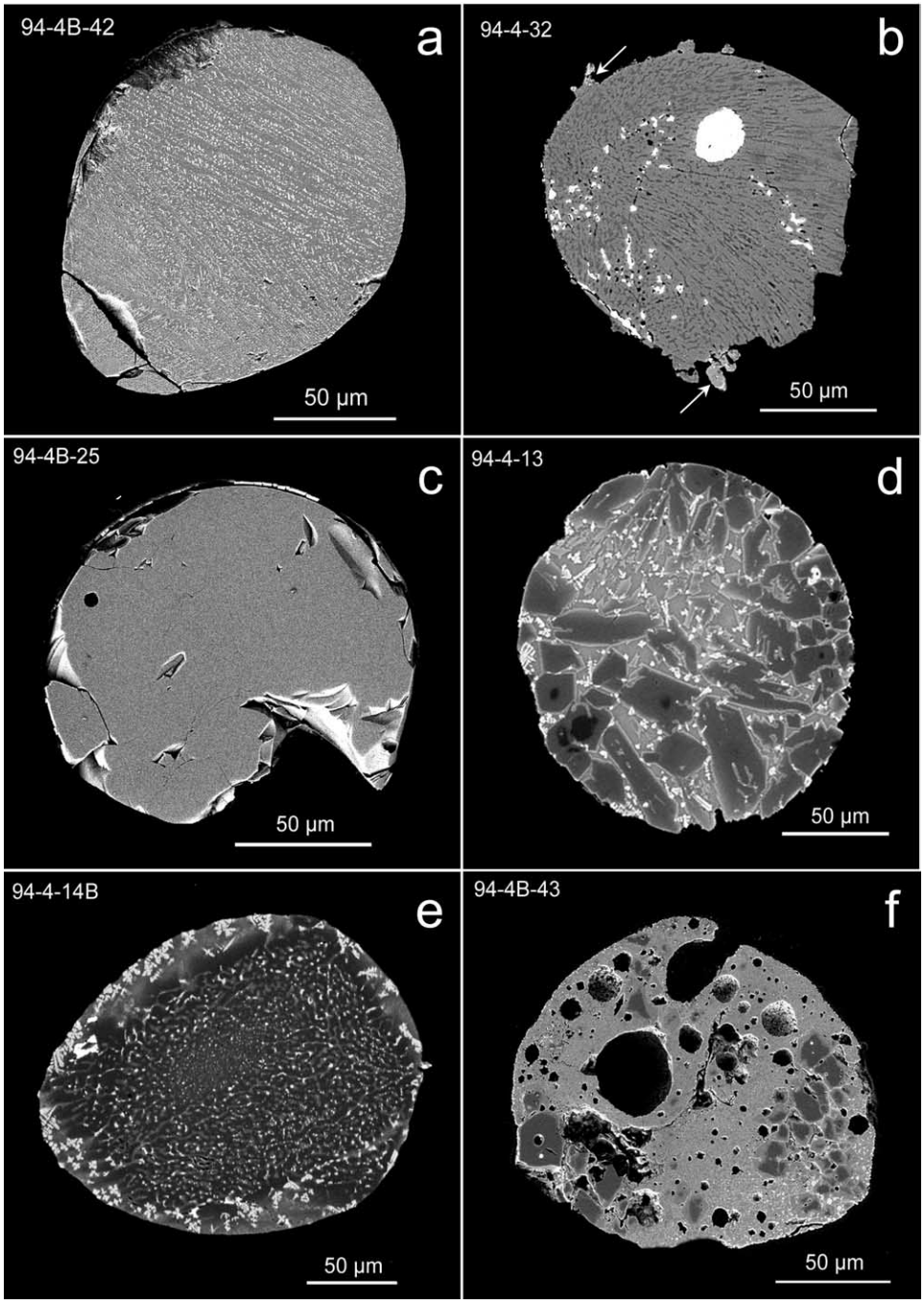

Fig. 11. Backscattered electron micrographs of polished sections of the textural types found in our sampling of type-S (stony) spherules. (a) Barred olivine (BO); (b) radial pyroxene spherule (RP) with pyroxene bars and feldspathic (plagioclase) glass. Bright spots are remnants of gold coating that was not totally removed by polishing after ion microprobe analysis. Small amounts of igneous rims are shown by white arrows; (c) Glass spherule (Gl); (d–f) porphyritic olivine spherules (PO); (d) PO spherule largely melted with a few relict forsteritic cores in the recrystallized olivine grains; (e) PO spherule with a very large unmelted core; and (f) partially melted PO spherule with relict forsteritic olivine grains.

graphic type. The fractionation of iron is small for both spherules (1.6 ± 0.5)‰/amu for S12 and (0.6 ± 0.2)‰/amu for S13 consistent with the generally small values of δ^{57}Fe reported by Taylor et al. (2002) for other *S*-type spherules. In both instances the fractionation of Cr isotopes is larger, (6.7 ± 0.6)‰/amu for S12 and (11.3 ± 0.6)‰/amu for S13, although not in any simple relation to the fractionation of Fe. We conclude that most of the particle melts were relatively well mixed, i.e., homogeneous on a scale of a few microns or more.

Table 7. *In situ* oxygen isotopic composition measured by ion microprobe in 13 stony cosmic spherules from Antarctica (94-4 and 94-4B series), and in one stony deep-sea spherule (KK297A-23). The data are arranged by textural type.

Sample	D* (μm)	Type[§]	Phases analyzed[¥]	$\delta^{18}O \pm \sigma$ (‰)[†]	$\delta^{17}O \pm \sigma$ (‰)[†]	$\Delta^{17}O \pm \sigma$ (‰)[†£]
94-4-11_1	195	BO	Ol + Gl + Mt	23.9 ± 1.4	12.0 ± 1.0	−0.4 ± 1.1
94-4-11_2	195	BO	Ol + Gl + Mt	19.8 ± 1.3	9.5 ± 1.0	−0.8 ± 1.1
94-4B_42_1	150	BO	Ol + Gl + Mt	26.6 ± 2.0	9.7 ± 1.4	−4.1 ± 1.1
94-4B-42_2	150	BO	Ol + Gl + Mt	27.7 ± 1.2	9.8 ± 1.1	−4.6 ± 1.1
94-4B-42_3	150	BO	Ol + Gl + Mt	29.0 ± 1.2	11.0 ± 1.2	−4.0 ± 1.2
KK297A-23_1	400	BO	Ol + Gl + Mt	23.6 ± 1.9	13.6 ± 1.2	1.3 ± 1.0
KK297A-23_2	400	BO	Ol + Gl + Mt	22.2 ± 1.8	11.7 ± 1.0	0.2 ± 0.6
KK297A-23_3	400	BO	Ol + Gl + Mt	20.5 ± 1.8	12.0 ± 1.0	1.3 ± 0.7
KK297A-23_4	400	BO	Ol + Gl + Mt	18.4 ± 1.8	10.8 ± 1.0	1.2 ± 0.6
94-4B-25_1	135	Gl	Gl	4.9 ± 1.2	−3.4 ± 1.4	−6.0 ± 1.3
94-4B-25_2	135	Gl	Gl	3.4 ± 1.2	−3.5 ± 1.4	−5.2 ± 1.3
94-4-32_1	140	RP	Px + Plag	3.7 ± 1.3	1.7 ± 0.8	−0.2 ± 0.8
94-4-32_2	140	RP	Px + Plag	7.2 ± 1.4	3.8 ± 1.1	0.1 ± 1.1
94-4-32_3	140	RP	Px + Plag	6.6 ± 1.6	2.0 ± 1.0	−1.4 ± 1.1
94-4-32_4	140	RP	Px + Plag	7.4 ± 1.2	3.6 ± 1.1	−0.3 ± 1.1
94-4-14_1	180	PO	Ol + Gl + Mt	22.3 ± 1.2	12.1 ± 0.7	0.5 ± 0.8
94-4-14_2	180	PO	Ol + Gl + Mt	20.1 ± 1.2	10.9 ± 0.7	0.5 ± 0.7
94-4B-45_1[a]	160	PO	Ol + Gl + Mt	24.2 ± 1.7	8.9 ± 1.5	−3.7 ± 1.4
94-4B-45_2	160	PO	Ol + Gl + Mt	23.4 ± 1.3	9.0 ± 1.1	−3.2 ± 1.1
94-4B_26_1[b]	160	PO	Ol + Gl	14.2 ± 1.1	6.4 ± 0.9	−0.9 ± 0.7
94-4B_26_2[b]	160	PO	Ol + Gl	18.7 ± 1.0	7.4 ± 0.8	−2.3 ± 0.7
94-4-13_1	185	PO	Ol + Gl + Mt	29.1 ± 1.4	13.8 ± 0.7	−1.4 ± 0.8
94-4-13_2	185	PO	Ol + Gl + Mt	29.8 ± 1.2	11.3 ± 0.9	−4.2 ± 0.9
94-4-8_1	125	PO	Ol + Gl + Mt	18.5 ± 1.2	10.6 ± 1.2	0.9 ± 1.2
94-4-8_2	125	PO	Ol + Gl + Mt	16.8 ± 1.3	10.6 ± 0.9	1.9 ± 0.9
94-4-14B_1	190	PO[‡]	Ol + Mx + Mt	8.9 ± 1.3	0.6 ± 0.8	−4.1 ± 0.9
94-4-14B_2	190	PO[‡]	Ol + Mx + Mt	0.7 ± 1.4	−2.9 ± 0.8	−3.2 ± 0.9
94-4B-6_1	140	PO[‡]	Ol + Mx	−0.1 ± 1.2	−4.2 ± 1.2	−4.1 ± 1.1
94-4B-12_1	130	PO[‡]	Ol + Gl	1.1 ± 1.2	−1.1 ± 1.0	−1.7 ± 0.9
94-4B-43_1	140	PO[‡]	$Fo_{98.8}$	13.4 ± 1.4	2.9 ± 1.7	−4.0 ± 1.7
94-4B-43_2	140	PO[‡]	$Fo_{98.7}$ + Mx	1.5 ± 1.3	−5.0 ± 1.4	−5.8 ± 1.3
94-4B_43_3	140	PO[‡]	$Fo_{98.6}$ + zoning	16.8 ± 1.9	4.7 ± 1.2	−4.0 ± 0.8
94-4B_43_4	140	PO[‡]	Mx	24.7 ± 1.9	10.1 ± 1.2	−2.8 ± 0.8
94-4B-43_5	140	PO[‡]	Fo + Mx	14.5 ± 2.5	2.4 ± 1.5	−5.2 ± 1.5

* Average diameter as measured on the polished section.

[§] Textural types of cosmic spherules: BO = barred olivine; Gl = Glass; RP = radial pyroxene; PO = porphyritic olivine; [‡] PO = Porphyritic olivine but only partially melted.

[¥] The ion microprobe beam spot included sometimes several phases : Ol = olivine; Gl = glass; Mt = magnetite; Px = pyroxene; Plag = plagioclase; Mx = matrix. The Fo numbers refer to the forsterite content (in mol%) of the olivine grains analyzed in spherule #94-4B-43. [a,b]Weighted mean of two and three analyses on the same spot, respectively.

[†] Relative to SMOW, errors are 1σ mean.

[£] $\Delta^{17}O \sim \delta^{17}O - 0.52 \times \delta^{18}O$.

6. DISCUSSION OF TYPE-S SPHERULES

6.1. Comparison with Other Oxygen Isotope Data

Clayton et al. (1986) analyzed four pooled samples of stony cosmic spherules from the deep-sea (KK1) collection; the samples contained from 42 to 315 particles each. The average values of $\delta^{18}O$ and $\delta^{17}O$ relative to SMOW for the four sets were (24 ± 1)‰ and (10 ± 1)‰, respectively. Each of these four measurements was effectively weighted by the cube of the average particle radius, which varied in the four splits. Even so, intersample variations of the oxygen isotopic abundances of the pooled samples are small, suggesting a weak dependence on particle radius.

For the 13 Antarctic and 1 deep-sea stony (type-S) spherules analyzed here, the measured values of $\delta^{18}O$ and $\delta^{17}O$ average, respectively, (16 ± 9)‰ and (6 ± 6)‰ relative to SMOW (Table 7 and Fig. 12). The large standard deviations of these averages reflect a spread in the data much larger than the uncertainties of the individual measurements (estimated to be ~1‰) and reaffirm the particle-to-particle variability evident in Figure 12. The oxygen data therefore indicate that our set of samples differs in a systematic way from the set (KK1) analyzed by Clayton et al. (1986). As now discussed, we believe that collection bias explains the difference.

Taylor et al. (2000) have compared the populations of particle types found in deep-sea (KK1) and in Antarctic surface collections. In the deep-sea collection, barred olivine and type-I spherules dominate, accounting for ~50 and 25% of all extraterrestrial particles. If we exclude the type-I particles, the percentage of barred olivine spherules in the deep-sea collection rises to 67%. Cryptocrystalline and glass particles make up less than 3% of the deep-sea total. In contrast, in the Antarctic surface collection, cryptocrystalline and glass particles occur in much greater abundance, 18%, as do relict grains and porphy-

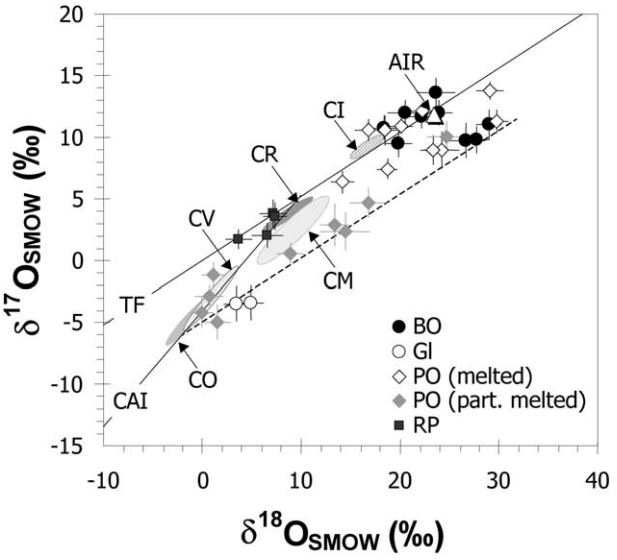

Fig. 12. Oxygen isotopic compositions of individual type-S spherules calculated relative to standard mean ocean water (SMOW). The solid line labeled TF is the terrestrial fractionation line anchored at SMOW and calculated from the relations

$$\delta(^{17,18}O = (\left[f_{retained}(^{16}O)\right]^{\alpha-1} - 1) \times 1000, \text{ where } \alpha = \sqrt{\frac{m(^{16}O)}{m(^{17,18}O)}}$$

and $f_{retained}$ is allowed to vary from 0.1 to 1.7; values of $f_{retained}$ greater than 1.0 correspond physically to mass gains from condensation. To a good approximation, $\delta^{17}O = 0.52 \times \delta^{18}O$. The line labeled CAI was read from Figure 2 of Clayton (1993); it has the form $\delta^{17}O = 0.938 \times \delta^{18}O - 4.06$. The slope 0.52 short dotted line represents the range of variation expected (relative to SMOW) in samples that underwent mass-dependent fractionation. Data for CI, CM, CR, and CO chondrites represent whole-rock analyses of meteorite falls taken from Rowe et al. (1994), Weisberg et al. (1993), Bischoff et al. (1993), and Clayton and Mayeda (1984, 1999, 2001). Most data for minerals from unmelted Antarctic meteorites lie between the TF and the CAI line with a lowest value of $\delta^{18}O = -11.3‰$ for non-refractory minerals (Engrand et al., 1999).

ritic and barred olivine spherules (Taylor et al., 2000). Under the circumstances, it makes more sense to compare the oxygen isotope abundances measured by Clayton et al. (1986), $\delta^{18}O = 24‰$ and $\delta^{17}O = 10‰$, with the average that we obtained for 3 barred olivine spherules, $\delta^{18}O(‰) = 24 \pm 4$ and $\delta^{17}O(‰) = 11 \pm 1$. The better agreement observed between these two sets of data suggests that the relatively large $\delta^{18,17}O$ values reported by Clayton et al. (1986) reflect the underrepresentation in the deep-sea collection of porphyritic, cryptocrystalline and glass particles, which were presumably destroyed by weathering. At the same time, the overall agreement for the barred olivine particles should not disguise the importance of the interparticle variability that we observe, a point discussed further in section 6.

Yada et al. (2002, 2003a–c) have recently reported ion microprobe oxygen isotopic analyses of Antarctic cosmic spherules from the Japanese collection. For the 36 stony spherules they analyzed, ~75% of the data plot on or close to the terrestrial fractionation line within analytical errors, with $\delta^{18}O$ values from ~0‰ to ~50‰, and $\delta^{17}O$ values ranging from ~1‰ to ~30‰. Two extreme values are found, one at $\delta^{18}O = 93‰$ slightly below the TF line, and the other with $\delta^{18}O \sim 50‰$ and $\Delta^{17}O = +13‰$. Yada et al. (2002, 2003a,b) interpret most of the data as resulting from large mass dependent fractionation due to evaporation of a large fraction of the grains.

6.2. Possible Mechanisms for Setting O Isotope Composition of Spherules

The isotopic data for oxygen are considered within the context of three possible mechanisms for setting their isotope composition. First, the spherules may have variable initial (pre-atmospheric entry) compositions, as is observed in whole-rock carbonaceous chondrites (e.g., Clayton and Mayeda, 1999). For example, some particles may have initially resembled CM chondrites and some CI chondrites (e.g., Kurat et al., 1994; Engrand and Maurette, 1998), or even some composition not represented in the current collection

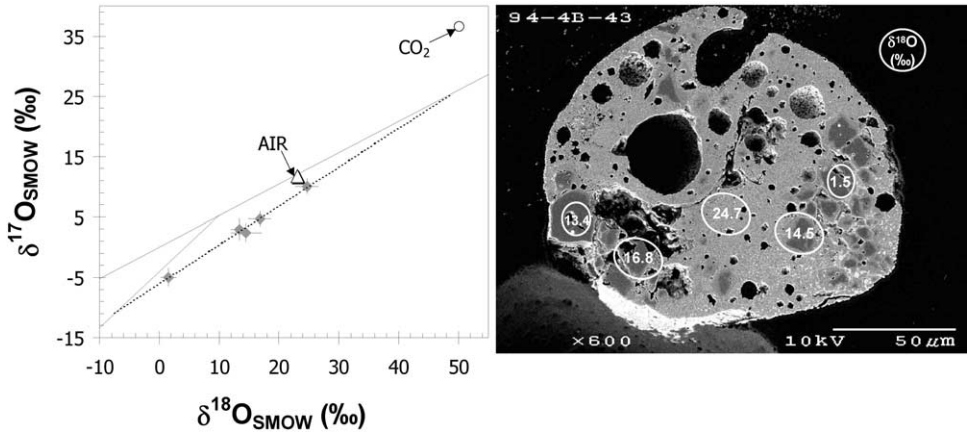

Fig. 13. Oxygen three isotope diagram of the porphyritic olivine partially melted spherule 94-4B-43. This spherule exhibits a range of variation in $\delta^{18}O$ values of more than 20‰. Two olivine grains with about the same composition ($Fo_{98.7}$ and $Fo_{98.8}$) have $\delta^{18}O$ values that differ by more than 10‰. A best fit through the data gives a linear equation: $y = 0.645x - 6.1273$, with $R^2 = 0.992$. The values for atmospheric air and atmospheric CO_2 at 60 km altitude are given for reference (Thiemens et al., 1995). The backscattered electron micrograph of this spherule is given on the right where the analysis areas (ellipses) are labeled with their corresponding $\delta^{18}O$ values.

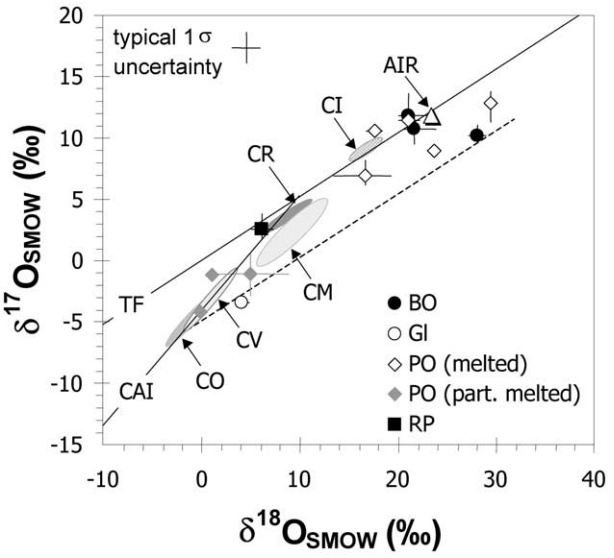

Fig. 14. Average oxygen isotopic compositions of individual type-S spherules calculated relative to standard mean ocean water (SMOW). The range bars associated with each data point give the variations from the mean within individual spherules, and do not represent the typical uncertainty for individual analyses, which is shown on the upper left corner of the plot. Data for spherule 94-4B-43 are given in Figure 13 and are not reported here. The solid line labeled TF is the terrestrial fractionation line. The line labeled CAI was read from Figure 2 of Clayton (1993); it has the form $\delta^{17}O = 0.938 \times \delta^{18}O - 4.06$. Data for CI, CM, CR, and CO chondrites represent whole-rock analyses of meteorite falls taken from Rowe et al. (1994), Weisberg et al. (1993), Bischoff et al. (1993), and Clayton and Mayeda (1984, 1999, 2001).

of meteorites. Second, the particles undoubtedly underwent some mass loss during atmospheric entry, and their isotopic compositions may have been fractionated during this event. Third, the particles may have exchanged isotopes with oxygen in the atmosphere. It is likely that the spherules record all three processes to varying degrees.

To assess the importance of these processes, the data of Figure 12 are replotted in Figure 14 (Table 8) as particle weighted means with range bars (excluding the one clearly heterogeneous particle 94-4B-43, which is discussed later). From Figure 14, we can define two main groups of particles: (1) the barred-olivine (BO) and the totally melted porphyritic olivine spherules (PO melted) have oxygen isotopic values that lie close to, but in many cases are slightly isotopically heavier than the field of CI chondrites and are also compatible with the values found for air; and (2) the types GI, RP, and PO partially melted spherules scatter along the CAI line, and close to established fields for bulk CR, CM or CO chondrites.

If we take as the starting material for each spherule the type of conventional carbonaceous chondrite that lies closest to it in the oxygen three-isotope plot (Fig. 12), then we do not need to calculate *large* evaporative losses of oxygen for most of the samples. The data for two of the BO and two of the melted PO spherules cited in (1) that plot close to the TF line can be explained by starting with CI-like material and either exchanging it with a phase high in $\delta^{18}O$ and $\delta^{17}O$ (atmospheric oxygen) or subjecting it to a small degree of mass-fractionation during melting and evaporation. This starting composition would be representative of bulk CI-like material, and not CI anhydrous minerals, which are rare and which have oxygen isotopic compositions close to the CAI mixing line (Leshin et al., 1997). The radial pyroxene, as well as the PO partially melted spherules that plot near the field of carbonaceous chondrites, likely contain dominantly indigenous extraterrestrial oxygen, which was essentially unfractionated during atmospheric entry heating. The glass spherule could also be explained by a CO-like precursor that underwent minimal mass fractionation. The only really puzzling samples that are difficult to explain in this scenario are the BO and the three PO spherules in group (1) that plot below the TF line (94-4B-26, 94-4B-42, 94-

Table 8. Average oxygen isotope compositions of, and possible precursors for type-S spherules.

Sample	Texture	$\delta^{18}O$ (‰)*	$\delta^{17}O$ (‰)*	f_{lost}+	Affinity
94-4-11	BO	$21.7^{+2.2}_{-1.9}$	$10.7^{+1.2}_{-1.3}$	0.20†	CI
94-4B-42	BO	$28.1^{+0.9}_{-1.4}$	$10.2^{+0.8}_{-0.5}$	0.70¥	CO/CV + fractionation or carbonate?
KK297-A-23	BO	$21.1^{+2.6}_{-2.7}$	$11.9^{+1.7}_{-1.1}$	0.18†	CI
94-4B-25	GI	$4.1^{+0.8}_{-0.7}$	$-3.4^{+0.0}_{-0.0}$	0.16¥	CO + slight fractionation?
94-4-32	RP	$6.2^{+1.2}_{-2.5}$	$2.5^{+1.3}_{-0.8}$		CM/CR
94-4-14	PO	$21.1^{+1.1}_{-1.1}$	$11.4^{+0.7}_{-0.5}$	0.19†	CI
94-4B-45	PO	$23.7^{+0.5}_{-0.3}$	$9.0^{+0.0}_{-0.0}$	0.64¥	CM/CV + fractionation or carbonate?
94-4B-26	PO	$16.7^{+2.7}_{-3.2}$	$6.9^{+1.2}_{-0.8}$	0.51¥	CM/CR + mixing/fractionation?
94-4-13	PO	$29.5^{+0.3}_{-0.4}$	$12.8^{+0.9}_{-1.6}$	0.71¥	CM/CV + fractionation or carbonate?
94-4-8	PO	$17.7^{+0.8}_{-0.9}$	$10.6^{+0.0}_{-0.0}$	0.06†	CI
94-4-14B	PO‡	$5.0^{+3.9}_{-4.3}$	$-1.1^{+1.7}_{-1.8}$		CM/CV
94-4B-6	PO‡	−0.1	−4.2		CV
94-4B-12	PO‡	1.1	−1.1		CO/CV
94-4B-43	PO‡	$11.9^{+12.8}_{-10.3}$	$3.6^{+6.4}_{-8.6}$		?

* Weighted mean value and range (when more than one analysis was made) for each particle. The precision of individual analyses is on the order of ~1 ‰, see Table 7.

+ Lost fraction calculated according to Wang *et al.* (2001) with average CI ($\delta^{18}O$ = 16.3‰) † or CO/CM ($\delta^{18}O$ = 0‰) ¥ starting compositions before evaporation.

4B-45 and 94-4-13). These spherules plot close to fractionation lines starting from CM- or CO-like compositions, but this would require large evaporative losses (see Section 6.5). They also plot close to mixing lines between CM- or CO-like compositions and the field of carbonates analyzed in CM chondrites (Brearley et al., 1999; Benedix et al., 2003) and in Orgueil and Tagish Lake (Engrand et al., 2001a,b; Leshin et al., 2001). As we cannot rule out the possibility of significant mass-dependent fractionation for these spherules, it would be helpful to know the isotopic compositions of the other elements they contain.

6.3. Relation between Oxygen Isotope Data and Spherule Texture

Taylor et al. (2000) have proposed a textural classification sequence for the type-S spherules that corresponds to increasing degrees of heating: relict-grain-bearing < porphyritic < barred olivine < cryptocrystalline < glass < Ca-Al-Ti rich or CAT. Our samples include one or more spherules of the porphyritic, barred olivine, and glass types. In agreement with this sequence, the data show that for the partially melted spherules porphyritic olivine, the average $\delta^{18}O = (4 \pm 5)‰$ and $\delta^{17}O = (-1 \pm 3)‰$ values are lower than the values found for the totally melted porphyritic olivine spherules (averages $\delta^{18}O = (22 \pm 5)‰$ and $\delta^{17}O = (10 \pm 2)‰$) which are in turn slightly lower than the mean isotopic values measured for barred-olivine spherules ($\delta^{18}O = (24 \pm 4)‰$ and $\delta^{17}O = (11 \pm 1)‰$).

On the other hand, to follow this sequence, we expect the glass particle 94-4B-25 to have high values of $\delta^{18}O$ and $\delta^{17}O$ contrary to observation (Table 7, Fig. 14). Relative to the BO spherules, however, this particle is more enriched in refractory elements such as Al and Ca, and contains less Fe, as expected from a higher temperature event. To explain the unexpectedly low isotopic fractionation of oxygen of this spherule, one can invoke very low values for $\delta^{18}O$ and $\delta^{17}O$ of the starting material, a loss by ablation and not evaporation during heating, or a starting composition with unusually high concentrations of Al and Ca. This spherule could also constitute a chondrule fragment that survived the atmospheric entry mostly unmelted. The preexisting refractory chemical composition of this spherule would have protected the spherule from a large amount of evaporation.

Our samples also include two particles with textures whose positions in the proposed heating sequence are unspecified, the radial pyroxene spherule 94-4-32 (Fig. 11b) and the porphyritic particle 94-4-14B (Fig. 11e). Among FeO-rich chondrules, radial-pyroxene chondrules tend to be less refractory than porphyritic types (Wasson, 1996), which is at least qualitatively consistent with our spherule observations, since the observed $\delta^{18}O$ and $\delta^{17}O$ values for the RP spherule average $(6.2 \pm 1.7)‰$, and $(2.8 \pm 1.1)‰$, respectively. The data for this particle actually plot in the field of unmelted minerals in Antarctic micrometeorites (Engrand et al., 1999) and we consider that this grain may constitute a remnant of a chondrule fragment that reached the Earth's surface unmelted. Interestingly, igneous material rims the top and bottom of spherule 94-4-32 (shown by arrows on Fig. 11b) that could have formed by atmospheric melting of matrix material that originally surrounded the chondrule (Genge, 2004). In addition to the candidate 94-4B-25 discussed above, this would be one of the few well preserved chondrules found in the Antarctic micrometeorite collections (e.g., Engrand and Maurette, 1998; Genge et al., 2005). One data point from the core of the porphyritic particle 94-4-14B plots very close to the CM whole-rock field on the oxygen three isotope diagram. The other data point taken in the melted rim of the particle 94-4-14B shows some isotopic fractionation. This grain could have remained largely unmelted during atmospheric entry, at least in the interior of the grain, and thereby kept most of its extraterrestrial oxygen.

6.4. Additional Evidence for Small Evaporative Losses of Oxygen from Type S Spherules

As a first evidence of small losses by evaporation in type-S spherules, we note that no correlation between the apparent size of the spherules and the degree of isotopic fractionation is found. One might expect such a correlation if evaporation were extensive, especially because a correlation *is* observed for our type C iron oxide spherules, which did undergo large degrees of evaporation (Fig. 3b).

Based on a consideration of the isotopic fractionations of elements other than oxygen, we also believe that the fractionation of oxygen isotopes by evaporation is small for most of our samples.

The iron isotopes in the two type-S spherules analyzed here are only weakly fractionated (Table 3). In a study of over 40 stony cosmic spherules, Taylor et al. (2002) found only 9 that showed significant fractionation of iron ($\Phi_{Fe} > 5‰$/amu). However, iron depletion observed in cosmic spherules is rather explained from the separation (and loss) of immiscible phases than from evaporation of significant amounts of iron (e.g. Brownlee, 1985; Genge and Grady, 1998; Alexander et al., 2002). The low degrees of iron isotopic fractionation observed are therefore a weak basis on which to draw conclusions about oxygen, which is not involved in the main process of iron loss.

While the Cr isotopes are appreciably fractionated, the Cr abundance is too low (as noted above) to have had much effect on oxygen isotope abundances, and, indeed, fractionation of Cr may involve sulfur rather than oxygen. Chromium only exhibits a chalcophile tendency at low oxygen fugacity. A likely cause of reduction would be the pyrolysis of carbonaceous material present in the incoming stony micrometeoroids, thus linking them to fine-grained micrometeorites.

If so, oxygen must evaporate in some form, however, and the next most volatile element that is a major partner for oxygen is silicon. Alexander et al. (2002) report the Mg, Si and Fe isotopic compositions in five stony CAT spherules which are very enriched in refractory elements and are thought to have been much more strongly heated than typical barred olivine spherules. For a given cosmic spherule they typically find relatively low degrees of isotopic fractionations $\Phi_{Mg}(\sim 0‰/amu) < \Phi_{Si}(\sim 2‰/amu) < \Phi_{Fe}(\sim 5‰/amu)$. In only one of these particles did the loss of Si reach more than 50%, with a Mg loss of ~40% and a loss of iron of ~100% (most of the iron is lost as immiscible phases formed during melting, see above). These CAT spherules being probably the most heated class of cosmic spherules, Alexander et al. (2002) state that the other stony micrometeorites and cosmic spherules will not have lost significant masses of Al, Mg, Si, or Ca by evaporation. Other attempts to detect isotopic fractionation of Mg isotopes in spherules (e.g., Davis et al., 1991; Misawa et al., 1992; Schnabel et al., 1999; Yada et al., 2003a) have yielded only a few positive results. These generally negative findings suggest that either the oxygen in the type-S spherules undergoes little mass-

dependent fractionation (the inference we favor), or that if it does fractionate, the fractionation occurs on a path not associated with Fe, Si, or Mg.

6.5. Evaporative Loss from Barred Olivine Spherules

For completeness, we calculate from the Rayleigh equation the likely degree of evaporative loss of oxygen from the barred olivine (BO) and the totally melted porphyritic olivine (PO) spherules of Figure 14 (Table 8). We assume homogeneous melts and the fractionation factor determined by Wang et al. (2001) and divide the objects into two subgroups. One subgroup comprises the BO and PO spherules (94-4-11, KK2-97A-23, 94-4-14 and 94-4-8) with values of $\delta^{18}O$ and $\delta^{17}O$ that can be reached by mass-dependent fractionation of oxygen with the isotopic composition found in CI chondrites (Fig. 14, Table 8). The calculated fractional losses for this group are relatively small, ranging from 0.1 (10%) to 0.2 (20%). The other subgroup, the spherules 94-4B-42, 94-4B-45, 94-4B-26, and 94-4-13, comprises the spherules with high values of $\delta^{18}O$ and $\delta^{17}O$, but which fall below the TF line (Fig. 14, Table 8). They are more consistent with mass-dependent fractionation of oxygen with the isotopic composition found in CO/CV and CM/CR meteorites. The calculated fractional losses for this group are larger, in the range from 0.5 to 0.7. We consider these fractions to be upper bounds.

6.6. Isotopically Heterogeneous Spherule 94-4B-43

The oxygen isotope abundances in porphyritic spherule 94-4B-43 vary significantly, with $\delta^{18}O$ ranging between 1.5‰ to 24.7‰. The data from this spherule are plotted in Figure 13 keyed to their locations in the particle. To interpret such a large range of isotopic values by a mass fractionation process (e.g., Rayleigh distillation) would imply total melting and homogenization of the particle, followed by the evaporation of a large fraction of the oxygen. This hypothesis is inconsistent with the texture and chemical composition of the spherule, which show that the particle did not equilibrate. The matrix of the spherule has an oxygen isotopic composition very close to that of air, which alternatively suggests isotopic mixing/exchange with atmospheric oxygen. The observed $\delta^{18}O$ values of 14.5‰ and 16.8‰ (Fig. 13) may be explained by physical mixing in the beam spot of relict forsterite grains (bearing extraterrestrial oxygen) and fractionated matrix. However, one forsteritic olivine grain ($Fo_{98.7}$) within this spherule has an oxygen isotopic composition ($\delta^{18}O = 1.5‰$) close to the field of the unmelted micrometeorites (Engrand et al., 1999) while a second olivine grain at the border of the CS which has nearly identical elemental composition ($Fo_{98.8}$) is ~10‰ heavier in $\delta^{18}O$ (13.4‰). To reproduce the measured oxygen isotopic compositions of the $Fo_{98.8}$ grain ($\delta^{18}O \sim 13.4‰$), one would need ~60% isotopic exchange between indigenous oxygen (postulated at $\delta^{18}O \sim 0‰$) and atmospheric oxygen ($\delta^{18}O \sim 23.5‰$) and/or oxygen coming from matrix which equilibrated with air. Gérard and Jaoul (1989) have measured the oxygen diffusion rates for San Carlos olivine (Fo_{90}). In our case ($Fo_{98.5}$), the oxygen diffusion coefficient has to be scaled from that of Gérard and Jaoul (1989) as the diffusion coefficient is proportional to the concentration of iron in the olivine to the power of one third (see Eqn. 4 in Gérard and Jaoul (1989)). For a 10 μm $Fo_{98.5}$ grain, the 60% isotopic exchange could be achieved within 40 s at 1800°C. These conditions are marginally compatible with those of atmospheric entry heating for cosmic spherules (e.g., Toppani et al., 2001). Although one might expect the spherule to be completely melted at this temperature and duration of heating, Greenwood and Hess (1995) suggest that in the case of flash heating refractory minerals like forsterite could melt in situ, within a preexisting melt of less refractory minerals (iron-rich matrix in this case) without complete mixing of the two components. In this case, the olivine grains are not truly "relict." Considering the temperature and duration of heating quoted above, ~35% of the Fe and Mg should have exchanged between the forsteritic olivines and the Fe-rich matrix, according to experiments by Chakraborty (1997). This result is compatible with the observation of Fe-rich zoning around the forsterite grains in this spherule (Fig. 13).

Thus, the somewhat puzzling oxygen isotopic composition of this peculiar spherule can be interpreted as a result of oxygen self-diffusion between the incident micrometeoroid and atmospheric oxygen at high temperature.

7. CONCLUSIONS

We have measured the O, Cr, Fe, Ni isotopes in eleven type-I (iron) deep-sea spherules, the oxygen isotopic composition of 13 type-S (stony) Antarctic and one stony deep-sea spherule, and the Fe and Cr isotopic composition of two other type-S deep-sea spherules. Type-I spherules show large enrichments of the heavier isotopes of O, Cr, Fe, Ni, by anywhere from a few ‰/amu to 50 ‰/amu. The isotopic fractionation and isotopic homogeneity of the type-I spherules are consistent with a Rayleigh distillation of the molten objects as they evaporate during their passage through the Earth's atmosphere. As heating and oxidation progress, the spherules lose their metallic cores. Later-stage melts are richer in oxygen and freeze to form solids with larger fractions of magnetite and magnetite rims. Larger degrees of isotopic fractionation generally correlate with texture and degree of oxidation.

Previous analyses of pooled type-I samples have established that oxygen isotopes fractionate in type-I spherules (Clayton et al., 1986), but not on average by so much as do the metals (e.g., Herzog et al., 1999). Our new results show directly that the isotopic fractionation of oxygen in individual spherules increases systematically with but lags behind that of the metals measured in the same spherules. We conclude that: 1) some metal evaporates and fractionates before oxygen can react with it and that as a result, the fractionation of metal jumps to an early lead that oxygen cannot overtake; and 2) during the later stages of spherule evolution, iron and chromium oxidize completely and thereafter evaporate as oxides, thereby fractionating the oxygen. A portion of the fractionation of oxygen, however may occur through a different mechanism, namely, a kinetic isotope effect associated with the chemical combination of atmospheric oxygen with the molten object. Assuming that the kinetic isotope effect lowers the $\delta^{18}O$ value by up to 8‰ (e.g., Clayton et al., 1986), we estimate that the oxidation of iron and chromium in the average type-I spherule was complete by the time that 10 to 40% of the iron had evaporated. Most of the evaporation of oxygen appears to be tied to that of Fe by virtue of iron's large abundance and because nickel, the next most abundant metal, resists oxidation longer.

The scarcity of type-I spherules with small degrees of mass-dependent isotopic fractionation in Fe, Cr, and Ni isotopic ratios

suggests that once the metallic melts have formed, their evaporation occurs very rapidly.

The oxygen isotope abundances of stony (type-S) cosmic spherules vary a great deal, by nearly 30‰ for $\delta^{18}O$, but not solely as a result of mass-dependent fractionation. Several circumstantial lines of evidence point to relatively small evaporative effects in many though not all type-S spherules. Those lines of evidence include good matches of the oxygen isotope data to known types of carbonaceous chondrites and the absence of common and large isotopic effects in other elements that ought to evaporate with oxygen (see Alexander et al., 2002; Taylor et al., 2002). However, despite the generally small degrees of isotopic fractionation so far observed for Fe, Si, and Mg in type-S spherules, it appears that some minor and trace elements may record evaporative losses and/or oxygen may exchange with air during melting. In the two type-S spherules analyzed isotopically for Cr, evaporative losses calculated from the Rayleigh equation exceed 50%.

Although total mass losses due to evaporation were probably small for most type-S spherules, typically <20% for major elements, heating was sufficiently pronounced and varied to have created a fairly well documented sequence of textural types (Taylor et al., 2000). Consistent with the proposed heating/textural sequence, porphyritic-partially melted spherules tend to have lower values of $\delta^{18}O$. In contrast to this sequence, a glass cosmic spherule has only slightly fractionated oxygen isotopic composition. It could be a largely unmelted chondrule fragment. Another of the type-S spherules studied, 94-4-32, has no assigned place in the textural hierarchy of heating. On the one hand, it looks similar to several strongly heated objects, while on the other its oxygen isotope composition is unfractionated and similar to those of many chondrules. We infer that this object is a fragment of a chondrule that survived unmelted upon atmospheric entry. The significance of this observation lies not only in the conclusion that the type-S spherules include chondrules, but also in the implication that improved understanding of how type-S spherules formed will allow us to distinguish more unusual and interesting objects.

Type-I spherules show generally larger degrees of isotopic fractionation than type-S spherules. Possible explanations include: a) the short duration of the heating pulse associated with the high volatile content of the type-S spherule precursors compared to type-I spherules; b) higher evaporation temperatures for at least a refractory portion of the silicates compared to that of iron metal or oxide; c) lower duration of heating of type-S spherules compared to type-I spherules as a consequence of their lower densities.

The isotopic results on these spherules, formed by transient heating at the top of the atmosphere, are interesting in their own right but they may also provide insight into other areas of study such as the origin of chondrules and perhaps even processes on Mars. Chondrules also form by transient heating but they do not show the levels of isotopic fractionation seen in the cosmic spherules. That they do not, provides clues to the nature of the relatively constrained conditions that produced chondrules. Cosmic spherules, accumulated over billions of years, must be highly abundant in some of the martian soils. This may be particularly true in cases where lag deposits form by winnowing processes. The isotopic character of the spherules could provide clues to past martian processes and environments. The presence of a significant abundance of spherules in a soil sample might also cause small but confusing effects in its bulk isotopic composition.

Acknowledgments—We thank G. Lofgren for his critical comments, which helped improve the manuscript. Insightful discussions with O. Jaoul, A. Toppani, and G. J. Greenwood are acknowledged. The paper was improved by thoughtful reviews of S. Taylor and M. J. Genge. This work was supported by grants from the NASA Cosmochemistry program (NAG5-11719 to GFH, NAG5-11809 to LAL). The UCLA ion microprobe facility is partially supported by a grant from the NSF Instrumentation and Facilities Program.

Associate editor: C. Koeberl

REFERENCES

Alexander C. M. O. D., Taylor S., Delaney J., Ma P., and Herzog G. F. (2002) Mass dependent fractionation of Mg, Si and Fe isotopes in five stony micrometeorites. *Geochim. Cosmochim. Acta* **66,** 173–183.

Anders E. and Grevesse N. (1989) Abundances of the elements: Meteoritic and solar. *Geochim. Cosmochim. Acta* **53,** 197–214.

Benedix G. K., Leshin L. A., Farquhar J., Jackson T. L., and Thiemens M. H. (2003) Carbonates in CM2 chondrites: Constraints on alteration conditions from oxygen isotopic compositions and petrographic observations. *Geochim. Cosmochim. Acta* **67,** 1577–1588.

Birck J.-L. and Allegre C.-J. (1985) Evidence for the presence of ^{53}Mn in the early solar system. *Geophys. Res. Lett.* **12,** 745–748.

Bischoff A., Palme H., Ash R. D., Clayton R. N., Schultz L., Herpers U., Stoffler D., Grady M. M., Pillinger C. T., Spettel B., Weber H., Grund T., Endress M., and Weber D. (1993) Paired Renazzo-type (CR) carbonaceous chondrites from the Sahara. *Geochim. Cosmochim. Acta* **57,** 1587–1603.

Brearley A. J., Saxton J. M., Lyon I. C., and Turner G. (1999) Carbonates in the Murchison CM chondrite: CL characteristics and oxygen isotopic compositions (abstract). *Lunar Planet. Sci.* **30,** 1301.

Brownlee D. E. (1985) Cosmic dust: Collection and research. *Ann. Rev. Earth Planet. Sci.* **13,** 147–173.

Brownlee D. E., Bates B., and Schramm L. (1997) The elemental composition of stony cosmic spherules. *Meteor. Planet. Sci.* **32,** 157–175.

Chakraborty S. (1997) Rates and mechanisms of Fe-Mg interdiffusion in olivine at 980°C–1300°C. *J. Geophys. Res.* **102,** *12,* 12,317–12,331.

Clayton R. N. and Mayeda T. K. (1984) The oxygen isotope record in Murchison and other carbonaceous chondrites. *Earth Planet. Sci. Lett.* **67,** 151–161.

Clayton R. N., Mayeda T. M., and Brownlee D. E. (1986) Oxygen isotopes in deep-sea spherules. *Earth Planet. Sci. Lett.* **79,** 235–240.

Clayton R. N. (1993) Oxygen isotopes in meteorites. *Ann. Rev. Earth Planet. Sci.* **21,** 115–149.

Clayton R. N. and Mayeda T. K. (1999) Oxygen isotope studies of carbonaceous chondrites. *Geochim. Cosmochim. Acta* **63,** 2089–2104.

Clayton R. N. and Mayeda T. K. (2001) Oxygen isotopic composition of the Tagish Lake carbonaceous chondrite (abstract). *Lunar Planet. Sci.* **32,** 1885.

Czajkowski J. (1987) Cosmo and geochemistry of the Jurassic hardgrounds. Ph.D. diss. University of California, San Diego.

Davis A. M., Clayton R. N., Mayeda T. K., and Brownlee D. E. (1991) Large mass fractionation of iron isotopes in cosmic spherules collected from deep-sea sediments (abstract). *Lunar Planet. Sci.* **22,** 281–282.

Davis A. M. and Brownlee D. E. (1993) Iron and nickel isotopic mass fractionation in deep-sea spherules (abstract). *Lunar Planet. Sci.* **24,** 373–374.

Delaney J., Herzog G. F., Ma P., Alexander C. M. O. D., and Taylor S. (2002) The fate of metal ejected from stony cosmic spherules: Low chrome on the range (abstract). *Meteor. Planet. Sci.* **37** (Suppl.), A41.

Duprat J., Engrand C., Maurette M., Gounelle M., Kurat G., and Leroux H. (2005) Friable micrometeorites from central Antarctica snow (abstract). *Lunar Planet. Sci.* **36,** 1678.

Engrand C. and Maurette M. (1998) Carbonaceous micrometeorites from Antarctica. *Meteor. Planet. Sci.* **33,** 565–580.

Engrand C., McKeegan K. D., and Leshin L. A. (1999) Oxygen isotopic compositions of individual minerals in Antarctic micrometeorites: Further links to carbonaceous chondrites. *Geochim. Cosmochim. Acta* **63,** 2623–2636.

Engrand C., Gounelle M., Duprat J., and Zolensky M. E. (2001a) In-situ oxygen isotopic composition of individual minerals in Tagish Lake, a new type 2 carbonaceous meteorite (abstract). *Lunar Planet. Sci.* **32,** 1568.

Engrand C., Gounelle M., and Zolensky M. E. (2001b) Oxygen isotopic composition of Tagish Lake (abstract). *Meteor. Planet. Sci.* **36** (Suppl.), A54.

Fahey A. J. (1988) Ion microprobe measurement of Mg, Ca, Ti and Fe isotopic ratios and trace element abundances in hibonite-bearing inclusions from primitive meteorites. Ph.D. diss. Washington University.

Genge M. J. (2004) Igneous rims on micrometeorites and the sizes of chondrules in main belt asteroids (abstract). *Lunar Planet. Sci.* **35,** 1102.

Genge M. J. and Grady M. M. (1998) Melted micrometeorites from Antarctic ice with evidence for the separation of immiscible Fe-Ni-S liquids during entry heating. *Meteor. Planet. Sci.* **33,** 425–434.

Genge M. J., Gileski A., and Grady M. M. (2005) Chondrules in Antarctic micrometeorites. *Meteor. Planet. Sci.* **40,** 225–238.

Gérard O. and Jaoul O. (1989) Oxygen diffusion in San Carlos olivine. *J. Geophys. Res.* **94,** 4119–4128.

Gonfiantini R., Stichler W., and Rozanski K. (1993) Standards and intercomparison materials distributed by the International Atomic Energy Agency for stable isotopes measurements. In *Reference and Intercomparison Materials for Stable Isotopes of Light Elements*, Vol. IAEA-Tecdoc-825, pp. 13–29. International Atomic Energy Agency.

Greenwood J. P. and Hess P. C. (1995) Dissolution and melting kinetics: Applications to chondrules (abstract). *Lunar Planet. Sci.* **26,** 505–506.

Herzog G. F., Xue S., Hall G. S., Nyquist L. E., Shih C. Y., Wiesmann H., and Brownlee D. E. (1999) Isotopic and elemental composition of iron, nickel and chromium in type-I deep-sea spherules: Implications for origin and composition of the parent micrometeoroids. *Geochim. Cosmochim. Acta* **63,** 1443–1457.

Kurat G., Koeberl C., Presper T., Brandstätter F., and Maurette M. (1994) Petrology and geochemistry of Antarctic micrometeorites. *Geochim. Cosmochim. Acta* **58,** 3879–3904.

Lal D. and Jull A. J. T. (2002) Atmospheric cosmic dust fluxes in the size range 10^{-4} to 10 centimeters. *Astrophys. J.* **576,** 1090–1097.

Leshin L. A., Rubin A. E., and McKeegan K. D. (1997) The oxygen isotopic composition of olivine and pyroxene from CI chondrites. *Geochim. Cosmochim. Acta* **61,** 835–845.

Leshin L. A., Farquhar J., Guan Y., Pizzarello S., Jackson T. L., and Thiemens M. H. (2001) Oxygen isotopic anatomy of Tagish Lake: Relationship to primary and secondary minerals in CI and CM chondrites (abstract). *Lunar Planet. Sci.* **32,** 1843.

Love S. G. and Brownlee D. E. (1993) A direct measurement of the terrestrial mass accretion rate of cosmic dust. *Science* **262,** 550–553.

Maurette M., Immel G., Hammer C., Harvey R., Kurat G., and Taylor S. (1994) Collection and curation of IDPs from the Greenland and Antarctic ice sheets. In *Analysis of Interplanetary Dust,* AIP Conference Proceedings, Vol. 310 (eds. M. E. Zolensky, T. L. Wilson, F. J. M. Rietmeijer, and G. J. Flynn), pp. 277–289. American Institute of Physics.

Misawa K., Yamakoshi K., and Nakamura N. (1992) Mg isotopic compositions of stony spherules from deep-sea sediments. *Geochem. J.* **26,** 29–36.

Nyquist L. E., Bansal B., Wiesmann H., and Shih C.-Y. (1994) Neodymium, strontium and chromium isotopic studies of the LEW86010 and Angra dos Reis meteorites and the chronology of the angrite parent body. *Meteoritics* **28,** 872–885.

Raisbeck G. M., Yiou F., Klein J., Middleton R., and Yamakoshi Y. (1982) Measurement of ^{26}Al and ^{10}Be in extraterrestrial matter by accelerator mass spectrometry. *Meteoritics* **17,** 270–271.

Rowe M. W., Clayton R. N., and Mayeda T. K. (1994) Oxygen isotopes in separated components of CI and CM meteorites. *Geochim. Cosmochim. Acta* **58,** 5341–5347.

Schnabel C., Herzog G. F., Taylor S., Field P., and Sherrell R. (1999) Magnesium isotope abundances in stony Antarctic micrometeorites. *Antarc. Meteorite Res.* **24,** 166–167.

Taylor S., Lever J. H., and Harvey R. P. (2000) Numbers, types and compositions of an unbiased collection of cosmic spherules. *Meteor. Planet. Sci.* **35,** 651–666.

Taylor S., Alexander C. M. O. D., Delaney J., Ma P., Herzog G. F., and Engrand C. (2002) Isotopic fractionation of Fe-57 in stony cosmic spherules: Implications for iron loss (abstract). *Lunar Planet. Sci.* **33,** 1136.

Thiemens M., Jackson T., Zipf E. C., Erdman P. W., and Van Egmond C. (1995) Carbon dioxide and oxygen isotope anomalies in the mesosphere and stratosphere. *Science* **270,** 969–972.

Toppani A., Libourel G., Engrand C., and Maurette M. (2001) Experimental simulation of atmospheric entry of micrometeorites. *Meteor. Planet. Sci.* **36,** 1377–1396.

Völkening J. and Papanastassiou D. A. (1989) Iron isotope anomalies. *Astrophys. J.* **347,** L43–L46.

Wang J., Davis A. M., Clayton R. N., and Mayeda T. K. (1994) Kinetic isotopic fractionation during the evaporation of the iron oxide from liquid state (abstract). *Lunar Planet. Sci.* **25,** 1459–1560.

Wang J., Davis A. M., Clayton R. N., Mayeda T. K., and Hashimoto A. (2001) Chemical and isotopic fractionation during the evaporation of the FeO-MgO-SiO_2-CaO-Al_2O_3-TiO_2 rare earth element melt system. *Geochim. Cosmochim. Acta* **65,** 479–494.

Wasson J. T. (1996) Chondrule formation: Energetics and length scales. In *Chondrules and the Protoplanetary Disk* (eds. R. H. Hewins, R. H. Jones, and E. R. D. Scott), pp. 45–54. Cambridge University Press.

Weisberg M. K., Prinz M., Clayton R. N., and Mayeda T. K. (1993) The CR (Renazzo-type) carbonaceous chondrite group and its implications. *Geochim. Cosmochim. Acta* **57,** 1567–1586.

Williamson J. H. (1968) Least-squares fitting of straight line. *Can. J. Phys.* **46,** 1845–1847.

Xue S., Herzog G. F., Hall G. S., Bi D., and Brownlee D. E. (1995) Nickel isotope abundances of type-I deep-sea spheres and of iron-nickel spherules from sediments in Alberta, Canada. *Geochim. Cosmochim. Acta* **59,** 4975–4981.

Yada T., Nakamura T., Sekiya M., and Takaoka N. (1996) Formation processes of magnetic spherules collected from deep-sea sediments—Observations and numerical simulations of the orbital evolution. *Proc. NIPR Symp. Antarc. Meteorites* **9,** 218–236.

Yada T., Matsumoto N., Nakamura T., Noguchi T., Setoyanagi T., Takaoka N., and Kojima H. (2002) Oxygen isotopic composition mineral grains in Antarctic micrometeorites and bulk spherules: A spherule having large Δ^{17}O (abstract). *Meteor. Planet. Sci.* **37** (Suppl.), A152.

Yada T., Nakamura T., Noguchi T., Ushikubo T., Hiyagon H., and Sugiura N. (2003a) Mg, Si and Fe fractionation observed in Antarctic silicate spherules. *Meteor. Planet. Sci.* **38** (Suppl.), A88.

Yada T., Nakamura T., Noguchi T., Ushikubo T., Matsumoto N., Kojima H., and Takaoka N. (2003b) Variations of oxygen isotopic compositions of silicate spherules collected from Antarctic blue ice (abstract). *Lunar Planet. Sci.* **34,** 1587.

Yada T., Nakamura T., Noguchi T., Ushikubo T., Matsumoto N., Kojima H., and Takaoka N. (2003c) Estimation for precursors of silicate spherules based on their oxygen isotopic compositions (abstract). In *International Symposium on Evolution of Solar System Materials: A New Perspective from Antarctic Meteorites*, pp. 146–147. National Institute of Polar Research, Tokyo, Japan.

Yiou F., Raisbeck G. M., and Brownlee D. E. (1985) ^{10}Be in iron type cosmic spherules: Evidence for a differentiated parent body (abstract). *Meteoritics* **20,** 791.

Geochimica et Cosmochimica Acta, Vol. 69, No. 13, pp. 3431–3443, 2005

0016-7037/05 $30.00 + .00

doi:10.1016/j.gca.2004.12.021

Hydrogen isotopic composition of water from fossil micrometeorites in howardites

Matthieu Gounelle,[1,2,3,*] Cécile Engrand,[1] Olivier Alard,[4] Philip A. Bland,[3,5] Michael E. Zolensky,[6] Sara S. Russell,[3] and Jean Duprat[1]

[1]CSNSM, Bâtiment 104, 91 405 Orsay Campus, France
[2]Université Paris XI, Bâtiment 104, 91 405 Orsay Campus, France
[3]Department of Mineralogy, The Natural History Museum, London SW7 5BD, UK
[4]Department of Earth Sciences, The Open University, Walton Hall, Milton Keynes, MK7 6AA, UK
[5]Department of Earth Science and Engineering, Exhibition Road, Imperial College, London SW7 2AZ, UK
[6]KT, NASA Johnson Space Center, Houston, TX 77058, USA

(*Received June* 23, 2004; *accepted in revised form December* 23, 2004)

Abstract—We have measured the hydrogen isotopic composition (D/H ratios) of the water from 13 carbonaceous chondritic microclasts (CCMs, size <1 mm) trapped in two howardites (Kapoeta and Yamato-793497) early in the evolution of Solar System. The division into tochilinite-rich; magnetite-rich, olivine-poor; magnetite-rich, olivine-rich CCM types is corroborated by the hydrogen isotopic compositions. Both mineralogy and hydrogen isotopic compositions demonstrate that tochilinite-rich CCMs represent CM2 chondritic matter. In contrast, there is no good match between the isotopic and mineralogical properties of the magnetite-rich CCMs and the known groups of carbonaceous chondrites, suggesting that magnetite-rich CCMs represent a new kind of chondritic matter, not yet sampled in meteorite collections. This demonstrates that the view of the asteroid belt revealed by the collection of meteorites is incomplete. The study of (micro)clasts offers a unique opportunity to better decipher the nature and relative abundance of asteroids.

The average hydrogen isotopic composition of water belonging to CCMs, D/H = $(152.0 \pm 4.8) \times 10^{-6}$ ($1\sigma_m$), is similar to that of Antarctic micrometeorites (AMMs), D/H = $(161.2 \pm 3.8) \times 10^{-6}$ ($1\sigma_m$). The similarity, in terms of mineralogy and hydrogen isotopic composition, between CCMs and AMMs demonstrates that the composition of the micrometeorites has not been modified over the whole history of the Solar System. It indicates that the composition of the micrometeorite flux onto Earth has been, and is, dominated by a mixture of CM2-like; magnetite-rich, olivine-poor; magnetite-rich, olivine-rich carbonaceous chondritic matter exemplified by CCMs found in howardites. Because CCMs have not suffered atmospheric entry, they provide an abundant source of pristine micrometeorites.

The average D/H ratio of the whole population of CCMs is identical within errors to that of the Earth ($149 \pm 3 \times 10^{-6}$). The match between the CCMs D/H ratio and that of the Earth is especially remarkable because 1) three different populations of CCMs are needed to make the D/H ratio of the Earth; 2) there is no single carbonaceous chondrite group for which a similar match exists. This observation suggests that CCMs population might be representative of the late veneer agent(s) that delivered water to the Earth.

1. INTRODUCTION

Volatile-rich extraterrestrial materials provide a unique opportunity for deciphering the origin of Solar System, the early evolution of asteroids, and the formation of the planets. Until the Stardust sample return mission brings back dust from the Wild 2 Jupiter family comet in 2006, the only volatile-rich extraterrestrial samples we have at hand are carbonaceous chondrites (e.g., McSween, 1979), cm-sized carbonaceous chondritic clasts within meteorites (e.g., Nakashima et al., 2003; Zolensky et al., 1992), micrometeorites collected in the polar ice caps (e.g., Maurette et al., 1991; Engrand and Maurette, 1998; Taylor et al., 1998; Nakamura, 1999; Duprat et al., 2003) and interplanetary dust particles (IDPs) in the stratosphere (e.g., Zolensky et al., 1994; Rietmeijer, 1998). In addition to these already well-characterized samples, a new source of volatile-rich extraterrestrial dust has been recently identified.

Gounelle et al. (2003) have reported the finding of 71 submillimeter-sized carbonaceous chondritic microclasts (CCMs) in howardites. Howardites are achondritic meteorites members of the HED (howardites-eucrites-diogenites) clan, and believed to sample the regolith of a differentiated asteroid, possibly 4 Vesta (Binzel and Xu, 1993). Although mm- to cm-sized clasts in howardites have been known and studied for a long time (e.g., Wilkening, 1973; Zolensky et al., 1996b), submillimeter-sized clasts have been only recently identified and are very little studied.

A mineralogical study has shown that CCMs are made of C2-like chondritic matter (Gounelle et al., 2003). These samples are worth further study for a number of reasons. First, CCMs provide a new, abundant, source of carbonaceous, volatile-rich micrometeorites. Second, they might offer a view of the asteroid belt significantly different from that given by meteorites, and potentially less biased. Third, unlike polar micrometeorites, CCMs have not suffered alteration due to atmospheric entry (e.g., Toppani et al., 2001), so they are relatively pristine with regard to their bulk chemical composition, mineralogy and isotopic composition. Fourth, CCMs have been shown to be *fossil* micrometeorites that were present in the inner Solar System very early in its history (Gounelle et al., 2003). As such, they can help us to probe the nature of Earth-

* Author to whom correspondence should be addressed (gounelle@csnsm.in2p3.fr).

Table 1. Summary of the mineralogy of carbonaceous chondritic microclasts.[a]

		Tochilinite poor, magnetite rich	
	Tochilinite rich, magnetite poor	Olivine-rich	Olivine-poor
CCMs	Y35, Y46, K9, Y50, K54, Y37	K3, K18, K24	Y1, Y22, Y8, Y43
Olivine	++++	++++	+
Fo%	39–96	1–99	98–99
Pyroxene	++++	++++	+
En%	87–98	4–98	95–98
Wo%	0–3	1–51	1–3
Carbonate (calcite)	++	++	−
Phyllosilicate (saponite, serpentine)	++++	++++	++++
Magnetite	+	++++	++++
Chromite	+	−	−
Fe-Ni sulfide (pyrrhotite, pentlandite)	+++	+++	++++
Metal	+	−	++++
Tochilinite	++++	−	−
Previous classification[b]	CM2-like	CR2-like	CR2-like
Related CCs	CM2s	CR2s, Tagish Lake	CI1s

[a] ++++ = very abundant; +++ = abundant; ++ = common; + = occurrence; − = absent. Fo%, En%, Wo% = range of forsterite, enstatite and wollastonite contents respectively.
[b] Gounelle et al. (2003).

impacting material in the early Solar System. Specifically, because they are rich in water-bearing minerals such as phyllosilicates, CCMs in howardites can provide clues to the origin of water on Earth, thought to have been delivered as a late veneer by an unspecified agent (e.g., Wänke, 1981; Chyba, 1990; Morbidelli et al., 2000).

In this paper, we report measurements of the hydrogen isotopic composition of the water in phyllosilicates of the CCMs found in howardites. The adopted analytical technique (ion microprobe equipped with a O^- beam) can exclusively measure the isotopic composition of hydrogen *water* (Deloule et al., 1991; Deloule and Robert, 1995), and excludes contributions from organic molecules. Despite this limitation, our data can still help to address the problem of the origin of the Earth water for two reasons. (1) When water was delivered on Earth by a late veneer agent, the Earth's atmosphere was significantly more reducing than it is now, and it might be that hydrogen bound in refractory extraterrestrial organic matter has never been a significant part of Earth's hydrologic cycle. (2) Even if organic hydrogen has been oxidized, water accounts for ~80% of the hydrogen present in CCs (Robert, 2002) and therefore, although organic matter is usually enriched in D relative to water, the bulk D/H ratio of CCMs should not be very different from the water D/H ratio (see table 1 of Robert, 2002).

The primary goal of this study is to better characterize the light element geochemistry of this new population of primitive objects: carbonaceous chondritic microclasts in howardites. In addition, this study may help improve the classification of CCMs, tentatively built from mineralogical data (Gounelle et al., 2003). Finally, because of the unique fossil nature of CCMs in howardites, their hydrogen isotopic composition may provide some clues about the nature of the late veneer agent that delivered water onto Earth.

2. EXPERIMENTAL METHODS

The mineralogy of carbonaceous chondritic microclasts has been studied in detail by Gounelle et al. (2003). For the present project, we made additional measurements of the matrix composition with a CAMECA SX 50 electron microprobe operated at a voltage acceleration of 15 kV, beam current of 10 nA and with a 5 μm defocused beam. The hydrogen isotopic composition was measured with the CRPG CAMECA IMS 1270 ion microprobe in Nancy (France) following the procedures outlined in Deloule et al. (1991), and utilized for analyses of meteorites and micrometeorites (Deloule and Robert, 1995; Engrand et al., 1999). Beam size was ~10 μm; the use of an O^- primary ion beam for these analyses enhances the emission of H^+ ions from the H-bearing silicate phases over that of organic H^+ ions by a factor of >100 (Deloule and Robert, 1995). Our analyses therefore provide the hydrogen isotopic composition of the structural water and hydroxyl radicals contained in the phyllosilicates (serpentine and saponite) abundant in the matrix of CCMs. For simplicity, we will refer below to the hydrogen isotopic composition of phyllosilicate water, omitting the hydroxyl radicals. The analytical uncertainty for these analyses (taking into account reproducibility of standards, correction of the instrumental mass fractionation and internal reproducibility) is of the order of 40‰.

3. RESULTS

3.1. Mineralogy

Gounelle et al. (2003) have reported the discovery of seventy-one carbonaceous chondritic microclasts with sizes ranging from 25 μm to 800 μm in three howardites (Kapoeta, Jodzie, and Yamato-793497). Approximately half of them are tochilinite-rich and contain no or very little magnetite, while the other half are magnetite-rich and contain no or very little tochilinite. The tochilinite-rich and magnetite-rich microclasts were tagged CM2-like and CR2-like microclasts, respectively. However, because the elucidation of possible genetic links with carbonaceous chondrite groups is one of the aims of the present work, we will not adopt here this interpretative terminology. Furthermore, within the magnetite-rich microclasts, we will from now on distinguish between olivine-poor and olivine-rich CCMs. This distinction is a first step in trying to resolve the classification ambiguity noted by Gounelle et al. (2003) for CR2-like CCMs. Below, we briefly describe the mineralogy of 13 CCMs from Yamato-793497 and Kapoeta selected for the hydrogen isotopic study, with the aim of justifying the terminology adopted above. Table 1 summarizes the mineralogy, classifica-

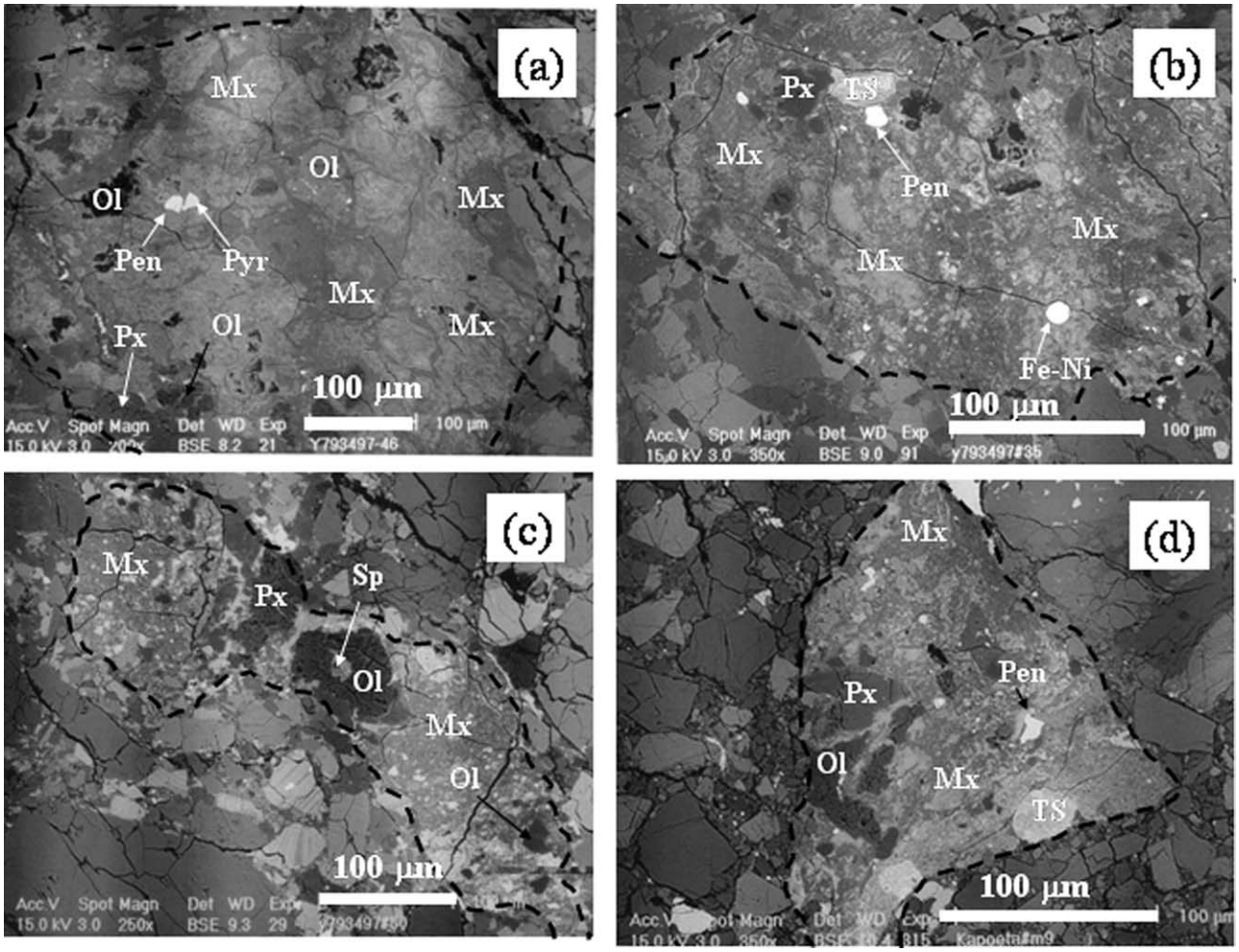

Fig. 1. Backscattered electron images of selected tochlinite-rich CCMs. Detailed mineralogical description is given in section 3.1 and summarized in Table 1. (a) Carbonaceous chondritic microclast 46 from the howardite Y793497 (Y46). (b) Carbonaceous chondritic microclast 35 from the howardite Y793497 (Y35). (c) Carbonaceous chondritic microclast 50 from the howardite Y793497 (Y50). (d) Carbonaceous chondritic microclast 9 from the howardite Kapoeta (K9). Mx, Ol, Px, Pen, Pyr, Fe-Ni, TS, Sp stand for matrix, olivine, pyroxene, pentlandite, pyrrhotite, iron-nickel metal, tochilinite-serpentine aggregate and spinel respectively.

tion and genetic links with carbonaceous chondrites (CCs) of the selected CCMs. Hereafter, CCMs belonging to the Yamato-793497 and Kapoeta howardites will be labeled with the prefix Y and K respectively.

3.1.1. *Mineralogy of Tochilinite-Rich CCMs*

Microclasts Y35, Y37 and Y46 have sizes up to 550 × 450 μm^2 and consist of a fine-grained phyllosilicate-rich matrix supporting rare low-calcium pyroxene ($En_{96}Wo_2$-$En_{98}Wo_0$) and olivine (Fo_{39}-Fo_{96}) grains, tochilinite, iron-nickel sulfides and metal (Fig. 1). The matrix consists of saponite, serpentine and tochilinite, with minor pentlandite and pyrrhotite (Table 2 and Fig. 4).

Microclast K9 (Fig. 1) has a size of 270 × 290 μm^2 and consists of a phyllosilicate-rich fine-grained matrix supporting abundant pyroxene ($En_{92}Wo_2$-$En_{97}Wo_1$) grains, iron-nickel sulfides, rare calcium carbonate and a complex round object made of a succession of intergrowths of serpentine and tochilinite. One grain of chromite sits at the edge of this complex object. The matrix consists of saponite, serpentine and tochilinite, with minor pentlandite and pyrrhotite (Table 2 and Fig. 4).

Microclast Y50 (Fig. 1) is 440 × 25 μm^2, and consists of a phyllosilicate-rich fine-grained matrix supporting olivine (Fo_{98-99}), pyroxene ($En_{87}Wo_3$-$En_{98}Wo_3$), spinel, magnetite, iron-nickel sulfides, and tochilinite. Phyllosilicates in the matrix are a mixture of serpentine and saponite (Table 2 and Fig. 4). A 5 μm spinel grain sits in a sulfide-rich mixture of serpentine and saponite rimmed by an olivine grain (Fo_{99}). This association can be viewed as a CAI similar to those found in CM2 chondrites (Lee and Greenwood, 1994; MacPherson and Davis, 1994). Tochilinite occurs together with serpentine as patches in the matrix.

Microclast K54 is 440 × 320 μm^2 wide, and consists of a phyllosilicate-rich fine-grained matrix supporting olivine-pyroxene aggregates, isolated olivine (Fo_{53-99}) and pyroxene ($En_{92-98}Wo_1$) grains, iron-nickel sulfides, and the interstratified serpentine-tochilinite phase (MacKinnon and Zolensky, 1984). A 100

Table 2. Selected electron microprobe analyses of carbonaceous chondritic microclasts matrices.[a]

	Magnetite-rich, olivine-rich CCMs					Magnetite-rich, olivine-poor CCMs					Tochilinite-rich CCMs					
	K24	K24	K18	K3	K3	Y1	Y1	Y43	Y43	Y8	Y8	K54	K54	K9	K9	Y46	Y46	Y50	Y50
Na_2O	0.16	0.09	0.06	0.08	0.30	0.30	0.08	0.15	0.17	0.10	0.56	0.48	0.09	0.12	0.07	0.08	0.00	0.07	0.12	0.11
MgO	15.9	12.8	19.6	20.4	22.3	25.5	12.9	13.9	10.1	15.5	15.8	25.8	18.0	10.7	13.5	13.8	37.7	14.7	11.3	10.9
Al_2O_3	2.43	2.28	10.4	9.62	3.68	3.32	3.87	2.61	4.27	5.42	6.32	5.65	2.10	2.21	2.39	2.18	0.03	2.63	2.72	2.57
SiO_2	31.8	39.1	35.4	36.2	37.4	46.8	37.1	35.8	35.2	22.5	33.3	36.8	31.3	20.7	29.0	26.3	37.5	34.4	35.9	37.6
P_2O_5	0.17	0.15	0.24	0.22	0.40	0.07	bd	0.05	0.11	0.12	0.18	0.39	0.06	bd	bd	bd	bd	0.60	0.11	0.30
S	1.47	0.19	0.04	0.06	3.84	0.09	1.97	1.78	1.44	0.43	0.87	1.36	1.29	7.50	2.17	3.54	bd	1.83	1.69	1.66
K_2O	0.19	0.18	0.16	0.20	0.44	0.38	0.11	0.15	0.30	0.18	0.31	0.24	0.06	bd	0.15	0.12	bd	bd	0.09	0.11
CaO	1.63	1.21	0.35	0.44	1.16	0.53	0.30	0.18	0.44	1.05	3.93	0.86	0.34	0.18	1.04	1.21	0.19	0.33	0.16	0.10
TiO_2	0.17	0.45	0.11	0.14	0.11	0.12	0.06	0.09	0.20	0.17	0.14	0.11	0.09	0.04	0.09	0.09	bd	0.11	0.07	0.11
Cr_2O_3	0.47	0.94	0.53	0.65	0.45	1.17	0.64	0.71	0.63	0.36	0.42	0.55	0.34	0.23	0.30	0.46	0.21	0.45	0.54	0.63
MnO	0.30	0.42	0.10	0.08	0.18	0.09	0.13	0.16	0.20	0.22	0.34	0.16	0.27	0.17	0.26	0.23	0.22	0.18	0.17	0.17
FeO	22.7	26.2	19.0	18.7	14.9	4.02	24.4	26.3	25.3	34.9	9.71	15.5	30.8	48.2	32.4	31.9	22.3	26.7	30.3	30.9
NiO	2.21	1.95	0.71	1.03	1.89	0.18	0.84	0.94	0.85	0.55	0.43	0.92	1.23	2.31	1.61	3.01	0.08	0.88	1.07	0.94
Total	**79.60**	**85.98**	**86.76**	**87.86**	**87.03**	**82.55**	**82.48**	**82.79**	**79.17**	**81.53**	**72.33**	**88.80**	**86.04**	**92.28**	**82.93**	**82.86**	**98.23**	**82.86**	**84.11**	**86.08**

[a] Data in wt%; bd = below detection limit.

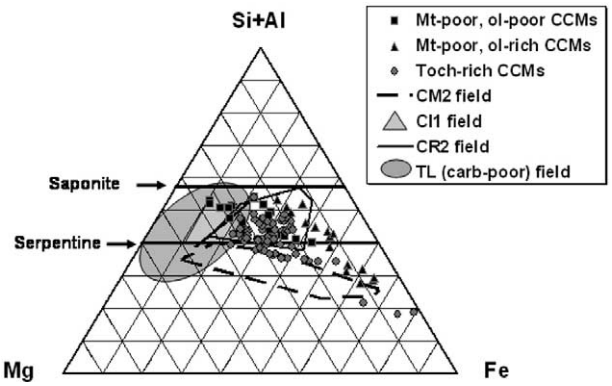

Fig. 2. The compositional variation of phyllosilicates in CCMs displayed on a Si+Al-Mg-Fe ternary diagram. Data defining the compositional field of CI1, CM2, CR2, Tagish Lake (carbonate-poor) carbonaceous chondrites are found in Tomeoka and Buseck (1988), Zolensky et al. (1993), Weisberg (1993) and Gounelle et al. (2001) respectively. Serpentine and saponite solid solutions are indicated for reference.

μm large round aggregate made of olivine (Fo_{99}), pyroxene ($En_{98}Wo_1$), serpentine, and iron sulfide, and rimmed by fine-grained serpentine assemblage was considered to be a chondrule by Gounelle et al. (2003). Phyllosilicates in the matrix are a mixture of serpentine and saponite (Table 2 and Fig. 4).

3.1.2. Mineralogy of magnetite-rich, olivine-rich CCMs

Microclast K3 is an ovoid (320 × 160 μm^2) microclast (Fig. 2) consisting of a relatively rare fine-grained phyllosilicate-rich matrix supporting a large (~100 μm) olivine (Fo_{1-99})-phyllosilicate-iron oxide-sulfide aggregate as well as isolated olivine (Fo_{99}), augite ($En_{61}Wo_{37}$), hedenbergite (En_4Wo_{51}-$En_{15}Wo_{50}$) and iron-nickel sulfide grains. Magnetite is very abundant, it occurs as euhedral grains of fairly pure composition associated with calcium carbonate and hedenbergite. Phyllosilicates in the matrix are serpentine and saponite (Table 2 and Fig. 4).

Microclast K18 is a large object (450 × 450 μm^2) consisting of a fine-grained phyllosilicate-rich matrix supporting olivine, pyroxene, magnetite and iron-nickel sulfides (Fig. 2). Matrix phyllosilicates consist of a mixture of saponite and serpentine (Table 2 and Fig. 4). Olivine (Fo_{98}) and pyroxene ($En_{98}Wo_1$) are common. Magnetite is very abundant; it occurs as plaquettes, framboids and anhedral grains. Pentlandite and minor pyrrhotite are common, they occur as isolated grains in the matrix and have also been found rimming serpentine + saponite assemblages.

Microclast K24 is a large object (800 × 500 μm^2) consisting of an abundant fine-grained phyllosilicate-rich matrix supporting a diversity of aggregates, isolated olivine (Fo_{98-100}) grains, iron-nickel sulfides, iron oxides enriched in P, Cr and Ni and magnetite displaying a variety of morphologies (Fig. 2). Phyllosilicates in the matrix are saponite and serpentine (Table 2). Unusual coarse phyllosilicate grains have been described by Gounelle et al. (2003) who suggested they were pseudomorphs after of olivine or pyroxene grains.

3.1.3. Magnetite-rich, olivine-poor CCMs

There are no significant differences between the different magnetite-rich-olivine-poor CCMs analyzed in the present

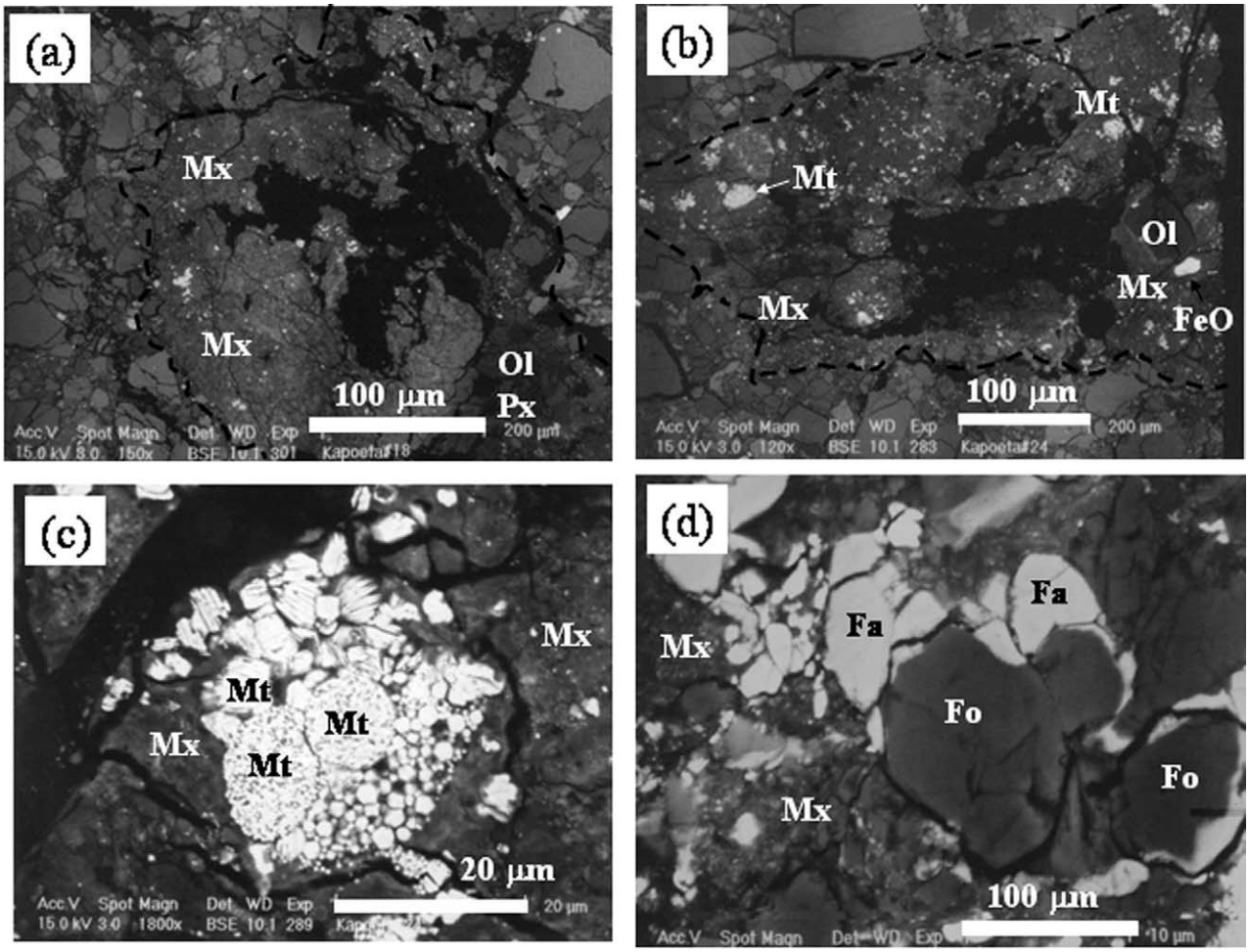

Fig. 3. Backscattered electron images of selected magnetite-rich, olivine-rich CCMs. Detailed mineralogical description is given in section 3.1 and summarized in Table 1. (a) Carbonaceous chondritic microclast 18 from the howardite Kapoeta (K18). (b) Carbonaceous chondritic microclast 24 from the howardite Kapoeta (K24). (c) Close up view of the carbonaceous chondritic microclast 24 from the howardite Kapoeta (K24). (d) Close up view of the carbonaceous chondritic microclast 3 from the howardite Kapoeta (K3). Mx, Ol, Px, Fo, Fa, Mt and FeO stand for matrix, olivine, pyroxene, forsterite, fayalite, magnetite and iron-oxide respectively. Dark areas in CCMs K18 and K24 correspond to epoxy.

study, except for a moderately varying magnetite abundance (Fig. 3). They have sizes up to 500 × 300 μm^2 and consist of an abundant phyllosilicate-rich matrix supporting magnetite and iron-nickel sulfides. Phyllosilicates are a mixture of saponite and serpentine (Table 2 and Fig. 4). Olivine and pyroxene grains are extremely rare (present mainly in Y1) and have very magnesium-rich compositions (Fo_{98-99} and $En_{95-98}Wo_{1-3}$ respectively). Magnetite occurs as framboidal aggregates, plaquettes, spherules and subhedral to euhedral grains. Magnetite is especially abundant in microclast Y8. Pyrrhotite is the most abundant sulfide; pentlandite and sulfides with a composition intermediate between that of pyrrhotite and pentlandite are rare. No carbonates were found.

3.2. Hydrogen Isotopic Composition

As stated in the introduction and in the experimental methods sections, the hydrogen isotopic composition of CCMs refers to that of the phyllosilicates' water and hydroxyl groups measured with the ion microprobe. The complete set of measured D/H ratios is shown in Table 3, while average values are displayed in Table 4 and Figure 5. The average D/H ratio of the whole population of CCMs is (152.0 ± 4.8) × 10^{-6} ($1\sigma_m$, n = 34). Tochilinite-rich CCMs have D/H ratios ranging from 117.6 × 10^{-6} to 138.4 × 10^{-6}, with an average value of (131.8 ± 2.3) × 10^{-6} ($1\sigma_m$, n = 14). Magnetite-rich, olivine-rich CCMs have D/H ratios ranging from 168.6 × 10^{-6} to 203.8 × 10^{-6}, with an average value of (180.8 ± 3.7) × 10^{-6} ($1\sigma_m$, n = 15). Magnetite-rich, olivine-poor CCMs have D/H ratios ranging from 112.8 × 10^{-6} to 170.1 × 10^{-6} with an average value of (137.7 ± 10.5) × 10^{-6} ($1\sigma_m$, n = 5). We observe a weak positive correlation between the modal abundance of anhydrous grains (olivine and pyroxene) of tochilinite-rich CCMs and their D/H ratio (Fig. 6).

4. DISCUSSION

4.1. Comparison of CCMs and Carbonaceous Chondrites

Mineralogical study of tochilinite-rich CCMs has demonstrated that they are linked to CM2 chondrites (see section 3,

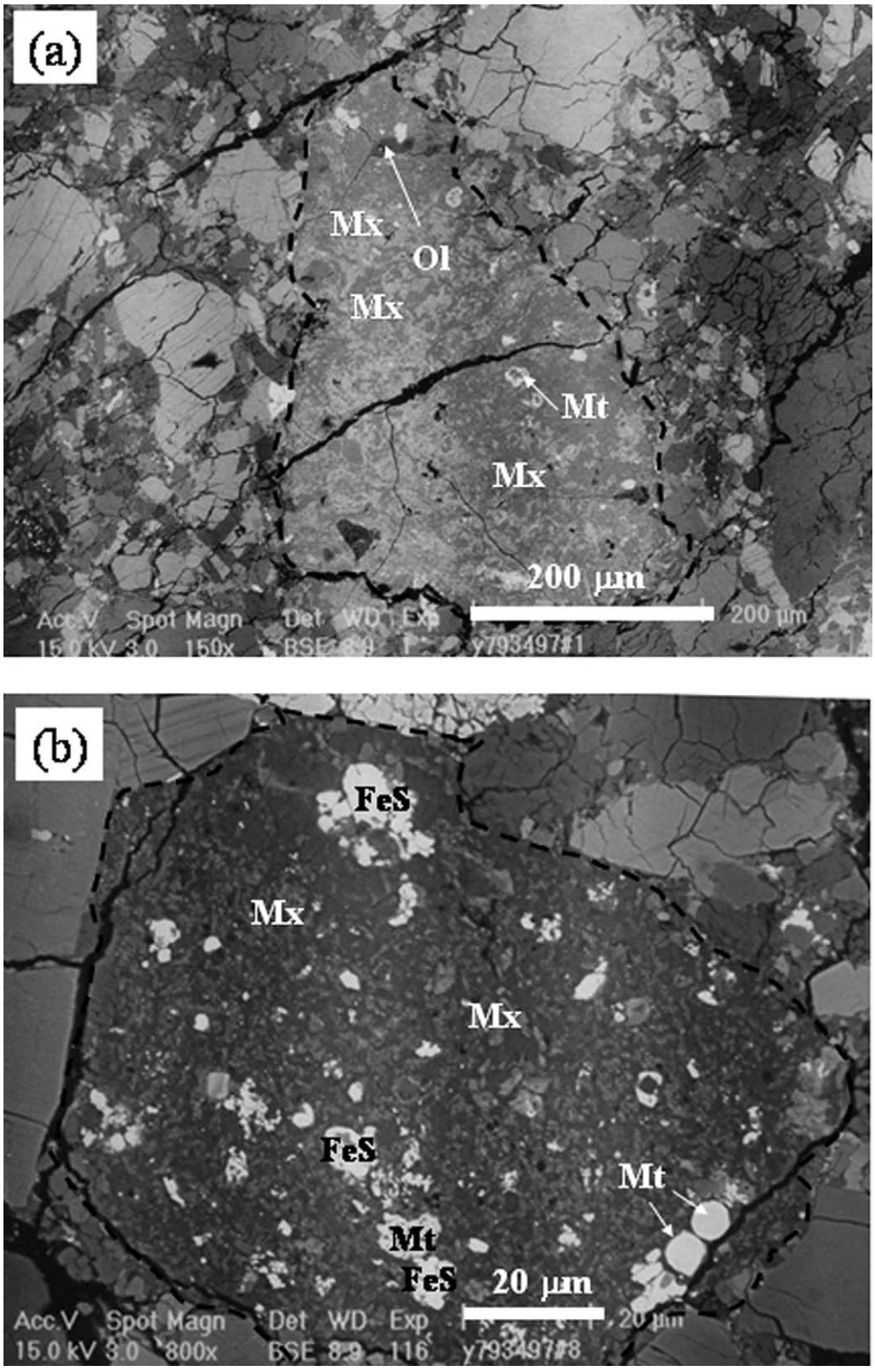

Fig. 4. Backscattered electron images of selected magnetite-rich, olivine-poor CCMs. Detailed mineralogical description is given in section 3.1 and summarized in Table 1. (a) Carbonaceous chondritic microclast 1 from the howardite Y793497 (Y1). (b) Carbonaceous chondritic microclast 8 from the howardite Y793497 (Y8). Mx, Ol, Mt, FeS stand for matrix, olivine, magnetite and iron-nickel sulfide respectively.

Table 3. Complete set of measured D/H ratios of carbonaceous chondritic microclasts in howardites.[a]

Mt-rich, ol-rich CCMs		Toch-rich CCMs		Mt-rich, ol-poor CCMs	
Analysis	D/H ($\times 10^6$)	Analysis	D/H ($\times 10^6$)	Analysis	D/H ($\times 10^6$)
K24_1	202.3	K54_1	134.7	Y1_1	112.8
K24_2	168.6	K54_2	137.9	Y1_2	117.5
K24_3	199	K54_3	128.1	Y43_1	140.1
K24_4	203.8	K54_4	156.8	Y22_1	147.9
K24_5	191.3	K9_1	128.1	Y8_1	170.1
K18_1	187.7	K9_2	127.1		
K18_2	185	K9_3	127		
K18_3	169.5	Y37_1	135.3		
K18_4	168.8	Y37_2	138.4		
K18_5	167.6	Y35_1	122.8		
K3_1	163.8	Y46_1	128.2		
K3_2	179.9	Y46_2	125.5		
K3_3	169.6	Y46_3	117.6		
K3_4	173.7	Y46_4	134.5		
		Y50_2	134.3		

[a] Errors on each data point are of the order of 4%. Mt, ol, and toch stand for magnetite, olivine, and tochilinite respectively.

Table 1, and Gounelle et al., 2003)). Minor mineralogical differences between tochilinite-rich CCMs and CM2 chondrites include the depletion of chondrules relative to CAIs and the high abundance of saponite in the former (Fig. 4). Magnetite-rich, olivine-rich CCMs are related to CR2 chondrites and the carbonate-poor lithology of the ungrouped C2 chondrite Tagish Lake (see section 3, Table 1, and Gounelle et al., 2003), but exhibit strong differences with these last two groups of chondrites. Compared to CR2 chondrites, they are more oxidized as shown by the rarity of metal grains (Table 1) and the high abundance of fayalitic olivine grains. Compared to the carbonate-poor lithology of the ungrouped

Table 4. D/H ratios of individual carbonaceous chondritic microclasts in howardites and averages for each mineralogical type.[a]

	D/H ($\times 10^6$)	1 σ_m	1σ_m (%)
K24	193.0	6.5	3.4
K18	175.7	4.4	2.5
K3	171.8	3.4	2.0
Magnetite rich, olivine rich	**180.8**	**3.7**	**2.0**
K54	139.4	6.1	4.4
K9	127.4	0.34	0.3
Y37	136.9	1.6	1.2
Y35	122.8	4.9	4.0
Y46	126.4	2.8	2.2
Y50	134.3	5.4	4.0
Tochilinite rich	**131.8**	**2.3**	**1.7**
Y1	115.0	2.3	2.0
Y8	170.1	6.8	4.0
Y43	140.1	5.6	4.0
Y22	147.9	5.9	4.0
Magnetite rich, olivine poor	**137.7**	**10.5**	**7.6**

[a] Errors are 1σ_m (i.e., 1 standard deviation of the mean). For the CCMs for which we have only one data point, the error is that of a single measure, i.e., 4% relative.

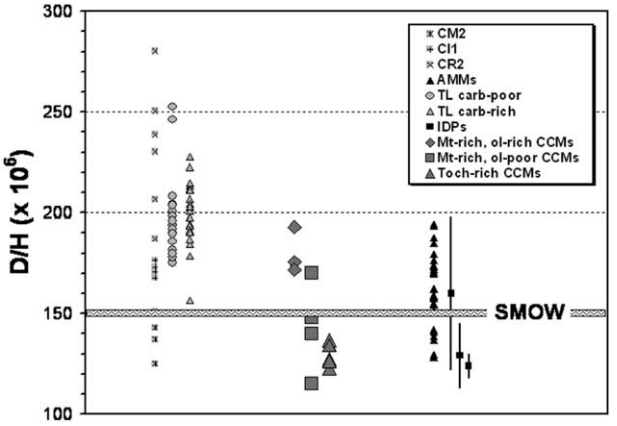

Fig. 5. Comparison of CCMs phyllosilicates' structural water D/H ratios with phyllosilicates' structural water D/H ratios of carbonaceous chondrites, and micrometeorites. For CCMs, each point is either a single measure, or the average of several data points (Table 4). Data for CM2 and CI1 chondrites are from Eiler and Kitchen (2004). Data for the two Tagish Lake lithologies are from Engrand et al. (2003). Data for AMMs and IDPs are from Engrand et al. (1999) and Aléon et al. (2001) respectively. For CR2 chondrites, we have not plotted the Renazzo data reported by Deloule and Robert (1995) because they are not tabulated. These data are compatible with those of Guan and Zolensky (1997). Error bars (except for the three IDPs) have not been plotted for sake of clarity. They are of the order of 4% relative for CCMs, AMMs and Tagish Lake (Engrand et al., 1999, 2003; this work), of 3% for CM2 and CI1 data (Eiler and Kitchen, 2004) and between 1 to 3% for CR2 chondrites. Standard Mean Ocean Water (SMOW) D/H ratio is indicated for reference.

C2 Tagish Lake (Gounelle et al., 2001), magnetite-rich, olivine-rich CCMs are depleted in chondrules, and have more magnesium-rich phyllosilicates (Fig. 4). Magnetite-rich, olivine-poor CCMs are related to CI1 chondrites (see section 3, Table 1 and Gounelle et al. (2003)). Compared to CI1 chondrites, they lack dolomite and have more iron-rich phyllosilicates (Fig. 4). Below, we compare CCMs' and CCs' D/H ratios to shed some light on the relationship between these two types of volatile-rich matter.

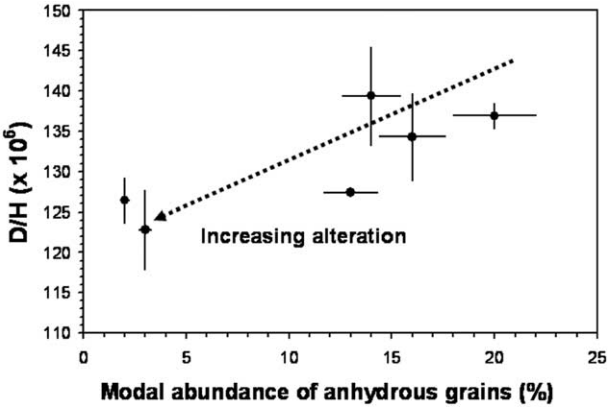

Fig. 6. D/H ratios plotted vs. the modal abundance of anhydrous grains for tochilinite-rich CCMs. This modal abundance is negatively correlated with the mineralogical alteration index defined for CM2 chondrites by Browning et al. (1996). Error bars on the modal abundance have been estimated to be 10% relative. The dashed line is a hand-drawn best fit curve.

Table 5. Average water D/H ratios of carbonaceous chondrites.[a]

	D/H ($\times 10^6$)	$1\sigma_m$	N	Reference
CI1	171.7	1.5	5	Eiler and Kitchen (2004)
CM2	141.3	4.8	5	Eiler and Kitchen (2004)
Tagish Lake carb. poor	197.4	4.4	20	Engrand et al. (2003)
Tagish Lake carb. rich	199.1	3.2	23	Engrand et al. (2003)
Tagish Lake (average)	198.3	2.6	43	Engrand et al. (2003)
Al Rais (CR2)	232.2	13.4	6	Guan and Zolensky (1997)

[a] The $1\sigma_m$ error is the standard error of the mean. N represents the number of data points from which we have calculated the average. For the CR2 chondrites, we have not reported the Renazzo data from Deloule and Robert (1995), because they are not tabulated. For the Al Rais data (Guan and Zolensky, 1997), we have not taken into account two points which are not definitely ascribed to phyllosilicates. The SMOW value adopted to transform data expressed as δD_{SMOW} in the litterature is 155.8×10^{-6} (Deloule and Robert, 1995).

The hydrogen isotopic composition of carbonaceous chondrites (CCs) has been the focus of extensive work for the last 50 yr. Some workers perform chemical treatment before isotopic measurements, providing thus a D/H ratio dominated by that of soluble and/or insoluble organic matter (e.g., Halbout et al., 1990; Ehrenfreund et al., 2001). Other studies provide bulk D/H ratios that do not distinguish between the two main hydrogen carrier phases of carbonaceous chondrites, organic molecules and water (e.g., Boato, 1954; Robert and Epstein, 1982; Kerridge, 1985; Robert et al., 1987). For consistency we will compare our data to similar datasets that report the water hydrogen isotopic composition, measured either using new step combustion microanalytical methods (Eiler and Kitchen, 2001, 2004), or the ion probe (Deloule and Robert, 1995; Guan and Zolensky, 1997; Engrand et al., 2003).

The D/H ratios of tochilinite-rich CCMs show little dispersion ($\sigma_m = 1.7\%$, Table 4 and Fig. 5), suggesting a quite homogeneous population. Tochilinite-rich CCMs and CM2 chondrites D/H ratios have similar variation ranges (117.6×10^{-6} to 138.4×10^{-6} and 125.1×10^{-6} to 151.0×10^{-6} respectively, Table 4, Fig. 5). Further, the average value D/H ratio of tochilinite-rich CCMs, $(131.8 \pm 3.7) \times 10^{-6}$ (Table 4), agrees well with that of CM2 chondrites, D/H = $(141.4 \pm 4.8) \times 10^{-6}$ (Table 5). Thus, the hydrogen isotopic composition of water confirms the CM2 classification inferred from mineralogy for tochilinite-rich CCMs. In addition, the rough positive correlation observed between the modal abundance of anhydrous grains of tochilinite-rich CCMs and their D/H ratio (Fig. 6) has also been observed by Eiler and Kitchen (2004) for CM2 chondrites. These authors have demonstrated that D/H ratios are anticorrelated with the mineralogical alteration index, itself anticorrelated with the modal abundance of anhydrous grains (Browning et al., 1996). The only persisting difference between tochilinite-rich CCMs and CM2 chondrites is the high abundance of saponite in the former. In this respect, tochilinite-rich CCMs compare to the CM2 chondrite Murray (Zolensky, 1993), to Bells, an unusual CM2 chondrite (Brearley, 1995), to Essebi and MAC-87300, unclassified C2 meteorites (Zolensky et al., 1993) and to the metamorphosed chondrites Y-86720 and B-7904 (Zolensky et al., 1993). We also note that hydrated clasts in the CBb chondrite QUE-94411 (Greshake et al., 2002) and CM1 clasts in Kaidun are also saponite-rich (Zolensky et al., 1996a; Zolensky and Ivanov, 2003).

The D/H ratios of magnetite-rich, olivine-rich CCMs show little dispersion ($\sigma_m = 2.0\%$, see Table 4 and Fig. 5), suggesting they form a quite homogeneous population. The D/H ratios of magnetite-rich, olivine-rich CCMs do not compare well to any of the carbonaceous chondrite groups with which they are mineralogically related. They have D/H ratios compatible with the low values of the carbonate-poor lithology of the ungrouped C2 chondrite Tagish Lake (Fig. 5), and of CR2 chondrites (Fig. 5). The average D/H ratio of magnetite-rich, olivine-rich CCMs ($137.7 \pm 10.5 \times 10^{-6}$, Table 4) is however different from the average D/H ratios of carbonate-poor lithology of the ungrouped C2 chondrite Tagish Lake ($197.4 \pm 4.4 \times 10^{-6}$, Table 5), and of the CR2 chondrites ($222.1 \pm 20.0 \times 10^{-6}$, Table 5).

The D/H ratios of magnetite-rich, olivine-poor CCMs show a higher dispersion ($\sigma_m = 7.6\%$ and Fig. 4), indicative of a more heterogeneous population. The limited size of our population (4 objects, and 5 D/H ratios measured) however precludes any definitive conclusions. With the exception of CCM Y8, magnetite-rich, olivine-poor have lower D/H ratios than CI1 chondrites, to which they are mineralogically related (Table 1). The high D/H value obtained for CCM Y8 (D/H = 170.1×10^{-6}, Table 4) overlaps with the lowest D/H ratios measured for Tagish Lake, Renazzo and Al Rais (Fig. 4). It is worth noting that this CCM group shows the lowest D/H ratio (D/H = 115.0×10^{-6}, Table 4) of any carbonaceous chondrite material.

Although the study of the hydrogen isotopic composition has not fully resolved the classification ambiguity of magnetite-rich CCMs (Gounelle et al., 2003 and section 3), the trends suggested by the mineralogical observations (Table 1) are confirmed by the isotopic data. Magnetite-rich, olivine-poor CCMs (linked to CR2 chondrites and the ungrouped chondrite Tagish Lake; Table 1) have lower D/H ratios than magnetite-rich, olivine-rich CCMs (linked to CI1 chondrites; Table 1). This is compatible with CI1 chondrites having lower D/H ratios than CR2 chondrites and the carbonate-poor lithology of the ungrouped C2 chondrite Tagish Lake. The large dispersion of the D/H values of magnetite-rich, olivine-poor CCMs, as well as a lower average value than CI1 chondrites prevents, however, a definitive CI1 classification for the magnetite-rich, olivine-poor CCMs. Similarly, the discrepancy between the average D/H ratios of magnetite-rich, olivine-rich CCMs and the ungrouped C2 chondrite Tagish Lake and CR2 chondrites does not allow a definitive association of magnetite-rich, olivine-poor CCMs with these chondrites.

Tochilinite-rich CCMs are, among the different CCMs subclasses, closest to a carbonaceous chondrites counterpart, the CM2 chondrites, in terms of mineralogy and hydrogen isotopic composition. This strengthens the conclusion that the CM2 chondrites, though exhibiting some variability, is a relatively

well identified and well-behaved chondrite group (Zolensky et al., 1997). On the other hand, the strong mineralogical and isotopic discrepancies between magnetite-rich, olivine-poor CCMs with CI1 chondrites and of magnetite-rich, olivine-rich CCMs with Tagish Lake (carbonate-poor) and CR2 chondrites suggest that there is an important component of C1 and C2 matter which is not sampled by carbonaceous chondrites currently available in our collections. The diversity of CCMs in howardites is reminiscent of the diversity of microclasts and clasts observed in the Kaidun microbreccia meteorite (Zolensky and Ivanov, 2003). The view of the asteroid belt offered by (micro)clasts seems to be different, and possibly more complete, than the one offered by meteorites.

4.2. Comparison of CCMs with Micrometeorites

Comparison of CCMs with micrometeorites is meaningful since both samples belong to the same size fraction (< 1 mm), and show strong mineralogical similarities (see Gounelle et al., 2003). To investigate the mineralogical relationship between micrometeorites and CCMs, we compare below the water D/H ratios of these two populations of submillimeter-sized extraterrestrial material.

The hydrogen isotopic composition of stratospheric interplanetary dust particles has been studied in great detail for the past 15 yr with the ion probe (for a recent review, see Messenger, 2002). The use of a Cs^+ beam (McKeegan et al., 1985; McKeegan et al., 1987; Messenger et al., 1996; Messenger, 2000; Aléon, 2001) prevents the possibility of distinguishing between phyllosilicates and organics as the source of H^+ (D^+) ions. Aléon et al. (2001) have however estimated the D/H ratio of IDPs water using regression lines between D/H and C/H ratios.

The study of Engrand et al. (1999) provides a large dataset for the hydrogen isotopic composition of phyllosilicates water from Antarctic micrometeorites (AMMs). Because AMMs have spent ~50 000 yr in the blue ice before collection (Maurette et al., 1990), and 8 h in contact with melted water during collection (Maurette et al., 1994), it is important to examine a possible hydrogen isotopic exchange of AMMs water with Antarctic water. Exchange and contamination experiments performed by Engrand and colleagues (Engrand et al., 1999) suggest that there is little isotopic exchange before and during collection. In addition, the isotopic composition of Antarctic ice is quite significantly lighter than the average value of AMMs ($\delta D_{SMOW} \sim -300$ ‰ for the water vs. $\delta D_{SMOW} \sim 0$ ‰ for AMMs; Engrand et al., 1999). This rules out hydrogen isotopic exchange between AMMs and Antarctic water to be responsible for the SMOW-like D/H ratio of AMMs.

An important observation is that the D/H variation range of CCMs ($112.8–203.8 \times 10^{-6}$) is almost exactly identical to that of a MMs ($128.4–194.5 \times 10^{-6}$; Fig. 5). Further, when average values of the whole populations are compared, the match between CCMs and MMs is good ($152.0 \pm 4.8 \times 10^{-6}$ and $161.2 \pm 3.8 \times 10^{-6}$ respectively). Within 2σ error bars, the two average values are identical. This match is not observed for any carbonaceous chondrites group. The similarity of D/H ratios of CCMs and micrometeorites appear to be a robust observation. Indeed, not only do CCMs and micrometeorites belong to the same size fraction and have comparable mineralogy (Gounelle et al., 2003); they also share the same water hydrogen isotopic composition.

The similarity between CCMs and micrometeorites suggests that the nature of the micrometeorites present in the inner Solar System has not changed over the history of the Solar System (see below for a discussion of the timing of incorporation of CCMs within howardites). The constancy of the micrometeorite composition is a remarkable fact, especially because the carbon- and water-rich micrometeoritic flux to Earth differs radically from the meteoritic one dominated by ordinary chondrites (Grady, 2000).

Astronomical evidence for the rarity of asteroids spectroscopically related to ordinary chondrites has been reviewed by Meibom and Clark (1999). Some researchers have proposed that S-type asteroids could be related to ordinary chondrites, but that they now appear spectroscopically diverse because of space weathering, i.e., bombardment of the asteroid surface by micrometeorites, cosmic rays, etc. (e.g., Chapman, 1996). Recently, Shestopalov and Golubeva (2004) analyzed experiments simulating space weathering (maturation) of ordinary chondrites; under no conditions could they bring the spectral properties of matured ordinary chondrites and S asteroids to match. They concluded that the difference between the reflectance spectra of ordinary chondrites and those of large main-belt S-type asteroids is determined not only by space weathering of asteroidal surfaces but also by systematic differences in the material composition (Shestopalov and Golubeva, 2004). On the other hand, Jedicke et al. (2004) have shown there exists a robust correlation between the dynamical age of S asteroid families and their color. The younger the family, the more similar its color is to ordinary chondrites. From these observations Jedicke and colleagues suggest that most S-complex asteroids could be ordinary chondrites parent bodies. In addition, the chemical and mineralogical properties of the S-asteroid Eros, visited by the NEAR spacecraft in 2000, matches that of ordinary chondrites (McCoy, 2001).

Regardless the abundance of ordinary chondrites asteroids in the asteroid belt, the long-term domination of carbonaceous chondritic matter in the micrometeorite flux is not understood yet. Current understanding on the micrometeorites production (by asteroidal collisions), transport (via Poynting-Robertson drag) and delivery onto Earth states that most of micrometeorites originate from a small number of asteroidal families (Kortenkamp et al., 2001). This would suggest that C-type asteroids, putative parent bodies of carbonaceous chondritic micrometeorites, have often (always?) dominated the dust production in the Solar System. In any case, the apparent constancy of the composition of the micrometeorite flux is an important constrain for models aiming at describing the origin and evolution of dust in the Solar System.

4.3. Implications for the Origin of Water on Earth

4.3.1. The fossil nature of CCMs

Carbonaceous chondritic microclasts are foreign *micrometeoritic objects* trapped on the HED parent asteroid. The exact timing of incorporation of microclasts in howardites is not known, but must have taken place before the lithification, or compaction, of howardites. Compaction ages of meteorites are poorly known but might range from a few Ma to a few 10 Ma

relative to the formation of the earliest solids (e.g., Caffe and MacDougall, 1988; Woolum and Hohenberg, 1993). It is therefore likely that carbonaceous chondritic microclasts have been incorporated in the howardite parent asteroid within the first 100 Ma of Solar System history. Additional arguments in favor of an early incorporation of carbonaceous chondritic microclasts are the overall decrease with time of the micrometeorites and meteorites flux (Hartmann et al., 2000), as well as the overall increase with time of relative velocities. In other words, micrometeorites were more numerous, and less likely to be destroyed during impact onto the howardite parent asteroid in early Solar System than later on. We note also that carbonates found in CI1 chondrites that are known to form ~20 Ma after the crystallization of the first solids (Endress et al., 1996) are absent from magnetite-rich, olivine-poor CCMs. This could be because CCMs have been ejected from their parent body before the epoch of carbonate formation, i.e., within the first 20 Ma of Solar System. Although we cannot constrain the trapping date better than within 100 Ma after the formation of the first solids, CCMs can be considered as *fossil micrometeorites* that have been trapped in the howardite parent asteroid in the early Solar System. As such, CCMs are, for the time being, the best proxy available to us of the matter that was present in inner Solar System when the Earth, and possibly other planets, was endowed with water.

4.3.2. Origin of the Earth's water and the late veneer(s)

The origin of water on Earth is still a matter of debate (Robert, 2001; Drake and Righter, 2002). Although some researchers contend that the Earth has accreted wet (Abe et al., 2000), the most likely origin is a late veneer of hydrous primitive bodies (e.g., Wänke, 1981; Chyba, 1990; Morbidelli et al., 2000). Two possible sources of water are usually considered: cometary ice, or structural water in phyllosilicates found in hydrous carbonaceous meteorites and micrometeorites. The large D/H ratio ($310 \pm 40 \times 10^{-6}$) in three Oort cloud cometary water (Eberhardt et al., 1995; Bockelée-Morvan et al., 1998; Meier et al., 1998) compared to the terrestrial value ($149 \pm 3 \times 10^{-6}$) probably excludes Oort cloud cometary ice as the major contributor to the late veneer. At present, the hydrogen isotopic composition of Jupiter family comets is unknown. Because of their lower D/H ratios, phyllosilicate-rich carbonaceous chondrite matter, in the form of micrometeorites (Maurette et al., 2000a,b), asteroids (e.g., Dauphas et al., 2000) or large planetary embryos (Morbidelli et al., 2000), is still a viable possibility.

The average D/H ratio of CCMs phyllosilicates water is $(152.0 \pm 4.8) \times 10^{-6}$ ($1\sigma_m$), which is indistinguishable within error from the terrestrial value ($149 \pm 3 \times 10^{-6}$). It is worth noting that this is the best match obtained so far for phyllosilicate structural water found in carbonaceous chondritic matter (Fig. 5). The average water D/H ratio of CI1 chondrites ($164.3 \pm 1.4 \times 10^{-6}$; Table 5), CR2 chondrites ($222.1 \pm 20.0 \times 10^{-6}$; Table 5) and the ungrouped C2 chondrite Tagish Lake ($198.3 \pm 2.3 \times 10^{-6}$; Table 5) are higher than that of the Earth. CM2 chondrites have a lower average D/H ratio ($135.2 \pm 4.6 \times 10^{-6}$; Table 5) than the Earth.

We would like to emphasize that the very good match between the average D/H ratio of carbonaceous chondritic microclasts and that of the Earth water can hardly be considered a coincidence. The match is even more remarkable since 1) there is no single carbonaceous chondrite group for which a similar match exists 2) three different kinds of microclasts are required to make the D/H ratio of the Earth. Carbonaceous chondritic microclasts could have therefore played a role in the endowment of Earth with water. If matter like carbonaceous chondritic microclasts in howardites has delivered the Earth's water, we must address three important questions:

1. What was the actual size range of the late veneer material? Maurette and coworkers (2000a,b) have suggested that dust was the dominant agent of the late veneer. Asteroid-sized objects are also a possibility, but have apparently been ruled out for dynamical reasons (Morbidelli et al., 2000). Morbidelli et al. (2000) have proposed that planetary embryos with lunar to martian masses were likely candidates for the origin of water on Earth. In such a case, CCMs could be fragments representative of these larger objects. While it has long been considered that large objects would impact Earth in a catastrophic fashion, leading to an appreciable loss of water (Ahrens, 1993), recent numerical simulations show that the retention factor of volatile compounds such as water could be as high as 80% (Genda and Abe, 2003). This leaves two contrasting mechanisms: a continuous supply of water (micrometeorites) and a stochastic delivery (embryos). Because only the *average* D/H value of three distinct CCMs populations match the D/H of the Earth, our data would at first sight support a continuous delivery of the Earth water by micrometeorites, rather than a stochastic one. Indeed, in the case of a stochastic event, it is expected that terrestrial water originates from the contribution of a unique impactor. It has however recently been proposed that carbonaceous chondrites of different types, and different isotopic compositions, can represent different depths of the same asteroid or embryo (Young et al., 1999). Because it is not yet clear if carbonaceous chondrites of different types belong to different parent bodies or to the same one, our data cannot help in identifying the size of the late veneer agent(s).

2. How do we reconcile hydrogen and osmium isotopic constraints on the late veneer material? The terrestrial mantle contains an excess of highly siderophile elements (HSEs) compared to equilibrium models of core-mantle segregation (e.g., Morgan et al., 2001). This HSE excess has been interpreted as originating from a late veneer of chondritic matter (Wänke, 1981). The carbonaceous chondrite matter that delivered water onto Earth would have codelivered between one and five times the needed amount of HSEs, depending on how well the late veneer is mixed in the upper mantle (Drake and Righter, 2002). A problem arises from the fact that the osmium isotopic composition of carbonaceous chondrites, $^{187}Os/^{188}Os < 0.1275$ (Walker et al., 2002b), is lower than that of the estimated primitive upper mantle (PUM, $^{187}Os/^{188}Os_{PUM} = 0.1296 \pm 0.0008$; (e.g., Meisel et al., 2001). If taken at face value, the PUM estimated osmium isotopic composition excludes carbonaceous chondrites as the HSE late veneer agent. With the caveat of possible errors in the core-mantle equilibrium models, we envision a range of "solutions" to the apparent conflict between H and Os isotopic evidence.

One possibility is that the osmium isotopic composition of the carbonaceous matter that was present in the inner Solar System 4.5 Ga ago might have been different than that of

carbonaceous chondrites falling on Earth today. Forthcoming measurements of the osmium isotopic composition of chondritic carbonaceous microclasts in howardites will help test this possibility.

Alternatively, the delivery of water to Earth might have occurred early enough in the Earth history that the siderophile elements brought together with the water have been incorporated to the core. The present excess of HSEs would have then be delivered by a second late veneer agent, with an osmium isotopic composition compatible with that of the PUM. This possibility could be considered part of a wet accretion scenario (Abe et al., 2000).

Finally, the precision of the PUM estimate might have been grossly overestimated. First the PUM may not represent the bulk silicate Earth (BSE) (Dauphas et al., 2002). Second, given the materials from which the PUM estimate has been derived (i.e., Proterozoic to Phanerozoic mantle xenoliths and massifs), it is at least possible that this estimate includes recycled components such as radiogenic subducted slabs mixed back to the mantle via convection (Walker et al., 2002a) and/or pyroxenitic components (Allègre and Turcotte, 1986; Meibom et al., 2002, 2004). Further, the basic tenet behind this estimate is that Os isotopes, due to the high compatibility of Os, are not affected by metasomatic events. However it has been recently demonstrated that, because of the high reactivity of sulfides, the main Os carrier phase in the mantle, this may not be the case (Alard et al., 2000). In addition, metasomatic alteration of the Os isotopic composition of the mantle toward more radiogenic values has been recently demonstrated to occur on a worldwide scale (Meibom and Frei, 2002; Meibom et al., 2003). Thus, once all quantitative and qualitative uncertainties are taken into account, the $^{187}Os/^{188}Os$ ratio of the Earth's mantle ranges between 0.125, as given by abyssal peridotites (Snow and Reisberg, 1995), and 0.130, as given by the PUM (Meisel et al., 2001). The value for carbonaceous chondrites ($^{187}Os/^{188}Os$ <0.1275) lies within these bounds, making it possible that the same carbonaceous chondrite late veneer agent has delivered both water and the excess of HSEs observed in the Earth's mantle.

3. What other atmophile elements were delivered together with water? This problem can be simply stated: there is no known sample in the meteorite collection whose abundances of volatile elements and compounds match exactly that of the Earth's atmosphere. It is for example well known that the present noble gases abundance and isotopic composition of the atmosphere is incompatible with a delivery by carbonaceous chondrite matter. In particular, the Earth is known to have an excess of xenon relative to the other noble gases when compared to carbonaceous chondrites. Understanding the origin of the Earth's atmosphere requires a detailed geochemical knowledge of the possible contributors, but also of the relative timescales of accretion, differentiation and atmosphere formation. It is well beyond the scope of the present paper, all the more so since the chemical and isotopic inventory of volatile elements and compounds in CCMs is still in its infancy.

5. SUMMARY

The hydrogen isotopic composition of water and hydroxyl compounds contained in 13 CCMs (divided in tochilinite-rich, magnetite-rich, olivine-poor and magnetite-rich, olivine-rich subclasses) has been measured with the ion probe. Both mineralogy and the hydrogen isotopic composition are consistent with the conclusion that tochilinite-rich CCMs represent true CM2 chondritic matter. On the other hand, the difficulty of finding a good isotopic and mineralogical match between magnetite-rich CCMs and any known group of carbonaceous chondrites suggests that magnetite-rich CCMs represent a new kind of chondritic matter, not yet sampled in the meteorite collection. This finding supports the idea that (micro)clasts in howardites and in other meteorites offer a less biased view of the asteroid belt than available meteorites.

The D/H variation range of CCMs ($112.8–203.8 \times 10^{-6}$) is almost exactly identical to that of Antarctic micrometeorites (AMMs) ($128.4–194.5 \times 10^{-6}$) and both populations have identical average D/H ratios within 2σ error bars. CCMs and AMMs belong to the same size fraction, have comparable mineralogy (Gounelle et al., 2003) and similar water hydrogen isotopic composition (this work). The similarity between CCMs and AMMs demonstrates that the nature of the micrometeorites has not been substantially modified. The micrometeorite flux composition has been and continues to be dominated by a mixture of CM2-like; magnetite-rich, olivine-poor; magnetite-rich, olivine-rich carbonaceous chondritic matter exemplified by CCMs found in howardites. Because CCMs have not suffered effects of atmospheric entry as AMMs have (Toppani et al., 2001), their properties can provide first hand information on micrometeorites' chemistry, mineralogy and isotopic composition.

CCMs are *fossil* micrometeorites, present in the early Solar system at a time close to that of the Earth's accretion of water. The average D/H ratio of the whole population of CCMs is $(152.0 \pm 4.8) \times 10^{-6}$ ($1\sigma_m$, $n = 34$). This value compares extremely well to that of the Earth, $(149 \pm 3) \times 10^{-6}$. The match between the CCMs D/H ratio and that of the Earth is especially remarkable because 1) three different populations of CCMs are needed to make the D/H ratio of the Earth; 2) there is no single carbonaceous chondrite group for which a similar match exists. This observation suggests that CCMs might be representative of the late veneer agent(s) that delivered water on Earth. Whether this late veneer agent took the form of planetary embryos or micrometeorites, and whether it codelivered other atmophile elements cannot be resolved from the present work. Constraints on the osmium isotopic composition of the Earth's mantle leaves room for a range of different carriers of the late veneer. It is therefore possible that the CCMs that have delivered the Earth's water have also contributed to the excess of HSEs observed in the mantle.

Acknowledgments—We are grateful to Dr Anders Meibom and an anonymous reviewer whose comments have considerably improved the manuscript. We are grateful to Dr. Koeberl for handling the manuscript. Fruitful conversations were held with Drs Michel Maurette and François Robert. The D/H measurements were made with the national ion microprobe facility Cameca IMS1270 at CRPG, Nancy. The help of Denis Mangin and Michel Champenois with the ion microprobe is greatly acknowledged. We acknowledge IN2P3, PNP, and IPEV for their continuous support of micrometeorite research at Orsay.

Associate editor: C. Koeberl

REFERENCES

Abe Y., Ohtani E., Okuchi T., Righter K., and Drake M. J. (2000) Water in the early Earth. In *Origin of the Earth and Moon* (eds. R. M. Canup and K. Righter), pp. 413–433. Arizona University Press.

Ahrens T. J. (1993) Impact erosion of terrestrial planetary atmospheres. *Ann. Rev. Earth Planet. Sci.* **21,** 525–555.

Alard O., Griffin W. L., Lorand J.-P., Jackson S. E., and O'Reilly S. Y. (2000) Non-chondritic distribution of the highly siderophile elements in mantle sulphides. *Nature* **407,** 891–894.

Aléon J., Engrand C., Robert F., and Chaussidon M. (2001) Clues to the origin of interplanetary dust particles from the isotopic study of their hydrogen-bearing phases. *Geochim. Cosmochim. Acta* **65,** 4399–4412.

Allègre C. J. and Turcotte D. L. (1986) Implications of two-component marble-cake mantle. *Nature* **323,** 123–127.

Binzel R. P. and Xu S. (1993) Chips off of Asteroid 4 Vesta : Evidence for the parent body of basaltic achondrite meteorites. *Science* **260,** 186–191.

Boato G. (1954) The isotopic composition of hydrogen and carbon in the carbonaceous chondrites. *Geochim. Cosmochim. Acta* **6,** 209–220.

Bockelée-Morvan D., Gautier D., Lis D. C., Young K., Keene J., Phillips T., Owen T., Crovisier J., Goldsmith P. F., Bergin E. A., Despois D., and Wooten A. (1998) Deuterated water in comet C/1996 B2 (Hyakutake) and its implications for the origin of comets. *Icarus* **133,** 147–162.

Brearley A. J. (1995) Aqueous alteration and brecciation in Bells, an unusual, saponite-bearing, CM chondrite. *Geochim. Cosmochim. Acta* **59,** 2291–2317.

Browning L. B., McSween H. Y., and Zolensky M. E. (1996) Correlated alteration effects in CM carbonaceous chondrites. *Geochim. Cosmochim. Acta* **60,** 2621–2633.

Caffe M. W. and MacDougall J. D. (1988) Compaction ages. In *Meteorites and Early Solar System* (eds. J. F. Kerridge and M. S. Matthews), pp. 289–298. Arizona University Press.

Chapman C. R. (1996) S-type asteroids, ordinary chondrites and space weathering: The evidence from *Galileo*'s fly-bys of Gaspra and Ida. *Meteor. Planet. Sci.* **31,** 699–725.

Chyba C. F. (1990) Impact delivery and erosion of planetary oceans in the early inner Solar System. *Nature* **343,** 129–133.

Dauphas N., Robert F., and Marty B. (2000) The late asteroidal and cometary bombardment of Earth as recorded in water deuterium to protium ratio. *Icarus* **148,** 508–512.

Dauphas N., Reisberg L., and Marty B. (2002) An alternative explanation for the distribution of highly siderophile elements in the Earth. *Geochem. J.* **36,** 409–419.

Deloule E., France-Lanord C., and Albarède F. (1991) D/H analysis of minerals by ion probe. *Geochim. Cosmochim. Acta* (special publication)**3,** 53–62.

Deloule E. and Robert F. (1995) Interstellar water in meteorites? *Geochim. Cosmochim. Acta* **59,** 4695–4706.

Drake M. J. and Righter K. (2002) Determining the composition of the Earth. *Nature* **416,** 39–44.

Duprat J., Engrand C., Maurette M., Gounelle M., Hammer C., and Kurat G. (2003) The CONCORDIA-collection: Pristine contemporary micrometeorites from central Antarctica surface snow (abstract). *Lunar Planet. Sci.***34,** 1727.

Eberhardt P., Reber M., Krankowsky D., and Hodges R. R. (1995) The D/H and $^{18}O/^{16}O$ ratios in water from comet P/Halley. *Astron. Astrophys.* **302,** 301–316.

Ehrenfreund P., Glavin D. P., Botta O., Cooper G., and Bada J. L. (2001) Extraterrestrial amino acids in Orgueil and Ivuna: Tracing the parent body of CI type carbonaceous chondrites. *Proc. Natl. Acad. Sci. USA* **98,** 2138–2141.

Eiler J. M. and Kitchen N. (2001) Hydrogen-isotope analysis of nanomole (picoliter) quantities of H_2O. *Geochim. Cosmochim. Acta* **65,** 4467–4479.

Eiler J. M. and Kitchen N. (2004) Hydrogen isotopic evidence for the origin and evolution of the carbonaceous chondrites. *Geochim. Cosmochim. Acta* **68,** 1395–1411.

Endress M., Zinner E. and Bischoff A. (1996) Early aqueous activity on primitive meteorite parent bodies. *Nature* **379,** 701–703.

Engrand C. and Maurette M. (1998) Carbonaceous micrometeorites from Antarctica. *Meteor. Planet. Sci.* **33,** 565–580.

Engrand C., Deloule E., Robert F., Maurette M., and Kurat G. (1999) Extraterrestrial water in micrometeorites and cosmic spherules from Antarctica : An ion microprobe study. *Meteor. Planet. Sci.* **34,** 773–787.

Engrand C., Gounelle M., Zolensky M. E., and Duprat J. (2003) About Tagish Lake as a potential parent-body for polar micrometeorites: Clues from their oxygen isotopic compositions (abstract). *Lunar Planet. Sci.* **34,** 1688.

Genda H. and Abe Y. (2003) Survival of a proto-atmosphere through the stage of giant impacts: The mechanical aspects. *Icarus* **164,** 149–162.

Gounelle M., Zolensky M. E., Tonui E., and Mikouchi T. (2001) Mineralogy of Togish Lake, a unique type 2 carbonaceous chondrite (abstract). *Lunar Planet. Sci.* **32,** 1616.

Gounelle M., Zolensky M. E., Liou J.-C., Bland P. A., and Alard O. (2003) Mineralogy of carbonaceous chondritic microclasts in howardites: Identification of C2 fossil micrometeorites. *Geochim. Cosmochim. Acta* **67,** 507–527.

Grady M. M. (2000) *Catalogue of Meteorites.* Cambridge University Press. 690 pp.

Greshake A., Krot A. N., Meibom A., Weisberg M. K., Zolensky M. E., and Keil K. (2002) Heavily-hydrated lithic clasts in CH chondrites and the related, metal-rich chondrites Queen Alexandra Range 94411 and Hammadah al Hamra 237. *Meteor. Planet. Sci.* **37,** 281–293.

Guan Y. and Zolensky M. E. (1997) The D/H ratios of round phyllosilicate and glass spherules in the Al Rais (CR) chondrite (abstract). *Lunar Planet. Sci. Conf.* **28,** 487–488.

Halbout J., Robert F., and Javoy M. (1990) Hydrogen and oxygen compositions in kerogen from the Orgueil meteorite: Clues to a solar origin. *Geochim. Cosmochim. Acta* **54,** 1453–1462.

Hartmann W. K., Ryder G., Dones L. and Grinspoon D. (2000) The time-dependent intense bombardment of the primordial Earth/Moon system. In *Origin of the Earth and Moon* (eds. R. M. Canup and K. Righter), pp. 493–512. University of Arizona Press.

Jedicke R., Nesvorny S., Whiteley R., Ivezic Z., and Juric M. (2004) An age-colour relationship for main-belt S-complex asteroid. *Nature* **429,** 275–277.

Kerridge J. F. (1985) Carbon, hydrogen and nitrogen in carbonaceous chondrites: Abundances and isotopic compositions in bulk samples. *Geochim. Cosmochim. Acta* **49,** 1707–1714.

Kortenkamp S. J., Dermott S. F., Fogle D. and Grogan K. (2001) Sources and orbital evolution of interplanetary dust accreted by the Earth. In *Accretion of Extraterrestrial Matter througout Earth's History* (eds. B. Peucker-Eherenbrink and B. Schmitz), pp. 13–30. Kluwer/Plenum.

Lee M. R. and Greenwood R. C. (1994) Alteration of calcium- and aluminium-rich inclusions in the Murray (CM2) carbonaceous chondrite. *Meteor. Planet. Sci.* **29,** 780–790.

MacKinnon I. D. R. and Zolensky M. E. (1984) Proposed structures for poorly characterized phases in CM2 carbonaceous chondrite meteorites. *Nature* **309,** 240–242.

MacPherson G. J. and Davis A. M. (1994) Refractory inclusions in the prototypical CM chondrite, Mighei. *Geochim. Cosmochim. Acta* **58,** 5599–5625.

Maurette M., Hammer C., and Pourchet M. (1990) Multidisciplinary investigations of new collections of Greenland and Antarctica micrometeorites. In *From Mantle to Meteorites*, pp. 87–126. Indian academy of sciences: Bangalore.

Maurette M., Olinger C., Christophe Michel-Lévy M., Kurat G., Pourchet M., Brandstätter F., and Bourot-Denise M. (1991) A collection of diverse micrometeorites recovered from 100 tons of Antarctic blue ice. *Nature* **351,** 44–47.

Maurette M., Immel G., Hammer C., Harvey R., Kurat G. and Taylor S. (1994) Collection and curation of IDPs from the Greenland and Antarctic ice sheets. In *Analysis of Interplanetary Dust, AIP Conference Proceedings,*Vol. 310 (eds. M. E. Zolensky, T. L. Wilson, F. J. M. Rietmeijer and G. J. Flynn), pp. 277–289. American Institute of Physics.

Maurette M., Gounelle M., Duprat J., Engrand C. and Matrajt G. (2000a) The "early-micrometeorites-accretion" scenario and the origin of the Earth's hydrosphere. In *Bioastronomy 99: A New Era in the Search for Life in the Universe* (eds. G. Lemarchand and K. Meech), pp. 263–284. Astronomical Society of the Pacific.

Maurette M., Duprat J., Engrand C., Kurat G., Gounelle M., Matrajt G., and Toppani A. (2000b) Accretion of neon, organics, CO_2, nitrogen and water from large interplanetary dust particles on the early Earth. *Planet. Space Sci.* **48,** 1117–1137.

McCoy T. J. (2001) The composition of 433 Eros: A mineralogical-chemical synthesis. *Meteor. Planet. Sci.* **36,** 1661–1672.

McKeegan K. D. (1987) Ion microprobe measurements of H, C, O, Mg and Si isotopic abundances in individual interplanetary dust particles. Ph.D. thesis, Washington University. 187 pp.

McKeegan K. D., Walker R. J., and Zinner E. (1985) Ion microprobe measurements of H, C, O, Mg and Si isotopic abundances in individual interplanetary dust particles. *Geochim. Cosmochim. Acta* **49,** 1971–1987.

McSween H. Y. J. (1979) Are carbonaceous chondrites primitive or processed? A review. *Rev. Geoph. Space Phys.* **17,** 1059–1078.

Meibom A. and Clark B. E. (1999) Evidence for the insignifiance of ordinary chondritic material in the asteroid belt. *Meteor. Planet. Sci.* **34,** 7–24.

Meibom A. and Frei R. (2002) Evidence for an ancient osmum isotopic reservoir in Earth. *Science* **296,** 516–518.

Meibom A., Sleep N. H., Chamberlain C. P., Coleman R. G., Frei R., Hren M. T., and Wooden J. L. (2002) Re-Os isotopic evidence for long-lived heterogeneity and equilibrium processes in Earth's upper mantle. *Nature* **419,** 705–708.

Meibom A., Anderson D. L., Sleep N. H., Frei R., Chamberlain C. P., Hren M. T., and Wooden J. L. (2003) Are high $^3He/^4He$ ratios in oceanic basalts an indicator of deep mantle plume components? *Earth Planet. Sci. Lett.* **208,** 197–204.

Meibom A., Frei R., and Sleep N. H. (2004) Osmium isotopic compositions of Os-rich platinum group element alloys from the Klamath and Siskiyou Mountains. *J. Geophys. Res.* **109,** B02203.

Meier R., Owen T. C., Matthews H. E., Jewitt D. C., Bockelée-Morvan D., Biver N., Crovisier J., and Gautier D. (1998) A determination of the HDO/H_2O ratio in comet C/1995 O1 (Hale-Bopp). *Science* **279,** 842–844.

Meisel T., Walker R. J., Irving A. J., and Lorand J.-P. (2001) Osmium isotopic compositions of mantle xenoliths: A global perspective. *Geochim. Cosmochim. Acta* **65,** 1311–1323.

Messenger S. (2000) Identification of molecular-cloud material in interplanetary dust particles. *Nature* **404,** 968–971.

Messenger S. (2002) Deuterium enrichments in interplanetary dust. *Planet. Space Sci.* **50,** 1221–1225.

Messenger S., Walker R. M., Clemett S. J., and Zare R. N. (1996) Deuterium enrichments in cluster IDPs (abstract). *Lunar Planet. Sci. Conf.* **27,** 867–868.

Morbidelli A., Chambers J. E., Lunine J., Petit J.-M., Robert F., Valsecchi G. B., and Cyr K. E. (2000) Source regions and time-scales for the origin of water on Earth. *Meteor. Planet. Sci.* **35,** 1309–1320.

Morgan J. W., Walker R. J., Brandon A. D., and Horan M. F. (2001) Siderophile elements in Earth's upper mantle and lunar breccias: Data synthesis suggests manifestations of the same late influx. *Meteor. Planet. Sci.* **36,** 1257–1276.

Nakamura T. (1999) Antarctic micrometeorites collected at the Dome Fuji Station. *Antarct. Meteor. Res.* **12,** 183–198.

Nakashima D., Nakamura T., and Noguchi T. (2003) Formation history of CI-like phyllosilicate-rich clasts in the Tsukuba meteorite inferred from mineralogy and noble gases signatures. *Earth Planet. Sci. Lett.* **212,** 321–336.

Rietmeijer F. J. M. (1998) Interplanetary dust particles. In *Planetary Materials*, Vol. 36 (ed. J. J. Papike), pp. 2.1–2.94. Mineralogical Society of America.

Robert F. (2001) The origin of water on Earth. *Science* **293,** 1056–1058.

Robert F. (2002) Water and organic matter D/H ratios in the solar system: A record of an early irradiation of the nebula? *Planet. Space Sci.* **50,** 1227–1234.

Robert F. and Epstein S. (1982) The concentration and isotopic composition of hydrogen, carbon and nitrogen in carbonaceous chondrites. *Geochim. Cosmochim. Acta* **46,** 81–95.

Robert F., Javoy M., Halbout J., Dimon B., and Merlivat L. (1987) Hydrogen isotope abundances in the solar system. Part II: Meteorites with terrestrial-like D/H ratio. *Geochim. Cosmochim. Acta* **51,** 1807–1822.

Shestopalov D. I. and Golubeva L. F. (2004) The optical maturation of a chondrite surface: Modeling for S-type asteroids and meteorites. *Solar System Res.* **38,** 203–211.

Snow J. E. and Reisberg L. (1995) Os isotopic systematics of the MORB mantle: Results from altered abyssal peridotites. *Earth Planet. Sci. Lett.* **133,** 411–421.

Taylor S., Lever J. H., and Harvey R. P. (1998) Accretion rate of cosmic spherules measured at South Pole. *Science* **392,** 899–903.

Tomeoka K. and Buseck P. R. (1988) Matrix mineralogy of the Orgueil CI carbonaceous chondrite. *Geochim. Cosmochim. Acta* **52,** 1627–1640.

Toppani A., Libourel G., Engrand C., and Maurette M. (2001) Experimental simulation of atmospheric entry of micrometeorites. *Meteor. Planet. Sci.* **36,** 1377–1396.

Walker R. J., Prichard H. M., Ishiwatari A., and Pimentel M. (2002a) The osmium isotopic composition of convecting upper mantle deduced from ophiolite chromites. *Geochim. Cosmochim. Acta* **66,** 329–345.

Walker R. J., Horan M. F., Morgan J. W., Becker H., Grossman J. N., and Rubin A. E. (2002b) Comparative ^{187}Re-^{187}Os systematics of chondrites: Implications regarding early solar system processes. *Geochim. Cosmochim. Acta* **66,** 4187–4201.

Wänke H. (1981) Constitution of terrestrial planets. *Phil. Trans. R. Soc. Lond. A* **303,** 287–302.

Weisberg M. K., Prinz M., Clayton R. N., and Mayeda T. K. (1993) The CR (Renazzo-type) carbonaceous chondrite and its implications. *Geochim. Cosmochim. Acta* **57,** 1567–1586.

Wilkening L. L. (1973) Foreign inclusions in stony meteorites—I. Carbonaceous chondritic xenoliths in the Kapoeta howardite. *Geochim. Cosmochim. Acta* **37,** 1985–1989.

Woolum D. S. and Hohenberg C. M. (1993) Energetic particle environment in the early solar system: Extremely long pre-compaction meteoritic ages or an enhanced early particle flux. In *Protostars and Planets III* (eds. E. H. Levy and J. I. Lunine), pp. 903–919. Arizona University Press.

Young E. D., Ash R. D., England P., and Rumble D. I. (1999) Fluid flow in chondritic parent bodies: Deciphering the compositions of planetesimals. *Science* **286,** 1331–1335.

Zolensky M., Barrett R., and Browning L. (1993) Mineralogy and composition of matrix and chondrule rims in carbonaceous chondrites. *Geochim. Cosmochim. Acta* **57,** 3123–3148.

Zolensky M., Hewins R. H., Mittlefehldt D. W., Lindstrom M. M., Xiao X., and Lipschutz M. E. (1992) Mineralogy, petrology and geochemistry of carbonaceous chondritic clasts in the LEW 85300 polymict eucrite. *Meteoritics* **27,** 596–604.

Zolensky M. E., Wilson T. L., Rietmeijer F. J. M., and Flynn G. J. (1994) *Analysis of Interplanetary Dust.* American Institute of Physics. 357 pp.

Zolensky M. E., Ivanov A. V., Yang V., and Ohsumi K. (1996a) The Kaidun meteorite : Mineralogy of an unusual CM1 clast. *Meteor. Planet. Sci.* **31,** 484–493.

Zolensky M. E., Weisberg M. K., Buchanan P. C., and Mittlefehldt D. W. (1996b) Mineralogy of carbonaceous chondrite clasts in HED achondrites and the Moon. *Meteor. Planet. Sci.* **31,** 518–537.

Zolensky M. E., Mittlefehldt D. W., Lipschutz M. E., Wang M.-S., Clayton R. N., Mayeda T. K., Grady M. M., Pillinger C., and Barber D. (1997) CM chondrites exhibit the complete petrologic range from type 2 to 1. *Geochim. Cosmochim. Acta* **61,** 5099–5115.

Zolensky M. and Ivanov A. (2003) The Kaidun microbreccia meteorite: A harvest from the inner and outer asteroid belt. *Chem. Geol.* **63,** 185–246.

Meteoritics & Planetary Science 40, Nr 6, 917–932 (2005)
Abstract available online at http://meteoritics.org

Small Antarctic micrometeorites: A mineralogical and in situ oxygen isotope study

Matthieu GOUNELLE[1, 2, 3*], Cécile ENGRAND[1, 5], Michel MAURETTE[1], Gero KURAT[4], Kevin D. McKEEGAN[5], and Franz BRANDSTÄTTER[4]

[1]CSNSM, Bâtiment 104, 91 405 Orsay Campus, France
[2]Université Paris XI, Bâtiment 104, 91 405 Orsay Campus, France
[3]Department of Mineralogy, The Natural History Museum, London SW7 5BD, UK
[4]Mineralogish-Petrographische Abteilung, Naturhistorisches Museum, Postfach 417, A-1014 Wien, Austria
[5]Department of Earth and Space Sciences, University of California—Los Angeles, Los Angeles, California 90095–1567, USA
[*]Corresponding author. E-mail: gounelle@csnsm.in2p3.fr

(Received 15 December 2004; revision accepted 05 April 2005)

Abstract–We have investigated the texture, bulk chemistry, mineralogy, as well as the anhydrous minerals oxygen isotopic composition of 67 small Antarctic micrometeorites (AMMs) collected at Cap Prudhomme, Antarctica, and belonging to the currently poorly studied size fraction 25–50 μm. When compared to larger (50–400 μm) micrometeorites collected at the same site in Antarctica with the same techniques, no significant differences are found between the two populations. We therefore conclude that the population of Cap Prudhomme AMMs is homogeneous over the size range 25–400 μm. In contrast, small AMMs have different textures, mineralogy, and oxygen isotopic compositions than those of stratospheric interplanetary dust particles (IDPs). Because small AMMs (<50 μm) overlap in size with IDPs, the differences between these two important sources of micrometeorites can no longer be attributed to a variation of the micrometeorite composition with size. Physical biases introduced by the collection procedures might account for these differences.

INTRODUCTION

Micrometeorites with sizes <1 mm account for most of the extraterrestrial matter accreting to Earth at present (Love and Brownlee 1993). Micrometeorites are a different and potentially more representative sample of the asteroid belt than meteorites, mainly because their dynamic evolution is controlled by Poynting-Robertson drag (Kortenkamp et al. 2001), as opposed to the conjunction of the Yarkovsky effect and orbital resonances with giant planets for meteorites (Vokrouhlicky and Farinella 2000). Prior to sample return from missions such as Stardust, which will bring back dust from comet Wild 2, and Hayabusa, which will sample the asteroid Itokawa, the main available micrometeorite sources are the polar ice caps and the stratosphere. Stratospheric interplanetary dust particles (IDPs) have been systematically collected by NASA at altitudes of ~20 km since 1981 (Brownlee 1985). Polar micrometeorites were first collected in the Greenland ice cap (e.g., Maurette et al. 1986). More recently, large numbers of micrometeorites have been collected in Antarctica in the blue ice fields of Terre Adélie, at Cap Prudhomme (e.g., Maurette et al. 1991) and at the nearby Astrolabe glacier (Gounelle et al. 1999), as well as at Yamato mountains (e.g., Terada et al. 2001). Water wells have provided micrometeorites at South Pole (Taylor et al. 1998), and at Dome Fuji (Nakamura et al. 1999). Recently Duprat et al. (2003) have collected micrometeorites in the surface snow in the Antarctic central regions (station CONCORDIA, Dome C).

All micrometeorite collections use complex procedures to recover relatively uncontaminated submillimeter dust from a diversity of environments. Different techniques are used for each environment, resulting in collections with their own characteristics, in terms of the number and nature of particles recovered. The differences are especially striking between Antarctic micrometeorites (AMMs) collected in blue ice (such as Cap Prudhomme) and the IDPs collected in the stratosphere. While IDPs are captured by using silicone oil-coated collectors attached on the wings of NASA U2 and ER2 stratospheric aircraft (Warren and Zolensky 1994), Cap Prudhomme micrometeorites are extracted from the blue ice after a procedure involving 1) melting blue ice with a steam

Table 1. Textural types of micrometeorites in the size fraction 25–50 μm. Xtal, fg, sc, and cs stand for crystalline, fine-grained, and scoriaceous micrometeorites, respectively.

Textural type	xtal	fg	sc	cs
Number of particles	10	42	8	7
Percentage relative to the extraterrestrial matter	15	63	12	10

generator, 2) mechanical pumping of the melt water, and 3) filtering of the water using three different mesh sizes: 25–50 μm, 50–100 μm, and 100–400 μm (Maurette et al. 1991). This results in Cap Prudhomme AMMs belonging to the size range of 25–400 μm, whereas IDPs are smaller than 50 μm (Rietmeijer 1998).

AMMs with sizes larger than 50 μm are very different from IDPs in terms of morphology and mineralogy (Engrand and Maurette 1998; Kurat et al. 1994b). For example, AMMs lack anhydrous chondritic porous particles, and often exhibit large isotopic anomalies (Messenger 2000), or hypothesized interstellar components, such as glass embedded with metal and sulfides (GEMS) (Bradley 1994; Bradley et al. 1999). Carbonates and sulfides, commonly found in IDPs (Tomeoka and Buseck 1985; Zolensky and Thomas 1995) are absent or rare in the Cap Prudomme AMMs collection (Duprat et al. 2003; Engrand and Maurette 1998).

Differences between AMMs and IDPs might be due to collection biases, to a temporal change in the composition of the micrometeorite flux onto the Earth, or to a variation of the micrometeorite composition with size. The latter possibility is strengthened by the fact that the numerous differences between micrometeorites (both stratospheric and polar) and meteorites indicate that the composition of extraterrestrial matter does indeed vary with size (Engrand and Maurette 1998; Rietmeijer 1998).

The goals of this paper are threefold. First, we want to characterize the morphology, bulk chemistry, mineralogy, and anhydrous grains oxygen isotopic composition of AMMs belonging to the small size fraction (25–50 μm), providing a large data set for samples described so far in only one abstract (Maurette et al. 1992b). Second, we will compare small AMMs with larger AMMs (50–400 mm), also collected at Cap Prudhomme. This comparison will enable us to assess if the AMMs population is homogeneous within the whole size range 25–400 μm, independently of collection biases. Third, because the 25–50 μm AMMs overlap in size with the largest IDPs, we will be able to directly compare AMMs and IDPs. This is an important step in understanding if the differences observed between large AMMs and IDPs can be ascribed to a size bias or is due to other causes.

SAMPLES AND INSTRUMENTAL METHODS

386 particles with sizes between 25 and 50 μm and that were collected at Cap Prudhomme during the 1991 field season (Maurette et al. 1992a) were first optically selected for their black color and irregular surface, and then were embedded in epoxy and polished. Broad selection criteria were used to ensure that no unusual extraterrestrial particle was missed. These particles were studied at the Vienna Naturhistorisches Museum with a scanning electron microscope (SEM) JEOL JSM-6400 run at 15 keV and equipped with a KEVEX energy dispersive X-ray (EDX) analysis system. Micrometeorites were identified from their chondritic EDX spectrum. Backscattered electron images (BSE) of selected micrometeorites were then taken with a PHILIPS XL 40 field emission gun scanning electron microscope at ONERA (Chatillon, France). The mineral grains and matrix of micrometeorites were analyzed using a SX100 CAMECA electron microprobe (EMP) operated at 15 kV with a beam current of 20 nA (Vienna University), and with a CAMEBAX EMP operated at 15 kV with a beam current of 10 nA (Paris University). All these analyses were performed using a focused beam with a diameter of ~1 μm. Bulk chemistry was determined with a SX100 CAMECA electron microprobe operated at 15 keV and 40 nA (Paris University), with a defocused beam ~30 μm. Detection limits are around 0.02 wt% for all elements. Natural as well as synthetic standards were used; data were corrected using the PAP Cameca program.

The oxygen isotopic composition of anhydrous minerals was determined with the UCLA CAMECA IMS 1270 following the procedures previously used for the analyses of larger micrometeorites (Engrand et al. 1999a). Data are expressed in the usual delta (per mil) unit, relative to the standard mean ocean water (SMOW). The precision of the analyses was of the order of ~1‰ for both $\delta^{17}O_{SMOW}$ and $\delta^{18}O_{SMOW}$. For the sake of simplicity, we will drop the index SMOW throughout this paper. Pyroxene and olivine analyses were corrected for matrix effect using the San Carlos olivine standard. Analyses of an enstatite standard under our experimental conditions show that relative variations of instrumental mass fractionation compared to San Carlos olivine are <1‰/amu.

RESULTS

Texture

Sixty-seven particles with an EDX spectrum compatible with a chondritic composition were found among the 386 particles. Micrometeorites were found to belong to the four textural types (Table 1) previously described by Kurat et al. (1994b): 10 crystalline AMMs consisting of an assemblage of anhydrous silicates (olivine and pyroxene), 42 fine-grained AMMs consisting of a phyllosilicate-rich matrix supporting olivine, pyroxene and accessory minerals, 8 scoriaceous AMMs consisting of a highly vesicular melt which contain

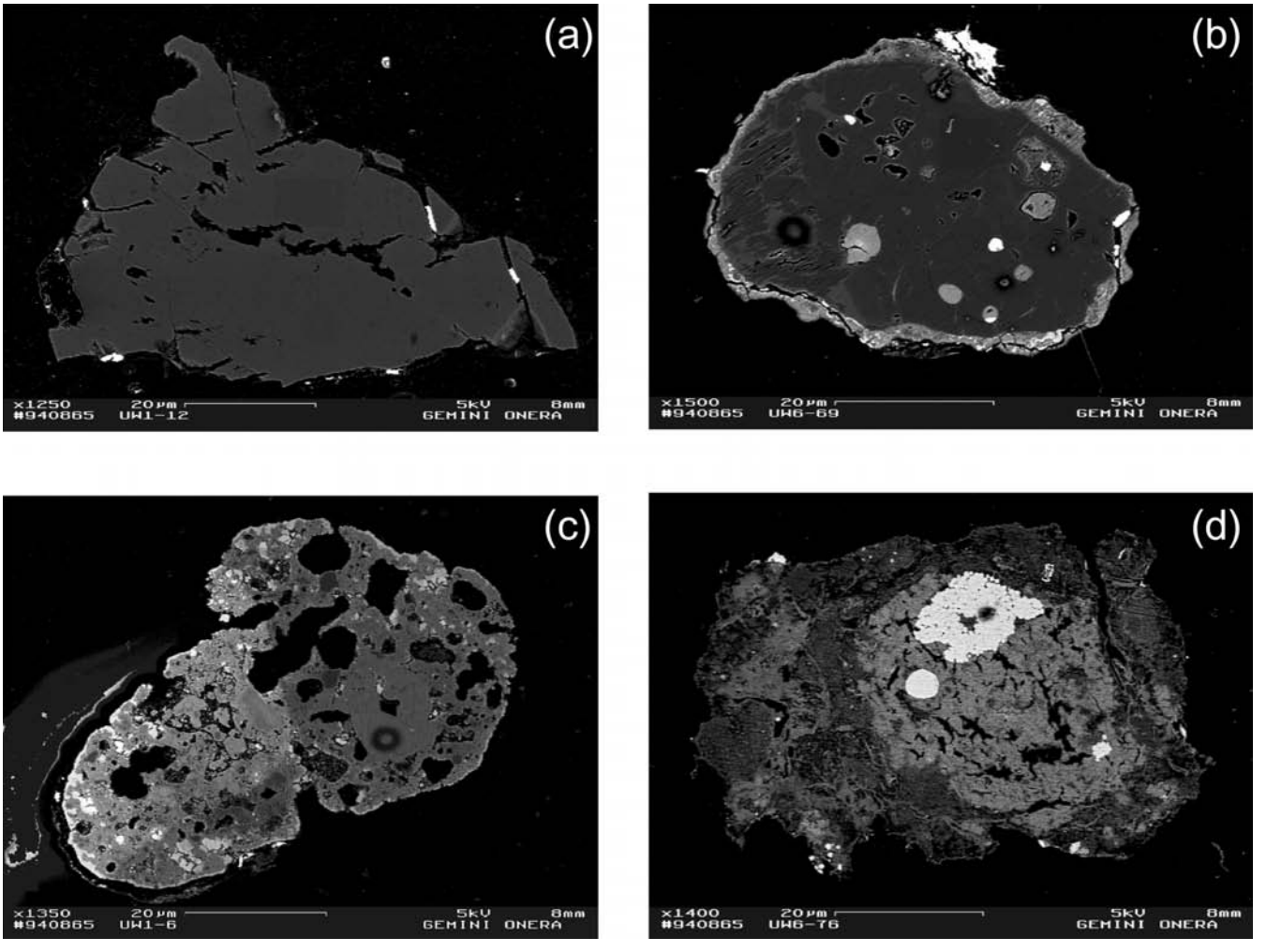

Fig. 1. Backscattered scanning electron images of 25–50 μm AMMs observed in polished sections: a) Crystalline micrometeorite with irregular morphology; b) Crystalline micrometeorite with round morphology; c) Scoriaceous micrometeorite; d) Fine-grained micrometeorite with magnetite framboids.

rare relic phases (olivine or pyroxene) (Fig. 1), and 7 cosmic spherules consisting of glass, olivine and magnetite assemblages. Both crystalline and fine-grained AMMs are considered as unmelted (UMMs) micrometeorites, contrary to scoriaceous micrometeorites and cosmic spherules that are partially and fully melted, respectively (Engrand and Maurette 1998).

Crystalline AMMs have morphologies varying from irregular to round (Fig. 1). Usually, irregular particles consist of a monocrystal, are highly cracked, and show no magnetite rim. Conversely, round grains display complex textures, e.g., porphyritic and poikilitic, and have a magnetite rim that is either discontinuous or completely surrounds the particle. Fine-grained AMMs have morphologies varying from irregular to round with a discontinuous to complete magnetite rim coating the external surface (Fig. 1). Scoriaceous AMMs have round to oval morphologies (Fig. 1), and most of them are coated with a magnetite rim either complete or discontinuous. Four cosmic spherules have perfectly round morphologies, two exhibit circular voids indicating the probable loss of a Fe-Ni nugget (Taylor et al. 2000), while one is broken. Magnetite rim appears in three spherules out of four.

Bulk Chemistry

The bulk chemistry of 38 randomly selected particles was determined using EMP with a defocused beam of approximately 30 μm. The bulk chemical compositions are reported in the Appendix and presented in Fig. 2 in the form of an atomic ternary diagram Mg-Fe-Si. Crystalline micrometeorites are very enriched in magnesium compared to fine-grained AMMs and scoriaceous micrometeorites. Fine-grained micrometeorites have varying compositions from very Mg-rich to very Fe-rich. Scoriaceous micrometeorites (with the exception of UW6-29) compositions overlap with fine-grained AMMs compositions. Cosmic spherules have a

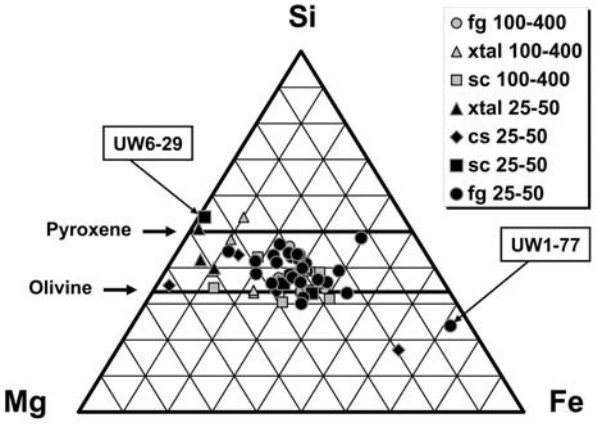

Fig. 2. An atomic ternary diagram (Si-Fe-Mg) showing the bulk compositions of small micrometeorites (data in the Appendix). A comparison is made with the bulk compositions of the large AMMs (Kurat et al. 1994) measured with the same technique (EMP defocused beam). The pyroxene and the olivine solid solutions are shown as solid lines.

very wide range of compositions, from very Fe-poor (UW1-66) to very iron-rich (UW1-28).

Mineralogy and Mineral Chemistry

Crystalline AMMs consist mainly of olivine and pyroxene set in a glass of feldspathic composition; accessory minerals are poorly defined iron oxyhydroxides, Fe-Ni metal, magnetite and low-Ni sulfides (very rare). Pyroxene is the most abundant mineral in crystalline AMMs (see Table 2 for compositions). Low-Ca pyroxenes are fairly iron-poor (0.91–6.82 wt% FeO) and have a highly variable CaO content (0.27–2.12 wt%). One pigeonite grain ($En_{91}Wo_6$) associated with iron-poor olivine (Fo_{97}) and one augite grain ($En_{54}Wo_2$) have been found. The pigeonite has a high Cr_2O_3 content (1.33 wt%) and a low FeO/MnO ratio (~3), whereas the augite has a moderate Cr_2O_3 content (0.53 wt%) and an intermediate FeO/MnO ratio (~38). Olivine is the second most abundant mineral in crystalline micrometeorites (see Table 3 for compositions). Most of the olivines are iron-rich (Fa_{15}–Fa_{36}), except for UW6-69, which has a forsteritic composition (Fo_{97}). All olivines are poor in Ni (NiO < 0.06 wt%) regardless of their iron content. The FeO/MnO ratio ranges from 60 to 80 for the iron-rich olivines and equals 10 for the forsteritic one. The CaO content is intermediary and varies between 0.10 and 0.39 wt%. The Cr_2O_3 content is highly variable (0.09–0.71 wt%), with the high chromium content corresponding to the forsteritic olivine. The Al_2O_3 content varies between 0.03 and 0.20 wt%. Accessory phases are usually too small for electron microprobe analyses. Magnetite is common in some particles as a thin (~1 μm) discontinuous or complete rim (Table 1 and Fig. 1). Iron oxyhydroxide occurs in voids and close to the particle surface. Low-Ni metal is enclosed in pyroxenes of variable composition ($En_{86}Wo_4$–$En_{98}Wo_1$). One low-Ni iron sulfide has been found.

Fine-grained AMMs consist of a fine-grained matrix supporting isolated pyroxene and olivine grains, magnetite, low-Ni iron sulfides, chromite, metal, and iron oxyhydroxides. The composition of matrix together with its variable EMP analysis totals (Table 4) suggests that it consists mainly of dehydrated phyllosilicates with a wide range of compositions and minor iron-nickel sulfides. Low-Ca pyroxene grains are the most abundant grains isolated in the matrix of fine-grained AMMs (see Table 2 for compositions). A predominant population has enstatitic compositions ($En_{94–99}Wo_3$) and a minor population is more iron-rich ($En_{84}Wo_0$). The CaO content ranges from 0.25 to 1.85 wt%. The FeO/MnO ratio ranges from 4 to 29. The Cr_2O_3 and TiO_2 contents are intermediate (0.09–1.00 wt% and 0.04–0.17 wt%, respectively) except for the iron-rich pyroxene ($En_{82}Wo_2$) that has a high TiO_2 content (0.64 wt%). One pigeonite was found; it has a low FeO/MnO ratio (~11) and a high Al_2O_3 content (4.05 wt%). Most of the olivines have (see Table 3 for compositions) a high iron content ($Fo_{78–82}$), while one is iron-poor (Fo_{97}). They have intermediary minor elements contents (Cr_2O_3 0.04–0.84 wt% and TiO_2 below 0.07 wt%), and their FeO/MnO ratio varies from 12 to 68. Accessory minerals are more abundant in fine-grained AMMs than in crystalline AMMs. Magnetite, besides being common as a rim at particle surface, often occurs as loose, subhedral grains in the matrix. A few Mg-rich magnetite grains have been found both in the matrix and in the rim. A magnetite rich in titanium (10.4 wt% TiO_2) has been found on the side of a particle associated with a magnetite of pure composition. Magnetite framboids have been found in the matrix of two fine-grained AMMs (Fig. 3). A Mg-phosphate has been found, but was too small to be analyzed with the electron microprobe. Because this grain is located in a particle void, it could be of terrestrial origin. Low-Ni iron sulfides, chromite, Fe-Ni metal, and iron oxyhydroxides (all rare) have been found in the matrix.

Scoriaceous small AMMs are dominated by glass, quenched olivine and quench magnetite—all too fine-grained to allow EMPA analysis. Accessory minerals, also very fine-grained, are low-Ni sulfides and chromium-rich magnetite. Very few relic grains have been found: just one fayalitic olivine (Fo_{63}) and one iron-poor low-Ca pyroxene ($En_{99}Wo_0$). The olivine has a quite high FeO/MnO ratio (~68) and is fairly poor in minor elements (except for CaO = 0.3 wt%). The pyroxene has a quite low FeO/MnO ratio (~11), is fairly poor in minor elements, and has a CaO content compatible with an orthopyroxene composition (0.13 wt%).

Cosmic spherules are dominated by glass, pyroxene, olivine, and magnetite. Most minerals are too small to provide reliable EMP data. The olivine (Table 3) is iron-rich ($Fo_{57–62}$). The glass is depleted in K_2O and Na_2O and has a high Ca content (Table 4).

Table 2. Analyses of pyroxenes from micrometeorites belonging to the 25–50 μm size fraction. Data in wt%. Xtal, fg, and sc stand for crystalline, fine-grained, and scoriaceous micrometeorites, respectively. B.d. stands for below detection limit.

Micrometeorite	UW1-12	UW6-74	UW5-93	UW6-69	UW3-56	UW6-53	UW6-53	UW1-44	UW6-29	UW5-104	UW5-104
Textural type	xtal	xtal	xtal	xtal	xtal	xtal	xtal	xtal	sc	fg	fg
SiO_2	58.8	55.1	52.3	56.6	55.8	58.5	58.2	57.6	59.1	56.0	58.1
TiO_2	0.03	0.22	0.26	0.12	0.17	0.10	0.11	0.09	0.04	0.11	0.08
Al_2O_3	0.31	1.65	1.17	1.23	1.38	0.66	0.63	0.96	0.15	1.44	0.46
Cr_2O_3	0.6	0.99	0.53	1.33	0.81	0.59	0.63	1.15	0.35	1.04	0.76
FeO	1.91	6.82	10.9	1.72	4.44	0.91	2.02	2.06	0.78	4.09	1.74
MnO	0.09	0.58	0.29	0.6	0.72	0.09	0.10	0.46	0.07	0.37	0.49
MgO	38.9	32.5	18.7	34.9	34.4	39.4	38.2	37.0	40.4	35.1	38.0
NiO	b.d.	b.d.	b.d.	b.d.	b.d.	b.d.	0.05	b.d.	b.d.	b.d.	b.d.
CaO	0.27	2.12	13.7	3.31	1.34	0.55	0.60	1.28	0.13	1.39	0.67
Na_2O	b.d.	b.d.	0.67	0.04	0.07	b.d.	b.d.	b.d.	b.d.	0.03	b.d.
K_2O	b.d.	b.d.	b.d.	0.03	b.d.	b.d.	b.d.	b.d.	b.d.	b.d.	b.d.
Total	100.91	99.98	98.52	99.88	99.12	100.79	100.53	100.61	101.02	99.57	100.32

Micrometeorite	UW5-104	UW5-104	UW6-12	UW1-69	UW3-23	UW6-18	UW5-62	UW6-85	UW6-55	UW5-93
Textural type	fg	fg	fg	fg	fg	fg	fg	fg	fg	fg
SiO_2	56.0	58.1	58.2	58.6	57.4	57.3	58.6	54.3	53.0	52.6
TiO_2	0.11	0.08	0.04	0.09	0.17	0.14	0.08	0.64	0.28	0.07
Al_2O_3	1.44	0.46	0.33	0.48	1.48	0.83	0.65	0.87	4.05	0.98
Cr_2O_3	1.04	0.76	0.69	0.60	1.00	0.53	0.67	0.45	1.31	0.78
FeO	4.09	1.74	3.63	1.29	2.12	2.33	0.63	11.1	7.3	4.26
MnO	0.37	0.49	0.13	0.17	0.55	0.11	0.21	0.51	0.62	0.26
MgO	35.1	38.0	37.4	39.0	36.2	38.0	39.0	30.9	29.6	38.7
NiO	b.d.	b.d.	b.d.	b.d.	b.d.	0.13	b.d.	b.d.	0.03	b.d.
CaO	1.39	0.67	0.25	0.57	1.85	0.62	0.63	0.82	3.1	1.29
Na_2O	0.03	b.d.	b.d.	b.d.	b.d.	b.d.	0.04	b.d.	b.d.	b.d.
K_2O	b.d.	b.d.	b.d.	b.d.	b.d.	b.d.	b.d.	b.d.	0.03	b.d.
Total	99.57	100.32	100.67	100.79	100.77	99.98	100.51	99.59	99.32	98.94

Table 3. Analyses of olivines from micrometeorites belonging to the 25–50 μm size fraction. Data in wt%. Xtal, fg, and sc stand for crystalline, fine-grained, and scoriaceous micrometeorites respectively. B.d. stands for below detection limit.

Micrometeorite	UW1-06	UW5-93	UW6-69	UW6-88	UW6-88	UW6-85	UW6-55	UW3-04	UW6-85	UW1-66
Textural type	sc	xtal	xtal	xtal	xtal	fg	fg	fg	fg	cs
SiO_2	35.8	35.2	41.1	37.9	39.1	38.7	40.6	41.3	37.7	35
TiO_2	b.d.	b.d.	0.04	b.d.	b.d.	0.05	0.03	b.d.	0.07	0.08
Al_2O_3	0.04	b.d.	0.2	0.13	0.06	b.d.	0.04	0.04	0.17	0.48
Cr_2O_3	0.09	0.09	0.71	0.47	0.26	0.04	0.31	0.76	0.83	0.46
FeO	32	31.7	2.5	19.8	14.04	16.7	11.4	2.84	19.9	32.1
MnO	0.47	0.4	0.24	0.29	0.22	0.43	0.67	0.23	0.39	0.22
MgO	30	31.4	54.1	40.5	45.6	43.2	45.8	54.7	39	29.3
NiO	b.d.	b.d.	b.d.	0.06	0.03	b.d.	b.d.	b.d.	0.14	0.06
CaO	0.31	0.25	0.39	0.12	0.1	b.d.	0.16	0.19	0.08	0.47
Na_2O	0.08	b.d.	b.d.	b.d.	b.d.	b.d.	b.d.	b.d.	b.d.	b.d.
K_2O	b.d.	b.d.	b.d.	b.d.	b.d.	b.d.	b.d.	b.d.	b.d.	b.d.
Total	98.79	99.04	99.28	99.27	99.41	99.12	99.01	100.06	98.28	98.21

Table 4. Representative analyses of matrix of fine-grained micrometeorites and glass of cosmic spherules. Data in wt%. Xtal, fg, sc, and cs stand for crystalline, fine-grained, scoriaceous, and cosmic spherules, respectively. B.d. stands for below detection limit. N.a. stands for non-analyzed.

Micrometeorite	UW1-03	UW1-03	UW1-74	UW3-03	UW3-28	UW5-96	UW5-104	UW3-25	UW6-92
Textural type	fg	fg	fg	fg	fg	fg	fg	cs	cs
SiO_2	30.3	37.7	39.3	27.1	27.3	35.6	33.3	47.9	38.6
TiO_2	0.11	0.09	0.19	0.11	0.06	0.13	0.1	0.23	0.13
Al_2O_3	3.36	1.65	2.55	2.71	3.25	2.43	2.71	3.01	3.93
Cr_2O_3	0.26	0.46	0.62	0.3	0.12	0.53	0.46	b.d.	b.d.
FeO	45.1	29.1	24.8	47.3	44.5	35.8	35.4	19.4	24.3
MnO	0.26	0.29	0.44	0.25	0.23	0.07	0.14	0.62	0.22
MgO	14.1	22.8	18.8	13.9	17.4	6.81	11.6	20.1	29.7
NiO	0.11	0.11	0.14	0.07	0.22	0.08	0.22	0.04	b.d.
CaO	1.13	0.55	0.85	0.1	0.59	0.4	0.4	5.18	1.25
Na_2O	0.2	0.16	0.58	0.05	0.03	0.54	0.51	b.d.	b.d.
K_2O	0.14	0.21	0.16	b.d.	b.d.	0.45	0.13	b.d.	b.d.
P_2O_5	0.14	0.28	b.d.	0.22	0.08	b.d.	b.d.	n.a.	n.a.
S	0.14	0.17	0.31	0.07	0.08	0.3	0.42	n.a.	n.a.
Total	95.35	93.57	88.74	92.18	93.86	83.14	85.39	96.46	98.27

The Oxygen Isotopic Composition of Anhydrous Minerals

The oxygen isotopic compositions of pyroxenes and olivines belonging to 8 crystalline, 5 fine-grained, and 1 scoriaceous micrometeorite are reported in Table 5 and shown on a three-isotope diagram in Fig. 4.

For olivine and pyroxene grains from crystalline micrometeorites, $\delta^{18}O$ varies from −11.0 to 1.0‰ and $\delta^{17}O$ varies from −11.7 to −0.80‰, respectively. For olivines and pyroxenes from fine-grained micrometeorites, $\delta^{18}O$ varies from −4.1 to 2.5‰ and $\delta^{17}O$ varies from −4.9 to 2.3‰, respectively. A single pyroxene grain large enough to be measured in a scoriaceous micrometeorite has $\delta^{18}O = 8.5 \pm 0.6$‰ (1σ) and $\delta^{17}O = 4.7 \pm 0.8$‰ (1σ).

No substantial differences have been observed between the oxygen isotopic composition of olivine and pyroxene (Table 5 and Fig. 4), although pyroxenes tend to show a somewhat larger range in $\delta^{18}O$ and $\delta^{17}O$ than olivine grains (Table 5 and Fig. 4).

Most of the analyzed grains plot between the terrestrial fractionation (TF) line and the carbonaceous chondrite anhydrous minerals (CCAM) line (Clayton et al. 1973). All analyses seem to be well-fitted by the Young and Russell (YR) line (Young and Russell 1998). The displacement from the TF line, expressed as $\Delta^{17}O$, varies from −6.0 to −1.0‰ and from −3.3 to 1.0‰ for crystalline and fine-grained micrometeorites, respectively. The pyroxene belonging to a scoriaceous micrometeorite has $\Delta^{17}O$ within uncertainty of terrestrial (0.3‰ ± 0.9‰). Different grains belonging to the same micrometeorite can have different oxygen isotopic compositions (see Table 5).

DISCUSSION

Comparison with Large AMMs

In order to assess whether or not there might be true differences between micrometeorites of different sizes, it is

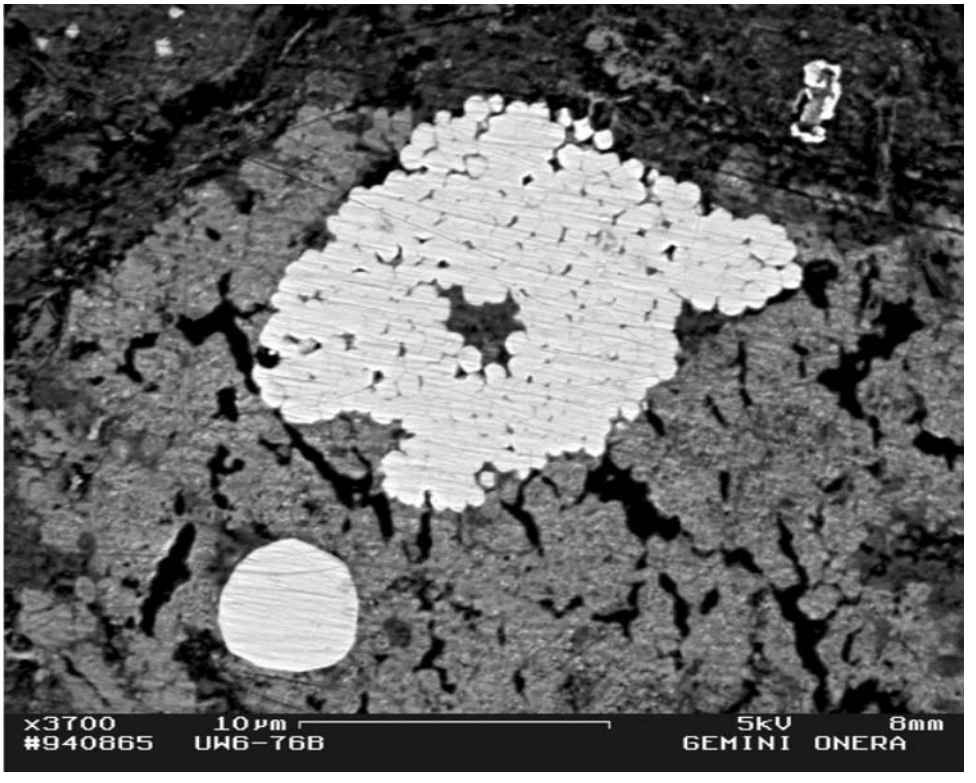

Fig. 3. Backscattered scanning electron image of the interior of a fine-grained micrometeorite. Magnetite framboids are embedded in dehydrated phyllosilicate.

important to first ascertain if AMMs of the 25–50 μm size fraction are true small micrometeorites or mere fragments of a larger size fraction generated during the collection procedure. The presence of a partial to complete magnetite rim on the majority of small micrometeorites (Fig. 1) is a good indicator for the 25–50 μm size fraction AMMs not being fragments of larger micrometeorites. However, this is not a definite criterion, since it depends critically on the sample preparation. Inappropriate polishing might fail to reveal magnetite rims (Toppani et al. 2001). A more reliable criterion is the presence or absence of glassy cosmic spherules. These objects are very fragile, and the presence of one glassy spherule out of seven cosmic spherules is an indication that micrometeorites endure minimum fragmentation during the collection procedure.

Small AMMs (25–50 μm size fraction) do not exhibit unusual textures when compared to the larger AMMs (50–400 μm size fraction): all of the 67 particles studied fall in the four textural groups previously defined by Kurat et al. (1994b). However, the relative abundance of textural types among the small AMMs differs significantly from that of larger AMMs. The unmelted micrometeorites group (fine-grained and crystalline) is by far the dominant population in the 25–50 μm size fraction, whereas larger AMMs display a roughly equal proportion of UMMs and partially melted AMMs (Engrand and Maurette 1998). The UMMs/scoria ratio is ~7 for the 25–50 μm size fraction and ~1 for the 50–400 size fraction (Engrand and Maurette 1998; Kurat et al. 1994b). Similarly, the abundance of cosmic spherules is lower in the small size fraction (10%) compared to the 100–400 μm size fraction (20%) (Engrand and Maurette 1998). These observations suggest that small particles are less heated during atmospheric entry than larger ones, in agreement with atmospheric entry models (Love and Brownlee 1991).

Though the overall chemical compositions of the two populations overlap well (Fig. 2), the bulk chemistry of small micrometeorites present minor differences with the bulk chemistry of large micrometeorites. One scoriaceous small micrometeorite (UW6-29) is conspicuously enriched in magnesium and silicon compared to large micrometeorites. However, this micrometeorite contains a large enstatite grain that displaces its bulk composition toward the enstatite pole (Mg-Si) of the ternary diagram. Two crystalline micrometeorites are also Mg-rich compared to large crystalline micrometeorites. Because enstatite monocrystals are common in the 25–50 μm size fraction, this observation does not constitute an intrinsic difference between small and large AMMs. One fine-grained micrometeorite (UW1-77) has a composition plotting outside the field defined by large micrometeorites (Fig. 2). Cosmic spherules have a wide range of compositions, compatible with that of other Antarctic spherules (Taylor et al. 2000).

Small crystalline AMMs display similar textural and mineralogical characteristics as their larger counterparts.

Table 5. Oxygen isotopic compositions of individual minerals in small AMMs (25–50 μm). Xtal, fg, and sc stand for crystalline, fine-grained, scoriaceous, micrometeorites, respectively. Px and ol stand for pyroxene and olivine, respectively.

Sample	Textural type	Mineral	Mineral composition	$\delta^{18}O$ (‰)[a]	1σ (‰)	$\delta^{17}O$ (‰)[a]	1σ (‰)	$\Delta^{17}O$ (‰)[b]
UW1-12	xtal	px	$En_{97}Wo_0$	–0.9	0.9	–3.0	0.8	–2.5
UW1-44_1	xtal	px	$Ens_{96}Wo_1$	–2.0	1.1	–3.3	0.9	–2.3
UW1-69_1	xtal	px	$En_{98}Wo_1$	0.3	1.4	–3.1	1.3	–3.3
UW3-23	fg	px	$En_{97}Wo_3$	1.0	0.9	–2.8	0.8	–3.3
UW3-4_1	fg	ol	Fo_{97}	1.6	1.1	–0.4	0.9	–1.2
UW3-60	xtal	px	$En_{92}Wo_9$	1.0	0.9	–1.6	0.7	–2.1
UW3-93_1	xtal	px	$En_{94}Wo_2$	0.4	1.1	–0.8	1.0	–1.0
UW6_53_1	fg	px	$En_{99}Wo_1$	–4.1	1.4	–4.9	1.5	–2.8
UW6_53_2	fg	px	$En_{97}Wo_1$	–1.5	1.2	–2.7	1.5	–1.9
UW6_55_1	fg	ol	Fo_{88}	0.6	1.3	0.5	1.4	0.2
UW6_55_2	fg	px	$En_{89}Wo_6$	2.0	1.3	1.7	1.4	0.7
UW6_69_1	xtal	px	$En_{97}Wo_6$	–3.6	1.2	–5.1	1.4	–3.2
UW6_69_2	xtal	ol	Fo_{98}	–4.2	1.6	–6.6	1.4	–4.4
UW6_74_1	xtal	ol	Fo_{90}	–2.4	1.4	–3.2	1.4	–2.0
UW6_85_1	fg	px	$En_{84}Wo_1$	0.6	1.0	0.3	1.0	0.0
UW6_85_2	fg	ol	Fo_{78}	2.5	1.4	2.3	1.6	1.0
UW6-29	sc	px	$En_{99}Wo_0$	8.5	0.6	4.7	0.8	0.3
UW3-56_1	xtal	px	$En_{93}Wo_3$	–11.0	0.9	–11.7	0.7	–6.0
UW3-56_2	xtal	px	$En_{89}Wo_2$	–4.9	1.2	–7.7	0.9	–5.2

[a]Relative to SMOW.
[b]$\Delta^{17}O = \delta^{17}O - 0.52 \times \delta^{18}O$.

Poikilitic and porphyritic textures described by Kurat (1994b) are found in addition to common, irregularly shaped particles. Olivines from small crystalline AMMs compare well to the olivine population described by Kurat et al. (1994b). They have completely overlapping iron contents ($Fo_{64–97}$ compared to $Fo_{63–98}$), compatible FeO/MnO ratios (60–80 compared to 15–130) and similar minor elements contents. Low-Ca pyroxene from the crystalline small AMMs show similar compositional ranges to pyroxene grains from large crystalline AMMs (Beckerling and Bischoff 1995). The iron content of pyroxene studied by Beckerling and Bischoff (1995) peaks at enstatitic compositions comparable to that of pyroxene grains from crystalline small AMMs. In addition, the FeO/MnO ratio in pyroxene from the subset of porphyritic and poikilitic particles analyzed by Beckerling and Bischoff (1995) ranges from 3 to 42 and includes the FeO/MnO range found in our study.

The mineralogy of fine-grained small AMMs is broadly similar to that of their larger counterparts. Relic pyroxene and olivine grains form two distinct compositional groups: an iron-poor group ($Fs_{<6}$ and $Fo_{<3}$, respectively) and an iron-rich group ($Fs_{>16}$ and $Fa_{>18}$, respectively), which have been reported by all AMMs researchers (e.g., Christophe Michel-Lévy and Bourot-Denise 1992; Genge et al. 1997; Kurat et al. 1994b; Steele 1992). The intermediate content of minor elements from relic olivine and pyroxene grains also matches the ranges of similar grains from larger AMMs (Fig. 5). Matrix compositions of fine-grained AMMs match the matrix analyses of phyllosilicate-like phases (Genge et al. 1997; Nakamura et al. 2001; Noguchi et al. 2002). Framboidal magnetite is present in two small fine-grained AMMs. These peculiar magnetite textures being typical of CI carbonaceous chondrites (Jedwab 1967; Kerridge 1970), their presence in an Antarctic micrometeorite has been used by Kurat et al. (1992) to define CI AMMs. These authors report 7 CI AMMs out of 110 UMMs (i.e., an abundance relative to UMMs of ~6%). Among small AMMs, the abundance of framboid-bearing AMMs is ~4% relative to UMMs. This figure is compatible with that of the larger size fraction given the statistical uncertainties due to our (relatively) small number of particles studied. Contrary to large AMMs (Engrand et al. 1999a; Greshake et al. 1996; Hoppe et al. 1995; Kurat et al. 1994a; Kurat et al. 1994c), no calcium-aluminium-rich inclusion (CAI) was found among small AMMs. However, this can easily be explained on statistical grounds, since the abundance of CAIs is ~0.4% in large AMMs (Gounelle 2000). Small AMMs have an average surface that is 10 times smaller than that of large AMMs. Consequently, we should have examined ~1000 small AMMs to expect one single CAI. As we studied only 67 of them, the absence of CAIs in our restricted set of particles is not conclusive.

The texture of scoriaceous small AMMs is identical to that of large scoriaceous AMMs. The mineralogy of scoriaceous small AMMs compares well to that of their larger counterparts. Kurat et al. (1994b) report fayalitic olivine ($Fo_{68–77}$) in scoriaceous particles, the composition of which is close to that of the only olivine we found among scoriaceous small AMMs (Fo_{63}). Pyroxene compositions from small

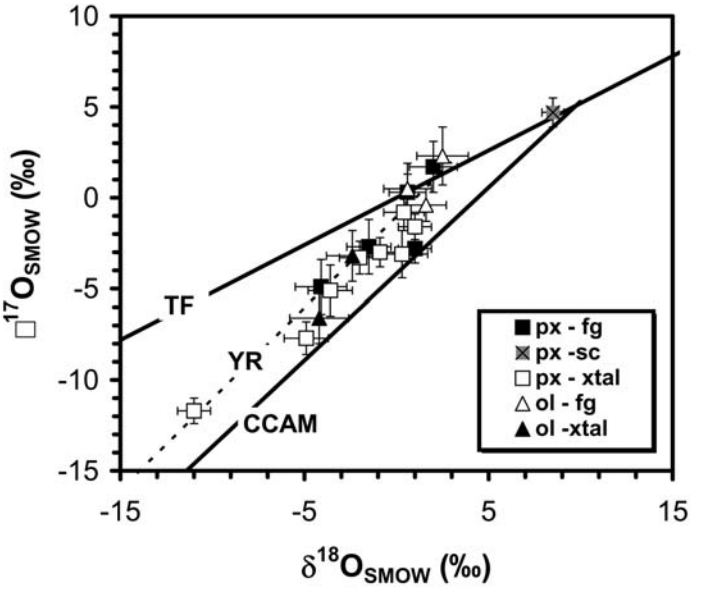

Fig. 4. Three-isotope diagram showing the oxygen isotopic composition of olivine and pyroxene grains belonging to 25–50 μm micrometeorites. The carbonaceous chondrite anhydrous minerals (CCAM) mixing line (Clayton et al. 1973), and the Young and Russell (YR) line (Young and Russell 1998) are shown for reference. Terrestrial samples lie along the terrestrial fractionation (TF) mixing line. Error bars are 1σ.

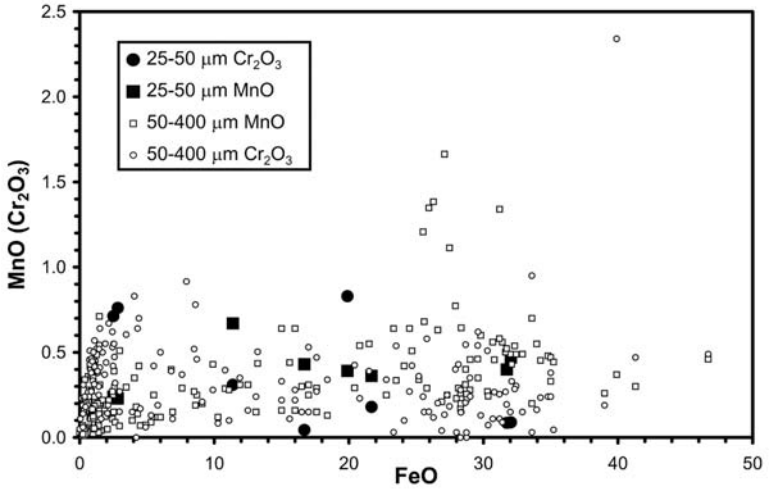

Fig. 5. Minor element contents (wt%) of olivine grains in 25–50 μm micrometeorites (this work) compared to 50–400 μm micrometeorites (data from Orsay and Vienna laboratories).

($En_{99}Wo_0$) and large ($En_{95-99}Wo_{0-1}$) AMMs are likewise similar.

Our cosmic spherule population is too small to meaningfully compare it with the cosmic spherules found in the 50–400 μm size fraction. It is worth noting, however, that all the textures we observe are compatible with the textures described for large Antarctic cosmic spherules (Taylor et al. 2000). In addition, the bulk composition of the 25–50 μm cosmic spherules (Fig. 2) matches that of larger cosmic spherules (Brownlee et al. 1997).

Figure 6 displays the oxygen isotopic composition of pyroxene and olivine grains belonging to small AMMs (this work) together with that of pyroxene and olivine grains belonging to large AMMs (Engrand et al. 1999a). Both populations have similar oxygen isotope systematics. The only minor difference is that in the 25–50 μm size fraction, the most ^{16}O-poor grain is a pyroxene, while in the 50–400 μm size fraction, it is an olivine. Olivine and pyroxene from small and large micrometeorites obviously sample the same oxygen isotopic reservoir.

Engrand et al. (1999c) have measured the hydrogen isotopic composition of six fine-grained and three

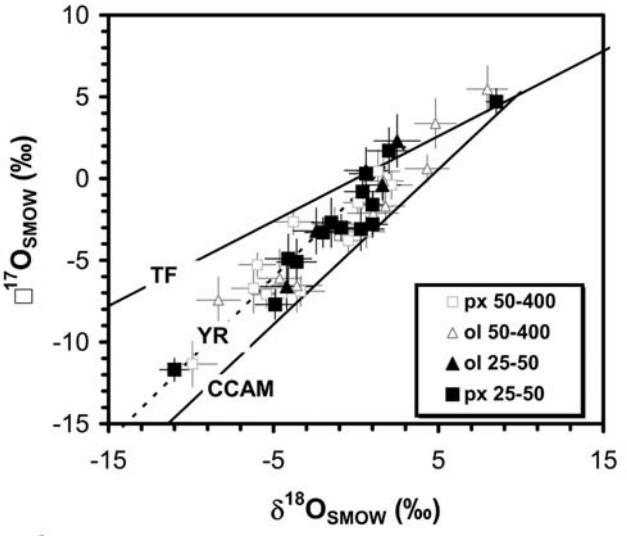

Fig. 6. Three-isotope plot showing the oxygen isotopic composition of olivine and pyroxene grains of the 25–50 μm and 50–400 μm micrometeorites. The carbonaceous chondrite anhydrous minerals (CCAM) mixing line (Clayton et al. 1973), and the Young and Russell (YR) line (Young and Russell 1998) are shown for reference. TF stands for terrestrial fractionation line. Error bars are 1σ.

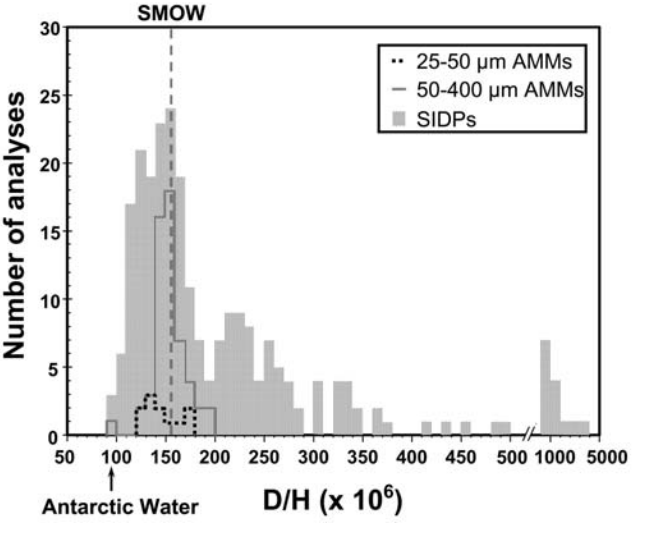

Fig. 7. The hydrogen isotopic composition of small (25–50 μm) AMMs compared to that of large AMMs (100–400 μm) and IDPs. Data from Engrand et al. (1999c) for the AMMs and Zinner et al. (1983), McKeegan et al. (1985), McKeegan (1987), Messenger (1997) for SIDPs.

scoriaceous micrometeorites belonging to the 25–50 μm size fraction (Fig. 7). Small AMMs have D/H ratios comparable to that of the Earth oceans (SMOW), and are similar to that of the large micrometeorites (Engrand et al. 1999c), compatible with a common origin between small and large micrometeorites.

Comparison with IDPs

There are important differences between IDPs and small (25–50 μm) AMMs in term of texture and morphology. The abundance of anhydrous particles among IDPs is higher, varying between 34% (Zolensky and Lindstrom 1992) and 50% (Bradley et al. 1988), compared to an abundance of crystalline micrometeorites among AMMs of 22% (this work). The presence of scoriaceous particles, abundant within the AMMs collection (Table 1) has not been reported within the IDPs collection (Rietmeijer 1998). Magnetite rims, which are common among the small AMMs, are rare among IDPs (Zolensky and Lindstrom 1992). These last two observations suggest that IDPs may have suffered less heating from atmospheric entry than have small AMMs (Keller et al. 1996).

Strong mineralogical differences between small AMMs and IDPs have also been identified. Carbonates in IDPs have been reported by many authors (Thomas et al. 1995; Tomeoka and Buseck 1985; Zolensky and Lindstrom 1992), while we have not found any carbonate among the 67 AMMs studied. Likewise, iron-nickel sulfides such as pyrrhotite and pentlandite have been reported to be abundant in IDPs (Dai and Bradley 2001; Thomas et al. 1995; Zolensky and Lindstrom 1992; Zolensky and Thomas 1995), while we found only two iron-nickel sulfide grains in the course of our study. Finally, low-iron-manganese-enriched (LIME) olivines (FeO/MnO < 1), ubiquitous in IDPs (Klöck et al. 1989), are absent from the small AMMs studied.

A key difference between IDPs and small micrometeorites concern the hydrogen isotope composition. Porous anhydrous cluster IDPs often exhibit large isotopic anomalies in hydrogen (e.g., Messenger 2000) that have not been found in the small size fraction of AMMs (Engrand et al. 1999c). Exchange and contamination experiments performed by Engrand et al. (1999c) have demonstrated that the terrestrial hydrogen isotopic composition of AMMs is not the result of exchange during the 50,000 year sojourn of AMMs within blue ice, or the 8 hour exposition to melted ice during recovery. The distinct hydrogen isotopic composition of AMMs and IDPs is therefore not due to the prolonged stay of AMMs within Antarctic ice, but has some other cause. It is possible that the difference arises from using different analytical techniques. Engrand et al. (1999c) used an O^- beam to measure the isotopic composition of hydrogen in AMMs, while a Cs^+ beam was used to characterize the hydrogen isotopic composition of IDPs (e.g., Messenger 2000; Mukhopadhyay and Nittler 2003). Deloule and Robert (1995) demonstrated that an O^- beam enhances the emission of H^+ ions from the H-bearing silicate phases over that of organic H^+ ions by a factor of >100 (cf. Gounelle et al. 2005), while transmission electron microscope studies performed by Keller et al. (2004) indicate that the D-rich matter in IDPs is organic. An exception are two cluster IDPs studied by Mukhopadhyay and Nittler (2003), which exhibit D-rich water. The apparent difference in hydrogen isotopic

composition between AMMs and IDPs could be in part due to a difference in the analytical techniques.

Although there has been recently a growing interest in measuring the oxygen isotopic composition of IDPs using ion probe imaging techniques (e.g., Aléon et al. 2001; Floss and Stadermann 2003; Messenger 1998; Messenger 1999), there have been relatively few ion probe studies on the oxygen isotopic composition of individual anhydrous grains in IDPs. Most of them are dedicated to refractory minerals such as spinel, corundum, or melilite (e.g., Greshake et al. 1996; McKeegan 1987). Engrand et al. (1999b) measured the oxygen isotopic composition of olivine and pyroxene in four IDPs. Seven analyses plot in the same field as AMMs in a three oxygen isotopes plot (Engrand et al. 1999b). One analysis—corresponding to a GEMs-rich particle—exhibits an enrichment in ^{16}O with $\delta^{18}O = -19.7 \pm 1.6$ (1σ) and $\delta^{17}O = -19.5 \pm 1.8‰$ (1σ). No similar enrichment has been discovered in small AMMs (this study). The only ^{16}O enrichments found so far in AMMs correspond to refractory minerals such as melilite and spinel (Engrand et al. 1999a; Hoppe et al. 1995; Kurat et al. 1994c). Messenger et al. (2003) have discovered recently very large oxygen isotope anomalies in six silicate grains using the NanoSIMS. Because of their rarity (6 out of 1031) and their small size, these circumstellar grains would not have been discovered using a conventional ion microprobe. Using similar techniques, Yada et al. (2004) have discovered a large (5 × 3 μm) presolar silicate in an AMM collected in Cap Prudhomme in 1988 (Maurette et al. 1991).

Although small AMMs bridge the size gap between large AMMs (>50 μm) and IDPs (<50 μm), only a small population of IDPs has sizes larger than 25 μm. Most of them are the so-called cluster IDPs that are often the bearers of the largest isotopic anomalies (e.g., Rietmeijer 1998). Most of the above comparisons between AMMs and IDPs are based on cluster IDPs, while comparison with noncluster IDPs implicitly assumes that there is a continuum between cluster and noncluster IDPs. In any case, comparing AMMs with sizes below 50 μm and IDPs establishes textural, morphological, mineralogical, and isotopic differences between these populations. Because the size of the samples studied overlap, the differences between AMMs and IDPs are not due to a size effect, but have other causes that we will outline in the next section.

CONCLUSIONS

We have investigated the texture, bulk chemistry, mineralogy, as well as the anhydrous grains oxygen isotopic composition of 67 micrometeorites collected at Cap Prudhomme, Antarctica and belonging to the size fraction 25–50 μm (small AMMs). Small AMMs can be classified in the same four textural classes as large AMMs (>100 μm) (Kurat et al. 1994b): crystalline, fine-grained, scoriaceous, and cosmic spherules. Bulk compositions of the major elements Fe, Mg, and Si show no striking differences with those of large micrometeorites. The mineralogy of a given textural class of small AMMs also compares well to that of large AMMs of the same textural class. Similarly, the oxygen isotopic compositions of olivine and pyroxene grains of small AMMs overlap those of large AMMs. Engrand et al. (1999c) had also shown that phyllosilicate water in both small and large AMMs had similar hydrogen isotopic compositions. To summarize, small AMMs (25–50 μm) strongly resemble larger AMMs (50–400 μm) in terms of texture, mineralogy, and isotopic composition. The AMMs population is thus compositionally homogeneous over the size range 25–400 μm. There is no change of the composition of the micrometeorite flux with size.

Small AMMs overlap in size with the largest IDPs and therefore can be directly compared to this other population of micrometeorites. Here we find that differences do exist between small AMMs and IDPs, especially in terms of texture and mineralogy. Minerals such as carbonates and iron-nickel sulfides, abundant within the IDPs, are not found in the small AMMs. The main difference, however, is the absence within the AMMs population of anhydrous, porous particles often exhibiting large isotopic anomalies in hydrogen and oxygen (Messenger 2000; Messenger et al. 2003). Because the sizes of small AMMs and IDPs overlap, the observed differences are not due to a size effect, but have other causes, such as physical biases introduced during collection techniques or a temporal variation in the composition of the micrometeorite flux.

A recent temporal change in the composition of the micrometeorite flux could explain the differences observed between AMMs and IDPs, since Cap Prudhomme micrometeorites sample the flux ~50,000 years ago (Maurette et al. 1994), while IDPs sample the present micrometeorite flux. A recent temporal change in the composition of the micrometeorite flux onto Earth is however difficult to assess. To establish such a change, one would need to collect 50,000-year-old micrometeorites with a technique that introduces biases similar to that of stratospheric collections. This seems difficult to achieve at the present time.

Assessing the biases introduced by the collection procedures in Antarctica and elsewhere is an important task for micrometeorites researchers (e.g., Duprat et al. 2003; Gounelle 2000; Maurette et al. 1994; Taylor et al. 1998). First, because micrometeorites are key samples for understanding the origin and evolution of the solar system, we want to have the most precise picture of the true population of micrometeorites accreting to Earth. Second, the determination of the micrometeorite mass flux onto Earth relies on a good collection efficiency and the minimization of the biases (Duprat et al. 2001; Gounelle 2000).

Physical biases can be due to the preferential destruction of certain particle types during collection procedures. For

example, it is likely that the pumps used in the Antarctic blue ice micrometeorites collections (Maurette et al. 1994) destroy the most friable particles found in the IDPs collection, such as the chondritic porous particles. Conversely, it is possible that hard particles, such as scoriaceous or crystalline micrometeorites, stick less efficiently to the silicon oil collectors used in stratospheric collections than the porous particles. The interaction of the terrestrial environment with micrometeorites can also introduce significant biases in the collection of micrometeorites. Some IDPs are known to be enriched in bromine relative to chondritic values (Rietmeijer 1998), which is indicative of possible atmospheric contamination. The absence of carbonates in Antarctic micrometeorites has been interpreted as resulting from the residence of micrometeorites with melt water, which might promote the dissolution of carbonates.

In the future, it is of outmost importance to develop micrometeorite collection procedures that minimize physical biases. In January 2002, Duprat et al. (2003) conducted a field trip in the central regions of Antarctica, at the station CONCORDIA (Dome C, S75° E123°). Because they collected micrometeorites in surface snow rather than in blue ice, and because they developed a procedure that does not involve mechanical pumping, the CONCORDIA collection may provide the most unbiased collection of Antarctic micrometeorites that can be compared to the stratospheric collection.

Acknowledgments–Dr. Mireille Christophe-Michel Lévy provided insightful comments. Mr. Boivin helped with the FEG-SEM kindly made available by ONERA (Chatillon, France). Drs. Theo Naftlos and Michel Fialin kindly helped with the EMP analyses in Vienna and Paris. The two reviewers, Drs. Larry Nittler and Mike Zolensky, as well as the associate editor, Dr. Scott Sandford, helped in improving the paper. We thank the IPEV, CNES, PNP and IN2P3 for continuous support. The UCLA ion microprobe laboratory is supported by grants from the NASA Cosmochemistry program and the Instrumentation and Facilities program of the NSF. This work was part of the Ph.D. thesis of M.G.

Editorial Handling—Dr. Scott Sanford

REFERENCES

Aléon J., Engrand C., Robert F., and Chaussidon M. 2001. Clues to the origin of interplanetary dust particles from the isotopic study of their hydrogen-bearing phases. *Geochimica et Cosmochimica Acta* 65:4399–4412.

Beckerling W. and Bischoff A. 1995. Occurence and composition of relict minerals in micrometeorites from Greenland and Antartica. Implications for their origins. *Planetary and Space Science* 43: 435–449.

Bradley J. P. 1994. Chemically anomalous preaccretionally irradiated grains in interplanetary dust from comets. *Science* 265:925–929.

Bradley J. P., Sandford S. A., and Walker R. M. 1988. Interplanetary dust. In *Meteorites and the early solar system*, edited by Kerridge J. F. and Matthews M. S. Tucson, Arizona: The University of Arizona Press. pp. 861–895.

Bradley J. P., Keller L. P., Snow T. P., Hanner M. S., Flynn G. J., Gezo J. C., Clemett S. J., Brownlee D. E., and Bowey J. E. 1999. An infrared spectral match between GEMS and interstellar grains. *Science* 285:1716–1718.

Brownlee D. E. 1985. Cosmic dust: Collection and research. *Annual Review of Earth and Planetary Sciences* 13:147–173.

Brownlee D. E., Bates B., and Schramm L. 1997. The elemental composition of stony cosmic spherules. *Meteoritics & Planetary Science* 32:157–175.

Christophe Michel-Lévy M. and Bourot-Denise M. 1992. Mineral composition in Antarctic and Greenland micrometeorites. *Meteoritics* 27:73–80.

Clayton R. N., Grossman L., and Mayeda T. K. 1973. A component of primitive nuclear composition in carbonaceous meteorites. *Science* 182:485–488.

Dai Z. R. and Bradley J. P. 2001. Iron-nickel sulfides in anhydrous interplanetary particles. *Geochimica et Cosmochimica Acta* 65: 3601–3612.

Deloule E. and Robert F. 1995. Interstellar water in meteorites? *Geochimica et Cosmochimica Acta* 59:4695–4706.

Duprat J., Engrand C., Maurette M., Gounelle M., Hammer C., and Kurat G. 2003. The CONCORDIA-collection: Pristine contemporary micrometeorites from central Antarctica surface snow (abstract #1727). 34th Lunar and Planetary Science Conference. CD-ROM.

Duprat J., Maurette M., Engrand C., Matrajt G., Immel G., Gounelle M., and Kurat G. 2001. An estimation of the contemporary micrometeorite flux obtained from surface snow samples collected in central Antarctica (abstract). *Meteoritics & Planetary Science* 36:A52.

Engrand C. and Maurette M. 1998. Carbonaceous micrometeorites from Antarctica. *Meteoritics & Planetary Science* 33:565–580.

Engrand C., McKeegan K. D., and Leshin L. A. 1999a. Oxygen isotopic compositions of individual minerals in Antarctic micrometeorites: Further links to carbonaceous chondrites. *Geochimica et Cosmochimica Acta* 63:2623–2636.

Engrand C., McKeegan K. D., Leshin L. A., Bradley J. P., and Brownlee D. E. 1999b. Oxygen isotopic compositions of interplanetary dust particles: ^{16}O-excess in a GEMS-rich IDP (abstract #1690). 30th Lunar and Planetary Science Conference. CD-ROM.

Engrand C., Deloule E., Robert F., Maurette M., and Kurat G. 1999c. Extraterrestrial water in micrometeorites and cosmic spherules from Antarctica: An ion microprobe study. *Meteoritics & Planetary Science* 34:773–787.

Floss C. and Stadermann F. J. 2003. Complementary carbon, nitrogen and oxygen isotopic imaging of interplanetary dust particles: Presolar grains and an indication of a carbon isotopic anomaly (abstract #1238). 34th Lunar and Planetary Science Conference. CD-ROM.

Genge M. J., Grady M. M., and Hutchison R. H. 1997. The textures and compositions of fine-grained micrometeorites: Implications for comparisons with meteorites. *Geochimica et Cosmochimica Acta* 61:5149–5162.

Gounelle M. 2000. Matière extraterrestre sur Terre: Des Océans aux protoétoiles. Ph.D. thesis, Université Paris, Paris, France.

Gounelle M., Maurette M., Engrand C., Brandstätter F., and Kurat G. 1999. Mineralogy of the 1998 Astrolabe Antarctic micrometeorite collection (abstract). *Meteoritics & Planetary Science* 34:A46.

Gounelle M., Engrand C., Alard O., Bland P. A., Zolensky M. E., Russell S. S., and Duprat J. Forthcoming. The hydrogen isotopic

composition of water from fossil micrometeorites. *Geochimica et Cosmochimica Acta*.
Greshake A., Hoppe P., and Bischoff A. 1996. Mineralogy, chemistry, and oxygen isotopes of refractory inclusions from stratospheric interplanetary dust particles and micrometeorites. *Meteoritics & Planetary Science* 31:739–748.
Hoppe P., Kurat G., Walter J., and Maurette M. 1995. Trace elements and oxygen isotopes in a CAI-bearing micrometeorite from Antarctica (abstract). 26th Lunar and Planetary Science Conference. pp. 623–624.
Jedwab J. 1967. La météorite en plaquettes des météorites carbonées d'Alais, Ivuna et Orgueil. *Earth and Planetary Science Letters* 2: 440–444.
Keller L. P., Thomas K. L., and McKay D. S. 1996. Mineralogical changes in IDPs resulting from atmospheric entry heating. In *Physics, chemistry, and dynamics of interplanetary dust*, vol. 104, edited by Gustafson B. S. and Hanner M. S. pp. 295–298.
Keller L. P., Messenger S., Flynn G. J., Clemett S. J., Wirick S., and Jacobsen C. 2004. The nature of molecular cloud material in interplanetary dust. *Geochimica et Cosmochimica Acta* 68:2577–2589.
Kerridge J. F. 1970. Some observations on the nature of magnetite in the Orgueil meteorite. *Earth and Planetary Science Letters* 9: 299–306.
Klöck W., Thomas K. L., McKay D. S., and Palme H. 1989. Unusual olivine and pyroxene composition in interplanetary dust and unequilibrated ordinary chondrite. *Nature* 339:126–128.
Kortenkamp S. J., Dermott S. F., Fogle D., and Grogan K. 2001. Sources and orbital evolution of interplanetary dust accreted by the Earth. In *Accretion of extraterrestrial matter throughout Earth's history*, edited by Peucker-Eherenbrink B. and Schmitz B. Kluwer/Plenum: New York. pp. 13–30.
Kurat G., Presper T., Brandstätter F., Maurette M., and Koeberl C. 1992. CI-like micrometeorites from Cap-Prudhomme, Antarctica (abstract). 23rd Lunar and Planetary Science Conference. pp. 747–748.
Kurat G., Hoppe P., and Maurette M. 1994a. Preliminary report on spinel-rich CAIs in an Antarctic micrometeorite (abstract). 25th Lunar and Planetary Science Conference. pp. 763–764.
Kurat G., Koeberl C., Presper T., Brandstätter F., and Maurette M. 1994b. Petrology and geochemistry of Antarctic micrometeorites. *Geochimica et Cosmochimica Acta* 58:3879–3904.
Kurat G., Hoppe P., Walter J., Engrand C., and Maurette M. 1994c. Oxygen isotopes in spinels from Antarctic micrometeorites (abstract). *Meteoritics* 29:487–488.
Love S. G. and Brownlee D. E. 1991. Heating and thermal transformation of micrometeoroids entering the Earth's atmosphere. *Icarus* 89:26–43.
Love S. G. and Brownlee D. E. 1993. A direct measurement of the terrestrial mass accretion rate of cosmic dust. *Science* 262:550–553.
Maurette M., Pourchet M., and Perreau M. 1992a. The 1991 EUROMET micrometeorite collection at Cap-Prudhomme, Antarctica. *Meteoritics* 27:473–475.
Maurette M., Brownlee D. E., Joswiak D. J., and Sutton S. R. 1992b. Antarctic micrometeorites smaller than 50 microns (abstract). 23rd Lunar and Planetary Science Conference. pp. 857–858.
Maurette M., Hammer C., Brownlee D. E., Reeh N., and Thomsen H. H. 1986. Placers of cosmic dust in the blue ice lakes of Greenland. *Science* 233:869–872.
Maurette M., Immel G., Hammer C., Harvey R., Kurat G., and Taylor S. 1994. Collection and curation of IDPs from the Greenland and Antarctic ice sheets. In *Analysis of interplanetary dust,* vol. 310, edited by Zolensky M. E., Wilson T. L., Rietmeijer F. J. M., and Flynn G. J. Houston: American Institute of Physics. pp. 277–289.
Maurette M., Olinger C., Christophe Michel-Lévy M., Kurat G., Pourchet M., Brandstätter F., and Bourot-Denise M. 1991. A collection of diverse micrometeorites recovered from 100 tons of Antarctic blue ice. *Nature* 351:44–47.
McKeegan K. D. 1987. Oxygen isotopes in refractory stratospheric dust particles: Proof of extraterrestrial origin. *Science* 237:1468–1471.
Messenger S. 1998. Oxygen isotopic imaging of interplanetary dust (abstract). *Meteoritics & Planetary Science* 33:A106.
Messenger S. 1999. Oxygen isotopic imaging of interplanetary dust by TOF-SIMS (abstract #1600). 29th Lunar and Planetary Science Conference. CD-ROM.
Messenger S. 2000. Identification of molecular-cloud material in interplanetary dust particles. *Nature* 404:968–971.
Messenger S., Keller L. P., Stadermann F. J., Walker R. J., and Zinner E. 2003. Samples of stars beyond the solar system: Silicate grains in interplanetary dust. *Science* 300:105–108.
Mukhopadhyay S. and Nittler L. R. 2003. D-rich water in interplanetary dust particles (abstract #1941). 34th Lunar and Planetary Science Conference. CD-ROM.
Nakamura T., Noguchi T., Yada T., Nakamuta Y., and Takaoka N. 2001. Bulk mineralogy of individual micrometeorites determined by X-ray diffraction analysis and transmission electron microscopy. *Geochimica et Cosmochimica Acta* 65: 4385–4397.
Nakamura T., Imae N., Nakai I., Noguchi T., Yano H., Terada K., Murakami T., Fukuoka T., Nogami K.-I., Ohashi H., Nozaki W., Hashimoto M., Kondo N., Matsuzaki H., Ichikawa O., and Ohmori R. 1999. Antarctic micrometeorites collected at the Dome Fuji Station. *Antarctic Meteorite Research* 12:183–198.
Noguchi T., Nakamura T., and Nozaki W. 2002. Mineralogy of phyllosilicate-rich micrometeorites and comparison with Tagish Lake and Sayama meteorites. *Earth and Planetary Science Letters* 202:229–246.
Rietmeijer F. J. M. 1998. Interplanetary dust particles. In *Planetary materials*, edited by Papike J. J. Washington, D.C.: Mineralogical Society of America. pp. 2-1–2-94.
Steele I. M. 1992. Olivine in Antarctic micrometeorites: Comparison with other extraterrestrial olivine. *Geochimica et Cosmochimica Acta* 56:2923–2929.
Taylor S., Lever J. H., and Harvey R. P. 1998. Accretion rate of cosmic spherules measured at South Pole. *Science* 392:899–903.
Taylor S., Lever J. H., and Harvey R. P. 2000. Numbers, types and compositions of an unbiased collection of cosmic spherules. *Meteoritics & Planetary Science* 35:651–666.
Terada K., Yada T., Kojima H., Noguchi T., Nakamura T., Murakami T., Yano H., Nozaki W., Nakamuta Y., Matsumoto N., Kamata J., Mori T., Nakai I., Sasaki M., Itabashi M., Setoyanagi T., Nagao K., Osawa T., Hiyagon H., Mizutani S., Fukuoka T., Nogami K.-I., Ohmori R., and Ohashi H. 2001. General characterization of Antarctic micrometeorites collected by the 39th Japanese Antarctic Research Expedition: Consortium studies of JARE AMMs (II). *Antarctic Meteorite Research* 14: 89–107.
Thomas K. L., Blandford G. E., Clemett S. J., Flynn G. J., Keller L. P., Klöck W., Maechling C. R., McKay D. S., Messenger S., Nier A. O., Schlutter D. J., Sutton S. R., Warren J. L., and Zare R. N. 1995. An asteroidal breccia: The anatomy of a cluster IDP. *Geochimica et Cosmochimica Acta* 59:2797–2815.
Tomeoka K. and Buseck P. R. 1985. Hydrated interplanetary dust particle linked with carbonaceous chondrites? *Nature* 314:338–340.
Toppani A., Libourel G., Engrand C., and Maurette M. 2001.

Experimental simulation of atmospheric entry of micrometeorites. *Meteoritics & Planetary Science* 36:1377–1396.

Vokrouhlicky D. and Farinella P. 2000. Efficient delivery of meteorites to the Earth from a wide range of asteroid parent bodies. *Nature* 407:606–608.

Warren J. L. and Zolensky M. E. 1994. Collection and curation of interplanetary dust particles recovered from the stratosphere by NASA. In *Analysis of interplanetary dust*, edited by Zolensky M. E., Wilson T. L., Rietmeijer F. J. M., and Flynn G. J. Houston: American Institute of Physics. pp. 245–253.

Yada T., Stadermann F. J., Floss C., Zinner E., and Olinger C. T. 2004. First presolar silicate discovered in an Antarctic micrometeorite (abstract #9056). Workshop on Chondrites and Protoplanetary Disk. CD-ROM.

Young E. D. and Russell S. S. 1998. Oxygen reservoirs in the early solar nebula inferred from an Allende CAI. *Science* 282:452–455.

Zolensky M. E. and Lindstrom D. J. 1992. Mineralogy of 12 large "chondritic" interplanetary dust particles. Proceedings, 22nd Lunar and Planetary Science Conference. pp. 161–169.

Zolensky M. E. and Thomas K. L. 1995. Iron and iron-nickel sulfides in chondritic interplanetary dust particles. *Geochimica et Cosmochimica Acta* 59:4707–4712.

APPENDIX

Appendix 1. Bulk analyses of micrometeorites belonging to the 25–50 μm size fraction. Data in wt%. Xtal, fg, and sc stand for crystalline, fine-grained, and scoriaceous micrometeorites, respectively. B.d. stands for below detection limit.

Micrometeorite	UW6-69	UW1-12	UW6-53	UW5-95	UW1-66	UW1-28	UW6-9	UW6-29	UW1-6
Textural type	xtal	xtal	xtal	cs	cs	cs	sc	sc	sc
SiO_2	46.8	54.1	46.4	33.4	33.2	12.2	23.0	56.6	21.8
TiO_2	0.10	0.07	0.06	0.10	0.10	0.13	0.07	0.05	0.05
Al_2O_3	1.24	0.34	1.09	2.49	0.98	5.05	3.01	3.60	2.89
Cr_2O_3	0.80	0.63	0.65	0.31	0.61	2.57	0.31	0.26	0.45
FeO	8.29	1.96	14.6	29.6	33.2	53.8	30.0	1.66	30.4
MnO	0.16	0.14	0.12	0.25	0.23	0.23	0.23	0.09	0.23
MgO	38.3	34.0	38.6	22.9	26.0	9.30	14.6	31.4	17.0
NiO	0.17	b.d.	0.65	0.72	b.d.	0.20	0.21	b.d.	0.23
CaO	0.60	0.30	0.76	1.26	0.49	0.15	0.36	0.44	0.44
Na_2O	0.07	b.d.	0.03	0.03	0.04	0.19	0.21	0.33	0.25
K_2O	b.d.	b.d.	b.d.	b.d.	0.04	0.07	0.10	0.16	0.06
S	0.10	b.d.	0.04	b.d.	0.03	0.17	0.23	0.11	0.80
Total	96.51	91.54	102.97	91.05	94.88	83.89	72.09	94.60	73.80

Micrometeorite	UW1-64	UW1-68	UW5-92	UW6-77	UW6-55	UW6-88	UW5-11	UW5-25	UW5-62
Textural type	fg	fg	fg	fg	fg	fg	fg	fg	fg
SiO_2	45.1	36.9	21.4	15.3	39.2	35.0	32.6	33.9	28.3
TiO_2	0.03	b.d.	0.05	b.d.	0.09	0.14	0.14	0.07	0.05
Al_2O_3	b.d.	0.03	1.68	1.03	6.98	5.36	2.49	2.84	2.04
Cr_2O_3	0.76	0.97	0.26	0.38	0.84	0.53	0.57	0.34	0.35
FeO	17.5	3.52	20.3	54.9	12.0	32.3	28.9	24.9	27.4
MnO	0.40	0.12	0.17	0.27	0.50	0.38	0.56	0.10	0.24
MgO	29.4	43.7	14.5	1.95	26.0	20.1	15.1	16.2	15.8
NiO	b.d.	b.d.	0.11	0.03	0.11	b.d.	0.44	0.15	0.30
CaO	b.d.	0.06	0.35	0.20	1.17	1.44	1.52	0.37	0.57
Na_2O	0.09	0.20	0.74	0.35	0.04	b.d.	0.25	0.09	0.24
K_2O	0.03	b.d.	0.43	0.27	b.d.	0.09	0.15	0.13	0.05
S	b.d.	b.d.	0.32	0.54	0.10	0.06	0.65	0.51	0.39
Total	93.31	85.49	59.99	74.67	86.93	95.34	82.73	79.08	75.34

Micrometeorite	UW5-78	UW5-85	UW5-96	UW5-97	UW5-104	UW6-12	UW6-18	UW6-43	UW6-76	UW1-74
Textural type	fg	fg	fg	fg	fg	fg	fg	fg	fg	fg
SiO_2	25.0	30.4	30.0	31.3	26.5	20.5	32.6	33.9	29.6	34.7
TiO_2	0.10	0.06	0.12	0.13	0.12	0.11	0.08	0.10	0.07	0.10
Al_2O_3	2.47	2.04	1.88	2.23	1.94	1.48	3.57	2.17	2.74	2.20
Cr_2O_3	0.33	0.31	0.65	0.41	0.42	0.39	0.60	0.49	0.44	0.60
FeO	31.4	16.3	29.3	24.9	31.4	32.6	28.9	20.6	27.9	25.9
MnO	0.19	0.29	b.d.	0.21	0.15	0.22	0.31	0.27	0.25	0.38

Appendix 1. *Continued.* Bulk analyses of micrometeorites belonging to the 25–50 μm size fraction. Data in wt%. Xtal, fg, and sc stand for crystalline, fine-grained, and scoriaceous micrometeorites, respectively. B.d. stands for below detection limit.

Micrometeorite	UW6-69	UW1-12	UW6-53	UW5-95	UW1-66	UW1-28	UW6-9	UW6-29	UW1-6	
MgO	12.2	19.2	5.16	14.5	9.93	9.68	19.2	18.0	17.7	15.4
NiO	0.78	0.43	0.05	0.23	0.23	0.58	0.22	0.53	0.65	0.16
CaO	0.52	1.36	0.31	0.86	0.39	0.47	0.96	0.29	0.12	0.98
Na_2O	0.15	1.86	0.47	0.72	0.43	0.97	0.10	0.92	0.37	0.69
K_2O	0.08	0.25	0.45	0.43	0.11	0.13	0.05	0.13	0.27	0.16
S	0.79	3.11	0.89	0.48	1.13	0.53	0.28	3.59	1.63	0.78
Total	73.21	72.50	68.39	75.91	71.62	67.13	86.59	77.40	80.10	81.27
Micrometeorite	UW6-82	UW6-83	UW6-85	UW6-87	UW6-95	UW6-108	UW1-3	UW1-5	UW1-8	UW1-62
Textural type	fg	fg	fg	fg	fg	fg	fg	fg	fg	fg
SiO_2	35.1	28.6	33.4	33.7	25.7	19.1	29.9	38.3	33.1	38.4
TiO_2	0.12	0.15	0.06	0.07	0.11	0.09	0.13	0.14	0.03	0.15
Al_2O_3	2.37	2.47	2.30	1.78	1.84	1.43	2.65	3.24	3.11	2.58
Cr_2O_3	0.71	0.43	0.48	0.14	0.47	0.41	0.29	0.63	0.37	0.62
FeO	22.70	30.30	22.90	28.90	19.60	25.00	34.50	21.70	30.20	26.20
MnO	0.26	0.21	0.34	0.32	0.08	0.20	0.23	0.13	0.27	0.20
MgO	25.20	17.10	18.80	24.60	11.30	13.60	15.20	17.40	16.60	17.90
NiO	0.17	0.09	0.24	0.46	0.05	0.11	0.21	0.14	0.39	0.17
CaO	0.22	0.21	0.88	1.00	0.06	0.41	0.81	0.43	0.35	0.43
Na_2O	0.23	0.33	0.82	0.28	0.51	0.26	0.28	0.58	0.70	0.69
K_2O	0.06	0.14	0.14	0.06	0.12	0.06	0.17	0.24	0.19	0.14
S	0.26	0.21	0.82	0.45	0.35	0.31	0.35	0.51	1.14	0.75
Total	87.13	80.04	80.37	91.31	59.84	60.66	84.37	82.93	85.31	87.48

Pergamon

Geochimica et Cosmochimica Acta, Vol. 65, No. 23, pp. 4399–4412, 2001

0016-7037/01 $20.00 + .00

PII S0016-7037(01)00720-7

Clues to the origin of interplanetary dust particles from the isotopic study of their hydrogen-bearing phases

JÉRÔME ALÉON,[1,*,†] CÉCILE ENGRAND,[2] FRANÇOIS ROBERT,[3,‡] and MARC CHAUSSIDON[1]

[1]Centre de Recherches Pétrographiques et Géochimiques-CNRS, 15 rue Notre Dame des Pauvres, BP 20, F-54501 Vandoeuvre-lès-Nancy, France
[2]Centre de Spectroscopie Nucléaire et de Spectrométrie de Masse, Bâtiment 104, F-91405 Orsay Campus, Orsay, France
[3]Laboratoire de Minéralogie, CNRS-URA736, Muséum National d'Histoire Naturelle, 61 rue Buffon, F-75005 Paris, France

(*Received November* 15, 2000; *accepted in revised form June* 8, 2001)

Abstract—Ion microprobe quantitative imaging was performed for H, D, ^{12,13}C, ^{16,18}O, ^{27}Al, and ^{28,29,30}Si in five stratospheric particles with a 1.5 × 1.5 μm spatial resolution to determine the carriers of high D/H ratios and to give new clues about the parent bodies of interplanetary dust particles (IDPs). Among these particles, four appear to be of extraterrestrial origin. Using imaging, the large variations of D/H ratios can be correlated at the micrometer scale with chemical composition so that endmembers can be identified. From the systematics of variation of C/H and D/H ratios, water present as hydroxyls in phyllosilicates (at C/H = 0) and three different types of organic matter (OM1, 2, and 3) were identified. Water exhibits D/H ratios lying in the chondritic domain (D/H ~150 × 10^{-6}), whereas OMs are enriched in deuterium. OM1 is similar to the macromolecular organic matter of carbonaceous chondrites (D/H = 250 × 10^{-6} and C/H = 1.5). OM2 (D/H = 1500 × 10^{-6} and C/H = 1.0) is close to cometary HCN. OM3 (D/H = 2000 × 10^{-6} and C/H = 3.0) is a highly condensed carbonaceous phase with no counterpart in known extraterrestrial objects. The C, O, and Si isotopic compositions are solar within ± 10%.

The identification of these phases allows a better understanding of the origin of D/H variations inferred for the protosolar nebula. The only mechanism that can explain such high D/H ratios is interstellar chemistry. However, D/H ratios in interplanetary dust organic matter remain lower than those measured in molecules from cold molecular clouds. This difference can be accounted for by an isotopic exchange with liquid water in IDP parent bodies. In addition, the close association of the chondritic component OM1 with the likely cometary component OM2 is evidence for a link between carbonaceous chondrites and comets. Although IDPs contain cometary organic matter, the water-D/H ratio is lower than that measured in comets (310 × 10^{-6}). IDPs seem thus constituted of various materials formed over a large range of heliocentric distances. *Copyright © 2001 Elsevier Science Ltd*

1. INTRODUCTION

In the past 25 yr it has been shown that the terrestrial atmosphere samples particles (size between 5 and 50 μm) from the interplanetary medium (Brownlee, 1985). Some of these interplanetary dust particles (IDPs) collected by stratospheric airplanes exhibit unequilibrated mineral assemblages with refractory anhydrous and hydrated minerals (Tomeoka and Buseck, 1985). Their enrichment in carbon relative to the carbonaceous chondrites reaches a factor up to 13, with a mean value of ~4 (Thomas et al., 1994). In addition, they show large deuterium excesses, which have been interpreted as resulting from interstellar chemistry (Zinner et al., 1983; McKeegan et al., 1985; Messenger and Walker, 1997; Messenger, 2000). Several attempts have been reported in the literature to determine the carrier phase of these high D/H ratios (Zinner et al., 1983; McKeegan et al., 1985; Nittler and Messenger, 1998; Messenger, 2000). It has been proposed that such a carrier was in the form of organic compounds: A SIMS study has shown that the C/O ratio is correlated with the D/H ratio (McKeegan et al., 1985) and a combined SIMS-TEM-XANES study (Keller et al., 2000) pointed out recently that the deuterium-rich phases and the organic-rich areas are related spatially.

Several questions remain open in the study of IDPs: (1) The carrier phase of the high D/H ratios has to be definitely identified. (2) Sources of IDPs in term of specific parent bodies are poorly understood. Based on entry velocities deduced from isotopic and mineralogic heating effects, a cometary and/or an asteroidal origin has been proposed (Brownlee, 1985; Sandford, 1986; Flynn, 1989; Nier and Schlutter, 1992). In addition, mineralogic similarities have been found between some IDPs and CI and CM chondrites (e.g., Bradley and Brownlee, 1991; Keller et al., 1992). (3) The processes responsible for the high and variable D/H ratios are not yet elucidated. In fact, it has been argued that such large deuterium enrichment is unlikely to take place in the protosolar nebula (Geiss and Reeves, 1981) and can only result from ion-molecule or grain surface reactions in cold molecular clouds (e.g., Tielens, 1983; Brown and Millar, 1989; Millar et al., 1989). However, as pointed out by Robert et al. (2000), an isotopic re-equilibration via exchange with the protosolar hydrogen may have lowered the interstellar water and organic D/H ratios (Mousis et al., 2000).

To answer these questions, ion microprobe (SIMS) isotopic imaging (McKeegan et al., 1987; Nittler and Messenger, 1998; Messenger, 2000) has been carried out for five individual interplanetary dust particles. Images of D and H were acquired for isotopic measurements, and images of Si, C, O, and Al were

* Author to whom correspondence should be addressed (aleon@oro.ess.ucla.edu).
† *Present address:* Department of Earth and Space Sciences, University of California Los Angeles, 595 Charles Young Drive, Los Angeles, CA 90095-1567, USA

Table 1. Measurement conditions.

Mass	Counting time	Number of cycles	Counting rate (cps)	Main interference	MRP[a]
H	3 s	50	9×10^3 to 2×10^4	–	1500
D	60/100 s	50	1 to 7	–	1500
^{12}C	1 s	50	1×10^4 to 5×10^4	–	3800
^{13}C	10 s	50	1×10^2 to 5×10^2	^{12}CH	3800
^{16}O	1 s	50	6×10^4 to 2×10^5	–	>5000
^{18}O	30 s	50	1×10^2 to 3×10^2	–	>5000
^{28}Si	3 s	50	9×10^3 to 3×10^4	^{27}AlH	4200
^{29}Si	15 s	50	4×10^2 to 1×10^3	^{28}SiH	4200
^{30}Si	15 s	50	2×10^2 to 5×10^2	^{29}SiH	4200

[a] Mass resolving power. See text for explanation of MRP settings.

acquired for quantitative elemental cartography. The aim of the present approach was to relate D/H ratios with the chemistry of hydrogen-bearing phases (organics and layer-lattice silicates) through image processing.

2. MATERIAL AND METHODS

2.1. Samples

Quantitative isotopic imaging was performed on five IDPs received from the NASA-JSC curation facility. The IDPs came from two different collectors: L2021 (particles A6 and K1) and L2036 (particles E22, R5, and R6). They were received on a glass plate in a small drop of silicon oil. The IDPs were rinsed with hexane and then crushed on clean gold foils. As demonstrated by the fact that high carbon and silicon intensities are never associated in ion images (see "Results"), the residual silicon oil has been removed to a level at which it remains undetectable in the analyses. The sample handling was done in the clean room facility at CSNSM in Orsay. After being crushed on the gold foils, the dimensions of A6, K1, E22, R5, and R6 were $\sim 5 \times 10$ μm, 20×20 μm, 5×10 μm, 50×60 μm and 5×15 μm, respectively. An amphibole (Illimaussaq), a type III kerogen (Mahakam Delta 48055), and an olivine (#313-1-Ol) were used as standards for H, C, O, and Si analyses. These standards were powdered to the 10 to 50 μm scale and mounted similarly to the samples. All the samples, including the standards, were coated with $\sim$200 Å of gold.

2.2. Isotopic Imaging Conditions

Measurements were performed with the Nancy Cameca IMS 1270 ion microprobe in a scanning ion imaging mode with automated peak jumping in monocollection (Aléon et al., 2001). The Cs^+ primary beam was focused to a $\sim$1.5- to 2-μm beam of 2 pA at 10 keV. Negative secondary ions were accelerated at -10 keV. A dynamic transfer operating system (DTOS) was used to compensate for the primary beam rastering on the sample and to obtain an immobile focused beam in the secondary optics. Different settings of the entrance and exit slits were used for each measured element to optimize the counting rates within the limitations (1) of a mass resolving power necessary to eliminate molecular interferences and (2) of a maximum of 10^6 counts per second (cps) on the electron multiplier (EM) to keep a linear response. The energy slit was kept wide open. Careful settings of the EM were performed: Pulse height distributions were acquired at the hydrogen mass for proper hydrogen isotope measurements. The EM dead time was electronically fixed to 44 ns.

2.2.1. Hydrogen isotopes

Using a Cs^+ primary beam strongly reduces the molecular interference at mass 2 between H_2^- and deuterium (McKeegan et al., 1985). In our measurements, H_2^- always remained below the detection limit due to the low primary intensity. Thus, we used wide-open entrance and exit slits to get the best deuterium collection efficiency, which corresponds to a mass resolving power (MRP) of M/ΔM of $\sim$1500 with the IMS 1270. To reduce possible contamination coming from the edge of the rastered area, a 4500-μm-wide field aperture located immediately after the transfer optics was used.

Before the analyses, the samples were heated overnight at $\sim$100°C in a vacuum of $\sim 10^{-7}$ to 10^{-8} Torr to remove adsorbed water contamination (Deloule et al., 1991). Organic volatile molecules might be lost during this step. During the analyses, the vacuum inside the sample chamber was kept between 10^{-10} and 10^{-9} Torr. In addition, a presputtering was systematically performed before each analysis.

Typical ion counts for hydrogen measurements were between 9×10^3 and 2×10^4 cps for H^- and between 1 and 7 cps for deuterium for bulk images (see Table 1 for analytical conditions). Measurements consisted of 10 blocks of five cycles each. During each cycle H^- was counted for 3 s and deuterium for 60 s or 100 s, depending on hydrogen concentrations in the samples. Since such long counting times were used for deuterium acquisition, the stability of the magnetic field was checked by repeating the mass calibration before each analysis until stable conditions were reached. No deviation from this calibration was ever observed at the end of hydrogen isotope measurements, indicating that the ion probe worked in stable conditions during all the analyses sessions. The thickness eroded during these measurements is typically on the order of few tens of nanometers.

To calibrate the instrumental mass fractionation (IMF) for the D/H ratio, amphiboles and kerogen standards were used. Matrix effects between layer-lattice silicates and organic matter remain within the precision of D/H measurement, i.e., $\pm$ 15% at the micrometer scale (Table 2). Thus, a single value of the instrumental mass fractionation was used for correction of the D/H images of IDPs. Matrix effects for C/H ratio in condensed

Table 2. Standards and precision of isotopic measurements.

Ratio	Reference ratio	Standard	IMF[a]	2σ (bulk)[a]	Systematic error[b]
D/H	155.76×10^{-6} (SMOW)	Illimaussaq[c] Mahakam Delta[d]	−110‰	50‰	150‰
$^{13}C/^{12}C$	1.1237×10^{-2} (PDB)	Mahakam Delta 48055[d]	+10‰	70‰	100‰
$^{18}O/^{16}O$	2.0052×10^{-3} (SMOW)	313-1-O1[e]	+35‰	17‰	50‰
$^{29}Si/^{28}Si$	5.0633×10^{-2}	313-1-O1[e]	0‰	8‰	30‰
$^{30}Si/^{28}Si$	3.357×10^{-2}	313-1-O1[e]	−25‰	8‰	30‰

[a] Given in δ notation where $\delta^n I = ((R/RT) - 1) \times 1000$ where R is the measured isotopic ratio and RT the corresponding terrestrial ratio taken as a reference ratio.
[b] The systematic error takes into account (1) matrix effects in the case of hydrogen and (2) the external error on standards. (3) It is then maximized assuming that the EM settings for D/H measurements are not optimized for other isotopes.
[c] Arfvedsonite.
[d] Type III kerogen.
[e] Olivine.

organic matter were investigated by Deloule and Robert (1995). They show that matrix effects remain < 10%. Ion yields for C/H ratio were thus corrected using the Mahakam Delta type III kerogen (IFP Nb. 48055) (Table 3). All IMFs are given in per mils related to a terrestrial reference in Table 2.

2.2.2. Isotopic survey of C, O, and Si

Conditions were optimized for hydrogen isotopes at the expense of those for other elements. Therefore, high-precision isotopic measurements were not expected for C, O, and Si. In fact, measurements on standards show that $^{13}C/^{12}C$, $^{18}O/^{16}O$, $^{29}Si/^{28}Si$, and $^{30}Si/^{28}Si$ are determined with a precision ranging from ± 3 to ± 10% (Table 2). Only departure of more than twice this systematic error should then be considered significant. As shown by Zinner (1998), presolar isotopic signatures can still be detected with such a low precision.

With our low primary beam intensity, the erosion is sufficiently slow to perform several measurements on the same grain. Si, O, and C isotope measurements were acquired separately to avoid hysteresis on the magnetic field due to large jumps of several atomic mass units. Position of the slits for Si and C were adjusted to remove interferences on mass 29 and 30, and on mass 13, respectively. For oxygen isotopic determination, it was necessary to work at high mass-resolving power (typically ~5000 or more) to reduce the signal below the EM limit. Measurement of ^{17}O was impossible due to the high dynamic range of O isotopes. Measurement conditions are shown in Table 1.

Table 3. Calibration of relative ion yield for C/H measurements.

Standard	Mahakam Delta 48055[a]
Mass $(C/H)_{true}$	17
Molar $(C/H)_{true}$	1.43
$C^-/H^-_{measured}$	3.20
α[b]	0.45
1σ reproducibility	11.5%

[a] Type III kerogen.
[b] α is the relative ion yield defined as molar $(C/H)_{true}/(C^-/H^-)_{measured}$.

2.2.3. Elemental cartography of C, O, Al, and Si

For each particle, all analyses were performed immediately after D/H acquisition. For C, O, and Si, the image of the more abundant isotope is used for cartography (see above and Table 1 for analytical conditions). ^{27}Al was measured in 10 cycles of 10 s at a MRP of ~4000. Typical count rates for Al were 20 to 80 cps. Note that these conditions are different from those currently used for Al measurements (Shimizu et al., 1978). For example, the count rates were low as required (1) for keeping analysis conditions as constant as possible and (2) by the low current required for D/H imaging.

2.3. Image Processing

To study quantitatively the isotopic and chemical variations in the IDPs, image processing was applied to the ion images, so that different micrometer-sized isotopic endmembers could be identified in each IDP. For a given mass, each image consisted of 50 subimage units (hereafter referred to as planes) corresponding to 50 cycles. Each image is composed of 256 × 256 pixels in which ion counts are coded in 16 bits on each pixel. Images were constructed at 400 Hz in an interlaced mode. In this mode, it is necessary to calibrate the time of ion flight for each mass to synchronize the rastering on the sample and that on the detector. Before processing, planes were summed in the Cameca software by blocks of five cycles. The image-processing software used in this study is Visilog 5.0 for Unix. This section is divided into several parts corresponding to the different steps of image processing.

2.3.1. Data storage and data extraction

Each pixel corresponds to a sample surface smaller than the primary beam area. Consequently, in the primary beam area, data for a given mass are randomly distributed over several pixels. Therefore, the proper area units from which numeric data can be extracted should consist of the minimum number of

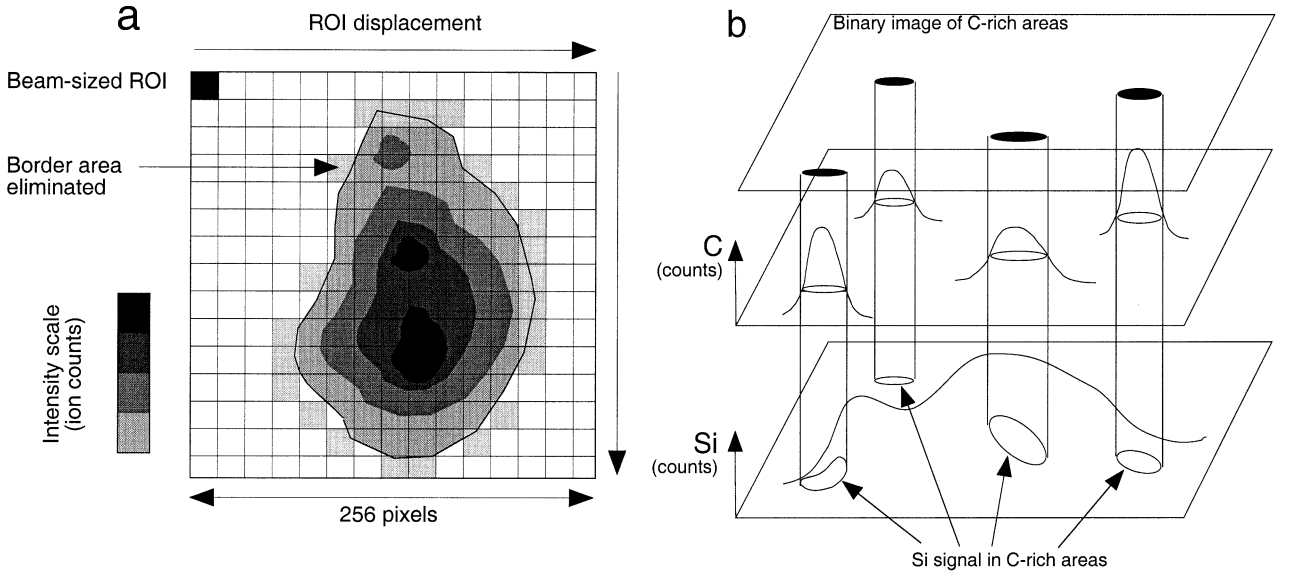

Fig. 1. Schematic drawing of the ion image processing. (a) ROIscript operations: A beam-sized ROI is rastered over the whole image and extracts mean secondary ion intensities for each primary beam position (see text). Border areas with insufficient intensities are eliminated. (b) The extraction of data using binary images is illustrated by an example in which the measurement of the Si intensities is restricted to carbon-rich areas.

pixels defined by the beam size. Images were processed in two steps. The first step consisted of defining the object inside the image and the second of extracting the data within this object. Objects are defined using binary images where pixels have a value of 1 inside the object and 0 outside. They can be either the whole IDP or a subzone of the IDP, e.g., deuterium-rich areas. There are two different ways to extract the data from the images: (1) simply by measuring the total ion counts inside objects preliminarily defined through binary images or (2) using a so-called ROI (region of interest) mathematical operator, which has the primary beam size and which is scanned through the whole image and records the ion counts inside its own area (Fig. 1a).

Binary images were constructed by thresholding the raw images. The displacement of the ROI through the image is achieved by a program written using processing operators of the software, to have a numeric procedure analogous to the rastering of the sample by the primary beam. Below, this program is referred to as ROIscript. It allows obtaining the whole range of elemental or isotopic variations in each IDP with lateral resolution defined by the size of the primary beam.

2.3.2. IDP image processing

Two different operations of image processing were performed: (1) The first is the extraction (at the ion beam scale) of all chemical and isotopic variations over the whole IDP; (2) the second is the extraction of chemical and isotopic ratios for areas exhibiting high concentration in C, D, or Si (Si and Al if high Al concentrations are observed).

The first operation was achieved by applying the ROIscript to all elemental and isotopic images (Fig. 1a). Border areas with low signal that could lead to aberrant values of analytical origin were discarded. The measurements obtained for each area are subsequently referred to as ROIs.

The second operation was obtained by thresholding the high concentration areas (Fig. 1b) to obtain binary images of these areas. This aim was to locate the organic- and silicate-rich areas on one hand and the deuterium excesses on the other. Thus, isotopic and elemental ratios could be calculated in these specific areas. Results show that this second operation corresponds to the extraction of the endmembers of the range given by the first operation. Binary images are referred to as masks (e.g., mask of silicon-rich areas means a binary image where pixels with a value of 1 locate silicon-rich areas).

Before these two operations, (1) the IDPs have to be isolated from the background without missing any phase. Therefore, C, Si, H, and O images are put to the same intensity level by normalization to the most intense image and summed to define an image that is assumed to take into account all major phases of the IDP. Applying a threshold to this image allows the elimination of the area surrounding the particle; (2) slight displacements between images could markedly affect the calculated isotopic ratios. Thus, these displacements were investigated using characteristic geometric details such as the edge of well-individualized subgrains. No shift was ever observed between two isotopes of the same element, and in only one case, a displacement occurred between two elements: the carbon image of E22 was slightly shifted compared to the H and deuterium images. In this case, the numeric correction of the shift does not cause a variation in the C/H ratio higher than the usual reproducibility on this quantity, i.e., $< 10\%$.

Bulk D/H ratios are calculated using the mask of the total IDP.

Once extracted from the raw images using these image processing operations, total ion counts are converted into counts per second and ratios (e.g., C/H) and finally corrected

Table 4. Correlation coefficients between O/H and Si/H.

IDP	R^2
K1	0.939
A6	0.932
E22	0.782
R6	0.785
R5	0.683

for instrumental mass fractionation (isotopic analyses) or ion yields (elemental cartography).

D/H ratios are given both in absolute ratios and in δD (‰) notation to ease the comparison with previous studies and astronomical data. The relationship between these two notations is given by the formula $\delta D = [(D/H)/(D/H)_{std} - 1] \times 1000$, where $(D/H)_{std}$ is the isotopic ratio of the standard mean ocean water (SMOW, 155.76×10^{-6}).

2.4. SEM Characterization

Particles were examined with a field emission gun scanning electron microscope (FEG-SEM) after isotopic analyses. EDS (energy dispersive X-ray spectrometry) spectra were acquired to check for chondritic signature of the particles. Low-resolution X-ray images of C, O, Mg, Al, Si, S, Ca, Cr, Fe, and Ni were also acquired for the five particles.

3. RESULTS

3.1. Sample Description: Chemistry and Morphology

In this section the chemistry and morphology of IDPs are described using H, C, O, Al, and Si ion images along with FEG-SEM work. Ion images revealed that all IDPs contain carbon-rich and silicon-rich phases. Correlations between Si/H and O/H revealed that the silicon-rich phases are silicates (Table 4). Correlation coefficients < 0.9 are due to the abundance of oxygen-rich organic matter (E22, R6) or oxides (R5). Hydrogen is associated with C and Si (see, e.g., Fig. 2) but preferentially with C, suggesting that carbon-rich phases are organic species but that phyllosilicates are also present in at least some IDPs. The usual association of H with C can be explained by (1) a low content in phyllosilicates and (2) a differential emission of H^- between organic matter and silicates, since H^- emission under Cs^+ sputtering is enhanced in organic matter relative to silicates, whereas it is the contrary with O^- sputtering (Deloule and Robert, 1995).

All particles but R6 have a chondritic EDS spectrum. R6 is a particle ~20 μm across made only of C-H-(O)-rich matter with three inclusions of Al-O-rich matter and one of Si-O.

E22 (~10 μm) presents high porosity and the highest carbon content of the five particles presently studied. Because this particle was fluffy before crushing, it is likely that such porosity is pristine and was not acquired during analysis by erosion with the ion beam. The EDS analysis revealed that the silicate phases (association of Si and O) are also magnesium rich.

A6 (~10 μm) shows a high porosity, which is probably also pristine. It consists mainly of silicate-rich material. Carbon-rich phases are located in small areas compared to Si, which is distributed almost everywhere. It is interesting to note that morphology and EDS spectra of the IDPs E22 and A6 are almost identical.

R5 is quite large for an IDP (~60 μm). Both a fine-grained and a compact smooth texture are observed. As with A6, R5 is mainly silicate rich. X-ray images show a large iron-rich area associated with O, without Si, and with a texture similar to framboidal magnetites. Silicon-rich areas are magnesium rich.

The size of K1 is ~20 μm. Its ion images show a rather uniform Si and O distribution interpreted as silicates, whereas C is restricted to areas of about the beam size (Fig. 2) One of these carbon-rich areas is extremely rich in both C and H. A large portion of the particle exhibits a strong ^{27}Al signal (Fig. 2). SEM examination revealed that large crystals could be seen between the fine-grained surface material. X-ray maps showed that the silicate background results in part from coarse-grained Mg silicate and in part from coarse-grained Ca, Al silicate.

3.2. Isotopic measurements of O, C, and Si

Results of isotopic measurements of Si, O, and C in the IDPs are summarized in Table 5. They all lie within solar values and fall in the range previously defined for IDPs and micrometeorites (McKeegan et al., 1985; McKeegan, 1987; Stadermann et al., 1989; Stadermann, 1990; Messenger, 1998; Engrand et al., 1999a). Isotopic compositions for Si, O, and C are homogeneous within each grain.

3.3. Hydrogen Isotopic Characterization

The studied IDPs present a large range of variation of D/H ratios (Table 6). Bulk D/H ratios (Table 6) reveal that three of the five particles studied exhibit significant deuterium enrichment. A6, K1, and E22 have bulk ratios of 287×10^{-6} ($\delta D = 842‰$), 294×10^{-6} (887‰) and 943×10^{-6} (5054‰), respectively, whereas R5 and R6 have bulk ratios which fall within the terrestrial range of 134×10^{-6} (−139‰) and 125×10^{-6} (−197‰), respectively. Deuterium excesses are present at the micrometer scale in K1, E22, and A6 (see Fig. 2 for K1) as first observed by McKeegan et al. (1987) in the IDP Butterfly. Direct comparison of the D, C, and Si images do not show obvious correlations. For instance, the deuterium-richest areas are not necessarily associated with the carbon-richest areas (A6, K1), but carbon is always present in deuterium-rich areas (Fig. 2).

The ROIscript was thus applied to all the images, and isotopic and elemental ratios were calculated for each ROI (see section 2.3.2.). If carbonaceous phases are carriers of deuterium enrichment (McKeegan et al., 1985; Keller et al., 2000), linear mixing correlations should exist between D/H and C/H ratios. The present IDPs show such relationships, which indicate mixing of several types of organic matter (having different C/H and D/H ratios) with phyllosilicates having C/H = 0 (Fig. 3). As a whole, (1) high C/H ratios seem to be linked with high D/H ratios, and (2) D/H ratios corresponding to C/H ratios close to 0 tend toward terrestrial values (~150×10^{-6}).

3.3.1. D/H results in individual IDPs

3.3.1.1. IDP K1

Repartition of ROIs in the D/H vs. C/H diagram fall in a triangle, suggesting that D/H ratios result from the mixing of at

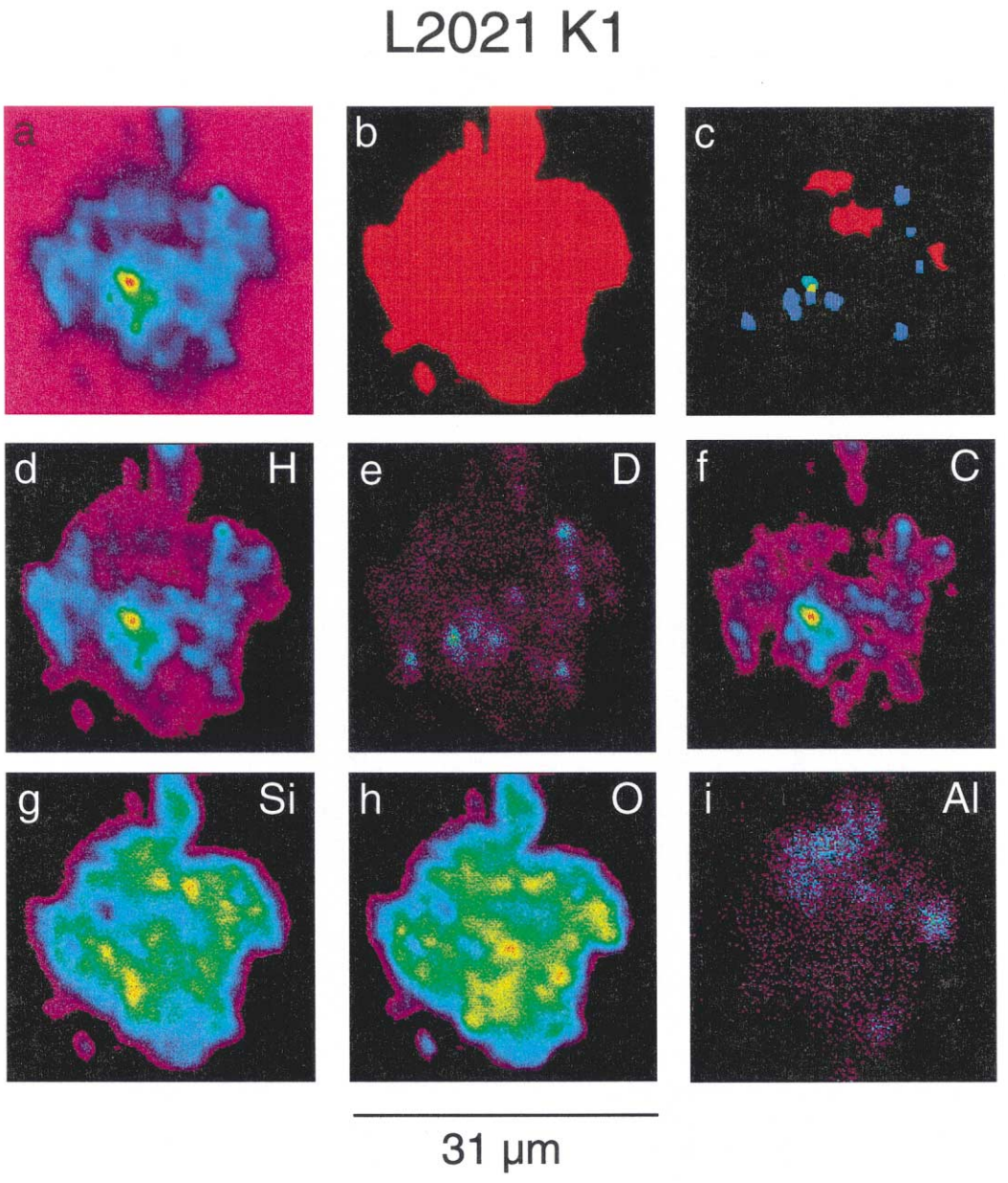

Fig. 2. Ion images of the IDP K1. (a) Whole IDP image given by the sum of normalized Si, H, C, and O (see text). (b) Mask of the total IDP resulting from the thresholding of Fig. 2a and representing the whole particle. (c) Masks of all enriched zones (see Fig. 1b). In red: Si-rich, Al-rich, and C-poor areas; in blue: deuterium-rich areas; in green: carbon-rich area. Note that one deuterium-rich area and the carbon-rich area are immediately adjacent; hence, their boundaries slightly overimpose (yellow). Ion images for H(d), D(e), C(f), Si(g), O(h), and Al(i).

least three endmembers (Fig. 3a). Selective extraction of deuterium-rich, carbon-rich, and silicon-rich areas from the images shows that these areas correspond to the triangle endmembers: a deuterium-rich endmember (D/H $\approx$ 1500 $\times$ 10^{-6}, C/H $\approx$ 1.0), a carbon-rich endmember (D/H $\approx$ 250 $\times$ 10^{-6}, C/H $\approx$ 1.5), and a silicon-rich endmember (D/H $\approx$ 180 $\times$ 10^{-6}, C/H $\approx$ 0.3) with D/H ratio close to terrestrial values. Furthermore, the deuterium-rich areas and the carbon-rich areas plot along a correlation.

3.3.1.2. IDP E22

Considering the ROIs, this IDP shows a positive correlation between D/H and C/H (Fig. 3b). As for K1, deuterium-rich, carbon-rich, and silicon-rich areas were extracted to define the endmembers. The first endmember corresponds to both deuterium-rich (D1, Table 6) and carbon-rich areas (D/H = 1880 $\times$ 10^{-6}, C/H $\approx$ 3.0). The second endmember is silicon rich with high D/H and C/H ratios (D/H $\approx$ 400 $\times$ 10^{-6}, C/H = 1.0). The deuterium-rich area D2 is responsible for the deviation of some ROIs from the trend. Silicon-rich phases present high D/H (up to 550 $\times$ 10^{-6}) and high C/H (up to 1.9) ratios compared to the other IDPs, which exhibit a silicon-rich phase with D/H $\leq$ 200 $\times$ 10^{-6} and C/H $<$ 0.5. But E22 exhibits the highest bulk

Table 5. Oxygen, carbon, and silicon isotopic ratios in the five analysed IDPs.

Isotopic ratio[a]	K1	E22	A6	R5	R6
$\delta^{18}O$	−25 ± 31	114 ± 49	−24 ± 16	14 ± 48	−45 ± 59
$\delta^{13}C$	−73 ± 55	−74 ± 22	−92 ± 47	−82 ± 117	−59 ± 27
$\delta^{29}Si$	−9 ± 30	−17 ± 38	−60 ± 60	6 ± 49	8 ± 31
$\delta^{30}Si$	−3 ± 21	−9 ± 33	−61 ± 61	−33 ± 58	−23 ± 19

[a] Mean values in ‰ of several areas defined by the ROIscript. Error bars represent the lateral variations within each IDP (1σ) at the beam scale. Values are given in deviation from a terrestrial reference (see Table 2).

carbon content and bulk D/H and C/H ratios. Therefore, a mixture of pure silicates (C/H = 0) with a minor amount of deuterium-rich organic matter (D/H = 1880×10^{-6}, C/H ≤ 3) in silicon-rich areas seems responsible for the high D/H and C/H ratios in these areas. This submicron mixing between silicates and organic matter, not resolved at the scale of the ion probe beam, is often encountered in IDPs (Bradley and Brownlee, 1986) and may reflect the fact that organic matter occurs as mantles around silicate grains (Wopenka, 1988). Note that although less obvious, this is also the case of the other analyzed IDPs for which the C/H ratio never reaches 0.

3.3.1.3. IDP A6

ROIs extracted from A6 present a rather simple correlation between D/H and C/H (Fig. 3c). The D/H ratio of the silicon-rich endmember (200×10^{-6} with C/H of ~0.4) is not far from terrestrial values. The second endmember (D/H ≈ 400×10^{-6}, C/H ≈ 0.7) is not well defined due to a slight difference in the D/H ratios between the deuterium-rich and carbon-rich areas, located immediately near each other, but not exactly similar.

3.3.1.4. IDP R5

R5 presents simple D/H vs. C/H patterns. Silicon-rich phases have a constant D/H ratio at terrestrial value with slightly

Table 6. D/H and C/H values of the 5 IDPs and of the deuterium, carbon, and silicon-rich areas within the particles.

IDP	Area[a]	C/H	σ C/H	D/H ($\times 10^{-6}$)	σ D/H ($\times 10^{-6}$)
K1	D1	1.16	0.13	1010	42
	D2	0.96	0.11	1150	87
	D3	1.00	0.12	1110	61
	D4	1.38	0.16	478	28
	D5	1.00	0.11	1120	48
	D6	1.21	0.14	528	27
	D7	1.03	0.12	1480	104
	D8	0.78	0.09	1510	116
	C1	1.51	0.17	253	18
	Si1	0.29	0.03	192	22
	Si2	0.47	0.05	174	8
	Si3	0.30	0.04	190	47
	Bulk	0.77	0.09	294	4
E22	C1-D1	2.94	0.32	1880	112
	D2	1.40	0.16	1670	120
	Si1	0.92	0.12	432	50
	Si2	1.90	0.21	556	41
	Bulk	1.57	0.18	943	69
A6	D1	0.64	0.08	449	6
	C1	0.70	0.08	329	8
	Si1	0.36	0.04	216	15
	Bulk	0.48	0.05	287	4
R5	il-Bulk	0.26	0.03	135	5
	il-C1	0.49	0.06	164	12
	il-C2	0.67	0.08	175	14
	il-C3	0.42	0.05	125	12
	il-Si1	0.23	0.03	136	11
	il-Si2	0.17	0.02	139	24
	il-Si3	0.41	0.05	141	22
	i3g1-Bulk	0.30	0.03	133	8
	i3-C1	0.33	0.04	141	16
	i3-C2	0.34	0.04	134	11
	i3-Si1	0.35	0.04	136	24
	i3-Si2	0.21	0.02	111	20
	i3-Si4	0.25	0.03	153	29
	i3g2-Bulk (i3-Si3)	0.11	0.01	144	11
R6	Bulk	2.34	0.27	125	3

[a] D stands for deuterium-rich; C for carbon-rich; Si for silicon-rich. In the case of R5, several images of several areas in the IDP have been acquired; il is image 1 and i3 image 3. Two distinct grains in image 3 are given by i3g1 and i3g2.

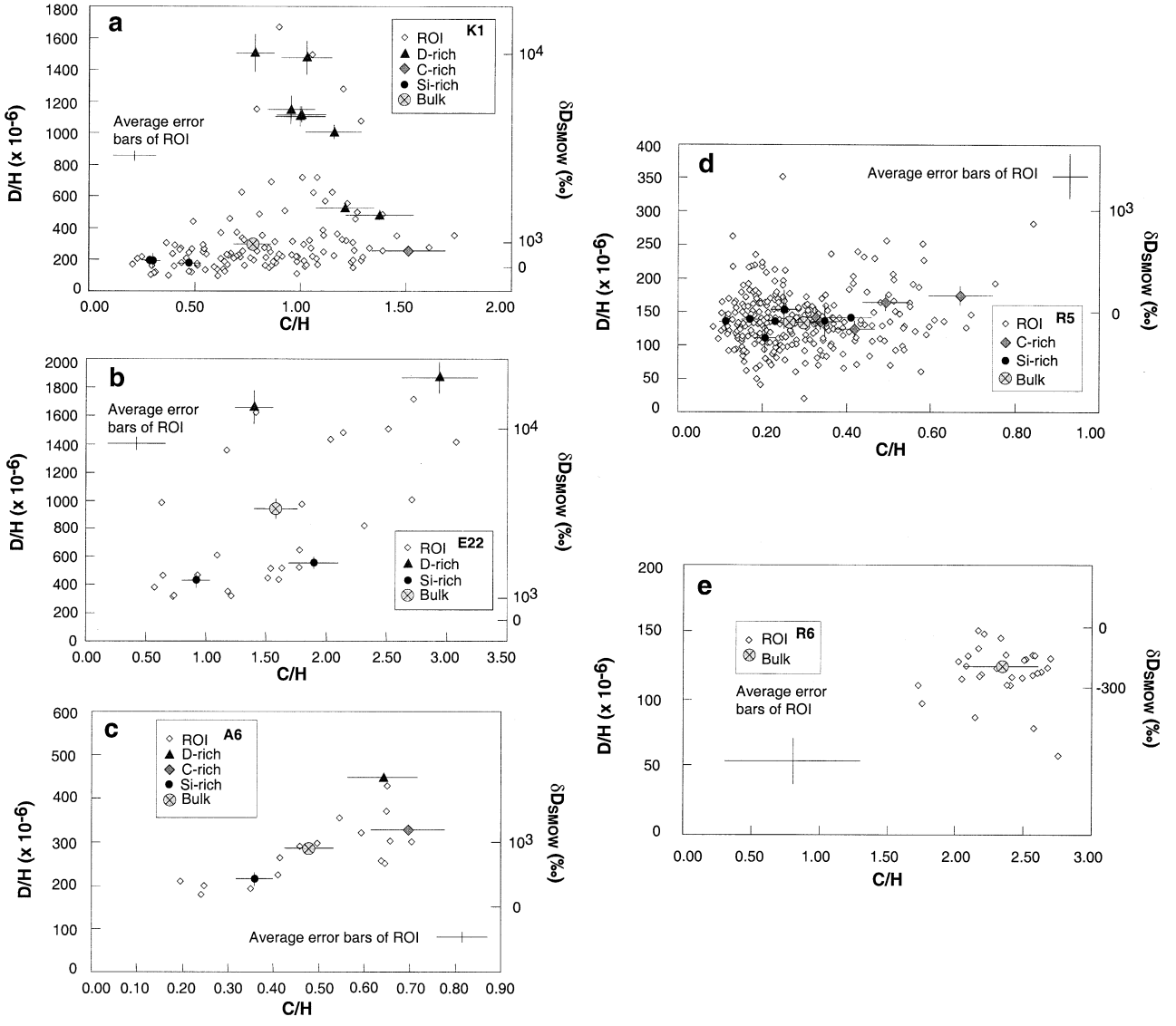

Fig. 3. D/H vs. C/H for the five analyzed particles. Open diamonds represent areas obtained by ROIscript processing; dark-gray triangles are deuterium-rich areas extracted from the deuterium images; gray diamonds are carbon-rich areas extracted from the C images; black circles are silicon-rich areas extracted from the Si images; crossed circles give the bulk value for each IDP. (a) K1. (b) E22. (c) A6. (d) R5 (to not overcrowd the figure, images i1 and i3 have not been distinguished). (e) R6 (only ROI areas and bulk value are shown).

varying C/H ratio between 0.1 and 0.4 (Fig. 3d). Most of the ROIs fall in the silicon-rich zone of the graph.

3.3.1.5. Particle R6.

R6 has a chemistry that is far from chondritic. Its D/H ratio of −193‰ falls at the lower limit of the terrestrial range of kerogens (down to −200‰; Fig. 3e). Furthermore, its homogeneous C/H ratio (2.3 ± 0.3) indicates that this particle is made from a limited number of carbonaceous species contrary to organic matter from IDPs (Wopenka, 1988; Clemett et al., 1993; Flynn et al., 2000; this work) or from carbonaceous chondrites, e.g., Robert and Newton (1996) and references therein. In addition, aluminum oxide grains are well-known contaminants in IDP collections and probably originate from rocket exhausts (e.g., McKeegan, 1986). Silica is rare in carbonaceous chondrites and has never been observed in IDPs, whereas quartz is an abundant component of continental dust (~10–20% in desert dust). Therefore, the mineral components of R6 (3 Al-O-rich grains and one Si-O-rich grain) are likely to be of terrestrial origin. Using ion microprobe imaging, terrestrial contaminant particles can thus be distinguished from IDPs. As a consequence, results for R6 are not taken into account in the following discussion.

3.3.2. Organic endmembers

Carbon-rich and deuterium-rich areas of A6, E22, and K1 allow the definition of three organic endmembers (Fig. 4). The trend defined by the deuterium-rich phases of IDP K1 can be interpreted as a mixing line between two different organic endmembers labeled OM1 and OM2 in Figure 4. OM1 has a

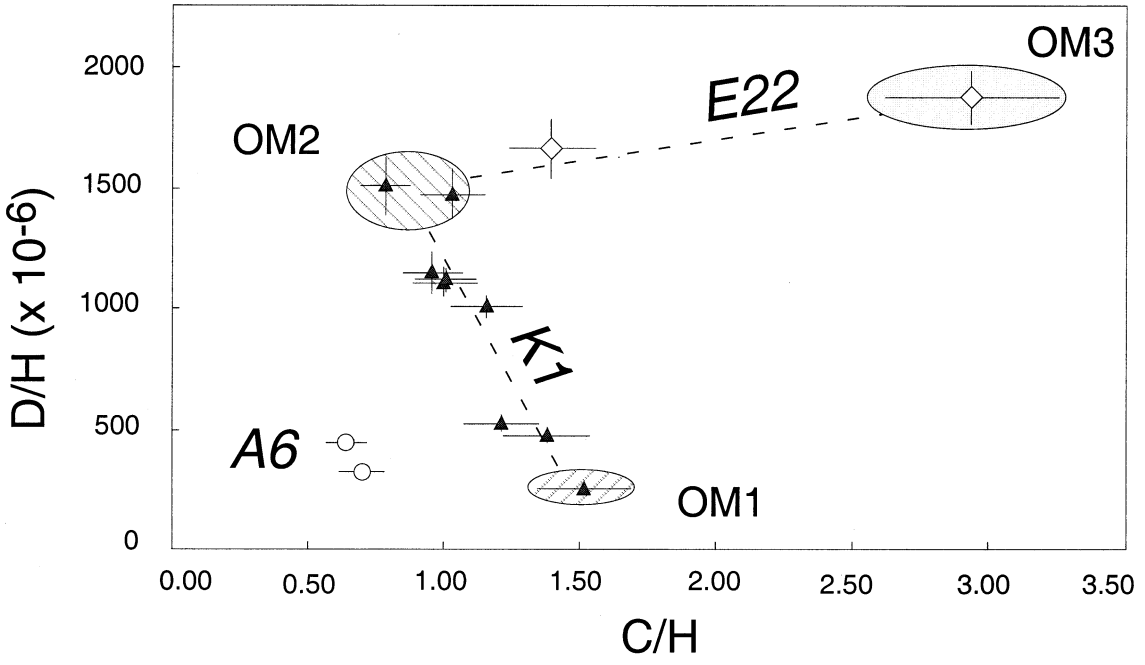

Fig. 4. D/H vs. C/H diagram of organic matter (OM) in the three deuterium-rich IDPs. Areas reported for each IDP are deuterium-rich and carbon-rich areas. Symbols stands for IDPs: triangles for K1, circles for A6, and diamonds for E22. Mixing model endmembers have been shaded and are referred to in the text as OM1, OM2, and OM3.

D/H ratio of $\sim 250 \times 10^{-6}$ and a C/H ratio of 1.5 ± 0.2, whereas D/H in OM2 is $\sim 1500 \times 10^{-6}$ with a C/H ratio of 1.0 ± 0.1. This is evidence that two types of deuterium-rich organic matter with different deuterium excesses coexist in the same IDP. In E22 a third type of organic matter appears. This organic matter has a C/H ratio of ~ 3 and a D/H value which reaches 1900×10^{-6}. This phase is labeled OM3 on Figure 4. Deuterium excesses of the carbon-rich and deuterium-rich phases of A6 can also be explained by a mixing between water and at least one of these three types of organic matter. The well-defined correlation in K1 and the high abundance of carbon in E22 indicate that the contribution of water in the carbon-rich areas is probably negligible.

3.3.3. The water endmember

Free water in IDPs, even if present in space, cannot be preserved in the laboratory. However, parent body alteration of silicates by water produces phyllosilicates whose hydroxyls keep a memory of the water D/H ratio. This D/H ratio can be obtained from the analysis of silicon-rich areas in the ion images. These silicon-rich areas represent a common endmember to the present IDPs and correspond to low C/H and low D/H ratios, except for E22 in which an organic signature is evidenced in silicon-rich areas (see section 3.3.1), suggesting that E22 silicates may be anhydrous. Although no mineralogic characterization of the silicates has been done, this suggests that the hydrogen-rich silicate endmember of K1, A6, and R5 represents phyllosilicates. Since submicron mixing with organic matter is likely in all IDPs, the D/H ratio of phyllosilicates can be obtained by extrapolating the correlations at C/H = 0 and is labeled D/H_{water}. Regression lines were calculated using the ROIs for each IDP. The K1 regression line is determined from the base of the mixing triangle, since most of the ROI plot in this area suggesting that this trend represents almost the whole IDP. Results are shown in Table 7. E22 yields a low-precision intercept: $D/H_{water} = 161^{+187}_{-161} \times 10^{-6}$. The value for R5 is undistinguishable from that of the bulk sample ($D/H_{water} = 124 \pm 6 \times 10^{-6}$ compared to $D/H_{bulk} = 135 \pm 5 \times 10^{-6}$). A6 and K1 have values in good agreement with that of R5 and fall in the chondritic range (~ 100–155×10^{-6}). K1,

Table 7. Parameters of the regression lines in the IDPs.

IDP	Slope (D atoms per C atoms)	σ slope	D/H at C/H=0	σ origin
R5	50×10^{-6}	18×10^{-6}	124×10^{-6}	6×10^{-6}
K1[a]	74×10^{-6}	18×10^{-6}	160×10^{-6}	16×10^{-6}
A6	304×10^{-6}	74×10^{-6}	129×10^{-6}	38×10^{-6}
E22	422×10^{-6}	108×10^{-6}	161×10^{-6}	187×10^{-6}

[a] Regression for K1 has not been calculated for the whole IDP but for the main basal trend (see text).

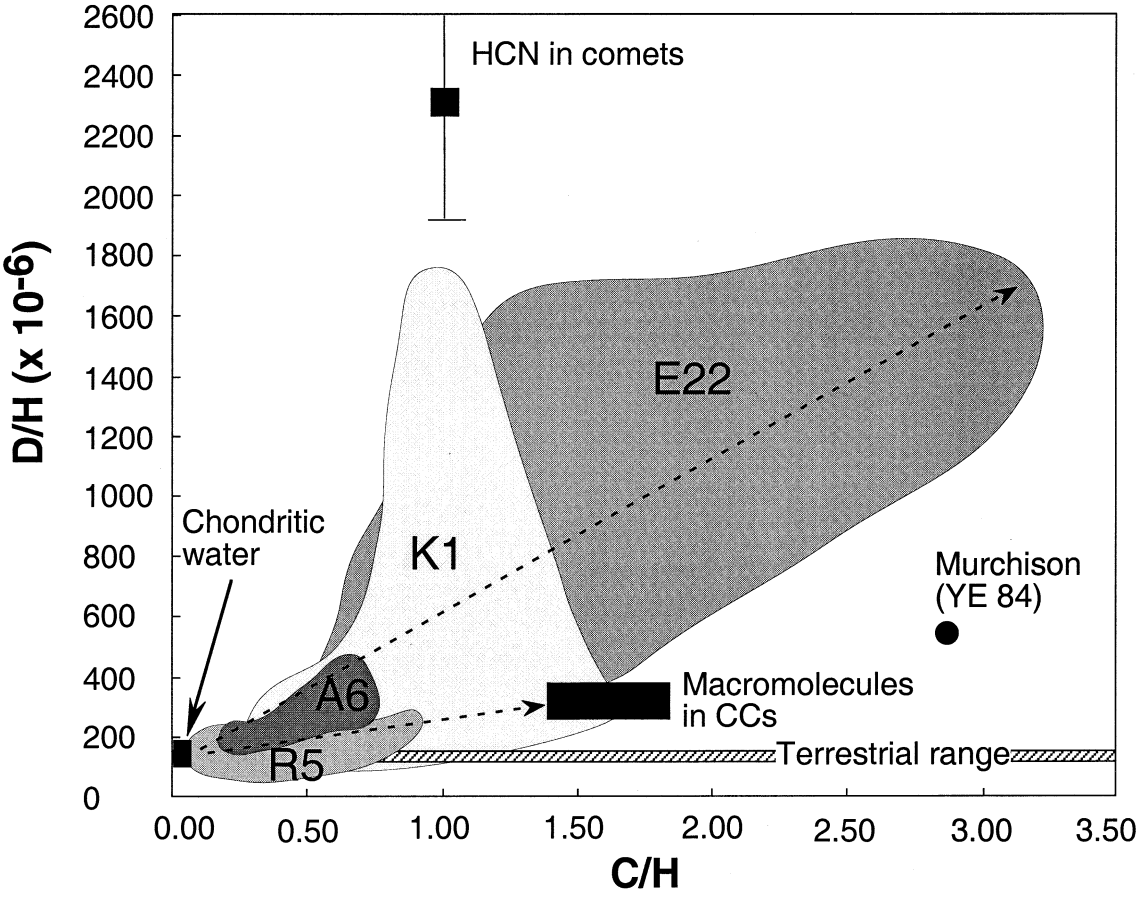

Fig. 5. D/H vs. C/H diagram with the domains defined by each IDP. Cometary HCN (in Hale-Bopp; Meier et al., 1998b). Macromolecules from carbonaceous chondrites. Refractory molecules from carbonaceous chondrites (Yang and Epstein, 1984), chondritic water (i.e., phyllosilicates in CCs) and terrestrial values are shown for comparison. Each domain seems governed by mixing between water and deuterium-rich organic matter.

which exhibits D/H ratios in carbonaceous phases up to 1500×10^{-6}, has a water D/H ratio falling also in the chondritic range ($160 \pm 16 \times 10^{-6}$).

4. DISCUSSION

4.1. Several interstellar organic components in IDPs

The use of C/H ratio to distinguish among several types of organic matter sheds light on the nature of these organic phases. Indeed, the C/H and D/H values of OM1 ($\sim$1.5 and 250×10^{-6}, respectively) are close to those observed in the macromolecular organic molecules of carbonaceous chondrites (Fig. 5): C/H = 1.39 in Orgueil and 1.33 in Murchison (Gardinier et al., 2000) with D/H $\sim 350 \times 10^{-6}$ (e.g., Robert and Epstein, 1982; Kerridge, 1983; Yang and Epstein, 1983). This implies that OM1 and the chondritic macromolecules have both common structural properties and common history, indicating in turn that this organic matter can be ascribed to the macromolecular organic matter found in carbonaceous chondrites. Furthermore, as in carbonaceous chondrites, this OM1 component is the dominant carbonaceous phase in K1. Small size units of aromatic polymers interconnected by short linear bridges have been shown to be the main moieties of this chondritic macromolecular organic matter (Gardinier et al., 2000).

Since OM2 has a C/H of 1.0 or slightly lower, aliphatic hydrocarbons should dominate this organic component. Aliphatic hydrocarbons have lower C/H ratios than aromatic hydrocarbons, since they are dominated by -CH_2 groups, i.e., a C/H of 0.5. This ratio can increase up to 1.0 due to heterosubstitution. The lowest C/H of aromatic hydrocarbons is 1.0 (C_6H_6, benzene) and increases with the number of cycles. Based on the similarity between D/H and C/H in OM2 and in cometary HCN ($1500 \pm 150 \times 10^{-6}$ and 1.0 ± 0.1 compared to $2300 \pm 400 \times 10^{-6}$ and 1.0; Fig. 5), OM2 might be constituted by nitrogen-rich molecules. Since pure HCN is probably no longer present in the sample because of its volatility at laboratory temperatures, these molecules could be the byproducts of HCN polymerization with a C/H ratio close to 1 (Minard et al., 1998). The wide occurrence in interstellar space of infrared signatures at 3.4 μm, similar to those of the carbonaceous chondrite macromolecules (Ehrenfreund et al., 1991; Pendleton et al., 1994), suggests that highly condensed organic matter such as polymers is an abundant form of carbon in the interstellar medium. Furthermore, nitrogen-rich refractory organic particles have been detected in comet Halley (Jessberger

et al., 1988). In that case, the polymerization process would have occurred by irradiation, either during the formation of the refractory crust, which is present at the surface of cometary nuclei, or in interstellar space before incorporation into cometary or meteoritic material.

With a C/H of ~3.0, OM3 has the highest C/H ratio observed in the four IDPs. Such a value is not far from that of the acid-treated residues of carbonaceous chondrites after their dehydrogenation by pyrolysis at 1000°C (Robert and Epstein, 1982) but implies, in turn, that OM3, to reach such a high C/H ratio, could have been heated up to 1000°C. Such a postulated thermal degradation is not compatible with the measured D/H ratio. Indeed, recent models of the evolution of a turbulent protosolar nebula show that at 1000°C, the macromolecular organic matter loses its interstellar D/H signature and re-equilibrates isotopically with the protosolar molecular hydrogen, reaching values of $\sim 10^{-4}$ (Mousis et al., 2000). This is clearly not the case with OM3 whose D/H ratio is among the highest solar system values and therefore cannot have been pyrolysed in the protosolar nebula. Thus, the high C/H and D/H ratios of OM3 indicate that its polymerization occurs in space at low temperature from simple interstellar molecules. This conclusion is also supported by the observation of Yang and Epstein (1984) who showed that a refractory organic component is present in Murchison with a high C/H ratio (2.81) and with the highest D/H ratio ever observed in CM and CI chondrites ($\delta D = 2584‰$, i.e., D/H $\approx 555 \times 10^{-6}$; Fig. 5).

4.2. Water in IDPs: Chondritic or Cometary?

The low D/H ratio of water in IDPs raises several problems, which are discussed below. Indeed, these values fall in the chondritic domain, but at least in IDP K1, this possible chondritic water is associated to the deuterium-rich HCN component, OM2. Comet Hale-Bopp is the only known object in the solar system having D/H and C/H ratios ($2300 \pm 400 \times 10^{-6}$ in HCN; Meier et al., 1998b) similar to those found in K1 and E22. Therefore, the presence of OM2 in these two IDPs could be regarded as an indication of their cometary origin. However, in contrast to the IDPs, the D/H ratio of water measured in the coma of comets is approximately twice the terrestrial value ($310 \pm 45 \times 10^{-6}$; Eberhardt et al., 1995; Bockelée-Morvan et al., 1998; Meier et al., 1998a). This apparent contradiction yields one or several of the following hypotheses: (1) Water ice in comets is heterogeneous in D/H ratios. (2) In comets, a difference in D/H ratios exists between water vapor in the coma and water ice in the nucleus. (3) The water D/H ratio in IDPs represents terrestrial contamination. (4) None of the four measured IDPs is cometary. These points are discussed in succession:

1. The dust in the region of comet formation can be viewed as a mixture of icy grains having different D/H ratios: interstellar grains with D/H of up to $720 \pm 120 \times 10^{-6}$ (i.e., interstellar water in LL3 chondrites; Deloule and Robert, 1995) mixed with chondritic-like grains (D/H $\sim 150 \times 10^{-6}$). In such an hypothesis, the cometary water D/H ratio ($310 \pm 45 \times 10^{-6}$) would correspond to a mixture of 70% ice, which originated from condensation in the inner solar system with a chondritic D/H ratio of $\sim 150 \times 10^{-6}$, and 30% of preserved interstellar ice with a D/H of $\sim 720 \times 10^{-6}$. This hypothesis is supported by the turbulent model of the protosolar nebula (Drouart et al., 1999), which shows that at the location of comet formation, the water vapor D/H ratio decreases with time via the injection of water vapor from the inner regions of the disk. Since the grains are coupled with the gas as long as their size does not exceed 1 cm, these results on vapor are valid for icy grains. It is also interesting to note that silicates (mostly olivine) in comets are both amorphous and crystalline (Crovisier et al., 1997; Wooden et al., 1999), which may indicate an interstellar and a protosolar origin, respectively. This suggests a similar mixing systematics for water ices, since interstellar ice is likely to be amorphous (e.g., Bar-Nun et al., 1985), whereas water condensed at ~150 K in the protosolar nebula should be crystalline. In such an interpretation, the water isotopic composition in comets is heterogeneous and somewhat similar to that observed in LL3 chondrites.
2. It is conceivable that during its outgassing from the nucleus, cometary water is enriched in deuterium via an isotopic exchange with deuterium-rich organic matter. The increase in the water D/H ratio from 150×10^{-6} (measured in IDPs) to 310×10^{-6} (measured in the coma) would require a maximum 8% exchange between organic hydrogen (taking a nominal D/H value of 2000×10^{-6}) and water. With 50% water in comets, this implies an exchange with 9 wt.% of organic carbon. Such a carbon concentration is in disagreement with the organic-to-water ratio measured in the coma (Biver et al., 1997) but compatible with the carbon-to-water ratio estimated for the grains. Detailed modeling of the transient water circulation in the nucleus, either at the perihelia (Benkhoff, 1999) or during accretion (Prialnik and Podolak, 1999), indicates that such an isotopic exchange between liquid water and organic matter can indeed take place. Durations for this isotopic exchange can be calculated from Eqn. 1 and 2 and are in the order of years. However, this interpretation requires a fine-tuning of several parameters and, in this respect, seems unlikely.
3. A sample contamination by laboratory vapor water also seems unlikely. The samples were heated under high vacuum in the sample chamber of the ion probe, and a presputtering was systematically performed before each analysis (see section 2.2.1.) An isotopic exchange with atmospheric water vapor during the atmospheric entry of IDPs is also unlikely. Indeed, contamination experiments have demonstrated that no isotopic exchange occurs on powdered material from the Orgueil CI chondrite immerged for 1 month in deuterated liquid water (Engrand et al., 1999b). Furthermore, isotopic exchange between water and clay minerals is negligible at room temperature (Savin and Epstein, 1970). Therefore, even the direct contact with liquid water should not affect the D/H ratio of clay minerals in IDPs. However, an addition of water to the sample cannot be totally excluded: IDPs exhibit a porous texture and their submicron grain size could provide enormous reactive specific surfaces for the adsorption of terrestrial water. Therefore, as far as the D/H ratio of water in IDPs is concerned, this crucial issue cannot be considered to be firmly solved. Further contamination simulation experiments with deuterium-rich

water are needed along with a mineralogic identification of the phyllosilicates.

4. The possibility that none of these IDPs are cometary is not unrealistic. Indeed, although no lower detection limit has been proposed, phyllosilicates are absent in the IR spectrum of comet Hale-Bopp (Wooden et al., 2000), indicating, in turn, that hydrated IDPs may not originate from comets. However, this observation implies that the D/H ratio in water is decoupled from that in organic matter. This second point is not supported by observations in meteorites for which CR and LL3 chondrites exhibit the highest D/H ratio both in water and in organic matter (Robert and Epstein, 1982; Yang and Epstein, 1983; Deloule and Robert, 1995). As for hypothesis 3, the mineralogic observation of phyllosilicates in these four IDPs is required for more definitive conclusions.

4.3. From Interstellar to Cometary and Chondritic D/H Ratios

The large D/H ratios observed in IDP organic matter can only be attributed to ion-molecule or gas-grain surface reactions in dense interstellar clouds (e.g., Tielens, 1983; Brown and Millar, 1989; Millar et al., 1989; Messenger, 2000). Previous determinations in small fragments of IDPs have exhibited high D/H ratios (e.g., Zinner et al., 1983; McKeegan et al., 1985; Messenger, 2000). In some of these fragments, the D/H ratio exceeds that measured in the present study for K1, A6, and even E22. Thus, organic molecules in IDPs define a large domain of variation, likely reflecting the different sources of IDPs in the solar system. Although the endmember of the IDP D/H distribution is similar to that reported in interstellar molecules, the mean D/H value in IDPs remains lower by a factor 5 to 10 than those measured in interstellar molecules from molecular clouds (see, for instance, the compilation of data in Robert et al., 2000). A key to this discrepancy is likely the isotopic exchanges that might have taken place between interstellar H-bearing compounds and solar system H_2 or water.

The kinetics of isotopic exchange between kerogens and either water or hydrogen can be determined using the results of Lécluse and Robert (1994) and Schimmelmann et al. (1999). The kinetics of isotopic exchange can be described by the following equation:

$$f(t) = \alpha(T) + [\, f_{t=0} - \alpha(T)] \exp (- P\ k^{-}(T)\ t) \qquad (1)$$

(Lécluse et al., 1996)

where f(t) is the deuterium enrichment factor $(D/H)_{ker}/(D/H)_m$ at time t with $(D/H)_{ker}$ the isotopic ratio of the kerogen and $(D/H)_m$ the isotopic ratio of the medium (H_2 or H_2O). α(T) is the equilibrium constant of the isotopic exchange reaction. P is the pressure expressed in atmospheres (given by the water or hydrogen pressure). k^{-}(T) is the kinetic rate constant of the reaction in $atm^{-1}.s^{-1}$. For an isotopic exchange between CH_4 and H_2, this constant obeys an Arrhenius law and has been experimentally determined to be:

$$k^{-}(T) = 6.1 \times 10^{-25} \exp (-4.38 \times 10^{3}/T) \qquad (2)$$

(Lécluse and Robert, 1994)

with k^{-}(T) in cm^3/s, given that k^{-}(T) [in cm^3/s] = k^{-}(T) [in $atm^{-1}.s^{-1}$] $\times$ T/(298 $\times$ 2.687 $\times$ 10^{19}) (Lécluse and Robert, 1994). In experiments where the isotopic exchange rates between kerogen samples and liquid water were measured (Schimmelmann et al., 1999), it is possible to determine k^{-}(600 K) by using Eqn. 1: 9.1 $\times$ 10^{-28} cm^3/s. This value is in agreement within a factor of two with k^{-}(600 K) calculated using Eqn. 2 (4.3 $\times$ 10^{-28} cm^3/s). Therefore, Eqn. 1 can be used with confidence to simulate an isotopic exchange during the maturation of a kerogen in liquid water.

In a parent body in which the isotopic exchange takes place between organic matter and liquid water, pressure and temperature are taken to be, respectively, 1 atm (i.e., close to water vapor pressure above liquid) and 353 K. The water D/H ratio is taken at the SMOW value (155 $\times$ 10^{-6}). The final organic D/H ratio is taken at the OM3 value (2000 $\times$ 10^{-6} or ~12,000‰) since it corresponds to the highest D/H measured in several IDPs, including Wiley at 12,000‰ and Roadrunner at 11,000‰ (Messenger, 2000) and Butterfly at > 9000‰ (McKeegan et al., 1987), and is within error of cometary HCN (2300 $\pm$ 400 $\times$ 10^{-6}; Meier et al., 1998b). In that case, only 24 months (or 71 yr at 273 K) of isotopic exchange are necessary to decrease the D/H ratio of OM3 from the highest D/H ratios observed in interstellar organic molecules (~1 $\times$ 10^{-1} in C_3H_2; Bell et al., 1988) down to 1.9 $\times$ 10^{-3}, i.e., down to the OM3 measured value. The isotopic exchange with liquid water is thus extremely fast and can significantly lower the interstellar D/H ratios during the parent body formation processes. The large range of D/H ratios of organic matter in IDPs and chondrites can therefore be produced from interstellar precursors by variable degrees of isotopic exchange, depending on the internal structures and temperatures of the parent body reached during accretion. Thus, the IDP Dragonfly described by Messenger (2000) is characterized by only a small extent of isotopic exchange, whereas the macromolecular organic matter in carbonaceous chondrites (i.e., OM1) was exchanged to a greater degree.

4.4. Links With Parent Bodies

New insights on the cometary or chondritic origin of IDPs might emerge from the slopes of the D/H vs. C/H correlations observed for the four IDPs (Table 7). In fact these correlations represent a mixing between water and the dominant organic phase whose origin can be specifically ascribed either to cometary or chondritic sources.

K1 and R5 have a slope one order of magnitude lower than those of IDPs E22 and A6. As OM2 (the likely cometary component) is a minor phase in K1, this slope corresponds to mixing between water and OM1, whereas it corresponds to mixing between water and OM3 for E22 and A6. Since OM3 has been ascribed (in section 4.1.) to interstellar organic polymers, parent bodies that could preserve such a phase are those formed in the external solar system, i.e., comets or extinct comet nuclei. Alternatively, the K1 and R5 organic matters are dominated by a component (OM1) whose C/H and D/H ratios are similar to those measured in the chondritic macromolecular organic matter, suggesting that the parent bodies of K1 and R5 have composition similar to carbonaceous chondrites. However, a contradiction arises from the presence of OM2 in K1:

Why does an IDP, which has major similarities to carbonaceous chondrites, exhibit such a minor cometary phase? This might suggest a link between carbonaceous chondrites and comets. Another question remains open as no chondritic counterpart has yet been observed for OM3: Why was not such a refractory phase preserved in the inner regions of the solar system, i.e., in carbonaceous chondrites?

5. CONCLUSIONS

At least three different organic components have been identified in the four IDPs studied in this work and all of these components carry deuterium excesses: (1) One is similar to the macromolecular organic matter of carbonaceous chondrites, (2) one is a highly condensed material likely synthesized via interstellar chemistry, which has not yet been observed in any extraterrestrial object, and (3) one may represent a heterosubstituted aliphatic material, such as an HCN polymer, based on the similarities with HCN detected in comet Hale-Bopp. Water is shown to have a chondritic D/H ratio.

Intricate mixing among these different components is observed at the micrometer scale. Mixing between water and the organic components provides a tool for identifying the source of individual particles, since the cometary and the meteoritic isotopic signatures can be distinguished. Finally, cometary components are found together with meteoritic macromolecular components, which suggests a link between carbonaceous chondrites and comets.

Acknowledgments—Janet Borg and Eric Quirico are thanked for providing us the samples and ample discussions on IDPs. Etienne Deloule gave helpful advice and comments on D/H measurements, and Denis Mangin is thanked for the great care he brought to the machine. We thank Tobias Owen and three anonymous reviewers for constructive comments that greatly improved this manuscript. This work also benefited from editorial advice by Rainer Wieler. This work was supported by the PNP INSU, the PCMI INSU, and the CNES Exobiology programs. This is CRPG-CNRS contribution 1533.

Associate editor: R. Wieler

REFERENCES

Aléon J., Chaussidon M., Champenois M., and Mangin D. (2001) Quantitative imaging of stable isotopes by ion microprobe. *Geostand. Newslett.*. in press.

Bar-Nun A., Hermann G., Laufer D., and Rappaport M.L. (1985) Trapping and release of gases by water ices, and implications for icy bodies. *Icarus* **63,** 317–332.

Bell M. B., Avery L. W., Matthews H. E., Feldman P. A., Watson J. K. G., Madden S. C., and Irvine W. M. (1988) A study of C_3HD in cold interstellar clouds. *Astrophys. J.* **326,** 924–930.

Benkhoff J. (1999) On the flux of water and minor volatiles from the surface of comet nuclei. *Space Sci. Rev.* **90,** 141–148.

Biver N., Bockelée-Morvan D., Colom P., Crovisier J., Davies J. K., Dent W. R. F., Despois D., Gérard E., Lellouch E., Rauer H., Moreno R., and Paubert G. (1997) Evolution of the outgassing of comet Hale-Bopp (C/1995 O1) from radio observations. *Science* **275,** 1915–1918.

Bockelée-Morvan D., Gautier D., Lis D. C., Young K., Keene J., Phillips T., Owen T., Crovisier J., Goldsmith P. F., Bergin E. A., Despois D., and Wooten A. (1998) Deuterated water in comet C/1996 B2 (Hyakutake) and its implications for the origin of comets. *Icarus* **133,** 147–162.

Bradley J. P. and Brownlee D. E. (1986) Cometary particles: Thin sectioning and electron beam analysis. *Science* **231,** 1542–1544.

Bradley J. P. and Brownlee D. E. (1991) An interplanetary dust particle linked directly to type CM meteorites and an asteroidal origin. *Science* **251,** 549–552.

Brown P. D. and Millar T. J. (1989) Models of the gas-grain interaction—deuterium chemistry. *Mon. Not. R. Astron. Soc.* **237,** 661–671.

Brownlee D. E. (1985) Cosmic dust: Collection and research. *Ann. Rev. Earth Planet. Sci.* **13,** 147–173.

Clemett S. J., Maechling C. R., Zare R. N., Swan P. D., and Walker R. M. (1993) Identification of complex aromatic molecules in individual interplanetary dust particles. *Science* **262,** 721–725.

Crovisier J., Leech K., Bockelée-Morvan D., Brooke T. Y., Hanner M. S. Altieri B., Keller H. U., and Lelouch E. (1997) The spectrum of comet Hale-Bopp (C/1995 O1) observed with the Infrared Space Observatory at 2.9 astronomical units from the Sun. *Science* **275,** 1904–1907.

Deloule E. and Robert F. (1995) Interstellar water in meteorites? *Geochim. Cosmochim. Acta* **59,** 4695–4706.

Deloule E., France-Lanord C., and Albarède F. (1991) D/H analysis of minerals by ion probe. In *Stable Isotope Geochemistry: A Tribute to Samuel Epstein* (ed. H. P. Taylor, Jr., J. R. O'Neil, and I. R. Kaplan), Spec. Pub. 3, pp. 53–62, Geochemical Society. San Antonio.

Drouart A., Dubrulle B., Gautier D., and Robert F. (1999) Structure and transport in the Solar Nebula from constraints on deuterium enrichment and giant planets formation. *Icarus* **140,** 129–155.

Eberhardt P., Reber M., Krankowsky D., and Hodges R. R. (1995) The D/H and $^{18}O/^{16}O$ ratios in water from comet P/Halley. *Astron. Astrophys.* **302,** 301–316.

Ehrenfreund P., Robert F., D'Hendencourt L., and Behar F. (1991) Comparison of interstellar and meteoritic organic matter at 3.4 μm. *Astron. Astrophys.* **252,** 712–717.

Engrand C., McKeegan K. D., Leshin L. A., Bradley J. P., and Brownlee D. E. (1999a) ^{16}O-excess in a GEMS-rich IDP. *Lunar Planet. Sci. XXX*, 1690 (abstr.), Lunar Planet. Inst., Houston. LPS Conf. 30 CD-ROM.

Engrand C., Deloule E., Robert F. Maurette M., and Kurat G. (1999b) Extraterrestrial water in micrometeorites and cosmic spherules from Antarctica: An ion microprobe study. *Meteorit. Planet. Sci.* **34,** 773–786.

Flynn G. J. (1989) Atmospheric entry heating: A criterion to distinguish between asteroidal and cometary sources of interplanetary dust. *Icarus* **77,** 287–310.

Flynn G. J., Keller L. P., Jacobsen C., Wirick S., and Miller M. A. (2000) *Organic carbon in interplanetary dust particles.* ASP Conf. Series, Bioastronomy '99—A New Era in Bioastronomy. **213,** 191–194. Astron. Soc. Pacific, San Francisco.

Gardinier A., Derenne S., Robert F., Behar F., Largeau C., and Maquet J. (2000) Solid state CP/MAS ^{13}C NMR of the insoluble organic matter of the Orgueil and Murchison meteorites: Quantitative study. *Earth Planet. Sci. Lett.* **184,** 9–21.

Geiss J. and Reeves H. (1981) Deuterium in the solar system. *Astron. Astrophys.* **93,** 189–199.

Jessberger E. K., Christoforidis A., and Kissel J. (1988) Aspects of the major element composition of Halley's dust. *Nature* **332,** 691–695.

Keller L. P., Thomas K. L., and McKay D. S. (1992) An interplanetary dust particle with links to CI chondrites. *Geochim. Cosmochim. Acta* **56,** 1409–1412.

Keller L. P., Messenger S., Flynn G. J., Jacobsen C., and Wirick S. (2000) Chemical and petrographic studies of molecular cloud materials preserved in interplanetary dust. *Meteorit. Planet. Sci.* **35,** A86–A87.

Kerridge J. F. (1983) Isotopic composition of carbonaceous-chondrite kerogen: Evidence for an interstellar origin of organic matter in meteorites. *Earth Planet. Sci. Lett.* **64,** 186–200.

Lécluse C. and Robert F. (1994) Hydrogen isotope exchange reaction rates: Origin of water in the inner solar system. *Geochim. Cosmochim. Acta* **58,** 2927–2939.

Lécluse C., Robert F., Gautier D., and Guiraud M. (1996) Deuterium enrichment in giant planets. *Planet. Space Sci.* **44,** 1579–1592.

McKeegan K. D. (1986) Hydrogen and magnesium isotopic abundances in aluminum-rich stratospheric dust particles. In *Lunar Planetary Science XVII*, pp. 539–540, Lunar Planet. Inst., Houston. LPS Conf. 17.

McKeegan K. D. (1987) Oxygen isotopes in refractory stratospheric

dust particles: Proof of extraterrestrial origin. *Science* **237,** 1468–1471.

McKeegan K. D., Walker R. M., and Zinner E. (1985) Ion microprobe isotopic measurements of individual interplanetary dust particles. *Geochim. Cosmochim. Acta* **49,** 1971–1987.

McKeegan K. D., Swan P., Walker R. M., Wopenka B., and Zinner E. (1987) Hydrogen isotopic variations in interplanetary dust particles. *Lunar Planet. Science XVIII*, pp. 627–628, Lunar Planet. Inst., Houston. LPS Conf. 18.

Meier R., Owen T. C., Matthews, H. E., Jewitt D. C., Bockelée-Morvan D., Biver N., Crovisier J., and Gautier D. (1998a) A determination of the HDO/H_2O ratio in comet C/1995 O1 (Hale-Bopp). *Science* **279,** 842–844.

Meier R., Owen T. C., Jewitt D. C., Matthews H. E., Senay M., Biver N., Bockelée-Morvan D., Crovisier J., and Gautier D. (1998b) Deuterium in Comet C/1995 O1 (Hale-Bopp): Detection of DCN. *Science* **279,** 1707–1710.

Messenger S. (1998) Oxygen isotopic imaging of interplanetary dust. *Meteorit. Planet. Sci.* **33,** A106—A107.

Messenger S. (2000) Identification of molecular-cloud material in interplanetary dust particles. *Nature* **404,** 968–971.

Messenger S. R. and Walker R. M. (1997) Evidence for molecular cloud material in meteorites and interplanetary dust. In *Astrophysical Implications of the Laboratory Study of Presolar Materials* (eds T. J. Bernatowicz and E. Zinner), pp. 545–564, AIP Conf. Proc. 402. Amer. Inst. Phys., Woodbury.

Millar T. J., Bennett A., and Herbst E. (1989) Deuterium fractionation in dense interstellar cloud. *Astrophys. J.* **340,** 906–920.

Minard R. D., Hatcher P. G., Gourley R. C., and Matthews C. N. (1998) Structural investigations of hydrogen cyanide polymers: New insights using TMAH thermochemolysis/GC-MS. *Origins Life Evol. B.* **28,** 461–473.

Mousis O., Gautier D., Bockelée-Morvan D., Robert F., Dubrulle B., and Drouart A. (2000) Constraints on the formation of comets from D/H ratios measured in H_2O and HCN. *Icarus* **148,** 513–525.

Nier A. O. and Schlutter D. J. (1992) Extraction of helium from individual interplanetary dust particles by step-heating. *Meteoritics* **27,** 166–173.

Nittler L. R. and Messenger S. R. (1998) Hydrogen and nitrogen isotopic imaging of interplanetary dust. *Lunar Planet. Science XXIX*, #1380(abstr.), Lunar Planet. Inst., Houston. LPS Conf. 29 CD-ROM.

Pendleton Y. J., Sandford S. A., Allamandola L. J., Tielens A. G. G. M., and Sellgren K. (1994) Near-infrared absorption spectroscopy of interstellar hydrocarbon grains. *Astrophys. J.* **437,** 683–696.

Prialnik D. and Podolak M. (1999) Changes in the structure of comet nuclei due to radioactive heating. *Space Sci. Rev.* **90,** 169–178.

Robert F. and Epstein S. (1982) The concentration and isotopic composition of hydrogen, carbon and nitrogen in carbonaceous meteorites. *Geochim. Cosmochim. Acta* **46,** 81–95.

Robert F. and Newton J. (1996) Carbonaceous species in extraterrestrial environments. *Condens. Matter News.* **5,** 8–27.

Robert F., Gautier D. and Dubrulle B. (2000) The solar system D/H ratios: Observations and theories. *Space Sci. Rev.* **92,** 201–224.

Sandford S. A. (1986) Solar flare track densities in interplanetary dust particles: The determination of an asteroidal versus cometary source of the zodiacal dust cloud. *Icarus* **68,** 377–394.

Savin S. M. and Epstein S. M. (1970) The oxygen and hydrogen isotope geochemistry of clay minerals. *Geochim. Cosmochim. Acta* **34,** 25–42.

Schimmelmann A., Lewan M. D., and Wintsch R. P. (1999) D/H isotope ratios of kerogen, bitumen, oil and water in hydrous pyrolysis of source rocks containing kerogen types I, II, IIS and III. *Geochim. Cosmochim. Acta* **63,** 3751–3766.

Shimizu N., Semet M. P., and Allègre C. J. (1978) Geochemical applications of quantitative ion-microprobe analysis. *Geochim. Cosmochim. Acta* **42,** 1321–1334.

Stadermann F. J. (1990) *Messung von Isotopen- und Elementhäufigkeiten in einzelnen Interplanetaren Staubteilchen mittels Sekundärionen-Massenspektrometrie*. Ph.D. thesis, Univ. Heidelberg, Germany.

Stadermann F. J., Walker R. M., and Zinner E. (1989) Ion microprobe measurements of nitrogen and carbon isotopic variations in individual IDPs. *Meteoritics* **24,** A327.

Thomas K. L., Keller L. P., Blanford G. E., and McKay D. S. (1994) Quantitative analyses of carbon in anhydrous and hydrated interplanetary dust particles. In *Analysis of Interplanetary Dust* (eds M. E. Zolensky, et al.), pp. 165–172, AIP Conf. Proc. 310. Amer. Inst. Phys., Woodbury.

Tielens A. G. G. M. (1983) Surface chemistry of deuterated molecules. *Astron. Astrophys.* **119,** 177–184.

Tomeoka K. and Buseck P. R. (1985) Hydrated interplanetary dust particle linked with carbonaceous chondrites? *Nature* **314,** 338–340.

Wopenka B. (1988) Raman observations on individual interplanetary dust particles. *Earth Planet. Sci. Lett.* **88,** 221–231.

Wooden D. H., Harker D. E., Woodward C. E., Butner H. M., Koike C., Witteborn F. C., and McMurtry C. W. (1999) Silicate mineralogy of the dust in the inner coma of comet C/1995 O1 (Hale-Bopp) pre- and post-perihelion. *Astrophys. J.* **517,** 1034–1058.

Wooden D. H., Butner H. M., Harker D. E., and Woodward C. E. (2000) Mg-rich silicate crystals in comet Hale-Bopp: ISM relics or solar nebula condensates? *Icarus* **143,** 126–137.

Yang J. and Epstein S. (1983) Interstellar organic matter in meteorites. *Geochim. Cosmochim. Acta* **47,** 2199–2216.

Yang J. and Epstein S. (1984) Relic interstellar grains in Murchison meteorite. *Nature* **311,** 544–547.

Zinner E. (1998) Stellar nucleosynthesis and the isotopic composition of presolar grains from primitive meteorites. *Annu. Rev. Earth Planet. Sci.* **26,** 147–188.

Zinner E., McKeegan K. D., and Walker R. M. (1983) Laboratory measurements of D/H ratios in interplanetary dust. *Nature* **305,** 119–121.

Available online at www.sciencedirect.com
ScienceDirect
Advances in Space Research 39 (2007) 605–611
ADVANCES IN SPACE RESEARCH (a COSPAR publication)
www.elsevier.com/locate/asr

Micrometeorites from Central Antarctic snow: The CONCORDIA collection

J. Duprat [a,*], C. Engrand [a], M. Maurette [a], G. Kurat [b], M. Gounelle [a], C. Hammer [c]

[a] CSNSM, Bat. 104, 91406 Orsay-Campus, France
[b] Inst. f. Geolog. Wissensch., Universität Wien, Althanstrasse 14, A-1090 Wien, Austria
[c] Department of Geophysics, Niels Bohr Institute, Copenhagen, DK 2100, Denmark

Received 1 October 2004; received in revised form 24 October 2005; accepted 1 May 2006

Abstract

We recovered micrometeorites from surface snow layers near the French-Italian station CONCORDIA. The unique weather and isolation conditions of Dome C allowed us to recover micrometeorites that are much better preserved than those extracted from blue ice fields. We have identified a new population of friable fine-grained micrometeorites; the absence of such particles in previous collections can be explained by their destruction by mechanical processes. In contrast to previous collections of micrometeorites, the particles from CONCORDIA Collection are characterized by a high content of Fe-sulfides and an undepleted CI elemental abundance pattern of their fine-grained matrix. These features suggest that micrometeorites from Dome C snow have endured much lower alteration from terrestrial weathering, unlike the micrometeorites recovered from near the margin of the Antarctic ice sheet (Adélie Land). The CONCORDIA particles have well constrained terrestrial ages and, given the low Dome C precipitation rate, the central regions of Antarctica provide a unique opportunity to search for particles from historical meteor showers.

Keywords: Dust grains; Micrometeorites; Interplanetary dust particles; Meteors showers; Terrestrial weathering

1. Introduction

Micrometeorites are extraterrestrial particles with sizes ranging from 20 μm up to a few 100 μm that survive atmospheric entry. They represent the present day dominant source of extraterrestrial material accreted by Earth (e.g., Love and Brownlee, 1993; Taylor et al., 1998). Their cosmogenic isotopic signature (^{26}Al, ^{10}Be) indicates that most of them traveled as small bodies in space and are not ablation products of meteorites (Raisbeck et al., 1986; Raisbeck and Yiou, 1987). Micrometeorites have been collected from different places: deep sea sediments, terrestrial sand, sedimentary rocks, Greenland lake sediments and Antarctic ice and snow (see Taylor and Lever, 2001 for a review). Isolated by the oceans of the southern hemisphere, Antarctica is well shielded from both natural and anthropological terrestrial dust of size larger than 20 μm, making it a prime place for the recovery of micrometeorites. Large collections of micrometeorites have been retrieved there, in particular on the coasts of Adélie Land (Maurette et al., 1991). Thanks to the current efforts of Polar institutes throughout the world, central Antarctica is becoming accessible, and several countries (Russia, Japan, US, Italy, France) now have scientific stations in the central regions of the continent (Vostok, Dome Fuji, South-Pole, Dome C). Recently, two micrometeorite collections have been retrieved from Antarctic snow, at South Pole Station (USA) (Taylor et al., 1998) and Dome Fuji (Japan) (Nakamura et al., 1999).

Beside ground-based collections, Interplanetary Dust Particles (IDPs) have been collected from the stratosphere by NASA since the 1970s (e.g., Brownlee, 1985; Bradley et al., 1988; Rietmeijer, 1998). In this paper, we restrict

* Corresponding author. Tel.: +33 1 69 15 52 83; fax: +33 1 69 15 50 08.
E-mail address: duprat@csnsm.in2p3.fr (J. Duprat).

0273-1177/$30 © 2006 COSPAR. Published by Elsevier Ltd. All rights reserved.
doi:10.1016/j.asr.2006.05.029

the use of the term micrometeorite to particles collected at the Earth's surface, whilst the acronym IDPs will be used for particles from the stratospheric collection. There are generally marked differences between micrometeorites and IDPs (size range, mineralogy, chemical composition, isotopic data, among other). All types of collections suffer biases related to collection techniques and/or weathering. We report here on an opportunity to significantly reduce the bias in micrometeorite collections by taking advantage on the unique characteristics of Dome C surface snow.

2. The CONCORDIA collection

During the last decade, the French and Italian polar institutes (Institut Polaire Français Expéditions Paul-Emile-Victor, IPEV, Programma Nazionale di Ricerche in Antartide, PNRA) have jointly constructed the CONCORDIA Station (S 75°, E 123°) located at Dome C (Fig. 1). Dome C is 1100 km away from the coast of Adélie Land at 3200 m altitude on the Antarctic plateau. The surface snow is separated from the bedrock by more than 3 km of ice. Dome C has a low and regular precipitation rate and is the location of the European Project for Ice Coring in Antarctica (EPICA) (Augustin et al., 2004).

2.1. Field work

We carried out two field trips at Dome C in January 2000 and January 2002 (DC00 and DC02, respectively) to recover micrometeorites from snow at the vicinity of the CONCORDIA station. We extracted manually the snow from different locations: a top layer (0–80 cm depth) at

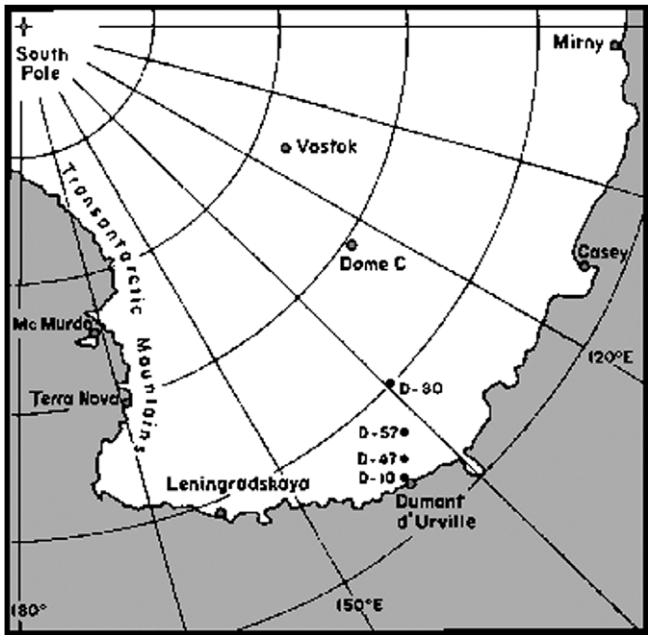

Fig. 1. Location of the CONCORDIA station at Dome C (S 75°, E 123°), on the central Eastern Antarctic plateau, 1100 km from the French station Dumont d'Urville.

Fig. 2. Snow sampling in a 5 m deep trench at the vicinity of CONCORDIA Station, Dome C, Antarctica, January 2002.

3 km upwind of the station, and from layers located at 3–4 m depth in clean trenches (see Fig. 2). The depth was chosen to collect snow layers from the years 1970 to 1980 (before the beginning of human activities at Dome C). Packed in 30 l sealed cans, the snow was taken back to CONCORDIA station on sledges, avoiding the use of any engine in the vicinity of the extraction point. We melted the snow at the CONCORDIA station using a dedicated stainless steel double tank snow smelter that was designed and built at CSNSM laboratory in Orsay, working with a 35 kW propane gas boiler. The dust was allowed to settle gently from the smelter onto a 30 μm mesh filter. The maximum time of exposure to water during the melting/sieving procedure ranged from 1 up to 20 h. During the entire sieving process, the water flow was kept low and did not involve any mechanical pumping. An inspection of each filter was performed for each melt. The contamination was monitored by checking that the number of collected particles per volume of snow did not exceed a few hundreds per 1 m^3 of snow. In a clean melt it was possible to perform a direct cosmic spherule counting. A single filter was used for each melt. The sorting of the filters is still going on and the results presented here do not include all the collected particles.

2.2. Results

We hand-picked all particles (including light coloured ones) in the size range of 30 up to 1000 μm under a binocular microscope. We left out only obvious contamination consisting essentially of textile fibres, plastic and metallic debris. All selected particles were analyzed using a JEOL 6400 analytical scanning electron microscope equipped with an energy dispersive X-ray spectrometer (EDXS) at the Natural History Museum in Vienna. So far, we have identified more than 400 particles of extraterrestrial origin. They all exhibit a chondritic-like composition as identified by the EDXS spectra showing O, Mg, Al, Si and Fe, as major elements with $Mg \gg Al$ and variable amounts of

Mg and Fe. These micrometeorites constitute the CONCORDIA Collection. In the collection performed at Dome C in 2000 (DC00) the ratio between extraterrestrial and terrestrial particles (ET/T) was 0.1, while improvements in the collection procedure in 2002 (DC02) yielded a ratio ranging from 0.1 up to 1.

In the CONCORDIA Collection we have recovered examples from the main families of micrometeorites defined by Kurat et al. (1994) and Engrand and Maurette (1998) (completely melted cosmic spherules, partially melted scoriaceous micrometeorites with vesicles, and unmelted fine-grained and crystalline micrometeorites). Within the fine-grained micrometeorites, we identified fluffy particles that have an external aspect similar to fluffy chondritic IDPs (see Fig. 3).

A large proportion (65%) of micrometeorites from the CONCORDIA Collection contain Fe-sulfides, observed at the surface of the micrometeorites as small melted spheres (1–5 μm) and in polished sections as large (10–15 μm) irregular rugged grains (Fig. 4). The sulfide grains were analysed using the Camparis University Cameca SX100 electron microprobe at 15 kV acceleration potential and a beam current of 10 nA. Most Fe-sulfide grains analysed are pyrrhotites, except one which has a composition intermediate between that of pyrrhotite and pentlandite. Within a fine-grained particle (particle 00-11-46), we also found a dolomite grain with a size of 4–5 μm (Fig. 4). To our knowledge, this is the first time a carbonate is reported in a polar micrometeorite. Finally, in order to compare the CONCORDIA Collection to previous collections performed on Blue Ice Fields, we extracted fine-grained particles from the Cap-Prud'homme (Maurette et al., 1994) and the Astrolabe collections (Gounelle et al., 1999a). We performed several analyses of the fine-grained matrix of these micrometeorites with the electron microprobe using a defocused (~5 μm) beam. Fig. 5 displays the abundance pattern of the average compositions in 13 major and minor elements from Na to Ni for a set of particles in each collection. The composition is normalised to the CI chondritic reference (Anders and Grevesse,

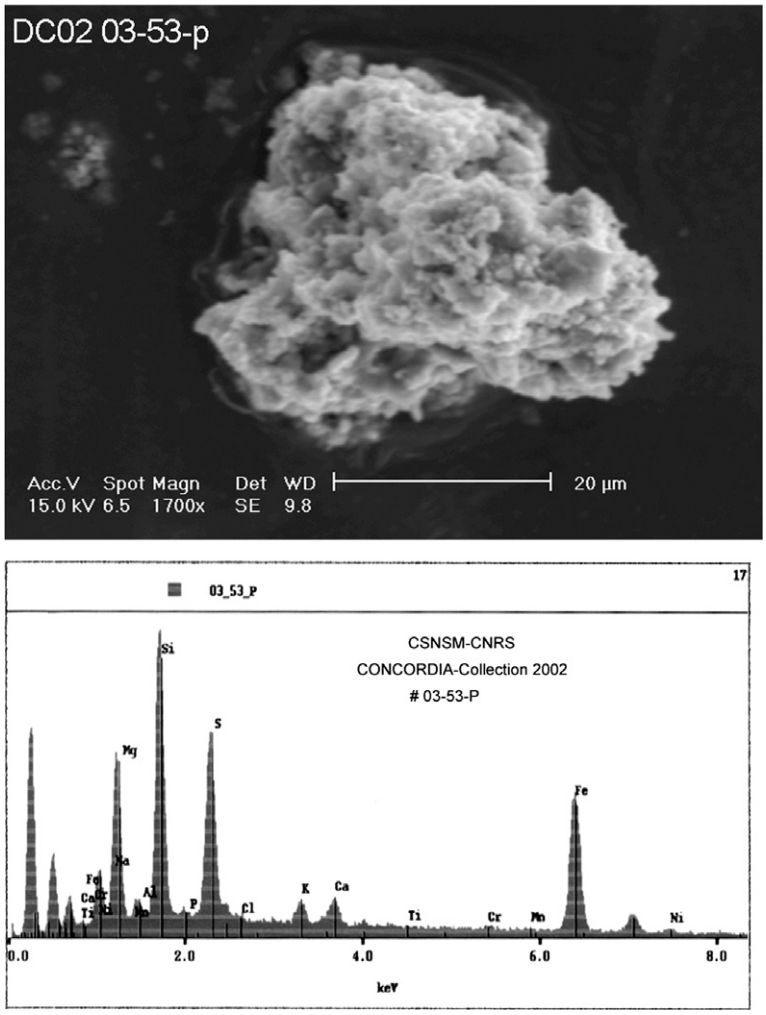

Fig. 3. Top, secondary electron image of a fine-grained micrometeorite from the CONCORDIA Collection performed at the Natural History Museum of Vienna using the JEOL 6400 SEM at 15 kV. Bottom, Energy Dispersive X-ray Spectrum (EDXS) of the particle's bulk composition, the analysis was repeated using a defocused beam on 2×2 μm areas at the surface of the particle.

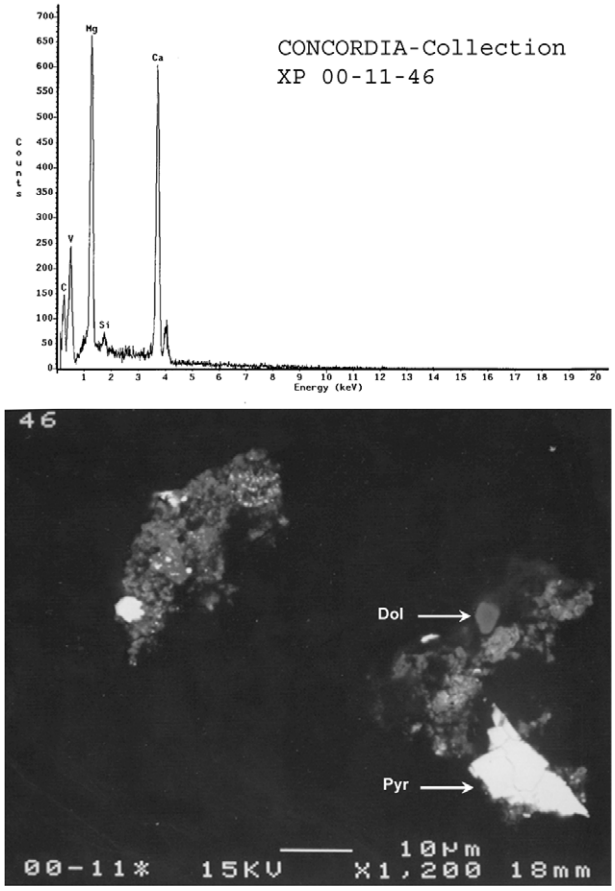

Fig. 4. Bottom, backscattered electron image of a polished section of the fine-grained particle 00-11-46. The large white inclusion is a Fe-sulfide, pyrrhotite (Pyr). The carbonate was identified as a dolomite (Dol). The energy dispersive X-ray spectrum (EDXS) of the dolomite is given in the top panel.

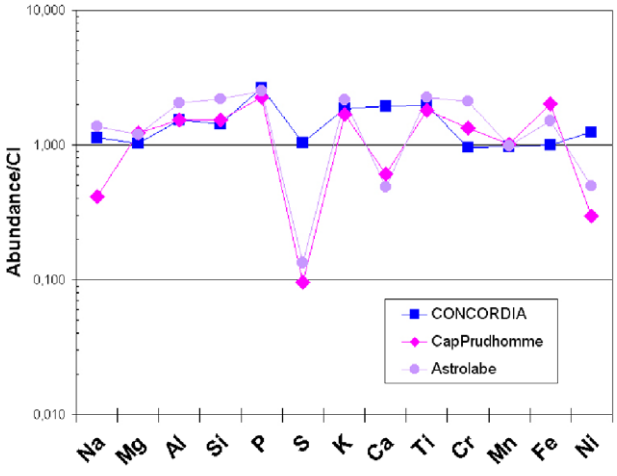

Fig. 5. Comparison of the fine-grained matrix average composition of CONCORDIA Collection micrometeorites with that of micrometeorites extracted from blue ice fields in Adélie Land (Cap Prud'homme and Astrolabe collections, CSNSM). Data obtained with the CAMECA SX100 electron microprobe at University Paris VI, using a ~5 µm defocused beam at 15 kV and 10 nA. All compositions are normalized to the reference composition of CI carbonaceous chondrites (Anders and Grevesse, 1989).

1989). The Cap-Prudhomme and Astrolabe data both show depletions in the abundances of S, Ca and Ni, as previously reported (Kurat et al., 1994), whereas the CONCORDIA data exhibit a pattern similar, within a factor of 2, to the CI reference value.

3. Discussion

In this section, we compare the results obtained on the CONCORDIA Collection to the micrometeorites collected from blue ice fields in Adélie Land (Maurette et al., 1994; Gounelle et al., 1999b) and to two other collections from Antarctic snow in the South-Pole Water Well (SPWW) (Taylor et al., 2000) and in the Dome Fuji Water Well (DFWW) (Nakamura et al., 1999).

3.1. High signal to background ratio

The order of magnitude improvement of the ET/T particle ratio in DC02 compared to DC00 indicates that most of the terrestrial particles found in Dome C snow come from contamination added during the fieldwork itself. In the DC02 field campaign, we improved the protocol using fibers free overalls, single-use gloves and careful washing of all tools. Still, we are convinced that, even in the DC02 collection, some contamination has still occurred, mainly during the melting/sieving procedure that we had to perform in difficult conditions in a tent. It is thus most probable that a higher ET/T ratio can be achieved in future micrometeorite collections at Dome C. By contrast with collections from Adélie Land that contains a large proportion of light-coloured morainic debris, the Dome C snow is completely isolated from the bedrock. Because of the dominant wind direction from the centre of the continent, blowing toward the coast, the Dome C snow is essentially free of terrestrial dust within the micrometeorites size range.

The two other collections from central Antarctic snow (SPWW and DFWW) exhibit higher contamination levels compared to the CONCORDIA data. In the DFWW collection extensive pre-sorting of the raw sample was necessary due to contamination incorporated during the transfer of the snow to the water tank (Nakamura et al., 1999). In the SPWW collection the ET/T ratio is of the order of 0.01 (Taylor et al., 1998). A key difference between these collections and the work presented here is that both SPWW and DFWW collections were obtained using the water supply of their station. The results obtained on the CONCORDIA Collection indicate that it is necessary to perform the collection in a dedicated smelter to reach the intrinsic high signal to background ratio of the central Antarctic snow. For particles with sizes larger than 20 µm, the dust in Dome C snow is essentially of extraterrestrial origin.

3.2. Mechanically undamaged micrometeorites

The CONCORDIA Collection contains friable fine-grained particles (Fig. 3). These particles are fragile and

sometime break apart during micro-manipulation under the binocular microscope. The lack of this type of particle in previous collections from blue ice fields can be explained by their destruction by mechanical damage at different stages in their transport in the ice, their collection and preparation (Gounelle et al., 2005). In collections performed in Adélie Land, the micrometeorites undergo different kinds of mechanical stresses: (i) in the ice flow until they reach the stagnant blue ice fields; (ii) during multiple cycles of freezing and thawing that occur when they reach the top surface of the blue ice (see below); (iii) during mechanical pumping of the water during their collection. Both SPWW and DFWW collections involved mechanical pumping which can create mechanical stress. Yet, Taylor et al. (2000) found a glassy cosmic spherule with a fragile tail suggesting that there is no evidence for extensive particle destruction in the SPWW collection. Another possible explanation can be related to the high signal/background ratio of the CONCORDIA Collection. In order to identify the CONCORDIA friable particles we selected almost all of the dust particles on the filters. Even if the friable particles of the CONCORDIA Collection exhibit external appearances similar to the fluffy chondritic IDPs (see Fig. 4), it would be premature to claim that these micrometeorites are of the very same type as the IDPs from stratospheric collection. Such a comparison requires a more detailed mineralogical and isotopic study. We are planning a systematic study of these new micrometeorites including a search for the Glass Embedded with Metal and Sulphides (GEMS) particles, abundant in chondritic porous anhydrous IDPs, and which could be of interstellar origin (Bradley, 1994; Bradley et al., 1999).

3.3. Minimal aqueous weathering

The CONCORDIA Collection exhibits a significantly larger proportion of micrometeorites containing Fe-sulfides (65%) than the blue ice field collections. In the Cap Prud'homme collection the proportion of micrometeorites containing such Fe-sulfides ranges from 10% to 20%. This high content of Fe-sulfides seems to be a characteristic of all collections from central Antarctic snow. They are reported in both unmelted micrometeorites and cosmic spherules from the SPWW collection (Taylor et al., 2000). Taking the data from the Japanese Collection (Nakamura et al., 2001), one can see that ~70% of the micrometeorites from the DFWW collection contain more than 1 wt.% of Fe-sulfides. Fe-sulfide is known to react with water (Pratt and Nesbitt, 1997). The high Fe-sulfide content thus suggests that the micrometeorites collected from Antarctic snow experienced a lower degree of terrestrial aqueous alteration than those from blue ice fields. This is corroborated by the first observation of a carbonate in a micrometeorite from the CONCORDIA Collection, as carbonates are easily dissolved in acidic water at low temperature. The aqueous alteration of micrometeorites collected in blue ice fields is most probably due to their concentration process at low depth in blue ice fields. Because they are dark colored, the micrometeorites efficiently absorb the sun light and melt a thin ice shell, causing them to sink until they stabilise at an equilibrium depth near the surface of the blue ice fields. This depth depends upon a combination of factors including ablation rate of the ice surface, local solar irradiation and the size of the particle. During thawing/freezing cycles the micrometeorites undergo terrestrial aqueous alteration in a confined environment, which is a process that can efficiently leach out soluble phases. This could explain the low abundance of Fe-sulfides and of carbonates in the blue ice field micrometeorite collections. In the CONCORDIA Collection, the particles endured liquid water only during the artificial snow melting time (a few hours) in the retrieval process. Because Fe-sulfide grains can straightforwardly be identified, their abundance is a powerful index for the degree of terrestrial weathering of micrometeorites.

These results prompted us to revisit the issue of depleted bulk composition in micrometeorites: the fine-grained matrix of micrometeorites collected in the ice at Cap-Prud'homme revealed a depletion in several elements (S, Ca, and Ni) compared to the CI reference composition (Kurat et al., 1994) (Fig. 5). These depletions could have arisen from various causes: terrestrial weathering, atmospheric entry effect or they may constitute a genuine characteristic of the micrometeorites. The CONCORDIA micrometeorites exhibit a composition pattern similar within a factor of 2 to the CI reference (Fig. 5). This result strongly support the hypothesis that the depletions reported in Blue Ice Fields collections are indeed be due to terrestrial weathering.

4. The search for cometary dust

The recognition of cometary dust particles from an identified parent body would represent a major breakthrough in our field of research. Beside major space missions such as STARDUST (NASA) (Brownlee et al., 2004) and ROSETTA (ESA) (Schwehm, 2004) different research teams are investigating recovery of cometary dust by various techniques such as: airborne collections (Messenger, 2002; Rietmeijer et al., 2003) or Antarctic snow collections (Duprat et al., 2001; Lever and Taylor, 2003). Central Antarctic regions can provide major advantages for this goal. At Dome C the precipitation rate is low and regular: about 3.5 g/cm^2/year (Pinglot et al., 1981; Petit et al., 1982). It is thus possible to recover micrometeorites by processing reasonable volumes of snow (a few m^3). Such volumes correspond to an equivalent surface of a few tens of m^2.year which is necessary to significantly reduce the statistical bias of the collection (Peucker-Ehrenbrink and Ravizza, 2000).

Thanks to the logistics available at CONCORDIA station, deep trenches (15 m) can be made permitting collection of samples with precipitation dates as old as three centuries. The terrestrial ages of micrometeorites at Dome C can be inferred from their collection depth with

a precision ranging from 1 to 3 years depending on the identification of a given annual snow horizon at the depth of extraction. We intend to use the deposits from the 1963–64 Agung volcanic eruption to pinpoint the 1966 layer corresponding to one of the most intense recent *Leonid* storms (Yeomans, 1981).

However, it is not straightforward to identify the *Leonid* signal in Dome C snow for several reasons. First, the radiant of the shower is located in the Northern Hemisphere, so Antarctica is clearly not best situated for being a good collector. A second major issue is the high average speed of the incoming cometary dust (70 km/s) which should result in the destruction of a large proportion of the particles at atmospheric entry, with the surviving particles likely to be melted cosmic spherules (Rietmeijer et al., 2003). We are currently investigating other meteor showers that could provide better candidates for a future Dome C collection. A critical problem also lies in the dilution of such a short time-scale signal in central Antarctic snow, due to low accumulation rate: within a snow layer of 1–2 consecutive years, precipitation over a few hours will be diluted by a factor of 10^4. With such a high dilution factor, the potential change in the particle flux intensity is likely to be below the precision of the background flux measurement.

A possible solution would be to search for dust with specific features expected for short period comets, such as cosmic ray irradiation ages from exposure in interplanetary space on the order of a few centuries. Such irradiation ages are orders of magnitude lower than those expected for the sporadic background dust (about 10^6 years). On time scales of a few centuries in interplanetary space, a particle will exhibit a saturated implantation of Solar Wind (SW) but a negligible implantation in Solar Energetic Particles (SEP). Moreover, its content of cosmogenic nuclei (^{21}Ne, ^{26}Al, ^{10}Be) produced by SEP and galactic cosmic rays will also be negligible. Therefore, we suggest searching for particles with ^{20}Ne/^{22}Ne ratio close to the SW value and a negligible content in ^{26}Al, ^{10}Be and cosmogenic ^{21}Ne (Cuillierier et al., 2002; Osawa and Nagao, 2002). The highly friable particles from CONCORDIA collection should have experienced less heating upon atmospheric entry than most other micrometeorites recovered so far on the Earth's surface, they may thus retain a noble gas inventory of a composition close to that of the pre-atmospheric micrometeoroid, and provide recognizable samples of particles released by short-period comets.

5. Conclusion

We performed two field trips in Antarctica to recover micrometeorites from Dome C snow in 2000 and 2002. We used a new collection technique that preserves the particles from mechanical damage. The results obtained from the CONCORDIA micrometeorites collection demonstrate the advantages of central Antarctic regions as sites to collect cosmic dust with a minimal terrestrial alteration. CONCORDIA micrometeorites appear to be pristine and contain minerals which are usually lacking in micrometeorites collected form blue ice fields (e.g., sulfides and carbonates). In addition, the collection of micrometeorites from the snow of Central Antarctic also contains fine-grained, fluffy micrometeorites, which are not present in the blue ice fields collections. Central Antarctic snow provides us with the best collector for micrometeorites and proper collection procedures should ensure that their populations can be retrieved in an unbiased way – opening a new window into the nature of interplanetary dust.

Collected micrometeorites have well constrained terrestrial ages. Given the average Dome C snow precipitation rate, the particles recovered from the top surface and from the low depth trenches belong to the contemporary dust flux encountered by our planet during the last century. It is worth noticing that this time period overlap that of collections of stratospheric interplanetary dust (IDPs). In central Antarctica, the precipitation rate is extremely low, it is thus technically possible to collect across large surfaces (corresponding to several tens m^2 year) from snow layers of up to 3 centuries ago, searching for signals from historical meteor showers. Noble gas analysis may provide a tool to identify micrometeorites with short exposure time in space (a few centuries) such as those expected from short period cometary dust trails.

Acknowledgements

We thank IPEV for financial and logistical support for polar expeditions. We are grateful to IPEV staff (S. Drapeau) and PNRA staff (C. Malagoli) and A. Landais (LSCE) for their help in the field. This work was supported in France by CNRS (PNP-INSU, IN2P3) and CNES and in Austria by FWF.

References

Anders, E., Grevesse, N. Abundances of the elements: meteoritic and solar. Geochim. Cosmochim. Acta 53, 197–214, 1989.

Augustin, L., Barbante, C., Barnes, P.R.F., et al. Eight glacial cycles from an Antarctic ice core. Nature 429 (6992), 623–628, 2004.

Bradley, J.P. Chemically anomalous preaccretionally irradiated grains in interplanetary dust from comets. Science 265, 925–929, 1994.

Bradley, J.P., Sandford, S.A., Walker, R.M. Interplanetary dust, in: Kerridge, J.F., Matthews, M.S. (Eds.), Meteorites and the early Solar System. The University of Arizona Press, Tucson, pp. 861–895, 1988.

Bradley, J.P., Keller, L.P., Snow, T.P., et al. An infrared spectral match between GEMS and interstellar grains. Science 285, 1716–1718, 1999.

Brownlee, D.E. Cosmic dust: collection and research. Ann. Rev. Earth Planet. Sci. 13, 147–173, 1985.

Brownlee, D.E., Horz, F., Newburn, R.L., et al. Surface of young jupiter family comet 81 P/Wild 2: view from the stardust spacecraft. Science 304 (5678), 1764–1769, 2004.

Cuillierier, R., Duprat, J., Maurette, M., et al. 2002. The crucial role of neon to identify cometary micrometeorites from historical and future Leonid showers trapped in Antarctica and Greenland snows (abstract). Lunar Planet. Sci. Conf. XXXIII: CD-ROM #1519.

Duprat, J., Hammer, C., Maurette, M., et al. 2001. Search for past and future frozen leonid showers in Antarctica and Greenland. Lunar Planet. Sci. Conf. XXXII: CD-ROM #1641.

Engrand, C., Maurette, M. Carbonaceous micrometeorites from Antarctica. Meteorit. Planet. Sci. 33, 565–580, 1998.

Gounelle, M., Maurette, M., Engrand, C., et al. Mineralogy of the 1998 Astrolabe Antarctic micrometeorite collection (abstract). Meteorit. Planet. Sci. 34 (Supp.), A46, 1999a.

Gounelle, M., Maurette, M., Kurat, G., et al., 1999b. Comparison of the 1998 "Cap Prudhomme" and "Astrolabe" Antarctic micrometeorite collections with the 1996 "South Pole" collection: preliminary implications (abstract). Lunar Planet. Sci. Conf. XXX: CD-ROM #1564.

Gounelle, M., Engrand, C., Maurette, M., et al. Small Antarctic micrometeorites: a mineralogical and in situ oxygen isotope study. Meteorit. Planet. Sci. 40 (6), 917–932, 2005.

Kurat, G., Koeberl, C., Presper, T., et al. Petrology and geochemistry of Antarctic micrometeorites. Geochim. Cosmochim. Acta 58, 3879–3904, 1994.

Lever, J.H., Taylor, S., 2003. Potential for a time-sequenced 100,000-year record of micrometeorites at south pole (abstract). Lunar Planet. Sci. Conf. XXXIV: CD-ROM #1644.

Love, S.G., Brownlee, D.E. A direct measurement of the terrestrial mass accretion rate of cosmic dust. Science 262, 550–553, 1993.

Maurette, M., Olinger, C., Christophe, M., Michel-Lévy, et al. A collection of diverse micrometeorites recovered from 100 tons of Antarctic blue ice. Nature 351, 44–47, 1991.

Maurette, M., Immel, G., Engrand, C., et al. The 1994 EUROMET collection of micrometeorites at Cap-Prudhomme, Antarctica (abstract). Meteoritics 29, 499, 1994.

Messenger, S. Opportunities for the stratospheric collection of dust from short-period comets. Meteorit. Planet. Sci. 37 (11), 1491–1506, 2002.

Nakamura, T., Imae, N., Nakai, I., et al. Antarctic micrometeorites collected at the Dome Fuji Station. Antarct. Meteorit. Res. 12, 183–198, 1999.

Nakamura, T., Noguchi, T., Yada, T., et al. Bulk mineralogy of individual micrometeorites determined by X-ray diffraction analysis and transmission electron microscopy. Geochim. Cosmochim. Acta 65, 4385–4397, 2001.

Osawa, T., Nagao, K. Noble gas compositions of Antarctic micrometeorites collected at the Dome Fuji Station in 1996 and 1997. Meteorit. Planet. Sci. 37, 911–936, 2002.

Petit, J.-R., Jouzel, J., Pourchet, M., et al. A detailed study of snow accumulation and stable isotope content in dome C (Antarctica). J. Geophys. Res. 87, 4301–4308, 1982.

Peucker-Ehrenbrink, B., Ravizza, G. The effects of sampling artifacts on cosmic dust flux estimates: a reevaluation of nonvolatile tracers (Os, Ir). Geochim. Cosmochim. Acta 64 (11), 1965–1970, 2000.

Pinglot, Pourchet, M., Merlivat, L., 1981. Gamma-ray bore-hole logging for determining radiactive fallout layers in snow. IAEA-SM-252/55.

Pratt, A.R., Nesbitt, H.W. Pyrrhotite leaching in acid mixtures of HCl and H_2SO_4. Am. J. Sci. 297, 807–828, 1997.

Raisbeck, G.M., Yiou, F. ^{10}Be and ^{26}Al in micrometeorites from greenland ice (abstract). Meteoritics 22, 485–486, 1987.

Raisbeck, G.M., Yiou, F., Bourles, D., et al. ^{10}Be and ^{26}Al in greenland cosmic spherules; evidence for irradiation in space as small objects and a probable cometary origin (abstract). Meteoritics, 487–488, 1986.

Rietmeijer, F.J.M. Interplanetary dust particles, in: Papike, J.J. (Ed.), Planetary Materials, vol. 36. Mineralogical Society of America, Washington, DC, pp. 2.1–2.94, 1998.

Rietmeijer, F.J.M., Pfeffer, M.A., Chizmadia, L., et al., 2003. Leonid dust spheres captured during the 2002 storm?. Lunar Planet. Sci. Conf. XXXIV: CDROM #1358.

Schwehm, G., 2004. The Rosetta Mission – a Status Report. 35th COSPAR Scientific Assembly, Paris, France, 3760.

Taylor, S., Lever, J.H. Seeking unbiased collections of modern and ancient micrometeorites, in: Peucker-Ehrenbrink, B., Schmitz, B. (Eds.), Accretion of Extraterrestrial Matter Throughout Earth's History. Kluwer Academic/Plenum Publishers, 2001.

Taylor, S., Lever, J.H., Harvey, R.P. Accretion rate of cosmic spherules measured at South Pole. Science 392, 899–903, 1998.

Taylor, S., Lever, J.H., Harvey, R.P. Numbers, types, and compositions of an unbiased collection of cosmic spherules. Meteorit. Planet. Sci. 35, 651–666, 2000.

Yeomans, D.K. Comet Tempel-Tuttle and the Leonid meteors. ICARUS 47 (3), 492–499, 1981.

Available online at www.sciencedirect.com
SCIENCE DIRECT®
Applied Surface Science 231–232 (2004) 883–887
applied surface science
www.elsevier.com/locate/apsusc

Multi-correlation analyses of TOF-SIMS spectra for mineralogical studies

C. Engrand[a], J. Lespagnol[b], P. Martin[b], L. Thirkell[b], R. Thomas[b,*]

[a]CSNSM, Bat104, Orsay Campus, F-91405 Orsay Cedex, France
[b]Laboratoire de Physique et Chimie de l'Environnement, 3A av. de la Recherche Scientifique, 45071 Orléans Cedex 2, France

Available online 25 May 2004

Abstract

A time-of-flight mass spectrometer (TOF-SIMS, COSIMA experiment) has been launched by ESA the 2nd March 2004, on board the comet bound spacecraft ''ROSETTA''. The scientific objectives of COSIMA are the determination of the compositions of cometary grains as well as the molecular analyses of their exposed organic compounds. These analyses will provide inorganic and organic data for pristine solar system material, which are crucial for models of solar system formation and evolution. The challenge is, from a mass spectrum, to determine the mineral(s) analysed, to trace back the origin and formation processes of the grains which will be ultimately analysed in situ in the comet by COSIMA. To prepare the interpretation of COSIMA spectra, we have evaluated a correlation algorithm between TOF-SIMS spectra, to estimate how the information can be used to characterise the mineral phase(s) analysed. As a first step in this work, we used mineralogical samples representative of minerals found on earth and in the solar system, silicate grains. These different minerals have rather similar mass spectrum, but experienced different formation conditions in the solar nebula. We will present this correlation algorithm, allowing an accurate study of the elements responsible for the correlation, and a rapid comparison with the classical principal component analysis (PCA) method.

Keywords: TOF-SIMS; Comet; In situ analysis; Correlation analysis

1. Introduction

In 1986, the French-Soviet spacecraft VEGA and the ESA GIOTTO mission made the first in situ observation of a comet (e.g. [1,2]). Comet Halley was investigated at the closest by GIOTTO which gave an image of the comet nucleus. However, the nearest approach was at about 600 km and the encounter where most observations took place lasted only ~1.5 h. Both VEGA and GIOTTO missions included an impact ionisation time-of-flight mass spectrometer onboard which revealed the presence of silicate dust and of organic compounds in much larger amounts and more complex forms than expected. The rather limited performances of the mass spectrometers and the very short observation duration at the closest distance did not allow a fine study of the cometary dust material. By examining comet 67P/Churyumov-Gerasimenko at only a few kilometres distance over a time span of a year, the ESA ROSETTA mission (launched the 2nd

* Corresponding author. Tel.: +33-2-38-25-53-03; fax: +33-2-38-49-46-72.
E-mail address: roger.thomas@univ-orleans.fr (R. Thomas).

0169-4332/$ – see front matter © 2004 Elsevier B.V. All rights reserved.
doi:10.1016/j.apsusc.2004.03.158

March 2004) will allow a major advance in cometary science.

Part of the ROSETTA scientific payload is COSIMA, a TOF-SIMS designed to obtain a mass resolution around 2000 for masses up to several 1000 amu, allowing the resolution of doublets between elementary peaks and molecular ions (for example $^{28}Si^+$ and $C_2H_4^+$). It automatically performs different tasks: (1) collect cometary dust grains on targets exposed to the cometary environment; (2) find the dust grains on the target surface; (3) move the target to place the dust grains in front of the mass analyser; (4) proceed to the analysis of the grain. The primary ion beam system uses a liquid metal $^{115}In^+$ ion source to produce a 8 keV primary ion beam, pulsed in 2 ns ion packets and focused to ~20 μm in diameter on the sample. COSIMA will provide data on the isotopic and chemical compositions of the organic and inorganic phases of the dust. The organic information will be interpreted by chemometric techniques and used in the frame of the heterogeneous chemistry of the interstellar medium. The interpretation of the inorganic part of spectrum (both isotopic and chemical information), will need the comparison with terrestrial and extraterrestrial samples (minerals and meteorites/micrometeorites) considered as references.

Interpretation of the spectra will not be easy, as from the complex cometary dust spectra one will have to: (1) extract the inorganic and the organic contributions; (2) recognise the individual components from an assemblage of different minerals.

As a first step, we propose to develop a method to differentiate mass spectra where the (numerous) minor peaks are also discriminating, not only the (few) major peaks. The purpose of this work is to estimate whether the "CORICO" software [3], based on multi-correlation calculations designed for large multi-variate analyses, can recognise different mineral phases having similar mass spectrum.

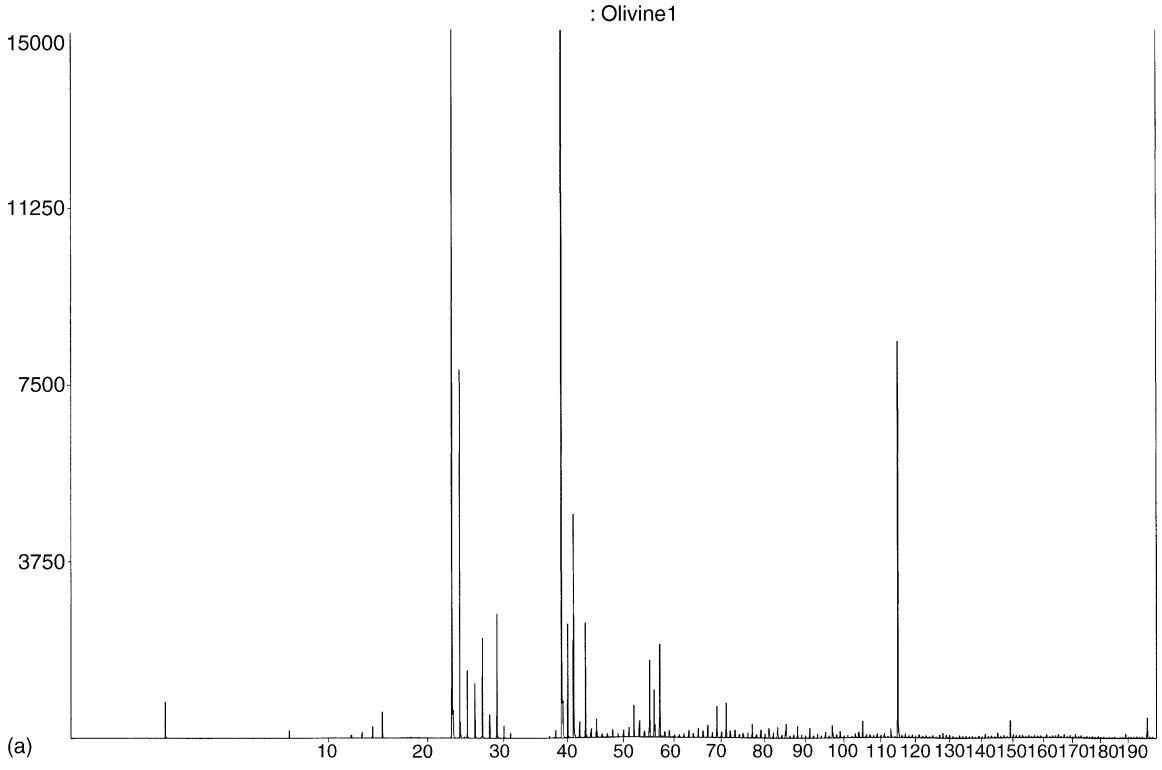

Fig. 1. Positive secondary ion laboratory TOF-SIMS spectra of an olivine grain (a) and of a Ca-rich pyroxene grain (b) pressed into a gold foil. Organic contamination is low. Except for the Ca^+ peak, the main differences are the Na^+ and K^+ peaks which are not structural elements but probably come from a human-made contamination during sample preparation. The presence of In^+ ions is due to implantation of primary ions.

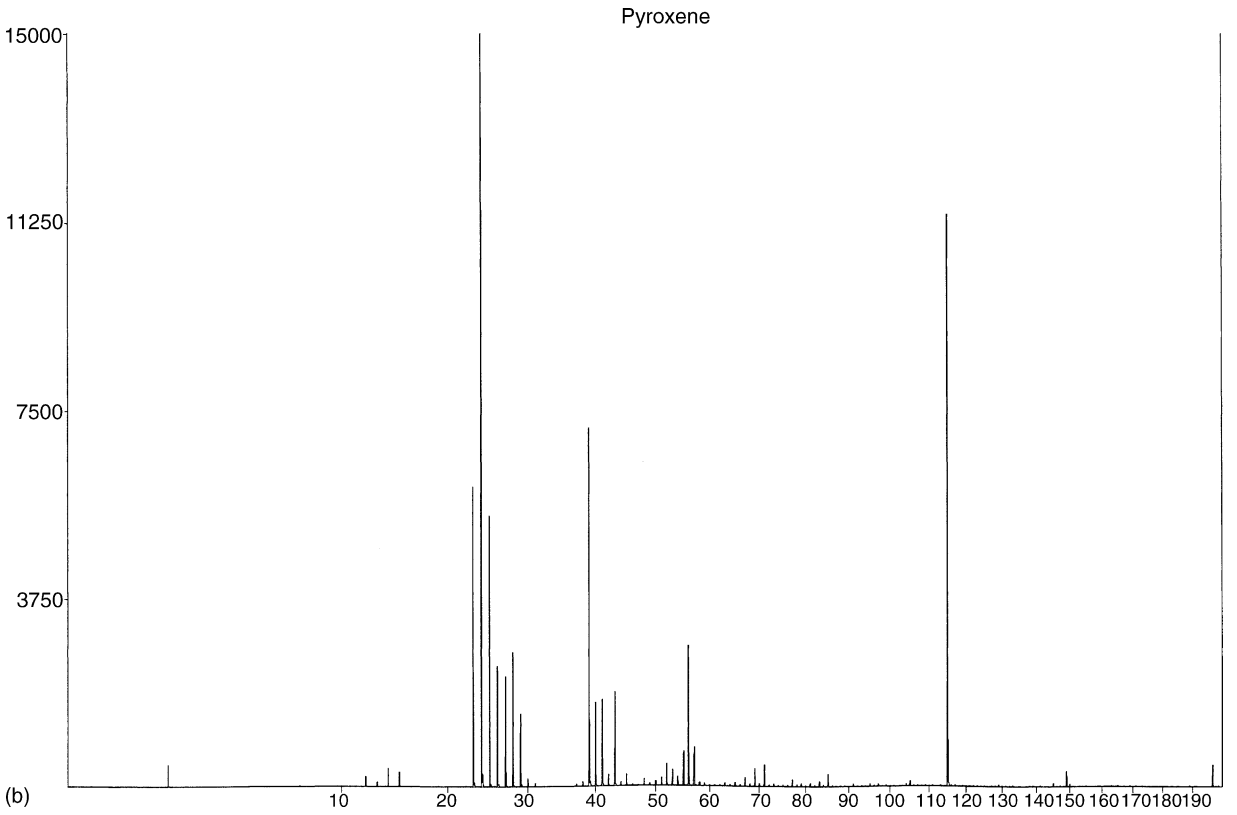

Fig. 1. (*Continued*).

2. Principle of the method and the CORICO software

A TOF-SIMS spectrum contains mass peaks, with a contribution of a few large peaks corresponding to the major elements and/or those with the highest ionisation probability and many small peaks representing the minor elements. A comparison between spectra considering only the major peaks would be largely biased, as one has to take into account the many small peaks present in the spectra. This can only be made with an adapted statistical tool. The main goal of the CORICO software is to compare several spectra over their whole mass range whatever the relative intensity of the peaks. The CORICO software takes into account conditional similarity (e.g. the ''memory effect'': if the spectrum X leaves a ''memory effect'' on spectra Y and Z, the software has to recognize it as a bias that would not be considered as a similarity to spectrum X). It gives equal weight to all individual spectra and mass peaks within them for the comparison. It can compare all the considered spectra to give an exhaustive review of the similarities and/or differences. It can identify the mass peaks responsible for these similarities or differences.

The correlation index and conditional correlation index are mathematical tools used for this purpose. In our experimental set-up, a spectrum consists of an histogram of 65 000 channels (2 ns per channel) representing the flight time of each ion from the target to the detector, hence its mass (Fig. 1). The data for ''m'' spectra are expressed as a matrix with ''m'' columns and 65 000 lines. Each column may be considered as a vector in the 65 000 dimension space.

CORICO calculates: (1) the symmetrical correlation matrix of the m vectors; (2) the correlation index between two spectra X and Y, $R(X,Y) = \sum_i X_i Y_i \Big/ \sqrt{\sum_i X_i^2} \sqrt{\sum_i Y_i^2}$, represents $\cos\theta$ where θ is the angle of the vector (spectrum) in the 65 000

dimensions space; (3) all the conditional correlation indexes between X and Y with regard to Z: $R(X,Y/Z) = [R(X,Y) - R(X,Z)R(Y,Z)]/\sqrt{1-R^2(X,Z)}\sqrt{1-R^2(Y,Z)}$. The conditional correlation index calculates the correlation between X and Y after deduction of the Z contribution in X and Y. It suppresses the ''memory effect'' bias, for example. With this correlation index, the risk of enhancing wrong similarities is very low.

The results are shown in a plot where individual spectra are linked if all the correlation indexes (including the conditional correlation index) are higher than a user given threshold. CORICO can determine the mass peaks contributing the most/least to the correlation. This specificity is essential in order to interpret the spectra with geochemical arguments.

3. Preliminary results

We acquired TOF-SIMS spectra of two kinds of terrestrial minerals, two olivine grains [$(Mg,Fe)_2SiO_4$] with different Mg/Fe ratios and one Ca-rich pyroxene [$CaMgSi_2O_6$]. These three minerals have fairly close chemical composition, but have different crystalline structure and were formed in different conditions. Olivine and pyroxene minerals are present on earth, but they are also the most common minerals in extra-terrestrial matter. Their relative abundance are a powerful criterion for meteorite taxonomy (e.g. [4]). Olivine grains were also found in comets from remote analysis, but Mg-rich pyroxene grains were only recently identified (e.g. [5]). It will therefore be important to discriminate between them from the COSIMA data. In this work, olivine and pyroxene grains were pressed into a gold foil for analysis. We took about ten spectra on each mineral (Fig. 1) and used the CORICO software to check whether it could differentiate between the two types of minerals from their mass spectrum.

A first run of CORICO on the 35 spectra showed that the correlation was mainly due to the In peak (primary ion implantation). For the second run, we took the In peak out of the calculation. The Na and K peaks became the major contributors to the correlation between spectra. These elements are typical of alkaline

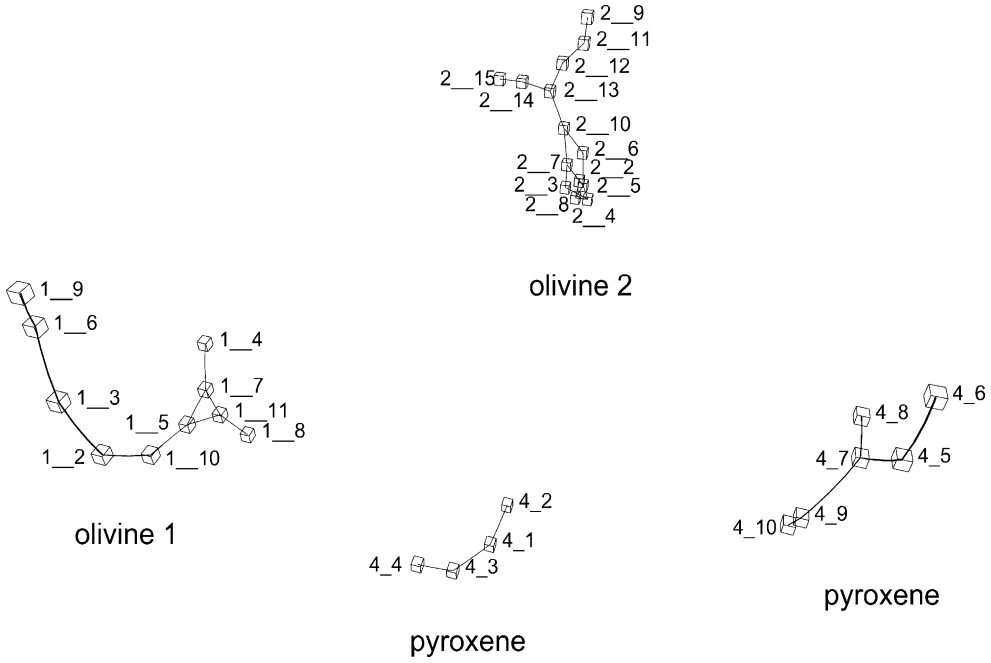

Fig. 2. CORICO correlation plot between 35 olivine and pyroxene spectra. The links between every spectrum numbers show that the conditional correlation and correlation indexes are higher than the threshold chosen by the user. The contributions of In, Na and K were withdrawn from the calculation.

surface contamination, but on the other hand they may be structural elements in minerals like feldspar. In our case, Na and K are not structural elements so we decided to remove them from the correlation, but this observation reveals the importance of sample preparation for TOF-SIMS analysis. Fig. 2 presents the results after removing Na and K from the correlation. We clearly separate the spectra in four groups:

- one distinct group for each olivine mineral. This expected result would be very difficult to obtain without an automatic procedure;
- two different groups for the Ca-rich pyroxene mineral, each one corresponding to the analyses of a different fragment of the same mineral. The contribution of Ca to each set of spectra makes the distinction between the two groups.

In this case, CORICO could discriminate between the olivine and the Ca-rich pyroxene, but showed a discrimination between two pyroxene fragments. This unexpected feature might result from a small natural heterogeneity between these two fragments that we will have to check with standard mineralogical analytical techniques.

4. Conclusion

In this preliminary work, we report the statistical treatment of TOF-SIMS spectra recorded from two different kinds of silicate which are abundant in extraterrestrial matter. The CORICO software used for this treatment: (1) shows the correlation between spectra of the same mineralogical composition; (2) identifies mass peaks which may introduce experimental bias (In, Na, K, etc.); (3) reveals unexpected differences in the analysis of two fragments of the same mineral (case of the Ca-rich pyroxene).

Such results could probably also be achieved with the more classical PCA method (principal component analysis). However, the CORICO software does not require a given choice of projection (score) which are difficult to interpret, as with the PCA method. With CORICO, the correlation indexes are all calculated in the same way and the elements relevant for the similarities and/or the differences observed between the spectra can be quantified.

Further work is needed to assess the limitations of CORICO, but these preliminary results are encouraging for the future interpretation of more complex in situ spectra of cometary grains by COSIMA around 2015.

Acknowledgements

We would like to thank ESA and all the ROSETTA participants for allowing this mission to be successfully launched. Special thanks go to J. Kissel and all the COSIMA team. This work is supported by CNES in France.

References

[1] J. Kissel, et al., Nature 321 (1986) 280–282.
[2] J. Kissel, et al., Nature 321 (1986) 336–337.
[3] M. Lesty, La Revue Modulad 22 (1999) 41–77.
[4] H.Y.J. McSween, Meteorites and their Parent Planets, 2nd ed., Cambridge University Press, Cambridge, London, 1999.
[5] D.H. Wooden, H.M. Butner, D.E. Harker, C.E. Woodward, Icarus 143 (2000) 126–137.

RAPID COMMUNICATIONS IN MASS SPECTROMETRY
Rapid Commun. Mass Spectrom. 2006; **20**: 1361–1368
Published online in Wiley InterScience (www.interscience.wiley.com) DOI: 10.1002/rcm.2448

Chemometric evaluation of time-of-flight secondary ion mass spectrometry data of minerals in the frame of future *in situ* analyses of cometary material by COSIMA onboard ROSETTA

Cecile Engrand[1], Jochen Kissel[2], Franz R. Krueger[3], Philippe Martin[4], Johan Silén[5], Laurent Thirkell[4], Roger Thomas[4] and Kurt Varmuza[6]*

[1]Centre de Spectrométrie Nucléaire et de Spectrométrie de Masse, CNRS-Univ. Paris XI, F-91405 Orsay Campus, France
[2]Max Planck Institute for Solar System Research, D-37191 Katlenburg-Lindau, Germany
[3]Ingenieurbureau Dr. Krueger, Messeler Strasse 24, D-64291 Darmstadt, Germany
[4]Laboratoire de Physique et de Chimie de l'Environnement, 3A av. de la Recherche Scientifique, F-45071 Orléans Cedex 2, France
[5]Finnish Meteorological Institute, FIN-00101 Helsinki, Finland
[6]Vienna University of Technology, Institute of Chemical Engineering, Laboratory for Chemometrics, A-1060 Vienna, Austria

Received 21 September 2005; Revised 17 February 2006; Accepted 17 February 2006

Chemometric data evaluation methods for time-of-flight secondary ion mass spectrometry (TOF-SIMS) have been tested for the characterization and classification of minerals. Potential applications of these methods include the expected data from cometary material to be measured by the COSIMA instrument onboard the ESA mission ROSETTA in the year 2014. Samples of the minerals serpentine, enstatite, olivine, and talc have been used as proxies for minerals existing in extraterrestrial matter. High mass resolution TOF-SIMS data allow the selection of peaks from inorganic ions relevant for minerals. Multivariate cluster analysis of peak intensity data by principal components analysis and the new method CORICO showed a good separation of the mineral classes. Classification by *k* nearest-neighbor classification (KNN) or binary decision trees (CART method) results in more than 90% correct class assignments in a leave-one-out cross validation.

This study contributes to the development of methods for the evaluation of time-of-flight secondary ion mass spectrometry (TOF-SIMS) data from mineralogical matter as expected from *in situ* measurements near a comet. Systematic investigations of minerals by TOF-SIMS are rare as usually other spectroscopic or crystallographic methods are preferentially used to characterize minerals.[1–3] For instance, metallic oxides have been analyzed by TOF-SIMS,[4,5] and an extensive overview of TOF-SIMS in cosmochemistry has been published,[6] but TOF-SIMS—together with chemometric methods—were not used in this case to recognize minerals. Furthermore, ratios of elemental concentrations—measured by laser ablation TOF-MS—have been used to characterize meteoritic material.[7]

Comets are considered the least differentiated bodies in our solar system. They still contain volatile material intimately mixed with highly refractory grains, as shown by previous *in situ* mass spectroscopic measurements near the comets Halley,[8] Hale-Bopp,[9,10] and Wild-2.[11] These results lent strong support to the models of J. Mayo Greenberg[12] on how a comet is made. While the high relative speed for the Halley fly-by missions allowed only a gross characterization of the organic material, the next mission with a dust mass spectrometer, STARDUST, allowed a more detailed analysis and the identification of a few more substance classes.[13] The *in situ* analytical technique applicable with fly-by missions is handicapped by the high relative speeds of more than 5 km/s of impacting dust particles; under these conditions, the mass of a particle has a large effect on the shape of the mass spectrum.[14]

For a more refined analysis of the physical structure and chemical composition of cometary material, a cold-sample return mission would be the best. In January 2006, the STARDUST cometary mission[15] returned a non-cooled sample of comet Wild 2 dust that will give us some insights on cometary matter. The ROSETTA mission is on its way to rendezvous with comet P67/Churyumov-Gerasimenko in the year 2014. A time-of-flight secondary ion mass spectrometer—named COSIMA—has been selected for *in situ* analyses of cometary dust onboard ROSETTA.

TOF-SIMS is an established laboratory technique, which gives access to the composition of the first few atomic layers of a sample. The method provides two advantageous features: (1) during ion formation, the information on the

**Correspondence to*: K. Varmuza, Vienna University of Technology, Institute of Chemical Engineering, Laboratory for Chemometrics, Getreidemarkt 9/166, A-1060 Vienna, Austria.
E-mail: kvarmuza@email.tuwien.ac.at
Contract/grant sponsor: CNES.

molecule's state on the surface is largely preserved, and (2) any volatile material adsorbed on the sample's surface is detectable. Previous analyses of cometary dust have shown the presence of abundant organic matter together with Mg-rich silicates.[8–11,13] It is thus expected that the COSIMA spectra of cometary dust will contain relevant information about inorganic and organic substance classes. Such complex spectra will be difficult to interpret and need the development of adequate data evaluation tools to be able to interpret the returned spectra.

In this study we analyzed mineral samples that could be relevant to extraterrestrial matter and comets. Antarctic micrometeorites (AMMs)[16,17] were proposed as calibration samples for COSIMA. They are generally composed of hydrous and anhydrous minerals mixed with a few weight percent (wt%) of carbonaceous matter and can be considered as good proxies for cometary dust. Because of the complex composition of cometary grains and AMMs, we chose to start this study by analyzing individual mineral grains, and evaluated the obtained data by chemometric methods.

The minerals include terrestrial analogues of the most abundant anhydrous silicates present in micrometeorites and in primitive meteorites, olivine and pyroxene grains.[16] The Mg-rich end-members of these minerals (forsterite and enstatite, respectively) have been identified in comets.[9,10] It is important to check whether COSIMA will be able to differentiate olivine from pyroxene since pyroxene was only recently identified in comets,[10] and as the olivine/pyroxene ratio is an important characteristic of meteorite classes. We also analyzed terrestrial hydrous minerals—considered as proxies for phyllosilicates in primitive meteorites and micrometeorites—to check whether or not it is possible to differentiate two minerals with close major elemental compositions, but one being anhydrous and the other hydrated (for instance, enstatite and talc).

For data evaluation we applied the rather new multivariate method CORICO, and we compared the results with results obtained by classical methods like principal components analysis (PCA) and classification by decision trees or *k* nearest neighbors (KNN).[18] Application of these data evaluation methods could be directly relevant to the data that will be returned by COSIMA. Chemometrics has been only rarely applied to TOF-SIMS data, for instance, in studies of inorganic material,[19] and aerosol particles,[20,21] as well as for image analysis of soldering inhomogeneities.[22] However, chemometrics has been extensively used with electron impact (EI) mass spectra of organic compounds,[23,24] even relevant to comet chemistry.[25,26] A review of the use of multivariate data analysis of TOF-SIMS data with emphasis on organic thin films has been published recently.[27]

EXPERIMENTAL

TOF-SIMS instrument

The time-of-flight secondary ion mass spectrometer used was built in the Laboratoire de Physique et Chimie de l'Environnement (LPCE), Orléans (France), as a laboratory model of the COSIMA instrument onboard the ROSETTA space mission, in particular for development and testing of the primary ion beam system. It has the same design parameters as the COSIMA instrument, and the performances of both instruments are very similar. The LPCE instrument is equipped with a liquid metal ion source containing an 8 keV $^{115}In^+$ or $^{69}Ga^+$ primary ion gun; the latter was used for this work. The beam is pulsed by a chopper and the pulses are compressed in time by a buncher to produce a pulse duration of 2–3 ns at the target; a pulse typically consists of 2000 ions. The beam is focused to a spot size of about 30 μm in diameter. Positive or negative secondary ions are accelerated by a potential of 3 keV resulting in about 3.2 μs flight time for hydrogen ions. A two-stage reflectron provides a maximum mass resolution $m/\Delta m$ of 2000 at half peak height at mass 100; drift path of secondary ions is about 240 cm. A micro-channel plate detector (MCP, F4292-06; Hammamatsu) is used for single ion detection. The system is operated at 1000 shots/s and typically yields 1–20 detected secondary ions per shot; so the acquisition of a spectrum with 10^6 detected ions requires 50–1000 s.

During analysis the vacuum is maintained at a pressure of 3×10^{-9} mbar using a cryogenic pump. Samples on gold substrates of size 1 cm × 1 cm are introduced by a linear manipulator device. The introduction chamber is connected to an oil-free turbo-molecular pump.

Samples

The four minerals used in this study are terrestrial samples (Table 1): an enstatite (Mg-rich end-member of the pyroxene series, collected on Corundum Hill, North Carolina), a Mg-rich olivine (San Carlos olivine), a serpentine sample (from Mollum, Norway), and talc (from the Lauzenac Museum, France). Averaged data from electron microprobe analyses are reported in Table 2. A Ca-rich pyroxene (diopside) was previously analyzed with the same analytical setup.[28]

Sample preparation and handling

In a TOF-SIMS instrument all secondary ions collected are produced from the first monolayers of the sample. The sputtering of less than one monolayer over the 30 μm diameter impact area can yield enough ions for a good spectrum. The high sensitivity of the method, however,

Table 1. Mineral samples

Class *i*	Mineral class	Theoretical formula	Empirical formula[a]	n_i[b]
1	Serpentine	$Mg_3[Si_2O_5](OH)_4$	$Mg_{2.6\text{-}2.8}Al_{0.2\text{-}0.5}[Si_{1.7\text{-}2.0}Fe_{0.10}O_{5.8\text{-}4.5}](OH)_{3.2\text{-}4.5}$[c]	12
2	Enstatite	$MgSiO_3$	$(Mg_{0.9}Fe_{0.1})Si_{1.0}O_3$	9
3	Olivine	$(Mg,Fe)_2SiO_4$	$(Mg_{1.8}Fe_{0.2})Si_{1.0}O_4$	9
4	Talc	$Mg_3Si_4O_{10}(OH)_2$	$Mg_{2.6}Si_{2.7\text{-}2.9}O_{4.8\text{-}4.1}(OH)_{7.2\text{-}7.9}$[c]	9

[a] Calculated from electron microprobe analyses data (Table 2).
[b] n_i is the number of TOF-SIMS spectra per mineral class; total number of spectra, *n*, is 39.
[c] For hydrated minerals the empirical formula was calculated by adding the (not analyzed) necessary amount of water in order to obtain a total of 100% for the data from electron microprobe analyses (Table 2).

DOI: 10.1002/rcm

Table 2. Average elemental abundances in weight percent (wt%) of the four minerals determined by electron microprobe analyses. Available standard deviations are given in parentheses

Mineral	Na	Mg	Al	Si	K	Ca	Ti	Cr	Mn	Fe	Ni	O	Total
Serpentine[a]	b.d.	23.0 (0.6)	3.1 (1.2)	18.7 (1.1)	b.d.	b.d.	b.d.	b.d.	b.d.	2.7 (0.2)	b.d.	40.1 (1.1)	87.7 (2.3)
Enstatite[b]	b.d.	21.0 (0.4)	0.3 (0.2)	27.0 (0.4)	b.d.	b.d.	b.d.	0.1	0.1	5.2 (0.3)	0.1	46.4 (0.3)	100.1 (0.8)
Olivine[c]	b.d.	29.9 (0.1)	b.d.	19.0 (0.1)	b.d.	0.1	b.d.	b.d.	0.1	7.5 (0.1)	0.3 (0.1)	43.7 (0.1)	100.7 (0.3)
Talc[d]	b.d.	18.2 (0.1)	b.d.	23.1 (0.5)	b.d.	b.d.	b.d.	b.d.	b.d.	0.3 (0.1)	b.d.	38.5 (0.6)	80.2 (1.0)

b.d., below detection limit of ~0.01 wt%
[a] Average of 20 analyses on two different grains.
[b] Average of 10 analyses on two different grains.
[c] Average of 5 analyses on a single grain.
[d] Average of 10 analyses on a single grain.

requires special effort on controlling the cleanliness of samples and instruments.[29]

Samples were prepared and stored under an atmosphere of dry nitrogen or filtered air in a laminar flow hood. Tools, sample holders and boxes were chemically cleaned by acetone and ethanol and heated up to 400–900°C for a few hours. The vacuum contaminants were monitored by a quadrupole mass spectrometer (Prisma QMS 200, Pfeiffer Vacuum). In the airlock of the TOF-SIMS system samples were heated in vacuum with an IR lamp. Sample surfaces were subsequently cleaned by using the primary ion beam in continuous operation mode (not pulsed) or with a UV laser (VSL-337ND-S; Laser Science Inc., USA). The cleaning efficiencies of the two techniques are strongly dependent on the nature of the contaminant, the nature of the sample, and the thickness of the contaminant. Plasticizers and lubricants like diisodecylphthalates and polydimethylsiloxanes are regularly detected with a TOF-SIMS instrument, and these kinds of compounds must not be present around samples during handling and storage.

Raw data treatment

A raw data mass spectrum consists of a histogram with 65 000 time channels (each 1.6 ns) with the number of detected ions in each channel. The objective of raw data treatment is to produce a peak list containing high-resolution masses and absolute intensities corresponding to the integral of a peak. The applied, newly developed algorithm for peak detection[29] from P2Asystems, Software TOF-LPCE (Vincennes, France), is based on the application of an appropriate threshold on the first derivative of a spectrum, and allows the identification of mass doublets resolved by the TOF. Peak positions in the time scale are transformed into the mass scale, and peaks with positions differing from each other by less than the mass resolution are grouped together.

CHEMOMETRICS

Application of multivariate data analysis methods requires the representation of each mass spectrum by a vector. Vector elements can be the intensities of selected peaks. A set of spectra defines a matrix $\boldsymbol{X}$ with a row for each spectrum (sample, object) and a column (variable, feature) for each selected mass. Various complementary chemometric methods have been used for exploratory data analysis (cluster analysis of mass spectra) as well as for classification (discrimination of mineral types). The performance of classification methods has been estimated by leave-one-out cross validation, which means that each of the objects is considered as an unknown; the classification rule is derived from the remaining data, and then applied to the selected unknown.[18,30,31]

Principal components analysis (PCA)

The standard method PCA has been used for exploratory data analysis. PCA gives linear projections of the feature space in the form of scatter plots with a point for each spectrum (score plot) or for each feature (loading plot).[18,31,32] The projection preserves best the Euclidean distances between the object points in the multidimensional feature space, with the Euclidean distance considered as a reciprocal measure of spectra similarity. Software products used for PCA were Unscrambler[33] and SCAN.[34]

CORICO method

CORICO (CORrelations ICOnography) is a non-linear mapping of the feature space onto a sphere; the algorithm is based on correlation coefficients calculated from vector pairs and on partial correlation coefficients.[35,36] The correlation coefficient is used as a measure of spectra similarity. The method can be used for cluster analysis and for classification; it has been successfully applied for instance in medicine,[37,38] but has been rarely used in chemometrics.[28] CORICO visualizes multivariate data in the form of scatter plots, with dots representing similar vectors being close to each other. Remarkable correlations, in the sense of CORICO, are indicated by connected dots. Groups of similar vectors (spectra) form clusters and are represented as a network of links. Software used was CORICO version 3.3.[36]

k nearest-neighbor (KNN) classification

This evident but powerful classification method is widely used in chemometrics. Classification of an unknown object is performed by searching the k objects in a database (with known object classes) that have smallest Euclidean distances (corresponding to highest spectral similarity) to the unknown. A majority voting among these neighbors gives the predicted class of the unknown. The optimum value of k is estimated by a cross validation procedure.[18,31,32] KNN classification is closely related to spectra similarity searches which for instance is routinely used with EI mass spectra.[23]

DOI: 10.1002/rcm

RCM

The software product used for KNN classifications was SCAN.[34]

CART decision tree

The CART (classification and regression trees)[30] method develops a binary decision tree from a training set of objects with known class memberships. For each decision a single, automatically selected feature is used and the objects are divided into two groups by applying a threshold; the final decisions in the tree guide to one of the classes to be separated. The classification procedure is easy to interpret, and the method is robust with respect to outliers. Selection of the used variables and determination of the thresholds are performed by an iterative algorithm. The software product used for CART was SCAN.[34]

RESULTS

Mass spectra

The data set used comprises 39 mass spectra from four groups of minerals (Table 1) and four additional spectra from the gold substrate in which the minerals have been crushed. These spectra contain peaks at 529 different masses between 1.00718 and 1089.63 Da originating from inorganic and organic ions. Figure 1 shows typical spectra for a serpentine and an olivine sample, each separated into a spectrum with inorganic ions (including C^+) and organic ions. The spectra of inorganic ions are dominated by background signals (Au^+ from the sample's substrate, Ga^+ from the primary ion beam source). The peaks relevant to the minerals are very similar in the two spectra. The spectra of organic ions are almost identical for both samples; they show typical hydrocarbon

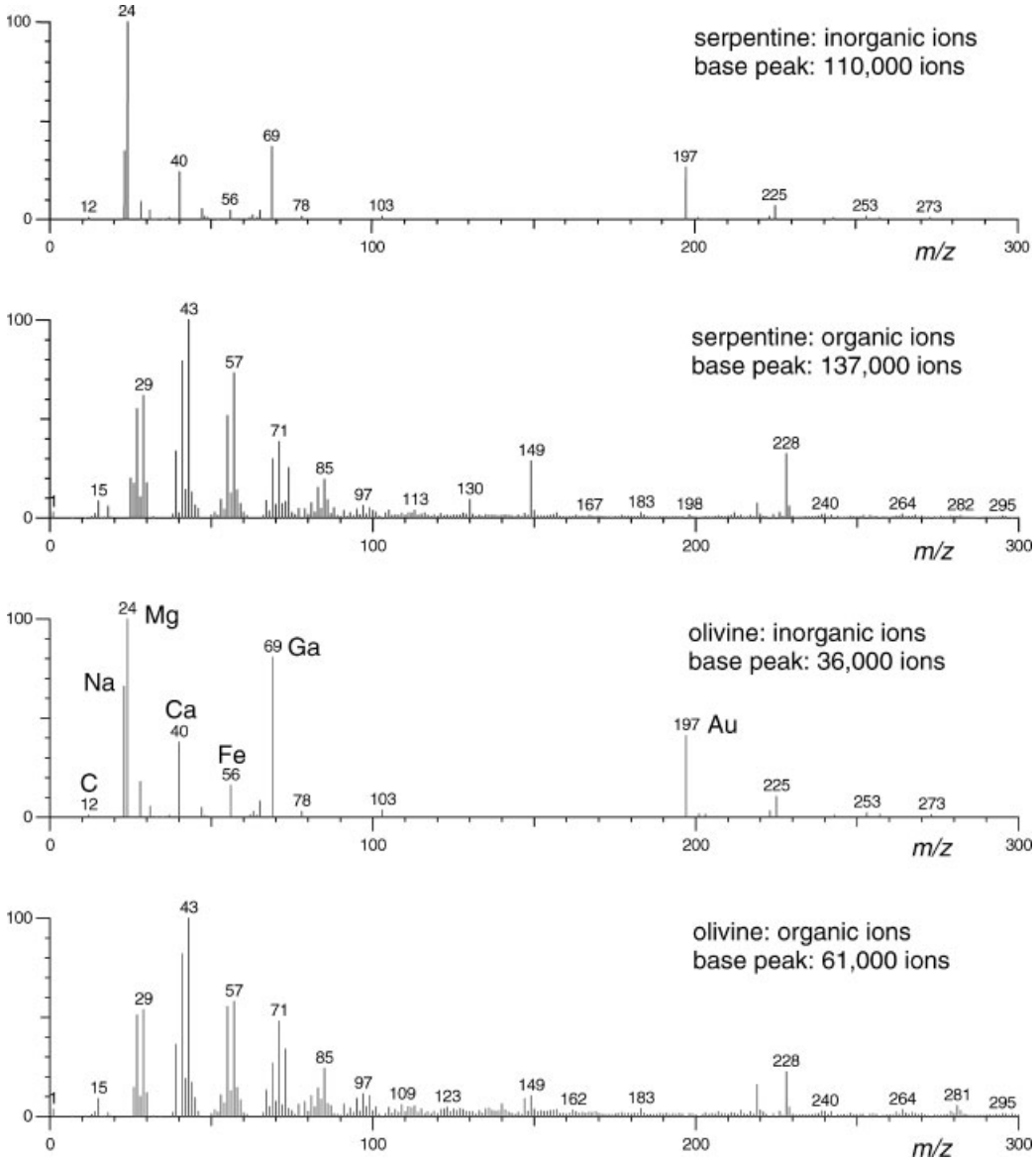

Figure 1. Examples of TOF-SIMS spectra of the serpentine and olivine samples. Inorganic and organic ions are separated into two spectra, each spectrum being scaled to base peak intensity; the numbers of detected ions of the base peaks are given to compare the yields of inorganic and organic ions. Only minor signals appear above *m/z* 300.

DOI: 10.1002/rcm

fragments and for instance the phthalate ion at m/z 149. Note that the ion yields for inorganic and organic ions are of the same order of magnitude in these data. From the spectra it is evident that the recognition of minerals requires a careful selection of peaks and the application of multivariate data analysis. Multivariate data analysis is able to consider peak intensities at many masses, and thereby provides a greater potential for clustering and classifying samples than for instance bivariate plots. Because an overall characterization of samples is important for cometary grains, data analysis in this study has been performed in two parts: using all peaks and using selected peaks considered to be relevant of the minerals.

Data analysis with all peaks

From data containing all 529 peak intensities a general picture of similarities between samples can be obtained by a cluster analysis. For data evaluation by PCA the peak intensities have been normalized to a constant sum of 100 in each spectrum. The score plot in Fig. 2 shows a clear separation of four talc samples from the other samples. In these four spectra peaks from $^{24}Mg^+$ and $^{28}Si^+$ have higher intensities than in other spectra, and these differences dominate the PCA score plot. Furthermore, eight of the 12 serpentine spectra form a compact cluster.

The CORICO software allows a background correction of the spectra by using data from blank gold substrates. The resulting diagram in Fig. 3 shows a good separation of the mineral classes, although—like with PCA—class information has not been used in the data treatment. In contrast to the PCA results, olivine and talc samples form distinct clusters in the CORICO plot. The only wrong assignments occur with two serpentine samples that are wrongly connected to the enstatite cluster. In summary, approximately 95% correct predictions of the four mineral classes can be expected by CORICO. The surprisingly good separation of some mineral classes – despite the fact that class information

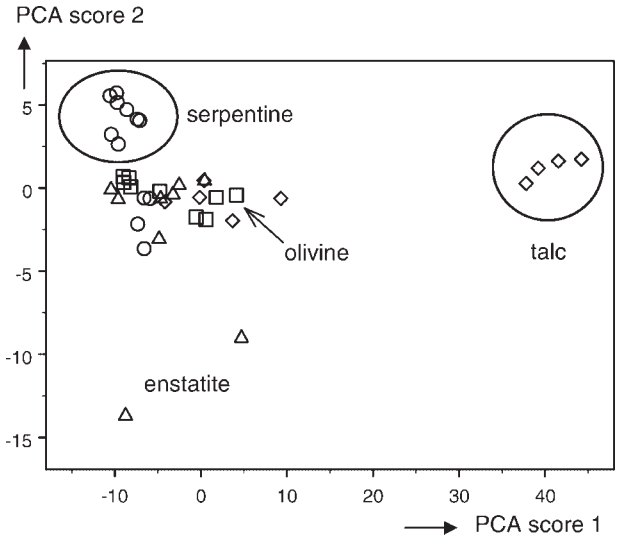

Figure 2. PCA score plot using all 529 peaks. Peak intensities have been normalized to a constant sum of 100 in each spectrum. First and second principal components preserve 86.5% and 4.0% of the total variance, respectively.

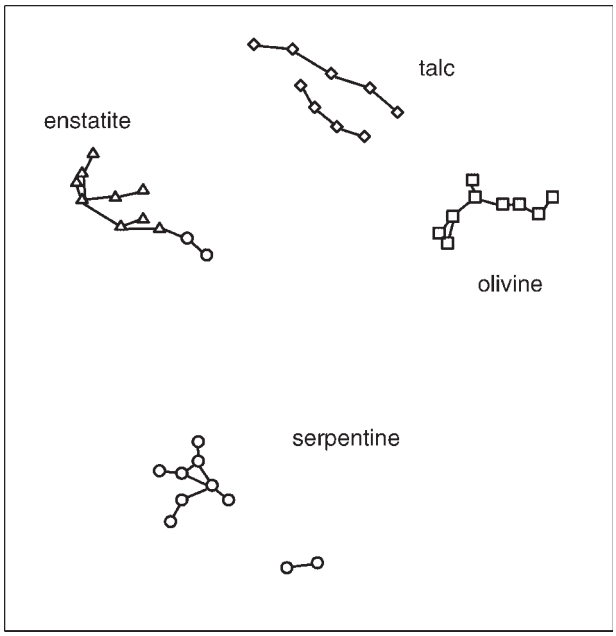

Figure 3. CORICO correlation plot for all 529 peaks with the intensities background corrected by using spectra from blank gold substrates.

was not used in data evaluation, and that organic peaks were not removed—can be explained by (1) significant differences in the peak patterns of mineral classes, and (2) by similar organic contaminations of the samples. However, the rather small data set available does not allow clarification of reasons for the ~5% wrong assignments. The most probable reason invoked could be the natural variation of the composition of mineral samples, but analytical errors, or an inadequate representation of the spectral data, cannot be excluded.

Data analysis with selected peaks

In chemometrics, the selection of variables is almost exclusively performed by applying mathematical criteria, for instance selection by maximum variance, maximum discrimination power, or maximum correlation with an object property or a class membership.[18,31] Genetic algorithms have also been applied to find good subsets of variables,[39] for instance for the recognition of substructures from EI mass spectra.[40] For this study mass spectral peaks have been selected that are potentially relevant for inorganic or mineral components in the samples. This selection is based on the chemical formulae of the ions as derived from the ion masses measured at a mass resolution of 2000. Two strategies for peak selection have been applied as follows. (1) No special knowledge about the type of inorganic compounds or minerals is assumed, and, consequently, all appropriate peaks from inorganic ions have been selected. This approach is suggested for the evaluation of data from cometary material. (2) The other strategy assumes that the sample belongs to one of a few known classes of inorganic compounds or minerals. In this case the selection aims at a small number of peaks, all potentially originating from the considered minerals, and yielding a high classification performance. In multivariate data analysis typically a larger set of variables is used for the discrimination of given classes

DOI: 10.1002/rcm

RCM

Table 3. Subset with 32 peaks of inorganic origin used for the discrimination of minerals. *m*, exact mass; Δ*m*, difference between experimental and exact mass. For peaks 11, 12 and 31 two different ions are given because they are not separated at the mass resolution of 2000

No.	Ion	*m*	Δ*m*
1	H	1.00782	−0.001
2	Li	7.01600	−0.002
3	O	15.99491	0.000
4	H_2O	18.01056	0.011
5	H_3O	19.01837	−0.003
6	^{23}Na	22.98978	−0.001
7	^{24}Mg	23.98504	−0.001
8	^{25}Mg	24.98584	0.015
9	^{26}Mg	25.98259	0.023
10	^{28}Si	27.97699	0.000
11	^{28}SiH	28.98475	−0.004
	^{29}Si	28.97649	0.004
12	^{29}SiH	29.98431	−0.010
	^{30}Si	29.97376	0.001
13	$^{28}SiH_3$	31.00036	−0.005
14	O_2	31.98982	−0.010
15	HO_2	32.99764	−0.011
16	H_2O_2	34.00546	−0.004
17	NaC	34.98978	−0.004
18	$NaCH_2$	37.00544	−0.009
19	$NaCH_3$	38.01326	−0.004
20	^{39}K	38.96371	−0.005
21	^{40}Ca	39.96259	0.000
22	^{41}K	40.96183	0.002
23	^{28}SiO	43.97181	−0.001
24	$^{28}SiNH_3$	45.00343	0.005
25	$^{28}SiH_2O$	45.98745	−0.003
26	$^{24}MgNa$	46.97480	−0.028
27	$^{24}Mg_2$	47.97000	−0.008
28	$^{24}Mg_2H$	48.97782	0.007
29	$^{24}Mg^{28}Si$	51.96190	−0.005
30	^{54}Fe	53.93961	0.002
31	^{56}Fe	55.93493	0.017
	$^{28}Si_2$	55.95380	−0.002
32	^{56}FeH	56.94272	−0.011

of samples; however, the final classification scheme may end up with only a few variables.

For a general characterization of the inorganic part of the samples a set of 32 peaks were selected as follows. Peaks from organic ions and peaks above *m*/*z* 60 were excluded. The resulting 32 peaks are listed in Table 3; they originate from the minerals but also from inorganic impurities or contaminations. Highest peak intensities were found for the atomic ions $^{24}Mg^+$ (32.9%), $^{23}Na^+$ (13.5%), $^{28}Si^+$ (13.5%), and $^{40}Ca^+$ (7.34%), with the intensities given as averages over the 39 spectra in percent of the sum of all 32 peak intensities.

Using the background-corrected data of these 32 selected peaks, CORICO separates well the mineral classes (Fig. 4). Spectra from olivine and talc form compact clusters; it can be expected that new spectra from these minerals can be correctly assigned. The serpentine samples form two clusters, one of them containing only serpentine, the other one being mixed with the enstatite group. From these results a total predictive ability for classification of 90% can be expected. The existence of four groups of minerals was found correctly, although class information was not used, and

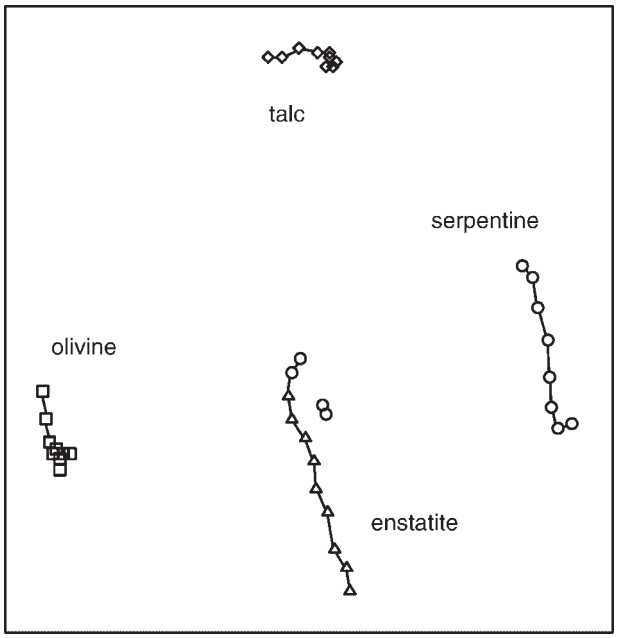

Figure 4. CORICO correlation plot using a selection of 32 peaks of inorganic origin (Table 3) with the intensities background corrected by using spectra from blank gold substrates.

although peak selection did not consider which elements are present in the minerals. The PCA score plot (not shown) obtained from the 32 selected peaks gives a less marked separation of the mineral classes than the CORICO plot; only the talc samples are clearly discriminated from the others. Obviously, the algorithm for background correction, together with the non-linear method as implemented in CORICO, are responsible for the improved cluster analysis results in comparison with PCA. Application of KNN classification to the 32 peak data (not background corrected) gives only three wrong results in leave-one-out cross validation, and thereby reaches a total predictive ability of 92.3%.

The second strategy applied for peak selection uses only peaks from ions containing the main elements Mg, Si, and Fe that are present in the four minerals. Ions containing oxygen and/or hydrogen give only minor signals and have not been considered. A data set containing only the intensities of the three peaks for $^{24}Mg^+$, $^{28}Si^+$, and $^{56}Fe^+ + {}^{28}Si_2^+$ (nos. 7, 10, and 31 in Table 3, respectively; note that $^{56}Fe^+$ and $^{28}Si_2^+$ cannot be separated at the used mass resolution of 2000) yields a good separation of the mineral classes. The original peak intensities of these three entities were normalized to a sum of 100 in each spectrum. The PCA score plot in Fig. 5 shows a complete separation of the talc and the olivine groups. Two of the serpentine spectra are located in the enstatite cluster. These two outliers have much lower relative intensities for $^{24}Mg^+$ (50% and 59%) than the other ten serpentines (67–88%), as well as much higher relative intensities for $^{28}Si^+$ (37 and 46%) than the other ten serpentines (7.8–29%). An explanation for these discrepancies cannot be given from the existing data; however, local contaminations may be a reason. The presence of outliers is a common situation in investigations of natural materials. In

DOI: 10.1002/rcm

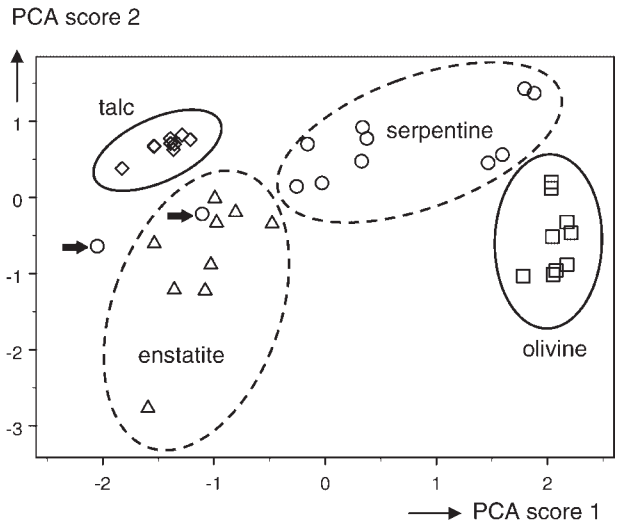

Figure 5. PCA score plot using intensities of the three peaks from ions $^{24}Mg^+$, $^{28}Si^+$, and $^{56}Fe^+ + {}^{28}Si_2^+$ (nos. 7, 10, and 31 in Table 3, respectively). Peak intensities are normalized to a constant sum of 100 in each spectrum. First and second principal components preserve 75.7% and 24.3% of the total variance, respectively. The mineral classes are well separated; bold face arrows indicate two serpentine outliers.

the present case they do not affect the overall good separation of the mineral classes.

A decision tree obtained by the CART method has a predictive ability of 92.3% (leave-one-out cross validation) with three erroneous classifications, namely the two serpentine outliers discussed above and one enstatite sample (Fig. 6(A)). A feature-feature plot (Fig. 6(B)) with the two variables that are used in the decision tree demonstrates the good separation of the mineral classes. The decision scheme for this plot—which is equivalent to the decision tree—allows a simple classification that can be summarized as follows. Assuming a sample belongs to one of the four investigated mineral classes, one has to normalize the peak intensities from ions $^{24}Mg^+$, $^{28}Si^+$, and $^{56}Fe^+ + {}^{28}Si_2^+$ to a sum of 100. If $[^{56}Fe^+ + {}^{28}Si_2^+]$ is lower than 2%, then the sample is predicted to be talc. If $[^{56}Fe^+ + {}^{28}Si_2^+]$ is higher than 8%, then olivine is a good candidate. If $[^{56}Fe^+ + {}^{28}Si_2^+]$ is between these two thresholds, one has to consider $[^{24}Mg^+]$; if $[^{24}Mg^+]$ is higher than 65% it is thought to be serpentine, or else it should be enstatite.

The classification thresholds found for $[^{56}Fe^+ + {}^{28}Si_2^+]$ correspond to the elemental wt% of iron which is 0.3 wt% for talc, 5.3 wt% for enstatite, 2.7 wt% for serpentine, and 7.5 wt% for olivine. This means that talc and olivine can be recognized in this data set by their mass spectral signal from $^{56}Fe^+$ ions (with contributions from $^{28}Si_2^+$ ions). Enstatite and serpentine are differentiated by their mass spectral signal from $^{24}Mg^+$ ions, although the elemental wt% (20.6 and 23.0, respectively) are rather similar for these minerals. In general, the relative intensities of secondary ions do not only depend on stoichiometry, but also for instance on crystallographic structure, and oxidation state of an element; more experimental data would be necessary to investigate these relationships.

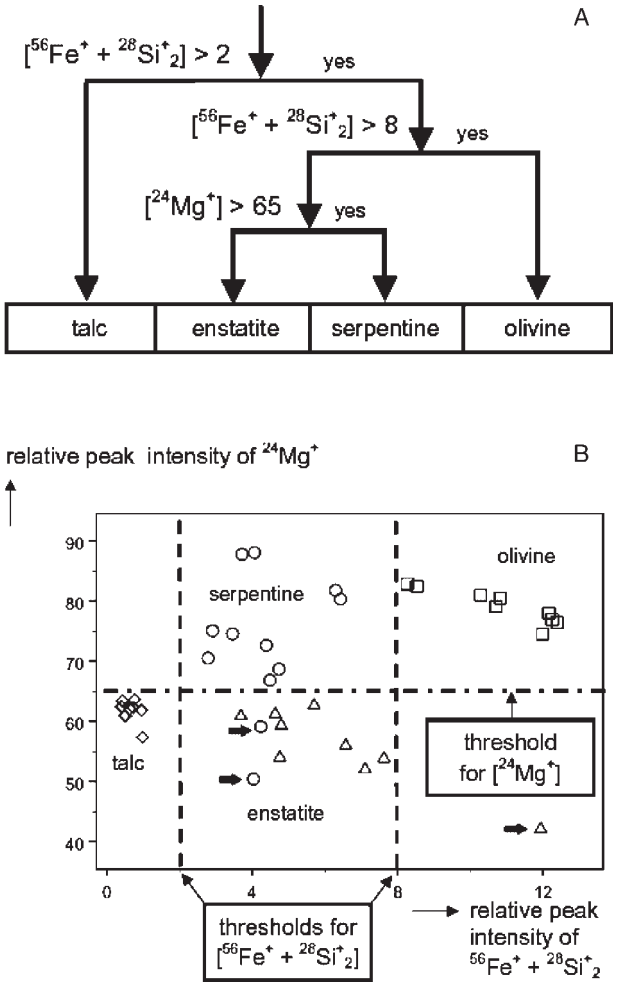

Figure 6. (A) Decision tree computed by the CART method. Except the two serpentine outliers and one enstatite sample all spectra are classified correctly with a total predictive ability of 92.3%. (B) Feature-feature plot with peak intensities of ions $^{56}Fe^+ + {}^{28}Si_2^+$ versus $^{24}Mg^+$. Peak intensities for ions $^{24}Mg^+$, $^{28}Si^+$, and $^{56}Fe^+ + {}^{28}Si_2^+$ (nos. 7, 10, and 31 in Table 3, respectively) are normalized to a constant sum of 100 in each spectrum. Bold face arrows indicate three wrong classifications.

CONCLUSIONS

TOF-SIMS data at high mass resolution are appropriate for a characterization of mineral samples by multivariate clustering. For the investigated data, the non-linear method CORICO gave somewhat more informative plots than the linear method PCA. Using all mass peaks (from inorganic and organic ions, partly originating from contaminations) provided an overview of the composition of the sample's surface. A selection of peaks from appropriate inorganic ions allowed a successful discrimination of the studied mineral classes serpentine, enstatite, olivine, and talc, widely independent from inorganic or organic contaminations. The predictive ability for classification—estimated by leave-one-out cross validation—exceeds 90% for KNN classification and a binary decision tree (CART); for these classifications only the relative intensities of ions $^{24}Mg^+$, $^{28}Si^+$, and $^{56}Fe^+ + {}^{28}Si_2^+$ were required. Error-free assignments have been obtained for olivine and talc samples;

DOI: 10.1002/rcm

in particular, olivine could be differentiated from the pyroxene (enstatite). It has been shown that TOF-SIMS together with multivariate data analysis is capable of discrimination in a one-step process between various minerals of similar kinds as they may exist in cosmic material.

We conclude that data from the COSIMA instrument will be principally appropriate to characterize inorganic cometary material by using the described chemometric methods. These results are complementary to studies with organic substances.[25,26] Furthermore, Antarctic micrometeorites—containing the studied minerals—may be appropriate reference samples for studies with analogous laboratory instruments to COSIMA. Future experiments will focus on mixtures of minerals and/or organics and careful sample preparation in order to avoid unnecessary surface contaminations.

Acknowledgements

This work is supported by CNES in France.

REFERENCES

1. Amici S, Piccioni G, Coradini A, Solazzo S. *Planet. Space Sci.* 2000; **48**: 401.
2. Brucato JR, Colangeli L, Mennella V, Palumbo P, Bussoletti E. *Planet. Space Sci.* 1999; **47**: 773.
3. Brucato JR, Mennella V, Colangeli L, Rotundi A, Palumbo P. *Planet. Space Sci.* 2002; **50**: 829.
4. Aubriet F, Poleunis C, Bertrand P. *J. Mass Spectrom.* 2001; **36**: 641.
5. Cuynen E, Van Vaeck L, Van Espen P. *Rapid Commun. Mass Spectrom.* 1999; **13**: 2287.
6. Stephan T. *Planet. Space Sci.* 2001; **49**: 859.
7. Brinckerhoff WB. *Planet. Space Sci.* 2005; **53**: 817.
8. Kissel J, Brownlee DE, Büchler K, Clark BC, Fechtig H, Grün E, Hornung K, Igenbergs EB, Jessberger EK, Krueger FR, Kuczera H, Mc Donnell JAM, Morfill GM, Rahe J, Schwehm GH, Sekanina Z, Utterback NG, Völk HJ, Zook HA. *Nature* 1986; **321**: 336.
9. Wooden DH, Butner HM, Harker DE, Woodward CE. *Icarus* 2000; **143**: 126.
10. Wooden DH, Harker DE, Woodward CE, Butner HM, Koike C, Witteborn FC, McMurtry CW. *Astrophys. J.* 1999; **517**: 1034.
11. Kissel J, Krueger FR, Silen J, Clark BC. *Science* 2004; **304**: 1774.
12. Greenberg JM. *Astron. Astrophys.* 1998; **330**: 375.
13. Krueger FR, Werther W, Kissel J, Schmid ER. *Rapid Commun. Mass Spectrom.* 2004; **18**: 103.
14. Kissel J, Krueger FR. *Appl. Phys. A* 1987; **42**: 69.
15. Brownlee DE, Horz F, Newburn RL, Zolensky M, Duxbury TC, Sandford S, Sekanina Z, Tsou P, Hanner MS, Clark BC, Green SF, Kissel J. *Science* 2004; **304**: 1764.
16. Kurat G, Koeberl C, Presper T, Brandstätter F, Maurette M. *Geochim. Cosmochim. Acta* 1994; **58**: 3879.
17. Engrand C, Maurette M. *Meteoritics Planet. Sci.* 1998; **33**: 565.
18. Vandeginste BGM, Massart DL, Buydens LCM, De Jong S, Smeyers-Verbeke J. *Handbook of Chemometrics and Qualimetrics*, part B. Elsevier: Amsterdam, 1998.
19. Hutter H, Grasserbauer M. *Chemom. Intell. Lab. Syst.* 1994; **24**: 99.
20. Xhoffer C, Bernard P, Van Grieken R. *Environ. Sci. Technol.* 1991; **25**: 1470.
21. Peterson RE, Tyler BJ. *Atmos. Environ.* 2002; **36**: 6041.
22. Latkoczy C, Hutter H, Grasserbauer M, Wilhartitz P. *Mikrochim. Acta* 1995; **119**: 1.
23. Varmuza K. In *Encyclopedia of Spectroscopy and Spectrometry*, Lindon JC, Tranter GE, Holmes JL (eds). Academic Press: London, 2000; 232.
24. Varmuza K, Werther W. *J. Chem. Inf. Comput. Sci.* 1996; **36**: 323.
25. Varmuza K, Kissel J, Krueger FR, Schmid ER. In *Advances in Mass Spectrometry*, vol. 15, Gelpi E (ed). John Wiley: Chichester, 2001; 229.
26. Werther W, Demuth W, Krueger FR, Kissel J, Schmid ER, Varmuza K. *J. Chemometrics* 2002; **16**: 99.
27. Wagner MS, Graham DJ, Ratner BD, Castner DG. *Surf. Sci.* 2004; **570**: 78.
28. Engrand C, Lespagnol J, Martin P, Thirkell L, Thomas R. *Appl. Surf. Sci.* 2004; **231**: 883.
29. Reich DF. In *ToF-SIMS: Surface Analysis by Mass Spectrometry*, Vickerman JC, Briggs D (eds). IM Publications: Chichester, 2001; 113.
30. Frank IE, Todeschini R. *The Data Analysis Handbook*. Elsevier: Amsterdam, 1994.
31. Massart DL, Vandeginste BGM, Buydens LCM, De Jong S, Smeyers-Verbeke J. *Handbook of Chemometrics and Qualimetrics*, part A. Elsevier: Amsterdam, 1997.
32. Varmuza K. In *The Encyclopedia of Computational Chemistry*, vol. 1, Schleyer PvR, Allinger NL, Clark T, Gasteiger J, Kollman PA, Schaefer IHF, Schreiner PR (eds). John Wiley: Chichester, 1998; 346.
33. Camo Process AS, *Software Unscrambler*, Oslo, Norway, 2002; http: //www.camo.no.
34. Minitab Inc., *Software SCAN*, State College, PA, USA, 1995.
35. Lesty M, Buat-Ménard P. *Les cahiers de l'analyse des données* 1982; **7**: 355.
36. Lesty M. *User guide CORICO*, version 3.3, Versailles, France, 2003.
37. Lesty C, Chleq C, Contesso G, Jacquillat C. *Anal. Quant. Cytol. Histol.* 1992; **14**: 175.
38. Lesty C, Pleau-Varet J, Kujas M. *J. Appl. Statistics* 2004; **31**: 191.
39. Leardi R. *J. Chemometrics* 2001; **15**: 559.
40. Yoshida H, Leardi R, Funatsu K, Varmuza K. *Anal. Chim. Acta* 2001; **446**: 483.

DOI: 10.1002/rcm

First discovery of meteoritic events in deep Antarctic (EPICA-Dome C) ice cores

Biancamaria Narcisi,[1] Jean Robert Petit,[2] and Cécile Engrand[3]

Received 25 May 2007; revised 10 July 2007; accepted 17 July 2007; published 11 August 2007.

[1] Two distinct dust layers in the EPICA-Dome C ice core (75°06′S, 123°21′E, East Antarctic Plateau) have been shown to relate to individual meteoritic events. Particles forming these layers, investigated by electron microprobe, show peculiar textural, mineralogical and geochemical features and closely resemble extraterrestrial debris in deep-sea sediments and polar caps. Preliminary estimates of cosmic debris input at the studied layers, obtained from Coulter Counter measurements, are 4–5 orders of magnitude greater than the yearly micrometeorite flux in East Antarctic snow and ice. The cosmic events are accurately dated through glaciological models at 434 ± 6 and 481 ± 6 ka, respectively and are located in the core climatic stratigraphy near the "Mid-Brunhes Event". This is the first report of well-dated cosmic horizons in deep Antarctic ice cores. It significantly improves the extraterrestrial record of Antarctica and opens new correlation perspectives between long climatic records of the South polar region. **Citation:** Narcisi, B., J. R. Petit, and C. Engrand (2007), First discovery of meteoritic events in deep Antarctic (EPICA-Dome C) ice cores, *Geophys. Res. Lett.*, *34*, L15502, doi:10.1029/2007GL030801.

1. Introduction

[2] Cosmic particulate matter in the form of interplanetary dust and micrometeorites constantly reaches the Earth surface and is found disseminated in diverse terrestrial deposits [e.g., *Blanchard et al.*, 1980; *Koeberl and Hagen*, 1989]. This material represents the dominant fraction of the present-day extraterrestrial flux [e.g., *Taylor et al.*, 2000] and its study provides information on solar system formation and evolution [*Brownlee*, 1985]. Traces of collisions having regional significance (e.g. impact craters and related ejecta sediments, conspicuous micrometeorite showers caused by passage of large meteoroids or comets) are greatly scattered in the geologic record [e.g., *Grieve*, 1997]. Nonetheless, their detection and study are very important to provide isochronous markers for stratigraphic correlations, and to address issues on future events and related environmental effects [e.g., *Toon et al.*, 1997].

[3] The Antarctic region represents the best site to collect small meteoritic particles because terrestrial input from surrounding deserts is very low [e.g., *Delmonte et al.*, 2002] and extreme environmental conditions prevent chemical weathering. Numerous characterization studies have been carried out on micrometeorites recovered from various Antarctic sites [e.g., *Maurette et al.*, 1991; *Taylor et al.*, 2000]. Recently, a new micrometeorite project has been launched at the permanent French-Italian station of Concordia, on the East Antarctic Plateau, where low accumulation rates allow collection of microparticles from reduced quantities of snow [*Duprat et al.*, 2005]. The bulk of previous and current Antarctic investigations focus on contemporary and recent continuous cosmic dust deliveries, which are incorporated in surface snow/firn layers, or the investigations focus on particle concentrations from blue ice and glacial sediments of unknown age. Little is known about microparticles in old dated Antarctic ice sections, although very valuable documentation on extraterrestrial steady fall and/or individual events is certainly archived in such ancient records [*Harvey et al.*, 1998; *Yada et al.*, 2004].

[4] Deep ice cores from the East Antarctic Plateau offer excellent opportunities to investigate past cosmic dust falls. This is because the recovered ice record (1) is continuous and extends back to several hundreds of thousands of years, (2) is stratigraphically coherent and not affected by ice flow disturbances, and (3) is provided with various paleoclimatic datasets and accurate age scale [e.g., *EPICA Community Members*, 2004], allowing for a reliable reconstruction of past accretion. However, so far, very limited work has been done on cosmic debris in deep East Antarctic cores [e.g., *Yiou et al.*, 1991].

[5] The aim of this paper is to document for the first time two extraterrestrial events from Middle Pleistocene sections of the EPICA-Dome C ice record, East Antarctic Plateau (75°06′S, 123°21′E). We show that these events occur as distinct dust layers consisting of cosmic debris with characteristic features. Since both events are precisely set into the detailed core chronostratigraphic record, we discuss the implications of our findings particularly for linking and dating of southern Hemisphere climatic records.

2. Materials and Methods

[6] The EPICA (European Project for Ice Coring in Antarctica) Dome C ice core, drilled down to 3260 m, has provided a continuous climatic record over the last eight glacial cycles, ca. 800 ka (Figure 1) [e.g., *EPICA Community Members*, 2004].

[7] The Dome C ice is generally very clear and the core contains less than twenty visible dust layers. The majority of these layers occur in the uppermost 2200 m and are composed of airborne volcanic ash produced by explosive

[1] Centro Ricerche Casaccia, Ente per le Nuove Technologie, l'Energia e l'Ambiente, Rome, Italy.
[2] Laboratoire de Glaciologie et Géophysique de l'Environnement, Centre National de la Recherche Scientifique, Saint Martin d'Hères, France.
[3] Centre de Spectrométrie Nucléaire et de Spectrométrie de Masse, Centre National de la Recherche Scientifique & Université Paris Sud, Orsay, France.

0094-8276/07/2007GL030801$05.00

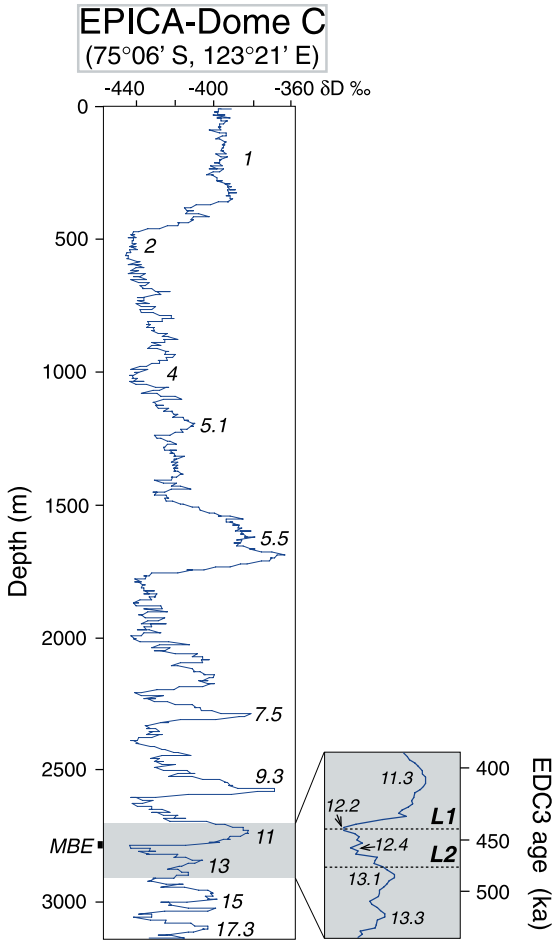

Figure 1. EPICA-Dome C δD record, which is a temperature proxy, with a few marine isotope stage numbers and the position of Mid-Brunhes Event (MBE) indicated [*EPICA Community Members*, 2004]. The box shows the stratigraphic position of studied layers (dashed lines). EDC3 core timescale is from *Parrenin et al.* [2007].

eruptions [*Narcisi et al.*, 2005]. The two discrete dust layers studied here lie at depths of 2788 and 2833 m, respectively (Figure 1). They were identified during core inspection and logging at Dome C and the related ice sections were analyzed in the field for their electrical properties [*Stauffer et al.*, 2004]. Both layers (hereafter L1 and L2) are visually very similar to tephra layers, i.e. they appear as dark, slightly undulated distinct strips with thickness in both cases of a few mm. Fine-scale laminations occurring in both layers could be to due eolian reworking prior to burial or more likely to ice stretching, as is also suggested by anomalies in the thinning function in the bottom 500 m of the core [*Parrenin et al.*, 2007]. The dust layers are precisely framed into the Dome C core chronostratigraphic record (Figure 1). L1 lies at the end of a cold period corresponding to Marine Isotope Stage (MIS) 12; based on the newly developed EDC3 core timescale [*Parrenin et al.*, 2007] its age is 434 ± 6 ka. L2 lies in late part of the interglacial MIS 13 and has an EDC3 age of 481 ± 6 ka.

[8] We have characterized the grain size, morphology, texture and composition of dust particles from both layers in order to assess their origin. The narrow core sections containing the two layers were processed in a class 100 clean room. After decontamination with deionized water and ice melting, grain size measurements were performed using a 256-channel Coulter Counter (for analytical procedures see *Delmonte et al.* [2002]). The particulate matter was recovered by filtration at 8 and 0.4 μm pore size and two or more filters per layer were prepared. Unpolished filters were used for particle external morphology and semi-quantitative major element analysis by scanning electron microscope equipped with an energy dispersive X-ray spectrometer (SEM-EDS). Filters embedded in epoxy resin and polished with microdiamond paste were used for examination of particle interior textures by SEM-EDS and for bulk quantitative elemental analysis by wavelength-dispersive X-ray spectrometry (WDS). For WDS microprobe working conditions see *Narcisi et al.* [2005]. Tens of particles were analyzed from each dust layer (Table 1).

3. Results and Interpretation

[9] Grain size measurements, and optical and electron microscope observations revealed that both layers consist of

Table 1. Major Oxide Composition of Particles in the EPICA-Dome C Dust Layers[a]

	Layer L1			Layer L2		
n	WDS Interior 22	EDS Surface 82	EDS Interior 25	WDS Interior 25	EDS Surface 46	EDS Interior 24
SiO_2	35.77 ± 2.24	1.8–56.8	9.9–42.3	31.40 ± 6.19	11.6–47.6	11.4–52.3
TiO_2	0.04 ± 0.02	bdl-1.7	bdl-0.5	0.10 ± 0.05	bdl-0.4	bdl-0.6
Al_2O_3	1.06 ± 0.87	bdl-8.4	bdl-7.4	1.89 ± 1.25	0.4–7.5	bdl-8.8
Cr_2O_3	0.38 ± 0.21	na	bdl-4.1	0.45 ± 0.22	na	bdl-4.1
FeO	27.94 ± 6.10	14.1–94.7	12.6–76.2	28.55 ± 9.50	16.4–74.6	6.8–70.0
MnO	0.35 ± 0.07	bdl-1.3	0.1–1.1	0.26 ± 0.06	bdl-1.0	bdl-0.4
MgO	29.95 ± 6.83	bdl-43.2	3.1–43.6	24.01 ± 8.82	4.3–39.6	4.4–43.9
CaO	0.81 ± 0.65	bdl-10.6	0.2–3.3	1.52 ± 1.09	0.2–6.8	0.2–5.5
Na_2O	0.25 ± 0.15	bdl-3.0	bdl-1.8	1.36 ± 1.33	bdl-4.6	bdl-6.1
K_2O	0.03 ± 0.02	bdl-0.9	bdl-0.3	0.06 ± 0.04	bdl-1.5	bdl-0.4
NiO	1.45 ± 0.66	bdl-10.5	0.3–3.3	1.82 ± 0.65	bdl-7.3	0.3–3.7
SO_3	0.38 ± 0.25	na	bdl-2.2	0.15 ± 0.10	na	bdl-2.0
Total	98.40 ± 2.32	100	100	91.58 ± 10.53	100	100

[a]Composition by either WDS (broad-beam analysis) or EDS (point analysis) microprobe is given as wt%, where *n* is the number of analyses from different particles. WDS data are presented as mean and standard deviation. EDS data are presented as range and are normalized to 100%. Total iron reported as FeO. bdl: below detection limit; na: not analyzed.

dark brown/black angular and rounded grains of large size (see auxiliary material).[1] SEM observations on the coarser particles indicate that sample L1 shows maximal grain size of ca. 100 μm. It is mostly composed of angular compact olivine particles, showing at times tiny metal inclusions. This sample also contains a minor proportion of spherical and angular particles, which are ca. 10 μm in size or larger and show internal porphyritic texture. Sample L2 has a modal value of the volume-size distribution of ca. 7–12 μm (Figure 2). Under the microscope, the coarser fractions consist mostly of spherical particles up to 25 μm in size, which are mostly glassy with magnetite dendrites (see auxiliary material). A minor grain population consists of olivine and pyroxene crystals with metal inclusions. They have angular shapes and sizes larger than the spheres (typically 30–40 μm, up to ca. 60 μm). Angular grains in layer L2 also include fragments of spheroidal particles with pronounced dendritic textures. Typical eolian dust (feldspars, quartz) in both samples is negligible and confined in the 2–3 μm size fraction.

[10] Microprobe analyses indicate that L1 and L2 are geochemically comparable to each other (Table 1 and Figure 3), suggesting a similar origin. Defocused beam WDS elemental composition of particle interiors from both layers is dominated by O, Si, Mg and Fe, with low contents of Al and Ca, and very low proportions of K and Ti and Ni and Cr commonly observable. EDS microprobe data on both particle surfaces and interiors display wide variations because they include point analyses from various mineral components and from glass, however they are broadly consistent with WDS values.

[11] The obtained results strongly suggest that the particles forming both studied layers have an extraterrestrial origin. The observed "coarse" grain size is not coherent with eolian deposition, since mineral aerosol input in East Antarctic ice is typically around 2 μm [*Delmonte et al.*, 2002] (Figure 2). Such grain size is in the range of airborne volcanic ash reaching the Antarctic interior [*Narcisi et al.*, 2005] (Figure 2), however neither shapes or geochemistry of the studied particles match features of Antarctic tephra layers (Figure 3). Spherical shapes are suggestive of melting processes during atmospheric entry and internal textures of the studied spheres, characterized by magnetite networks enclosing silicate glass, are a distinctive feature of cosmic spherules from various sites [e.g., *Blanchard et al.*, 1980; *Koeberl and Hagen*, 1989]. Porphyritic textures and mineral assemblages of the angular particles are consistent with unmelted and partially-melted micrometeorites at various terrestrial locations [e.g., *Beckerling and Bischoff*, 1995]. A volcanic origin can be excluded because englacial tephra layers in distal East Antarctic sites are almost devoid of phenocrysts [*Narcisi et al.*, 2005]. Therefore, the observed mafic crystals with tiny metal inclusions are relicts of the precursor body that were not completely melted during passage through Earth's atmosphere. Finally, the obtained "chondritic" elemental composition is well comparable with various collections of cosmic particles and rule out either a volcanic or a continental nature of the studied grains (Figure 3). The elemental abundances do not fit those of

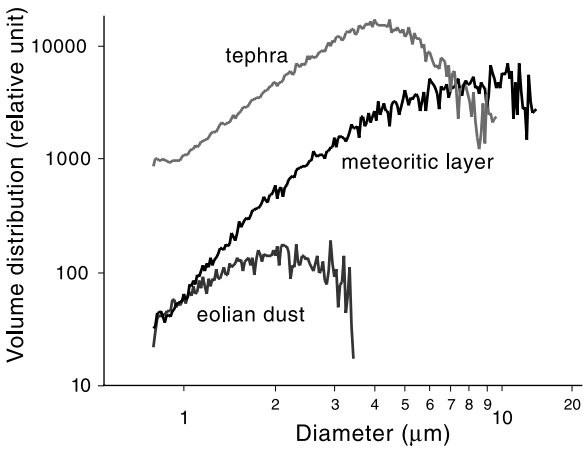

Figure 2. Volume-size distribution of meteoritic layer L2 compared to typical tephra and eolian dust samples from the EPICA-Dome C core. In the meteoritic layer, 19,822 particles with diameter larger than 0.7 μm were counted. 1700 particles have a diameter larger than 5 μm, and 398 larger than 8 μm. Less than 3 particles were counted for sizes larger than 13 μm.

microtektites (Figure 3), indicating that the L1 and L2 Dome C particles are truly cosmic debris produced from meteoroid entry into the atmosphere, and not impact ejecta.

[12] From particle concentration obtained by Coulter Counter measurements of the 0.7–13 μm fraction, we estimate a micrometeorite input at the event forming L2 of ca. 0.3 g m^{-2}. A similar value can be expected also for the other studied event, since the two layers show comparable thickness and granulometry. This debris amount is 4 orders of magnitude greater than the yearly contemporary micrometeorite flux recorded at Dome C for particles larger than 30 μm (ca. 0.01 mg m^{-2}) [*Duprat et al.*, 2006] and 4–5 orders of magnitude greater than the annual cosmic particle input in East Antarctic ice during the last 200 ka (from ca. 0.003 to ca. 0.05 mg m^{-2}) [*Yiou et al.*, 1991; *Yada et al.*, 2004].

4. Discussion and Conclusion

[13] Cosmic dust allows the deduction of the composition of primitive solar system material, estimate the accretion rates of extraterrestrial matter, and establish stratigraphic correlations. The latter purpose can be achieved if particles are related to single depositional events. In this respect, the copiousness of cosmic debris, which is confined within the studied layers and is not mixed with significant extraneous (i.e. terrestrial) matter, already suggests relation to individual meteoritic falls rather than to steady input. Our findings are clearly different from previous micrometeorite records in Antarctic cores, which were related to a few cosmic microparticles from large ice sections [*Yiou et al.*, 1991]. In addition, the ice core stratigraphy is continuous and undisturbed [*EPICA Community Members*, 2004], leading to exclude selective secondary concentration of cosmic particles of normal continuous fall from surrounding ice. Surface phenomena at the EPICA site can influence the ice record only at a year timescale [*Barnes et al.*, 2006]. Therefore, the possibility of a hiatus of snow accumulation

[1] Auxiliary materials are available in the HTML. doi:10.1029/2007GL030801.

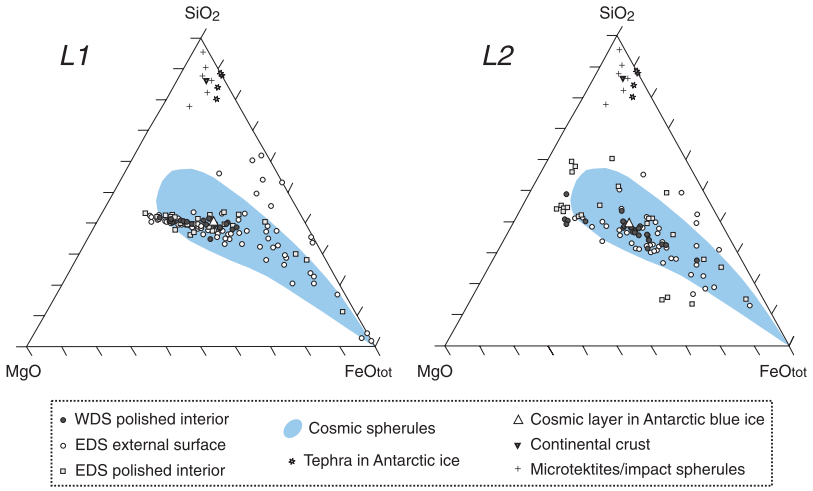

Figure 3. Comparison of grain-specific chemical analyses from this study with Greenland/deep sea cosmic spheres [*Maurette et al.*, 1986], tephra layers in Antarctic ice [*Narcisi et al.*, 2005], cosmic layer detected in Victoria Land blue ice [*Harvey et al.*, 1998], average composition of the continental crust [*Wedepohl*, 1995], and Australasian microtektites/impact spherules [*Glass et al.*, 2004].

for a time interval sufficient to concentrate the constant micrometeorite deposition in a discrete layer (using the above input estimate this interval would be at least a few thousands of years) is ruled out. We therefore conclude that both layers represent individual meteoritic events. In both cases, the debris produced by meteoroid disruption fell out onto the Dome C surface and then became part of the ice record with no significant stratigraphic displacement.

[14] Considering that micrometeoritic fallout in ancient Antarctic ice is largely undocumented, and that fall events are uncommon phenomena in the Earth record, our detection of two distinct Middle Pleistocene events at one site and within a short geological time interval (ca. 50 ka) is an outstanding finding. Our unexpected discovery provides the first evidence of meteoritic events in Antarctic ice cores and represents a major step towards reconstruction of extraterrestrial stratigraphic record of the Antarctic continent, which is to date largely unknown.

[15] Astrophysical implications of our findings will be discussed elsewhere. Here we focus mainly on potential implications for correlation purposes. The two meteoritic horizons show distinctive particle features and lie in precise chronostratigraphic positions within the core climatic record (Figure 1). Therefore, similarly to airborne volcanic ash layers, they form valuable marker beds for independent link and dating of stratigraphies from different sites. Depending on the scale of the identified events (local meteorite showers or large events of regional scale), our discovery can enhance correlation perspectives between long Antarctic ice climatic records and even circumpolar sequences. In this respect, note that the Dome C events are stratigraphically located in the vicinity of the so-called Mid-Brunhes Event (MBE), roughly corresponding to the transition between MIS 12 and MIS 11 (Figure 1), which marks a notable amplitude and duration change of climate cycles with respect to the previous periods [e.g., *EPICA Community Members*, 2004]. The cosmic horizons could be used to unambiguously compare South polar climatic archives from different realms across this peculiar transition [e.g., *Hodell et al.*, 2003], and therefore help clarify the causes of the Event. The occurrence of micrometeorite horizons close to this distinct climate change may also renew the debate on a possible relationship between climate and extraterrestrial dust accretion [*Muller and MacDonald*, 1997], although the presented data certainly are not sufficient to draw any conclusion. Lastly, meteoritic debris is suitable for radioisotope dating [*Nishiizumi et al.*, 1989], however the high uncertainties on cosmogenic terrestrial ages of Middle Pleistocene material (typically several tens of thousands of years) limit interest in the application of such dating methods to the studied layers.

[16] From preliminary examination of known extraterrestrial events in the southern Hemisphere, there are no suitable counterparts of the Dome C events. The Eltanin impact (ca. 2.15 Ma) [*Gersonde et al.*, 1997], the event responsible for the Australasian microtektite layer (ca. 0.8 Ma) [e.g., *Glass et al.*, 2004], and the 2.3–2.7 Ma meteoritic event recorded in Victoria Land blue ice [*Harvey et al.*, 1998] are too old to be related. Impact events in Australia and South Africa do not show matching ages [*Haines*, 2005; *Reimold et al.*, 1998] and the 445-ka Argentinean event [*Schultz et al.*, 2004] most likely was not large enough for connection with Dome C layers.

[17] In conclusion, although magnitude and geographic extent of detected events are not known, the new EPICA-Dome C findings significantly increase knowledge on Antarctic meteoritic events in geological times and provide unique time-synchronous markers for potential stratigraphic correlations in the South polar region. More generally, the long Antarctic ice records are mines of detailed geological information and our discovery confirms their extraordinary capacity to archive environmental facts of the various types.

[18] **Acknowledgments.** This research was supported by the Antarctic National Research Program (PNRA) under the Project on Glaciology. The EPICA drilling operations at Dome C benefited from the support of the French-Italian Concordia Station. We thank the scientific and logistic personnel involved in the Dome C fieldwork, M. Tonelli (CIGS, Modena) and F. Olmi (CNR, Florence, deceased) for assistance during SEM-EDS and WDS microprobe analysis, respectively, and two anonymous reviewers

for constructive comments. This work is a contribution to the "European Project for Ice Coring in Antarctica" (EPICA), a joint European Science Foundation/European Commission scientific program, funded by the EU (EPICA-MIS) and by national contributions from Belgium, Denmark, France, Germany, Italy, the Netherlands, Norway, Sweden, Switzerland and the United Kingdom. This is EPICA publication 180.

References

Barnes, P. R. F., E. W. Wolff, and R. Mulvaney (2006), A 44 kyr paleoroughness record of the Antarctic surface, *J. Geophys. Res.*, *111*, D03102, doi:10.1029/2005JD006349.

Beckerling, W., and A. Bischoff (1995), Occurrence and composition of relict minerals in micrometeorites from Greenland and Antarctica: Implications for their origins, *Planet. Space Sci.*, *43*(3–4), 435–449.

Blanchard, M. B., D. E. Brownlee, T. E. Bunch, P. W. Hodge, and F. T. Kyte (1980), Meteoroid ablation spheres from deep-sea sediments, *Earth Planet. Sci. Lett.*, *46*, 178–190.

Brownlee, D. E. (1985), Cosmic dust: Collection and research, *Annu. Rev. Earth Planet. Sci.*, *13*, 147–173.

Delmonte, B., J. R. Petit, and V. Maggi (2002), Glacial to Holocene implications of the new 27000-year dust record from the EPICA Dome C (East Antarctica) ice core, *Clim. Dyn.*, *18*, 647–660.

Duprat, J., C. Engrand, M. Maurette, M. Gounelle, G. Kurat, and C. Hammer (2005), The Micrometeorite Program at Dome C, in *Dome C Astronomy and Astrophysics Meeting*, *EAS Publ. Ser.*, vol. 14, edited by M. Giard et al., pp. 51–56, EDP Sci., Les Ulis, France.

Duprat, J., C. Engrand, M. Maurette, F. Naulin, G. Kurat, and M. Gounelle (2006), The micrometeorite mass flux as recorded in Dome C central Antarctic surface snow, *Meteorit. Planet. Sci.*, *41 Suppl.*, A48.

EPICA Community Members (2004), Eight glacial cycles from an Antarctic ice core, *Nature*, *429*, 623–628.

Gersonde, R., et al. (1997), Geological record and reconstruction of the late Pliocene impact of the Eltanin asteroid in the Southern Ocean, *Nature*, *390*, 357–363.

Glass, B. P., H. Huber, and C. Koeberl (2004), Geochemistry of Cenozoic microtektites and clinopyroxene-bearing spherules, *Geochim. Cosmochim. Acta*, *68*, 3971–4004.

Grieve, R. A. F. (1997), Extraterrestrial impact events: The record in the rocks and the stratigraphic column, *Palaeogeogr. Palaeoclimatol. Palaeoecol.*, *132*, 5–23.

Haines, P. W. (2005), Impact cratering and distal ejecta: The Australian record, *Aust. J. Earth Sci.*, *52*, 481–507.

Harvey, R. P., N. W. Dunbar, W. C. McIntosh, R. P. Esser, K. Nishiizumi, S. Taylor, and M. W. Caffee (1998), Meteoritic event recorded in Antarctic ice, *Geology*, *26*(7), 607–610.

Hodell, D. A., S. L. Kanfoush, K. A. Venz, C. D. Charles, and F. J. Sierro (2003), The Mid-Brunhes transition in ODP sites 1089 and 1090 (Subantarctic South Atlantic), in *Earth's Climate and Orbital Eccentricity: The Marine Isotope Stage 11 Question*, *Geophys. Monogr. Ser.*, vol. 137, edited by A. W. Droxler et al., pp. 113–129, AGU, Washington, D. C.

Koeberl, C., and E. H. Hagen (1989), Extraterrestrial spherules in glacial sediment from the Transantarctic Mountains, Antarctica: Structure, mineralogy, and chemical composition, *Geochim. Cosmochim. Acta*, *53*, 937–944.

Maurette, M., C. Hammer, D. E. Brownlee, N. Reeh, and H. H. Thomsen (1986), Placers of cosmic dust in the blue ice lakes of Greenland, *Science*, *233*, 869–872.

Maurette, M., C. Olinger, M. Christophe Michel-Lévy, G. Kurat, M. Pourchet, F. Brandstätter, and M. Bourot-Denise (1991), A collection of diverse micrometeorites recovered from 100 tonnes of Antarctic blue ice, *Nature*, *351*, 44–47.

Muller, R. A., and G. J. MacDonald (1997), Glacial cycles and astronomical forcing, *Science*, *277*, 215–218.

Narcisi, B., J. R. Petit, B. Delmonte, I. Basile-Doelsch, and V. Maggi (2005), Characteristics and sources of tephra layers in the EPICA-Dome C ice record (East Antarctica): Implications for past atmospheric circulation and ice core stratigraphic correlations, *Earth Planet. Sci. Lett.*, *239*, 253–265.

Nishiizumi, K., D. Elmore, and P. W. Kubik (1989), Update on terrestrial ages of Antarctic meteorites, *Earth Planet. Sci. Lett.*, *93*, 299–313.

Parrenin, F., et al. (2007), The EDC3 chronology for the EPICA Dome C ice core, *Clim. Past*, in press.

Reimold, W. U., C. Koeberl, and J. S. V. Reddering (1998), The 1992 drill core from the Kalkkop impact crater, Eastern Cape Province, South Africa: Stratigraphy, petrography, geochemistry and age, *J. Afr. Earth Sci.*, *26*(4), 573–592.

Schultz, P. H., M. Zárate, B. Hames, C. Koeberl, T. Bunch, D. Storzer, P. Renne, and J. Wittke (2004), The Quaternary impact record from the Pampas, Argentina, *Earth Planet. Sci. Lett.*, *219*, 221–238.

Stauffer, B., J. Flückiger, E. Wolff, and P. Barnes (2004), The EPICA deep ice cores: First results and perspectives, *Ann. Glaciol.*, *39*, 93–100.

Taylor, S., J. H. Lever, and R. P. Harvey (2000), Numbers, types, and compositions of an unbiased collection of cosmic spherules, *Meteorit. Planet. Sci.*, *35*, 651–666.

Toon, O. B., K. Zahnle, D. Morrison, R. P. Turco, and C. Covey (1997), Environmental perturbations caused by the impacts of asteroids and comets, *Rev. Geophys.*, *35*(1), 41–78.

Wedepohl, K. H. (1995), The composition of the continental crust, *Geochim. Cosmochim. Acta*, *59*, 1217–1232.

Yada, T., T. Nakamura, N. Takaoka, T. Noguchi, K. Terada, H. Yano, T. Nakazawa, and H. Kojima (2004), The global accretion rate of extraterrestrial materials in the last glacial period estimated from the abundance of micrometeorites in Antarctic glacier ice, *Earth Planets Space*, *56*(1), 67–79.

Yiou, F., G. M. Raisbeck, and C. Jéhanno (1991), The micrometeorite flux to the earth during the last ~200,000 years as deduced from cosmic spherule concentration in Antarctic ice cores, *Meteoritics*, *26*, 412.

C. Engrand, Centre de Spectrométrie Nucléaire et de Spectrométrie de Masse, UMR8609 Centre National de la Recherche Scientifique & Université Paris Sud, Bâtiment 104, F-91405 Orsay Campus, France.

B. Narcisi, Centro Ricerche Casaccia, Ente per le Nuove Technologie, l'Energia e l'Ambiente, Via Anguillarese 301, I-00123 Roma, Italy. (narcisi@casaccia.enea.it)

J. R. Petit, Laboratoire de Glaciologie et Géophysique de l'Environnement, Centre National de la Recherche Scientifique, BP 96, F-38402 Saint Martin d'Hères, France.

Glossaire – 1

Termes scientifiques	
AIB	*α-Amino IsoButyric acid*. Acide aminé formé de façon abiotique, présent en faible concentrations dans les météorites et micrométéorites.
Åkermanite	Pôle magnésien de la mélilite : $Ca_2MgSi_2O_7$ (voir aussi Gehlenite).
Albite	Feldspath sodique : $NaAlSi_3O_8$ (voir aussi Anorthite et Orthose).
Anorthite	Feldspath calcique : $CaAl_2Si_2O_8$ (voir aussi Anorthite et Orthose).
BSE	*BackScattered Electron* (image). : image en microscopie électronique à balayage donnant une information sur la masse moléculaire moyenne locale de l'échantillon ("image en Z").
CAI	*Ca-Al-rich inclusion*. Ces inclusions réfractaires sont les premiers assemblages minéraux formés dans le système solaire, probablement par condensation à partir d'un gaz. Elles sont formées à très haute température et présentes en faibles abondances dans les météorites.
CCs	Classe des Chondrites Carbonées (météorites primitives).
CHON	Particules riches en C, H, O, N détectées dans la comète Halley par les missions spatiales Giotto et Vega (1986).
CI	Clan des chondrites carbonées de la famille d'Ivuna. Groupe pétrologique non précisé.
CI1	Clan des chondrites carbonées de la famille d'Ivuna. Groupe pétrologique 1.
CI2	Clan des chondrites carbonées de la famille d'Ivuna. Groupe pétrologique 2.
Clinopyroxène	Famille des pyroxènes de structure monoclinique. Formule générale: $(Mg,Fe,Ca)_2Si_2O_6$.
CM	Clan des chondrites carbonées de la famille de Murray. Groupe pétrologique non précisé.
CM2	Clan des chondrites carbonées de la famille de Murray. Groupe pétrologique 2.
Co-I	Co-Investigator (Missions spatiales).
Co-PI	Co-Principal Investigator (Missions spatiales).
CR2	Clan des chondrites carbonées de la famille de Renazzo. Groupe pétrologique 2.
CS	*Cosmic Spherule* : micrométéorite ayant globalement fondu lors de l'entrée atmosphérique et ayant acquis une forme arrondie.
CV	Clan de chondrites carbonées de la famille de Vigarano.
δD	Ecart relatif entre la composition isotopique de l'hydrogène d'un échantillon et une référence, exprimée en pourmil (‰). $\delta D = [(D/H_{échantillon})/(D/H_{référence}) - 1] \times 1000$. En général on utilise SMOW (*Standard Mean Ocean Water*) comme valeur de référence.
Diopside	Pyroxène riche en calcium de la famille des clinopyroxènes. Formule : $CaMgSi_2O_6$.
$\delta^{18}O$, $\delta^{17}O$	Ecart relatif entre le rapport $^{18}O/^{16}O$ ou $^{17}O/^{16}O$ d'un échantillon et d'une référence, exprimée en pourmil (‰). $\delta^{18}O = [(^{18}O/^{16}O_{échantillon})/(^{18}O/^{17}O_{référence}) - 1] \times 1000$. En général on utilise SMOW (*Standard Mean Ocean Water*) comme valeur de référence.
Effet de Matrice	Effet instrumental (élémentaire ou isotopique) qui modifie la réponse instrumentale en fonction de la nature du matériau analysé (minéraux de compositions ou de structures cristallines différentes, matière organique…).
EMMA	*Early MicroMeteorite Accretion*. Scénario développé par M. Maurette d'accrétion des éléments volatils par les micrométéorites sur la Terre primitive.
En_{XX}	Valeur permettant de visualiser la teneur en Mg d'un pyroxène $(Mg,Fe)SiO_3$ par rapport au pole pur Enstatite (En : $MgSiO_3$) : $XX = [Mg/(Mg+Fe)]$ (en atomes).
Enstatite (En)	Pôle magnésien des pyroxènes. Formule : $MgSiO_3$ (voir Ferrosilite pour le pôle riche en fer).
Fayalite (Fa)	Pôle riche en fer des olivines. Formule : Fe_2SiO_4 (voir Forstérite pour le pôle magnésien).
Fassaite	Pyroxène réfractaire riche en calcium et en titane observé dans les météorites. Parfois aussi appelé Augite. Formule générale : $(Ca,Na)(Mg,Fe,Al,Ti)(Si,Al)_2O_6$.
Feldspath	Famille d'aluminosilicates dont les trois pôles sont l'Orthose ($KAlSi_3O_8$), l'Albite ($NaAlSi_3O_8$) et l'Anorthite ($CaAl_2Si_2O_8$).

Glossaire – 1 (suite)

Termes scientifiques	
Ferrosilite (Fs)	Pôle riche en fer des pyroxènes. Formule : $FeSiO_3$ (voir Enstatite pour le pôle magnésien). N'existe pas à l'état naturel sur Terre.
Fg	*Fine-grained* : classe texturale des micrométéorites à grains fins.
FgC	*Fine-grained Compact* : classe texturale des micrométéorites non fondues présentant une structure à grains fins compacte.
FgF	*Fine-grained Fluffy* : classe texturale des micrométéorites présentant une structure à grains fins fragile et poreuse (collection Concordia).
Forsterite (Fo)	Pôle magnésien de l'olivine. Formule : Mg_2SiO_4 (voir Fayalite pour le pôle riche en fer).
Fo (nombre)	Valeur permettant de visualiser la teneur en Mg d'une olivine $(Mg,Fe)_2SiO_4$ par rapport au pôle pur de Forsterite (Fo : Mg_2SiO_4): Fo = [Mg/(Mg+Fe)] (en atomes).
Fractionnement instrumental	Effet isotopique introduit par l'instrument de mesure qui fait différer la valeur mesurée de la valeur vraie de l'échantillon (voir aussi IMF).
FWHM-G	*Full Width at Half Maximum* (largeur à mi-hauteur) de la bande G du carbone en spectroscopie Raman.
Gehlenite	Pôle alumineux de la mélilite $Ca_2Al(AlSi)O_7$ (voir aussi Åkermanite).
HED	Groupe d'achondrites basaltiques (*Howardites, Eucrites, Diogenites*).
IDPs	*Interplanetary Dust Particles*. Poussières cosmiques (tailles < 50 µm) collectées dans la stratosphère terrestre par la NASA.
IMF	*Instrumental Mass Fractionation* (voir Fractionnement instrumental).
Kamacite	Alliage de Fe-Ni pauvre en Ni (5 at% < Ni < 10 at%)
MC-ICPMS	*Multi-Collector Inductively Coupled Plasma Mass Spectrometry.* Technique de spectrométrie de masse en phase gazeuse, à détection parallèle.
MEB	Microscopie Electronique à Balayage.
Mélilite	Famille de minéraux réfractaires de formule générale $(Ca,Na)_2(Al,Mg,Fe)[(Al,Si)SiO_7]$. Les pôles principaux sont l'Åkermanite et la Gehlenite.
MET	Microscopie Electronique en Transmission.
MMA	MicroMétéorite Antarctique.
MM	MicroMétéorite.
MO1, MO2, MO3	Matière Organique 1, 2 et 3, comme définies dans *Aléon et al., 2001.*
NBS28	Standard utilisé pour la composition isotopique du silicium (NIST).
Olivine	Famille de silicates ferromagnésiens de structure orthorhombique de formule $(Mg,Fe)_2SiO_4$.
Orthopyroxène	pyroxène de structure orthorhombique, de formule générale $(Mg,Fe)SiO_3$.
Orthose	Feldspath potassique : $KAlSi_3O_8$ (voir aussi Albite et Anorthite).
Pentlandite	Sulfure de fer : $(Fe,Ni)_9S_8$.
PI	Principal Investigator (Missions spatiales).
Pyroxène	Famille de silicates ferromagnésiens de structure monoclinique (clinopyroxènes) ou orthorhombique (orthopyroxènes), formule courante $(Mg,Fe,Ca)_2Si_2O_6$.
Pyrrhotite	Sulfure de fer : $Fe_{(1-x)}S$ avec x = 0 – 0,17.
San Carlos	Olivine courante du manteau terrestre, riche en magnésium.
Sc	*Scoria* : classe texturale des micrométéorites partiellement fondues lors de l'entrée atmosphérique présentant des vésicules provenant du dégazage d'espèces volatiles.
SE	*Secondary Electron* (image) : image en microscopie électronique à balayage donnant une information fine sur la topographie de l'échantillon
SMOW	*Standard Mean Ocean Water* : valeurs de références pour les isotopes de l'oxygène et de l'hydrogène. $D/H_{SMOW} = 0,00015576$; $^{18}O/^{16}O_{SMOW} = 0,0020052$; $^{17}O/^{16}O_{SMOW} = 0,00038288$
Taenite	Alliage de Fe-Ni riche en Ni (20 at% <Ni < 65 at %)
TF Line	*Terrestrial Fractionation Line*. Pour les isotopes de l'oxygène, droite de pente ~ 1/2 définie par le fractionnement isotopique dépendant de la masse des isotopes de l'oxygène (^{16}O, ^{17}O, et ^{18}O) lors de transformations physiques (évaporation, condensation…). Sauf pour quelques exceptions (ozone…), tous les échantillons terrestres se placent sur cette droite.
Troilite	Sulfure de fer : FeS.
ω_oG	Position de la bande G du carbone en spectroscopie Raman.

Glossaire – 2

Instruments/missions	
Cameca IMS1270	Microsonde ionique à grand rayon commercialisée par Cameca. Facilité nationale au CRPG de Nancy.
Concordia	Station polaire franco-italienne des régions centrales antarctiques, ouverte à partir de 2004 aux hivernages et site prometteur pour les observations astronomiques. Lieu de collecte des micrométéorites Concordia (dans la neige).
CORICO	Logiciel d'analyse statistique de spectres (voir Lesty 1999).
COSIMA	Cometary Secondary Ion Mass Analyzer. Microsonde ionique à temps de vol implémentée sur l'orbiteur de la mission cométaire Rosetta ayant rendez-vous avec 67P/Churyumov-Gerasimenko en 2014.
Cosmic Vision	Programme de l'ESA pour l'exploration du système solaire.
Dôme C	Lieu géographique de la station Concordia dans les régions centrales antarctiques.
EPICA-Dôme C	Forage profond réalisé par la communauté scientifique européenne à des fins d'études climatologiques.
Giotto	Mission spatiale ayant étudié la comète de Halley (1986)
ILMA	Ion Laser Mass Analyzer. Spectromètre de Masse proposé dans le cadre de la mission spatiale MARCO POLO (Cosmic Vision).
IMS-Orsay	Microsonde ionique - prototype de laboratoire - basée sur un instrument commercial Cameca IMS4F initialement au laboratoire du physique des solides d'Orsay (équipe de G. Slodzian), et déménagée au CSNSM fin 2002.
MARCO POLO	Mission spatiale de retour d'échantillon et d'analyse d'astéroïde carboné proposée dans le cadre du programme Cosmic Vision de l'ESA, avec possibilité de coopération avec l'agence spatiale japonaise (JAXA).
ROSETTA	Mission spatiale d'analyse in situ de la comète 67P/Churyumov-Gerasimenko. Lancement en 2004, rendez-vous en 2014.
SIMS	*Secondary Ion Mass Spectrometry*. Technique de spectrométrie de masse par pulvérisation ionique, initialement mise au point par G. Slodzian. Autre nom de la microsonde ionique.
STARDUST	Mission spatiale de retour d'échantillons de la comète 81P/Wild 2 (NASA). Retour des échantillons sur Terre en Janvier 2006.
TOF-SIMS	SIMS avec spectromètre de masse à temps de vol (*Time-Of-Flight*).
Vega	Mission spatiale ayant étudié la comète de Halley (1986).

Glossaire – 3

Laboratoires/agences	
ANVAR	Agence Nationale de Valorisation de la Recherche.
CNES	Centre National d'Etudes Spatiales. Agence spatiale française.
CRPG	Centre de Recherches Pétrographiques et Géochimiques (Nancy).
CSNSM	Centre de Spectrométrie Nucléaire et de Spectrométrie de Masse (Orsay).
ENEA	Agence Nationale pour les Nouvelles Technologies, l'Energie et l'Environnement (Rome, Italie).
ESA	*European Space Agency*. Agence Spatiale Européenne.
GDR Exobiologie	Groupement de Recherche Exobiologie (maintenant remplacé par la SFE, Société Française d'Exobiologie).
IMCCE	Institut de Mécanique Céleste et de Calcul des Ephémerides, Paris.
ISAS	Institute of Space and Astronautical Science. Institut de recherche spatiale japonais.
JAXA	Japanese Aerospace eXploration Agency. Agence Spatiale japonaise.
JSC	Johnson Space Center (NASA Houston).
LGGE	Laboratoire de Glaciologie et de Géophysique de l'Environnement (Grenoble).
LPG	Laboratoire de Planétologie de Grenoble
LISA	Laboratoire Inter-universitaire des Systèmes Atmosphériques (Créteil).
LPCE	Laboratoire de Physique et Chimie de l'Environnement (maintenant 'et de l'Espace', LPC2E, Orléans).
LSPES	Laboratoire de Structure et Propriétés de l'Etat Solide (Lille).
MPI	Max Planck Institut (Allemagne).
NASA	National Aeronautics and Space Administration.
SFE	Société Française d'Exobiologie.
SWT	Science Working Team (Mission Rosetta).